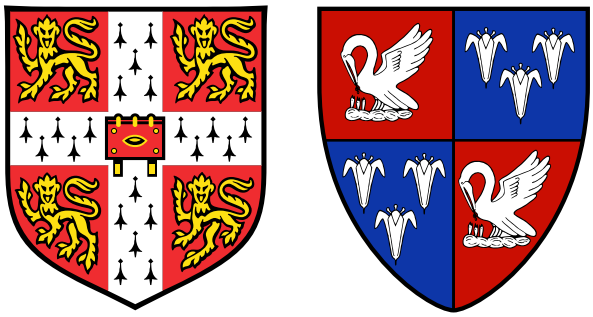
Exploring the Function of Cytochrome c_{6A}



Darius Gregor Kosmützky

Department of Biochemistry
University of Cambridge

This dissertation is submitted for the degree of
Doctor of Philosophy

Corpus Christi College September 2024

Declaration

This thesis is the result of my own work and includes nothing which is the outcome of work done in collaboration except as declared in the preface and specified in the text. It is not substantially the same as any work that has already been submitted, or is being concurrently submitted, for any degree, diploma or other qualification at the University of Cambridge or any other University or similar institution except as declared in the preface and specified in the text. It does not exceed the prescribed word limit for the relevant Degree Committee.

Darius Gregor Kosmützky
September 2024

Exploring the Function of Cytochrome c_{6A} - Abstract

by Darius Kosmützky

The electron transfer protein cytochrome c_6 (c_6) of photosynthesis was believed to have been lost in plants until a ubiquitous and highly conserved homologue, named cytochrome c_{6A} (c_{6A}), was identified. Soon after its discovery, c_{6A} was shown to be unable to replace c_6 (or plastocyanin) functionally in the photosynthetic electron transfer chain (PETC), despite their significant structural homology. Since then only few studies have revealed additional insights about c_{6A}. Thus its function remains unknown, although the high sequence conservation of c_{6A} across the green lineage points towards an important role. In this study, the function of c_{6A} in the green alga *Chlamydomonas reinhardtii* was explored. A wide range of microbiological, biochemical, and biophysical techniques was employed to compare c_{6A} knock-out and overexpression strains to the wild-type background.

Exposure to a harsh fluctuating light regime, named DISCO Light, in photomixotrophy was found to lead to a growth penalty in the absence of c_{6A}. No other significant growth phenotypes could be observed in continuous light, continuous darkness, or milder fluctuating light regimes in photoautotrophic or photomixotrophic conditions.

The light dependency of the growth phenotype and homology of c_{6A} to c_6 prompted in-depth analyses of the PETC using absorbance and fluorescence spectrometry. In the absence of c_{6A}, the light harvesting balance between PSI and PSII was shifted in favour of PSII and the PQ pool was more reduced, even in light conditions that did not cause a growth phenotype. While state transitions were at least in principle functional, the shift in light harvesting towards PSII was still present in conditions that would normally lead to state 1 or state 2. The more reduced PQ pool was found to have a prominent effect on the redox kinetics of *b* hemes in the cytochrome b_6f complex in response to light, while the Q cycle appeared functional. In DISCO Light, the c_{6A}-dependent phenotype of an altered light harvesting balance was amplified, the photochemical activity of PSII was lower without c_{6A}, and elevated NPQ levels suggested increased stress levels in the absence of c_{6A}. These insights explain the observed growth penalty which could be caused by the altered light harvesting balance, leading to a more reduced PQ pool, and ultimately increased damage through photooxidative stress in the absence of c_{6A}.

To investigate further a possible mechanism of action, the localisation and interactions of c_{6A} were studied. Using subcellular fractionation and immunofluorescence microscopy c_{6A} was found in the thylakoid lumen. Co-immunoprecipitation studies did not reveal any stable complexes, consistent with a function for c_{6A} through transient interactions. Examination of the effect of c_{6A} on complexes of the thylakoid membrane showed a putative LHC-less PSI complex that was more prominent in the absence of c_{6A}.

Western blot analysis indicated that the abundances of PSI and PSII core proteins were unlikely to account for the increased presence of this PSI complex, indicating that changes to the light harvesting antennae are more likely underlying this observation. Reduced abundance of PTOX2, a 'safety valve' for excess electrons in the PETC, was detected in the absence of c_{6A}, potentially contributing to the observed difference in PQ pool redox state. RNAseq revealed c_{6A}-dependent changes in transcript levels of genes associated with circadian rhythm, chloroplast thylakoid components including light-harvesting complex subunits, and thiol-based redox regulation, even in conditions that did not cause a growth phenotype. In addition, in DISCO Light, a decreased expression of oxidative stress response genes in the c_{6A} knock-out compared to wild-type was found, which could further contribute to the observed growth phenotype. Correspondingly, a transient increase in abundance of the stress-related NPQ effector LHCSR3 and the prominent emergence of PsbA breakdown products in the absence of c_{6A} in DISCO Light also indicated increased oxidative stress.

Previous hypotheses for the function of c_{6A} proposed that it is a replacement for plastocyanin, a safety valve for transfer of excess electrons, a high light signalling protein or, via its conserved disulfide bridge, a redox-regulator in the thylakoid lumen. The latter appeared the most likely in the light of the results of this study and the model for this was developed further. It is proposed that c_{6A} influences photosynthetic performance via fine-tuning the redox state of thiol-based redox regulation targets in the lumen, like the state transition kinase STT7 and the PSII subunit PSBO. It is further suggested that the ability of c_{6A} to transfer electrons via its bound heme and the disulphide bridge to multiple electron acceptors provides an additional degree of flexibility, important to maintain the complex luminal redox homeostasis, especially under stressful environmental conditions.

Hier wie dort ist die lebendige Natur die beste Lehrerin und Erzieherin.
Here, like there, living nature is the best teacher and nurturer.

Arnold & Carolina Dodel-Port, 1883



A passionflower (Passiflora) illustrated by Carolina Dodel-Port for the "Atlas der Botanik", in which many beautiful illustrations of plants and algae can be found together with informative text about their biology. The atlas was published in 1883 together with Dodel-Port's husband Arnold Dodel-Port who was a professor of botany in Zürich [1]. Despite there only being scaffold assemblies of Passiflora genomes available at the time of writing, a BLAST search of the scaffold assembly of the Passiflora edulis genome revealed a sequence homologous to cytochrome c_{6A} of Arabidopsis thaliana.

Acknowledgements

First and foremost I would like to express my deep gratitude to my supervisor Prof. Christopher Howe. He has been instrumental in bringing this PhD project to fruition. During a great number of meetings, scientific discussions, and theory exchanges I learned a lot from him. His kind support during my scientific journey made for a very enjoyable PhD experience. And last but not least, Chris, thanks for showing me how to ~~correctly~~ split infinitives correctly.

My PhD would have not been possible without the financial support of various funding bodies. I am grateful to the Gates Cambridge Trust, the Benn W Levy Fund of the Department of Biochemistry, the Cambridge Philosophical Society, the Genetics Society, the Biochemical Society, Corpus Christi College Cambridge, and AlgaeUK.

I have relied on the help of a great number of people and as all of their contributions to my PhD coming this far are important, I would like to list them in decreasing order of distance from my desk space in the Hopkins Building of the Department of Biochemistry to prevent any wrong impression of decreasing importance.

The funding listed above has enabled me to visit many exciting places with fascinating conferences and importantly supported two research visits to the University of Turku where I was able to generate the data for chapter 4. I would like to thank Prof. Yagut Allahverdiyeva for hosting me in her group in Turku, for the helpful scientific discussions, for organising additional financial support, and for various antibody aliquots. I am deeply indebted to Dr. Laura Wey who taught me a lot about photosynthesis, how to use the biophysics equipment to investigate it, and how to analyse the complex data outputs. Dr. Wey also performed the 77 K chlorophyll fluorescence measurements presented in section 4.2.2.1 with samples sent from Cambridge. Furthermore, I would like to give thanks to Dr. Lauri Nikkanen is a great source of knowledge on all things biophysics, and a great source of patience throughout various MIMS measurements. Speaking of MIMS, I would like to thank Michal Hubáček for helping me out in the final days of my second Turku visit. Additionally, thank you to Dr. Martina Jokel-Toivanen for providing me with *flv* mutant strains and advice on *C. reinhardtii*. Thanks to the all members of the Photosynthetic Microbes group and the wider Molecular Plant Biology unit for making me feel so welcome in Turku, kiitos!

Support from across Europe came from Prof. Gilles Peltier (Marseille) who kindly provided an aliquot of the NDA2 antibody. The project presented here, relied on a modified *C. reinhardtii* strain that was created by Dr. Aron Ferenczi in Dr. Attila Molnar's group at the University of Edinburgh. I would like to thank them for this vital contribution. I am grateful to Dr. Sandrine Bujaldon from Prof. Francis-André Wollman's group (Paris, yes it is closer than Edinburgh!) for sending an aliquot of the PTOX2 antibody.

In Cambridge many people were helping me, too. Thanks to Prof. Ben Luisi (Sanger Building) for his insightful feedback during the meetings of my Postgraduate Thesis Panel (PTP). I would like to express my gratitude to Dr. Katrin Geisler from Prof. Alison Smith's group in the Department of Plant Sciences (3rd floor) for various lab protocols, the fluorescent *C. reinhardtii* strains I used as controls in chapter 5, and the supportive and insightful scientific discussions. I would also like to acknowledge Dr. Lorraine Archer for her help and the whole Smith group for having me in lab meetings to learn more about microalgae. I would like to thank Prof. Alison Smith for facilitating all this and for providing helpful feedback on various parts of my work as part of my PTP. Also in the Plant Sciences department, I thank Dr. Julia Walter from Dr. Johannes Kromdijk's group (1st floor) who has kindly taken the time to teach me the secrets of blue native PAGE and to help me find the antibodies originally raised by Prof. John C. Gray. Moving closer to my desk, I am grateful to Prof. Ross Waller and his lab members Dr. Brandon Mercado-Saavedra and Sara Chelaghma (ground floor Hopkins Building) for access and introduction to the confocal microscope. Prof. Paul Dupree is next closest (1st floor Hopkins Building) and I would like to thank him for helpful discussions during my PTP meetings. My thanks also to the rest of the Dupree group (Darragh, Alberto E, Henry, Dora, Yoshi, Nadine, Parveen *et al.*) for creating a nice working atmosphere. I am thankful for the support of the Howe lab members (Wendy, Adrian, Stephen, Paolo, Joel, and Loris) and the various students we hosted over the time of my PhD. Especially, I would like to thank Alexandre Mann for being on "Team c_{6A}" for his Master's project and creating and testing constructs mentioned in section 3.2.2. Special thanks to Dr. Alberto Scarampi (same office at the window) for measuring algae cultures when I was ill or away and for the scientific advice on Golden Gate and beyond. Closest is Dr. Joshua Lawrence (same office opposite side), who I am grateful to for various occasions of diving deep into biophysical data trying to make sense of it and theorising about the function of c_{6A}.

Leaving the workplace and ordering-by-distance behind, this PhD endeavour would not have been possible without a little help from my friends. Through being in Cambridge and part of Corpus Christi College, I met many wonderful people. Cristina, Albi, and Michal, thank you for being home away from home, surviving a pandemic together, and teaching me how to play the guitar and Briscola. Thanks to the rest of the extended Selwyn gang, too. I want to thank Dora for being there throughout, Lukas for all the chats, Nils for the tennis outings, Kitty for her encouragement, and Morgan for always having an open ear for me. I would like to express my deep gratitude to my partner and friend Emma for making me laugh, brainstorming science together, and reminding me of the lovely things in life during the harder times. I'm incredibly grateful for the joy and comfort I have found in the friends I got to meet before moving to the UK and have been fortunate enough to keep ever since. A heartfelt thanks to Hannes, Nicole, Moritz, Miriam, Simon, Robert, Jan, Darja, and Robin. Last, I want to thank my family in Germany for their everlasting support. Tausend Dank an Irene, Erich, Alina, Kevin, Corinna und Daniel, sowie auch an meine kleine Nichte Lucia für's Mich-zum-lachen-bringen während der Schreibphase!

Publications & Conference Presentations

The research presented in this thesis was in preparation for publication in scientific journals at the time of writing. A list of publications the author contributed to during the time this research was carried out, is shown below.

D. Kosmützky, L. T. Wey, L. Nikkanen, Y. Allahverdiyeva and C. J. Howe, "Cytochrome c_{6A} is Important for Growth under Fluctuating Light and Maintaining the Redox Balance of the Photosynthetic Electron Transfer Chain in *Chlamydomonas reinhardtii*". In preparation.

T. K. Baikie, **D. Kosmützky**, J. M. Lawrence, V. Gray, C. Schnedermann, R. Horton, J. D. Collins, H. Medipally, B. Witek, M. M. Nowaczyk, et al., "Ultrafast *In vivo* Transient Absorption Spectroscopy", arXiv (2023).

I. Nimmo, K. Geisler, A. C. Barbrook, F. H. Kleiner, A. Scarampi, **D. Kosmützky**, E. Nisbet, and C. J. Howe, "Establishment of a Novel Set of Vectors for Transformation of the Dinoflagellate *Amphidinium carterae*", bioRxiv (2022).

B. Slater*, **D. Kosmützky***, R. E. R. Nisbet, and C. J. Howe, "The Evolution of the Cytochrome c_6 Family of Photosynthetic Electron Transfer Proteins", Genome Biology and Evolution 13, 1–12 (2021). (*co-first authors)

Parts of the research presented in this thesis have been presented at scientific conferences listed below.

Second European Congress on Photosynthesis Research in Padua, Italy (June 2024)
Winner "Best Poster Award" and selected speaker for the "Young Session": "Stayin' Alive in the DISCO Light: Cytochrome c_{6A} Impacts Photosynthetic Electron Flow and Growth in Fluctuating Light of *Chlamydomonas reinhardtii*"

Plastid Preview in Oxford, UK (September 2023)
Selected speaker: "Stayin' Alive in the DISCO Light: Unravelling the Mystery of Cytochrome c_{6A} in *Chlamydomonas reinhardtii*"

Gordon Research Conference - Photosynthesis in Newry (ME), USA (July 2023)
Poster presentation: "Stayin' Alive in the DISCO Light: Unravelling the Mystery of Cytochrome c_{6A} in *Chlamydomonas reinhardtii*"

School of Molecular and Biophysical Bases of Photosynthesis in Venice, Italy (May 2022)
Oral presentation: "Function of Cytochrome c_{6A}"

Chlamy 2020+1 in Ile-des-Embiez, France (September 2021)
Poster presentation: "Chlamy in the Spotlight - Transcriptomic Response to High Light in *C. reinhardtii*"

Table of contents

Declaration iii

Exploring the Function of Cytochrome c_{6A} - Abstract v

Acknowledgements ix

Publications & Conference Presentations xi

List of figures xxi

List of tables xxv

Acronyms / Abbreviations xxvii

1 General Introduction 1

1.1 The model organism *Chlamydomonas reinhardtii* 1

1.1.1 *C. reinhardtii* in the laboratory 3

1.2 Photosynthesis in *C. reinhardtii* 4

1.2.1 Linear electron flow & the Calvin-Benson-Bassham cycle 5

1.2.2 Alternative electron flow pathways 8

1.2.3 Non-photochemical quenching 12

1.2.4 The impact of acetate on photosynthesis in *C. reinhardtii* 17

1.2.5 Redox regulation in the thylakoid lumen 18

1.3 The soluble electron transfer proteins plastocyanin and cytochrome c_6 . . . 21

1.4 Cytochrome c_{6A} 21

1.4.1 Discovery 21

1.4.2 Structure and physical properties 22

1.4.3 Conservation in the green lineage, further homologues & phylogenetic history 24

1.4.4 Localisation & interaction partners 25

1.4.5 Proposed functions 26

1.4.6 CRISPR-mediated c_{6A} knock-out in *C. reinhardtii* 28

1.5 Overall aims and structure of the study 29

2 Materials & Methods **31**

2.1 Algae strains & growth conditions 31

2.1.1 *Chlamydomonas reinhardtii* strains 31

2.1.2 Growth of *C. reinhardtii* 31

2.2 Molecular biology techniques 34

2.2.1 DNA extraction from *C. reinhardtii* 34

2.2.2 RNA extraction from *C. reinhardtii* 35

2.2.3 Colony PCR of *C. reinhardtii* 36

2.2.4 Golden Gate assembly of constructs for transformation of *C. reinhardtii* 38

2.2.5 Transformation of *C. reinhardtii* 40

2.3 Biochemical analyses 40

2.3.1 Chlorophyll quantification in *C. reinhardtii* samples 40

2.3.2 Determination of acetate concentration in *C. reinhardtii* medium . . 40

2.3.3 Chloroplast and thylakoid isolation from *C. reinhardtii* 41

2.3.4 Fractionation of *C. reinhardtii* chloroplasts 41

2.4 Protein Analyses 42

2.4.1 Protein extraction from *C. reinhardtii* 42

2.4.2 Protein gel electrophoresis 42

2.4.3 Membrane transfer and immunoblotting 43

2.4.4 Co-immunoprecipitation of FLAG-tagged proteins and putative interaction partners from *C. reinhardtii* lysates 45

2.4.5 Blue native PAGE of *C. reinhardtii* thylakoids 45

2.4.6 Second dimension SDS-PAGE of BN-PAGE 46

2.5 Microscopy 47

2.5.1 Fluorescence microscopy 47

2.5.2 Immunofluorescence staining & microscopy of *C. reinhardtii* 47

2.6 Spectrometric methods 48

2.6.1 Measurement of light intensity 48

2.6.2 Measurement of fluorescent protein expression 48

2.6.3 Low temperature fluorescence spectroscopy of *C. reinhardtii* 48

2.6.4 Pulse-amplitude modulation (PAM) fluorometry of *C. reinhardtii* . 49

2.6.5 Chlorophyll fluorescence induction spectroscopy (OJIP) of *C. reinhardtii* 49

2.6.6 P700 differential absorbance spectrometry of *C. reinhardtii* 50

2.6.7 Coupled fluorescence and absorption spectrometry monitoring PSII and PSI of *C. reinhardtii* 50

2.6.8 DUAL-KLAS-NIR absorbance spectrometry of *C. reinhardtii* . . . 51

2.6.9 Cytochrome b_6f differential absorbance spectrometry of *C. reinhardtii* using a Joliot type spectrometer (JTS) 52

2.6.10 Electrochromic shift (ECS) measurements of *C. reinhardtii* 53

2.6.11 Membrane inlet mass spectrometry of *C. reinhardtii* 54

2.7 Sequencing 54

2.7.1 Sanger sequencing 54

2.7.2 Whole genome sequencing of *C. reinhardtii* 54

2.7.3 RNA sequencing of isolated RNA from *C. reinhardtii* 55

2.8 Bioinformatic methods 55

2.8.1 General data analysis, visualisation and statistics 55

2.8.2 Whole genome sequencing analysis and single nucleotide polymorphism (SNP) analysis 55

2.8.3 RNA sequencing analysis 56

3 Creation and characterisation of cytochrome c_{6A} mutant strains in *C. reinhardtii* 57

3.1 Introduction 57

3.1.1 A brief history of *C. reinhardtii* laboratory strains 57

3.1.2 Growth of *C. reinhardtii* in the presence of acetate 58

3.1.3 Growth of *C. reinhardtii* under fluctuating light conditions 59

3.1.4 Aims 62

3.2 Results & Discussion 62

3.2.1 A CRISPR-edited *C. reinhardtii* strain was confirmed to be a cytochrome c_{6A} knock-out via PCR and whole genome sequencing . . 62

3.2.2 A Golden Gate c_{6A} overexpression construct led to c_{6A} expression in *C. reinhardtii* c_{6A}-KO 64

3.2.3 Comparison of growth of *C. reinhardtii* cytochrome c_{6A} mutant strains 66

3.3 Conclusion & Outlook 75

4 Biophysical investigation of cytochrome c_{6A} mutant strains in *C. reinhardtii* 77

4.1 Introduction 77

4.1.1 Fluorescence spectrometric approaches for probing the PETC . . . 77

4.1.2 Absorbance spectrometric approaches for probing the PETC 82

4.1.3 Membrane-inlet mass spectrometry 87

4.1.4 Aims 88

4.2 Results & Discussion 88

4.2.1 The effect of c_{6A} on the photosynthetic electron transfer chain of *C. reinhardtii* in continuous light 88

4.2.2 The effect of c_{6A} on the photosynthetic electron transfer chain of *C. reinhardtii* in DISCO Light 108

4.3 Conclusion & Outlook 119

4.3.1 Summary of findings from biophysical investigation of the PETC of *C. reinhardtii* c_{6A} mutant strains 119

4.3.2 Further work 120

5 Localisation of cytochrome c_{6A} and its effect on thylakoid membrane complexes 123

5.1 Introduction 123

5.1.1 Subcellular architecture of *C. reinhardtii* 123

5.1.2 Protein complexes in the thylakoid membrane of *C. reinhardtii* . . . 124

5.1.3 Aims 127

5.2 Results & Discussion 127

5.2.1 Localisation of cytochrome c_{6A} in *C. reinhardtii* 127

5.2.2 Co-immunoprecipitation of putative interaction partners of c_{6A} in *C. reinhardtii* does not reveal any stable interactions 139

5.2.3 The effect of cytochrome c_{6A} on protein complexes of the thylakoid membrane in *C. reinhardtii* 144

5.3 Conclusion & Outlook 151

5.3.1 Summary of findings 151

5.3.2 Further work 153

6 Protein and transcript levels of cytochrome c_{6A} mutant strains in *C. reinhardtii* 155

6.1 Introduction 155

6.1.1 Responses to stressful light in *C. reinhardtii* 155

6.1.2 Effect of stress and other environmental conditions on transcript levels of cytochrome c_{6A} 156

6.1.3 Aims 158

6.2 Results & Discussion 158

6.2.1 The effect of c_{6A} on the abundance of selected proteins associated with photosynthesis 159

6.2.2 Transcriptomic analysis of *C. reinhardtii* c_{6A} mutant strains exposed to DISCO Light 169

6.2.3 Comparison of protein and transcript levels of *C. reinhardtii* c_{6A} mutant strains 192

6.3 Conclusion & Outlook 196

6.3.1 Summary of findings 196

6.3.2 Further work 197

7 General Conclusions & Outlook 199

7.1 Summary of findings 199

7.2 Findings in the light of proposed functions 204

7.2.1 Cytochrome c_{6A} as a replacement for plastocyanin? 205

7.2.2 Cytochrome c_{6A} as part of a high light signalling response? 206

7.2.3 Cytochrome c_{6A} as safety valve for excess electrons? 206

7.2.4 Cytochrome c_{6A} as part of thiol-based redox regulation? 207

7.3 Working hypothesis for the function of cytochrome c_{6A} 209

7.3.1 Putative regulation targets of c_{6A} 210

7.3.2 Putative downstream electron acceptors from c_{6A} 214

7.3.3 Cytochrome c_{6A} is a soluble mediator in the complex thiol-based redox regulation network in the thylakoid lumen and fine-tunes STT7 activity and PSBO stability 218

7.3.4 Challenges to the hypothesis and open questions 218

7.4 Further work 220

7.4.1 Testing the thiol-based redox regulation hypothesis 220

7.4.2 The function of c_{6A} beyond *C. reinhardtii* 222

7.4.3 The function of other c_6-like cytochromes 224

References **227**

Appendix A Plasmid maps **255**

Appendix B Additional WGS data **259**

Appendix C Additional mass-spectrometric data of 2D-PAGE spots **263**

Appendix D PonceauS stains of membranes used for western blots **271**

Appendix E RNAseq quality control details **275**

List of figures

1.1 Phylogenetic relationships among the main lineages of Viridiplantae 2

1.2 Historic print of the *Chlamydomonas* genus 3

1.3 The photosynthetic electron transfer chain 5

1.4 The different routes of cyclic electron flow in *C. reinhardtii* 9

1.5 The different water-to-water cycles in *C. reinhardtii* 10

1.6 Mechanism of response to excess light in *C. reinhardtii* 13

1.7 Principle of state transitions and activation of the STT7 kinase in *C. reinhardtii* 15

1.8 Thiol-based redox regulation in the thylakoid lumen 19

1.9 Structure and sequence conservation in the green lineage of c_{6A} 23

1.10 Ancestry model for the cytochrome c_6 family in photosynthetic organisms . 24

1.11 The *CYC4* gene during the process of CRISPR/Cpf1 modification 28

2.1 PCR cycling protocol used for *C. reinhardtii* colony PCR 36

2.2 Golden Gate assembly thermocycler protocol 39

3.1 Ancestry of *C. reinhardtii* laboratory strains 58

3.2 Genetic analyses of c_{6A}-KO and WT 63

3.3 Creation of a cytochrome c_{6A}-overexpression strain 65

3.4 Growth curves of c_{6A}-KO and WT under continuous light conditions 67

3.5 Introducing DISCO Light, a harsh fluctuating light regime 69

3.6 Growth curves of c_{6A}-KO and WT under darkness and fluctuating light regimes 71

3.7 Chlorophyll and acetate content of c_{6A}-KO and WT cultures 73

4.1 A chlorophyll fluorescence trace from a PAM fluorescence measurement . . 79

4.2 Example OJIP curves of *C. reinhardtii* 81

4.3 Principle of the P700 saturating pulse method 83

4.4 Principle of measuring cytochrome b_6f redox kinetics with a JTS 85

4.5 Principles of pmf measurements using electrochromic shift (ECS) 86

4.6 77 K chlorophyll fluorescence spectra of c_{6A} mutant strains and WT 89

4.7 77K measurements of state transitions in c_{6A}-KO and WT 91

4.8 PSII and PSI parameter light curves of c_{6A} mutant strains and WT 93

4.9 Redox changes of Pc, P700, and Fd of c_{6A}-KO and WT 96

4.10 OJIP curves of c_{6A} mutant strains and WT 98

4.11 Redox changes of *b* hemes, Cyt *f*, and Pc in c_{6A} mutant strains and WT . . 100

4.12 Further measurements of *b* hemes redox changes in c_{6A} mutants and WT . . 103

4.13 ECS measurements of c_{6A} mutant strains and WT 106

4.14 O_2 flux measurements of c_{6A} mutant strains and WT 107

4.15 77 K spectra of c_{6A} mutant strains and WT grown under DISCO Light . . . 109

4.16 PSII parameters of c_{6A}-KO and WT under DISCO Light conditions 111

4.17 ECS of c_{6A} mutant strains and WT under DISCO Light conditions 115

4.18 PSI parameters of c_{6A}-KO and WT under DISCO Light conditions 117

5.1 Diagram of the *C. reinhardtii* cell 124

5.2 Creation of a mVenus-tagged cytochrome c_{6A} expression strain 128

5.3 Fluorescence microscopy of a putative c_{6A}-mVenus overexpressing strain . 130

5.4 Images of the gradients used for subcellular fractionation of *C. reinhardtii* . 131

5.5 Fluorescence microscopy of subcellular fractions of a c_{6A}-FLAG strain . . 133

5.6 Immunoblot analyses of subcellular fractions of a c_{6A}-FLAG strain 135

5.7 Immunofluorescence localisation of c_{6A}-FLAG 138

5.8 Co-IP of FLAG-tagged proteins from a c_{6A}-FLAG strain grown in continuous light conditions 140

5.9 Co-IP of FLAG-tagged proteins from a c_{6A}-FLAG strain grown in DISCO Light conditions 143

5.10 BN-PAGE analysis of thylakoid membrane complexes from c_{6A} mutant strains and WT 145

5.11 2D-PAGE analysis of a BN-PAGE lane from c_{6A}-KO 147

5.12 2D-PAGE analyses of futher BN-PAGE lanes from c_{6A} mutant strains and WT 149

6.1 Experimental setup for the investigation of protein and transcript levels of c_{6A} mutant strains and WT grown in continuous light or DISCO Light . . . 159

6.2 Immunoblot analyses of proteins isolated from c_{6A} mutant strains and WT grown in continuous light conditions 160

6.3 Immunoblot analyses of proteins isolated on day 2 from c_{6A} mutant strains and WT grown in DISCO Light conditions 164

6.4 Immunoblot analyses of proteins isolated on day 4 from c_{6A} mutant strains and WT grown in DISCO Light conditions 167

6.5 Expression of *CYC4* in the RNAseq experiment 171

6.6 Principal Component Analysis (PCA) of the RNAseq count data 172

6.7 Comparisons of gene expression between strains and/or conditions 173

6.8 Heatmap of the 225 DEGs from c_{6A}-KO versus WT in continuous light . . 179

6.9 Venn diagram of DEGs from c_{6A}-KO versus WT 180

6.10 Heatmap of the 372 DEGs from c_{6A}-KO versus WT in DISCO light 184

6.11 GO enrichment analysis for DEGs from WT DISCO Light versus continuous light 186

6.12 GO enrichment analysis for DEGs from c_{6A}-KO comparing DISCO Light versus continuous light 188

6.13 Heatmap of the top 250 DEGs that were unique to "c_{6A}-KO DISCO vs continuous light" 189

6.14 Heatmap of genes encoding proteins associated with photosynthesis 191

6.15 Comparison of protein and transcript levels of selected genes 194

7.1 Selected parts of thiol-based redox regulation in the thylakoid lumen 209

7.2 Hypothesis: putative target proteins of c_{6A} in the thylakoid lumen 211

7.3 Hypothesis: downstream electron acceptors of c_{6A} in the thylakoid lumen . 215

7.4 Hypothesis: cytochrome c_{6A} as redox-regulator in the thylakoid lumen . . . 217

A.1 Plasmid maps of pDK plasmids 258

B.1 Quality assessment graphs of whole genome sequencing data on WT 260

B.2 Quality assessment graphs of whole genome sequencing data on c_{6A}-KO . . 261

B.3 Exon read count comparison between WT and c_{6A}-KO 262

D.1 PonceauS total protein stain of protein samples from continuous light . . . 271

D.2 PonceauS total protein stain of protein samples from DISCO Light Day 2 . 272

D.3 PonceauS total protein stain of protein samples from DISCO Light day 4 . . 273

E.1 Gel electrophoresis of RNA samples 276

List of tables

2.1 Recipe for TP/TAP media 32

2.2 Recipe for Beijerinck salts solution 32

2.3 Recipe for Hutner's trace elements solution 33

2.4 Experimental light conditions 34

2.5 Recipe for DNA extraction buffer 35

2.6 Recipe for RNA gel-loading buffer 36

2.7 Components of a *C. reinhardtii* colony PCR reaction 37

2.8 Primer sequences 37

2.9 Recipe for Tris-Borate-EDTA (TBE) buffer 38

2.10 Golden Gate acceptor plasmids 39

2.11 Components of a Golden Gate assembly reaction 39

2.12 Antibodies 44

2.13 Voltage and time specifications for BN-PAGE 46

2.14 Light intensities and exposure times for light response curves 51

2.15 Chemicals used to affect the PETC in *C. reinhardtii* during JTS experiments 53

3.1 Fluctuating light phenotypes 60

3.2 Photosystem II quantum yields of c_{6A}-KO and WT 68

4.1 Photosynthetic parameters and their calculation 80

5.1 Proteins that could be unspecifically anti-FLAG immunoprecipitated 141

6.1 Expression of *CYC4* under various conditions 157

6.2 Number of DEGs in the RNAseq experiment 173

6.3 Top 10 upregulated DEGs comparing c_{6A}-KO to WT in continuous light . . 175

6.4 Top 10 downregulated DEGs comparing c_{6A}-KO to WT in continuous light 177

6.5 Top 10 upregulated DEGs comparing c_{6A}-KO to WT in DISCO light 181

6.6 Top 10 downregulated DEGs comparing c_{6A}-KO to WT in DISCO light . . 182

6.7 Other notable downregulated genes in c_{6A}-KO unique to DISCO Light . . . 183

6.8 Differential expression of selected genes associated with photosynthesis . . 195

7.1 Summary of findings of the study 201

B.1 Results of fastQC quality assessment of the whole genome sequencing data 259

C.1 Identified proteins from peptides found in the spot assigned to PsaA 263

C.2 Identified proteins from peptides found in the spot assigned to PSAL 264

C.3 Identified proteins from peptides found in the spot assigned to PsbC 265

C.4 Identified proteins from peptides found in the spot assigned to PetD 266

C.5 Identified proteins from peptides found in the spot assigned to LHCA1 . . . 267

C.6 Identified proteins from peptides found in the spot assigned to PRX1 268

C.7 Identified proteins from peptides found in the yellow circled spot 269

E.1 Nanodrop measurements of RNA samples used for RNAseq 275

E.2 RNA sample quality as determined by Novogene 277

E.3 Read quality measures of RNAseq samples 278

Acronyms / Abbreviations

β-DM	β-Dodecyl maltoside
A. thaliana	*Arabidopsis thaliana*
2D-PAGE	Two-dimensional BN-PAGE/SDS-PAGE
AEF	Alternative electron flow
ANOVA	Analysis of Variance
ATP	Adenosine triphosphate
BN-PAGE	Blue native PAGE
C. reinhardtii	*Chlamydomonas reinhardtii*
c_6	Cytochrome c_6
c_{6A}	Cytochrome c_{6A}
c_{6B}	Cytochrome c_{6B}
CBB cycle	Calvin-Benson-Bassham cycle
CDS	Coding sequence
CEF	Cyclic electron flow
Co-IP	Co-immunoprecipitation
Cpf1	CRISPR-associated endonuclease in Prevotella and Francisella 1
CRISPR	Clustered Regularly Interspaced Short Palindromic Repeats
cw15	Cell wall-less mutation in *C. reinhardtii*
DBMIB	Dibromothymoquinone
DCMU	3-(3,4-dichlorophenyl)-1,1-dimethylurea
DEG	Differentially expressed gene
DIRK	Dark interval relaxation kinetic
DISCO Light	Darkness Interrupted by Short COntinuous Light
DMP	Differential model plot
DNA	Deoxyribonucleic acid
ECS	Electrochromic shift
EDTA	Ethylenediaminetetraacetatic acid disodium salt

FLV	Flavodiiron protein
FNR	Ferredoxin-$NADP^+$ reductase
FTR	Ferredoxin-thioredoxin reductase
GAPDH	Glyceraldehyde-3-phosphate dehydrogenase
GO	Gene ontology
IAA	Isoamyl alcohol
JTS	Joliot-type spectrometry
KO	Knock-out
LB	Lysogeny broth
LC-MS/MS	Liquid chromatography coupled mass spectrometry
LEF	Linear electron flow
LHCI(I)	Light harvesting complex I(I)
LIP	Loop insertion peptide
MIMS	Membrane inlet mass spectrometry
MS	Mass spectrometry
mt	Mating type
MV	Methyl viologen
n-PG	n-Propyl gallate
NAD(P)H	Nicotinamide adenine dinucleotide (phosphate)
NPQ	Regulated non-photochemical quenching
OD_{750nm}	Optical density at 750 nm
OE	Overexpression
OEC	Oxygen-evolving cluster
PAGE	Polyacrylamide gel electrophoresis
PAM	Pulse-amplitude modulation
PAR	Photosynthetically active radiation
PBS	Phosphate-buffered saline
PCR	Polymerase chain reaction
PETC	Photosynthetic electron transfer chain
pmf	Proton motive force

PMSF	Phenylmethylsulphonyl fluoride
PQ	Plastoquinone
PSI(I)	Photosystem I(I)
qE	Energy-dependent quenching
qI	Photoinhibitory quenching
qT	State transition quenching
qZ	Zeaxanthin-dependent quenching
rETR	Relative electron transfer rate
R_f	In gel mobility measure
RNA	Ribonucleic acid
RNP	Ribonucleoprotein
ROS	Reactive oxygen species
RT	Room temperature
RuBisCO	Ribulose-1,5-bisphosphate carboxylase/oxygenase
RuBP	Ribulose-1,5-bisphosphate
SD	Standard deviation
SE	Standard error
SDS	Sodium dodecyl sulfate
SNP	Single nucleotide polymorphism
SP	Saturating pulse
ST or MT	Single or multiple turnover flash
TAP	Tris-Acetate-Phosphate
TBS	Tris-buffered saline
TP	Tris-Phosphate
WGS	Whole genome sequencing
WT	Wild-type
WWC	Water-to-water cycle
Y2H	Yeast-two-hybrid

1

General Introduction

1.1 The model organism *Chlamydomonas reinhardtii*

The green lineage, or Viridiplantae, encompasses all green algae and plants, representing an enormous diversity of species inhabiting vital roles in ecosystems both on land and in aquatic environments [2]. The unicellular ancestor of the green lineage emerged following an endosymbiotic event that also led to the development of the red (Rhodophyta) and glaucophyte (Glaucophyta) lineages [3]. While research into the phylogeny of Viridiplantae is still ongoing (e.g. [4]), two primary lineages have long been recognised: the Chlorophyta and the Streptophyta (figure 1.1) [5, 6]. Streptophyta include the Charophyta, a paraphyletic group of freshwater algae, and the land plants (Embryophyta). Chlorophyta primarily consist of unicellular planktonic algae that diversified predominantly in marine environments. This latter lineage gave rise to the Prasinophyta and the morphologically and ecologically diverse core chlorophytes. Within the core chlorophytes lies the class Chlorophyceae, which includes the order Chlamydomonales, phylogenetic 'home' to the model organism *Chlamydomonas reinhardtii* (*C. reinhardtii*) used in this study.

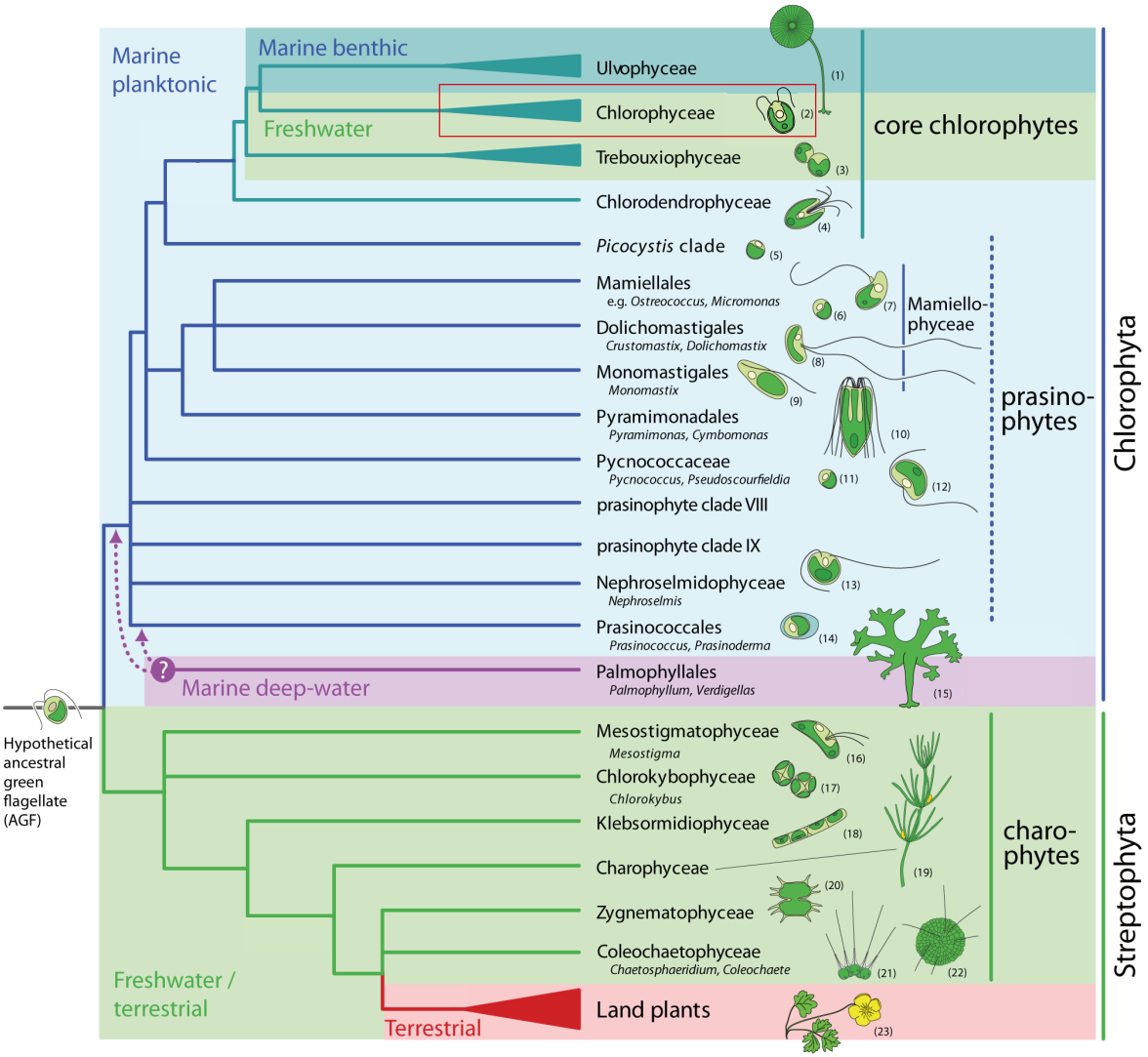


Figure 1.1: Phylogenetic relationships among the main lineages of Viridiplantae. The tree topology is a composite of accepted relationships based on molecular phylogenetic evidence. Uncertain phylogenetic relationships are indicated by dotted lines. The class of the model organism used here, *C. reinhardtii*, is indicated by a red box. Drawings illustrate representatives of each lineage: (1) *Acetabularia*, (2) *Chlamydomonas*, (3) *Chlorella*, (4) *Tetraselmis*, (5) *Picocystis*, (6) *Ostreococcus*, (7) *Micromonas*, (8) *Crustomastix*, (9) *Monomastix*, (10) *Pyramimonas*, (11) *Pycnococcus*, (12) *Pseudoscourfieldia*, (13) *Nephroselmis*, (14) *Prasinococcus*, (15) *Verdigellas*, (16) *Mesostigma*, (17) *Chlorokybus*, (18) *Klebsormidium*, (19) *Chara*, (20) *Xanthidium*, (21) *Chaetosphaeridium*, (22) *Coleochaete*, (23) *Ranunculus*. Adapted from Leliaert *et al.* (2011) [6].

The genus *Chlamydomonas* was named in 1838 by Christian Gottfried Ehrenberg (originally *Chlamidomonas* as Ehrenberg was German, figure 1.2) [7]. In 1888, the species *C. reinhardtii* was named by the French botanist Pierre Dangeard, in honour of Ludwig Reinhard, a Ukrainian botanist who had published on the mating of algae [8, 9]. The origin of the *C. reinhardtii* laboratory strains used today lies in a potato field in Massachusetts, USA.

In 1945, Gilbert Smith isolated *C. reinhardtii* from soil samples and his strain 137c went on to be a widespread photosynthetic model organism [8].



Figure 1.2: Print from copper-plate engravings of members of the *Chlamydomonas* genus illustrated by Ehrenberg. The species was identified as *Chlamidomonas pulvisculus* but renamed *Chlamydomonas reinhardtii* in 1888. From Ehrenberg (1838) [7].

1.1.1 *C. reinhardtii* in the laboratory

Nearly two centuries after its genus was first named and 80 years after the isolation of the present-day laboratory strain, *C. reinhardtii* has become a widely used model organism in plant biology, thanks to several key advantages.

One significant reason for the popularity of *C. reinhardtii* is its ease of handling in laboratory settings. *C. reinhardtii* can grow in liquid and solid media at moderate temperatures of 20-25 °C, with a shorter generation time than plants [10]. Furthermore, it grows photoautotrophically, as well as under photomixotrophic and heterotrophic conditions in the presence of acetate [8]. *C. reinhardtii* can reproduce both asexually and sexually. Asexual reproduction is advantageous for experiments that require genetically identical cells, while sexual reproduction has been instrumental in genetic research, enabling the crossing of different strains to create new mutants.

Another asset is its fully sequenced haploid genome, which consists of 121 Mb and is annotated with gene identifiers and additional information [11, 12]. However, the latter is limited as over 30% of loci are devoid of any curated annotation [13]. The latest version of the assembly also includes mitochondrial and chloroplast genomes. This complete genome has provided the foundation for extensive transcriptomic studies mainly relying on RNA sequencing (RNAseq), which have explored how *C. reinhardtii* responds to various environmental conditions as well as how genetic mutations influence the transcriptome. For example, investigations of gene expression changes include the impact of the cell and diurnal cycles [14, 15], different CO_2 [16] or nitrogen [17] levels, and stress factors such as added hydrogen peroxide (H_2O_2) [18] or salt [19]. Mutant strains like *sta6*, affecting the responses to nitrogen, have also been extensively studied [20]. In fact, a meta-analysis of gene expression studies revealed that 80% of *C. reinhardtii* genes were differentially expressed in at least one of seven experimental conditions [21]. Further enhancing its utility in genetic studies, *C. reinhardtii* can be transformed using various methods, including *Agrobacterium tumefaciens*-mediated transformation (similar to plants), glass beads, biolistics (the main method used for chloroplast and mitochondria transformation), and electroporation [22]. However, integration of exogenous DNA into the nuclear genome of *C. reinhardtii* is characterised by low rates of homologous recombination, leading to random integration of DNA fragments [23, 24]. With CRISPR-based genome editing tools, genetic modification in *C. reinhardtii* has become more precise [23, 25]. Moreover, molecular cloning tools have provided a suite of building blocks for genetic engineering, enabling the creation of mutant strains and the expression of exogenous genes in *C. reinhardtii* [26].

In summary, *C. reinhardtii* has various characteristics that make it a popular model organism, particularly in photosynthesis research. A wide range of techniques used to study photosynthesis can also be readily applied to *C. reinhardtii*, some of which will be introduced in detail in chapter 4.

1.2 Photosynthesis in *C. reinhardtii*

Photosynthesis is a fundamental process that sustains life on Earth by converting light energy into chemical energy. At the core of this process is the photosynthetic electron transfer chain (PETC), which facilitates the production of reducing equivalents (NADPH) and ATP through the movement of electrons and protons within and across the thylakoid membrane of photosynthetic organisms [27]. The products of the PETC are subsequently primarily used in the Calvin-Benson-Bassham cycle to fix CO_2 and provide carbon skeletons for cell metabolism.

1.2.1 Linear electron flow & the Calvin-Benson-Bassham cycle

The conventional linear electron flow (LEF) through the PETC relies on the coordinated function of four major complexes: Photosystem II (PSII), cytochrome b_6f, Photosystem I (PSI), and ATP synthase (figure 1.3).

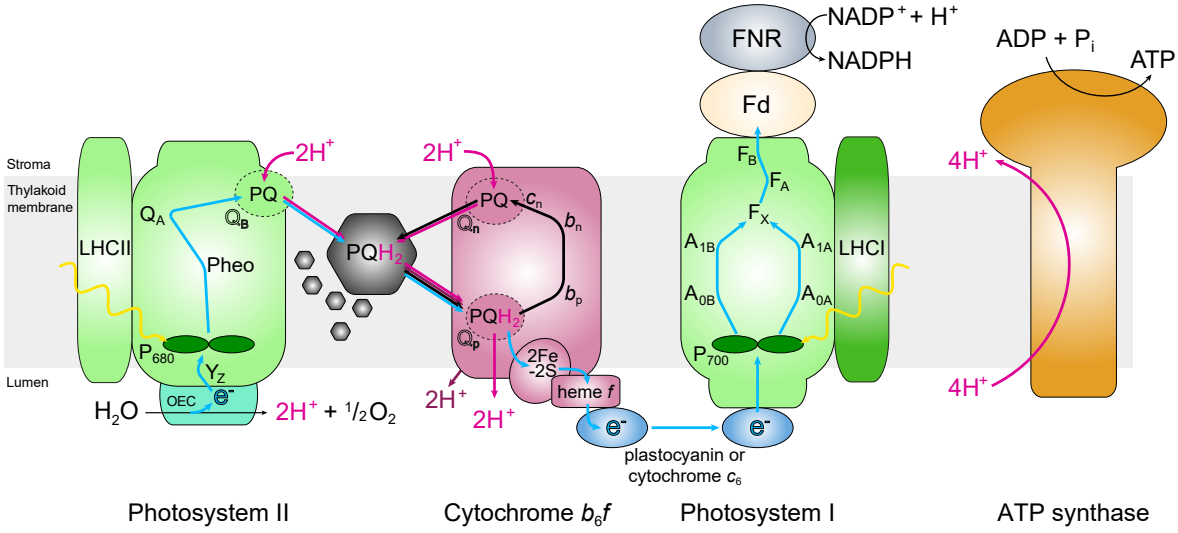


Figure 1.3: Diagram of the photosynthetic electron transfer chain. Blue coloured arrows indicate linear electron flow with transfer of two electrons up to the Q_p site of b_6f and the transfer of one electron thereafter. Pink arrows represent proton movement. The Q cycle is indicated by black arrows. The second oxidation of PQH_2 needed for one reduction of PQ at the Q_n site releases two additional protons into the lumen (dark pink arrow). PQ binding pockets at PSII and b_6f are marked by broken circles. The PQ pool is depicted by grey hexagonal shapes. Further details can be found in the text.

PSII is positioned at the start of LEF [28]. It is a multi-subunit complex that includes specific antenna proteins known as light-harvesting complex II (LHCII), which contain primarily chlorophyll pigments responsible for capturing light energy. When photons are absorbed by these chlorophyll pigments, an electron is excited. This excitation is then passed on to a special chlorophyll pair, P680, located in the PSII reaction centre, where charge separation occurs. Following this initial step, the excited electrons from two photochemical cycles are transferred via pheophytin and a tightly bound plastoquinone (Q_A) to a plastoquinone (PQ) molecule in the Q_B binding pocket. The electron transfer from Q_A to Q_B is facilitated by a non-heme iron coordinated by histidine residues of the PSII core subunits and a bicarbonate anion. The subsequent release of reduced plastoquinone (PQH_2) from Q_B involves the uptake of two protons from the stroma, contributing to the generation of a proton gradient across the thylakoid membrane. The $P680^+$ that results from charge separation is reduced by electrons that are derived from the oxidation of water and transferred to $P680^+$ via a specific tyrosine residue of the PsbA D1 subunit (Y_Z). The water-splitting reaction is catalysed by the oxygen-

evolving manganese cluster (OEC) on the luminal side of PSII. The protons released into the lumen from this reaction contribute further to the generation of the proton gradient as part of the proton motive force (pmf).

Following PSII, the next component in the PETC is the cytochrome b_6f (b_6f) complex [29–31], a dimeric complex composed of four major subunits (cytochrome b_6, cytochrome *f*, the Rieske iron-sulphur protein, and subunit IV) along with four smaller subunits. This complex plays a pivotal role in connecting PSII and PSI while contributing to the pmf generation. PQH_2, generated by photochemical reactions at PSII, diffuses through the membrane and is oxidised at the Q_p site of the b_6f complex (figure 1.3). This oxidation process releases two protons into the thylakoid lumen, further contributing to the pmf. The oxidation of PQH_2 releases two electrons and occurs in two steps, involving the formation of a transient semiquinone. The two electrons are bifurcated at the point of the Q_p site: one enters the so-called high-potential chain to the iron-sulphur cluster (2Fe-2S) in the Rieske protein and then to the heme group in cytochrome *f* while the other is fed into the low-potential chain for the Q cycle. Within the Q cycle, electrons are transferred via hemes b_p and b_n to heme c_n, which is located near the Q_n site [32] (figure 1.3). The Q cycle contributes to the pmf as PQ at the Q_n site is reduced, and protonated with protons from the stroma. Because of the electron bifurcation into low and high potential chain, two oxidation reactions at Q_p are needed for the reduction of one PQ at Q_n. The position of b_6f between PSII and PSI also enables its involvement in various regulatory mechanisms of photosynthesis. One such regulatory mechanism is photosynthetic control, which is a feedback system that helps prevent photooxidative damage to PSI. Preventing damage to PSI is important, as PSI lacks a rapid repair cycle, in contrast to PSII. Photosynthetic control is induced in excess light, which causes a low luminal pH. Under these conditions, protonation of a histidine residue in the Q_p pocket of b_6f reduces the rate of PQH_2 oxidation by preventing the release of protons, thus limiting the electron flow and protecting PSI from over-reduction [29].

After the b_6f complex, LEF continues to PSI (figure 1.3) [28]. In *C. reinhardtii*, the electron transfer from b_6f to PSI is facilitated by the soluble electron carriers plastocyanin or cytochrome c_6, depending on copper availability (section 1.3). These carriers interact with cytochrome *f* at the b_6f complex and the PSAF subunit of PSI, leading to the reduction of oxidised $P700^+$ which is produced through light-induced charge separation. PSI has a heterodimeric core structure composed of PsaA and PsaB, which form two mirror-symmetry-related cofactor chains. Both of these chains are capable of facilitating electron transport. Like PSII, PSI is also equipped with light-harvesting antennae (light-harvesting complex I, LHCI) which capture light energy and transfer it to the special chlorophyll pair, P700. Once P700 is excited, the electron is transferred to one of the primary acceptor chlorophylls *a* ($A_{0A/B}$). From A_0, the electron moves to phylloquinones $A_{1A/B}$, which are in slightly different structural

environments in the two PSI subunits. Subsequently, the bifurcated electron transfer paths rejoin at the iron-sulphur cluster F_X. The electron is further transferred via the iron-sulphur clusters F_A and F_B until it reaches ferredoxin, a soluble protein of the chloroplast stroma. Ferredoxin then serves as a substrate for the ferredoxin-$NADP^+$ reductase (FNR), which is responsible for reducing $NADP^+$ to NADPH. In addition to being a substrate for FNR, ferredoxin also provides electrons for various metabolic processes, such as nitrogen, sulphur, and carbon assimilation, amino acid synthesis, and thioredoxin-dependent regulation. Additionally, ferredoxin plays a part in alternative electron flow pathways such as cyclic electron flow and Mehler-like reactions (section 1.2.2) [33].

The final complex of LEF, the ATP synthase, is not strictly involved in electron transfer but makes use of the pmf generated by LEF. The proton gradient created by water splitting and the Q cycle is harnessed to drive the synthesis of ATP from ADP and inorganic phosphate [34]. The ATP synthase consists of multiple subunits that are grouped into F_o and F_1 parts. F_o sits in the membrane and contains the proton binding sites, while F_1 extends into the stroma and is responsible for the binding of the adenine nucleotides. Thermodynamic measurements have determined that 4 protons are needed for the rotation of the ATP synthase to form one ATP [35]. In contrast, 4.7 protons are needed per ATP based on the ratio between the number of proton binding sites on the c-subunit-ring in F_o to the catalytic nucleotide binding sites on the β-subunits in F_1. It was thus suggested that some energy from the pmf is also utilised for other processes than ATP synthesis, possibly the activation of the ATP synthase itself [35]. In darkness, to prevent the chloroplast ATP synthase running in reverse and thereby hydrolysing ATP, it is deactivated by the formation of a disulphide bond on the γ-subunit on the stromal side. This regulatory mechanism is facilitated by the thioredoxin system that relies on ferredoxin as electron donor.

The outputs of LEF, ATP and NADPH, are used in downstream metabolism, most importantly in the Calvin-Benson-Bassham (CBB) cycle [33]. In the CBB cycle, Ribulose-1,5-bisphosphate carboxylase/oxygenase (RuBisCO) fixes inorganic carbon in the form of CO_2 and thereby provides carbon skeletons for a variety of cellular processes. RuBisCO works in conjunction with other enzymes that make up the CBB cycle, a process tightly regulated by the thioredoxin system. Key enzymes regulated by thioredoxin include RuBisCO activase (important for RuBisCO function but not directly part of the CBB cycle), glyceraldehyde-3-phosphate dehydrogenase (GAPDH), and several enzymes involved in the regeneration of ribulose-1,5-bisphosphate (RuBP). These enzymes include fructose-1,6-bisphosphate phosphatase (FBPase), sedoheptulose-1,7-bisphosphate phosphatase (SBPase), and phosphoribulokinase (PRK). The regeneration of RuBP, the essential substrate for carbon fixation by RuBisCO, is a complex process involving eight enzymes catalysing ten reactions [36]. In this phase, three-carbon molecules known as triose phosphates are reshuffled

and converted into the five-carbon sugar RuBP. The efficiency of RuBP regeneration is crucial for maintaining the flow of the CBB cycle and, thus, the overall process of photosynthesis. Enhancing the efficiency of RuBP regeneration has therefore been a topic of interest for improving carbon assimilation and ultimately crop yields [36].

LEF produces ATP and NADPH in a fixed ratio. While this may be optimal under certain conditions, photosynthetic organisms including *C. reinhardtii* are exposed to a great variety of environmental changes, including nutrient availability and dynamic light conditions. These changes will cause different metabolic needs and photosynthetic outputs of the cell. With a fixed ratio of ATP to NADPH it becomes clear that LEF does not provide the cell enough flexibility to cope with dynamic environments. The flexibility needed in ATP/NADPH production ratio and responses of the PETC to changing environments is achieved via alternative electron flows (AEFs, section 1.2.2) as well as the quenching of excess energy known as non-photochemical quenching (NPQ, section 1.2.3).

1.2.2 Alternative electron flow pathways

AEFs include cyclic electron flow (CEF) pathways and water-to-water cycles (WWCs). As described below, activity of AEFs leads to a change in NADPH/ATP ratio and can provide important routes for safe dissipation of excess energy.

1.2.2.1 Cyclic electron flow

Oxidised $P700^+$ in PSI is quickly reduced after continuous illumination, even in the presence of the PSII inhibitor DCMU [37]. This suggests that an electron transfer mechanism other than LEF must exist that does not involve 'new' electrons from water splitting that are fed into the PETC. In CEF, electrons are 'recycled' before the production of NADPH or directly re-introduced from NADPH into the PETC. As a result, no NADPH is produced but ATP synthesis still occurs because of the proton gradient generated by the b_6f complex (figure 1.4). Multiple mechanisms involving different proteins have been proposed for CEF in *C. reinhardtii*.

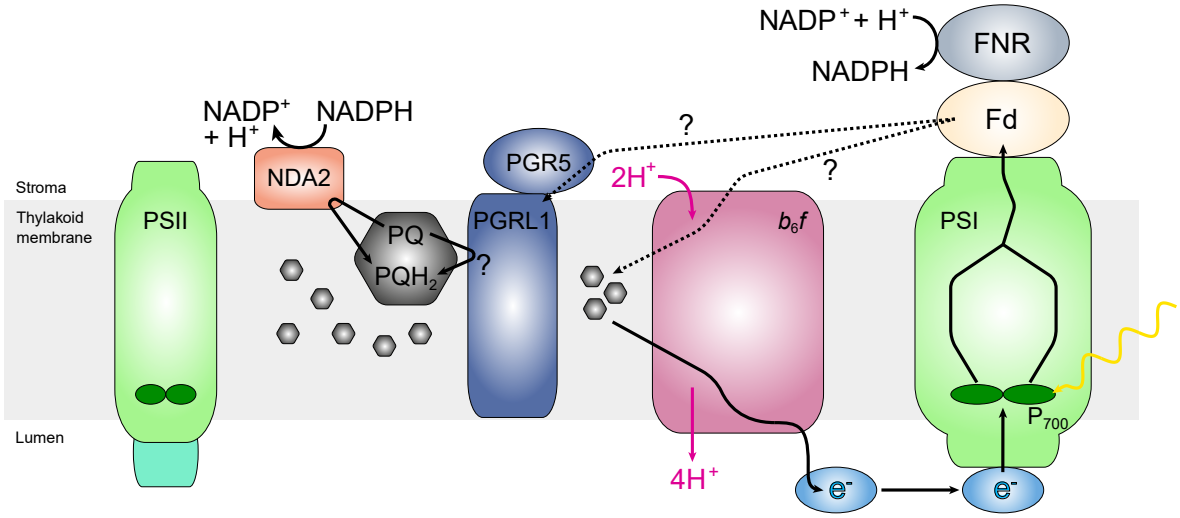


Figure 1.4: Diagram of the different routes of cyclic electron flow in *C. reinhardtii*. Electron transfer between the different CEF components is shown by black arrows and broken lines with question marks indicate uncertainty about the connection drawn. Proton movement via the b_6f complex is marked in pink. The PQ pool is depicted by grey hexagonal shapes. Further details can be found in the text.

In *C. reinhardtii*, NDA2 can contribute to CEF [38, 39]. NDA2 is a thylakoid membrane-bound NADPH dehydrogenase facing the stroma which catalyses the non-photochemical electron transfer from NADPH to PQ. As a type II NADPH dehydrogenase, NDA2 does not exhibit proton-pumping activity, in contrast to its type I counterparts in plants and cyanobacteria.

The proteins PGR5 and PGRL1 are also implicated in CEF activity in *C. reinhardtii*. PGRL1 is an integral thylakoid membrane protein and contains six redox-active and stroma-exposed cysteine residues which were found to be important for its activity [40, 41]. The *Arabidopsis thaliana* (*A. thaliana*) homologue of PGRL1 has been shown to reduce ferredoxin and oxidise the PQ analogue 2,6-dimethyl-*p*-benzoquinone (DMBQ) *in vitro* [41]. The interaction partner of PGRL1, PGR5, is a small, stroma-localised, and soluble protein initially discovered in a mutant defective in the NPQ mechanism qE (section 1.2.3) [42]. Whether the PGR5/PGRL1 complex is directly involved in the electron transfer reactions of CEF or rather assumes a regulatory role in *C. reinhardtii* remains a subject of debate [43, 44]. There is also speculation that PGR5/PGRL1 may regulate the association of a supercomplex involving the b_6f complex, PSI, and FNR, which has been found in *C. reinhardtii* [45, 46].

A potential third CEF pathway has been proposed, involving the direct reinjection of electrons from stromal reductants into the Q_n site of the b_6f complex via heme c_n. In this process, a plastoquinone molecule is reduced by one electron from stromal reductants and another electron from *b* hemes within the b_6f complex [47, 48]. This mechanism aligns with

the original Q-cycle proposed by Mitchell [49], though it differs from the Q-cycle mechanism introduced above. Additionally, it has been suggested that PGR5 may play a role in regulating the switch between these two Q cycles mechanisms [50].

In summary, while CEF is important for the metabolic flexibility of photosynthetic organisms like *C. reinhardtii*, its precise mechanisms are still a matter of research.

1.2.2.2 Water-to-water cycles

As with CEF, the water-to-water cycles (WWCs) do not result in a net gain of NADPH, which is why they are also called pseudo-cyclic electron flow mechanisms. Here, electrons from water oxidation at PSII are rerouted from LEF and eventually transferred back onto oxygen, re-generating water (figure 1.5).

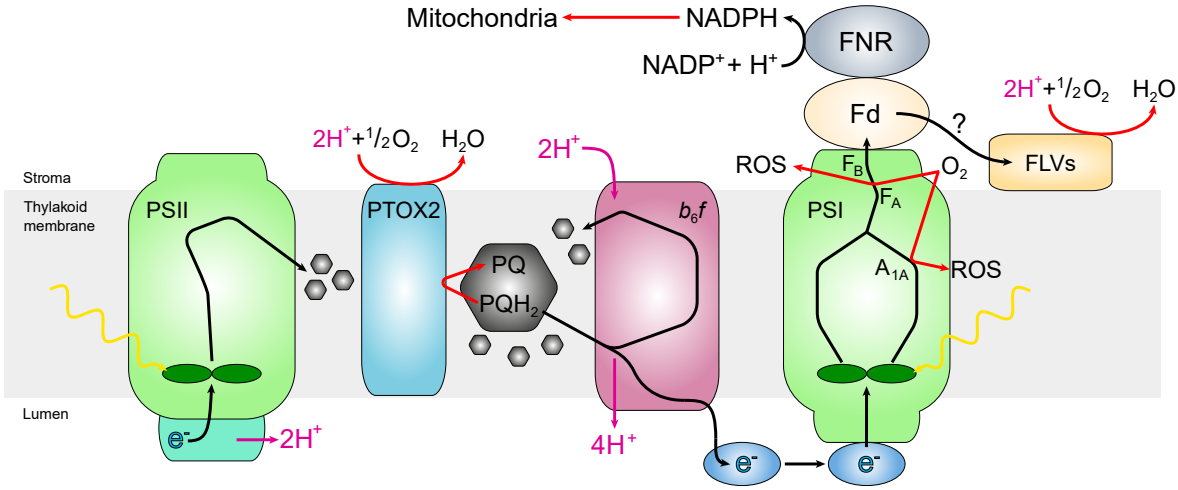


Figure 1.5: Diagram of the different water-to-water cycles in *C. reinhardtii*. Red arrows mark the different WWC reactions, electron flow is marked by black arrows and proton movement is depicted in pink. The PQ pool is depicted by grey hexagonal shapes. Further details can be found in the text.

The plastid terminal oxidase PTOX2 facilitates a WWC. This stroma-facing membrane protein can oxidise PQH_2, removing electrons from the PQ pool and transferring them to oxygen [51, 52]. PTOX2 can act as a safety valve under conditions of over-reduced PQ pools, though it operates at a much lower electron flux rate than PSII in *C. reinhardtii* [51, 53]. Moreover, PTOX2 has been suggested to help balance the redox state of the PQ pool during dark-light transitions, as evidenced by the growth phenotype of *ptox2* mutants under fluctuating light conditions [53]. While in *A. thaliana*, PTOX activity is modulated by cysteine residues in the C-terminal domain, *C. reinhardtii* PTOX2 lacks this domain [54]. Regulation of PTOX2 activity in *C. reinhardtii* therefore remains to be investigated. In the

absence of PSII activity—such as during darkness—PTOX2, in combination with NDA2, forms a chlororespiratory pathway transferring electrons from NADPH to oxygen via the PQ pool. However, since NDA2 does not possess proton-pumping activity, the process is non-electrogenic, i.e. does not lead to generation of a pmf.

Another pathway facilitating a WWC is the Mehler reaction, first described in 1951 [55]. Mehler postulated a process in which electrons from PSI are transferred to oxygen, leading to the production of hydrogen peroxide (H_2O_2) [55]. Later it was found that such a reaction proceeds via the transient formation of a superoxide anion radical ($O_2^{\bullet -}$) , which is then disproportionated into H_2O_2 and O_2 by the stromal and membrane-bound superoxide dismutase [56]. Superoxide and H_2O_2 belong to the class of molecules known as reactive oxygen species (ROS). H_2O_2 can act as a signalling molecule [57, 58] or be scavenged by enzymes such as ascorbate peroxidase, peroxiredoxins, and glutathione peroxidase, ultimately converting it back into water and completing the water-water cycle [59]. Initially, ferredoxin was thought to be the electron donor for the Mehler reaction but recent studies have implicated the iron-sulphur clusters F_A/F_B and especially the phylloquinone A_{1A} as more likely donors [60]. The physiological relevance of the Mehler reaction *in vivo* remains an open question in *C. reinhardtii*, because much of the oxygen uptake once attributed to the Mehler reaction is now thought to be caused by the activity of flavodiiron proteins (FLVs).

The activity of FLVs is therefore also known as the Mehler-like reaction. The first identified FLVs were cyanobacterial [61] and two sets of FLVs have been found. Flv1 and Flv3 as well as Flv2 and Flv4 form functional heterodimers catalysing the reduction of oxygen to water at the acceptor side of PSI, however with different time periods of activity and kinetics [62]. Flv1/3 were found to be essential for the survival under fluctuating light conditions, as they provide an important electron sink during the initial phase of photosynthetic induction before full activation of the CBB cycle [63]. The *C. reinhardtii* FLVs, FLVA and FLVB, are homologues of the cyanobacterial Flv1 and Flv3 [64] and were also characterised as essential for growth under fluctuating light conditions [65]. No FLV activity has been detected under steady-state illumination [66]. In contrast to the Mehler reaction, FLVs alleviate PSI acceptor side limitation without the generation of harmful ROS. Interestingly, the exact electron donor for FLVs is still debated. Potential candidates in cyanobacteria include ferredoxin or the iron-sulphur clusters within PSI [67]. Regulation of FLV activity in cyanobacteria was recently found to rely on the extent of the pmf across the thylakoid membrane [68].

Finally, another variation of WWCs involves cooperation between the chloroplast and mitochondria through chloroplast-mitochondria electron flow (CMEF). In this pathway, reducing equivalents from the PETC are shuttled to mitochondria via the malate/oxaloacetate shuttle.

Malate is then fed into the Krebs cycle, where its electrons are ultimately used to reduce oxygen to water in the mitochondrial electron transfer chain, thus closing the water-to-water cycle. Plastid malate dehydrogenase (MDH), which catalyses the reduction of oxaloacetate to malate, is redox-regulated by thioredoxins connecting CMEF and PETC activity [69]. A recent study demonstrated that CMEF also plays a role in energising the carbon-concentration mechanism of *C. reinhardtii* [70].

Together, these diverse water-to-water cycle pathways provide essential flexibility for the electron flow in the PETC.

1.2.3 Non-photochemical quenching

When photosynthetic electron transfer becomes saturated, especially under high light conditions, ROS can form. One source of ROS can be excited chlorophylls that are not efficiently used for photochemical reactions (photochemical quenching) and thus transfer their energy onto oxygen, generating highly reactive singlet oxygen. To prevent the harmful effects of ROS formation, *C. reinhardtii* and other photosynthetic organisms possess various strategies for photoprotection (figure 1.6) [71, 72]. Among these, non-photochemical quenching (NPQ) of chlorophyll fluorescence dissipates excess energy from excited chlorophylls as heat, preventing oxidative damage.

There are multiple NPQ mechanisms that act on different timescales, ranging from rapid responses in seconds to long-term adaptations over days. This range of mechanisms allows *C. reinhardtii* to respond effectively to diverse light fluctuations, from sudden changes caused by sun, clouds, overhanging vegetation, soil and water movements to the more gradual shifts of diurnal cycles. The major types of NPQ include energy-dependent quenching (qE), zeaxanthin-dependent quenching (qZ), state transition quenching (qT), and photoinhibitory quenching (qI). An additional type of NPQ called qH, involving a slowly reversible quenching in LHCII, was recently identified in *A. thaliana* [73, 74]. However, qH has not yet been described in *C. reinhardtii*.

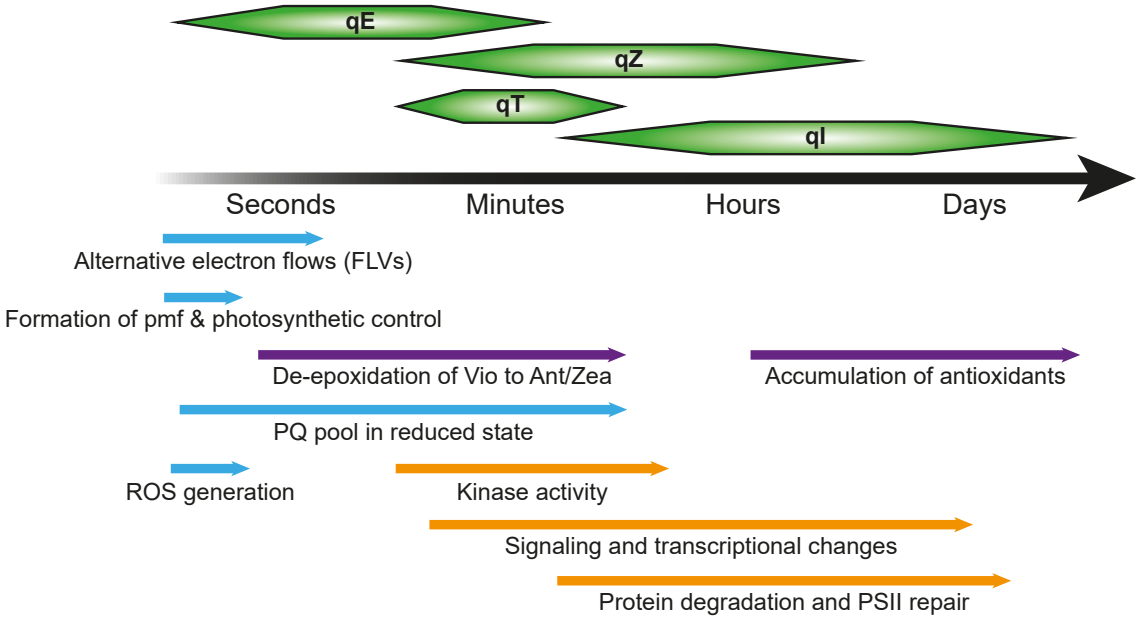


Figure 1.6: Time scales of different responses to excess light in *C. reinhardtii*. The different processes of non-photochemical quenching (NPQ) are shown in green at the top. Alternative electron flows (AEFs, especially FLVs), pmf formation, photosynthetic control, and ROS formation can be observed with the onset of high light while the PQ pool is reduced quickly after (blue arrows). De-epoxidation of the carotenoid violaxanthin (Vio) to antheraxanthin (Ant) and zeaxanthin (Zea) is a requirement for qZ (section 1.2.3.2) and happens over the timescale of seconds and minutes. Other antioxidants such as further carotenoids, ascorbate, glutathione, and ROS scavenger proteins accumulate over the course of hours to days (purple arrows). Changes involving protein activity (like that of the STT7 kinase, section 1.2.3.3) and transcriptional adjustments take place over the timescale of minutes to days (orange arrows). Adapted from [72].

1.2.3.1 Energy-dependent quenching qE

The most rapid form of NPQ is qE, which is triggered within seconds in response to high light exposure. The formation of a pH gradient across the thylakoid membrane is a requirement for qE activity. In plants, the PSBS protein is essential for qE, but in *C. reinhardtii* the role of PSBS remains less clear. While PSBS is known to contribute somewhat to qE in *C. reinhardtii*, it may do so by reorganising thylakoid structures [75]. The primary effectors of qE in *C. reinhardtii* are the light-harvesting complex stress related proteins LHCSR1 and LHCSR3 [76]. LHCSR3 is especially important, as mutants lacking LHCSR3 show much more severe impairment in qE than LHCSR1 mutants [77, 78]. LHCSR3 binds pigments such as chlorophylls and carotenoids (lutein, zeaxanthin or violaxanthin) and its activity relies on its pH-sensing capability that enables it to respond to changes in lumen pH [79]. When the luminal pH drops, LHCSR3 gets protonated and protects the photosynthetic apparatus by quenching excited chlorophylls within a PSII-LHCII-LHCSR3 supercomplex [80]. LHCSR3

has also been shown to contribute to PSI quenching [81]. Excitation energy quenching in LHCSR3 likely involves a bound lutein molecule, which can form a radical cation and provide a route for rapid excitation energy quenching [76]. Next to lutein, zeaxanthin was also implicated in LHCSR3-dependent quenching [82]. LHCSR3 is encoded by two genes, *LHCSR3A* and *LHCSR3B*, which produce identical proteins [77]. The expression of LHCSR3 is regulated by various factors, including blue light, the circadian rhythm, and CO_2 concentration [71, 75, 83, 84]. *C. reinhardtii* cells grown under constant low light conditions show limited qE capacity due to a lack of LHCSR expression [77]. Notably, the calcium sensor CAS is necessary for the induction of LHCSR3 expression [85], further highlighting the complex regulatory network that controls NPQ in response to environmental cues.

1.2.3.2 Zeaxanthin-dependent quenching qZ

Zeaxanthin-dependent quenching qZ is induced on a timescale of minutes [72]. It relies on the xanthophyll cycle involving the carotenoids zeaxanthin, antheraxanthin, and violaxanthin. The formation of a pH gradient in response to light triggers the de-epoxidation of violaxanthin to zeaxanthin via antheraxanthin, catalysed by the enzyme violaxanthin de-epoxidase (VDE). Zeaxanthin is then believed to bind to LHC antennae proteins, and likely also LHCSR3, to perform constitutive quenching of excited chlorophyll molecules [82]. Once zeaxanthin has accumulated, qZ becomes independent of the pH gradient. Through the activity of the zeaxanthin epoxidase (ZEP) under low light conditions zeaxanthin can be epoxidised to violaxanthin, making qZ a reversible process [71]. The plant VDE is localised in the thylakoid lumen and underlies thiol-based redox regulation, as it is most stable when its cysteines are oxidised forming six disulphide bonds [86, 87]. In contrast, *C. reinhardtii* contains an atypical VDE called chlorophycean VDE (CVDE) which is not homologous to VDE [88]. CVDE was shown to be stromal localised [88] and its activity was not inhibited by dithiothreitol (DTT), suggesting that it is not thiol-regulated [89]. The mechanism of qZ regulation therefore seems to differ between *C. reinhardtii* and plants.

1.2.3.3 State transition quenching qT

State transitions refer to a mechanism that regulates the distribution of LHCII between PSII and PSI, thus helping to maintain the light harvesting balance between the two photosystems [90]. When LHCII migrate from PSII to PSI, a decrease in chlorophyll fluorescence can be observed, making state transitions a contributor to NPQ on a time scale of minutes. LHCII migration is dependent on their phosphorylation status which is ultimately controlled by the redox state of the PQ pool. When the PQ pool is highly reduced, more LHCII complexes are

phosphorylated and attach to PSI (state 2), whereas when the PQ pool is in a more oxidised state, LHCII are not phosphorylated and associate with PSII (state 1). While the names 'state 1' and 'state 2' suggest a binary shift, a continuum of intermediate states exists [91]. Phosphorylation and de-phosphorylation of LHCII proteins is mediated by the kinase STT7 and two phosphatases, respectively (figure 1.7).

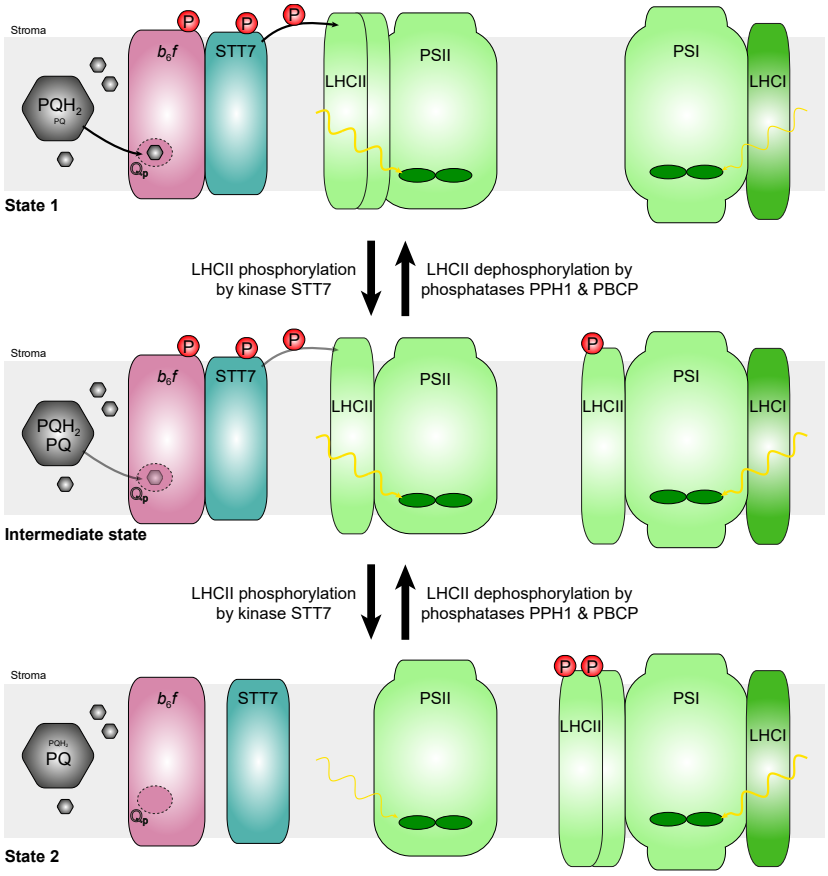


Figure 1.7: Principle of state transitions and activation of the STT7 kinase in *C. reinhardtii*. Starting in state 1 at the top, the LHCII proteins are not phosphorylated and therefore associated with PSII. If the PQ pool gets reduced (PQH_2 larger than PQ), activation of STT7 occurs (see text) and LHCII proteins get phosphorylated. In an intermediate state, the LHCII phosphorylation status and the PQ pool redox state are balanced. In state 2, LHCII phosphorylation is at its maximum and LHCII complexes largely associate with PSI increasing its antenna size. If, in response, the PQ pool gets more oxidised (PQ larger than PQH_2), dephosphorylation of LHCII proteins occurs, catalysed by phosphatases. Phosphatase activity thus leads back towards intermediate states and state 1.

The most prominent phosphorylation targets of STT7 are LHCII proteins [92, 93]. Up to 80% of LHCII proteins dissociate from PSII upon phosphorylation [94]. These migratory antennae can then associate with PSI-LHCI complexes. However, it was also found that not all phosphorylated LHCII antennae associate with PSI. Some form unassociated quenching antennae that can also contribute to qT [45, 95]. Furthermore, LHCSR3 was shown to be a phosphorylation target of STT7 [96] and in its phosphorylated form, LHCRS3 was suggested

to be involved in quenching of LHCII associated with PSI [81]. The mechanisms of qE and qT could therefore be connected. The activated STT7 kinase was also found to exhibit autophosphorylation on the stromal side upon transition to state 2 [97, 98]. However, this was not essential for the LHCII kinase activity as determined by mutant studies [98]. STT7 was further shown to be necessary for the phosphorylation of subunit IV of b_6f [96] and the b_6f-associated PETO protein [99].

The inverse reaction of de-phosphorylation of LHCII proteins is catalysed by the phosphatases PPH1 and PBCP [100], about which much less is known than their kinase counterpart.

The activation and regulation of the STT7 kinase has been at the centre of many studies on state transitions. It is activated upon the binding of PQH_2 to the luminal Q_p site of the b_6f complex. This initiates a conformational change involving the Rieske protein and allows the docking of STT7 to the b_6f complex [101]. An open question remains of how exactly the activation signal originating in the luminal Q_p site is transmitted to the stromal side, where the phosphorylation domain of STT7 can be found [29]. Two evolutionarily conserved and lumen-exposed cysteine residues of STT7 were shown to form a disulphide bridge, essential for kinase activity [93, 102]. Interestingly in high light, downregulation of LHCII phosphorylation can be observed [103]. The activity of STT7 could thus be limited in high light by the reduction of the disulphide bridge, which was proposed to be mediated by CCDA and HCF164, two thylakoid membrane proteins known to be involved in the assembly of the b_6f complex [104]. They would transmit a high light signal from the stromal thioredoxin system to the luminal cysteine residues of STT7 limiting its activity [104]. However, it was subsequently shown that the disulphide bridge is maintained even under high light conditions [102]. The mechanism of STT7 activation was thus suggested to involve the formation of two intermolecular disulphide bridges leading to a STT7 homodimer with kinase activity [102]. This homodimer was proposed to be unstable, reverting back to two monomers with an intramolecular disulphide bridge each when the Q_p site is unoccupied resulting in an inactive kinase [102]. How the kinase is inactivated in high light remains to be established conclusively [90]. With the lumen thiol oxidoreductase LTO1 a new possible regulator of STT7 was identified, as LTO1 was shown to oxidise the disulphide bridge of the *A. thaliana* homologue STN7 *in vitro* [105]. The maintenance of oxidised STN7 is thus probably a prerequisite for the proposed switch between intra- and intermolecular disulphide bridges. An influence of LTO1 on state transitions was further supported by the *lto1* knock-out exhibiting reduced, although not completely abolished qT [105].

Experimentally, state transitions can be induced by exposing *C. reinhardtii* to different conditions. In dark, oxygen-rich conditions or in the presence of the PSII inhibitor DCMU and light, *C. reinhardtii* exhibits state 1 [106]. State 2 is induced in darkness and anaerobic

conditions, where the PQ pool is reduced by electrons from fermentative processes [107]. In *C. reinhardtii*, these changes are more pronounced than those caused by variations in light quality [108].

1.2.3.4 Photoinhibitory quenching qI

Photoinhibitory quenching qI represents the slowest mechanism of NPQ and is closely linked to photoinhibition at PSII [109]. Under high light conditions, PSII experiences photodamage, particularly to the PsbA D1 protein in the PSII reaction centre. This leads to a decrease of chlorophyll fluorescence over the course of minutes to hours. Rather than replacing the entire complex, an efficient repair system replaces only the damaged PsbA subunit [110]. The speed of this repair process is governed by environmental factors and the energetic state of the chloroplast, with repair rates slowing significantly under excessive light conditions [111]. A critical aspect of the repair cycle is the degradation of the damaged PsbA, which is mediated by the FTSH protease [112]. Mutations in FTSH lead to a marked slowdown in the relaxation of qI, indicating that qI is primarily localised to the PSII reaction centre [113]. Additionally, the dissociation of PSII subunits PSBO, PSBP, and PSBQ has been shown to correlate with the cleavage of PsbA, potentially constituting the rate-limiting step of the degradation process [114]. Interestingly, PSBO contains a luminal oxidised disulphide bridge that is essential for its structural integrity [115], linking qI to thiol-based redox regulation.

1.2.4 The impact of acetate on photosynthesis in *C. reinhardtii*

As mentioned above, *C. reinhardtii* can also grow photomixotrophically and heterotrophically in the presence of acetate. Acetate provides a carbon source for *C. reinhardtii* and therefore influences the energetic status of the cell. Overall, *C. reinhardtii* cultures exposed to acetate exhibit a decrease in photosynthetic oxygen evolution and carbon fixation to about 50-70% of the levels of cultures without acetate [116, 117]. At the same time, respiration is stimulated, although this was only found in some studies [116, 118] and not in another [117]. Addition of acetate also led to increased re-reduction rates of PSI even in the presence of the PSII inhibitor DCMU. This effect was independent of light exposure, suggesting that reducing equivalents from acetate metabolism in the mitochondria are shuttled to the chloroplast via the oxaloacetate-malate shuttle where NDA2 activity can lead to the reduction of the PQ pool, as part of a chlororespiratory pathway [118]. Consequently, with a more reduced PQ pool, qT could be observed as cells transitioned from state 1 into state 2 [118–120]. However, a

sustained transition to state 2 was not observed for long-term photomixotrophic cultures [120]. Furthermore, addition of acetate was accompanied by a changed ATP/NADPH ratio in favour of NADPH [119] which could be explained by the metabolism of acetate. Interestingly, enhanced cyclic electron flow was found in the presence of acetate, possibly in response to a changed ATP/NADPH ratio [121]. While the maximum PSII efficiency, F_v/F_m, did not change through addition of acetate [117], a decrease of PSII core protein abundance was observed over the course of 8 hours [119]. This could be connected to the observed decrease in ROS production in the presence of acetate, because PSII produces more ROS when the PQ pool is more reduced. However, the reduction in ROS generation was also suggested to be caused by acetate replacing the bicarbonate in PSII changing the environment of Q_A and Q_B, leading to charge recombination rather than ROS formation [120]. Finally, in isolated spinach chloroplasts, acetate was also shown to compete with the essential water oxidation cofactor chloride at the OEC of PSII, thereby decreasing the rate of reduction of the acceptor tyrosine [122].

In summary, the presence of acetate affects photosynthetic processes through various suggested mechanisms of action. Studies on photosynthesis that rely on photomixotrophic growth of *C. reinhardtii* should therefore take into account these effects when interpreting results.

1.2.5 Redox regulation in the thylakoid lumen

The ferredoxin-thioredoxin system for redox regulation in the stroma is well characterised. Ferredoxin (Fd) is reduced by PSI and acts as an electron donor to thioredoxin (Trx), a reaction catalysed by the ferredoxin-thioredoxin reductase (FTR, figure 1.8 **1**). The ferredoxin-thioredoxin system thus translates light signals into thiol signals for redox regulation of proteins [123], some of which were mentioned throughout the introduction above. In the lumen, thiol-based regulation is less well described [124, 125]. Especially in *C. reinhardtii* more studies are needed to understand completely the processes involved. Nevertheless, some parts of this complex regulation system have been clarified, mainly using other model organisms like *A. thaliana*.

The thylakoid lumen presents unique redox challenges, as it is acidified during light exposure, influencing redox potential and protein activity. Unlike in the stroma, where thiol-regulated proteins are generally active in their reduced form (thiol), luminal proteins are more often active in their oxidised state (disulphide) [126]. Although the precise transfer mechanisms are not fully known yet, evidence suggests that machinery exists enabling thiol-disulphide redox exchanges between stroma and lumen. From the perspective of luminal

proteins, this involves the movement of reduction equivalents into the lumen to reduce (and often deactivate) proteins and electrons out of the lumen to oxidise (often activate) them.

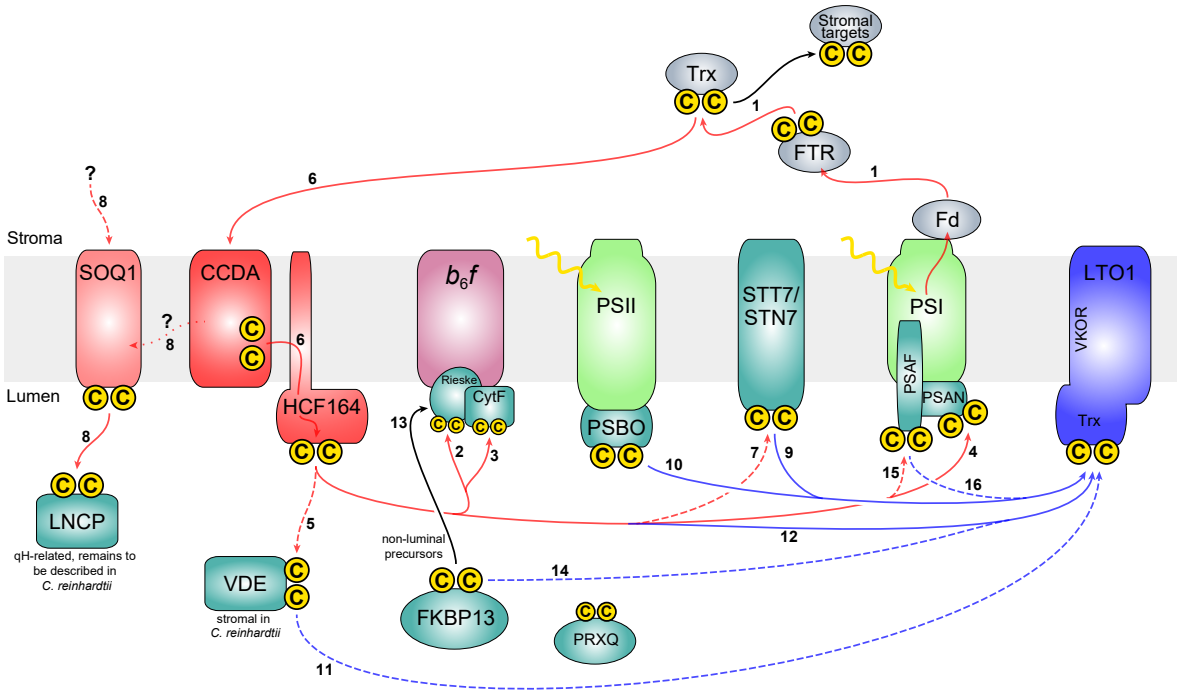


Figure 1.8: Components of thiol-based redox regulation in the thylakoid lumen of plants and algae. Luminal target proteins of thiol-based redox regulation are shown in turquoise (LNCP, VDE, FKBP13, Rieske protein, CytF, PRXQ, PSBO, STT7/STN7, PSAF, and PSAN). The reductive pathway via CCDA, HCF164, and SOQ1 influencing the redox state of the thiol(s)/disulphide(s) (yellow C for cysteine) is marked red and the oxidative pathway via LTO1 is shown in blue. The numbers on the arrows are referred to in the text and suggested connections with limited experimental evidence are represented as broken lines. The dotted line with a question mark indicates a speculation.

Several components for the reduction of disulphides to thiols have been identified in the thylakoid lumen and membrane. HCF164 (also known as CCS5 in *C. reinhardtii*) possesses a thioredoxin-like domain in the lumen. It plays a role in reducing disulphides in target proteins such as the Rieske protein, cytochrome *f*, and the PSI subunit PSAN (figure 1.8 **2**, **3** and **4**, respectively) and is involved in the assembly of the cytochrome b_6f complex [127, 128]. HCF164 was furthermore proposed to be the reducing effector for VDE, inactivating the enzyme (figure 1.8 **5**) [124]. The reducing equivalents HCF164 transfers to target proteins were found to originate from CCDA (CCDA1 in *C. reinhardtii*), a thylakoid membrane protein that transfers reducing equivalents from the stroma to the lumen (figure 1.8 **6**). CCDA interacts with stromal thioredoxins and ultimately facilitates b_6f assembly [129, 130]. The observation that overexpression of thioredoxin results in a more reduced state for STN7 [131] (STT7 in *C. reinhardtii*) led to the suggestion that HCF164 can also reduce STN7/STT7 (figure 1.8 **7**). The SOQ1 (Suppressor of Quenching) protein has been identified as a luminal protein

anchored to the thylakoid membrane and transferring reducing equivalents from the stroma (and possibly CCDA) to the luminal plastid lipocalin LCNP, which is involved in qH in *A. thaliana* (figure 1.8 **8**) [74]. The *C. reinhardtii* homologue of SOQ1 (Cre13.g586050) remains to be further investigated.

For the oxidative system of redox regulation in the lumen, LTO1 has been identified as a key effector. It oxidises target proteins, such as STN7 [105] and PSBO [132] and interacts, at least *in vitro*, with VDE [133], the *C. reinhardtii* homologue of which is, however, localised in the stroma (figure 1.8 **9**, **10**, and **11**, respectively). The membrane protein LTO1 has two functional domains, one thioredoxin-like (Trx) domain in the lumen and one vitamin K epoxide reductase (VKOR) domain in the thylakoid membrane [132]. Interestingly, also interaction and thiol/disulphide exchanges between HCF164 and the thioredoxin-like domain of LTO1 were reported *in vitro* [133] (figure 1.8 **12**). Two other possible mechanisms for oxidation of target proteins were proposed. One involved oxygen produced at the OEC of PSII [126] and the other the luminal cytochrome c_{6A} transferring electrons from oxidation of target proteins to plastocyanin and thus back into the PETC (section 1.4) [134].

Multiple further (putative) target proteins of thiol-based redox regulation in the lumen were identified. FKBP13 (FKBP16E in *C. reinhardtii*) is a luminal immunophilin whose non-luminal precursors are implicated in the biogenesis of the b_6f complex [135] (figure 1.8 **13**). It exhibits thiol-based regulation of its peptidyl-prolyl isomerase activity [136] and is likely a target protein of LTO1 [133] (figure 1.8 **14**). The peroxiredoxin PRXQ (PRX6 in *C. reinhardtii*) was also found in the thylakoid lumen [137] and with its cysteine residues could be involved in redox regulation. It is conceivable that FKBP13 and PRXQ could assume the position of a soluble electron carrier for connecting membrane-bound components such as LTO1 or HCF164 with target proteins. Lastly, the PSI subunit PSAF was suggested to be involved in the redox regulation of ROS formation at PSI. PSAF possesses two luminal cysteine residues that could form a disulphide bridge, a potential target for HCF164 and LTO1 [138] (figure 1.8 **15** and **16**, respectively).

In summary, the thylakoid lumen exhibits a complex network of thiol-based redox regulation. However, several open questions remain. For example, while LTO1 is thought to oxidise target proteins, the fate of electrons from these reactions is still unknown. Additionally, the fact that redox midpoint potentials shift with pH makes the thylakoid lumen a challenging environment for thiol-based regulation [124]. Components that assist in fine-tuning the redox state of target proteins even in an acidic lumen remain to be identified.

1.3 The soluble electron transfer proteins plastocyanin and cytochrome c_6

As introduced above, photosynthesis relies on the action of the PETC. For the PETC to function, soluble electron transfer proteins are essential. This class of proteins includes well-studied proteins such as plastocyanin and cytochrome c_6 (c_6), which transfer electrons from the cytochrome b_6f complex to photosystem I. Additionally, there are proteins in this class, such as cytochrome c_{6A}, cytochrome c_M or other c_6-like proteins whose function is unknown [139]. All these proteins are metalloproteins, containing either iron or copper.

The type I copper protein plastocyanin is found in plants, eukaryotic algae, and cyanobacteria. In eukaryotes, plastocyanin is nuclear encoded and its mature form consists of ~100 amino acids (10.5 kDa). Interaction, with and thereby electron transfer between, cytochrome b_6f and PSI is facilitated by its high redox midpoint potential (+370 mV), a conserved negatively charged region and the solvent exposed region known as “hydrophobic patch” [140].

As functional alternative for plastocyanin in most cyanobacteria and some eukaryotic algae the heme-containing cytochrome c_6 (c_6) is expressed under copper-limiting conditions [21, 141]. Except for some red algae [142], it is generally nuclear encoded. Cytochrome c_6 has a highly conserved CxxCH heme binding motif, consists of 83-89 amino acids (10 kDa), and forms four α-helices connected by three loops [143]. Like plastocyanin, c_6 exhibits a negatively charged surface region facilitating interaction with cytochrome b_6f and PSI. The redox midpoint potential of +350 mV allows electron transfer by c_6 between those proteins, likely via the solvent-exposed part of the heme group [140].

1.4 Cytochrome c_{6A}

1.4.1 Discovery

Prior to the discovery of c_{6A}, it was thought that plants solely relied on plastocyanin for electron transfer between b_6f and PSI and that they did not have a c_6-like protein. In 2002, two independent reports of the discovery of c_6-like proteins in plants changed this paradigm. First, analyses of expressed sequence tag (EST) databases revealed c_6-like sequences in a number of plant species, such as *A. thaliana*, rice, and soybean [144]. These sequences all contained a heme-binding motif, an iron-ligating methionine, and a novel insertion of twelve

amino acids with two conserved cysteine residues that was not found in cyanobacterial or algal c_6 sequences. This insertion was later called 'loop insertion peptide' (LIP) [145]. Together with the observation of a different distribution of charged amino acid residues between c_6 and c_{6A}, it was suggested that c_{6A} would assume a distinct function from c_6 and plastocyanin. A second group discovered a c_6-like sequence in *A. thaliana* when looking for interaction partners of the chloroplast immunophilin FKBP13 in a yeast-two-hybrid (Y2H) assay [146]. FKBP13 was found to interact with the Rieske protein of b_6f, and absence of FKBP13 led to increased Rieske protein abundance [135]. While mutant plants of c_{6A} did not show a particular phenotype under standard conditions, evidence was presented that suggested that c_{6A} is able to replace plastocyanin functionally *in vitro*, although this was later called into question [147–149]. The model organism used in this study, *C. reinhardtii*, was found to possess both c_6 and c_{6A}, further suggesting different functions for c_6 and c_{6A} [150].

1.4.2 Structure and physical properties

The structure of c_{6A} was solved by X-ray crystallography soon after the discovery of the protein [151, 152]. It was found that c_{6A} is a typical class I *c*-type cytochrome consisting of four α-helices and a heme group, with an overall structure very similar to c_6 (figure 1.9). No structural differences were seen between the heme-oxidised and -reduced version of c_{6A}. While c_{6A} and c_6 are homologues, some important structural differences remain (figure 1.9). The loop insertion peptide (LIP) is a surface-located well-defined loop with a conserved disulphide bridge which is only found in c_{6A} [145]. From determination of the stability of various mutant proteins, the LIP was found to be of structural importance [151, 153]. The disulphide bridge in the LIP was predicted to contribute to the stability of the protein, rather than being catalytic [153, 154]. However, a catalytic role can not be excluded. Additionally, amino acid residue 52 (position in *A. thaliana*) is a hydrophobic valine, leucine, or isoleucine in c_{6A}, whereas it is hydrophilic glutamine in c_6 (green diamond in figure 1.9). This single amino acid difference is responsible for a change of ~100 mV in the redox midpoint potential, which could be explained by the residue's impact on the water arrangement in the heme binding pocket [155]. The redox-midpoint potential of c_{6A} (+140 mV [156] or +71 mV [155]) was found to be approximately 220-250 mV lower than that of plastocyanin or c_6 (+365 mV [156] or +325 mV [155]), depending on the experimental method. This large difference renders it unlikely that c_{6A} acts as functional replacement for plastocyanin in plants and algae. Furthermore, while c_6 and plastocyanin have strongly negatively charged surfaces at points of interaction with PSI, c_{6A} has a strongly positive surface charge there [147]. Finally, the isoelectric point (pI) of plastocyanin and c_{6A} is different (5.1 vs. 4.1 in *A. thaliana*, respectively) which, together with different surface charges, indicates different interactions [156].

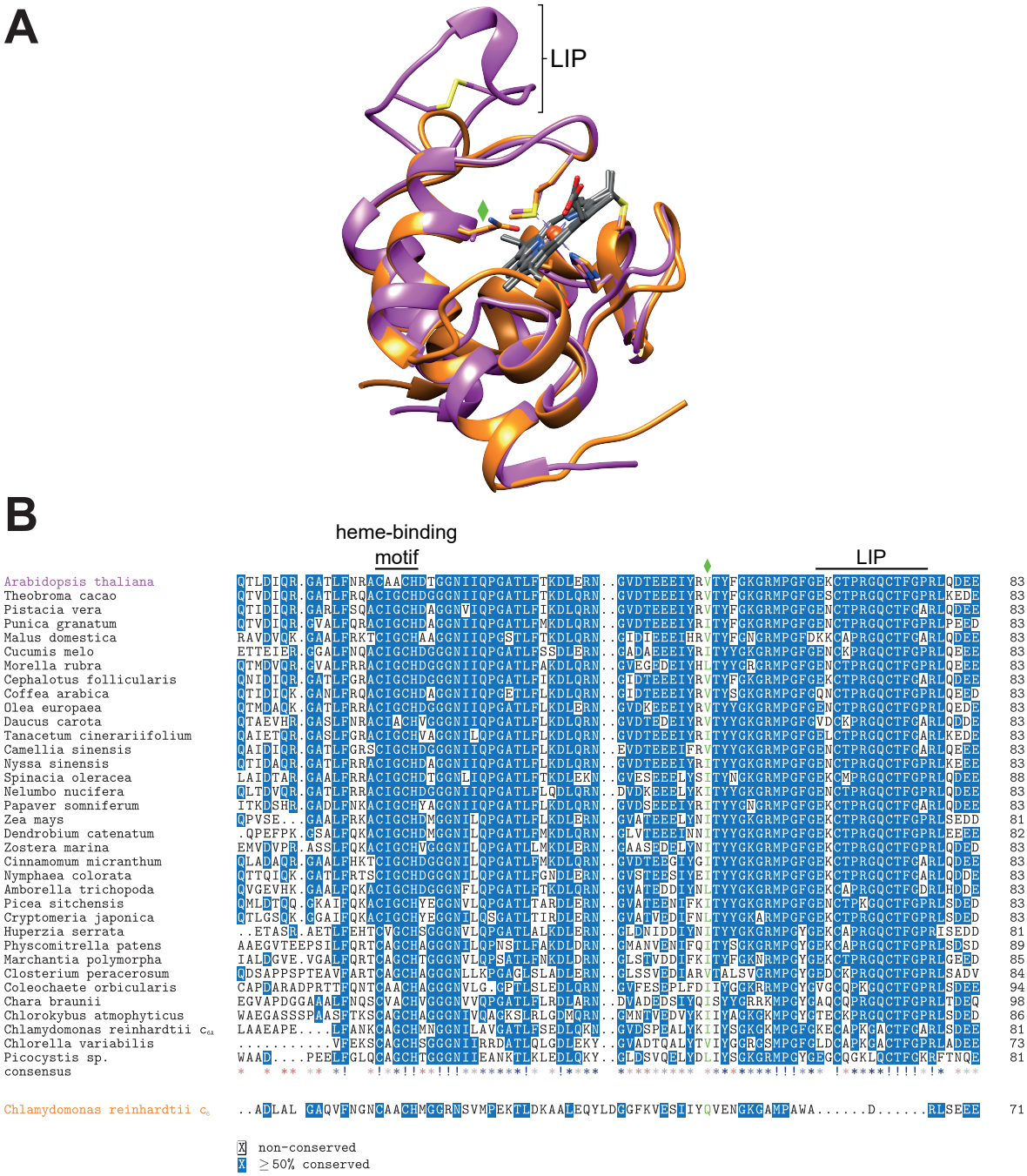


Figure 1.9: Structure and sequence conservation in the green lineage of c_{6A}. (**A**) Overlay of the crystal structures of c_6 from *C. reinhardtii* (orange, PDB: 1CYJ [157]) and c_{6A} from *A. thaliana* (purple, PDB: 2CE0 [152]). The position of the LIP is noted with the disulphide bridge formed between the two conserved cysteine residues (yellow sticks). The amino acid residues at position 52 are shown as stick model and are labelled with a green diamond. (**B**) Alignment of the mature c_{6A} protein sequences from 26 different species of the green lineage. Amino acids that are conserved in over 50% of the sequences are coloured in blue and symbols in the consensus line indicate levels of conservation (exclamation marks: complete conservation, asterisks: red (lower) to blue (higher) conservation of over 50%). The number on the right specifies the position of the last shown amino acid in the respective protein sequence. Heme-binding motif and LIP are marked above the alignment and the residue 52 (in *A. thaliana*) is coloured green. For comparison, the c_6 sequence of *C. reinhardtii* is also aligned below the c_{6A} alignment.

1.4.3 Conservation in the green lineage, further homologues & phylogenetic history

The sequence of c_{6A} has a similar level of conservation across the green lineage to that of plastocyanin, suggesting an important role for c_{6A} within green photosynthetic eukaryotes (figure 1.9B). Following the discovery of c_{6A} in Viridiplantae, database searches also led to the discovery of more c_6-like proteins in cyanobacteria [158]. Both cytochromes c_{6B} (c_{6B}) and c_{6C} have lower redox midpoint potentials than c_6 and a hydrophobic amino acid residue at position 52. However, unlike c_{6A} they do not possess a LIP [159–161]. They were first described as distinct proteins but were later proposed to be orthologues of the same protein in different species of cyanobacteria and thus will be referred to as c_{6B} only [162]. Phylogenetic analyses of sequences of the cytochrome c family including c_6, c_{6A}, c_M, c_{550} and c_{555}, demonstrated that c_{6A} sequences represent a monophyletic group, which is distinct from c_6 [150].

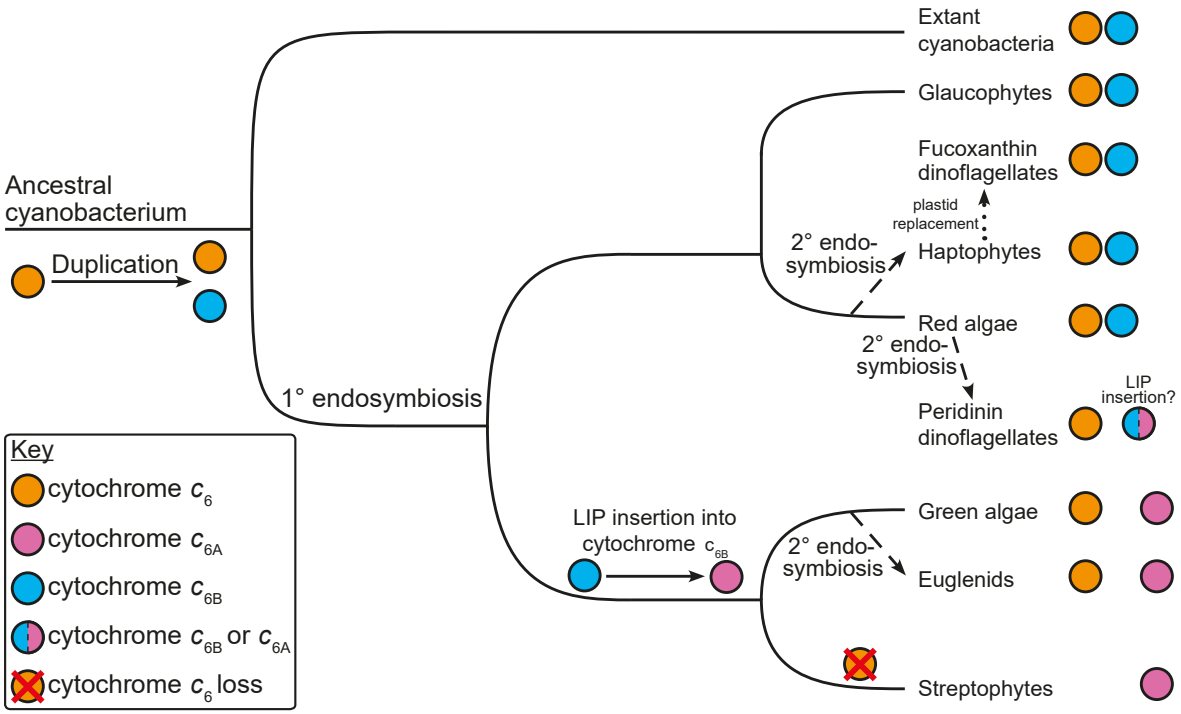


Figure 1.10: Ancestry model for the cytochrome c_6 family of proteins in photosynthetic organisms. Duplication and mutation of c_6 in an ancestral cyanobacterium led to the evolution of c_{6B}, which remains present in extant cyanobacteria. Both genes were transferred to photosynthetic eukaryotes at the primary endosymbiosis that gave rise to green, red and glaucophyte chloroplasts. While in the red and glaucophyte lineage c_{6B} can still be found, in the green lineage c_{6A} emerged, likely as result of insertion of the LIP into c_{6B}. Green algae kept both c_6 and c_{6A} sequences, whereas streptophytes (charophyte algae and land plants) lost c_6. Multiple c_{6A} or c_{6B} sequences could also be found in dinoflagellates, raising the possibility of a novel LIP insertion. Adapted from [162].

A further phylogenetic study showed that c_{6B} is likely to have evolved from a duplicated c_6 at an early stage of cyanobacterial evolution, indicating that the low redox midpoint potential shared by c_{6A} and c_{6B} appeared early in their evolutionary history. Cytochrome c_{6A} forms a monophyletic group within c_{6B}, suggesting that insertion of the LIP into c_{6B} resulted in c_{6A}, early in the green eukaryotic lineage (figure 1.10) [162].

Additionally, another c_6-like protein, first designated cytochrome $c_{6\text{-}3}$ and later cytochrome c_{6D}, with a similarly high redox midpoint potential to c_6 was found in filamentous cyanobacteria [163, 164]. While it belongs to the c_6-like family, c_{6D} is suggested to have a distinct function from c_6, c_{6A}, or c_{6B} [163].

1.4.4 Localisation & interaction partners

Cytochrome c_{6A} was discovered through interaction with FKBP13, a protein localised in the thylakoid lumen, which led to the proposal that c_{6A} is also a luminal protein [146].

In *A. thaliana*, c_{6A} was found to be uniquely localised to sensory plastids rather than mesophyll chloroplasts [165]. Sensory plastids are specialised organelles for stress sensing and signalling [166]. These plastids are smaller than primarily photosynthetic plastids, like the chloroplasts found in mesophyll cells, and have a distinct proteome [165]. Facilitated by the actin cytoskeleton sensory plastids can position close to the nucleus, potentially aiding in retrograde signalling. This signalling may be related to ROS, although the exact pathways remain unclear [166, 167]. While c_{6A}'s specific location within sensory plastids has not been established, its identification in these specialised organelles suggests a role in signalling rather than conventional involvement in the PETC. During the course of the research presented here, c_{6A} was detected in the soluble fraction of the thylakoid lumen of *A. thaliana* [168]. This finding came from a sample that did not differentiate between sensory plastids and mesophyll chloroplasts.

In *C. reinhardtii*, the localisation of c_{6A} has been less studied. Bioinformatic predictions suggested that c_{6A} is located in the chloroplast but did not provide a clear indication of a specific location within the chloroplast [169]. Immunofluorescence microscopy confirmed that c_{6A} is indeed found in the chloroplast, but again, no specific sub-compartment within the chloroplast could be identified [169].

Taken together, a thylakoid luminal localisation for c_{6A} seems likely, also for *C. reinhardtii*. However, direct evidence for a luminal localisation within *C. reinhardtii* is still missing. Furthermore, investigating the localisation in *C. reinhardtii* is important in the light of

C. reinhardtii possessing only a singular chloroplast in contrast to the large number of multiple types of plastids in *A. thaliana*.

In contrast to its homologue cytochrome c_6, c_{6A} cannot effectively reduce PSI, rendering interaction between c_{6A} and PSI unlikely [147]. Cytochrome c_{6A} was found to interact with itself in a Y2H assay [148]. Furthermore, c_{6A} was shown to be able to reduce plastocyanin *in vitro* [152]. Although an interaction was not seen in Y2H, the authors noted that this may reflect the difficulty of detecting transient interactions with this method [148]. A possible interaction between c_{6A} and plastocyanin was further characterised by nuclear magnetic resonance (NMR) titrations of the two proteins. Weak interaction with a binding constant K_d of 2.01 mM was detected, consistent with a transient interaction. Interestingly, three amino acid residues of the LIP (R70, G71 & F75 in *A. thaliana* c_{6A}) and one residue close to a solvent-exposed edge of the heme (G30 in *A. thaliana* c_{6A}) were found to be relatively more involved in a putative interaction than other amino acid residues [169]. These interaction sites would be consistent with electron transfer between c_{6A} and plastocyanin via the disulphide bridge in the LIP or the heme ligand. The Y2H assay that led to co-discovery of c_{6A} [146] suggested interaction between the redox-regulated FKBP13 and c_{6A}. This interaction could not be reproduced in a second Y2H assay, however, the same methodological limitations as above apply [170]. Another interaction candidate of c_{6A}, LTO1, was found *in vitro* using Y2H [133]. This lumen thiol oxidoreductase was shown also to interact with the state transition kinase STN7 *in vivo* in *A. thaliana* and FKBP13 *in vitro* [105, 133]. Subsequent surface plasmon resonance (SPR) measurements did not support interaction between c_{6A} and LTO1. However, the formation of inclusion bodies when expressing c_{6A} for SPR experiments was also reported, which might have prevented its normal fold and thus normal interactions [133]. Conclusive and especially *in vivo* data on interaction partners of c_{6A} is therefore still missing.

1.4.5 Proposed functions

Since the discovery of c_{6A} multiple hypotheses about its function were proposed. That c_{6A} is a functional replacement for plastocyanin or c_6 in the PETC is unlikely for four different reasons. First, c_{6A}'s low redox midpoint potential prevents it from oxidising cytochrome *f* [147]. Second, only an insignificant direct reduction rate of PSI by c_{6A} was found *in vitro* [149], possibly due to an inappropriate surface charge of c_{6A} [144, 147]. Third, c_{6A} has a low abundance making it unlikely to replace the highly abundant plastocyanin [169, 171]. Last, *A. thaliana* lacking plastocyanin was unable to grow photoautotrophically and even overexpression of c_{6A} could not rescue this phenotype [149]. The latter contrasts with the findings of Gupta *et al*. (2002), where *A. thaliana* lacking plastocyanin exhibited diminished growth, with lethality

occurring only when c_{6A} was also missing [146]. This difference can likely be explained by the methods used in each study: Gupta *et al*. (2002) used RNA interference (RNAi) to reduce plastocyanin levels, which may have left a small amount of plastocyanin, undetectable by western blot. The study by Weigel *et al*. (2003) on the other hand, used T-DNA insertion lines that completely disrupted the plastocyanin genes, resulting in a true knock-out [149].

Cytochrome c_{6A} was hypothesised to be involved in redox-regulatory mechanisms via its observed interaction partner FKBP13 [145]. While c_{6A}'s interaction with FBKP13 could not be reproduced [170], the conserved cysteine residues in the surface-exposed LIP could interact with other proteins, too. In fact, c_{6A} was proposed to facilitate the formation of disulphide bridges in the thylakoid lumen passing on electrons from the oxidation of target proteins to plastocyanin [134]. This would help maintaining luminal proteins in their active, oxidised state [126]. Two findings challenge this hypothesis. First, no interaction with plastocyanin could be found in a Y2H assay [148], however, transient interactions might not have been captured. Second, the comparison of bond angles with other disulphide bridges suggested that the disulphide bridge in the LIP is structural rather than catalytic [153]. However, there is also no evidence disproving catalytic activity of the disulphide bridge *in vivo*.

A role as a 'safety valve' for excess electrons was suggested for c_{6A}, where c_{6A} could help alleviate high light stress [172]. Interaction with the PQ pool as requirement for this function was shown for other soluble proteins such as the chloroplast sensor kinase CSK [173]. Support for this hypothesis was found in a small reduction of growth under high light of *A. thaliana* lacking c_{6A}, suggesting that c_{6A} is important for the response to high light [174]. The high light growth phenotype was recoverable by overexpression of c_{6A} in the knock-out background. Interestingly, the overexpression strain showed slightly reduced growth compared to wild type and knock-out under low light conditions. These results were interpreted as such that c_{6A} could take electrons from the PQ pool and transfer them onto plastocyanin, bypassing the b_6f complex. Under high light, this would alleviate stress, while under standard and low light less b_6f activity would lead to a lower pmf causing reduced energy production via the ATP synthase and thus reduced growth [174]. A similar high light growth phenotype for the absence of c_{6A} was not found in *C. reinhardtii* and the exposure to high light did not drastically increase the transcript abundance of the very low abundant c_{6A} [171]. The low overall abundance indicates a very limited safety valve capacity, fundamentally questioning this hypothesis [169, 171]. Nevertheless, a safety valve function cannot be excluded for conditions with increased expression of c_{6A}.

The low abundance of c_{6A} and the high light growth phenotype in *A. thaliana* could be reconciled if rather than being a safety valve, c_{6A} were involved in signalling mechanisms in response to high light. This was suggested following the analysis of c_{6A}-dependent tran-

scriptomic changes in response to high light conditions in *C. reinhardtii*, where mainly genes implicated in the carbon concentration mechanism, NPQ, and phototaxis were affected [171].

Finally, c_{6A} was recently suspected to be involved in luminal redox regulation of ROS generation at the level of PSI in plants [138]. However, measurements of ROS generation that supported involvement of LTO1 and CCDA in regulation of light-induced ROS formation at PSI did not show a similar result for c_{6A} [138].

In summary, while some functional hypotheses for c_{6A} have been proposed, conclusive evidence for a specific function is still lacking.

1.4.6 CRISPR-mediated c_{6A} knock-out in *C. reinhardtii*

Employing the CRISPR/Cpf1 method for genetic modification of *C. reinhardtii* [25], collaborators (Aron Ferenczi and Attila Molnar, University of Edinburgh) have created a c_{6A} (*CYC4* gene) knock-out strain as shown in figure 1.11. The method relies on preassembled recombinant complexes of the endonuclease Cpf1 and guide RNAs (sgRNA) as ribonucleoproteins (RNPs). The double strand break-inducing enzyme Cpf1 is not expressed in the cell but rather transiently introduced by electroporation. The RNPs are thus quickly degraded in the cell, resulting in limited endonuclease activity and off-target effects [23]. The insertion of a multiple stop codon through the provided single stranded DNA repair template as well as the removal of the ribosome binding site and the start codon should prevent functional protein from being produced. The knock-out locus can be detected by PCR, as it is 696 bp shorter than the wild-type locus.

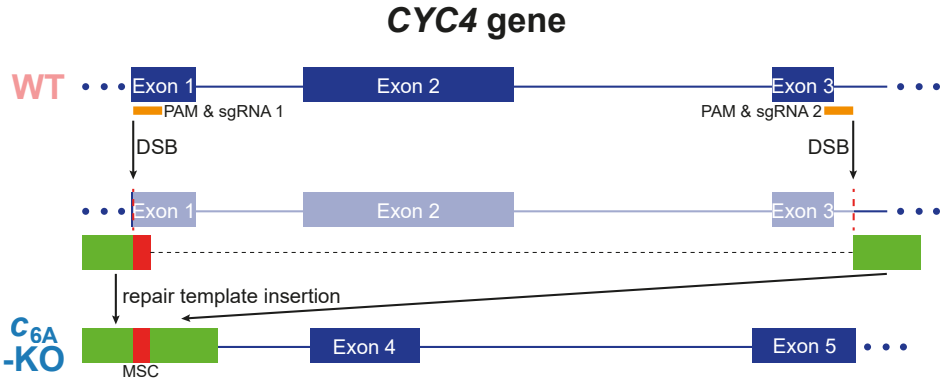


Figure 1.11: The *CYC4* gene (Cre16.g670950) during the process of CRISPR/Cpf1 modification. Two double strand breaks (DSB) are introduced in the *CYC4* gene encoding c_{6A} by employing sgRNAs to guide the Cpf1 enzyme to the protospacer adjacent motif (PAM) sites, one in the 5'UTR and the other in Exon 3. The provided repair template with homologous regions (green) and a multiple stop codon (MSC, red) is then inserted resulting in a deletion of 708 bp of *CYC4* and addition of 12 bp from the MSC.

1.5 Overall aims and structure of the study

While advances in studying cytochrome c_{6A} have been made, its function remains to be elucidated (section 1.4). The overall aim of this study is thus to explore the function of cytochrome c_{6A} in *C. reinhardtii*. For this, *C. reinhardtii* strains lacking or overexpressing c_{6A} are established and confirmed (chapter 3). These strains are the basis for the subsequent characterisation of c_{6A}'s effects on growth, photosynthesis, thylakoid membrane complexes, and the protein and transcript levels of *C. reinhardtii*. Additionally, the subcellular localisation and interaction partners of c_{6A} are investigated. The materials and methods utilised in this study are detailed in chapter 2.

In chapter 3, in addition to the establishment of *C. reinhardtii* c_{6A} mutant strains, these strains are tested for their growth under various conditions, including stressful fluctuating high light.

Chapter 4 contains a detailed biophysical analysis of the PETC of *C. reinhardtii* c_{6A} mutant strains. This was motivated by a possible connection of c_{6A} with photosynthesis and includes studies under standard light as well as fluctuating light conditions. Various spectrometric techniques are used to study c_{6A}'s effect on the function of the major complexes of the PETC (PSII, b_6f, PSI and ATP synthase) as well as on important energetic balances of photosynthesis (light-harvesting, PQ pool).

In chapter 5, localisation and interaction partners of c_{6A} as well as its effect on thylakoid membrane complexes are investigated. As there is some uncertainty about the exact location of c_{6A} in *C. reinhardtii* subcellular fractionation and immunofluorescence microscopy are used to investigate its localisation. Interaction partners of c_{6A} are also still elusive. Co-immunoprecipitation is therefore employed in the search for putative interaction partners. To characterise the effect of c_{6A} on photosynthesis further, blue native gel electrophoresis is used to determine c_{6A}-dependent differences in the thylakoid membrane complexes of *C. reinhardtii*.

Chapter 6 then details the investigation of c_{6A}'s effect on protein and transcript levels of *C. reinhardtii* in standard and fluctuating light conditions. Immunoblots show how c_{6A} affects abundances of proteins associated with photosynthesis and RNAseq analysis provides a broader image of c_{6A}'s effect on *C. reinhardtii* with a focus on genes related to photosynthesis.

Finally, in chapter 7, functional implications of the obtained findings are discussed and result in an updated working hypothesis for the function of c_{6A}.

2

Materials & Methods

2.1 Algae strains & growth conditions

2.1.1 *Chlamydomonas reinhardtii* strains

The *C. reinhardtii* cell wall-less wild-type strain CC-1883 (WT) and the cytochrome c_{6A} knock-out strain Uex55 (c_{6A}-KO, CC-1883 background) were obtained from Aron Ferenczi (laboratory of Attila Molnar, University of Edinburgh).

2.1.2 Growth of *C. reinhardtii*

2.1.2.1 Maintenance

C. reinhardtii strains were maintained on Tris-Acetate-Phosphate (TAP, table 2.1) medium with Hutner's trace element solution (table 2.3, [175]) supplemented with 1.5% agar at 30 $\mu mol_{photons}$ m^{-2} s^{-1} and 25 °C. For longer-term storage cultures were kept on TAP slants on the lab window-sill at room temperature. Liquid cultures were grown at 30 $\mu mol_{photons}$ m^{-2} s^{-1} 25 °C and 120 rpm in AlgaeTron AG130 or AG230 incubators (Photon System Instruments) unless otherwise specified.

Table 2.1: Recipe for TP/TAP media. Beijerinck salts, Hutner's Trace Elements, and phosphate buffer were autoclave-sterilised before mixing. After preparation of the medium, it was autoclaved again for sterilisation.

Component	TAP	TP
Beijerinck salts (40x, table 2.2)	25 mL	25 mL
Hutner's Trace Elements (table 2.3)	1 mL	1 mL
1 M KPO_4 pH 7, consisting of 250 mL 1 M K_2HPO_4 + 170 mL 1 M KH_2PO_4	1 mL	1 mL
Tris Base	2.42 g	2.42 g
Glacial acetic acid (TAP only)	1.15 mL (26 mM)	-
dH_2O	fill up to 1 L	fill up to 1 L
Adjust to pH 7 with	KOH	HCl

Table 2.2: Recipe for Beijerinck salts solution (40x). Once the salts were dissolved, the solution was autoclaved for sterilisation.

Component	Amount
NH_4Cl	16 g
$CaCl_2 \cdot 2H_2O$	2 g
$MgSO_4 \cdot 7H_2O$	4 g
dH_2O	fill up to 1 L

Table 2.3: Recipe for Hutner's trace elements solution.

Component	Amount
H_3BO_3	11.40 g
$ZnSO_4 \cdot 7H_2O$	22.00 g
$MnCl_2 \cdot 4H_2O$	5.06 g
$FeSO_4 \cdot 7H_2O$	4.99 g
$CoCl_2 \cdot 6H_2O$	1.61 g
$CuSO_4 \cdot 5H_2O$	1.57 g
$(NH_4)_6Mo_7O_{24}$	1.10 g
dH_2O	fill up to 1 L

2.1.2.2 Experimental growth curves

For experimental cultures, triplicates of 30 mL medium (Tris-phosphate (TP) medium, table 2.1) for photoautotrophic, and TAP for photomixotrophic conditions) were inoculated with *C. reinhardtii* strains to OD_{750nm} = 0.1. The cultures were then subjected to the experimental conditions (table 2.4). All experimental cultures were subcultured at least twice in standard conditions before exposure to experimental conditions. Optical density of *C. reinhardtii* cultures was monitored at 750 nm (OD_{750nm}) with a Genesys 10S (Thermo Scientific) or UV-1800 spectrophotometer (Shimadzu). Some experimental cultures were monitored for their PSII fluorescence yield with a FluorPen (Photon System Instruments).

Table 2.4: Experimental light conditions in the AlgaeTron AG130 and AG230 growth chambers utilising white light.

Name	Light regime
standard growth light	continuous 30 $\mu mol_{photons}\ m^{-2}\ s^{-1}$
high light	continuous 700 $\mu mol_{photons}\ m^{-2}\ s^{-1}$
darkness	continuous 0 $\mu mol_{photons}\ m^{-2}\ s^{-1}$
2 min on/off	alternating 2 min 700 $\mu mol_{photons}\ m^{-2}\ s^{-1}$ & 2 min darkness
12 s on/off	alternating 12 s 700 $\mu mol_{photons}\ m^{-2}\ s^{-1}$ & 12 s darkness
DISCO Light	alternating 2 min darkness & 2 min 12 s 700 $\mu mol_{photons}\ m^{-2}\ s^{-1}$/ 12 s off (figure 3.5)

2.2 Molecular biology techniques

2.2.1 DNA extraction from *C. reinhardtii*

Genomic DNA from *C. reinhardtii* cells was obtained by phenol:chloroform extraction following an established protocol (Dr. Katrin Geisler, personal communication). *C. reinhardtii* cells from standard growth conditions in TAP (50 mL) were harvested at mid-exponential growth phase (1000 xg, 5 min) and resuspended in extraction buffer (300 µL, table 2.5). The cell suspension was vigorously mixed (30 s) and incubated at 37 °C for 2 h with occasional shaking. Subsequently, the suspension was extracted with a phenol:chloroform:isoamyl alcohol (IAA, 25:24:1) mixture for 5 min with shaking and separated by centrifugation (15000 xg, 3 min, room temperature (RT)). The organic phase was extracted twice more with extraction buffer and the aqueous phases were combined before extraction with a chloroform:IAA (24:1) mixture. The resultant aqueous phase was incubated with RNAse A (2 µL 10 mg/mL) for 10 min at 37 °C and extracted again with the chloroform:IAA mixture. A one-tenth volume of sodium acetate (3 M, pH 4.8) was added to the aqueous phase and mixed briefly before 2.5 volumes of ice-cold absolute ethanol were added to the sample. Incubation overnight at -20 °C resulted in a DNA precipitate, which was harvested by centrifugation (15000 xg,

30 min, RT), washed with ethanol (70%), air-dried, and resuspended in Tris-HCl (10mM, pH 7.5). The concentration of the extracted DNA was estimated using a NanoDrop1000 (Thermo Fisher Scientific) and integrity was confirmed by gel electrophoresis.

Table 2.5: Recipe for DNA extraction buffer.

Component	Amount
Tris base	157.6 mg
EDTA	730.6 mg
NaCl	146.1 mg
Proteinase K (20 mg/mL)	1 µL
SDS	1.0 mg
dH_2O	fill up to 50 mL

2.2.2 RNA extraction from *C. reinhardtii*

Mid-exponential phase *C. reinhardtii* cultures (5 mL) were harvested by centrifugation at 1000 xg for 5 min. After disposal of the supernatant the cell concentrate was snap-frozen in liquid nitrogen. The frozen pellet was resuspended in 1 mL of TRIzol reagent (Thermo Fisher Scientific) and stored until further use at -80 °C. The TRIzol suspension was mixed with 1 mL of ethanol in preparation for RNA purification using the Direct-zol RNA Miniprep kit (Zymo Research) following the manufacturer's instructions. The optional DNase treatment and two additional wash steps were included: one wash with 0.4 mL of RNA Wash Buffer before the DNase treatment and another wash with 0.4 mL of Direct-zol RNA PreWash Buffer after the first pre-wash. The resulting concentrations and the 260/280, 260/230 ratios were subsequently estimated using a NanoDrop1000 (Thermo Fisher Scientific).

Integrity of the extracted RNA was confirmed by gel electrophoresis. Briefly, 1% agarose was dissolved in Tris-Acetate-EDTA buffer (TAE, Invitrogen), the mixture was poured into an appropriate mould and stained using SYBR DNA Gel Stain (1X final concentration, Invitrogen). 400 ng of RNA were diluted to 5 µL with water, 10 µL of a specific loading buffer (table 2.6) were added and the solution was subsequently transferred into prepared wells of the gel. HyperLadder 1 kb (Bioline) was used as a size marker. The loaded samples were subsequently subjected to electrophoresis for 45 min at 100 V.

Table 2.6: Recipe for RNA gel-loading buffer (1.5x).

Component	Amount
Formamide	9.5 mg
Bromophenol blue (2.5%, w/v)	100 µL
Xylene cyanol FF (2.5%, w/v)	100 µL
EDTA (pH 8, 0.25 M)	200 µL

2.2.3 Colony PCR of *C. reinhardtii*

Colony PCR on *C. reinhardtii* was performed using the Phire Plant Direct PCR kit (Thermo Fisher) and following manufacturer's instructions. 2 µL of liquid *C. reinhardtii* culture were mixed with 20 µL of dilution buffer, stored for at least 30 min at -20 °C and thawed again under shaking at 4 °C. 2 µL of this mixture were used as template for the PCR reaction mixture as specified in table 2.7. The cycling protocol is shown in figure 2.1. Primers used and their respective annealing temperatures and extension times are summarised in table 2.8. The PCR result was analysed by gel electrophoresis, for which 1% agarose was dissolved in Tris-Borate-EDTA (TBE) buffer (table 2.9). The mixture was poured into an appropriate mould and stained using SYBR Safe DNA Gel Stain (1X final concentration, Invitrogen). Hyperladder 1 kb plus (Bioline) was used as size marker. 15 µL of PCR product mixed with 3 µL of loading dye (6x, NEB) were transferred into prepared wells and subjected to electrophoresis for 45 min at 100 V.

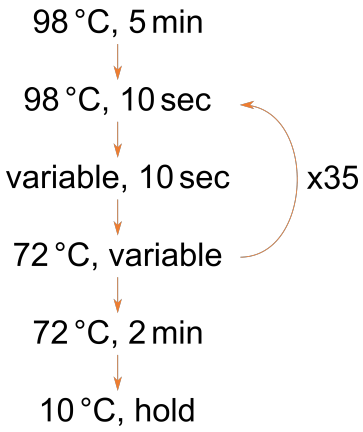


Figure 2.1: PCR cycling protocol used for *C. reinhardtii* colony PCR with Phire Plant direct PCR kit. The annealing temperature as well as the extension time are specific for primer pairs used and can be found in table 2.8.

Table 2.7: Components of a *C. reinhardtii* colony PCR reaction.

Component	Volume (µL)
Autoclaved, milliQ H2O	5.0
2X Phire Plant PCR Buffer	10.0
Forward Primer (10 µM)	1.0
Reverse Primer (10 µM)	1.0
Culture supernatant from dilution buffer	2.0
Phire Hot Start II DNA Polymerase	0.4
DMSO	0.6
Total volume	20.0

Table 2.8: Primers, their sequence and respective annealing temperatures and extension times as used for colony PCR of *C. reinhardtii*.

Name	**Sequence** (5'→3')	$T_{Annealing}$ (°C)	$t_{Extension}$ (s)
c6A-KO check fw	GAGACGCTACGCTGCATGT	65	45
c6A-KO check rev	CACTTCCTCGCGCTGCATA		
pDKM trafo check fw	TCTTTCTCCATGGGCGGGCT	69	70
pDKM trafo check rev	CCCTCGGTCACATGTGCATCC		

Table 2.9: Recipe for Tris-Borate-EDTA (TBE) buffer.

Component	Amount (g)
Tris base	12.11
Boric acid	6.18
EDTA	0.74
dH_2O	fill up to 1 L

2.2.4 Golden Gate assembly of constructs for transformation of *C. reinhardtii*

All pDK plasmids (see appendix A.1) were assembled following the molecular cloning (MoClo) syntax [26, 176]. The c_{6A}-overexpression constructs (pDKM-000 (FLAG) & pDKM-001 (mVenus)) were assembled using MoClo parts pCM0-016 (*PSAD* promoter), pDK0-002 (*CYC4* gene with introns), pCM0-094 (C-terminal triple FLAG tag) or pCM-102 (C-terminal mVenus tag), and pCM0-114 (*PSAD* terminator). The *CYC4* gene coding for c_{6A} with two intronic *Bsa*I restriction sites altered (GAGACC $\rightarrow$ GAAACC) was synthesized (Twist Bioscience). All the remaining parts have been described before [26] including the acceptor plasmids used (table 2.10).

DNA assembly reactions were mixed in PCR tubes (table 2.11) and subsequently placed in a thermocycler (figure 2.2). The assembly reaction was used to transform chemically competent *E. coli* 5α cells (NEB) by heat-shock following manufacturer's instructions. Cells were subsequently plated onto LB medium supplemented with 2% agarose, the appropriate antibiotic (60 µg/mL spectinomycin for level 0, 100 µg/mL carbenicillin for level 1, 50 µg/mL kanamycin for Level M) as well as IPTG (1 mM) and X-Gal (80 µg/mL) for blue-white screening for Level 0/1. After overnight incubation at 37 °C, white colonies were subcultured in liquid LB medium supplemented with appropriate antibiotics. Plasmid DNA was isolated after 18 h of incubation (37 °C, 200 rpm) using the GeneJET Plasmid Miniprep Kit (Thermo Fisher). The plasmid DNA sequence was confirmed by Sanger sequencing (Sequencing facility, Department of Biochemistry, University of Cambridge).

Table 2.10: Golden Gate acceptor plasmids used, their respective level and antibiotic resistance in *E. coli* as well as what they were used for.

Acceptor plasmid	Level	used for	Resistance in *E. coli*
pAGM1287	0	coding sequence (CDS) cloning	Spectinomycin
pICH47742	1	Level 1 position 2	Carbenicillin
pAGM4723	M	Level M assembly	Kanamycin

Table 2.11: Components of a Golden Gate assembly reaction.

Component	Amount
Buffer G	2 µL
Bovine Serum Albumin (2 mg/mL)	2 µL
ATP (10 mM)	2 µL
Restriction enzyme (BbsI for Level 0 & M, BsaI for Level 1, 20 U/µL)	1 µL
T4 DNA Ligase (5 U/µL)	1 µL
Backbone plasmid	75 ng
Insert plasmids	2:1 molar ratio to backbone

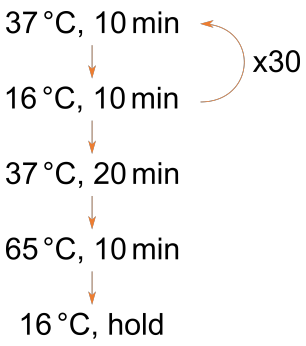


Figure 2.2: Golden Gate assembly thermocycler protocol.

2.2.5 Transformation of *C. reinhardtii*

Transformation by electroporation was carried out as previously described [26]. Briefly, a *C. reinhardtii* culture (standard growth conditions) with OD_{750nm} ~1 was concentrated 100-fold by centrifugation and resuspension in TAP with 60 mM sucrose. 250 µL were then incubated with 1 µg of linearised DNA (by digestion with PmeI) for 10 min on ice in an electroporation cuvette (0.4 cm gap, BioRad) prior to electroporation with a BioRad Gene Pulser. Cells were allowed to recover in 10 mL TAP with 60 mM sucrose for 16 h in a shaking incubator (2 $\mu mol_{photons}$ m^{-2} s^{-1}, 120 rpm, 25 °C) and plated for selection on TAP-agar plates with paromomycin (10 µg/mL).

2.3 Biochemical analyses

2.3.1 Chlorophyll quantification in *C. reinhardtii* samples

A 200 µL sample from a *C. reinhardtii* culture was mixed with 800 µL acetone (resulting in a dilution factor of 5), vigorously mixed for 20 s and centrifuged for 3 min at 13000 xg. The supernatant was isolated and its absorbance at 663 nm and 645 nm was measured against an 80% acetone blank. The concentration of chlorophyll *a*, *b* and total was calculated as in formulas 2.1 to 2.3 [177] where D is the dilution factor (here D = 5).

$$\text{Chl } a \text{ (µg/mL)} = (OD_{663} * 12.7 - OD_{645} * 2.69) * D \tag{2.1}$$

$$\text{Chl } b \text{ (µg/mL)} = (OD_{645} * 22.9 - OD_{663} * 4.68) * D \tag{2.2}$$

$$\text{Total chl (µg/mL)} = \text{chl } a + \text{chl } b \tag{2.3}$$

2.3.2 Determination of acetate concentration in *C. reinhardtii* medium

A sample of a *C. reinhardtii* culture was centrifuged for 3 min at 13000 xg to pellet cells. The concentration of acetate in the supernatant medium was then measured using an acetate enzymatic test kit (K-ACETRM, Megazyme) following the manufacturer's instructions, using a third of all volumes specified.

2.3.3 Chloroplast and thylakoid isolation from *C. reinhardtii*

Thylakoid membranes from *C. reinhardtii* cultures were isolated as described before [178]. Briefly, photomixotrophically (TAP) grown cells were harvested, washed with HEPES-KOH (50 mM, pH 7.5) and diluted to 1.5 mg/ml total chlorophyll. Subsequently, cells were disrupted in an isolation buffer by pressing the cell suspension through a syringe needle (27-gauge × 1/2 inch). Thylakoids were then separated from chloroplasts and other cell components by centrifugation on a discontinuous Percoll gradient. For blue native PAGE analysis of thylakoid protein complexes (section 2.4.5), the washed thylakoid fraction was then stored at -80 °C after snap-freezing in liquid nitrogen. For further fractionation of *C. reinhardtii* chloroplasts (section 2.3.4), the washed chloroplast fraction was kept at +4 °C overnight awaiting fractionation.

Samples of washed fractions were investigated under an inverted confocal fluorescence microscope (Nikon Eclipse Ti) using a 100X oil immersion lens, acquiring images in bright field and a chlorophyll autofluorescence channel (635 nm excitation, red emission filter).

2.3.4 Fractionation of *C. reinhardtii* chloroplasts

Previously isolated chloroplasts (section 2.3.3) were further separated into stroma and thylakoid fractions as previously described [179]. In brief, chloroplasts were osmotically lysed and centrifuged on a discontinuous sucrose gradient (0.6 and 1.0 M), yielding the stromal fraction as material that did not enter the gradient on the top. The pellet was again centrifuged on a discontinuous sucrose gradient (1.3 and 1.8 M) to further purify thylakoids. The stromal fraction was washed with final sample buffer (10 mM tricine, pH 7.8, 0.2 mM EDTA, 60 mM KCl, 5 mM β-mercaptoethanol, and 20% glycerol) and concentrated with a centrifugal concentrator (Vivaspin 2 3000 MWCO, Merck) until roughly 100 µL final sample volume was reached (usually 2-3 h, 10600 xg, 4 °C).

After centrifuging the thylakoid fraction to wash away remaining sucrose, half of it was resuspended in proteinase buffer (50 mM Tris, 7.5 mM $CaCl_2$, pH 8.8) and subjected to a Proteinase K treatment with or without membrane permeabilising detergent Triton X-100. For this, Triton X-100 (0.5% final concentration) treated samples were incubated with the detergent on ice for 10 min before adding Proteinase K (50 µg/mL final concentration) to both samples, with or without Triton X-100, and incubating at 21 °C for 30 min with gentle mixing every 5 min. With the addition of PMSF (9 mM final concentration) proteolysis was interrupted. Finally, protein from all sample stages except the stromal fraction (whole cell, chloroplast, thylakoids, thylakoids+proteinase, thylakoids+proteinase+Triton) was extracted

from the samples. Samples were resuspended in RIPA lysis buffer [180] with freshly added PMSF (1 mM final concentration) and subjected to bead-beating (~100 µL of 425-600 µm beads) for 5 cycles of 1 min bead-beating and 1 min on ice. The lysate was pelleted (1 min, 2000 xg) before the supernatant was centrifuged again for 5 min at 15000 xg. The resulting supernatant was then flash frozen and stored at -80 °C until further use.

2.4 Protein Analyses

2.4.1 Protein extraction from *C. reinhardtii*

A known volume of *C. reinhardtii* cells at a desired growth stage was harvested by centrifugation at 1000 xg for 5 min. The pellet was subsequently resuspended in RIPA lysis buffer [180] with freshly added PMSF (1mM final concentration) to reach a calculated OD_{750nm} of 50. The chlorophyll content was measured as in section 2.3.1, but here 10 µL of sample were mixed with 40 µL of acetone and 1 mL of 80% acetone, resulting in a dilution factor D of 105. Protein samples were then adjusted to the same total chlorophyll concentration with RIPA buffer and frozen at -20 °C for at least 1.5 h or overnight, followed by thawing on ice to complete cell lysis. Protein concentration was determined using a Bradford assay (Merck) according to manufacturer's instructions diluting the protein samples 5- to 10-fold [181].

2.4.2 Protein gel electrophoresis

Previously extracted protein samples from *C. reinhardtii* (sections 2.4.1 & 2.3.4) were subjected to denaturing gel electrophoresis (SDS-PAGE). All samples were diluted to 1 µg/µL protein with RIPA buffer before being mixed with 4x Lämmli buffer [182] and incubated for 30 min (50 °C, 600 rpm). After centrifuging the samples (12000 xg, 1 min) to remove insoluble material, samples were loaded to the desired amount into wells of polyacrylamide gels (Mini-PROTEAN TGX Stain-Free, BioRad). PageRuler Plus (7 µL, Thermo Scientific) was used as size marker. Electrophoresis was carried out at 4 °C and 200 V for about 50 min. The gel was imaged in a ChemiDoc MP imaging system (BioRad) using the Stain Free setting and 5 min activation time. Some gels were stained with Pierce™ Silver Stain for Mass Spectrometry (Thermo Scientific).

2.4.3 Membrane transfer and immunoblotting

Transfer of protein from polyacrylamide gels onto polyvinylidene fluoride (PVDF) membranes was carried out using the iBlot dry transfer apparatus, following the manufacturer's instructions and using program P3 for 5 min. Membranes were then probed for successful transfer with PonceauS (Thermo Scientific) as per manufacturer's instructions and imaged with the ChemiDoc MP imaging system (BioRad). Depending on need, membranes were cut at this stage to allow for multiple antibody exposures. Following the PonceauS destaining, membranes were blocked in 5% milk in Tris-buffered saline with 0.1% Tween 20 (TBS-T) for 1 h at room temperature with gentle shaking. After washing membranes once with TBS-T to remove remnants of blocking agent, membranes were incubated with specific primary antibody solutions in 5% milk TBS-T (except PTOX2, table 2.12). Subsequently, membranes were washed with TBS-T (5x 5 min) and incubated for 1.5 h at room temperature with species-specific horseradish peroxidase-linked secondary antibody in 5% milk TBS-T (table 2.12). After washing membranes thrice in TBS-T and once in TBS (10 min each), they were incubated with chemiluminescence substrate (SuperSignal™ West Pico PLUS Chemiluminescent Substrate, Thermo Scientific) and imaged using a ChemiDoc MP imaging system (BioRad).

Some membranes were stripped of bound antibodies with two washes (5 min each) in mild stripping buffer (0.2 M glycine, 0.05% SDS, 0.5% Tween-20, pH 2.2) followed by three washes in TBS-T (10 min each) after which blocking and immunodetection were carried out as above.

Table 2.12: Primary and secondary antibodies used and their specifications, source, catalogue number, species the antibody was raised in, molecular weight of the target protein (MW), dilution of the antibody (in TBS-T with 5% milk except for PTOX2) and incubation conditions for antibody exposure. Antibodies with an "AS..." catalogue number can be sourced from Agrisera. The antibodies originally raised by John C. Gray were obtained from the Kromdijk group (Department of Plant Sciences, University of Cambridge).

	Antibody	Source	Catalogue number	Species	MW (kDa)	Dilution	Incubation
primary	AtpB	Y. Allahverdiyeva	AS05085	rabbit	52	1:5000	O/N 4 ℃
	CytF	Y. Allahverdiyeva	AS06119	rabbit	32	1:5000	O/N 4 ℃
	FLAG	Sigma-Aldrich	F3165	mouse	NA	1:5000	O/N 4 ℃
	LHCSR3	Agrisera	AS142766	rabbit	20	1:2000	O/N 4 ℃
	NDA2	G. Peltier	NA	rabbit	70	1:5000	O/N 4 ℃
	Plastocyanin	John C. Gray	R37/10	rabbit	10	1:2000	O/N 4 ℃
	PsaB	Agrisera	AS10695	rabbit	82	1:1000	O/N 4 ℃ + 1 h RT
	PsbA D1	Y. Allahverdiyeva	AS05084	rabbit	28	1:10000	O/N 4 ℃
	PSBO	John C. Gray	R45/5	rabbit	33	1:1000	O/N 4 ℃
	PTOX2	S. Bujaldon & F. Wollman	NA	rabbit	44	1:500 (3% milk in PBS-T)	O/N 4 ℃ + 1 h RT
	RbcL	Y. Allahverdiyeva	AS03037	rabbit	52	1:5000	O/N 4 ℃
	RuBisCO	John C. Gray	R2/2	rabbit	52	1:1000	O/N 4 ℃

	Antibody	Source	Catalogue number	Species	MW (kDa)	Dilution	Incubation
secondary	Goat anti-Mouse IgG	Immuno-Reagents	GtxMu-003-DHRPX	Goat	NA	1:5000	1.5 h RT
	Goat anti-Rabbit IgG	BioRad	1706515	Goat	NA	1:10000	1.5 h RT

2.4.4 Co-immunoprecipitation of FLAG-tagged proteins and putative interaction partners from *C. reinhardtii* lysates

C. reinhardtii cultures from mid exponential growth phase were harvested by centrifugation (1000 xg, 5 min) and the pellets were resuspended in RIPA lysis buffer [180] with freshly added PMSF (1 mM final concentration) and DNAse I (final concentration 100 U/mL). Cells were lysed by bead-beating (~100 µL of 425-600 µm beads) for 5 cycles of 1 min bead-beating and 1 min on ice. The lysate was pelleted (1 min, 2000 xg) before the supernatant was centrifuged again for 5 min at 15000 xg. The cleared lysate was then diluted with dilution buffer (10 mM Tris/Cl pH 7.5, 150 mM NaCl, 0.5 mM EDTA) and protein concentration was determined with a Bradford assay as before (section 2.4.1). For co-immunoprecipitation of FLAG-tagged proteins and putative interaction partners in the lysates, DYKDDDDK Fab-Trap™ Agarose beads (Chromotek) were utilised as per manufacturer's instructions with at least 4 washes and elution with 2x SDS sample buffer.

2.4.5 Blue native PAGE of *C. reinhardtii* thylakoids

Isolated thylakoids from *C. reinhardtii* (section 2.3.3) were subjected to blue native polyacrylamide gel electrophoresis (BN-PAGE) following an adaptation from Dr Julia Walter (Department of Plant Sciences, University of Cambridge) of a published protocol (personal communication, [183]). Firstly, thylakoid samples were diluted with resuspension buffer (25 mM Bis-Tris/HCl (pH 7.0), 20% (w/v) glycerol, 0.25 mg/ml Pefabloc, and 10 mM sodium fluoride) to a chlorophyll concentration of 0.53 µg/µL and to a total of 6 µg chlorophyll. An equal volume of β-dodecyl maltoside (β-DM, 2% in resuspension buffer) was added to each

sample and the thylakoid membranes were solubilised by gentle pipetting for 2 min. After centrifugation (4 °C, 18000 xg, 20 min) samples were mixed with a one-tenth volume of sample loading buffer (100 mM Bis-Tris/HCl (pH 7.0), 0.5 M ACA, 30% (w/v) sucrose and 50 mg/ml Serva Blue G) and loaded into the wells of a NativePAGE 3-12% Bis-Tris protein gel (Invitrogen). Electrophoresis was carried out with specific anode buffer (50 mM Bis-Tris/HCl, pH 7.0) and cathode buffer containing Serva Blue G dye (50 mM Tricine, 15 mM Bis-Tris/HCl, pH 7.0, and 0.01% Serva Blue G) at 4 °C as specified in table 2.13. After the 30 min at 125 V, the blue cathode buffer was replaced by the same cathode buffer but without Serva Blue G. The last step was prolonged to 5 h if additional separation of bands of interest was needed.

Table 2.13: Voltage and time specifications for BN-PAGE.

Step	Voltage (V)	Time (min)
1	75	30
2	100	30
3	125	30
4	150	60
5	175	30
6	200	60

2.4.6 Second dimension SDS-PAGE of BN-PAGE

Gel electrophoretic separation of complexes in BN-PAGE lanes on a second dimension SDS-PAGE was carried out as previously described [183, 184], although 12% polyacrylamide gels were used here. Gels were stained with Pierce™ Silver Stain for Mass Spectrometry (Thermo Scientific). After staining, gels were stored at 4 °C in 1% acetic acid until individual spots were excised and sent for analysis with liquid chromatography coupled mass spectrometry (LC-MS/MS). LC-MS/MS analysis was carried out by the Cambridge Centre for Proteomics (Biochemistry Department, University of Cambridge).

2.5 Microscopy

2.5.1 Fluorescence microscopy

Samples of *C. reinhardtii* cultures or isolated components were sealed on a microscopy slide with a cover slip and nail polish and investigated for fluorescence using the 100X oil immersion lens of an inverted confocal fluorescence microscope (Nikon Eclipse Ti). Chlorophyll fluorescence (635 nm excitation, red emission filter), mVenus fluorescence (525 nm excitation, yellow emission filter) and a brightfield image were recorded.

2.5.2 Immunofluorescence staining & microscopy of *C. reinhardtii*

Immunofluorescence staining of *C. reinhardtii* cells carried out here was adapted from Yamano *et al*. [185]. The methanol incubation step was left out to retain chlorophyll in the samples serving as a chloroplast marker. A 100 µL sample of *C. reinhardtii* culture (grown under standard conditions to OD_{750nm} ~2) was allowed to air-dry on a polylysine covered glass microscopy slide (VWR) before cells were permeabilised by incubation in PBS-T (Phosphate-buffered saline with 0.1% Tween 20) in a Coplin jar for 10 min. All following fixing, blocking and staining steps were executed in a humid atmosphere provided by a closed Petri dish lined with wetted tissue. For all washing steps a Coplin jar was used. The samples were fixed by adding PBS containing 4% (w/v) formaldehyde (100 µL for 10 min, then another 100 µL were added for 10 more min) and then washed twice in PBS and air-dried (5 min each). Using 5% BSA in PBS, the cells were blocked for 1 h before washing and air-drying as before. Primary antibody solution in PBS-T was applied for 1 h (mouse anti-FLAG: 1:2500 (B3111, Sigma)). Following PBS-T washes (5x 3 min), the samples were incubated in the dark for 1 h with PBS-T containing secondary antibody (Goat anti-Mouse IgG Alexa Fluor™ 488: 1:200 (A11029, Invitrogen)). Further PBS-T washes (5x 3 min) were followed by application of mounting medium (8 µL 20 mM Tris, pH 8.0, 50% glycerol), addition of a coverslip and sealing the coverslip with nail polish.

An inverted confocal fluorescence microscope (Nikon Eclipse Ti) was used to investigate the stained slides. Brightfield and epifluorescence images were taken with a 20X or 100X oil immersion lens. AlexaFluor 488 signal was recorded in a YFP channel (500 nm excitation (73% intensity), yellow emission filter, 500 ms exposure) while another channel was used for chlorophyll autofluorescence (635 nm excitation (31% intensity), red emission filter, 500 ms exposure). Images were acquired as z-stacks (acquisition every 0.3 µm) and the

fluorescence signals were deconvoluted using the Richardson-Lucy method and 20 iterations in the NIS-Elements Advanced Research Software (Nikon).

2.6 Spectrometric methods

2.6.1 Measurement of light intensity

Light intensity as experienced by algae cultures and samples in incubators and spectrometric instruments was recorded with a LI-250A (LI-COR) or SKP200 (Skye Instruments) light meter.

2.6.2 Measurement of fluorescent protein expression

Aliquots of *C. reinhardtii* cultures were tested for expression of mVenus in a 96-well plate with a CLARIOstar Plus plate reader (BMG Labtech). Fluorescence values of mVenus (515 nm excitation, 550 nm emission) and chlorophyll (440 nm excitation, 680 nm emission) were recorded for each well.

2.6.3 Low temperature fluorescence spectroscopy of *C. reinhardtii*

77K fluorescence emission spectra were recorded with a QE Pro spectrophotometer (Ocean Optics, Dunedin, FL, USA). Cell samples (200 µL) frozen in liquid N_2 were excited with blue light (440 nm). Raw spectra were normalised to the photosystem II (PSII) fluorescence peak at 685 nm.

2.6.3.1 Growth samples

C. reinhardtii cells were harvested and total chlorophyll concentration was adjusted to 5 µg/mL with fresh medium (TP or TAP). Cells were then frozen in liquid N_2 for measurement.

2.6.3.2 State transition experiment

For the state transition experiment (section 4.2.1.2), *C. reinhardtii* cells grown in TAP under standard conditions were adjusted to 5 µg/mL total chlorophyll with fresh medium. Anoxia (state 2 inducing) samples were adjusted with medium containing glucose (final concentration 20 mM) and Glucose Oxidase (final concentration 50 U/mL) that was purged with N_2 for 3 min. The final samples were again purged with N_2 before being sealed. Oxia (state 1 inducing) samples were adjusted with unchanged medium and left unsealed. All samples were then shaken for 30 min in darkness before being frozen in liquid N_2 for fluorescence measurement.

2.6.4 Pulse-amplitude modulation (PAM) fluorometry of *C. reinhardtii*

Whole-cell chlorophyll fluorescence of *C. reinhardtii* was measured with a pulse amplitude-modulated spectrometer (Dual-PAM-100, Walz). Prior to measurements, cells were resuspended in TAP and the chlorophyll concentration was adjusted to 20 µg/mL. After recovery under standard growth conditions for at least 30 min, measurements were performed in a quartz cuvette at 25 °C with stirring and samples were initially incubated in darkness for 5 min before the blue fluorescence measuring light (Intensity 12, 28 $\mu mol_{photons}\ m^{-2}\ s^{-1}$) was turned on. Saturating pulses (Intensity 5, 5000 $\mu mol_{photons}\ m^{-2}\ s^{-1}$, 500 ms width) for PSII parameter determination were applied with stirring turned off. DISCO Light conditions (section 2.1.2, figure 3.5) in the DUAL-PAM-100 were achieved by alternating 2 min darkness followed by 2 min consisting of 12 s high light (690 $\mu mol_{photons}\ m^{-2}\ s^{-1}$) and 12 s darkness alternations. Saturating pulses were applied in the middle of each 12 s phase or three times during the 2 min dark phases. Photosynthetic parameters were calculated as described previously [186].

2.6.5 Chlorophyll fluorescence induction spectroscopy (OJIP) of *C. reinhardtii*

Whole cell chlorophyll fluorescence induction (OJIP) of *C. reinhardtii* was measured with a FL3500 fluorometer (Photon System Instruments). Prior to measurement, cells were resuspended in TAP and chlorophyll concentration was adjusted to 20 µg/mL. After recovery under standard growth conditions for at least 30 min, chlorophyll concentration was adjusted to 5 µg/mL with or without DCMU (10 µM final concentration). After 15 min incubation in darkness, fluorescence induction in response to red light (984 $\mu mol_{photons}\ m^{-2}\ s^{-1}$, 45% A-voltage)

was recorded for 120 s. Raw fluorescence data was double normalised to fluorescence at time point 0 and the maximum fluorescence value to compare the kinetics between samples [187].

2.6.6 P700 differential absorbance spectrometry of *C. reinhardtii*

Whole-cell P700 absorbance of *C. reinhardtii* was measured with a pulse amplitude-modulated spectrometer (Dual-PAM-100, Walz). Prior to measurements, cells were resuspended in TAP and the chlorophyll concentration was adjusted to 20 µg/mL. After recovery under standard growth conditions for at least 30 min, 2 mL of the cell suspension were filtered onto glass fibre filters (WHA1822025, Whatman) and 100 µL fresh TAP were added to keep the filter moist. Measurements were performed using leaf clamps holding the filter and samples were initially incubated in darkness for 5 min before the P700 measuring light (Intensity 15) was turned on. Saturating pulses and DISCO Light treatment were identical to those used in the PSII fluorescence measurements (section 2.6.4). P700 SP-evaluation settings were adjusted to 7 ms delay and 10 ms width and photosynthetic parameters were calculated as described previously [188].

2.6.7 Coupled fluorescence and absorption spectrometry monitoring PSII and PSI of *C. reinhardtii*

Whole-cell P700 absorbance and chlorophyll fluorescence of *C. reinhardtii* were measured with a pulse amplitude-modulated spectrometer (Dual-PAM-100, Walz). For the light curves (section 4.2.1.3), algal samples on glass fibre filters were prepared as in section 2.6.6 and both fluorescence (Intensity 12, 28 $\mu mol_{photons}\ m^{-2}\ s^{-1}$) and P700 measuring light (Intensity 15) were turned on after 5 min incubation in darkness. Samples filters were held by leaf clamps and saturating pulses, P700 SP-evaluation settings and calculation of parameters were the same as in sections 2.6.4 & 2.6.6.

The internal light curve protocol of the Dual-PAM-100 (Walz) was adjusted to the measured light intensities and times in table 2.14.

Table 2.14: Light intensities and exposure times for measurements of light response curves with *C. reinhardtii*.

Step	**Light intensity** ($\mu mol_{photons}\ m^{-2}\ s^{-1}$)	**Time** (s)
1	0	30
2	11	30
3	29	30
4	68	30
5	155	30
6	217	30
7	307	30
8	378	30
9	477	30
10	772	30
11	1197	30

2.6.8 DUAL-KLAS-NIR absorbance spectrometry of *C. reinhardtii*

Whole-cell differential absorbance at the wavelength pairs 780–820, 820–870, 840–965 and 870–965 nm was measured simultaneously with a DUAL-KLAS-NIR spectrometer (Walz). From these, plastocyanin, P700 and ferredoxin redox changes were deconvoluted using differential model plots (DMPs; [189–191]). Due to the presence of flavodiiron proteins in WT *C. reinhardtii* reoxidation of ferredoxin is very fast and affects DMP acquisition. Thus, DMPs were measured using the *flvAB* knock-out strain of *C. reinhardtii* grown photoautotrophically (Martina Jokel, Turku University). Additionally, the plastocyanin DMP was recorded with DCMU treated samples (10 µM final concentration). Otherwise, DMPs were recorded following the manufacturer's instructions. Algal samples on glass fibre filters were prepared as in section 2.6.6 and measurements were carried out using leaf clamps after 20 min of incubation in the dark followed by 30 s illumination with red light (503 $\mu mol_{photons}\ m^{-2}\ s^{-1}$). Redox changes were then recorded using the NIRmax script of the instrument software, consisting of 3 s red actinic light (200 $\mu mol_{photons}\ m^{-2}\ s^{-1}$), with a saturating pulse after

200 ms to reduce ferredoxin fully. Following 4 s of darkness thereafter, 10 s of far-red light actinic illumination and a saturating pulse at the end allowed for full oxidation of P700 and plastocyanin. The differential wavelength signals were deconvoluted, normalised to the respective maximum redox change and signal-to-noise ratio was improved with a Savitzky-Golay filter [192].

2.6.9 Cytochrome b_6f differential absorbance spectrometry of *C. reinhardtii* using a Joliot type spectrometer (JTS)

Plastocyanin, cytochrome *f*, and *b* heme redox kinetics were determined in whole *C. reinhardtii* cells by deconvoluting absorbance changes at 546, 554, 563, and 573 nm that were measured using a JTS-10 pump probe spectrophotometer (BioLogic) and appropriate 10 nm FWHM (full width at half maximum) interference filters. BG39 filters (Schott) were used to shield the light detectors from scattered light. Deconvolution was performed with the JTS-10 software. Prior to measurements, cells were resuspended in fresh medium to a total chlorophyll concentration of 20 µg/mL. After recovery under standard growth conditions for at least 30 min, Ficoll 400 was added to a final concentration of 10%. In some cases, other chemicals were added to affect parts of the PETC at the same time as Ficoll (table 2.15). Cells were dark-adapted for 3 min before measurement with each interference filter and then illuminated with 5 s of green light (500 $\mu mol_{photons}\ m^{-2}\ s^{-1}$). Flashes of white detection light were administered during 300 µs dark intervals in actinic illumination. Every recording was corrected for any detection light impact by subtracting a trace with actinic light turned off. During analysis, the signal-to-noise ratio was improved with a Savitzky-Golay filter [192].

Table 2.15: Chemicals used to affect the PETC in *C. reinhardtii* during JTS experiments, their primary effect, final concentrations and references for concentrations used.

Chemical	Primary effect on PETC	Final concentration	Ref.
3-(3,4-dichlorophenyl)-1,1-dimethylurea (DCMU)	blocks the Q_B site of PSII	10 µM	[193]
Methyl viologen (MV)	artificial electron acceptor from PSI	10 mM	[50, 193]
N-propyl gallate (n-PG)	inhibits PTOX2	1 mM	[51, 194]
2,5-dibromo-3-methyl-6-isopropyl-p-benzoquinone (DBMIB)	blocks the Q_p site in cytochrome b_6f	20 µM	[193]

2.6.10 Electrochromic shift (ECS) measurements of *C. reinhardtii*

Changes in the proton motive force and contributing factors, vH^+ and gH^+, were determined with a Dual-PAM-100 (Walz) by measuring absorbance changes at 515 nm, known as electrochromic shift (ECS; [195–197]). Dark interval relaxation kinetics (DIRKs) were recorded by interrupting actinic light exposure for 450 ms with darkness. Prior to measurements, *C. reinhardtii* cells were resuspended in fresh medium and the total chlorophyll concentration was adjusted to 20 µg/mL. After recovery under standard growth conditions for at least 30 min, Ficoll 400 was added to a final concentration of 10%. Cells were dark-adapted for 10 min before measurement and measurements started with a single turnover flash (100 µs) used later for normalisation of the ECS signal. For the standard growth condition induction experiment (section 4.2.1.7) red actinic light (53 $\mu mol_{photons}\ m^{-2}\ s^{-1}$) was turned on and DIRKs recorded every 5 s for 30 s and every 10 s thereafter. For the DISCO Light experiment (section 4.2.2.3), the light regime as in section 2.6.4 was used, but instead of saturating pulses, DIRKs were recorded. At the end of the protocol, slow relaxation of the ECS signal in darkness was recorded for 1 min and used later for analysis of partitioning the pmf into ΔpH and $\Delta\Psi$ [198, 199]. Analysis of kinetic data was carried out using OriginPro (Version 2024, OriginLab Corporation). The first 20 ms of the DIRK were fitted with a linear regression, the absolute slope of which corresponds to the proton pumping activity (vH^+, [200]), while the inverse of the time constant of the first order exponential decay fit of a DIRK corresponds to the activity of the ATP-Synthase (gH^+, [195]).

2.6.11 Membrane inlet mass spectrometry of *C. reinhardtii*

Gas exchange of $^{16}O_2$ (m/z 32) and $^{18}O_2$ (m/z 36) was measured *in vivo* using membrane inlet mass spectrometry (MIMS) as described before [201, 202]. Prior to measurements, *C. reinhardtii* cells were resuspended in fresh medium (TAP) and the total chlorophyll concentration was adjusted to 20 µg/mL. After recovery under standard growth conditions for at least 30 min, cells were supplemented with $^{18}O_2$ at an equivalent concentration to $^{16}O_2$ and incubated in darkness for 15 to 20 min, 5 min of which represent the start of the recorded traces. After 5 min of white actinic light (500 $\mu mol_{photons}\ m^{-2}\ s^{-1}$) gas exchange was recorded for another 5 min in darkness.

The minimum and maximum O_2 signal were calibrated in ultrapure water. The gas exchange rates were calculated according to Beckmann *et al*. [203]. To enable accurate determination of rates, a mathematical offset was applied to account for the fluctuating concentrations of the $^{18}O_2$ and $^{16}O_2$ isotopologues throughout the experiment [204]. During analysis, the signal-to-noise ratio was improved with a Savitzky-Golay filter [192].

2.7 Sequencing

2.7.1 Sanger sequencing

Sanger sequencing of DNA (plasmids and PCR products) was carried out by the DNA sequencing facility (Department of Biochemistry, University of Cambridge).

2.7.2 Whole genome sequencing of *C. reinhardtii*

Genomic DNA from *C. reinhardtii* (section 2.2.1) was used for whole genome sequencing carried out by Novogene (Cambridge, UK). Novogene subjected samples to quality control, library preparation, and Illumina sequencing (PE-150 technology).

2.7.3 RNA sequencing of isolated RNA from *C. reinhardtii*

Whole cell RNA from *C. reinhardtii* (section 2.2.2) was used for RNA sequencing carried out by Novogene (Cambridge, UK). Novogene subjected samples to quality control, directional poly-A enriching library preparation, and Illumina sequencing (PE-150 technology).

2.8 Bioinformatic methods

2.8.1 General data analysis, visualisation and statistics

Analysis, visualisation and statistical analyses were carried out using R and RStudio, unless otherwise specified [205, 206]. Key packages to mention include tidyverse [207], ggplot2 [208], ggpubr [209], and rstatix [210].

2.8.2 Whole genome sequencing analysis and single nucleotide polymorphism (SNP) analysis

Raw fastq files were obtained from Novogene. After confirming their quality using FastQC [211], BBDuk in Geneious Prime was used to trim adapter sequences, low quality (< 30 quality value) and short reads (<10 bp). Subsequently, reads were aligned to the latest genome assembly for *C. reinhardtii* from JGI (CC-4532 v6.1, [11]) with the Geneious Mapper.

Comparative read count analysis was performed using SeqMonk [212] and Integrative genomics viewer was used for coverage visualisation [213].

Analysis of variants was carried out with the "Find Variations/SNPs" tool in Geneious and the following settings: minimum coverage 10, minimum variant frequency 90% (to focus on differences between strains), maximum variant p-value 10^{-6}, minimum strand-bias p-value 10^{-5} when exceeding 65% bias. SNPs were subsequently filtered with a custom Python script to include only non-synonymous mutations in coding regions of the genome.

2.8.3 RNA sequencing analysis

Raw fastq files were obtained from Novogene. After confirming their quality using FastQC [211], the latest genome assembly for *C. reinhardtii* from JGI (CC-4532 v6.1, [11]) was used to build the reference genome and raw reads were aligned with hisat2 [214]. Alignment was confirmed and read assignment statistics were calculated with picard tools [215]. A quality control summary was created with multiQC [216]. Count data for genetic features was extracted using featureCounts [217] and the latest gff3 reference file for *C. reinhardtii* from JGI. The featureCounts table was analysed in R, where analysis of differential expression was performed with DEseq2 [218]. Visualisation of differential expression data relied on ggplot2 [208] and ComplexHeatmap [219], while ShinyGO [220] and topGO [221] were used for gene ontology enrichment .

3

Creation and characterisation of cytochrome c_{6A} mutant strains in *C. reinhardtii*

3.1 Introduction

3.1.1 A brief history of *C. reinhardtii* laboratory strains

Three major lines of *C. reinhardtii* "wild-type" strains emerged in the years after the first isolation of *C. reinhardtii* 137c by Gilbert Smith due to samples being sent across the world: the "Sager" line, the "Cambridge" line and the "Ebersold/Levine" line (figure 3.1). Today's most commonly used wild type strains CC-125 and CC-124 (mating type (mt) + and –, respectively) originated from the "Ebersold/Levine" line. Early in this line, strains accumulated mutations preventing them from utilising nitrate (nit1 and nit2).

As more *C. reinhardtii* strains were crossed and mutants created, crosses between strains from the three lines were also carried out. The strains used in the work presented here, CC-1883 (WT) and CC-4532 (for its *C. reinhardtii* reference genome v6.1) are products of such inter-line crossings. The cell wall-less ("cw15") CC-1883 originates from a cross of CC-1690 21 gr mt+ (Sager line, salmon) with CC-1615 cw15 nit2 mt- which is ultimately a descendant of CC-400 cw15 mt+ (Ebersold/Levine line, salmon) (figure 3.1) [222]. CC-4532 was recently used to establish the latest *C. reinhardtii* reference genome [11] and is a putative subclone of CC-621 NO mt- (Ebersold/Levine line, burgundy). It is believed to originate from a cross between 21gr mt+ (Sager line, burgundy) and 137c mt- (Ebersold/Levine line, burgundy, figure 3.1) [223, 224].

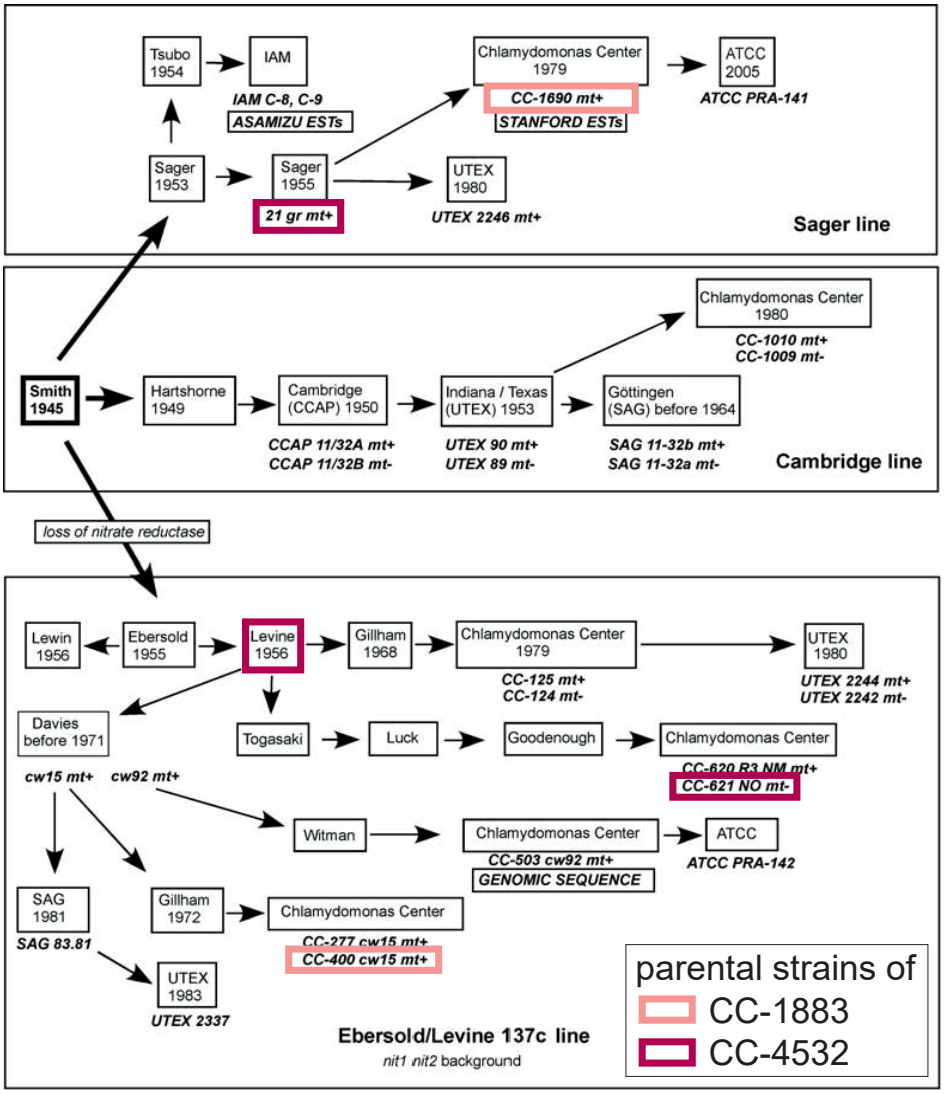


Figure 3.1: *C. reinhardtii* wild-type laboratory strains derived from an isolate of G. M. Smith in 1945. The putative parental strains of CC-1883 (WT) and CC-4532 (*C. reinhardtii* genome v6.1) are marked in salmon and burgundy, respectively. Adapted from [223].

Although CC-1883 and CC-4532 are both "wild-type" *C. reinhardtii* strains, it can be expected that they differ significantly in both genotype and phenotype as suggested by their ancestry. This glimpse of *C. reinhardtii* strain history showcases how vital it is for phenotypic studies of mutants to utilise the background strain used to create the mutant, rather than a "wild-type" strain of any variety.

3.1.2 Growth of *C. reinhardtii* in the presence of acetate

Many members of the genus *Chlamydomonas* can grow heterotrophically on acetate in darkness, however, an equally large number was found not to be capable of heterotrophic

growth [225]. The ability of *C. reinhardtii* to grow in darkness on acetate and still keep a fully functional PETC has contributed to its success as model organism, as strains of *C. reinhardtii* mutant in photosynthesis could be kept alive and studied where obligate phototrophs would have died [226].

Assimilation of acetate in *C. reinhardtii* proceeds via the following route. Exogenous acetate is incorporated into acetyl coenzyme A (acetyl-CoA) in an ATP-dependent manner via acetyl-CoA synthetase or acetate kinase and phosphate acetyltransferase. The ATP needed for assimilation of acetate in the dark is provided only in aerobic conditions that allow respiration [227]. The assimilated acetate, now in the form of acetyl-CoA is fed into the glyoxylate or Szent–Györgyi–Krebs cycles, ultimately supporting the production of ATP and reducing equivalents allowing biomass formation [226].

C. reinhardtii can also grow photomixotrophically relying on photosynthesis and exogenous acetate at the same time. Under such conditions, cells are characterised by reduced photosynthetic capacity but an increased growth rate compared to photoautotrophic conditions. Once acetate in the medium is depleted, *C. reinhardtii* cultures reach stationary phase [228]. The processes of acetate assimilation and photosynthesis are connected, as acetate photoassimilation has been shown to be supported by cyclic electron flow [121, 226]. Furthermore, the presence of acetate can lead to a more reduced state of the PQ pool, because reducing equivalents from the Szent–Györgyi–Krebs cycle can be exchanged between mitochondria and chloroplasts via the malate-oxaloacetate shuttle and fed into the PETC likely via the NADPH dehydrogenase NDA2 [118, 119, 229].

3.1.3 Growth of *C. reinhardtii* under fluctuating light conditions

Photosynthetic organisms are exposed to variations of light intensity in their natural environments. These include diurnal cycles but also more rapid light fluctuations caused by the sun, clouds, overhanging vegetation, and in the case of the alga *C. reinhardtii* also soil and water movements [8, 230]. Additionally, fluctuating light conditions are a common experience for photosynthetic microorganisms when grown in photobioreactors for biotechnological purposes. This is due to the constant mixing of high-density cultures, resulting in fast movements between dark and light zones within the vessel [231].

For *C. reinhardtii*, studies uncovered a stark effect of fluctuating light regimes on its ability to grow. When exposed to a 12 s on/ 12 s off cycle with light intensities of 600-700 $\mu mol_{photons}\ m^{-2}\ s^{-1}$ in photoautotrophic conditions, *C. reinhardtii* growth rates reached only ~30% of rates achieved under continuous illumination [232]. A more comprehensive

study of fluctuating light frequencies and their impact on growth of photosynthetic organisms *C. reinhardtii* and the cyanobacterium *Synechococcus elongatus* revealed a growth penalty caused by fluctuating light with frequencies in the range of 0.01 to 0.1 Hz (i.e. 10-100 s on/off) [233]. The authors concluded that regulation of photosynthesis caused this growth penalty with RuBP regeneration being the dominant limiting factor at timescales of 5 to 250 s on/off cycles. Interestingly, photomixotrophy partly alleviated the observed growth penalty, as the presence of an organic carbon source decreases the need for carbon fixation via the CBB cycle. The additional trophic mode thus increases *C. reinhardtii*'s chances of survival under difficult light conditions.

Additional to studies with wild-type cells, various *C. reinhardtii* mutants have been found to exhibit a growth penalty only when exposed to fluctuating light, implicating the respective knocked-out proteins in processes allowing algal growth in such conditions (table 3.1).

Table 3.1: Proteins in *C. reinhardtii* or *A. thaliana* (STN7 only) whose knock-out lead to a growth penalty compared to the respective background strain under fluctuating light. For better readability the light intensity unit "$\mu mol_{photons}\ m^{-2}\ s^{-1}$" was omitted.

Affected protein	Phenotype causing fluctuating light regime	Reference
PGRL1	5 min 20 & 1 min 600	[65]
PGR5	5 min 20 & 1 min 200	[65]
FLVA/B	5 min 20 & 1 min 200	[65]
APX2	5 min 50 & 1 min 600	[234]
STT7	no phenotype for 1, 10 or 30 min 620/dark	[235]
STN7(*A. thaliana*)	5 min 60 & 1 min 600	[236]
	1 h 50 & 1 h 240	[237]
LHCSR3	1 min 620 & 1 min dark	[235]
	10 min 500 & 10 min dark	[238]
PTOX2	1 min 300 & 1 min dark	[53]

For example, Jokel *et al.* (2018) investigated the impact of fluctuating light regimes on the growth of *C. reinhardtii* without PGRL1, PGR5 or FLVA/B [65]. PGRL1 and PGR5 have both been implicated in CEF, however, a debate remains about the specific mechanism

of their action [44]. In *C. reinhardtii*, growth penalties have been found for mutants strains lacking PGRL1 or PGR5 under fluctuating light regimes with low light to high light transitions (table 3.1) [65]. A similar fluctuating light regime led to a severe growth penalty for the FLVA/B knock-out (table 3.1). These findings contributed to determining that FLVA and FLVB together provide an alternative electron pathway to conventional LEF. FLVA/B prevent acceptor side limitation of PSI upon dark-to-light transitions by reducing O_2 with electrons likely from ferredoxin [66, 239]. A knock-out of APX2 was also found to affect growth of *C. reinhardtii* under a similar fluctuating light regime as for FLVA/B [234]. APX2 is an ascorbate peroxidase–related protein that regulates the levels of plastocyanin in *C. reinhardtii* and thereby has a more indirect but nevertheless important impact on the PETC [240].

Low light to high light transitions also affect the growth of a knock-out of STN7 in *A. thaliana* (table 3.1), while a knock-out of the homologue STT7 in *C. reinhardtii* did not produce a growth defect under 1, 10 or 30 min on/off cycles [235]. STT7 and STN7 are the kinases that allow state transitions in *C. reinhardtii* and *A. thaliana* respectively by phosphorylating LHCII proteins and could therefore be expected to be important for light conditions that require dynamic adaptation [90]. Wientjes *et al.* (2013) suggested that in *C. reinhardtii* state transitions are more important for short-term fluctuating light conditions, while in plants they are more useful for long-term adaptations as under nearly all light conditions in plants some LHCII antennae were found associated with PSI [241]. However, this would be contrary to the observed phenotypes, as a STT7 knock-out in *C. reinhardtii* did not show a growth penalty in short-term fluctuating light [235], while a STN7 knock-out in *A. thaliana* did [236, 237].

Energy dependent quenching, qE, of NPQ is another mechanism for adaptation to stressful light conditions and in *C. reinhardtii* is mainly facilitated by the protein LHCSR3 [71]. For a mutant lacking LHCSR3 a growth penalty was found when exposed to 1 or 10 min on/off light cycles (table 3.1).

Finally, the terminal oxidase PTOX2 has also been associated with survival of *C. reinhardtii* under fluctuating light conditions. PTOX2 has been found to be the major oxidase involved in chlororespiration in *C. reinhardtii* [51]. Without PTOX2, *C. reinhardtii* exhibits a growth defect when exposed to 1 min on/off light cycles (table 3.1).

In summary, studies of fluctuating light have increased our understanding of photosynthetic processes by uncovering roles in regulation mechanisms and involvement of different proteins in alternative electron pathways.

3.1.4 Aims

To provide a basis for investigating the function of c_{6A}, c_{6A} mutant strains (c_{6A} knock-out and c_{6A} overexpression) were created and confirmed via PCR, whole genome sequencing (WGS), and western blots. Given the possible role of c_{6A} in photosynthesis and associated processes, it was important to determine if the presence of the protein affected the ability of *C. reinhardtii* cells to survive under a range of conditions. To this end, the c_{6A} mutant strains were analysed for their growth under different conditions, including various fluctuating light regimes and heterotrophy.

3.2 Results & Discussion

3.2.1 A CRISPR-edited *C. reinhardtii* strain was confirmed to be a cytochrome c_{6A} knock-out via PCR and whole genome sequencing

The *C. reinhardtii* wild-type strain CC-1883 (aka "Edincw15", "WT" hereafter) was subjected to a CRISPR/Cpf1 mediated knock-out of the c_{6A} gene *CYC4* and resulted in the Uex55 strain ("c_{6A}-KO" hereafter, section 1.4.6, Ferenczi & Molnar, University of Edinburgh). To confirm the knock-out, the c_{6A} locus of c_{6A}-KO and WT were examined by colony PCR (figure 3.2A). Primers were used that spanned the whole c_{6A} gene (*CYC4*, Cre16.g670950) binding 245 bp upstream and 75 bp downstream of *CYC4*, respectively (c6A-KO check fw & rev, table 2.8). For WT, the PCR led to a band at 2.5 kb which corresponded well with the expected size of 2469 bp. For c_{6A}-KO, a band of around 1.7 kb was visible, consistent with the expected size of 1773 bp following the CRISPR induced deletion of 708 bp and addition of a 12 bp multiple stop codon. The c_{6A} knock-out could therefore be confirmed for the c_{6A}-KO strain. The PCR protocol shown here was regularly carried out throughout the duration of experiments to ensure the genotypic difference between c_{6A}-KO and WT.

To verify the PCR and check for off-target effects of the CRISPR system, both c_{6A}-KO and WT were subjected to WGS. DNA was extracted from photomixotrophically grown cultures under standard conditions. The DNA was found to be of sufficient quality via NanoDrop quantification and gel electrophoresis and subsequently sequenced by Novogene. Assessment of the raw reads confirming high quality sequencing as provided by Novogene and fastQC analysis can be found in the appendix (table B.1, figures B.1 & B.2). The WGS data showed a high coverage of the c_{6A} locus (> 50x) for both strains (figure 3.2B). The whole locus was covered by reads in WT, while c_{6A}-KO lacked all reads for exon 2 and intron 2. Reads in

exon 1, intron 2 and exon 3 exhibited mismatches (coloured bars in figure 3.2B) as they contain the introduced multiple stop codon (section 1.4.6) and bases of exon 1 and intron 2 for reads in exon 3 and vice versa. The WGS therefore confirmed the knock-out covering exon 1 to exon 3 in the c_{6A} locus in c_{6A}-KO. The lack of any reads for the knocked-out region also confirmed that the deleted part had not reintegrated somewhere else in the genome, as the short read alignment would have placed those reads within the *CYC4* locus.

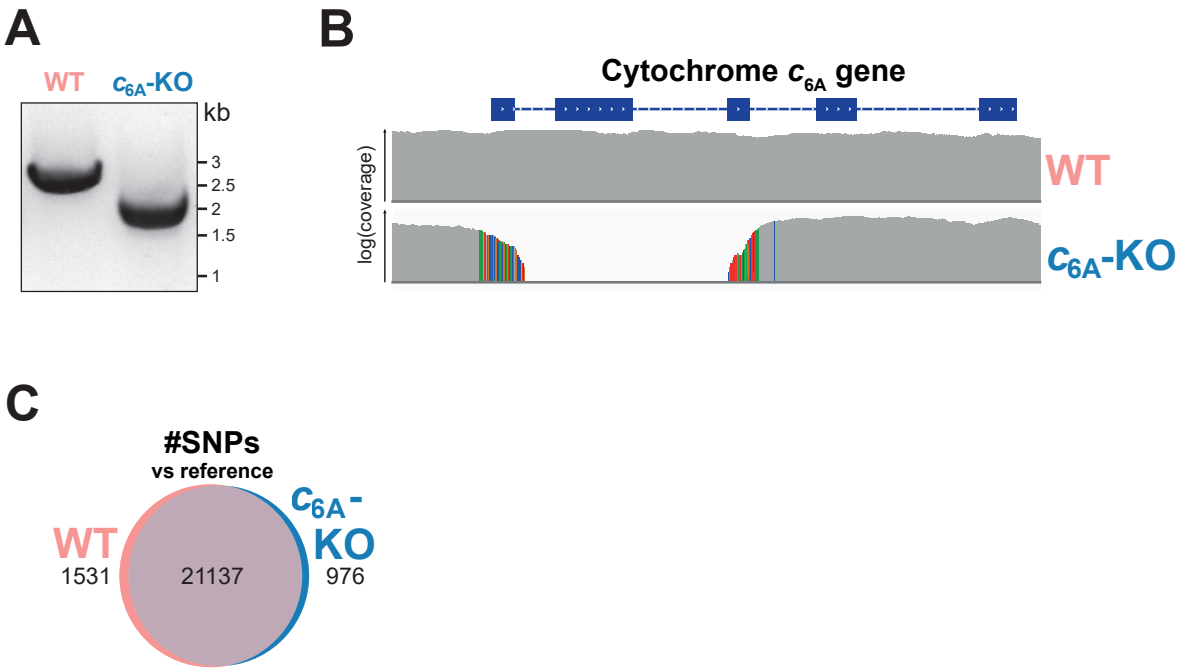


Figure 3.2: Genetic analyses of c_{6A}-KO and WT. (**A**) PCR with primers spanning the whole *CYC4* locus revealed a shortened locus (~1.7 kb) in c_{6A}-KO compared to WT (~2.5 kb). (**B**) Whole genome sequencing analysis of the *CYC4* locus confirmed the CRISPR-induced deletion of exon 1 to 3 in c_{6A}-KO as seen from the coverage plot. (**C**) The number of single nucleotide variants versus the reference strain was compared between c_{6A}-KO and WT. SNPs were filtered for coverage of >10, variant frequency of >90%, to be only of non-synonymous nature and found only found in coding sequence (CDS) regions.

To look for further off-target effects like exon deletions similar to the deletions at the c_{6A} locus comparative analysis of read counts was carried out with SeqMonk. While compared to the reference genome there were exon deletions in both c_{6A}-KO and WT, *CYC4* remained the only gene with exon deletion in only one of the strains (appendix figure B.3). Furthermore, and importantly for photosynthetic organisms, the plastid genome was found to be intact and identical in both c_{6A}-KO and WT, just as the mitochondrial genome.

Even though there were no larger deletions other than c_{6A}, analysis of single nucleotide polymorphisms (SNPs) revealed a substantial degree of variation between WT, c_{6A}-KO and the strain used to create the reference genome (CC-4532, figure 3.2C). To study the most significant SNPs, they were filtered to have a coverage of >10, variant frequency of >90%,

to be only of non-synonymous nature and found in coding sequence (CDS) regions. The high number of differences (>20000 SNPs) from the reference strain CC-4532 might be expected as there is a long and complicated lineage history of *C. reinhardtii* laboratory strains (section 3.1.1) [8]. The last common ancestor between the strains used for this study and the reference CC-4532 probably predates 1985 when CC-1883 (WT) was first taken into the Chlamydomonas Center collection [222]. Similarly high numbers of variations have been found previously when the genomes of various *C. reinhardtii* wild type strains were compared amongst themselves [242]. Comparing c_{6A}-KO and WT, however, also identified many unique SNPs (976 for c_{6A}-KO and 1531 for WT), indicating a high rate of mutation since the establishment of the knock-out strain. These SNPs corresponded to 75 and 123 uniquely affected genes in the c_{6A}-KO and WT, respectively. The only gene of those that displayed a start codon loss was *CYC4* and no genes related to photosynthesis were among the list.

In summary, the c_{6A} knock-out has been confirmed for c_{6A}-KO using PCR and WGS and while variations between c_{6A}-KO and WT exist, comparisons of the two strains will be informative for determining the function of c_{6A}. Further certainty about c_{6A}-dependent differences could be obtained by rescuing the c_{6A} knock-out with an overexpression construct.

3.2.2 A Golden Gate c_{6A} overexpression construct led to c_{6A} expression in *C. reinhardtii* c_{6A}-KO

Golden Gate cloning was used to create a FLAG tagged c_{6A} overexpression construct named pDKM-000 (figure 3.3A). A resistance to the antibiotic paromomycin was conferred by the *ParoR* gene under the control of a chimeric *HSP70A*/*RBCS2* promoter (PHR) and the *RBCS2* terminator (TRBCS) [26]. The strong constitutive *PSAD* promoter and terminator (PPSAD & TPSAD) [26] direct the expression of the native *C. reinhardtii* c_{6A} sequence (including introns) with a C-terminal FLAG tag. The epitope FLAG tag was chosen due to its small size, good immunoreactivity, and confirmed functionality in chloroplasts [243].

Correct assembly of the construct was verified by Sanger sequencing. The c_{6A}-KO strain was then transformed with the construct and a number of colonies were obtained. Successful transformation of the c_{6A}-KO strain with the construct was tested by colony PCR on three of the colonies (figure 3.3B). Primers were used that should bind inside the construct (arrows in 3.3A) and produce a fragment of 2880 bp. For colonies 1 and 3 the presence of the construct could be confirmed, while colony 2 seemed to have a smaller PCR product indicating unsuccessful introduction of the whole construct, although this might have been a loading effect.

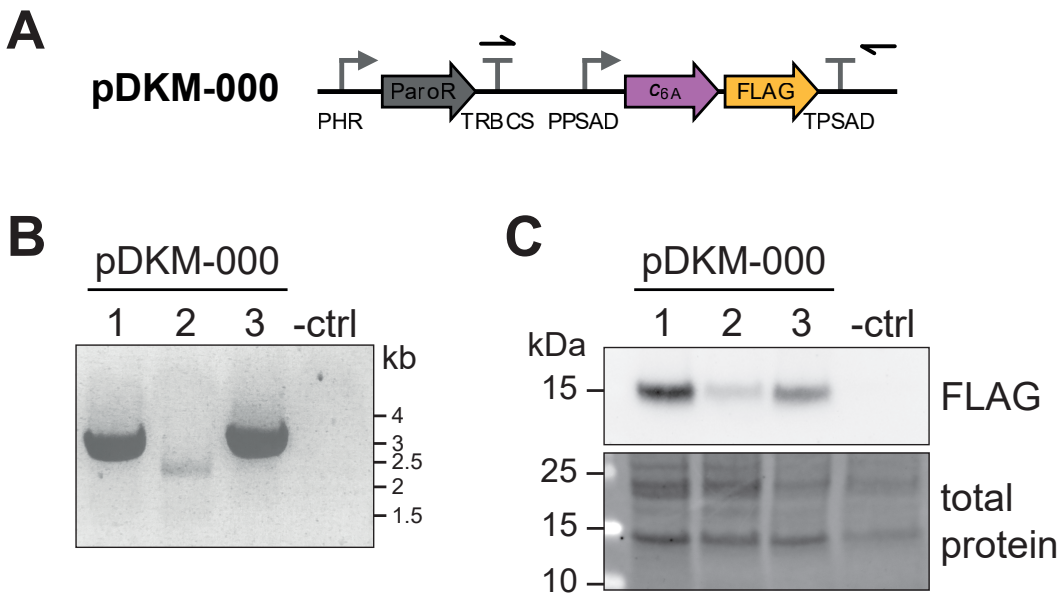


Figure 3.3: Creation of a cytochrome c_{6A}-overexpression strain. (**A**) The c_{6A}-overexpression construct pDKM-000 was created using Golden Gate cloning and contains a paromomycin antibiotic resistance cassette and a C-terminally FLAG tagged c_{6A}-overexpression cassette. The sizes of the coloured arrows are not representative of the DNA fragment size. The antibiotic resistance gene was under the control of the *HR* promoter and *RBCS2* terminator, while expression of c_{6A}-FLAG was driven by the *PSAD* promoter and terminator. The black half-arrows indicate the positions of primers used for colony PCR. (**B**) Colony PCR of three individual *C. reinhardtii* transformants confirmed the existence of the pDKM-000 c_{6A}-overexpression cassette in colonies 1 and 3. The negative control was a colony from the untransformed background strain. (**C**) Western blot with an anti-FLAG antibody could confirm c_{6A}-FLAG expression on protein level for all three transformants. An untransformed strain was used as negative control (-ctrl). Total protein was visualised using the stain-free method (BioRad) and is shown as a loading control.

Because the presence of the construct as shown by PCR cannot guarantee correctly expressed and processed protein, an immunoblot was employed to test for expression of c_{6A}-FLAG protein (figure 3.3C). Protein samples from all three colonies showed a band at just under 15 kDa when the blot was probed with the anti-FLAG antibody. This corresponds well to the expected size of c_{6A}-FLAG without its predicted signal peptide of 13.5 kDa (cut site VLA/AEA, TargetP2.0). Unprocessed c_{6A}-FLAG has a molecular weight of 20.8 kDa. Taken together, this indicates that, in addition to c_{6A}-FLAG being expressed, the processing of the protein and thus its localisation is likely as normal. Even though all three colonies seemed to express c_{6A}-FLAG, the colony PCR result (figure 3.3B) had led to exclusion of colony 2. Colony 3 was chosen as representative c_{6A} overexpression strain and named c_{6A}-OE for future experiments. While comparison of protein levels with WT was not possible as c_{6A} could not be detected using western blots, the strain c_{6A}-OE was later also found to exhibit a ~14-fold higher c_{6A} transcript abundance than WT (section 6.2.2.1), confirming that it is indeed a c_{6A}-overexpression strain.

Constructs other than pDKM-000 with different promoter/terminator combinations, such as from the *BTUB* gene encoding β-tubulin, were also created and tested by Alexandre Mann. Overall, it was found that pDKM-000 led to the most reliable c_{6A} overexpression, based on immunoblot analyses.

In summary, a c_{6A} overexpressing strain (c_{6A}-OE) was created and could be confirmed to express processed c_{6A} with a C-terminal FLAG-tag.

3.2.3 Comparison of growth of *C. reinhardtii* cytochrome c_{6A} mutant strains

Having established and confirmed mutant strains of c_{6A} in *C. reinhardtii*, the effect of c_{6A} on growth of *C. reinhardtii* was investigated under various conditions.

3.2.3.1 Cytochrome c_{6A} does not affect growth of *C. reinhardtii* under continuous light conditions

Growth of c_{6A} mutant strains in liquid medium was tested under continuous light conditions by measuring the optical density of cultures at 750 nm (OD_{750nm}, figure 3.4). Photomixotrophic and photoautotrophic cultures were exposed to continuous standard growth light (30 $\mu mol_{photons}$ m^{-2} s^{-1}) as well as continuous high light (700 $\mu mol_{photons}$ m^{-2} s^{-1}). Both c_{6A}-KO and WT reached maximum optical densities of around 2 and 0.6 in photomixotrophic and -autotrophic conditions respectively, independent of the light regime. No significant growth difference between c_{6A}-KO and WT was found in photomixotrophy, although c_{6A}-KO tended to exhibit slightly lower cell densities when reaching the stationary growth phase in high light conditions. Statistical testing was performed with repeated measure ANOVAs and pairwise comparisons per time point if the p-value for the interaction effect of time and strain on OD_{750nm} in the ANOVA was significant ($p_{time:strain} < 0.05$). No statistically significant differences between the strains were found for either photomixotrophic or photoautotrophic conditions, in agreement with the absence of visual differences.

Compared to photomixotrophy, photoautotrophic growth was slower and cultures reached lower cell densities. While photomixotrophic cultures reached stationary phase after two days of growth, photoautotrophically grown cultures started to tail off on day 4. It is well-known that photomixotrophy usually leads to higher growth rates of *C. reinhardtii*, as photomixotrophy provides acetate as additional carbon source, while photoautotrophic cultures solely rely on photosynthetically driven carbon fixation [121].

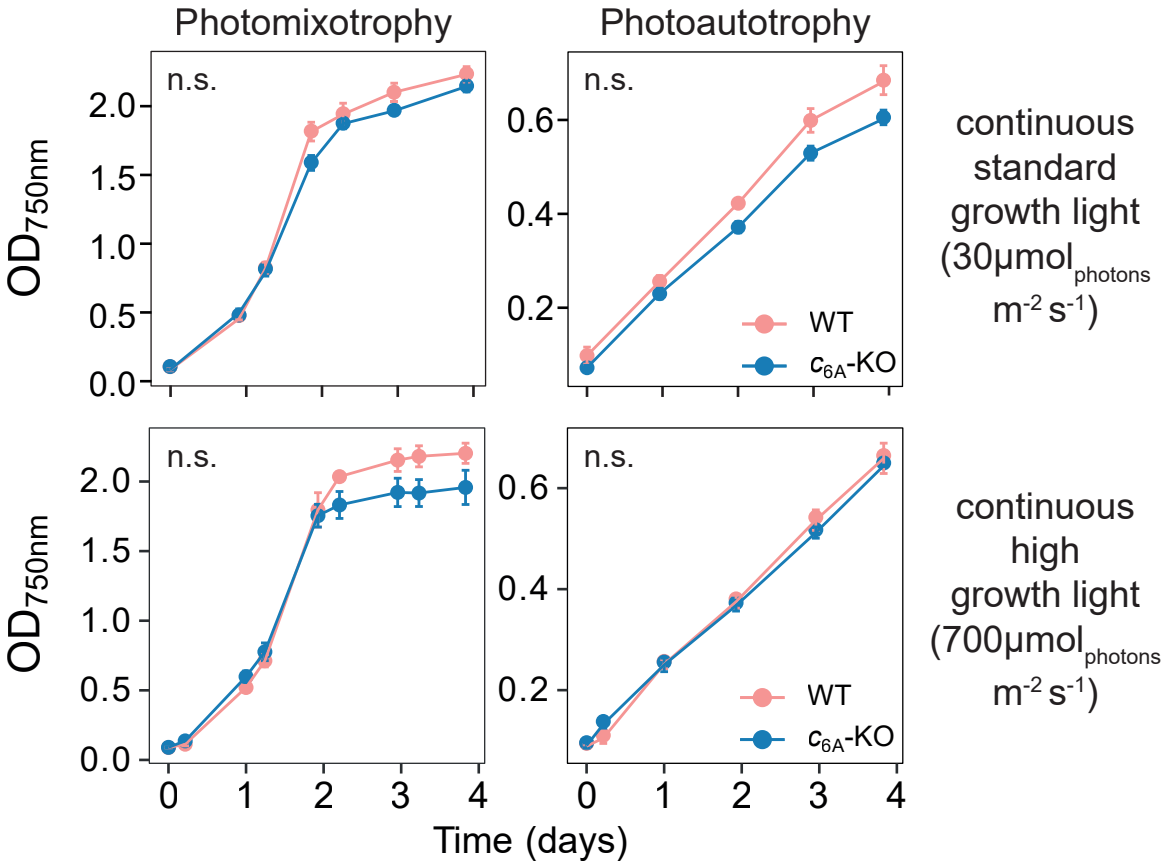


Figure 3.4: Growth curves of c_{6A}-KO and WT under continuous light conditions. The strains were grown in either photomixotrophy or photoautotrophy and exposed to standard or high continuous light conditions (30 and 700 $\mu mol_{photons}$ m^{-2} s^{-1} respectively) and tested for optical density (OD_{750nm}) throughout (N=3 $\pm$ SD). Statistical testing was carried out with repeated measure ANOVA. For interaction term $p_{time:strain}$ values lower than 0.05, pairwise t-tests at each time point were performed out as post-hoc test. No significant differences were found here ("n.s.").

To monitor not only biomass via OD_{750nm} measurements but also photosynthetic capacity, values of photosystem II quantum yield (Y(II)) were determined on day 2 of growth. They showed no difference between the strains, although higher light intensity led to decreased PSII quantum yield (table 3.2). The observation of lower Y(II) for higher growth light without an observable growth penalty suggests that the high continuous growth light oversaturates light harvesting while not being too high to cause damage to the cell.

Table 3.2: Photosystem II quantum yields (Y(II)) measured for *C. reinhardtii* cultures depending on the light condition (n = 3 ± SD).

Condition	WT	c_{6A}-KO
Standard photomixotrophy	0.74 ± 0.01	0.75 ± 0.01
High light photomixotrophy	0.40 ± 0.04	0.38 ± 0.04
High light photoautotrophy	0.42 ± 0.02	0.44 ± 0.01

Growth rates as well as maximum cell density of c_{6A}-OE under standard continuous light in photomixotrophy were found to be no different from c_{6A}-KO and WT (data not shown). As no phenotype for the c_{6A}-KO was found under the other conditions either, investigation of growth of the overexpression strain under those conditions was not carried out.

3.2.3.2 Cytochrome c_{6A} confers a growth advantage under a fluctuating light regime called DISCO Light

As continuous light did not show any differences between c_{6A}-KO and WT, a harsh fluctuating light regime was devised to test if c_{6A} is needed for survival under stressful light conditions. DISCO Light (for Darkness Interrupted by Short COntinuous Light) consists of 2 alternating phases, 2 min of darkness followed by 2 min of alternating 12 s high light pulses of 700 $\mu mol_{photons}$ m^{-2} s^{-1} and 12 s darkness (figure 3.5A). Under these light conditions all three strains (WT, c_{6A}-KO & c_{6A}-OE) grew significantly worse than under continuous illumination, indicating that DISCO Light causes stress for *C. reinhardtii*. This is supported by the fact that none of the strains grew in photoautotrophic conditions when exposed to DISCO Light, in contrast to continuous light.

In photomixotrophy DISCO Light exposure led to a reproducible phenotype where c_{6A}-KO grew more slowly and to lower cell densities than WT (figure 3.5B). Statistical testing with repeated measure ANOVA and subsequent pairwise t-test per time point revealed a significant difference ($p < 0.05$) between c_{6A}-KO and WT on day 1. For the subsequent days some variance between replicates of WT led to pairwise t-test p values of above 0.05 but below 0.1 (hash signs), signifying a consistent trend. Additionally, by day 3 WT cultures were more than 1.5 times as dense as KO cultures on average, based on OD_{750nm}, making the difference readily distinguishable by eye (figure 3.5C). This phenotype was consistently observed over the course of subsequent experiments aiming to investigate it further (section 4.2.2). The growth penalty

induced by the absence of c_{6A} could be recovered by overexpressing c_{6A} (figure 3.5B), with significantly higher cell densities for c_{6A}-OE compared to c_{6A}-KO observed from day 1. This confirmed that the DISCO Light growth difference was c_{6A}-dependent. Many proteins have been identified to be involved in photosynthesis because of their importance for growth under fluctuating light (section 3.1.3). The DISCO Light phenotype for c_{6A} therefore implies an involvement of c_{6A} in photosynthetic processes.

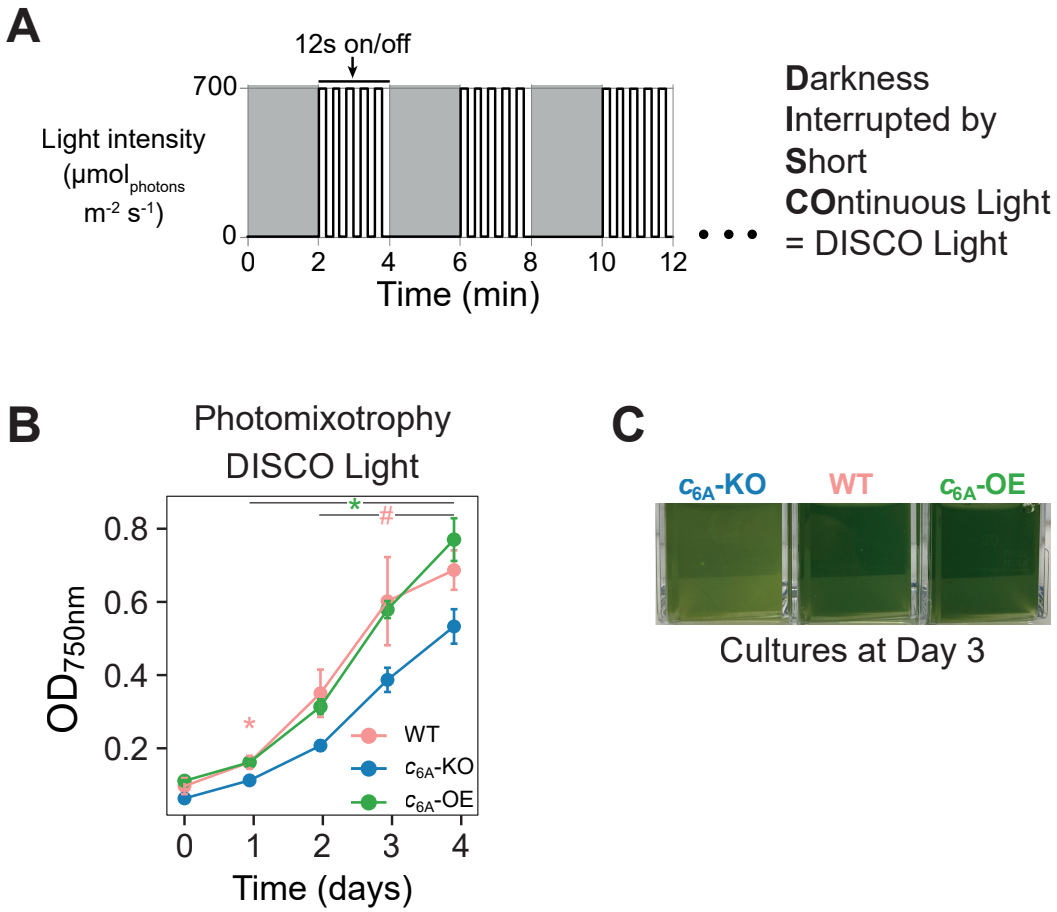


Figure 3.5: Introducing DISCO Light, a harsh fluctuating light regime. (**A**) DISCO Light (**D**arkness **I**nterrupted by **S**hort **CO**ntinuous Light) consists of alternating 2 min darkness followed by 2 min of high light pulses (12 s high light (700 $\mu mol_{photons}$ m^{-2} s^{-1}) & 12 s darkness). (**B**) Optical density (OD_{750nm}) growth curve of c_{6A} mutant strains under DISCO Light shows reduced growth of the c_{6A}-KO strain compared to WT and c_{6A}-OE (N=3 $\pm$ SD). Statistical testing was carried out with repeated measure ANOVA. Subsequent pairwise t-tests at each time point were performed as post-hoc test comparing WT (pink) or c_{6A}-OE (green) against c_{6A}-KO ($p < 0.05$: *, $p < 0.1$: #). (**C**) By eye, the cultures of the three strains at day 3 of growth are different in density.

3.2.3.3 The DISCO Light growth phenotype could not be reproduced by simpler fluctuating light regimes or darkness

DISCO Light is a combination of simpler light regimes that could give rise to the observed growth effect without the need for the complexity of DISCO Light and might even cause a difference when cultures are grown photoautotrophically. Growth of c_{6A}-KO and WT was therefore investigated under darkness, 2 min on/off light cycles, and 12 s on/off light cycles.

DISCO Light consists of 75% darkness, so the growth defect in DISCO Light could result if heterotrophic growth were compromised (section 3.1.2). While c_{6A}-KO showed slightly less cell density on average, no significant growth difference between WT and KO was found when grown in darkness with acetate (figure 3.6A). WT and c_{6A}-KO grew up to a maximum OD_{750nm} of about 0.8-0.9 in heterotrophic conditions which was followed by a decline in density, indicating the exhaustion of available acetate in the media. Interestingly, both c_{6A}-KO and WT grew slightly faster and to higher cell densities in heterotrophic conditions than under DISCO Light (figure 3.5B), underlining the stressful effect of fluctuating light. The lack of a phenotype under heterotrophic growth conditions means that the c_{6A}-dependent difference observed under DISCO Light is also light dependent. The absence of a difference between strains also renders it unlikely that c_{6A} is involved directly in acetate metabolism.

Another component of DISCO Light is a cycle of 2 min high light & 2 min darkness (figure 3.6B). Exposed to such a light regime and photomixotrophy, c_{6A}-KO and WT cultures only showed a significant difference in growth on day 3 which was not part of a consistent trend. The cultures reached stationary phase at day 4 of growth which is considerably slower than under continuous light. While the maximum culture density of just over 1.5 was also decreased compared to standard growth conditions (~2, figure 3.4), both WT and KO grew substantially faster and to higher optical densities than when grown in DISCO Light. The 2 min cycle can therefore also be ruled out as sole source of the DISCO Light phenotype.

Interestingly, photoautotrophic cultures of c_{6A}-KO and WT showed growth under the 2 min cycle while they would not under DISCO Light. The significant difference in optical density observed here suggests that the KO grew better than WT, although this difference is not reflected in the respective growth rates (compare slope of growth curves in figure 3.6B photoautotrophy). It is therefore suspected that this difference was an artifact of culturing rather than a true c_{6A}-dependent phenotype. Similar to photomixotrophic conditions, both strains exhibited a growth penalty in photoautotrophy in the 2 min cycle compared to continuous light, in agreement with previous findings [233].

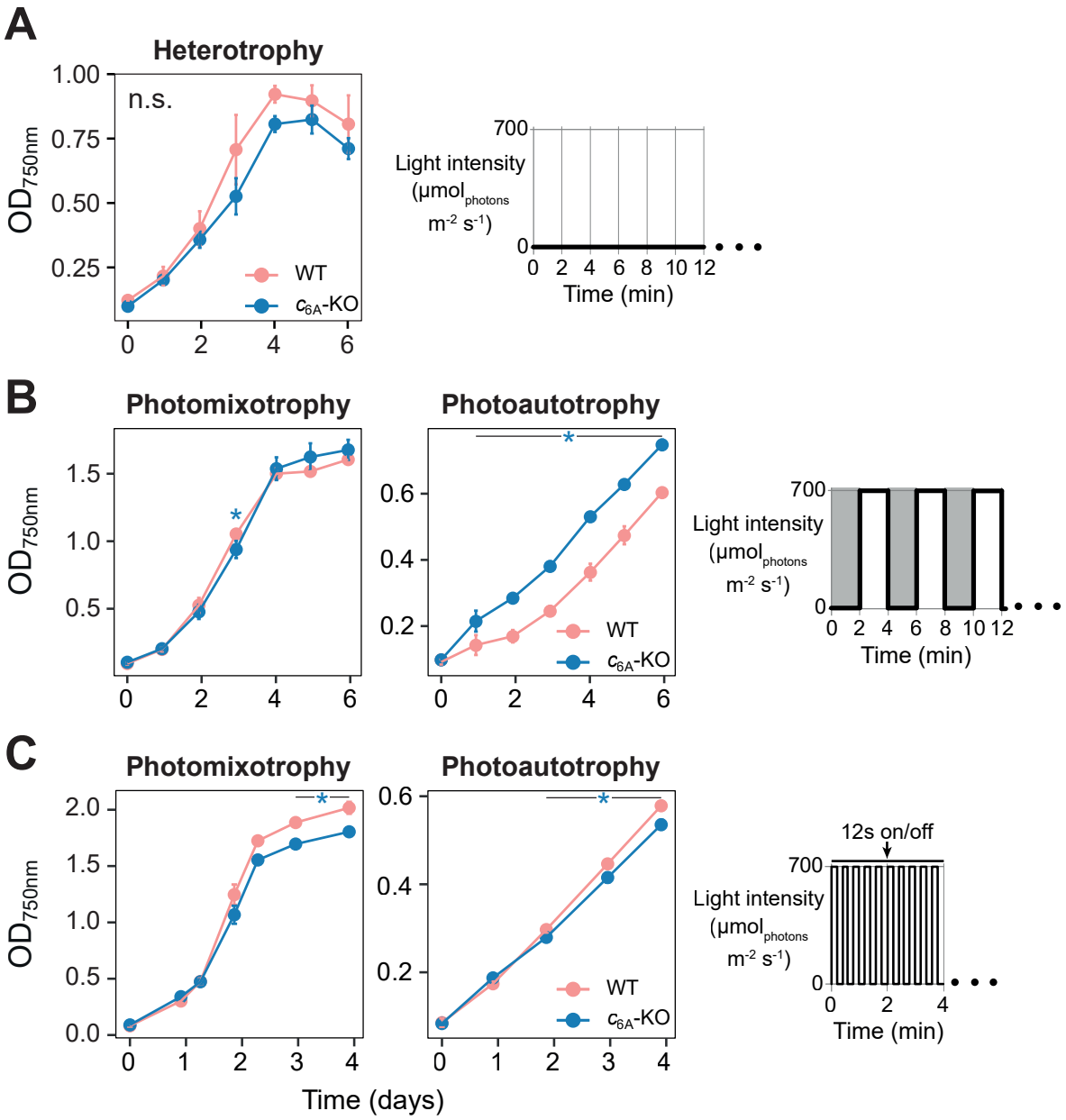


Figure 3.6: Growth curves of c_{6A}-KO and WT under darkness and two fluctuating light regimes. (**A**) Cultures were grown heterotrophically in darkness, photomixotrophically and photoautotrophically under (**B**) a 2 min on/off fluctuating light regime, or under (**C**) a 12 s on/off fluctuating light regime and tested for their optical density (OD_{750nm}) throughout (N=3 $\pm$ SD). For both fluctuating light regimes, light intensity of 700 $\mu mol_{photons}$ m^{-2} s^{-1} was used when the light was on, as shown in the light regime panels. Statistical testing was carried out with repeated measure ANOVA. For interaction term $p_{time:strain}$ values lower than 0.05, t-tests at each time point were performed as post-hoc test, comparing c_{6A}-KO against WT ($p < 0.05$: *).

The last component of DISCO Light is a cycle of 12 s high light & 12 s darkness (figure 3.6C). In photoautotrophic conditions, a significant difference between c_{6A}-KO and WT was found for days 2 to 4. However, this was not distinguishable by eye at any point as

the magnitude of difference was very small (less than 0.05 at all time points). Similarly, in photomixotrophy only small but statistically significant differences appeared from day 3. Both strains reached stationary phase at a similar density level of nearly 2, to that reached when grown under standard conditions, just half a day later than under continuous light. Surprisingly, this suggests that the seemingly stressful 12 s high light fluctuating light regime did not cause major difficulties for WT or c_{6A}-KO. It is possible that a 12 s light fluctuation is so fast that inactivation of photosynthetic processes due to darkness does not take place in *C. reinhardtii*. Graham *et al.* (2017) estimated deactivation rates for RuBP regeneration and RuBisCO to be on the scale of 100 and 10000 s, respectively [233]. However, the only small impact on growth under photoautotrophic conditions seen here is not in agreement with previous findings, as Janssen *et al.* (2000) found a reduced growth rate under a 12 s on/off fluctuating light regime for *C. reinhardtii* [232]. The dissimilarity might be explained by a difference in experimental method, as Janssen *et al.* (2000) utilised a different *C. reinhardtii* strain and a turbidostat setup for their cultures. Additionally, their experimental cultures were exposed to the fluctuating light regime during the light hours of a diurnal 16 h light/8 h dark cycle.

In summary, none of the components of DISCO Light alone was found to reproduce the DISCO Light phenotype. The phenotype found in DISCO Light is therefore likely a consequence of the combination of these light regimes.

3.2.3.4 The DISCO Light growth phenotype is reflected in chlorophyll content and acetate consumption

To investigate the DISCO Light phenotype further, c_{6A}-KO and WT cultures were assessed for total chlorophyll content per volume or per OD_{750nm}, as well as for acetate consumption when grown under DISCO Light or continuous light conditions (figure 3.7). Under continuous light conditions in both photomixotrophy and photoautotrophy, the chlorophyll content per volume followed the same pattern as OD_{750nm} with chlorophyll content in photoautotrophy being lower than in photomixotrophy (~12 µg/mL vs ~58 µg/mL on day 3, respectively). No significant difference between c_{6A}-KO and WT was found in chlorophyll content in photoautotrophy while there was one significantly different time point in the exponential phase when grown in photomixotrophy. However, this was not part of a sustained trend. On the other hand, DISCO Light exposure led to a difference in chlorophyll content between c_{6A}-KO and WT that mirrored the trend of optical density measurements. Already on day 1, c_{6A}-KO exhibited a significantly lower chlorophyll content per volume than WT. By day 3, WT had nearly double the amount of total chlorophyll than the c_{6A}-KO strain, however, variability between replicates rendered this difference not statistically significant. At day 4, the lower

chlorophyll content per volume in c_{6A}-KO was statistically significant. As a photosynthetic organism that uses chlorophylls for light harvesting, *C. reinhardtii* can be expected to display increased chlorophyll content with increases of culture density. The similarity of findings between OD_{750nm} and chlorophyll measurements is therefore not surprising. Nevertheless, it underlines that DISCO Light treatment causes a c_{6A}-dependent phenotype.

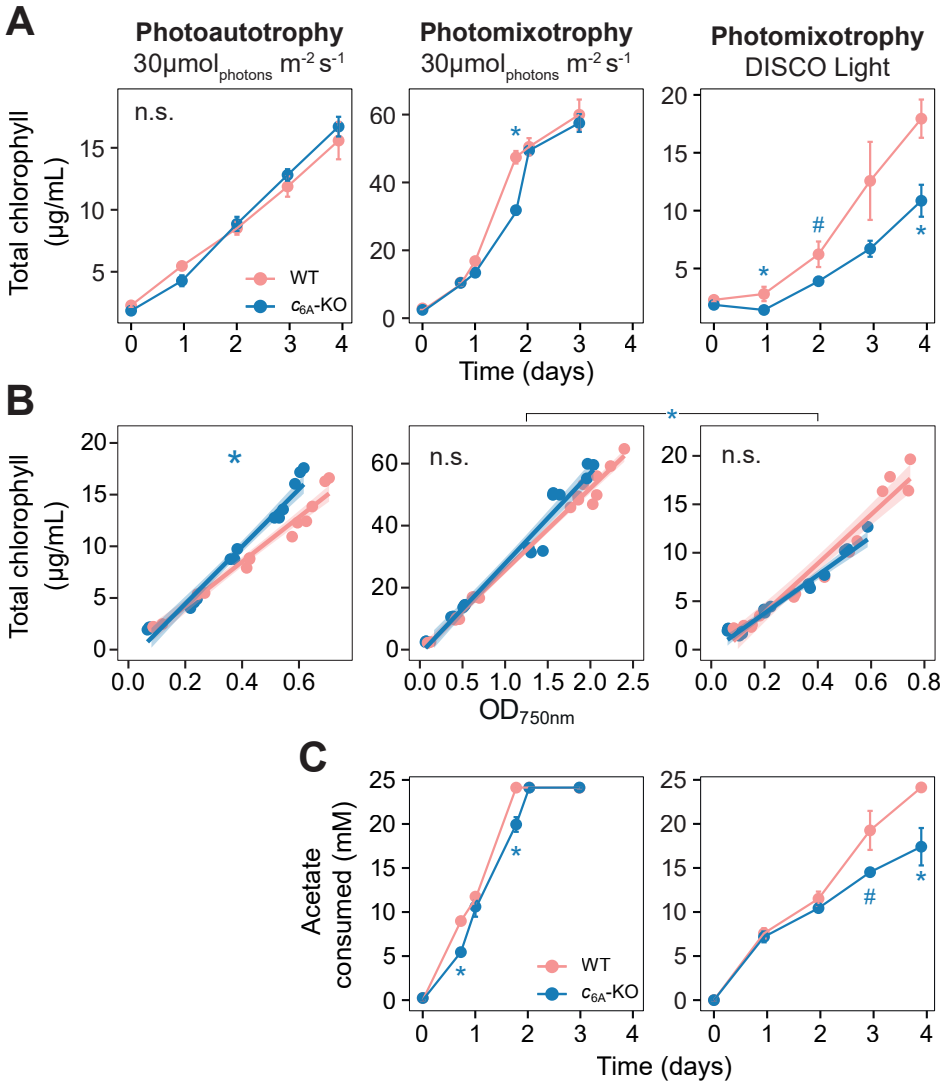


Figure 3.7: Chlorophyll content per volume or OD_{750nm} and consumed acetate of c_{6A}-KO and WT when grown under different conditions. Cultures were grown in DISCO Light or standard growth light in photomixotrophy or photoautotrophy and tested for (**A**) chlorophyll content per volume (**B**) chlorophyll content per OD_{750nm} and (**C**) consumed acetate throughout (N=3 $\pm$ SD). The maximum possible value of consumed acetate was measured to be 24.1 mM (at day 0). Due to the absence of acetate in the media, acetate was not measured for photoautotrophic cultures. For the time course data (chlorophyll per volume & consumed acetate) statistical testing was carried out with repeated measure ANOVA. Pairwise t-tests at each time point were carried out as post-hoc test, comparing c_{6A}-KO against WT ($p < 0.05$: *, $p < 0.1$: #). For the chlorophyll per OD unit data, three-way ANOVA with OD, strain, and light condition of the linear fits was carried out. The results of emmeans post-hoc testing with pairwise comparisons is indicated by asterisks ($p < 0.05$: *).

The chlorophyll content per optical density unit was assessed by linear regression which results in a proxy measure for chlorophyll content per cell (figure 3.7). No statistically significant difference was found between c_{6A}-KO and WT in photomixotrophy under either continuous or DISCO Light. However, the linear regressions were significantly different between the two conditions. This indicates that DISCO Light caused a change in chlorophyll per cell content compared to continuous light independent of the strain identity. A statistically significant difference between c_{6A}-KO and WT was found for chlorophyll per OD_{750nm} in photoautotrophic conditions. This small difference would require further experiments to confirm a c_{6A}-dependent effect.

Under photomixotrophic conditions, *C. reinhardtii* can utilise the supplied acetate as a carbon source. Measurements of acetate concentration in the growth medium showed that within less than two days, all acetate in the media was consumed by c_{6A}-KO and WT strains when grown in continuous light. While c_{6A}-KO had consumed significantly less acetate at two time points, the overall trend was very similar between c_{6A} and WT. The depletion of acetate in the media also coincided with the reaching of stationary phase of the cultures, in agreement with previous findings [228]. In contrast, when exposed to DISCO Light, the c_{6A}-KO consumed consistently less acetate than WT. However, this was only apparent from day 3 of growth and statistically significant from day 4, which was later than the appearance of the difference in OD_{750nm}. This suggests that altered acetate consumption is a consequence of the DISCO Light phenotype rather than a cause. It is likely that slower growth also leads to slower acetate consumption, as less cells are present that could take up the acetate.

3.2.3.5 Discussion of the DISCO Light phenotype

As shown in the sections above, DISCO Light, a harsh fluctuating light regime, causes a c_{6A}-dependent growth penalty for *C. reinhardtii* in photomixotrophy. This is reflected by culture densities, chlorophyll contents per volume and acetate consumption. Interestingly, only the combination of two fluctuating light regimes (2 min on/off & 12 s on/off) leads to a growth phenotype while each of them alone does not show c_{6A}-dependent effects. This is also a noteworthy difference from other mutants sensitive to fluctuating light (section 3.1.3), as no growth phenotype could be found for c_{6A} mutants when grown under conditions similar to previously explored fluctuating light regimes that led to growth deficiencies for other mutants (data not shown for a 5 min 20 $\mu mol_{photons}\ m^{-2}\ s^{-1}$ & 1 min 600 $\mu mol_{photons}\ m^{-2}\ s^{-1}$ light cycle). DISCO Light's longer dark phases (2 min) together with the short 12 s light phases might not allow for sustained activation of the dark reactions of photosynthesis that are vital for cell growth. This would also explain why no photoautotrophic growth was observed under DISCO Light. For example, Graham *et al.* (2017) estimated light-dependent RuBisCO activation

rates in the range of 100-1000 s [233]. Graham *et al.* (2017) attributed the growth penalty of fluctuating light in the time frame of 12 s to 2 min mainly to RuBP regeneration through modelling approaches [233]. The observed c_{6A}-dependent growth phenotype therefore may suggest a connection between c_{6A} and RuBP regeneration, which is ATP dependent and controlled via the thioredoxin-ferredoxin system [244]. This system ultimately relays redox state information from the PETC to target proteins. As a redox-active protein itself, c_{6A} could thus be involved in redox regulation processes.

3.2.3.6 Usefulness of DISCO Light

Past studies have shown a growth penalty for *C. reinhardtii* when exposed to regular fluctuating light cycles (including 12 s or 2 min on/off light cycles) [232, 233]. Here, DISCO Light combines the two and causes a major growth penalty compared to continuous light and less complex fluctuating light regimes even for WT. This suggests that fluctuating light that possesses multiple frequencies presents even larger challenges to photosynthetic organisms. More complex fluctuating light regimes that cause a phenotypic difference between mutant and wild-type strains, as is the case for c_{6A}, could therefore prove immensely useful to study previously unknown mechanisms of photosynthesis. Additionally, investigation of photosynthetic organisms under fluctuating light conditions more like those seen in nature could be insightful and may be more directly relevant to agricultural settings (e.g. [245, 246]). Graham *et al.* (2017) suggested that the effect of environmental conditions that are changing due to human caused global warming might also be underestimated when utilising continuous light for investigations instead of more natural fluctuating light conditions [233].

3.3 Conclusion & Outlook

To provide a basis for investigation of the function of c_{6A}, mutant strains of c_{6A} in *C. reinhardtii* were successfully created and confirmed. A CRISPR-mediated c_{6A} knock-out strain was shown to lack the targeted knock-out region by PCR and WGS, and a c_{6A}-overexpression construct used for transformation of the c_{6A}-KO was shown to express processed c_{6A}-FLAG. Using these c_{6A} mutant strains in comparison to WT a c_{6A}-dependent phenotype for growth under DISCO Light was found, laying the base for an in-depth analysis of possible causes. The light dependency of the observed phenotype suggests a connection between the function of c_{6A} and photosynthesis. Chapter 4 therefore delves into biophysical investigation of photosynthetic processes in the c_{6A} mutant strains. A direct connection to acetate metabolism was found to be unlikely, while an involvement of c_{6A} in redox regulation emerged as a possibility.

Future experiments relating to DISCO Light and growth phenotypes could entail the testing of more fluctuating light regimes including the imitation of fluctuations that naturally occurs for *C. reinhardtii*. Furthermore, testing DISCO Light exposure in other photosynthetic species in combination with usage of c_{6A} mutant strains will elucidate the conservation of c_{6A}'s function across the green lineage.

4

Biophysical investigation of cytochrome c_{6A} mutant strains in *C. reinhardtii*

4.1 Introduction

The observed phenotype for c_{6A} in DISCO Light was found to be dependent on light and therefore links c_{6A} to photosynthesis. This link is further supported by c_{6A}'s homology to the well characterised electron carrier protein cytochrome c_6 which takes on an important role in the PETC transferring electrons from b_6f to PSI. Additionally, c_{6A}'s proposed localisation in the thylakoid lumen further underpins a possible involvement in photosynthesis. For these reasons, the PETC of c_{6A} mutant strains of *C. reinhardtii* was investigated. Various spectrometry techniques were employed to gain detailed quantitative insight into the processes of the PETC. These techniques rely on the fact that photosynthetically active light absorbed by photosynthetic organisms drives electron flow through the PETC. This electron flow causes redox changes that correlate with changes in absorbance or fluorescence properties. Thus, electron flow through the PETC can be measured by monitoring optical properties with spectrometric methods. Methods used here are introduced below.

4.1.1 Fluorescence spectrometric approaches for probing the PETC

Chlorophylls are the main light harvesting pigments of photosynthetic eukaryotes in the green lineage. As such, their fluorescence emission is widely used as a tool for investigating the PETC.

4.1.1.1 Low temperature (77 K) chlorophyll fluorometry

At room temperature, one relatively broad chlorophyll fluorescence peak at ~684 nm is dominant, which is attributed to PSII fluorescence [247]. In contrast, at the low temperature of liquid N_2 (77 K) multiple narrower chlorophyll fluorescence peaks appear that can be assigned to the different parts of PSII and PSI antennae.

In *C. reinhardtii*, the chlorophyll emission spectrum at 77 K consists of two major peaks. The emission peak at 685 nm with a shoulder at 695 nm was assigned to chlorophylls in CP43 and CP47 of PSII, respectively [108, 248, 249]. The second major peak at ca. 715 nm originates from PSI cores [250, 251]. An additional blue-shifted shoulder of the CP43 peak was found at ~681 nm and attributed to free LHCII proteins that are not stably bound to PSII [252, 253]. All these attributions mostly rely on investigation of isolated complexes and exact assignment of fluorescence peaks *in vivo* is still a matter of research [187]. Nevertheless, PSI and PSII peaks are clearly distinguishable and the more antennae bound to the fluorescence emitting cores, the more fluorescence is detected. The binding of light harvesting antennae like LHCI and LHCII therefore has a major impact on the observed fluorescence peaks.

As PSI can be excited by PSII emission, which would lead to overestimation of PSI fluorescence, very dilute samples of *C. reinhardtii* are utilised for the recording of 77 K spectra. During analysis, 77 K spectra are often normalised to the dominant PSII peak at 685 nm because the raw fluorescence values can differ between replicates due to the exact chlorophyll content, positioning of the fluorescence probe and exact excitation light intensity. The output is then a PSI/PSII fluorescence ratio that informs on the relative abundances of PSI and PSII and their bound antennae, i.e. is a measure for the light harvesting balance between the photosystems. These characteristics make 77 K spectra a popular tool for the investigation of state transitions. When LHCII proteins are bound to PSII (state 1), a lower PSI/PSII ratio is observed, while LHCII antennae bound to PSI (state 2) lead to a relative increase in PSI fluorescence [237, 254, 255].

4.1.1.2 Pulse amplitude modulated fluorometry

The light absorbed by photosynthetic organism can drive photosynthesis, be dissipated as heat or be re-emitted as fluorescence. Measurement of the fluorescence yield resulting from excitation by incident light contains information about photochemistry and heat dissipation, because these three processes are in competition [256, 257]. With regard to quenching of fluorescence, the effect of photochemistry is therefore called photochemical quenching and the effect of heat dissipation non-photochemical quenching. To investigate photochemical and

non-photochemical quenching, pulse amplitude modulated (PAM) chlorophyll fluorometry can be utilised. The PAM technique uses very short measuring excitation light pulses (µs range) in combination with a fluorescence detector that is synchronised to the excitation light pulses and therefore highly selective for the fluorescence caused by the measuring light (low-intensity light that does not significantly drive photosynthesis) rather than the fluorescence caused by actinic light (continuous light that drives photosynthesis). This allows for accurate fluorescence measurements in the dark as well as during high actinic illumination [258]. Application of a short but saturating light pulse (SP) leads to a complete suppression of photochemical quenching, as all PSII reaction centres are closed as a consequence. This allows deconvolution of photochemistry and non-photochemical quenching the latter of which can be regulated (NPQ) or unregulated (NO). Multiple parameters of photosynthesis can be derived from the fluorescence values measured (figure 4.1, table 4.1) [186].

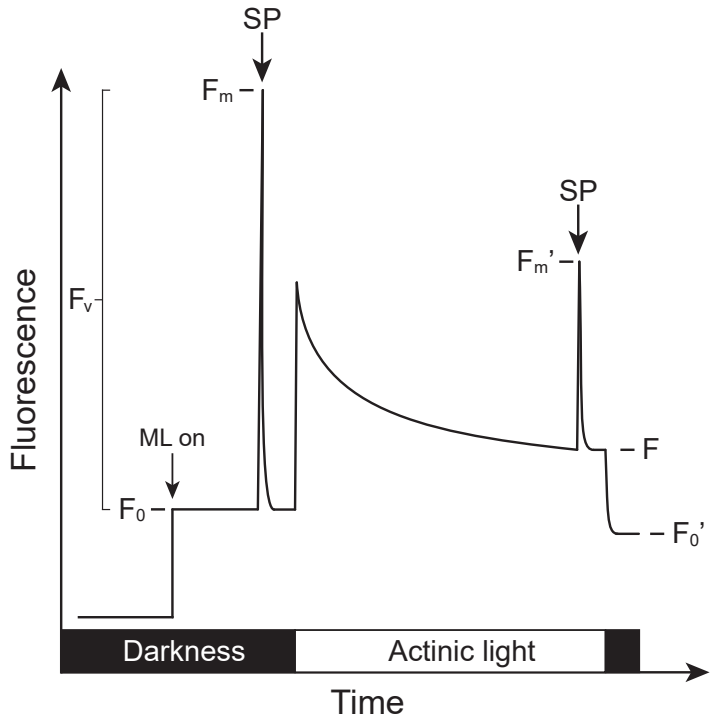


Figure 4.1: Diagram of a chlorophyll fluorescence trace from a PAM fluorescence measurement. Typically, a dark-adapted sample is investigated and at first the measuring light (ML) is turned on, giving the minimum fluorescence yield F_0. Application of a saturating pulse (SP) in darkness is used to determine the maximum fluorescence F_m before actinic light is turned on. The difference between F_m and F_0 is called variable fluorescence (F_v). SP application in actinic light gives the maximum fluorescence yield in the light F_m' and the steady state fluorescence yield F' in the light is measured just before SP application. Once actinic light is turned off, the minimal fluorescence yield of the illuminated sample F_0' is determined. F_0' should ideally be measured with far-red light exposure to re-oxidise the PSII acceptor side. If the experimental setup does not allow this, an approximation can be used: $F_0' = F_0 / ((F_m - F_0)/F_m + F_0/F_m')$ [259].

The steady-state fluorescence yield of the light exposed sample (F') is measured before SP application and has been found to be informative of the reduction state of the intersystem electron transfer chain, including the PQ pool [260]. The effective PSII quantum yield Y(II) reflects the fraction of light energy used for photochemistry under the conditions tested. After dark adaptation, Y(II) reaches its maximum value, known as F_v/F_m, representing the maximum PSII quantum yield. Y(II), Y(NPQ) and Y(NO) sum to 1, informing on the partitioning of absorbed light [261]. The higher Y(II), the more of the energy absorbed is therefore used for photochemistry in PSII. On the other hand, low Y(II) values do not necessarily indicate a condition that negatively affects an organisms fitness but suggests that PSII photochemistry is closer to saturated, causing more incident light to be dissipated as heat and fluorescence. By multiplying Y(II) with the incident light intensity, the relative electron transfer rate through PSII rETR(II) is obtained. Typically, rETR(II) saturates at species-specific light intensities and a lowered rETR(II) at high light intensities may indicate photoinhibition at PSII [262]. The quantum yield of regulated non-photochemical energy dissipation Y(NPQ) involves the mechanisms introduced above (section 1.2.3). A high Y(NPQ) value indicates that the light intensity is excessive but also signifies that the photosynthetic organism is still able to protect itself by dissipating excess excitation energy. This dissipation prevents the formation of ROS, which could damage the complexes of the PETC [71]. The quantum yield of non-regulated energy loss Y(NO) includes energy lost as heat and fluorescence. A high Y(NO) value suggests that both photochemistry and regulated NPQ are inefficient, indicating the organism's difficulty in managing the light conditions. This inefficiency often precedes or accompanies damage to PSII [186].

Table 4.1: Photosynthetic parameters and their calculation from fluorescence values shown in figure 4.1 [186]. PAR = photosynthetically active radiation (incident light intensity).

Parameter	Description	Formula
F'	steady-state fluorescence yield	F'
Y(II)	PSII quantum yield	$\frac{F'_m - F'}{F'_m}$
Y(NPQ)	Quantum yield of regulated non-photochemical quenching	$\frac{F'}{F'_m} - \frac{F'}{F_m}$
Y(NO)	Quantum yield of unregulated non-photochemical quenching	$\frac{F'}{F_m}$
1-qL	Fraction of reduced Q_A (proxy for PQ pool)	$1 - (\frac{F'_m - F'}{F'_m - F'_0} * \frac{F'_0}{F})$
rETR(II)	relative electron transfer rate through PSII	$Y(II) * PAR$

The parameter 1-qL indicates the fraction of reduced Q_A, the primary quinone electron acceptor in PSII. Assuming Q_A is in redox equilibrium with the PQ pool, a higher 1-qL value suggests a more reduced PQ pool [187, 261, 263]. Another parameter for Q_A redox state is qP, which is calculated assuming different prerequisites. Debate continues over which of these two methods is preferable [187] and the work presented here focuses on 1-qL.
Together, these parameters offer a comprehensive understanding of the state and efficiency of PSII under various light conditions as determined by PAM fluorescence measurements.

4.1.1.3 Direct chlorophyll fluorescence induction measurements (OJIP fluorometry)

Strong illumination of green photosynthetic eukaryotes leads to an increase of their emitted chlorophyll fluorescence to a maximum within 200-300 ms. On a logarithmic scale and normalised to minimum and maximum fluorescence, this fluorescence rise exhibits multiple characteristic phases (O-J-I-P) that are informative of the state of the PETC (figure 4.2) [187]. The early phase (from 0 to 2-3 ms, "OJ") is associated with the reduction of Q_A and Q_B at the acceptor side of PSII. During the "JI" phase (from 2-3 to ~30 ms), the PQ pool is reduced and the last phase ("IP", ~30 to ~300 ms) represents reduction of PSI and surrounding electron acceptors [247]. Consequently, the values measured with OJIP curves are sensitive to changes of the underlying processes. For example, addition of DCMU (red in figure 4.2) leads to maximum fluorescence at the inflection point J, as electron transfer from Q_A is blocked. Furthermore, a more reduced PQ pool was found to lead to higher fluorescence values at J [264] while PSI content influences the "IP" phase [265].

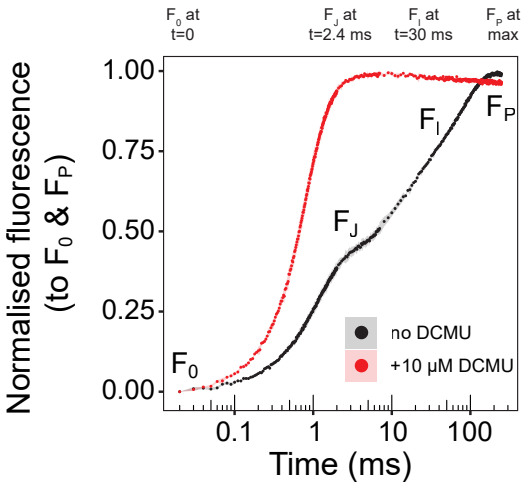


Figure 4.2: Example chlorophyll fluorescence induction measurement (OJIP curves) of *C. reinhardtii* WT. Chlorophyll fluorescence of photomixotrophic exponential growth phase cultures was measured in response to red light (984 $\mu mol_{photons}\ m^{-2}\ s^{-1}$) in a FL3500 fluorometer with or without DCMU (10 µM) (N=3 ± SD). Double normalised OJIP curves are shown and O, J, I and P points of fluorescence are marked.

4.1.2 Absorbance spectrometric approaches for probing the PETC

4.1.2.1 P700 differential absorbance spectrometry

To investigate PSI performance, P700 differential absorbance spectrometry can be employed. This well-established technique relies on the absorbance differences between reduced P700 and oxidised $P700^{+}$. While the biggest change in absorbance difference is found around 700 nm, differential absorption measurements in the near infrared are used for P700 measurements in a Dual-PAM-100, because no interference with photosynthetic pigments occurs. Two wavelengths are measured: 830 nm as sample wavelength near the maximum light-induced absorbance change in the infrared and 875 nm as reference wavelength at the edge of the absorbance maximum correcting for not P700-specific absorbance changes [266]. However, plastocyanin redox changes also cause differential absorbance in this wavelength area, contributing to the observed P700 signal [188].

As the wavelengths of PAM fluorescence and P700 measurements do not overlap, simultaneous measurement of PSII and PSI parameters is possible when utilising a Dual-PAM-100. Similar to PAM fluorescence for PSII, the effect of saturating pulses (SP) on P700 absorbance can be used to determine PSI parameters (figure 4.3). First, the maximum oxidisable P700 P_M is determined from a dark-adapted sample (equivalent to F_m in fluorescence) by exposure to far-red light and application of a saturating pulse. Subsequently, the oxidation state of P700 during actinic light ($P700_{ox}$) and the maximum P700 signal from application of a SP (P_M') are used to calculate photosystem I quantum yield Y(I), donor-side limitation Y(ND), and acceptor-side limitation Y(NA) (formulas 4.1 to 4.4) [188, 267].

$$Y(I) = \frac{P'_M - P700_{ox}}{P_M} \tag{4.1}$$

$$Y(ND) = \frac{P700_{ox}}{P_M} \tag{4.2}$$

$$Y(NA) = \frac{P_M - P'_M}{P_M} \tag{4.3}$$

$$Y(I) + Y(ND) + Y(NA) = 1 \tag{4.4}$$

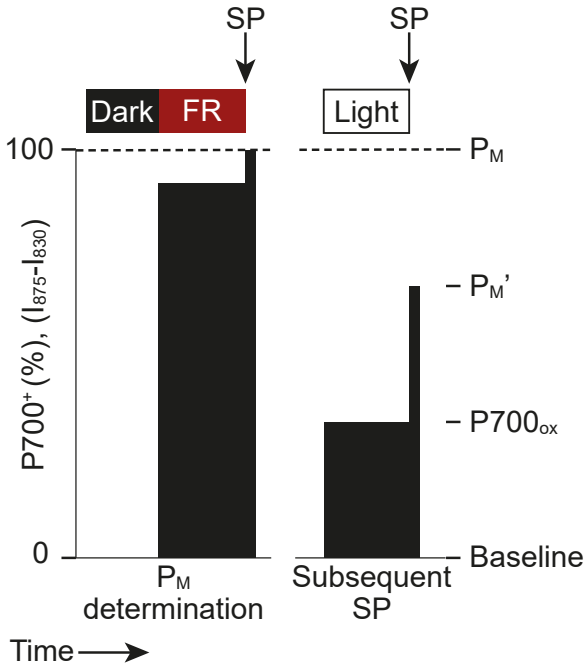


Figure 4.3: Principle of the P700 saturating pulse method for determination of PSI parameters. Differential absorbance (I_{875}-I_{830}) informs on the redox state of P700 and determination of the maximum oxidisable P700 (P_M) allows normalisation. P_M is reached through illumination with far-red light (FR) and application of a saturating pulse (SP). $P700^+$ levels before ($P700_{ox}$) and during subsequent saturating pulses (P_M') in actinic light (right part) can then be used to calculate Y(I), Y(ND), and Y(NA). Adapted from [267].

These three parameters give a measure for the usage of light energy by PSI and sum to 1. Photosystem I quantum yield Y(I) describes the fraction of open PSI that is available for photochemistry. By multiplying Y(I) with the incident light intensity, the relative electron transfer rate through PSI rETR(I) is obtained. Similar to rETR(II), rETR(I) saturates at a certain light intensity and a lowered rETR(I) at high light intensities may indicate damage at PSI. Donor-side limitation Y(ND) reflects the fraction of PSI that is closed due to a shortage of electrons re-reducing $P700^+$. Donor-side limitation is a mechanism for controlling PSI activity and is tightly connected to photosynthetic control at the cytochrome b_6f complex and PSII activity. At high light intensities, PSI tends to be donor-side limited to protect it from damage through ROS that can evolve in case of prolonged excited states of P700, i.e. acceptor side limitation. Acceptor-side limitation Y(NA) indicates the fraction of PSI that are unavailable for photochemistry due to lack of electron acceptors that would oxidise P700. Y(NA) levels are therefore influenced by dark adaptation (as carbon fixation is turned off) or changes to carbon fixation and other electron accepting processes downstream of PSI. At lower light intensities, the acceptor side is the main limitation of PSI photochemistry [188].

A similar principle to the P700 measurements presented above but with more sets of differential wavelength measurements allows deconvolution of P700, plastocyanin, and

ferredoxin signals using a DUAL-KLAS-NIR spectrometer [189]. Four wavelength pairs (785-840 nm, 810-870 nm, 870-970 nm & 795-970 nm) are recorded simultaneously and deconvolution with the help of differential model plots yields redox kinetics in response to light of PSI and its donor and acceptor sides. The differential model plots are recorded during conditions where redox changes in only one of the contributors are visible. For example, this could be done with P700 under far-red light exposure, when all three contributors are largely oxidised. A 5 µs light pulse is applied that does not have a major impact on plastocyanin or ferredoxin redox states but causes a difference in the P700 signal. As cyanobacteria and algae have FLVs that present another fast electron acceptor downstream of PSI and would therefore disturb the ferredoxin signal, the differential model plots should be recorded with strains that were modified to lack FLVs [67, 201].

Utilising DUAL-KLAS-NIR spectrometry, detailed studies of the PSI donor and acceptor sides were carried out in plants [268–270] and cyanobacteria [67, 201, 271, 272], while similar analyses for *C. reinhardtii* are yet to be published.

4.1.2.2 Joliot-type spectrometry (JTS) of cytochrome b_6f

Samples of photosynthetic organisms are highly absorbent, highly scattering, and photoactive, making it difficult to balance the need for sufficient light to measure properties of photosynthetic organisms without directly influencing photosynthetic processes. The Joliot-type pump-probe spectrometer overcomes this challenge by using very short intense light pulses for measurement that generate strong signals while minimising actinic effects. A Joliot-type spectrometer also incorporates an optical setup that includes a reference port that can be adjusted for each sample to cancel out scattering effects [273]. The scatter cancellation requires the assumption that prior to actinic illumination, no photochemically induced redox change occurs, i.e. the samples need to be dark-adapted.

To measure the redox kinetics of the cytochrome b_6f complex, light-induced absorption changes of the two *b* hemes and cytochrome *f* of b_6f are tracked at specific wavelengths (563 nm for *b* hemes and 554 nm for cytochrome *f*). Due to potential broad baseline changes, additional baseline measurements between 546 nm and 573 nm are needed (figure 4.4). While plastocyanin is included in these baseline measurements at 573 nm, it is not the primary focus. Overall, determination of b_6f redox kinetics requires measuring four different wavelengths, translating into three filter changes for one sample in older Joliot-type spectrometers.

The redox kinetics of *b* hemes and cytochrome *f* have been extensively studied using JTS. These measurements have been pivotal in advancing our understanding of b_6f function, including the Q-cycle, photosynthetic control, and cyclic electron flow [50, 271, 274–276].

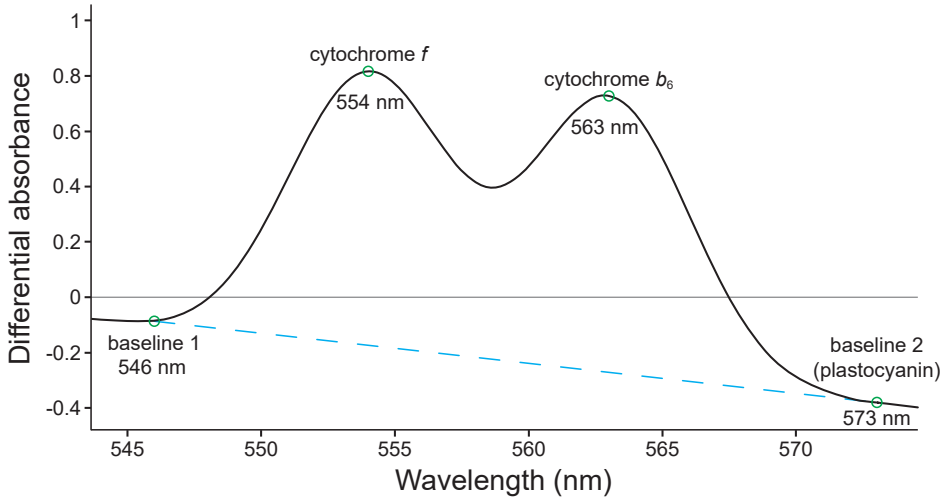


Figure 4.4: Principle of measuring cytochrome b_6f redox kinetics with a JTS. Shown is the differential absorbance of cytochrome *f* and cytochrome b_6 comparing oxidised and reduced states, as well as the baseline recorded for correction of the values, where baseline 2 records changes in plastocyanin redox state. Adapted from [273].

4.1.2.3 Electrochromic shift differential absorbance spectrometry

The activity of the PETC, i.e. the movement of electrons and protons through and across the thylakoid membrane results in the generation of the proton motive force (pmf). The pmf comprises a proton gradient (ΔpH) and an electric field (ΔΨ) component and is mainly dissipated by the ATP synthase to drive ATP synthesis [277]. The electric field component leads to specific absorbance changes of the carotenoid pigments in the membrane, a phenomenon known as electrochromic shift (ECS). The measurement of ECS signals in response to light can therefore inform on the electric field and thus the pmf that exists across the thylakoid membrane [198]. The specific ECS spectrum is species-dependent, as thylakoid membranes of different species have different pigment compositions. For *C. reinhardtii*, as for the organism the ECS signal was first described in, *Chlorella*, the absorbance change at 515 nm is recorded [278].

With the introduction of dark interval relaxation kinetics (DIRK) in ECS measurements, quantitative measurements of proton movement across the membrane in actinic light were made possible [279]. Under continuous illumination the ECS signal is in a steady-state, so that pmf generation (light-induced electron and proton transfer) and dissipation (mostly ATP synthesis) are equal. DIRK measurements involve turning off the actinic light for a short

time period (<1 s), during which the decay of the ECS signal is measured (figure 4.5A). In these measurements, the difference between the light and dark level reflects the magnitude of pmf. Additionally, the initial slope of the ECS decay is proportional to the proton pumping activity in the light and is therefore called proton flux vH^+. The proton conductivity gH^+ correlates with the inverse time constant of the decay and gives a measure of the ATP synthase activity [200, 280, 281]. DIRK measurements on mutant strains of photosynthetic organisms have provided insights into fundamental aspects of photosynthesis, like regulation of the ATP synthase and cyclic electron flow [269, 282], or flavodiiron proteins [201, 283].

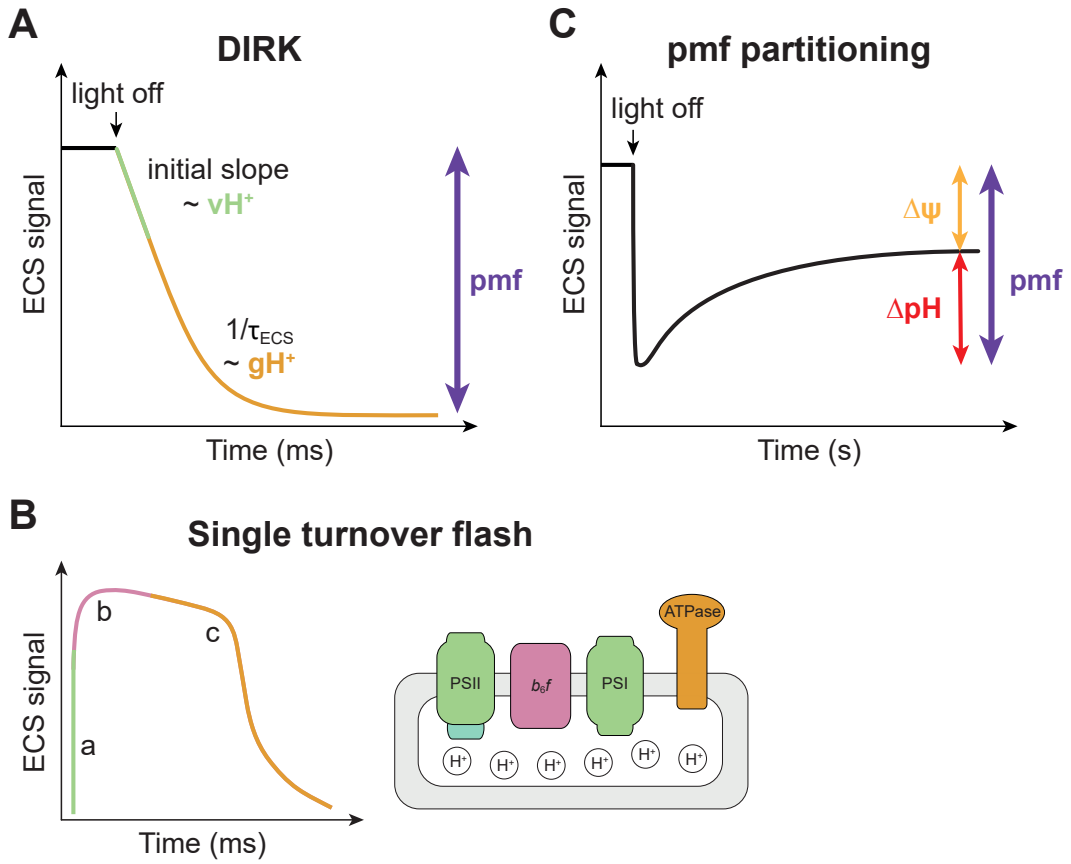


Figure 4.5: Principles of pmf measurements using electrochromic shift (ECS). (**A**) The analysis of dark interval relaxation kinetics (DIRK) yields information on the magnitude of pmf, the proton flux vH^+ of proton pumping in the light, and the proton conductivity gH^+ through the ATP synthase. (**B**) The application of a single turnover flash leads to a transient rise of the ECS signal, where phases a, b and c are associated with photosystem, b_6f complex, and ATP synthase activity, respectively. (**C**) On a longer timescale, the partitioning of the pmf reveals the contribution of ΔpH and $\Delta\Psi$. Adapted from [198].

The pmf measurement is ideally normalised to a single turnover flash to ensure comparability [284]. The ECS response to such a flash also contains information on the status of the PETC (figure 4.5B) [198] as it comprises three distinct phases over the initial ~100 ms [285]. Phase 'a' occurs within the first 100 µs after the flash (too rapid to be resolved) and corresponds

to an increase in the electric field due to charge separation by the photosystems. Phase 'b' which unfolds over milliseconds, shows a slower increase until reaching a steady state which turns into a decline, reflecting the activity of the cytochrome b_6f complex. Phase 'c' involves the dissipation of the electric field due to ionic flux, primarily through the ATP synthase.

In contrast to the very fast response of ECS to a single flash, the slow relaxation of the ECS signal during prolonged darkness after a continuous light exposure can be used to determine the contribution of ΔpH and ΔΨ to the pmf (figure 4.5C) [199]. After the first fast drop in ECS signal, as observed during a DIRK, in prolonged darkness the ECS signal shows an increase to a steady-state level in dark within roughly one minute. This increase has been interpreted as the dissipation of the ΔpH component, which takes longer than the dissipation of the electrical gradient as it requires the flux of counter ions across the thylakoid membrane. This partitioning of pmf has therefore been instrumental in characterisation of ion channels in thylakoid membranes [246, 286].

4.1.3 Membrane-inlet mass spectrometry

The connection of a suspension of a photosynthetic microorganism with a mass spectrometer, separated by a gas-permeable membrane, allows for the real-time investigation of gas exchange within said suspension. While many gases can and have been analysed, most of the applications of this membrane-inlet mass spectrometry (MIMS) focus on measurements of oxygen [287]. In *C. reinhardtii*, various processes contribute to oxygen gas fluxes. Most importantly, photosynthetic water splitting accounts for oxygen evolution, while respiration causes oxygen consumption. Additionally, some processes associated with photosynthesis also consume oxygen: the Mehler and Mehler-like reactions as well as photo- and chlororespiration. The sensitivity of mass spectrometry is leveraged to distinguish between oxygen uptake and production flows by spiking samples with $^{18}O_2$. All produced oxygen originates from water with the naturally much more abundant isotope ^{16}O, whilst oxygen consuming processes will lead to the uptake of both isotopic forms of oxygen. As MIMS is a time-resolved technique, oxygen flux rates can be calculated from the total measured gas concentrations, elucidating different mechanisms and limitations of oxygen consumption or evolution. Employing this approach with mutant strains of microalgae or cyanobacteria, the roles of various proteins in oxygen fluxes can be clarified, such as the light-dependent oxygen uptake of flavodiiron proteins [63, 66].

4.1.4 Aims

To investigate a possible involvement of c_{6A} in photosynthesis in *C. reinhardtii*, the PETC of c_{6A} mutant strains and WT was examined employing the wide range of spectrometric approaches introduced above. First, the effect of c_{6A} on the PETC under continuous light was investigated, following the hypothesis that a role for c_{6A} exists under these conditions even if its absence did not lead to an obvious growth phenotype. Second, the reason for the observed growth phenotype under DISCO Light was dissected with biophysical examination of the PETC of c_{6A} mutant strains and WT exposed to DISCO Light. In both sections, the light harvesting balance between the photosystems is examined by 77 K chlorophyll fluorometry, photosystems performances are analysed with PAM fluorometry and differential absorbance spectroscopy, and the pmf is studied with ECS spectrometry. Additionally, for samples grown in continuous light, a detailed analysis of the PQ pool redox state, cytochrome b_6f redox kinetics, and oxygen gas exchange was carried out.

4.2 Results & Discussion

4.2.1 The effect of c_{6A} on the photosynthetic electron transfer chain of *C. reinhardtii* in continuous light

The investigation of the PETC of *C. reinhardtii* under continuous standard growth light, i.e. when not stressed, might provide insights into c_{6A}'s putative function in photosynthesis that are more generally applicable than findings obtained when the alga is exposed to stressful light, like DISCO Light. Furthermore, it is important to establish a baseline of differences in continuous light to be able to infer effects on *C. reinhardtii* of DISCO Light as well as how c_{6A} might affect a response of *C. reinhardtii* to DISCO Light. As the differences in growth phenotype between c_{6A} mutant strains and WT were observed under photomixotrophic conditions, most biophysical experiments focused on investigating the *C. reinhardtii* strains under such conditions also.

4.2.1.1 Cytochrome c_{6A} is important to maintain a normal light harvesting balance between photosystems I and II in photomixotrophy

To investigate if c_{6A} affects the light harvesting balance between PSI and PSII under continuous illumination, low temperature chlorophyll fluorescence spectra were recorded.

Samples were taken from photoautotrophic and photomixotrophic cultures in the exponential growth phase, fluorescence was measured, and raw spectra were normalised to the PSII-associated peak at 685 nm (figure 4.6).

In photoautotrophy (figure 4.6A), nearly congruent fluorescence traces for c_{6A}-KO and WT could be observed with PSII and PSI peaks in the expected regions. The ratio between PSI and PSII fluorescence was very similar between the two strains (1.25-1.3), suggesting that in photoautotrophy, c_{6A} does not affect the light harvesting balance of *C. reinhardtii*.

In photomixotrophy (figure 4.6B), WT displayed an unchanged PSI/PSII ratio compared to photoautotrophic conditions of about 1.2. Importantly, c_{6A}-KO showed a significantly lower PSI/PSII ratio (0.95) than WT and than c_{6A}-KO in photoautotrophy, also making the CP47-associated peak at 695 nm more prominent. The c_{6A}-OE strain rescued this c_{6A}-KO phenotype back to WT levels. Cytochrome c_{6A} thus has an impact on the light harvesting balance of *C. reinhardtii* in photomixotrophy. Since the data were normalised to the PSII-associated peak, the observed differences could originate from variations in the fluorescence associated with either photosystem. A smaller PSI/PSII ratio could be due to an increase in PSII fluorescence or a decrease in PSI fluorescence. Addition of a known amount of a fluorescent dye could be used for normalisation in future 77 K experiments, allowing a more detailed comparison of PSI and PSII fluorescence changes.

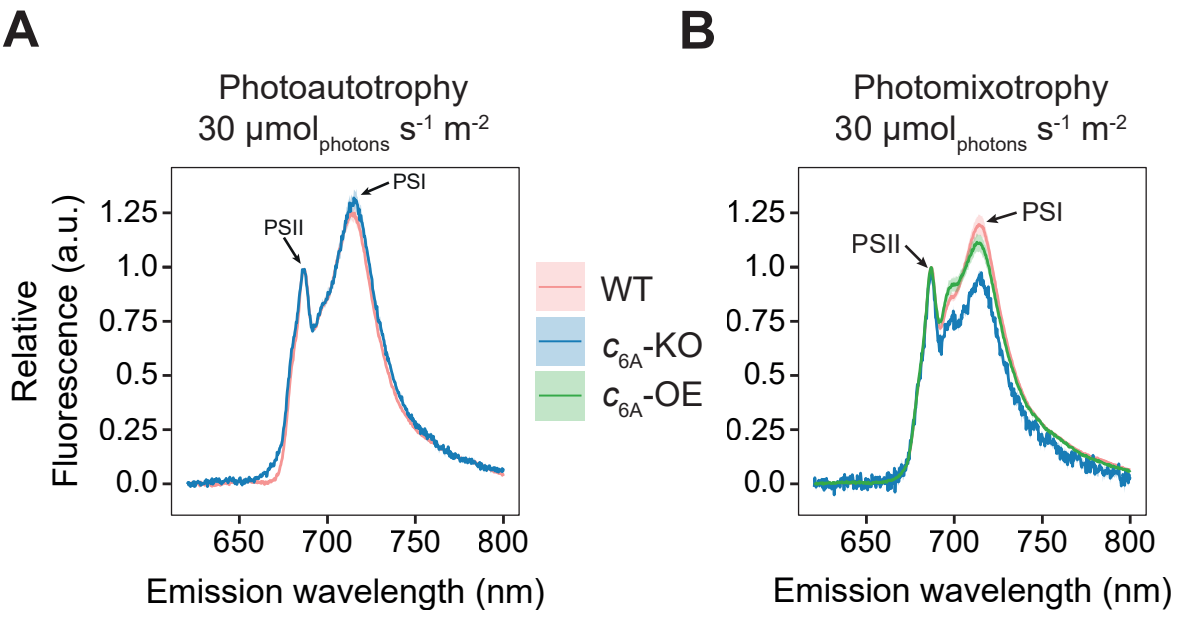


Figure 4.6: Low temperature (77 K) chlorophyll fluorescence spectra of *C. reinhardtii* c_{6A} mutant strains and WT. Cultures were grown under continuous light in (**A**) photoautotrophy or (**B**) photomixotrophy. Samples were taken during exponential growth phases, adjusted to 5 µg/mL chlorophyll and frozen (N=3 ± SE). Raw fluorescence spectra were normalised to the PSII-associated peak at 685 nm. The most prominent PSI and PSII fluorescence peaks are indicated by black arrows.

The observation that c_{6A} affects the light harvesting properties under photomixotrophic conditions is the first time a phenotype for c_{6A} has been observed under standard growth conditions. Hence, the role of c_{6A} can indeed be dissected under these conditions. However, the loss of c_{6A} translates into a growth phenotype only under more challenging light conditions (section 3.2.3). This suggests that the function of c_{6A} could be connected to adapting the light harvesting balance in response to more stressful light conditions, under which it provides a fitness advantage. Furthermore, an effect of c_{6A} on the PSI/PSII ratio could not be observed under photoautotrophic conditions but only in photomixotrophy with acetate as external source of reducing equivalents. This indicates that c_{6A} is particularly important in more reducing conditions. Interestingly, no difference in PSI/PSII ratio between photoautotrophic and photomixotrophic conditions was seen for WT. While acetate has a reducing effect on the PQ pool, *C. reinhardtii* exhibits only short-term transition into state 2 (on the scale of minutes) with more PSI fluorescence upon addition of acetate [120]. In cultures fully adapted to photomixotrophy or photoautotrophy, no difference in PSI/PSII ratio could be found [120]. Here, fully adapted cultures were used, indicating that the c_{6A}-dependent difference likely reflects a long-term alteration of the light-harvesting balance rather than a short-term response to changed acetate levels.

The c_{6A}-dependent difference in light harvesting balance in photomixotrophy found here could be due to several factors and will be discussed in further sections and chapters. These factors include variations in the composition or content of photosystems and antennae, or altered state transitions, all of which are intimately connected with photosynthetic electron flow and not mutually exclusive.

4.2.1.2 Cytochrome c_{6A} does not detrimentally affect the ability for state transitions of *C. reinhardtii* in photomixotrophy

To test if an altered ability for state transitions could be the reason for the observed c_{6A}-dependent light harvesting phenotype, low temperature chlorophyll fluorescence spectra of culture samples were recorded after exposure to conditions promoting the two different states of state transitions. Dark anoxia treatment was employed to promote state 2 where a more reduced PQ pool ultimately leads to an increased PSI fluorescence signal in relation to PSII fluorescence (broken lines in figure 4.7). Vigorous shaking in dark oxic conditions was used to induce state 1 by oxidising the PQ pool and ultimately increasing the PSII fluorescence relative to PSI fluorescence (solid lines in figure 4.7) [106].

WT and c_{6A}-KO were tested for their state transition ability. Both strains showed the expected behaviour with state 1 inducing conditions resulting in more PSII fluorescence,

while state 2 inducing conditions led to higher PSI fluorescence of around 30% more in state 2 than in state 1. The considerable fluorescence difference between states 1 and 2 inducing conditions is not found in strains mutant in proteins directly involved in state transitions in *C. reinhardtii*, like the STT7 kinase or the PPH1 and PBCP phosphatases. In both, state 1 and state 2 inducing conditions, *C. reinhardtii* appears stuck in state 1 or state 2 for STT7 or the phosphatases, respectively [93, 100]. The presence of a difference between states for c_{6A}-KO thus shows that under photomixotrophic conditions the ability for state transitions is not affected by c_{6A}. However, the observed relative PSI fluorescence in the c_{6A}-KO was always lower than the WT equivalent. Where WT exhibited normalised PSI fluorescence of 1.12 in state 2 conditions, c_{6A}-KO reached 1.02. Similarly, under state 1 conditions, WT PSI fluorescence was over 0.84, while the c_{6A}-KO showed a PSI fluorescence value of 0.77. This supports the finding of changed light harvesting properties from section 4.2.1.1.

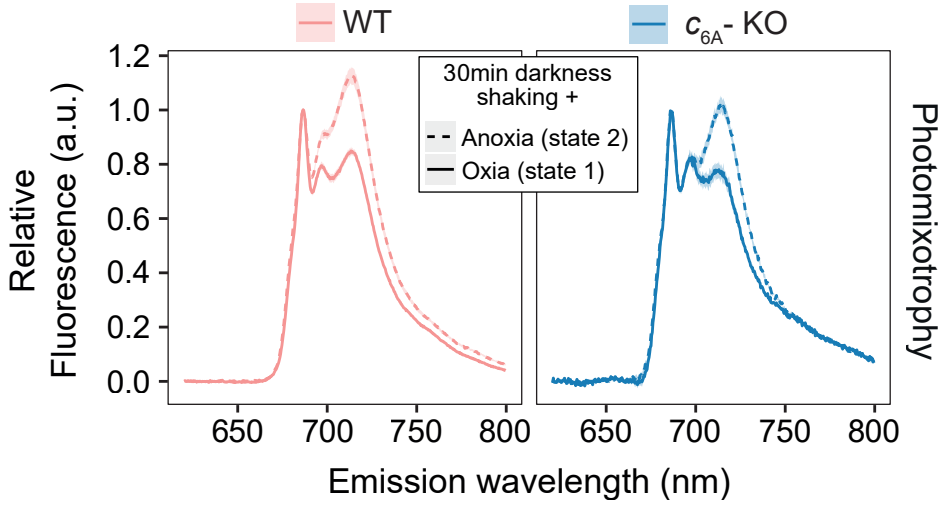


Figure 4.7: Low temperature (77 K) chlorophyll fluorescence spectra of c_{6A}-KO and WT exposed to state 1 or 2 inducing conditions. Cultures were grown to exponential phase under continuous light (30 $\mu mol_{photons}$ m^{-2} s^{-1}) in photomixotrophy, adjusted to 5 µg/mL chlorophyll and then exposed to 30 min of darkness and anoxia (state 2 inducing) or oxia (state 1 inducing) before freezing (N=3 $\pm$ SE). Anoxia was achieved by using N_2 purged media supplemented with glucose oxidase and glucose in closed tubes. Oxia was achieved by vigorous shaking of open tubes.

While the ability for state transitions did not seem detrimentally affected in absence of c_{6A}, an effect of c_{6A} on the rates with which state transitions occur cannot be excluded. Here, 30 min exposure to state inducing conditions led to a similar magnitude of change in relative PSI fluorescence between c_{6A}-KO and WT. However, fluorescence monitoring showed that state transitions start occurring within 2 to 4 min upon increased reduction of the PQ pool [93, 100]. A time-resolved measurement of state transitions would therefore be necessary to further investigate if c_{6A} affects the rate of state transition. Furthermore, generally less phosphorylated LHCII proteins in c_{6A}-KO, independent of the induced state, could lead to

the observed difference in relative PSI fluorescence. Examining the phosphorylation status of LHCII antennae would thus be useful to determine the effect of c_{6A} on state transitions.

In summary, an altered ability for state transitions in the c_{6A}-KO as the origin for the light harvesting balance phenotype was found to be unlikely, while c_{6A}-dependent differences in light harvesting balance prevailed in both states of state transitions and an effect of c_{6A} on rates of state transitions could not be excluded.

4.2.1.3 The effect of cytochrome c_{6A} on PSII and PSI function in continuous light

To investigate if the observed c_{6A}-dependent difference in light harvesting balance is also reflected in functionality of PSI or PSII, the light dependency of central photosynthetic parameters was measured (figure 4.8). To allow simultaneous measurement of PSI and PSII parameters, photomixotrophic exponential growth phase culture samples of WT, c_{6A}-KO and c_{6A}-OE were applied to glass fibre filters. This led to steady traces with high signal-to-noise ratios for both the P700 differential absorption and chlorophyll fluorescence signal measured with a Dual-PAM-100 spectrometer.

Firstly, the PSII quantum yield Y(II) was found to decrease in all strains with increasing light intensities (figure 4.8A). This is a normal behaviour for photosynthetic organisms and due to the limitations for electron transfer downstream of PSII [247]. Importantly, the maximum PSII quantum yield (when illumination (PAR) is 0) was not different between the strains (ranging from 0.72 - 0.76), in agreement with earlier Y(II) determination experiments (section 3.2.3.1). At higher light intensities (from 217 $\mu mol_{photons}\ m^{-2}\ s^{-1}$ upwards) c_{6A}-OE showed a significantly higher Y(II) than c_{6A}-KO, although the difference was small. Together with the absence of a difference between c_{6A}-KO and WT this suggests that different expression levels of c_{6A} could affect PSII function differently and higher levels of c_{6A} could seemingly improve the photochemical quantum yield of PSII at higher light intensities. Whether the elevated Y(II) leads to a growth advantage for c_{6A}-OE could be tested by exposing cultures to 500 $\mu mol_{photons}\ m^{-2}\ s^{-1}$ growth light, where the difference is the largest. The increased Y(II) values for c_{6A}-OE also translated into a significantly increased relative electron transfer rate (rETRII) under higher light intensities (figure 4.8A). Onset of photoinhibition could be observed for all strains from 378 $\mu mol_{photons}\ m^{-2}\ s^{-1}$, as evidenced by the declining slope of rETRII.

When examining levels of non-photochemical quenching Y(NPQ) (figure 4.8A), an increase with light intensity was observed for all strains which is to be expected as NPQ is a light-induced phenomenon with a greater effect at higher light intensities [71]. Additionally,

c_{6A}-KO had a significantly increased NPQ level compared to WT from the onset of light and throughout all light intensities tested. This NPQ phenotype was partially alleviated by overexpressing c_{6A}, as evidenced by the NPQ trace of c_{6A}-OE. Especially under lower light intensities, a significant decrease of NPQ levels was observed for c_{6A}-OE compared to c_{6A}-KO. If NPQ function were negatively affected by c_{6A}, a lowered NPQ response to light compared to WT would have been expected for c_{6A}-KO, as observed for example in a *C. reinhardtii* mutant lacking LHCSR3 [235]. Therefore, the observed increase in NPQ in c_{6A}-KO suggest that NPQ mechanisms in absence of c_{6A} are functional, while it also points to increased stress in c_{6A}-KO.

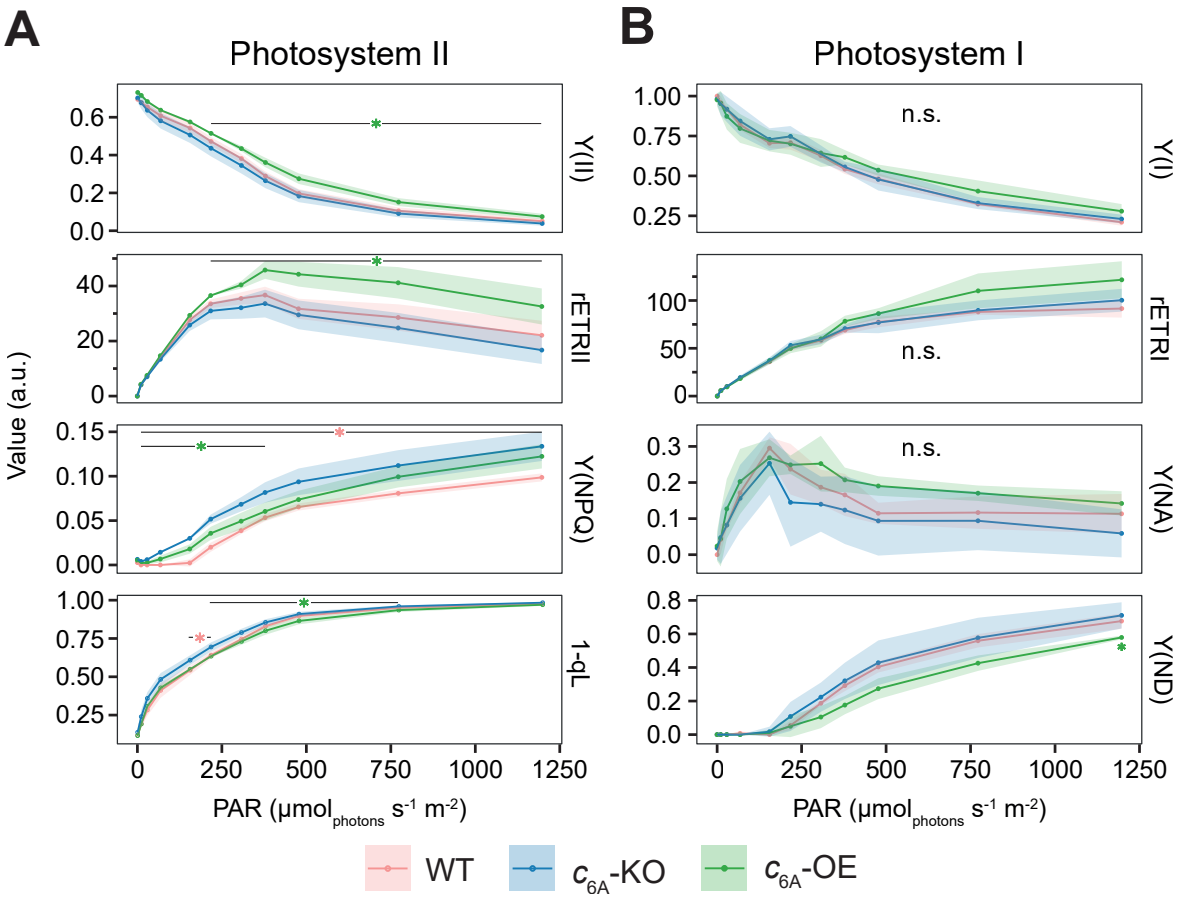


Figure 4.8: Light response curves of different photosystem II and I parameters of c_{6A} mutant strains and WT. (**A**) Photomixotrophic exponential growth phase cultures were measured for their photosystem II quantum yield Y(II), relative electron transfer rate rETRII, regulated non-photochemical quenching Y(NPQ), and Q_A reduction state 1-qL (a proxy for the PQ pool redox state) using a Dual-PAM-100. (**B**) Simultaneously, the samples were also assessed for their photosystem I quantum yield Y(I), rETRI, acceptor side limitation Y(NA) and donor-side limitation Y(ND). The relative electron transfer rates (rETR) for PSII and PSI were calculated as photosystem quantum yield x PAR (N=3 $\pm$ SD). Non-significance is indicated by "n.s." and coloured asterisks mark a significant difference ($p < 0.05$) of WT or c_{6A}-OE to c_{6A}-KO as determined by repeated measure ANOVA and pairwise t-tests as post-hoc test if the ANOVA $p_{PAR:strain}$ value was below 0.05.

The value of 1-qL is a proxy measurement for the redox state of the PQ pool as it describes how reduced Q_A in PSII is. As Q_A is in a redox equilibrium with the PQ pool, it can be inferred that the higher 1-qL the more reduced the PQ pool (figure 4.8A) [187, 261, 263]. As expected with increasing light intensities, 1-qL also grew to a maximum just below 1 (fully reduced Q_A) for all strains. Interestingly, the c_{6A}-KO showed a slight but significant increase at intermediary light intensities compared to the WT, indicating a more reduced PQ pool in the absence of c_{6A}. A significant increase was also found for c_{6A}-KO compared to c_{6A}-OE at light intensities from 217 to 772 $\mu mol_{photons}\ m^{-2}\ s^{-1}$. A more reduced PQ pool could be the consequence of a light harvesting imbalance in favour of PSII, as observed for c_{6A}-KO in section 4.2.1.1. However, a more reduced PQ pool, as inferred from 1-qL measurements, was also observed for a *C. reinhardtii* mutant that is impaired in starch accumulation (*sta6*) [239, 276]. This underlines that the PQ pool redox balance is influenced by a multitude of factors which c_{6A} could influence. Furthermore, caution has to be applied in relation to the 1-qL parameter. It is only a proxy measurement of the PQ pool, hence more detailed plastoquinone pool measurements were carried out later to examine further the above findings (section 4.2.1.5).

Overall, only small c_{6A}-dependent differences were found for PSII parameters in continuous light which is in agreement with the absence of a growth phenotype under continuous light conditions. Nevertheless, overexpression of c_{6A} led to a slightly increased Y(II) in higher light, while increased NPQ levels and a somewhat more reduced PQ pool were found in the absence of c_{6A}.

Simultaneous to PSII parameter determination, parameters of photosystem I performance were investigated (figure 4.8B). For all three strains, Y(I) was found to decrease with increasing light intensity, while electron transfer limitations around PSI, Y(NA) and Y(ND), increase. No significant difference was found between the strains for Y(I) which also translated to a lack of significant differences in rETRI. For all strains, acceptor side limitation Y(NA) rose quickly with the light intensity to its maximum at around 155 $\mu mol_{photons}\ m^{-2}\ s^{-1}$ and then stabilised to a lower level at higher light intensities. PSI donor side limitation Y(ND) showed a positive correlation with light intensities greater than 217 $\mu mol_{photons}\ m^{-2}\ s^{-1}$. With increasing light intensities, decreasing Y(II) (figure 4.8A) is logically followed by increased donor side limitation at PSI. No significant difference was found here between the strains, except for c_{6A}-OE at the highest light intensity. The c_{6A}-OE strain was found to generally trend at lower Y(ND) values, which can be readily explained by the slightly increased Y(II).

Taken together, these results suggest that c_{6A} does not affect PSI function directly under continuous illumination.

4.2.1.4 Electron flow around photosystem I of *C. reinhardtii* in photomixotrophy as determined by DUAL-KLAS-NIR spectrometry

No c_{6A}-dependent PSI impairment was found when investigating PSI parameters in continuous light (section 4.2.1.3). However, the P700 absorption signal as measured by the Dual-PAM-100 contains contributions of plastocyanin and ferredoxin also, which could affect the accuracy of PSI measurements. DUAL-KLAS-NIR spectrometer measurements allow for a more detailed investigation of PSI, deconvoluting signals from plastocyanin, P700, and ferredoxin. This requires the recording of differential model plots that contain redox changes in only one of the components. After acquiring differential model plots with photoautotrophic cultures to maximise the signal-to-noise ratio, c_{6A}-KO and WT were compared for their plastocyanin, P700, and ferredoxin redox kinetics (figure 4.9) making these data the first reported deconvoluted DUAL-KLAS-NIR traces for *C. reinhardtii*.

For plastocyanin, the redox kinetics showed a complex profile with parts of it exhibiting unexpected behaviour possibly due to technical problems with deconvolution. The detailed reasons for this unexpected behaviour remain to be determined. For both strains, a multiple turnover flash (MT, asterisks in figure 4.9) and subsequent red light illumination led to moderate oxidation, as expected. The c_{6A}-KO strain showed a higher extent of oxidation due to red light than WT. When the actinic light was turned off, a quick partial re-reduction of plastocyanin was observed. Subsequently, the signal suggested a slow oxidation of plastocyanin in the dark, the reasons for which remain to be clarified. Then, in far-red light, an apparent reduction was seen. This is also unusual in that oxidation would be expected here instead. Finally, the second MT transiently oxidised plastocyanin to its maximum value used for normalisation after which plastocyanin was quickly re-reduced and continued being reduced in darkness at a similar rate as in far-red light.

In contrast to plastocyanin, the trace of redox kinetics of P700 largely followed the expected pattern in both c_{6A}-KO and WT. Red and far-red light led to about 75% of maximal oxidation of P700 while the initial oxidation rate in far-red light was higher than the red light equivalent. The second MT then caused maximum oxidation of P700 and fast re-reduction to a baseline level occurred once the light was turned off. No major differences in P700 redox kinetics were found between c_{6A}-KO and WT.

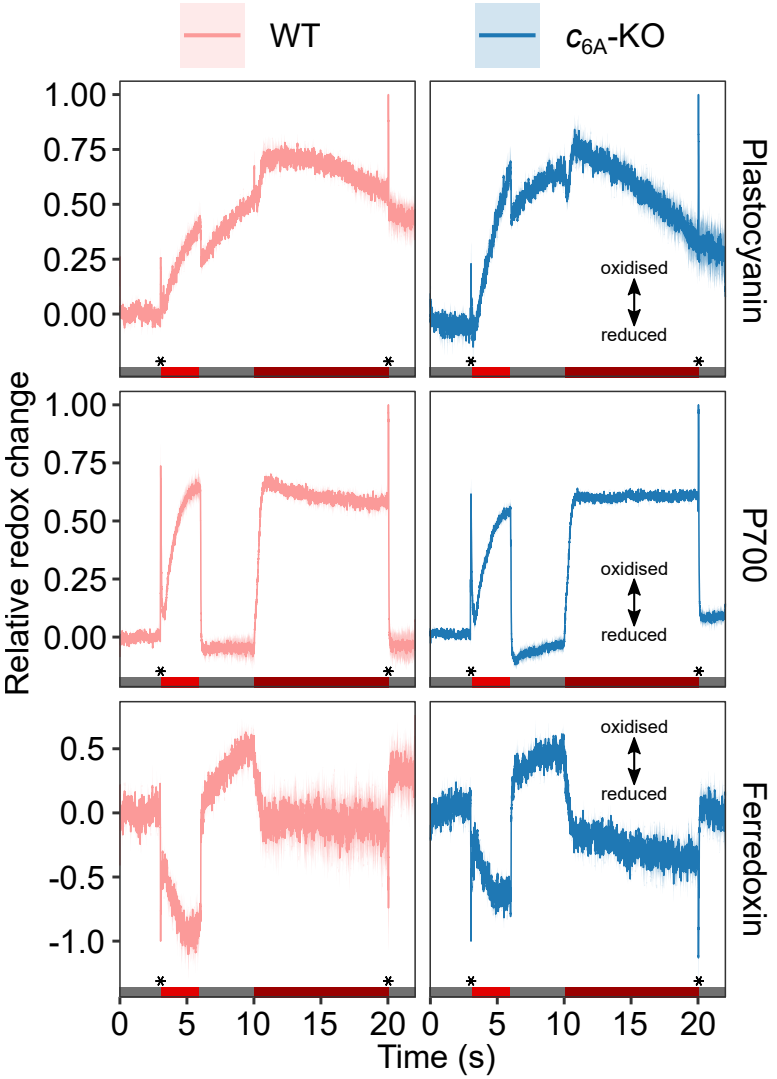


Figure 4.9: Relative redox changes of plastocyanin, P700, and ferredoxin of c_{6A}-KO and WT. Photomixotrophic exponential growth phase cultures were exposed to a NIRmax protocol in a DUAL-KLAS-NIR spectrometer (N=3 $\pm$ SD). Absolute values of each component were normalised to the value at which the light conditions cause the respective maximum redox change. Grey, red and dark red bars at the bottom indicate the light regime of the NIRmax protocol; darkness, red light or far-red light, respectively. Asterisks symbolise application of a multiple turnover flash.

Similarly to P700, the ferredoxin relative redox change mostly aligned with expected redox changes. Here, the first multiple turnover flash was used for normalisation of the signal as it usually leads to the largest redox change. Indeed, the MT led to a great reduction of ferredoxin, although the maximum was also reached during red light illumination (WT) or surpassed by the second MT flash (c_{6A}-KO). As expected, red and far-red light illumination caused reduction of ferredoxin, with red light reducing ferredoxin in WT to a slightly larger extent than in c_{6A}-KO. Ferredoxin was then quickly re-oxidised when the light was turned off. This is expected as the downstream reactions from ferredoxin are not light dependent

and therefore, it can still transfer electrons. The apparent oxidation during the second dark phase to a higher level than the starting point indicates inadequate length of dark adaptation before the experiment or could be due to signal deconvolution problems as suspected for the plastocyanin trace.

Overall, the investigation of electron flow around PSI using a DUAL-KLAS-NIR spectrometer suggested that small differences in plastocyanin and ferredoxin redox changes might exist between c_{6A}-KO and WT. However, signal deconvolution issues and inappropriate dark adaptation may have caused artefacts. To obtain maximum signal-to-noise ratio, differential model plots were measured using photoautotrophic cultures, while the experiments were carried out with photomixotrophic cultures. This possibly contributed to deconvolution issues, because the presence of acetate affects the metabolism and photosynthetic machinery of *C. reinhardtii*. More robust differential model plots could be obtained by utilising the same culture conditions for experiment and model, although a photoautotrophic sample also showed similar unexpected behaviour (data not shown). Once deconvolution issues are removed, confirmation of the differences described above and investigation of PSI under different conditions (such as DISCO Light) could prove informative.

4.2.1.5 Cytochrome c_{6A} affects the redox state of the plastoquinone pool in *C. reinhardtii* under photomixotrophic conditions

An increased 1-qL value was found for c_{6A}-KO in the light response curves, indicating a more reduced PQ pool in the absence of c_{6A} (section 4.2.1.3). This finding was further investigated with more sensitive chlorophyll fluorescence induction measurements, also known as OJIP curves. These measurements - and especially the fluorescence value F_J from an OJIP curve - contain information on the redox state of the PQ pool [264]. Therefore, OJIP curves were recorded of samples from WT, c_{6A}-KO and c_{6A}-OE grown photomixotrophically under standard conditions (figure 4.10). Samples with or without DCMU were compared, as DCMU blocks the Q_B site in PSII and any differences that remain would be due to changes within the first steps of photosynthetic electron transfer.

Raw fluorescence values were recorded for samples with or without DCMU (figure 4.10A). While all strains started at similar fluorescence values, after 200 ms c_{6A}-OE showed increased maximum fluorescence compared to c_{6A}-KO, which in turn had higher raw maximum fluorescence than WT. The same order was observed for samples with DCMU, where all strains exhibited maximum fluorescence after about 3 ms.

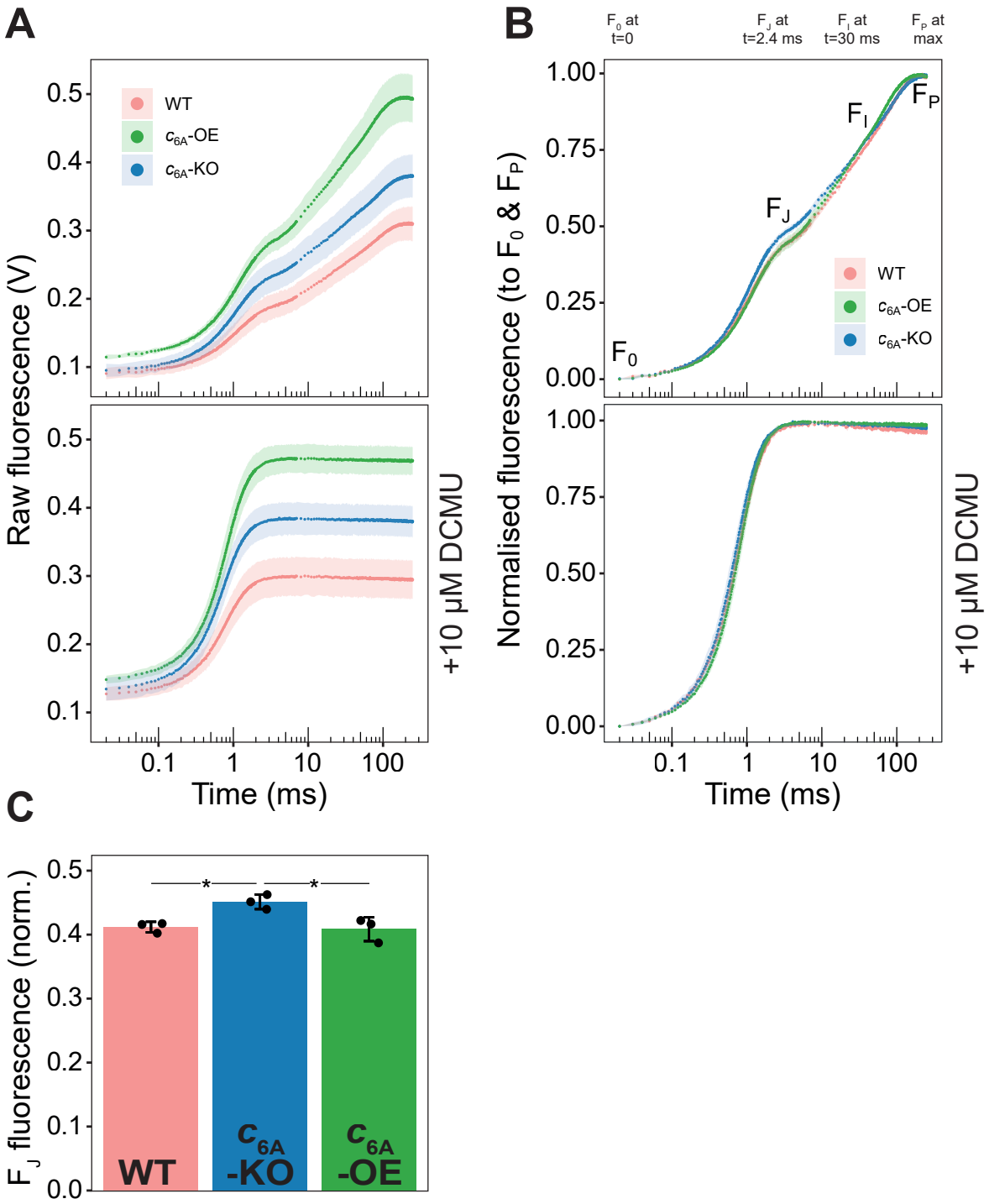


Figure 4.10: Chlorophyll fluorescence induction measurements (OJIP curves) of *C. reinhardtii* c_{6A} mutant strains and WT. (**A**) Chlorophyll fluorescence of photomixotrophic exponential growth phase cultures was measured in response to red light (984 $\mu mol_{photons}$ m^{-2} s^{-1}) in a FL3500 fluorometer with or without DCMU (10 µM) (N=3 ± SD). (**B**) Raw fluorescence data from (A) was used to determine double normalised OJIP curves where fluorescence values were normalised to F_0 and F_P. (**C**) The normalised fluorescence at inflection point F_J (2.4 ms) is shown separately. Asterisks indicate a significant difference ($p < 0.05$) as determined by one-way ANOVA and pairwise t-test.

To compare the kinetics between samples, OJIP curves are often double normalised, to the baseline fluorescence F_0 and the maximum value F_P (figure 4.10B) [247]. When double normalised, the fluorescence traces of WT, c_{6A}-KO and c_{6A}-OE showed a significant difference with an increase of the F_J fluorescence in c_{6A}-KO compared to WT and c_{6A}-OE. No other significant differences could be observed. The absence of a difference at F_I which is associated with PSI electron transfer [265], supports previous findings of c_{6A} not majorly affecting PSI (section 4.2.1.3). The samples with DCMU did not show any differences in fluorescence kinetics between the strains when double normalised.

For easier inspection, the double normalised fluorescence values of F_J at 2.4 ms were plotted again in figure 4.10C. The c_{6A}-KO exhibited elevated F_J fluorescence, significantly increased by 10% compared to WT and c_{6A}-OE. As higher F_J values correlate with a more reduced PQ pool [264], the c_{6A}-dependent difference in F_J suggests that c_{6A} is needed to maintain a normal redox balance of the PQ pool in *C. reinhardtii* under photomixotrophy, confirming the previous indication of a more reduced PQ pool in absence of c_{6A} (section 4.2.1.3).

In summary, an involvement of c_{6A} in the redox balance of the PQ pool was found using OJIP curves. The more reduced state of the PQ pool in absence of c_{6A} could be due to various factors. A light harvesting imbalance in favour of PSII as found earlier (section 4.2.1.1) could lead to a more reduced PQ pool [288]. However, inhibition of electron transfer downstream of the PQ pool could also lead to a more reduced state. If this were the case, it would be unlikely to be linked to PSI as no differences could be observed there (section 4.2.1.3). An effect on the cytochrome b_6f complex situated between the PQ pool and PSI in electron transfer could also be the reason for a more reduced PQ pool in the absence of c_{6A} [239]. Other complexes of the thylakoid membrane, such as the plastid terminal oxidase PTOX2, can also influence the redox state of the PQ pool. [51].

4.2.1.6 Cytochrome c_{6A} absence leads to altered redox kinetics of the *b* hemes in cytochrome b_6f of *C. reinhardtii*

To investigate if c_{6A} influences electron flow through the cytochrome b_6f complex, either directly or through its effect on the PQ pool redox state, the redox kinetics of the cytochrome b_6f complex were measured upon light exposure. Using a Joliot-type spectrometer (JTS), the differential absorbance values of four different measurement wavelengths can be used to deconvolute the redox changes of the *b* hemes and cytochrome *f*, with plastocyanin redox changes featuring in one of the baseline measurements (section 4.1.2.2). Photoautotrophic and photomixotrophic samples of WT, c_{6A}-KO and c_{6A}-OE were tested (figure 4.11).

In photoautotrophy, the *b* hemes reduction peak within 100 ms of light in c_{6A}-KO was on average half of the equivalent WT and c_{6A}-OE peaks. While c_{6A}-OE exhibited re-oxidation to the level of c_{6A}-KO in 600 ms, WT stayed at a similar redox level after its initial reduction peak. Especially the c_{6A}-dependent difference seen for the first reduction peak is noteworthy, as it suggests a difference in electron flow at the onset of light, the effects of which would be greater in fluctuating light conditions. The observation described above is the first time in this study that a c_{6A}-associated phenotype was found under photoautotrophic conditions.

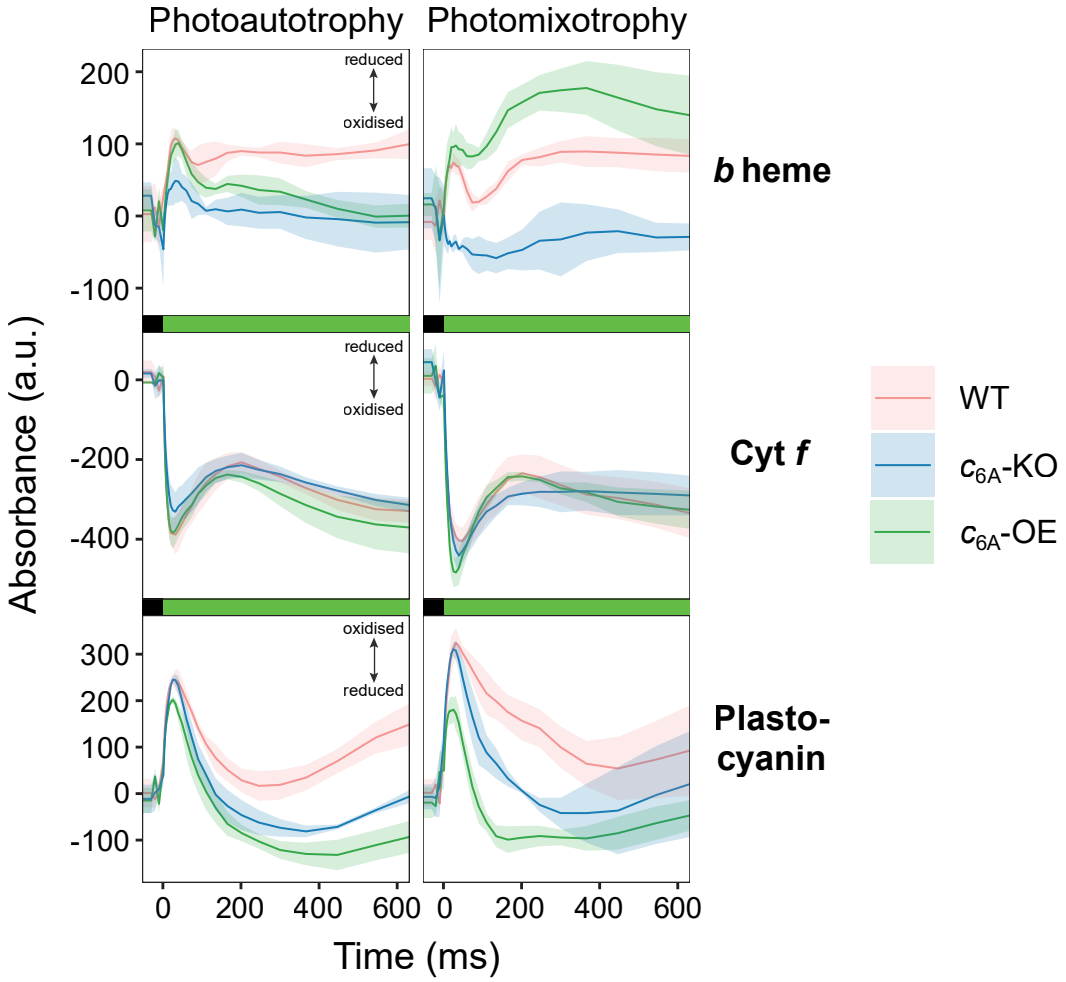


Figure 4.11: Redox changes of *b* hemes, cytochrome *f*, and plastocyanin in *C. reinhardtii* c_{6A} mutant strains and WT. Photoautotrophic or photomixotrophic exponential growth phase cultures were exposed to green light (500 $\mu mol_{photons}$ m^{-2} s^{-1}, green bar) in a JTS spectrometer and redox changes were recorded for ~600 ms (N=3 $\pm$ SD). Data is baselined to the dark level by default (black bar).

Photomixotrophic cultures exhibited an increased difference in *b* hemes redox kinetics between c_{6A}-KO and WT/c_{6A}-OE. While both WT and c_{6A}-OE had a similar reduction peak within 100 ms and subsequently exhibited an oxidation-reduction pattern, the *b* hemes in c_{6A}-

KO showed slight oxidation at the onset of light and then underwent only small re-reduction within the margin of error. Additionally, the steady-state levels at 600 ms were different, with WT and c_{6A}-OE showing a much more reduced state than c_{6A}-KO. It can be inferred that c_{6A} significantly affects *b* heme electron flow when first exposed to light, especially in presence of acetate. Previous studies have shown that, as found for c_{6A}-KO compared to WT/c_{6A}-OE, altered *b* hemes redox kinetics are observed when the redox state of the PQ pool is changed. A more reduced PQ pool leads to less intense reduction peaks upon light exposure and even apparent oxidation of *b* hemes [274, 275, 289]. The latter is due to *b* hemes being pre-reduced in conditions with a highly reduced PQ pool. The more reduced PQ pool in c_{6A}-KO may therefore explain the observed differences in *b* hemes redox kinetics. The difference in *b* hemes redox kinetics seen here between photoautotrophy and photomixotrophy could also be explained by the PQ pool redox difference. It can be expected that the PQ pool is more reduced with external acetate present, exacerbating the effect on *b* hemes redox kinetics. The observation of affected *b* hemes redox kinetics and its connection to the PQ pool will be further investigated later in this section.

While the differences in *b* hemes redox kinetics between the strains are substantial, cytochrome *f* (Cyt *f*) followed a similar redox kinetics pattern for all strains in both photoautotrophy and photomixotrophy without significant differences. In photoautotrophy, the onset of light led to an oxidation peak which was only slightly smaller in c_{6A}-KO in photoautotrophy. Furthermore, the oxidation peak in photomixotrophic conditions was slightly but not substantially different between all strains and overall larger than in photoautotrophic cultures. The peak was followed by a re-reduction in the light and arrival at a steady state level by 600 ms. The electron flow through cytochrome *f* did not seem to be majorly affected by c_{6A}. This suggests that the linear electron flow to PSI is unaffected by c_{6A}, in agreement with previous results of PSI performance (section 4.2.1.3).

For plastocyanin, photoautotrophic and photomixotrophic cultures of all strains exhibited a similar shape of redox kinetics. However, the oxidation peak just after the onset of light was decreased in c_{6A}-OE compared to c_{6A}-KO and WT. While all strains showed a substantial re-reduction within 300 ms, plastocyanin was in a more oxidised state in WT than c_{6A}-KO and c_{6A}-OE by 600 ms. Investigation of the redox kinetics for longer timescales than 600 ms revealed a drift for the plastocyanin measurements that led to large differences even between replicates of the same strain. Further experiments would be needed to determine the reason for this drift but it is likely to have affected also the early time points of the measurements shown here. This, together with the stark c_{6A}-dependent difference found for *b* hemes and the absence of differences for cytochrome *f*, led to subsequent experiments focusing on the characterisation of *b* hemes redox kinetics.

To dissect further the c_{6A}-dependent *b* hemes phenotype, photomixotrophic cultures of WT, c_{6A}-KO and c_{6A}-OE were exposed to various chemicals affecting the PETC - and thus the redox state of the PQ pool - and tested for their *b* hemes redox kinetics in response to light (figure 4.12). The result for photomixotrophic cultures without added chemicals is included again for reference.

First, DCMU was added. DCMU is a widely-used competitive inhibitor of the PSII Q_B site and causes a more oxidised PQ pool as PSII activity is disrupted [290]. A more oxidised PQ pool should lead to increased reduction of *b* hemes upon light exposure even if PSII is inactive as the electron pull from PSI would drive redox reactions in the b_6f complex until the PQ pool is completely oxidised. For the redox kinetics of the *b* hemes, DCMU addition led to only slightly increased reduction peaks within 100 ms for c_{6A}-OE and WT compared to without DCMU. The PQ pool in those strains was therefore likely relatively oxidised even without DCMU addition. A different picture was found for c_{6A}-KO where instead of the oxidation without DCMU, a reduction peak with DCMU was apparent. A more reduced PQ pool in absence of c_{6A} would also be more susceptible to changes induced by DCMU. Furthermore, the second reduction increase around ~200 ms seen for WT and c_{6A}-OE in photomixotrophy in the absence of DCMU was not present with DCMU in any strain, indicating that this second rise is connected to PSII activity. The first peak in *b* hemes redox kinetics in response to light is therefore likely PSI-dependent. Finally, all three strains reached a similar steady-state at 600 ms, with c_{6A}-OE trending at slightly more reduced levels. Taken together, these changes caused by DCMU addition indicate that the c_{6A}-dependent difference is at least partly dependent on sustained PSII activity and further supports the hypothesis that the differences observed in photomixotrophy without inhibitors are connected to the PQ pool redox state.

Another set of samples was supplemented with methyl viologen (MV) which acts as an artificial electron acceptor from PSI. As MV relieves any acceptor side limitation from PSI and diminishes cyclic electron flow it also causes a more oxidised PQ pool [291]. A small c_{6A}-dependent difference in the first reduction peak was also found here, although the c_{6A}-KO trace again showed a pronounced reduction. In steady-state after 600 ms, all three strains remained at a similar reduction level as WT without MV, which can be expected from sustained PSII activity. The absence of a strain-dependent difference here indicates that additional to PSII activity, a certain acceptor side limitation at PSI needs to be present for the c_{6A}-dependent difference to emerge. Removing PSI acceptor side limitation and CEF would alleviate the effect of a more reduced PQ pool redox state. The findings therefore again contribute to explaining the c_{6A}-dependent difference in *b* hemes redox kinetics with an altered PQ pool redox state.

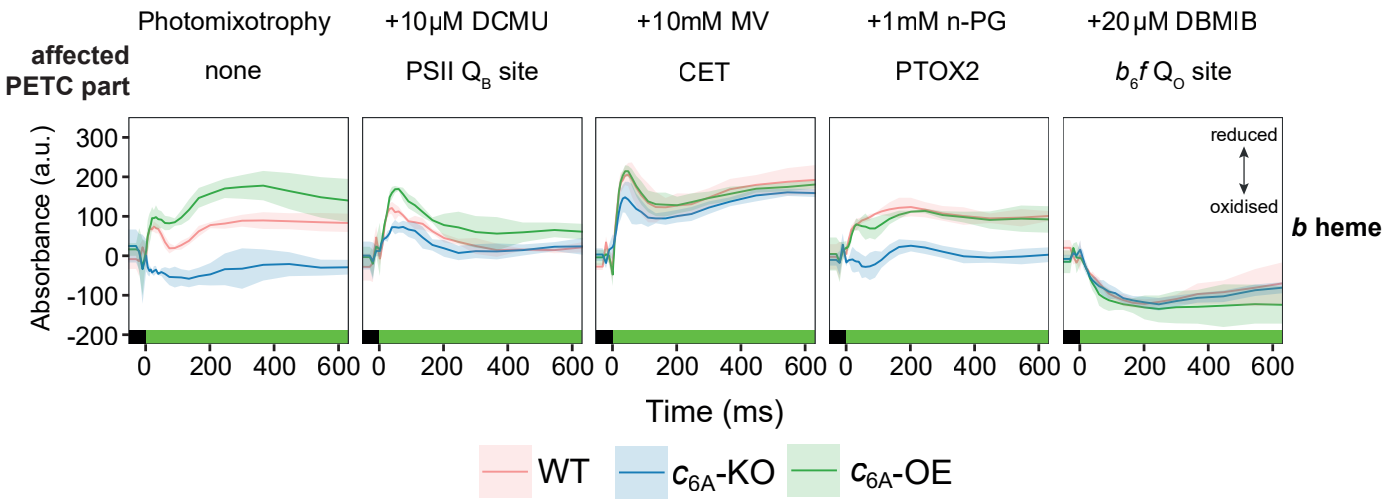


Figure 4.12: Redox changes of *b* hemes in *C. reinhardtii* c_{6A} mutant strains and WT with or without addition of various chemicals affecting the PETC. Photomixotrophic exponential growth phase cultures were exposed to green light (500 $\mu mol_{photons}$ m^{-2} s^{-1}, green bar) in a JTS spectrometer and redox changes were recorded for ~600 ms (N=3 $\pm$ SD). Data is baselined to the dark level by default (black bar). Chemicals were added to the final concentrations specified in the figure and the PETC part they affect is noted for reference.

To control for the possibility that c_{6A} affects the function of the plastid terminal oxidase PTOX2, the PTOX2 inhibitor n-propyl gallate (n-PG) was added to WT, c_{6A}-KO and c_{6A}-OE samples. PTOX2 can contribute to PQ pool oxidation by transferring electrons from the PQ pool to oxygen [51]. A different PTOX2 activity therefore could explain differences in PQ pool redox state and *b* hemes redox kinetics. The *b* hemes redox kinetics of samples with n-PG were overall similar to the ones without n-PG, which suggests that the effect of PTOX2 on the PQ pool redox balance is small in the conditions used here. The c_{6A}-KO showed a slight oxidation upon light exposure followed by a small reduction transient. WT and c_{6A}-OE exhibited *b* hemes reduction upon light exposure. Interestingly, the oxidation transient around ~100 ms observed in photomixotrophic conditions was not found in WT anymore, while it was present in c_{6A}-OE. Similar to samples without n-PG, the steady-state level after 600 ms was different between c_{6A}-KO and WT/c_{6A}-OE. These results suggest that the function of c_{6A} is not directly linked with PTOX2 activity, as the c_{6A}-dependent differences remained, even when PTOX2 was inhibited.

To investigate if the observed oxidation of *b* hemes upon light exposure in c_{6A}-KO arises from altered reduction or altered oxidation of the *b* hemes, the luminal plastoquinone binding site at the b_6f complex (Q_p site) was blocked using dibromothymoquinone (DBMIB) [292]. An inhibitor binding to the Q_p site would lead to prevention of reduction of *b* hemes as no electrons can enter the Q-cycle. Any difference between strains that remains despite a blocked Q_p site could therefore be attributed to alterations on the Q_n site, where *b* hemes

are oxidised. Here, the blockage led to an equalisation of the *b* hemes redox kinetics of all three strains, which then only exhibited oxidation to a steady state within 200 ms rather than the more complex reduction-oxidation-reduction profile as observed without DBMIB. The c_{6A}-dependent difference without DBMIB could thus be associated with the reduction of *b* hemes rather than their oxidation. However, the observed oxidation of *b* hemes independent of the strain identity was unexpected, as blocking the Q_p site should theoretically lead to a standstill of the Q-cycle. No electrons could be fed into the Q-cycle and PSII activity would cause reduction of the PQ pool preventing oxidation of the low-potential chain at the Q_n site. This conundrum can be explained by the fact that DBMIB has been found to act also as inhibitor of PSII [293]. Blocked PSII would lead to a more oxidised PQ pool which would allow for oxidation of *b* hemes via the Q_n site. Additionally, as DBMIB is a quinone itself, it can be hypothesised that it would accept electrons leading to oxidation of *b* hemes. In either case, if c_{6A} were affecting the oxidation of *b* hemes rather than their reduction, a strain-dependent difference would have been expected here still.

In summary, a significant effect of c_{6A} on the redox kinetics of *b* hemes was discovered, particularly pronounced in photomixotrophy. The c_{6A}-dependent differences were shown to depend on PSII activity and a PSI acceptor side limitation or CEF. While the involvement of PTOX2 was deemed unlikely, c_{6A} was hypothesised to affect *b* hemes reduction rather than oxidation. All results could be explained by the finding of a more reduced PQ pool in the absence of c_{6A} and the effect of the different chemicals on the redox state of the PQ pool. This is in agreement with earlier findings and further supports the hypothesis that c_{6A} is important for maintaining a normal PQ pool redox state in *C. reinhardtii*.

However, altered *b* hemes redox kinetics could also be due to affected Q-cycle function, which in turn could lead to a more reduced PQ pool if electrons accumulated before the defect. A slower or broken Q-cycle, for example caused by a missing heme c_n, would lead to a decrease of proton pumping across the thylakoid membrane, a lower pmf and ultimately less ATP production and growth, especially under photoautotrophic conditions [275]. No growth phenotype in line with a broken Q-cycle (such as a severe growth penalty under photoautotrophic conditions) was found for c_{6A} suggesting that in c_{6A}-KO the Q-cycle is at least functional in principle. Nevertheless, from the data presented thus far, an effect of c_{6A} on Q-cycle function cannot be excluded and was investigated further (section 4.2.1.7).

4.2.1.7 Cytochrome c_{6A} does not affect the proton motive force in *C. reinhardtii* under photomixotrophic conditions

The investigation of *b* hemes redox kinetics (section 4.2.1.6) raised the question if the absence of c_{6A} affected Q-cycle function. As the Q-cycle sits within the b_6f complex and therefore in the middle of the PETC, an altered Q-cycle should show a significant effect on photosynthetic electron transfer. The Q-cycle is an important part of the generation of the proton motive force (pmf), due to the protonation steps involved. Determining the pmf with ECS measurements can therefore be informative of Q-cycle function. Here, ECS measurements of c_{6A} mutant strains and WT were carried out with the recording of dark interval relaxation kinetics (DIRKs) to determine pmf, proton flux (vH^+), and proton conductivity (gH^+). Samples were dark-adapted and subsequently exposed to continuous standard growth light in a Dual-PAM-100 with a P515 measuring head (figure 4.13).

For pmf (figure 4.13A), all strains reached a peak within the first ten seconds of light exposure followed by a relaxation to a relatively steady level after about 70 s. This pattern is in agreement with previous studies and reflects the difference in rates between quasi-instantaneous proton pumping and slower pmf dissipation via the ATP synthase [198]. No statistically significant differences were found between the strains, except for one data point in the steady state where c_{6A}-OE showed a slightly elevated pmf compared to c_{6A}-KO. Proton flux (vH^+) was also determined (figure 4.13B) to test for a defect in the Q cycle. No significant differences between the strains were found. The same was the case for proton conductivity, indicative of ATP synthase activity (gH^+, figure 4.13C), where for all strains an inverse trend to that of pmf could be observed, showing the up-regulation of the ATP synthase in light.

Overall, the ECS measurements and especially the absence of a difference in vH^+ render it unlikely that c_{6A} is involved in Q-cycle function under the conditions tested. However, pmf and also vH^+ are not direct measurements of the Q-cycle and are affected by other processes which might mask any c_{6A}-dependent effects. It is also possible that c_{6A}-dependent differences could be found more rapidly after the onset of illumination than on the timescale studied here. The first DIRK was recorded ~1.5 s after turning on the light, while the difference in *b* hemes redox kinetics was visible within the first 600 ms. An effect at these millisecond timescales would have a significant impact under conditions of multiple dark-to-light transitions. The parameters measured here were therefore also investigated under DISCO Light (section 4.2.2.3).

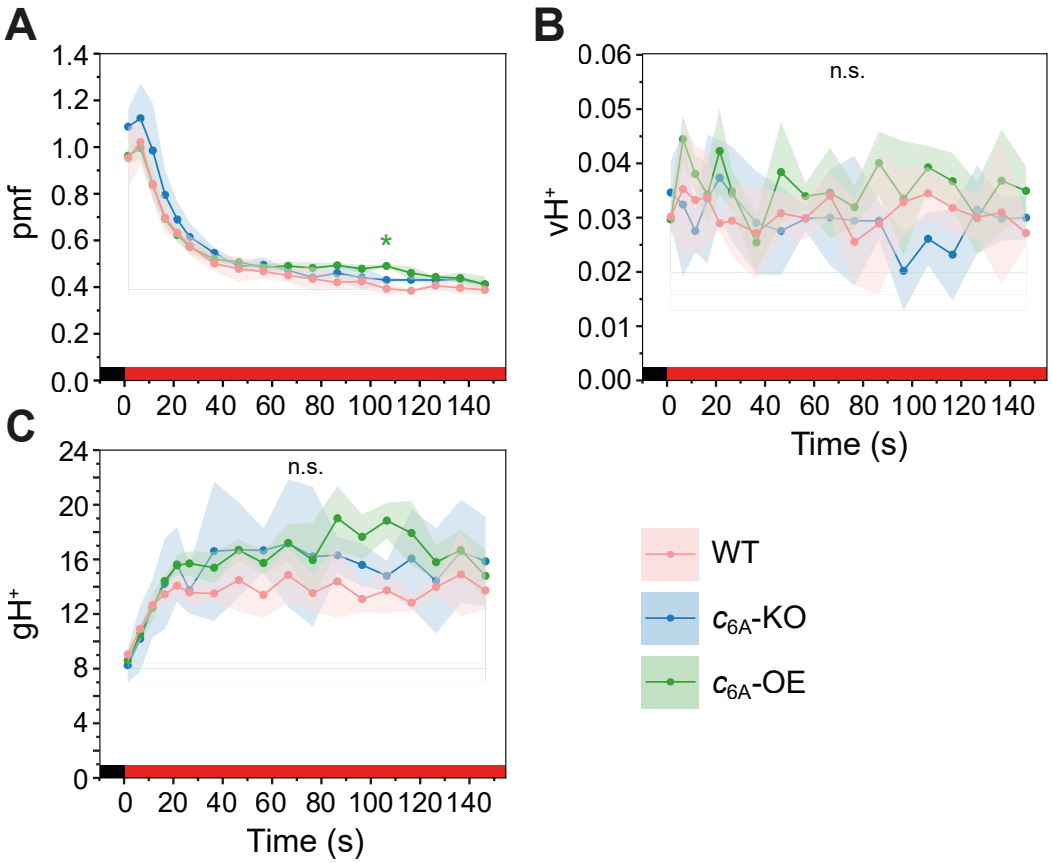


Figure 4.13: Electrochromic shift (ECS) measurements of *C. reinhardtii* c_{6A} mutant strains and WT. Dark-adapted, photomixotrophic exponential growth phase cultures were exposed to continuous red light (53 $\mu mol_{photons}$ m^{-2} s^{-1} red bar) in a Dual-PAM-100 spectrometer with a P515 measuring head (N=3 $\pm$ SD). Dark interval relaxation kinetics (DIRK, indicated by points) were used to determine (**A**) proton motive force pmf, (**B**) proton pumping activity vH^+, and (**C**) ATP synthase activity gH^+. The pmf data is normalised to the ECS signal change caused by a single turnover flash before the continuous illumination. Non-significance is indicated by "n.s." and the green coloured asterisk marks a significant difference ($p < 0.05$) of c_{6A}-OE to c_{6A}-KO as determined by repeated measure ANOVA and pairwise t-test.

4.2.1.8 Cytochrome c_{6A} does not affect oxygen gas exchange of *C. reinhardtii* under photomixotrophic conditions

The PQ pool redox state is not only affected by photosynthesis but also by respiratory processes, especially in photomixotrophic conditions, as reduction equivalents can be shuttled between chloroplast and mitochondria [193, 294]. Furthermore, the plastid terminal oxidase PTOX2 can affect the PQ pool redox state [295]. Both, respiration and PTOX2 consume oxygen. Hence, measuring oxygen gas exchange would help determining if elevated respiration or PTOX2 activity could lead to the observation of a more reduced PQ pool in c_{6A}-KO. The rates of oxygen gas exchange from respiration and photosynthesis in c_{6A} mutant strains and

WT were measured using membrane-inlet mass spectrometry (figure 4.14). Photomixotrophic culture samples were exposed to a dark-light-dark treatment of 5 min each, while gas exchange was recorded. Differentiation of oxygen consumption and production fluxes was enabled through spiking of the samples with $^{18}O_2$.

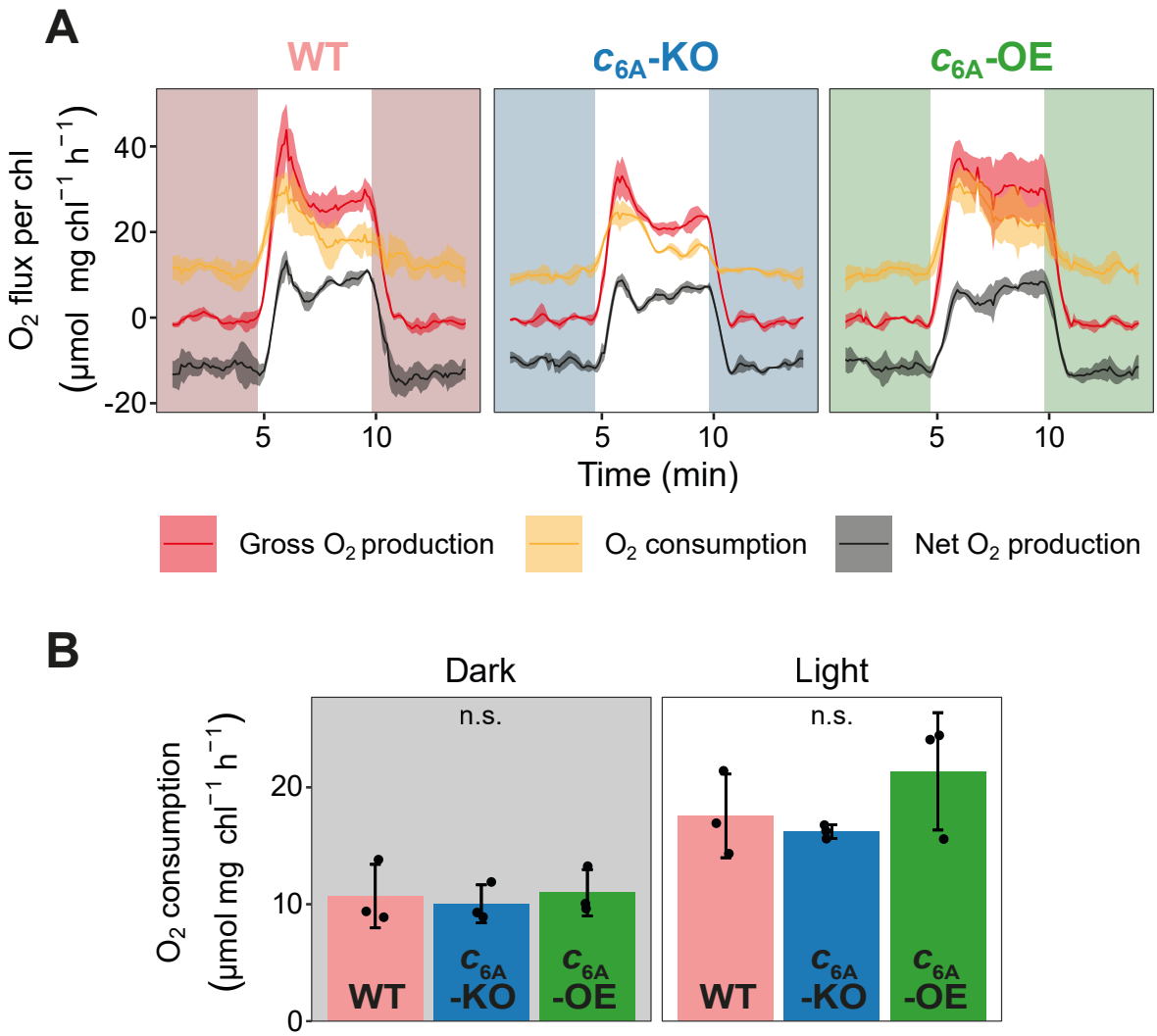


Figure 4.14: O_2 flux measurements of *C. reinhardtii* c_{6A} mutant strains and WT. (**A**) Photomixotrophic exponential growth phase cultures were exposed to 5 min darkness (grey shaded coloured boxes), 5 min white light (white boxes, 500 $\mu mol_{photons}$ m^{-2} s^{-1}), and 5 min darkness in a custom-built membrane inlet mass spectrometer. Spiking of the samples with $^{18}O_2$ allowed the deconvolution of oxygen fluxes into production and consumption (red and yellow in each plot, respectively). Net O_2 production (black) was calculated as the difference between production and consumption. (**B**) The oxygen consumption rates in dark and light were calculated as averages of the two last minutes in the first dark phase and the last minute in the light phase, respectively. Statistical analysis with ANOVA showed no significant differences between the strains. Shown here are the rates per mg chlorophyll and hour (N=3 $\pm$ SD).

When investigating the time resolved oxygen flux rates (figure 4.14A), no differences between the strains were observed in the first 5 min of darkness. A steady level of oxygen consumption (yellow) indicated active respiration, while no oxygen evolution (red) was observed. Upon light exposure, all strains showed a similar peak in oxygen production as well as oxygen consumption, followed by relaxation to steady-state levels. After light was turned off (at ~10 min), oxygen evolution returned to zero in all strains and a sustained oxygen consumption was found at a similar level as in the first dark phase.

To focus on oxygen consumption processes, rates in dark and light were calculated as averages of the two last minutes in the first dark phase and the last minute in the light phase, respectively (figure 4.14B). Oxygen uptake in the dark is mainly driven by respiration with a possible contribution from chlororespiration (i.e. PTOX2) [51]. No difference between the strains could be found here, suggesting that respiratory processes and PTOX2 activity are unlikely to be contributing to the c_{6A}-dependent differences found in earlier sections. This is in agreement with the finding that PTOX2 involvement in the c_{6A}-dependent differences in the redox kinetics of *b* hemes was found to be unlikely (section 4.2.1.6). Oxygen consumption in the light has contributions from respiration, PTOX2 activity, and Mehler and Mehler-like reactions [65, 287]. Also here, no significant c_{6A}-dependent difference was found, indicating that neither of those processes are likely to contribute to c_{6A} phenotypes, nor do they seem affected by different c_{6A} levels.

Overall, oxygen gas exchange measurements did not indicate a significant role for respiration or PTOX2 in the previously described c_{6A}-dependent differences. It was also found unlikely that c_{6A} influences respiration or oxygen evolution under the conditions tested.

4.2.2 The effect of c_{6A} on the photosynthetic electron transfer chain of *C. reinhardtii* in DISCO Light

Multiple effects of c_{6A} on the PETC have been found under continuous light that could be important for the emergence of the growth phenotype under DISCO Light (section 3.2.3.2). To identify the cause of the c_{6A}-dependent growth phenotype under DISCO Light, the PETC was investigated of *C. reinhardtii* cultures either grown in DISCO Light or exposed to DISCO Light for the first time during the measurements.

4.2.2.1 The c_{6A}-dependent phenotype in light harvesting balance is amplified by growth in DISCO Light

A c_{6A}-dependent phenotype in light harvesting balance has been found under photomixotrophic conditions in continuous light (section 4.2.1.1), raising the question how the phenotype develops under DISCO Light where an additional growth phenotype was observed. Therefore, samples from WT, c_{6A}-KO and c_{6A}-OE cultures grown in DISCO Light were examined at days 0, 2 and 4 of growth for their chlorophyll fluorescence at 77 K (figure 4.15).

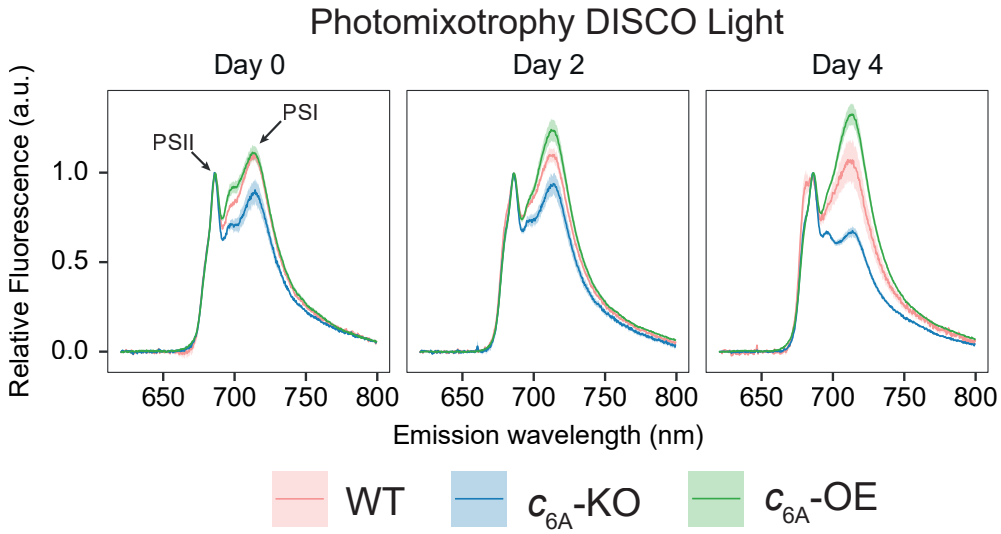


Figure 4.15: Low temperature (77 K) chlorophyll fluorescence spectra of *C. reinhardtii* c_{6A} mutant strains and WT grown under DISCO Light. Samples were taken on day 0 (equivalent to photomixotrophic standard light conditions), day 2 and day 4, adjusted to 5 µg/mL chlorophyll and frozen (N=3 ± SE). Raw fluorescence spectra were normalised to the PSII-associated peak at 685 nm. The most prominent PSI and PSII fluorescence peaks are indicated by black arrows. The fluorescence measurement of prepared samples was carried out by Dr. Laura Wey (University of Turku, Finland).

The 77 K spectra at day 0 were acquired from cultures that were not yet exposed to DISCO Light and therefore resemble the ones from cultures grown in continuous light (section 4.2.1.1). Here, the c_{6A}-KO strain exhibited a lower PSI/PSII fluorescence ratio than WT and c_{6A}-OE. The fluorescence traces at day 2 looked similar to day 0, with a lower PSI/PSII fluorescence ratio for c_{6A}-KO than WT and c_{6A}-OE. However, c_{6A}-OE showed a slightly increased PSI/PSII ratio compared to WT. On day 4, the difference between c_{6A}-KO and WT/c_{6A}-OE became greatly enlarged. While WT and c_{6A}-OE had a relatively steady PSI/PSII fluorescence ratio compared to day 2 of about 1.05 and 1.3, respectively, c_{6A}-KO exhibited a drastic decrease to ~0.65. Interestingly, on day 4, WT showed a shoulder peak blue-shifted from the main PSII peak at 685 nm. This peak at ~681 nm could be assigned to free LHCII proteins [253],

suggesting that in WT detachment of LHCII proteins from photosystems occurs as response to DISCO Light. The different reactions to DISCO Light observed here also reflect the growth phenotype with increasing differences between c_{6A}-KO and WT/c_{6A}-OE over the course of DISCO Light exposure. An increased imbalance of light harvesting would also have an effect on the balance of the PQ pool and could represent an origin for the detected c_{6A}-dependent phenotype.

In summary, DISCO Light seems to enhance dramatically the c_{6A}-dependent difference observed under continuous light, as c_{6A}-OE had a steady increase of PSI/PSII fluorescence ratio over the course of 4 days, while the ratio decreased within 4 days in c_{6A}-KO.

4.2.2.2 Cytochrome c_{6A} is important for normal photosystem II function in DISCO Light

The more reduced PQ pool seen in the absence of c_{6A} and under continuous light raised the question if this would affect PSII performance under more difficult light conditions like DISCO Light. Samples from WT and c_{6A}-KO grown in photomixotrophy under continuous light were therefore exposed to a DISCO Light regime in a Dual-PAM-100 spectrometer while chlorophyll fluorescence was measured to infer PSII parameters (figure 4.16).

Firstly, Y(II) was examined (figure 4.16A). The first point in the dark (time = 0) reflects the maximum PSII quantum yields of c_{6A}-KO and WT and no differences were found, which is in agreement with previous measurements (sections 4.2.1.3 & 3.2.3.1). When exposed to DISCO Light, however, a difference between c_{6A}-KO and WT emerged. While in dark phases (grey boxes and points above 0.5 in white boxes) Y(II) was equal between the strains, the 12 s light phases of DISCO Light caused a substantial difference between c_{6A}-KO and WT. WT steadily had Y(II) values of around 0.2, while c_{6A}-KO showed quantum yields below 0.1. This halving of Y(II) could serve as explanation for the growth difference observed between c_{6A}-KO and WT, as c_{6A} absence seems to lead to less ability to carry out PSII photochemistry. It is interesting to note that this lower Y(II) value is visible right from the start of DISCO Light exposure. The first saturating pulse for Y(II) measurement was applied after 5 s of exposure to light of 690 $\mu mol_{photons}\ m^{-2}\ s^{-1}$. Although no c_{6A}-dependent Y(II) difference was seen at the same light intensity in the continuous light curve measurements (section 4.2.1.3), in the latter experiments samples were exposed to increasing light intensities for 30 s each. This suggests that c_{6A} is important when *C. reinhardtii* is first exposed to light coming from darkness, while other adaptation processes would mask its effect during continuous light exposure. This hypothesis would also explain why there was no growth phenotype under continuous light, although there were detectable differences in the PETC.

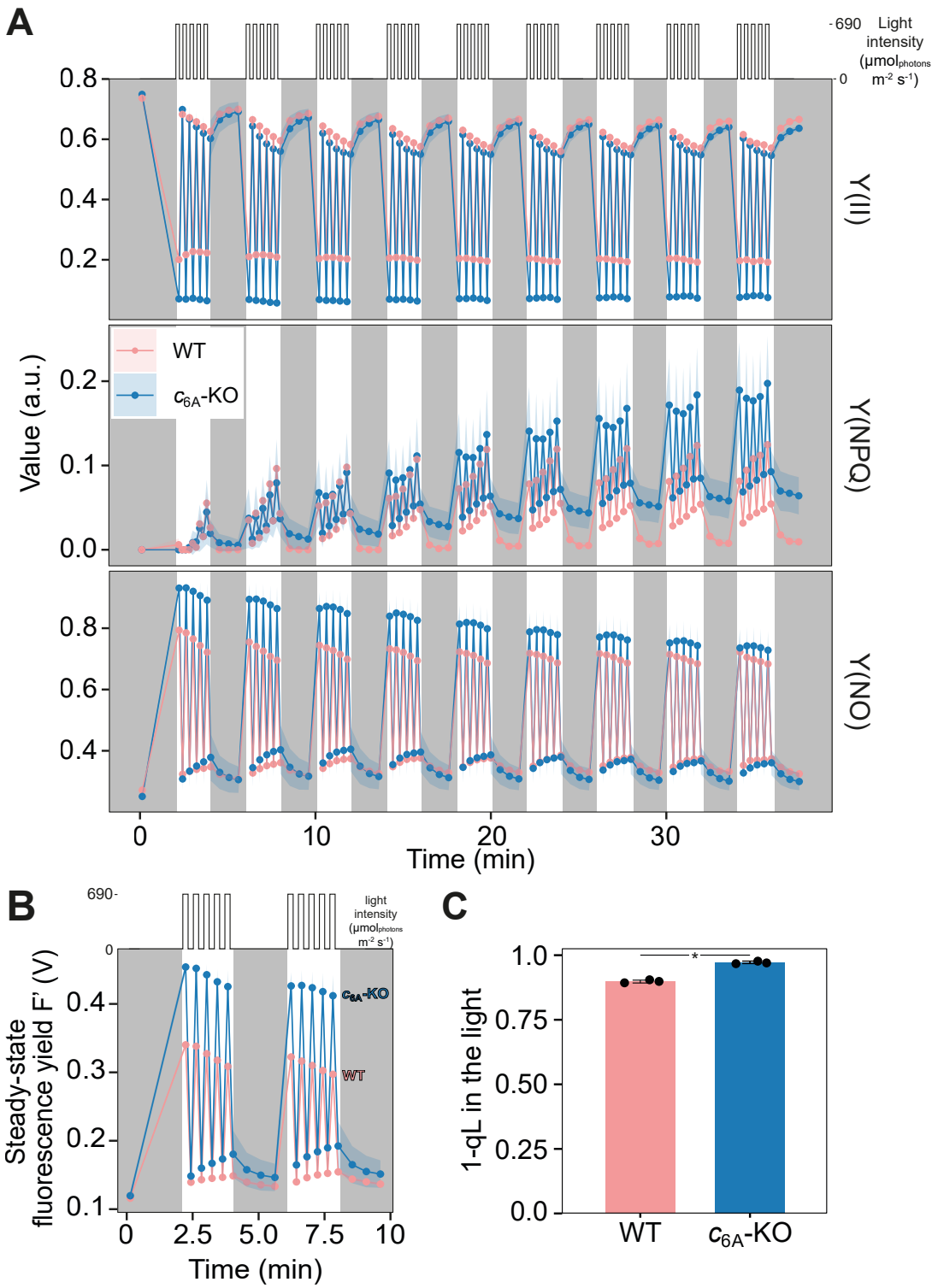


Figure 4.16: Measurements of photosystem II parameters of c_{6A}-KO and WT under DISCO Light conditions. (**A**) Photomixotrophic exponential growth phase cultures were exposed to a DISCO Light regime in a Dual-PAM-100 spectrometer where grey boxes represent darkness and white boxes represent 2 min of 12 s on/off as depicted above the Y(II) panel (N=3 ± SD). The effect of saturating pulses on chlorophyll fluorescence was used to calculate photosystem II quantum yield Y(II), regulated non-photochemical quenching Y(NPQ), and unregulated non-photochemical quenching Y(NO). (**B**) Raw steady-state fluorescence yield F' in volts (V) and (**C**) 1-qL values in the light phases were recorded simultaneously to (A) and averaged per replicate (N=3 ± SD, asterisk: significant difference ($p < 0.001$) as determined by t-test).

A lower Y(II) value, as found here in the absence of c_{6A}, indicates the existence of a blockade of electron transfer downstream of PSII. A block could be as far away as the PSI acceptor side (e.g. as seen for mutant strains without FLV proteins [65]) or as close as the PQ pool (e.g. as seen for the *tpt3* and *sta6* mutants with a more reduced PQ pool [276, 296]). From earlier results, a more reduced PQ pool seemed likely but measurements of PSI activity (section 4.2.2.4) and the PQ pool redox state (see below) under DISCO Light were carried out to clarify the reason for the lower PSII quantum yield.

For the regulated non-photochemical Y(NPQ) (figure 4.16A), differences between c_{6A}-KO and WT emerged over the course of 40 min DISCO Light. At the beginning, dark-adapted samples from both strains exhibited Y(NPQ) values of 0, however with increasing time, c_{6A}-KO showed an increased Y(NPQ) level compared to WT. While WT Y(NPQ) relaxed in dark phases to nearly zero, even after 35 min in DISCO Light, c_{6A}-KO had a sustained Y(NPQ) response in the dark. This c_{6A}-dependent difference is in agreement with previous observations (section 4.2.1.3) and points to increased stress levels in absence of c_{6A} while NPQ mechanisms are functional.

Increased stress levels in the absence of c_{6A} were also found when examining non-regulated non-photochemical quenching Y(NO) (figure 4.16A). This parameter describes the fraction of energy that is neither used for photochemistry nor released in a regulated way via NPQ. Elevated Y(NO) therefore highlights substantial difficulties of the algae with the light conditions and points to PSII damage that is imminent or has already occurred [186]. At the start of DISCO Light exposure, over 90% of light energy was dissipated in a non-regulated fashion in c_{6A}-KO, while WT had values of below 80%. A relaxation of Y(NO) levels in c_{6A}-KO occurred over the course of 40 min DISCO Light, eventually nearing WT levels of about 70%, as the regulated process of NPQ took over.

The parameters discussed above were calculated from fluorescence traces after application of saturating pulses. However, the raw fluorescence also contains valuable information if, like here, samples are normalised to have the same chlorophyll amount. The value of steady-state fluorescence yield F', i.e. the fluorescence yield during illumination with the actinic light treatment before application of a saturating pulse, is influenced by, amongst other things, the redox state of the PQ pool, as the PQ pool is in a redox equilibrium with Q_A in PSII [247, 263]. F' during DISCO Light exposure was therefore compared between c_{6A}-KO and WT (figure 4.16B). The increase of F' in reaction to actinic light was clearly visible for both strains. While WT exhibited fluorescence values of around 0.3 volts (V), c_{6A}-KO basal fluorescence was increased to over 0.4 V in the light phases. From investigation of the saturating pulse kinetics traces, this increased F' was also found to contribute to the lower Y(II) values described above and indicates that the lower Y(II) is likely due to a more reduced PQ pool

in c_{6A}-KO. Increased F' values were also observed in *A. thaliana* for multiple mutants of proteins involved in photosynthesis, like STN7 or PGR5 [260]. The authors explained this observation with the imbalance of light harvesting in these mutants that leads to accumulation of electrons between the two photosystems, i.e. a more reduced PQ pool.

Another indicator for the redox state of the PQ pool is the value 1-qL (figure 4.16C) [261]. For WT, a high value of 0.9 for 1-qL indicated that Q_A and in extension the PQ pool is highly reduced in the light. The c_{6A}-KO, however, surpassed this highly reduced state exhibiting 1-qL values of around 0.975 in the light. A more reduced Q_A could also lead to more damage to PSII via the formation of ROS [297], possibly contributing to the observed growth penalty. The finding of a more reduced PQ pool in the absence of c_{6A}, in turn leading to more reduced Q_A, is in agreement with previous chlorophyll fluorescence analyses, like OJIP and light curves (sections 4.2.1.5 & 4.2.1.3).

Taken together, the investigation of PSII under DISCO Light revealed that a more reduced PQ pool in c_{6A}-KO seems likely to cause a lower PSII quantum yield and ultimately leads to a growth phenotype under these conditions. The absence of a growth phenotype under continuous light conditions suggests that the effect that c_{6A} has on the PQ pool and PSII can be alleviated by other mechanisms if *C. reinhardtii* is not exposed to stressful dark-light transitions.

4.2.2.3 The proton motive force is not affected by c_{6A} in DISCO Light

Measurements of *b* hemes redox kinetics suggested that c_{6A} might be involved in the normal function of the Q-cycle, although no evidence could be found for this hypothesis when measuring pmf via ECS under continuous light. However, exposure to stressful light conditions like DISCO Light might lead to the emergence of c_{6A}-dependent differences. Additionally, a lower Y(II), as observed for c_{6A}-KO under DISCO Light, could also lead to a lower pmf, ultimately causing a growth phenotype due to lowered ATP synthesis. Photomixotrophic cultures of WT, c_{6A}-KO and c_{6A}-OE grown in continuous light were therefore exposed to a DISCO Light regime in a Dual-PAM-100 with a P515 measuring head. DIRKs were recorded in every light phase to determine pmf, proton flux (vH^+), and proton conductivity (gH^+). In the dark phases no DIRK could be recorded, because no actinic light was present that could have been turned off (figure 4.17).

In the first fluctuating light phase of DISCO Light, all strains exhibited high levels of pmf in the first 12 s (figure 4.17A). The subsequent 12 s light phases of the first fluctuating light phase, led to a reduction of pmf by around 25% for all strains. After the subsequent

dark phases, all strains exhibited the same pattern with similar starting values as in the first fluctuating light phase but a slightly faster decrease to a level that was held in the last two 12 s light phases. No statistically significant differences were found for pmf, although the WT trended at slightly increased pmf values compared to the c_{6A} mutant strains. The downward trend during the fluctuating light phase indicates that there is an up-regulation of pmf dissipation, although the return to starting levels after each 2 min dark phase suggests that no sustained activation of pmf dissipation is taking place.

Monitoring of proton flux (vH^+) did not reveal any significant differences between WT, c_{6A}-KO, and c_{6A}-OE (figure 4.17B). For all three strains, during the three fluctuating light phases, a small increase of vH^+ was followed by a decrease to near starting levels. The proton conductivity (gH^+) exhibited an inverse trend to pmf, increasing during the fluctuating light phases to a maximum and returning to close to the original levels after the 2 min dark phases (figure 4.17C). Again, no statistically significant differences between the strains were found. The return to near starting levels after the dark phases suggests that 2 min of darkness are enough to return the ATP synthase into a nearly fully dark-adapted state in *C. reinhardtii*. While the 12 s dark periods did not seem to lead to a down regulation of ATP synthase activity, 2 min dark led to a near reset. This could be important for explaining why a growth phenotype was observed for DISCO Light but not under a 12 s on/off cycle.

The pmf measurements described above were normalised to the magnitude of ECS change caused by a single turnover (ST) flash. The ECS signal in response to this ST flash also contains valuable information about electron transfer in the PETC and was therefore compared between WT, c_{6A}-KO and c_{6A}-OE (figure 4.17D). No differences between the strains were observed. All three strains exhibited a fast rise in ECS signal in direct response to the ST flash on an unresolved timescale (known as "a" phase, associated with charge separation in PSI and PSII), followed by a small increase and steady state ("b" phase, associated with b_6f electron flow) and a slow decay of the ECS signal ("c" phase, associated with charge leakage through ATP synthase) [198]. The absence of differences between the strains renders it unlikely that any of those processes are directly affected by c_{6A}. Especially the "b" phase similarities between all strains gives evidence to discard the hypothesis that c_{6A} is affecting the Q-cycle directly.

After the exposure to the DISCO Light regime (figure 4.17A-C), relaxation of the ECS signal in darkness was recorded to determine ΔpH and $\Delta\Psi$ contributions (figure 4.17E). All strains exhibited a partitioning of pmf slightly in favour of ΔpH but close to the 1:1 ratio reported before for *C. reinhardtii* [277], without showing significant differences between them. This suggests that ion channels are not specifically involved in the c_{6A}-dependent differences observed.

In summary, no c_{6A}-dependent differences were found in ECS measurements under DISCO Light, making direct involvement of c_{6A} in processes of pmf generation and dissipation seem unlikely. Thus, these processes are likely not the reason for the observed growth phenotype. Additionally, it suggests that the growth phenotype is not due to ATP synthesis limitation.

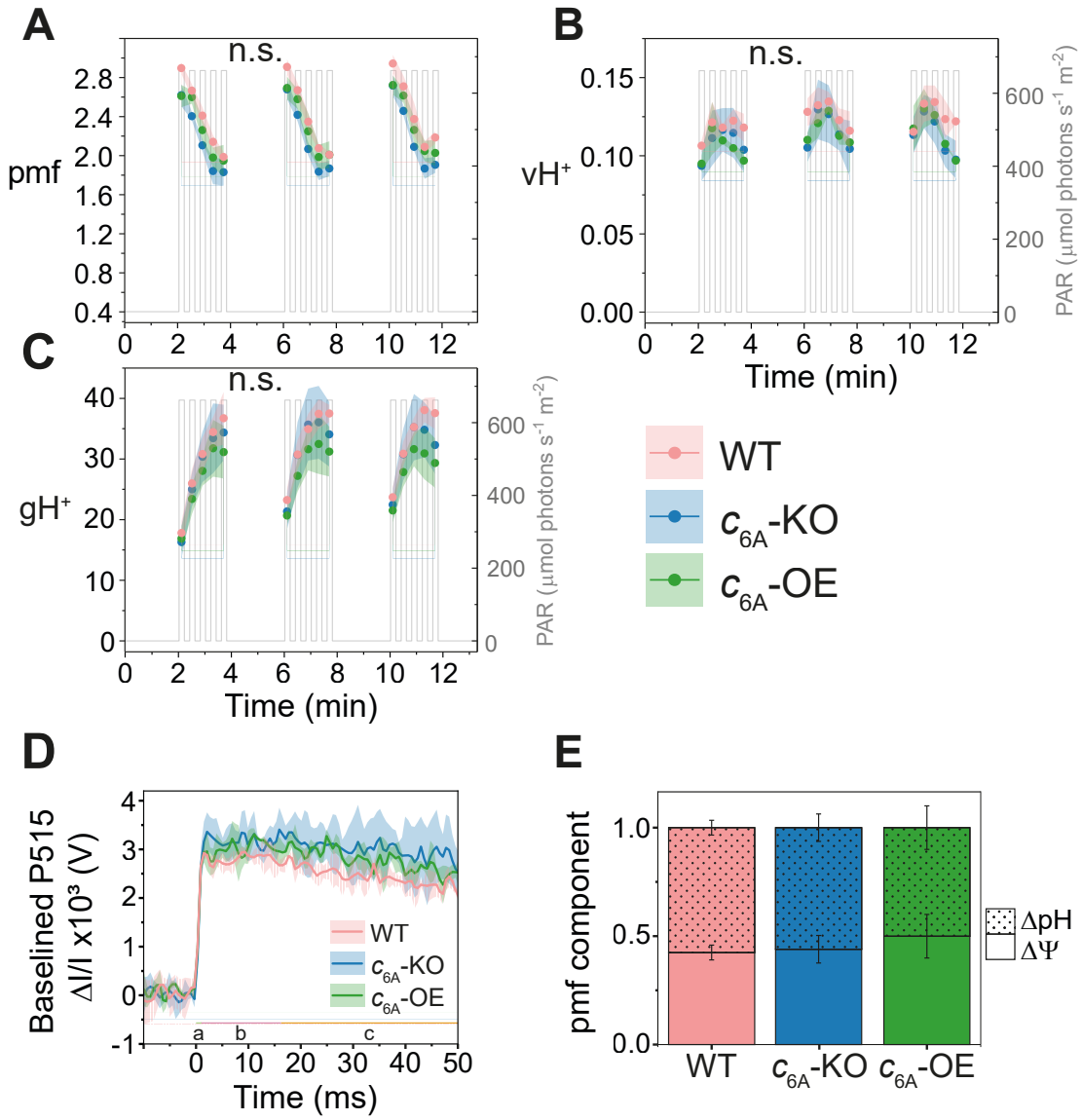


Figure 4.17: Electrochromic shift measurements (ECS) of *C. reinhardtii* c_{6A} mutant strains and WT under DISCO Light. Photomixotrophic exponential growth phase cultures were exposed to a DISCO Light regime (grey traces in A-C) in a Dual-PAM-100 spectrometer (N=3 ± SD). Dark interval relaxation kinetics (DIRKs, indicated by points) were used to determine (**A**) proton motive force pmf (normalised to the ECS signal of a single turnover flash in D), (**B**) proton flux vH^+, and (**C**) proton conductivity gH^+ and recorded in the middle of each 12 s light phase of the DISCO Light protocol. (**D**) The ECS response to a single turnover flash (applied at t = 0 ms) was recorded before the start of the DISCO Light protocol and the different phases (a-c, section 4.1.2.3) are marked for reference. (**E**) The partition of pmf into ΔpH and ΔΨ was determined at the end of the light protocol. No significant differences were found when employing repeated measure ANOVAs (for A-C).

4.2.2.4 Cytochrome c_{6A} does not majorly affect PSI function in DISCO Light

To investigate if there is an effect of c_{6A} on PSI that could explain the growth phenotype under DISCO Light conditions, samples from c_{6A}-KO and WT grown photomixotrophically in continuous light were exposed to a DISCO Light regime in a Dual-PAM-100 spectrometer while P700 differential absorbance was recorded. Application of saturating pulses allowed the determination of PSI quantum yield Y(I), acceptor-side limitation Y(NA) and donor-side limitation Y(ND) in light and dark phases of DISCO Light (figure 4.18A).

Firstly, PSI quantum yield Y(I) was examined (figure 4.18A). In the light phases of DISCO Light (values below 0.25 in the white boxes) no difference between c_{6A}-KO and WT could be observed and values for both strains changed from just under 0.2 to about 0.125 over the course of a 40 min exposure. This decrease indicates DISCO Light leads to less electron flow through PSI. A more pronounced decrease of Y(I) was found for dark periods, where values for c_{6A}-KO and WT decreased from over 0.8 to around 0.5 with a slightly steeper slope for WT than c_{6A}-KO, although with only marginal differences between the strains.

Acceptor side limitation Y(NA) (figure 4.18A) rose quickly with light exposure for both c_{6A}-KO and WT, having been initially higher in the light phases for c_{6A}-KO. The sustained increase of Y(NA) even during darkness accounts for the decrease of Y(I) in darkness over the 40 min of the experiment. Interestingly, in WT, Y(NA) levels fluctuated with light and dark exposure throughout 40 min of DISCO Light, while in c_{6A}-KO Y(NA) levels were the same between light and dark after 20 min but increasing slightly with time and averaging at the same levels Y(NA) in WT. The high and increasing acceptor side limitation found here for both strains indicates that electron sinks on the acceptor side of PSI, like the CBB cycle or alternative electron flow routes including CEF, are not fully active or upregulated in *C. reinhardtii* when exposed to DISCO Light and reducing equivalents are building up on the acceptor side of PSI. Sustained electron transfer away from PSI seems therefore not to occur which could lead to damage at PSI [60]. An explanation for the absence of fluctuations in Y(NA) in c_{6A}-KO compared to WT could be the more reduced PQ pool in c_{6A}-KO. While in WT, a portion of ferredoxin could be re-oxidised in the dark periods via CEF, in c_{6A}-KO the more reduced PQ pool would much reduce the extent of this re-oxidation via CEF.

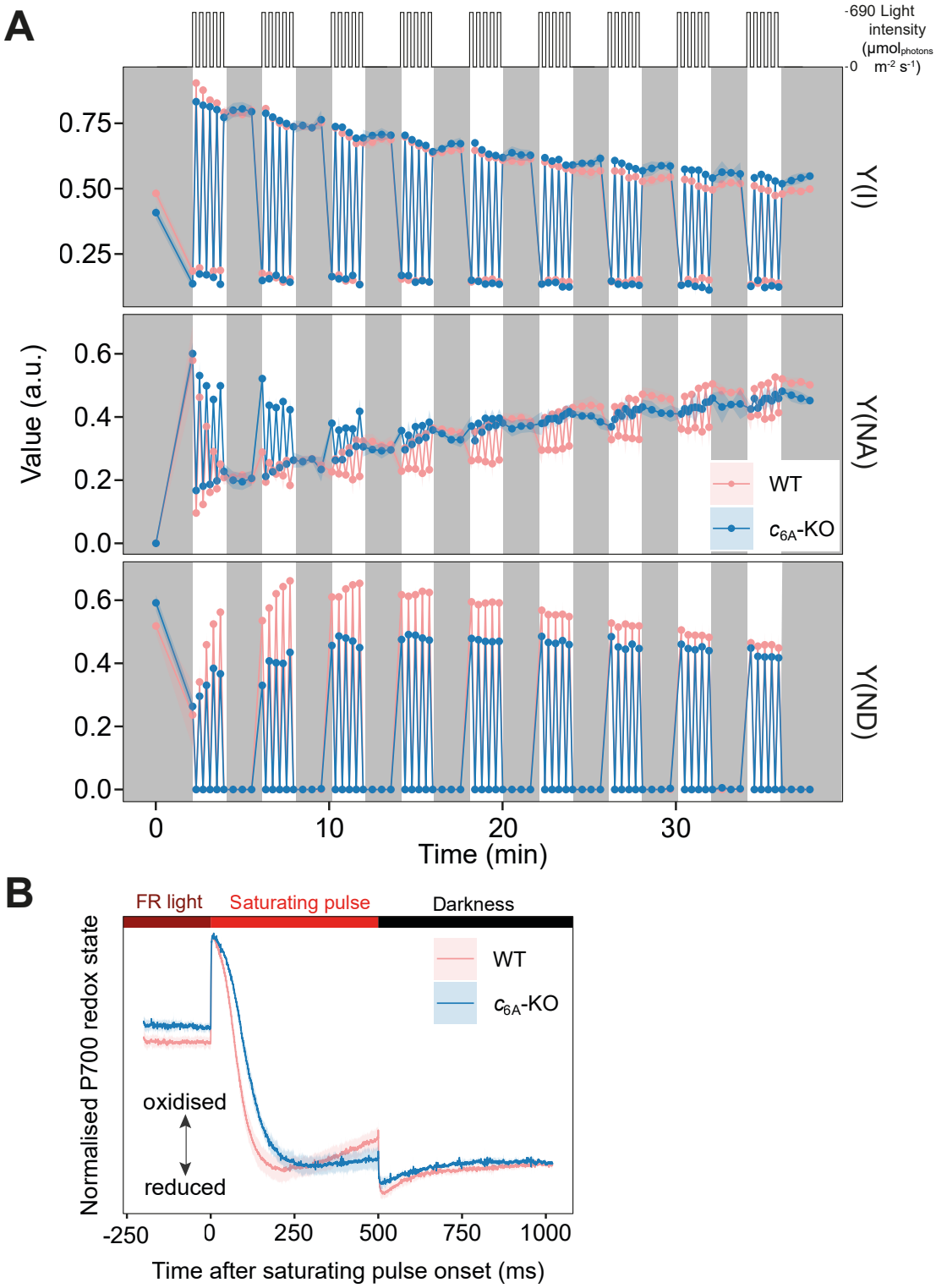


Figure 4.18: Measurements of photosystem I parameters of c_{6A}-KO and WT under DISCO Light conditions. Photomixotrophic exponential growth phase cultures were applied to a glass fibre filter and exposed to a DISCO Light regime in a Dual-PAM-100 spectrometer where grey boxes represent darkness and white boxes represent 2 min of 12 s on/off as depicted above the Y(I) panel (N=3 ± SD). (**A**) The effect of saturating pulses on P700 differential absorbance was used to calculate photosystem I quantum yield Y(I), acceptor-side limitation Y(NA) and donor-side limitation Y(ND). (**B**) Fast kinetics traces of P_M determination (12s far-red (FR) light, 500ms saturating pulse, then dark) of the samples in (A) were normalised to maximum and dark level.

The most pronounced differences for PSI parameters between c_{6A}-KO and WT were observed in donor-side limitation Y(ND) in the light phases of DISCO Light (figure 4.18A). While WT exhibited a fast increase to Y(ND) levels of over 0.6 within 8 min, c_{6A}-KO showed a smaller increase to a relatively constant level of less than 0.5. After 40 min of DISCO Light, Y(ND) of WT had decreased to similar levels as Y(ND) of c_{6A}-KO. This c_{6A}-dependent difference could be explained by a more reduced PQ pool in c_{6A}-KO as found before. A low PSI/PSII ratio as observed in section 4.2.1.1 would also align with these findings, as a more reduced donor-side of PSI in red light could be observed due to increased relative PSII activity.

The first data point in darkness in figure 4.18A reflects the measurement of P_M, the maximum oxidised level of P700, where 12 s of far-red light were followed by a saturating pulse. Here, a small difference between c_{6A}-KO and WT was observed which could be further resolved with the normalised fast kinetics traces of the saturating pulse employed for measurement (figure 4.18B). The slightly more oxidised level of P700 in c_{6A}-KO under far-red illumination translated into an increased donor-side limitation and lower Y(I) compared to WT, as seen in figure 4.18A. The subsequent reduction by the saturating pulse is also somewhat slower in c_{6A}-KO than in WT, agreeing with an increased donor-side limitation after pre-exposure to far-red light. As far-red light primarily excites PSI, a decrease in electron flow back to the donor-side of PSI is likely underlying this observation. A lower amount of PSI associated antennae or inhibited CEF could therefore contribute to the observed increase in Y(ND) of c_{6A}-KO under far-red light, the former being consistent with 77K fluorescence measurements (sections Section 4.2.1.1 & 4.2.2.1). For a direct inhibitory effect of c_{6A} on CEF, a sustained increase in Y(NA) during actinic light exposure for c_{6A}-KO would be expected, as has been observed for a knockout of PGR5 [65]. This is not the case here, rendering it unlikely that c_{6A} is directly involved in CEF. Additionally, the higher Y(ND) due to far-red light is in contrast to the lower donor-side limitation of c_{6A}-KO when exposed to the red light of the DISCO Light protocol. This indicates that the c_{6A}-dependent difference in photosynthesis is affected by the balance of light mainly exciting PSI or PSII. An imbalance between PSI and PSII light harvesting (section 4.2.1.1) could therefore help explain this observation.

In summary, it can be concluded that PSI function is not majorly influenced by c_{6A}, with the few observed changes in PSI activity in c_{6A}-KO (including decreased donor-side limitation) being consistent with an over-reduced PQ pool. Hence, a difference in PSI function is unlikely to contribute to the emergence of the DISCO Light growth phenotype. Additionally, it can be inferred that the lowered PSII quantum yield in c_{6A}-KO is not due to malfunction of PSI.

4.3 Conclusion & Outlook

4.3.1 Summary of findings from biophysical investigation of the PETC of *C. reinhardtii* c_{6A} mutant strains

Employing a wide range of biophysical techniques, multiple effects of c_{6A} on the PETC of *C. reinhardtii* were discovered under continuous light, despite the absence of an obvious a growth phenotype. Firstly, a c_{6A}-dependent difference in light harvesting balance in photomixotrophic conditions was found using 77 K fluorescence (section 4.2.1.1). This difference was shown not to be due to major state transitions defects in c_{6A}-KO in photomixotrophy, however altered state transition rates could not be excluded (section 4.2.1.2). The origins of the observed light harvesting balance difference therefore remain to be investigated further (see chapters 5 & 6 for biochemical analyses). Light response curves of photosystem performance revealed no influence of c_{6A} on PSI and only slight effects on PSII functionality in continuous light, although elevated NPQ and a more reduced PQ pool were found in the absence of c_{6A} (section 4.2.1.3). Employing OJIP curves, the finding of a more reduced PQ pool in the absence of c_{6A} was once again established (section 4.2.1.5). The most prominent c_{6A}-dependent difference was found in the redox kinetics of *b* hemes, where in photomixotrophy light exposure led to oxidation of *b* hemes in the absence of c_{6A}, contrasting the normal light-induced reduction in WT and c_{6A}-OE (section 4.2.1.6). The changes to *b* hemes redox kinetics could be explained by the difference in PQ pool redox state and were found to be unlikely due to a dysfunctional Q-cycle, as determined by ECS measurements (section 4.2.1.7). Finally, oxygen measurements rendered unlikely an involvement of respiratory processes and PTOX2 activity in c_{6A}-dependent differences (section 4.2.1.8).

Taken together, a role for c_{6A} in the maintenance of a normal PQ pool redox state and light harvesting balance emerges. These two fundamental balances of photosynthesis are tightly linked. A more reduced PQ pool in c_{6A}-KO could be consequence of an altered light harvesting balance in favour of PSII, e.g. as found in the lower PSI/PSII fluorescence ratio. On the other hand, a more reduced PQ pool should lead to changes in light harvesting by promoting state transitions towards PSI, contradicting the 77 K fluorescence data collected here. This result implicates state transitions in the effect of c_{6A} on the PETC. Additionally, a more reduced PQ pool could also affect PSII performance, although altered PSII performance was not found when exposed to continuous light.

When exposed to DISCO Light, however, PSII performance was indeed affected, as evidenced by a lower PSII quantum yield in absence of c_{6A} (section 4.2.2.2), further supporting

the PQ pool hypothesis and providing an explanation for the DISCO Light growth phenotype. Furthermore, an increased NPQ level was observed in the absence of c_{6A}, indicating increased stress levels in c_{6A}-KO. Additional DISCO Light investigation showed that the c_{6A}-dependent light harvesting balance phenotype observed under continuous light was amplified when *C. reinhardtii* was grown under DISCO Light (section 4.2.2.1). PSI parameter determination suggested that PSI is not likely to be the underlying reason for the DISCO Light growth phenotype but further supported the PQ pool hypothesis (section 4.2.2.4). The generation and dissipation of the pmf was not affected by c_{6A} under DISCO Light conditions making ATP limitation unlikely to underlie the DISCO Light phenotype (section 4.2.2.3). It is unclear how the pmf remains unchanged in c_{6A}-KO under DISCO Light, despite a lower PSII activity being observed. It suggests that water splitting continues as normal contributing to pmf, while some of the electrons released from it cannot be used for photochemistry as the PQ pool is already more reduced than normal. This could lead to ROS production at PSII [297] and thereby lead to a growth penalty. Alternatively, a sub-optimal ATP/NADPH ratio could also be underlying the growth difference.

4.3.2 Further work

Future work should entail experiments that study further biophysical findings presented above as well as explore the established routes towards a detailed mechanistic understanding of the function of c_{6A}.

For the former, direct HPLC measurement of the PQ pool redox state [298] of c_{6A} mutant strains would be invaluable, to confirm c_{6A}'s involvement in the PQ pool redox balance. A complementary approach to 77 K fluorescence spectra for estimation of PSI/PSII ratio can be found in ECS measurements. Quantifying the ECS in response to a single turnover flash with or without PSII-blocking reagents allows the calculation of the ratio of active reaction centres [198]. While the ability for state transitions was in principle present in c_{6A}-KO, a more detailed time-resolved investigation of state transitions should be carried out with chlorophyll fluorescence measurements to examine the reason for the lowered PSI/PSII ratio in both states in the absence of c_{6A}. Furthermore, examining the phosphorylation status of LHCII antennae would be helpful in clarifying any involvement of the kinase or phosphatases facilitating state transitions. That the absence of c_{6A} is the reason for the lower PSII quantum yield when exposed to DISCO Light could be validated by repeating the same experiment with c_{6A}-OE. Measuring oxygen evolution of c_{6A} mutant strains when exposed to DISCO Light would provide a further way to investigate if the lowered PSII quantum yield is the reason for the growth phenotype. A more precise MIMS recording under DISCO Light would

enable distinction between lower PSII activity and more ROS production that could both lead to apparent lower oxygen evolution as measured by an oxygen electrode. Measuring ROS as well as NADPH and ATP levels (feasible with commercially available reagents) would allow for further investigation of the DISCO Light growth penalty and how it is connected to photosynthetic processes. Finally, determination of PSII and PSI parameters of c_{6A} mutant strains grown under DISCO Light would inform on the status of the PETC after exposure to DISCO Light for multiple days.

To increase our understanding of c_{6A}'s mechanism of action, further studies should question how c_{6A} influences the PQ pool. The indication found here that an altered light harvesting balance could be the reason, should be investigated first. Characterising the composition of the thylakoid membrane of c_{6A} mutant strains will clarify if an imbalance of photosystem complexes exists due to c_{6A} absence (section 5.2.3). This could also aid in determining reasons for the c_{6A}-dependent difference in light harvesting. Analyses on c_{6A}-dependent changes of protein and transcript level could then inform on a putative regulatory role of c_{6A} in response to difficult light conditions (chapter 6).

5

Localisation of cytochrome c_{6A} and its effect on thylakoid membrane complexes

5.1 Introduction

5.1.1 Subcellular architecture of *C. reinhardtii*

The eukaryotic unicellular freshwater alga *C. reinhardtii* is a popular model organism in plant biology and exhibits a specific cellular structure (figure 5.1) [230, 299]. A typical *C. reinhardtii* cell is 5-10 µm in diameter and surrounded by a cell membrane and a cell wall, except for strains that are cell wall-less (cw15, section 3.1.1). Like other eukaryotes, *C. reinhardtii* cells contain a nucleus, mitochondria and Golgi bodies. Two anterior cilia are assembled from the basal bodies and facilitate movement through phototaxis, influenced by the eyespot. The cilia also play a crucial role in the organism's mating processes. The water balance of the cell is maintained through the activity of contractile vacuoles. The most prominent organelle of *C. reinhardtii* is its cup-shaped chloroplast that takes up a large part of the cell (~40% of the cell volume). In the basal area of the chloroplast is situated the pyrenoid, a carbon concentrating organelle and location of carbon fixation. This stromal structure is surrounded by a starch sheath. The presence of additional starch granules in the chloroplast stroma depends on the growth conditions. Plastoglobules, which are spherules of protein and lipids, are also frequently observed within the chloroplast.

The inner architecture of the chloroplast is defined by an extensive network of thylakoid membranes [300]. These membranes, which span the entire chloroplast, are mostly arranged in a parallel, lamellar configuration. While some thylakoids are stacked (ranging from 2 to 15 layers, typically 3 to 5), they are always interconnected by individual lamellae, akin to stromal lamellae found in plants. The thylakoid membranes house the photosynthetic machinery, which is differentially distributed between stacked and unstacked regions [301]. Special thylakoids are found traversing the pyrenoid as bundles of tubules. These tubules

are thought to be important for delivering CO_2 to RuBisCO which is mainly localised in the pyrenoid [302]. Importantly, the lumen of these thylakoids is continuous with that of the surrounding thylakoids outside of the pyrenoid. In consequence, soluble luminal proteins, such as plastocyanin, are evenly distributed throughout pyrenoid-traversing and chloroplastic thylakoids.

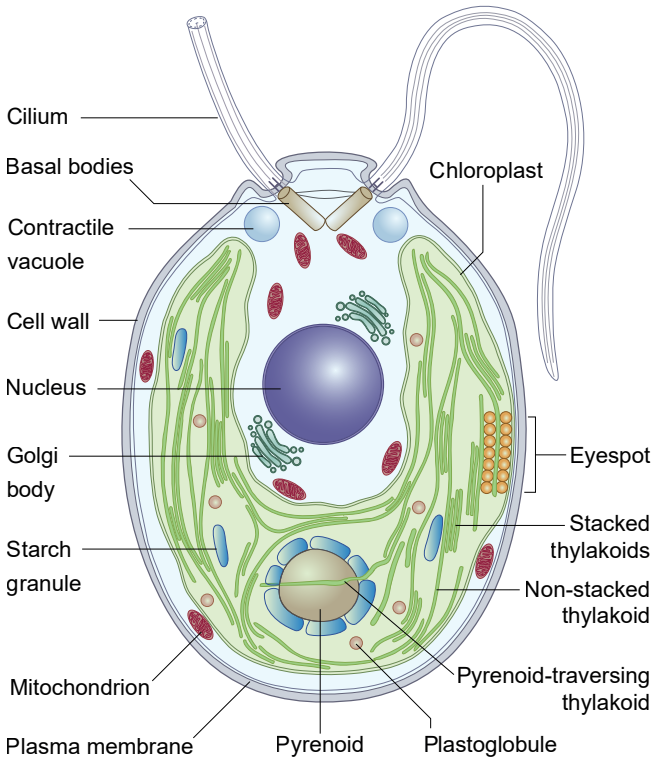


Figure 5.1: Diagram of the *C. reinhardtii* cell. Shown is an example of a walled cell with labels specifying the subcellular structures. Adapted from [230].

5.1.2 Protein complexes in the thylakoid membrane of *C. reinhardtii*

The thylakoid membranes of *C. reinhardtii* have a very high protein concentration of about 70% by area [303]. Most of these proteins are the complexes of photosynthetic electron transfer: PSII, PSI, their associated light-harvesting antennae LHCII and LHCI, the cytochrome b_6f complex and the ATP synthase.

PSII complexes of *C. reinhardtii* have been studied extensively [28, 300]. The dimeric PSII core complex (C2) consists of major subunits D1, D2, CP43, and CP47, along with 17 additional subunits. The additional subunits are membrane intrinsic or associated on the luminal side, such as the oxygen-evolving enhancer with the PSBO, PSBP and PSBQ subunits [304, 305]. The light-harvesting complex of PSII, LHCII, can form homodimeric symmetric PSII-LHCII complexes with the PSII core. Minor antenna proteins, CP26 and

CP29, maintain tight associations with the PSII core, while the LHCII subunits, LHCBM1-9, form a peripheral light-harvesting system. LHCII can form trimers that bind the PSII core with varying affinities, classified as strong (S), moderate (M), or loose (L). Consequently, PSII-LHCII complexes can exist in multiple configurations, with $C_2S_2M_2L_2$ being the largest known complex [305, 306], though the exact composition can change depending on light conditions [254].

C. reinhardtii's PSI complexes have also been of great interest [28, 300]. The PSI monomeric core comprises two large homologous subunits, PsaA and PsaB, along with several smaller subunits (PsaC-PsaL, PSAN, and PSAO)[307]. The LHCI antenna system, consisting of 9-10 *LHCA* gene products, forms belts around the PSI core. Up to ten LHCI complexes can bind to PSI, creating the large PSI-LHCI complex [308, 309]. Under certain conditions, such as state 2, a PSI-LHCI-LHCII supercomplex can form [310]. Additionally, PSI-LHCI dimers and PSI-LHCI-b_6f complexes have been identified, the latter of which was suggested to be involved in cyclic electron flow [46, 311].

As well as these chlorophyll-containing complexes, other proteins can also be found in the thylakoid membrane of *C. reinhardtii*. These include the cytochrome b_6f complex and the ATP synthase [301, 312]. Furthermore, NDA2, a chloroplast NADPH dehydrogenase that reduces the plastoquinone (PQ) pool can be found associated with the thylakoid membrane on the stromal side [38, 39].

The assembly of all these protein complexes involves a sophisticated process where proteins encoded in both the chloroplast and the nucleus must be correctly integrated into the thylakoid membrane. This process ensures the proper binding of pigments and other cofactors, critical for the functional integrity of the photosynthetic apparatus [313].

Isolation of the above listed complexes from *C. reinhardtii* can be achieved through detergent solubilisation followed by separation on a sucrose gradient or blue native PAGE (BN-PAGE). There are multiple methods to identify resolved complexes from a BN-PAGE. The classic approach of a second dimension SDS-PAGE (2D-PAGE) separates complex components by denaturing gel electrophoresis of a BN-PAGE lane. The resulting spot pattern in a vertical line below the BN-PAGE band is characteristic of the complex found in the band and can be further investigated using mass-spectrometry or immunoblots to identify proteins and ultimately the complex corresponding to the BN-PAGE band. The more recent technique of complexome profiling employs direct mass-spectrometric analysis of BN-PAGE bands to determine the composition of complexes and elucidate migration profiles of hundreds of proteins [314, 315]. Published data utilising both methods provide valuable comparisons for complex migration patterns.

In species like *A. thaliana* and *Synechocystis sp.* PCC 6803, well-characterised 2D-PAGE reference maps exist, with mass spectrometry (MS) data available for comparison [183, 316, 317]. However, *C. reinhardtii* exhibits unique photosystem-light harvesting complex arrangements, resulting in distinct banding patterns on BN-PAGE. This uniqueness underscores the necessity for species-specific reference maps to compare thylakoid membrane complex compositions accurately between experiments. For *C. reinhardtii*, only one notable investigation by Rexroth *et al.* (2003) was found that provided such a reference map of 2D-PAGE with subsequent MS identification [312]. There, identified complexes in order of decreasing size include: PSII-LHCII, PSI-LHCI, PSII dimer, ATP synthase, PSI, PSII monomer and LHCII trimer. Multiple PSII-LCHII complexes with varying amounts of bound antennae were observed. Some PSII cores were found even without the minor antennae. The PSI-LHCI complex was notably larger than those in plants and under photomixotrophic conditions, the authors observed PSI only without LHCI and did not observe PSI-LHCI. In contrast, under photoautotrophic conditions they observed PSI both with and without LHCI. Some spots on the published gels remained unidentified, even within assigned bands, emphasising that data on the exact composition of BN-PAGE bands was still missing. Another study reported 2D analysis with subsequent MS identification but did not present the underlying data [318]. Complexes identified in order of decreasing size included PSII-LHCII, PSI-LHCI, PSII dimer, ATP synthase, RuBisCO, PSI, PSII monomer, LHCII trimer, and LHCII monomer. Subsequent studies have often relied on previous literature for assignments or utilised western blot identification of bands, however often without sufficient detail on how bands were identified to allow others to assess the accuracy [319–324]. Despite these limitations, the overall order of bands by size has remained consistent, with PSII-LHCII being larger than the PSI-LHCI complex at the large end of the banding pattern and the smallest band corresponding to LHCII monomers.

Overall, this order is consistent with complexome profiling studies on *C. reinhardtii* thylakoids [325, 326]. However, some important differences are also apparent. While most BN-PAGE analyses mentioned above clearly separated PSII-LHCII and PSI-LHCI complexes, complexome profiling revealed multiple bands of both PSII-LHCII and PSI-LHCI. This resulted in PSI-LHCI and PSII-LHCII complexes overlapping in size order which could be due to variable amounts of antennae binding to the cores. PSII-LHCII complexes were generally larger than PSI-LHCI complexes, although one prominent band showed components of both photosystem-light harvesting complexes. It is therefore possible that different complexes migrate similarly on BN-PAGE. Interestingly, in one of the above complexome profiling studies where supplementary material was accessible at the time of writing, no c_{6A} was found in the mass-spectrometric analyses, suggesting that it does not form stable complexes with thylakoid membrane proteins [326].

5.1.3 Aims

The previously observed effects of c_{6A} on photosynthesis suggested that it has an impact on the light harvesting balance between the photosystems found in the thylakoid membrane (chapter 4). To examine this further, c_{6A}'s localisation in relation to the thylakoid membrane was investigated, a search for putative interaction partners was carried out, and c_{6A}'s effect on the formation of thylakoid membrane complexes was analysed.

5.2 Results & Discussion

5.2.1 Localisation of cytochrome c_{6A} in *C. reinhardtii*

To investigate the localisation of cytochrome c_{6A} within the cell of *C. reinhardtii*, three approaches were employed: fluorescent protein tagging, subcellular fractionation with subsequent immunodetection, and immunofluorescence.

5.2.1.1 Fluorescent protein-tagged localisation studies

A construct for expression of a fusion protein of c_{6A}-mVenus was created with Golden Gate cloning (pDKM-001, figure 5.2A). Paromomycin resistance was conferred through the *ParoR* gene, expression of which was directed by the chimeric *HR* promoter and the *RBCS2* terminator [26]. The expression of the native *C. reinhardtii* c_{6A} sequence (including introns) with a C-terminal mVenus tag was driven by the strong constitutive *PSAD* promoter and terminator [26]. The mVenus part also contained the artificially introduced intron 2 from the *RBCS2* gene that was found to increase transgene expression [327]. The fluorescent mVenus tag was chosen as its excitation and emission maxima do not overlap with chlorophyll fluorescence and because it has been shown to be functional in the chloroplast [26, 328].

Correct assembly of the construct was verified by Sanger sequencing. *C. reinhardtii* was then transformed with pDKM-001 and a number of paromomycin-resistant colonies were obtained. The presence of the construct in the transformants obtained was tested with colony PCR on twelve colonies (figure 5.2B). Primers were used that should bind inside the construct and produce a fragment of 3914 bp (arrows in 5.2A). For colonies 1, 5, 6, 10, and 12 the presence of the construct could be confirmed (figure 5.2B).

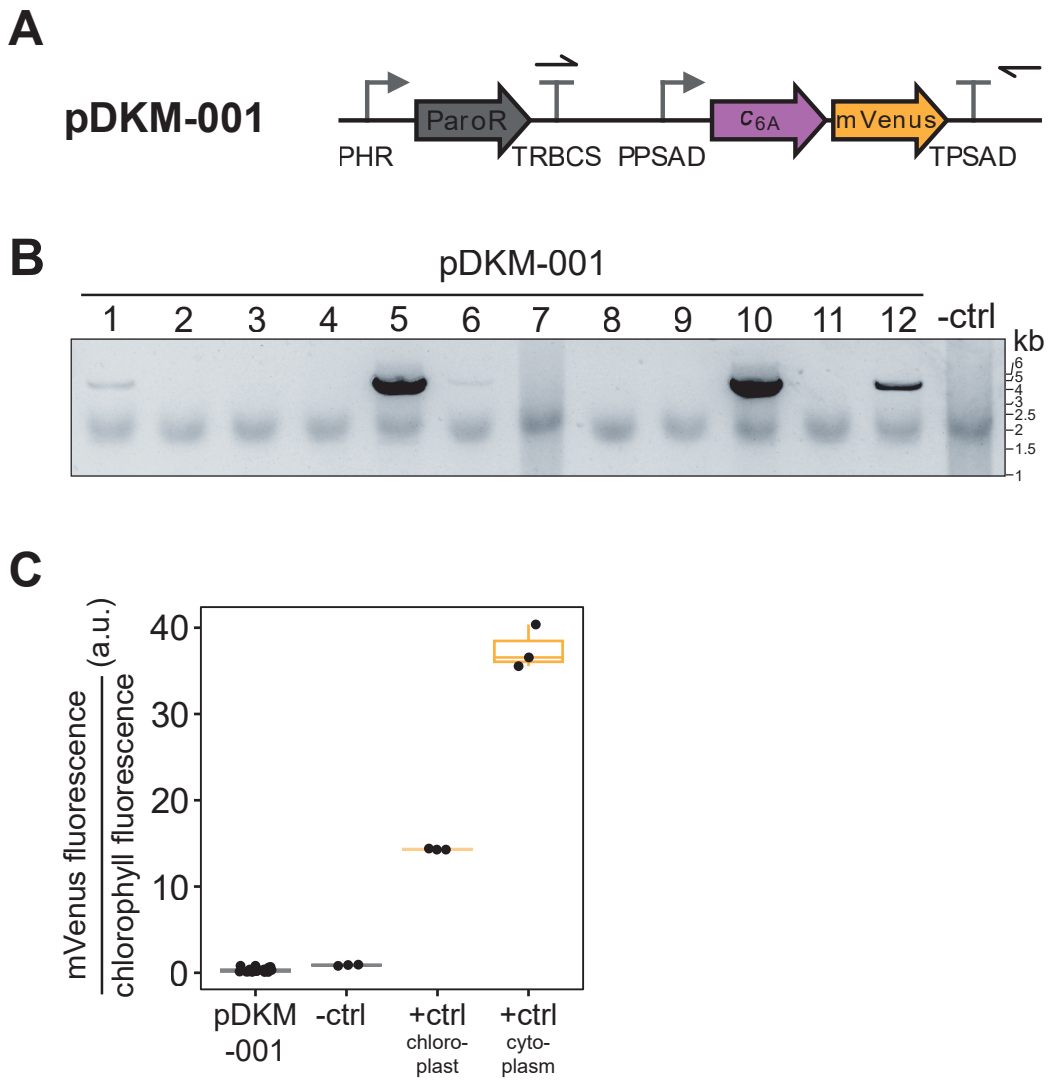


Figure 5.2: Creation of a mVenus-tagged cytochrome c_{6A} expression strain. (**A**) The c_{6A}-mVenus expression construct pDKM-001 was created using Golden Gate cloning and contains a paromomycin antibiotic resistance cassette and a c_{6A}-expression cassette with a C-terminal mVenus tag (the size of the coloured arrows is not representative of the DNA fragment size). The antibiotic resistance gene was under the control of the *HR* promoter and *RBCS2* terminator, while expression of c_{6A}-mVenus was directed by the *PSAD* promoter and terminator. The black half-arrows indicate the positions of primers used for colony PCR. (**B**) Colony PCR of 12 individual *C. reinhardtii* transformants confirmed the existence of the pDKM-001 c_{6A}-mVenus expression cassette in colonies 1, 5, 6, 10 and 12 (expected size: 3914 bp). The negative control (-ctrl) was the untransformed background strain. (**C**) Fluorescence of mVenus normalised to chlorophyll fluorescence was measured for single transformants (points) grown in a 96 well plate. The negative control (-ctrl) was the untransformed background strain and positive controls have been transformed with a construct for expression of chloroplastic or cytoplasmic mVenus (gift from Dr. Katrin Geisler, University of Cambridge).

To assess if presence of the construct also led to protein expression, mVenus fluorescence was measured from all colonies picked from the transformation plate after growth for 10 days

in photomixotrophic medium with supplemented antibiotic in a 96-well plate. Fluorescence of mVenus was normalised to chlorophyll fluorescence to correct for different cell densities of samples and an untransformed control (-ctrl) as well as two positive controls (+ctrl) were included in the measurements (figure 5.2C). The positive controls consisted of two *C. reinhardtii* strains that expressed mVenus localised to the chloroplast and the cytoplasm, respectively (gift from Dr. Katrin Geisler, University of Cambridge). The transformed colonies (pDKM-001) showed similarly low normalised mVenus fluorescence as the negative control (< 1). The positive controls, chloroplastic and cytoplasmic mVenus-expressing strains, exhibited 14- to 40-fold more mVenus fluorescence than chlorophyll fluorescence, respectively. Despite successful transformation, expression of a fluorescently tagged c_{6A} could thus not be confirmed with bulk fluorescence measurements.

Because the transformants shown in figure 5.2 were discarded after the negative results of the bulk fluorescence measurement, new samples were obtained by transformation to investigate if this lack of fluorescence in bulk was also reflected at the single cell level. Fluorescence microscopy of paromomycin-resistant pDKM-001 colonies as well as negative and positive controls was conducted (figure 5.3). The figure shows representative images after investigating samples from seven different paromomycin-resistant colonies. Utilising the same exposures for all samples, mVenus and chlorophyll fluorescence were recorded as well as a brightfield image. The transformants did not show fluorescence above the background level for mVenus, while in the chlorophyll channel the structure of the chloroplast was clearly distinguishable. This was the same observation as for the untransformed negative control. The positive control with cytoplasmic mVenus expression exhibited significantly more mVenus fluorescence that was localised to *C. reinhardtii* cells and did not overlap with the detected chlorophyll fluorescence signal, confirming the cytoplasmic localisation of mVenus in this sample. Fluorescence of c_{6A}-mVenus could thus not be detected in the transformants on a single cell level either.

Other constructs designed for the expression of c_{6A}-mVenus fusion proteins were also tested. These used three different approaches. First, a different mVenus part was used without the inserted intron *RBCS2*i2 but with a linker encoding six amino acids (GSGSGS) between c_{6A} and mVenus (Katrin Geisler, University of Cambridge). Second, only the region encoding the putative signal peptide of c_{6A} (from start to including VLA, TargetP2.0) was C-terminally tagged with the mVenus part with the *RBCS2*i2 intron. Lastly, an available Venus- and triple FLAG tagged construct with the c_{6A} gene (pLM005-Cre16.g670950-Venus-3xFLAG) was obtained from the repository of a large *C. reinhardtii* protein localisation project [329]. With these three other constructs the same absence of mVenus fluorescence was found as with pDKM-001 when investigated with bulk measurements in a plate reader and on single cell level using fluorescence microscopy.

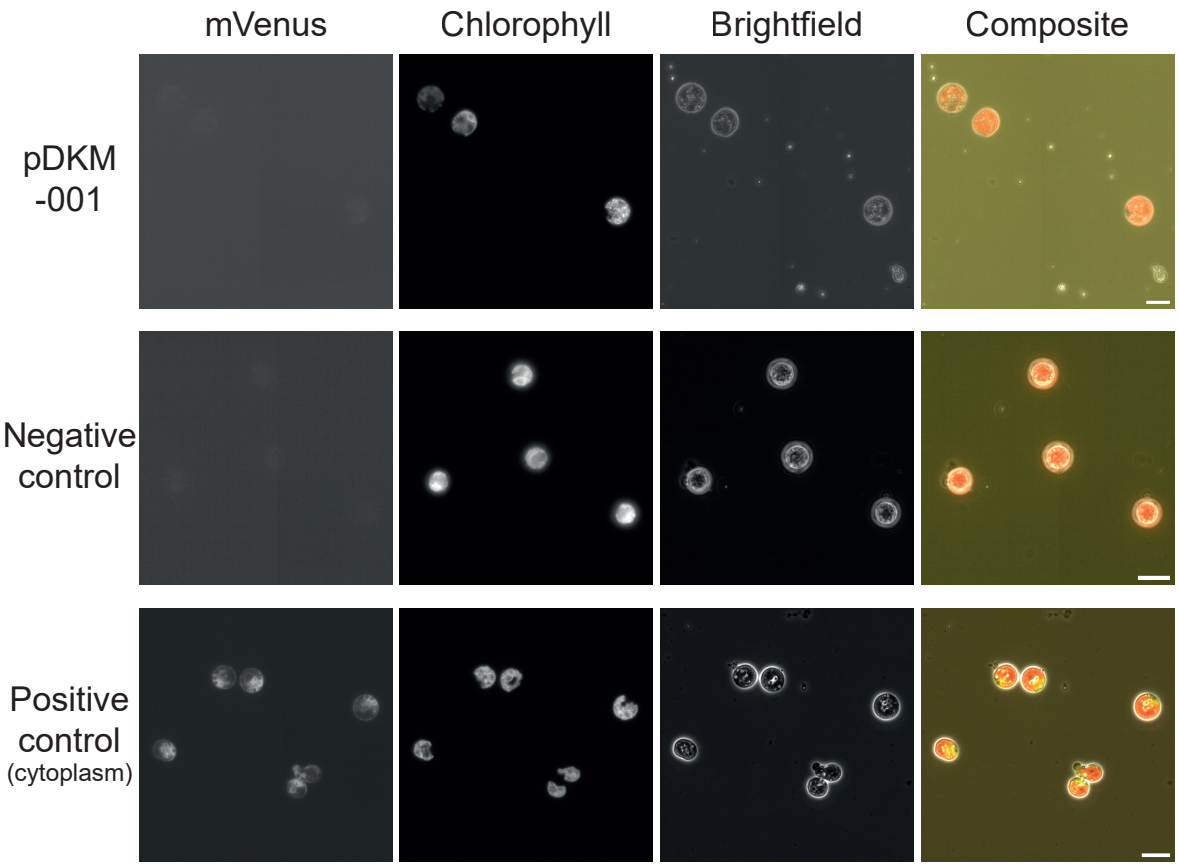


Figure 5.3: Fluorescence and brightfield microscopy of a putative c_{6A}-mVenus over-expressing *C. reinhardtii* strain (pDKM-001). One representative image is shown here, from seven individual transformants in total. The negative control was the untransformed background strain of pDKM-001 and the positive control expressed cytoplasmic mVenus (Dr Katrin Geisler, University of Cambridge). Using a 100x oil immersion lens, fluorescence was imaged for mVenus (525 nm excitation, yellow emission filter, 1 s exposure) and chlorophyll (635 nm excitation, red filter, 68 ms exposure) and a brightfield image was recorded as well (scale bar = 10 µm). In the composite, mVenus and chlorophyll fluorescence are shown in yellow and red, respectively.

The absence of mVenus fluorescence in successfully transformed *C. reinhardtii* could be due to various reasons. A lack of transcription of the transgene would lead to no protein and therefore no fluorescence. This is, however, unlikely to be the reason here, as other very similar constructs, such as pDKM-000 (section 3.2.2), led to sustained transgene expression. Nevertheless, reverse transcription (RT)-PCR on RNA from pDKM-001 transformants would be necessary to exclude this possibility conclusively. If there were transgene transcript, a fault in translation or protein folding could have led to the absence of mVenus fluorescence. A wrongly folded mVenus fusion protein would not fluoresce and might even be degraded.

Additionally, the import into or the environment of the proposed location of c_{6A}, the thylakoid lumen could present another challenge for correctly folding c_{6A}-mVenus into its fluorescent structure. However, other proteins that are similarly sized to c_{6A} (e.g. PSBP3,

PsbH or CYN20B) were found to be localised in the thylakoid lumen by fluorescently tagging them with Venus [282]. The reason for the absence of fluorescence could be further investigated by determining if the fusion protein is present by immunoblotting, which could also be a basis for further localisation studies utilising immunoreactivity-based techniques. However, a smaller tag than mVenus like a FLAG-tag would be more appropriate for these types of experiments.

In summary, a construct for overexpressing the fusion protein c_{6A}-mVenus was successfully introduced into *C. reinhardtii*. However, no mVenus fluorescence could be found, preventing localisation studies that relied on a fluorescently labelled c_{6A}.

5.2.1.2 Subcellular fractionation of *C. reinhardtii* overexpressing c_{6A}-FLAG suggests a thylakoid luminal localisation for c_{6A}

As an alternative approach to determining the localisation of c_{6A} within *C. reinhardtii* subcellular fractionation and subsequent immunoblotting were performed. Focusing on the putative localisation of c_{6A} within the chloroplast, the c_{6A}-FLAG overexpressing strain c_{6A}-OE (section 3.2.2) was used to isolate chloroplasts and then fractionate them. To obtain chloroplasts, cells were disrupted and fractionated on a Percoll gradient (figure 5.4).

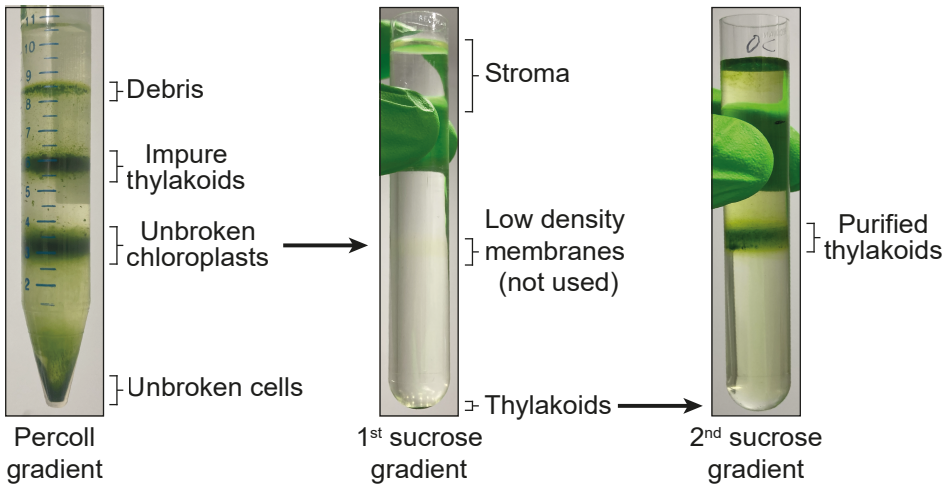


Figure 5.4: Images of the gradients used for subcellular fractionation of *C. reinhardtii*. Disrupted cells were fractionated on a Percoll gradient to obtain unbroken chloroplasts, which were subsequently osmotically lysed and fractionated into stroma (material that did not enter the sucrose gradient), low density membranes, and thylakoids (1st sucrose gradient). After isolation, the stroma fraction was concentrated in a centrifugal concentrator (3 kDa molecular weight cutoff). The low density membranes were not used further but the pellet with thylakoids was purified on a second sucrose gradient. The tubes were held up for imaging while wearing green coloured gloves.

The chloroplast fraction was then osmotically lysed and separated into stroma and thylakoid fractions using sucrose gradients following an established protocol [179]. The material from lysed chloroplasts that did not enter the sucrose gradient was isolated as the stromal fraction. This colour-less fraction was subsequently concentrated with a centrifugal concentrator. The low-density membranes isolated in the first sucrose gradient were not examined further, while the pellet contained thylakoids that were ultimately isolated from the interface of a second sucrose gradient. The resulting fractions of chloroplasts and thylakoids as well as a whole cell sample were investigated under a fluorescence microscope, to confirm their structural composition. Chlorophyll fluorescence and brightfield images were recorded and representative images are shown in figure 5.5.

In the whole cell fraction, chlorophyll fluorescence revealed the characteristic cup shape of the chloroplast, including a clear boundary for the pyrenoid. Brightfield imaging showed cell sizes ranging between 5 and 10 µm as well as visible flagella and the pyrenoid as a dark circular structure (black and white arrow in the brightfield image of the whole cells sample, respectively). The composite images exhibited some areas of the cells without chlorophyll fluorescence, suggesting an intact cellular structure.

Chlorophyll fluorescence of the chloroplast fraction showed similar structures as in the whole cells with thylakoid membranes and an area of lower fluorescence indicating presence of a pyrenoid (white arrows in the chlorophyll image of the chloroplast fraction). In brightfield images chloroplasts appeared smaller than whole cells, without visible flagella and a less prominent pyrenoid structure, possibly indicating disturbance of the pyrenoid structure during the isolation. In the composite image, except for one structure indicated by a black arrow, no structure exhibited areas lacking chlorophyll fluorescence suggesting largely successful separation of chloroplasts from unbroken whole cells. Another structure appeared different from other chloroplasts, possibly representing further breakage and release of thylakoid membranes (white arrow in the composite image of the chloroplast fraction). Other efforts for *C. reinhardtii* fractionation have resulted in fractions of similarly intact chloroplasts [178].

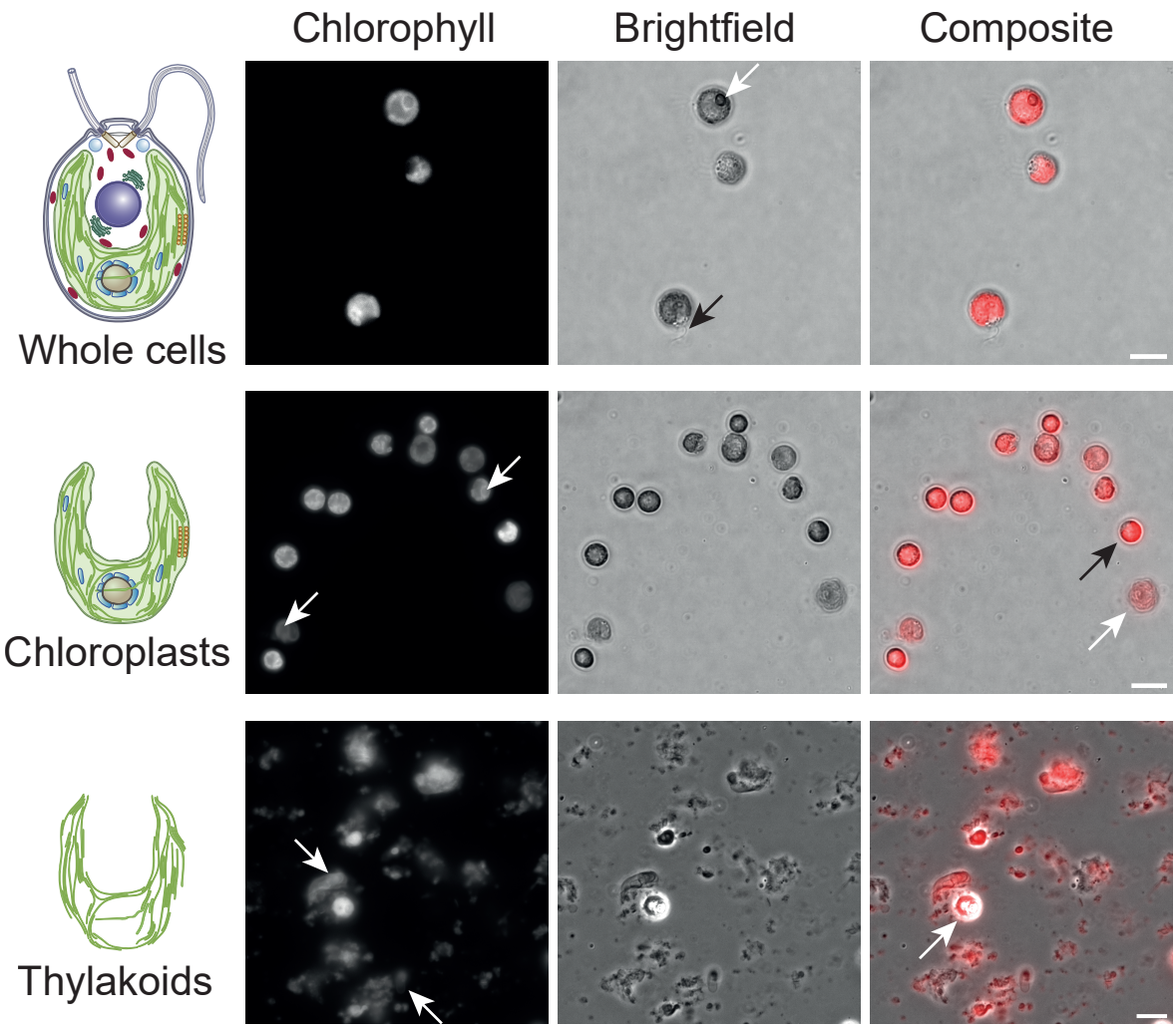


Figure 5.5: Fluorescence and brightfield microscopy of different subcellular fractions of a c_{6A}-FLAG overexpressing *C. reinhardtii* strain (c_{6A}-OE). Whole cells, chloroplasts and thylakoids were obtained by subcellular fractionation. Using a 100x oil immersion lens, fluorescence was imaged for chlorophyll (635 nm excitation, red filter, 40 ms exposure) and a brightfield image was recorded as well (scale bar = 10 µm). In the composite image, chlorophyll fluorescence is shown in red. The black and white arrows indicate specific structures mentioned in the text. Whole cells: white arrow - pyrenoid, black arrow - flagella. Chloroplasts: white arrows in chlorophyll image - pyrenoid area, black and white arrows in composite image - possibly unbroken cell and a putatively broken chloroplast, respectively. Thylakoids: white arrows in chlorophyll image - balloon-like structures, white arrow in composite image - possibly unbroken chloroplast.

In the thylakoid fraction, the regular structures observed in whole cells and chloroplasts were absent. Chlorophyll fluorescence appeared cloud-like and, in some areas, exhibited balloon-like structures with fluorescence enriched at the borders (white arrows in chlorophyll image of the thylakoids fraction). Many small fluorescent particles were also detected. Brightfield imaging showed no regular structures compared to whole cells and chloroplasts, except for one, potentially unbroken chloroplast (white arrow in the composite image of

the thylakoids fraction). It would be expected that isolated membranes would lack regular organisation. Together with the composite image, where all structures exhibited chlorophyll fluorescence, it could be concluded that these structures are chlorophyll-containing thylakoid membranes.

In summary, subcellular fractions of c_{6A}-OE could be isolated. From fluorescence microscopy, thylakoid and chloroplast fractions were found to exhibit low cross-contamination levels, providing a good basis for further analyses of the isolated fractions.

To investigate the proposed localisation of c_{6A} in the thylakoid lumen, a sample of the thylakoid fraction was treated with proteinase K, which digests all proteins that are not inside the thylakoid lumen, assuming intact thylakoid membranes. An additional sample was treated with proteinase K and Triton X-100, the latter of which permeabilises membranes and thus makes the thylakoid lumen accessible to the proteinase. A protein that is located in the lumen should thus be found in the sample with proteinase treatment but not in the sample with proteinase and Triton treatment. To determine the localisation of c_{6A}-FLAG in the previously isolated fractions and therefore within *C. reinhardtii*, denaturing protein gel electrophoresis and immunoblotting of the fractions was carried out (figure 5.6). Protein concentrations were measured with a Bradford assay to allow for equal protein loading for gel electrophoresis.

The stain-free method (BioRad) revealed total protein in all samples with different patterns over the protein size range investigated (10 to 70 kDa). While whole cell and chloroplast extracts appeared similar, the stromal fraction exhibited a highly abundant band just above 55 kDa, later identified as the large RuBisCO subunit. The untreated thylakoid fraction exhibited fewer high molecular weight protein bands and more abundant bands between 15 and 35 kDa. Proteinase treatment reduced overall protein abundance in the sample while proteinase+Triton treatment led to near complete disappearance of protein bands. For the treated thylakoid fractions, although proteinase was expected to decrease the overall protein content, the normalization to equal loading may have been affected by the presence of the proteinase, itself being a protein.
To investigate the purity of the fractions and aid in the determination of c_{6A}'s localisation, four different compartment markers were utilized. First, utilising a RuBisCO antibody as a stroma marker [302], a band at 55 kDa corresponding to the large RuBisCO subunit was found in whole cells, chloroplasts, and the stromal fraction but not in the thylakoid fractions. As RuBisCO is a highly abundant protein, its absence from the thylakoid fractions suggests that the thylakoid fractions were unlikely to be contaminated with stromal proteins.

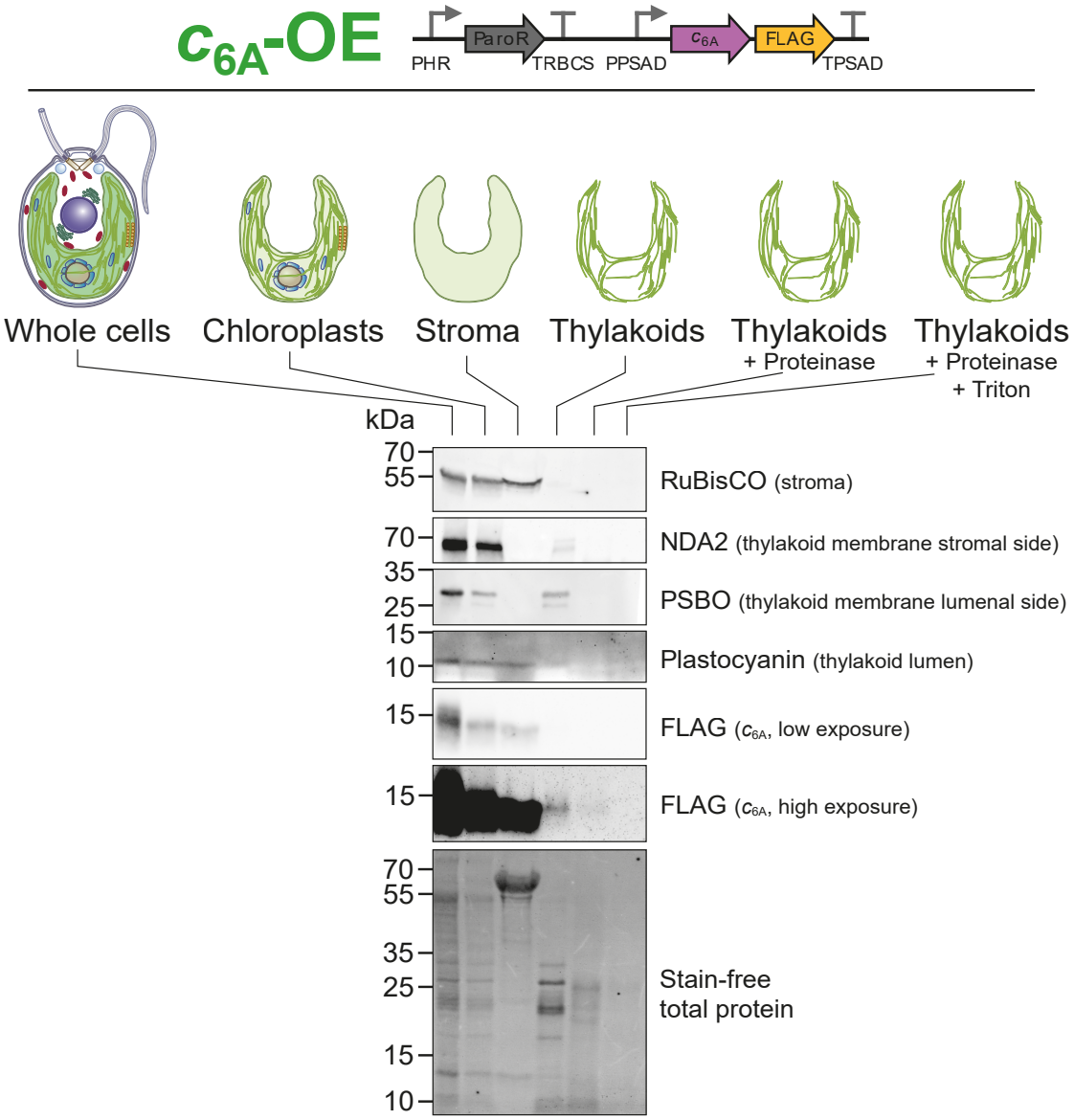


Figure 5.6: Immunoblot analyses of subcellular fractions of a c_{6A}-FLAG overexpressing *C. reinhardtii* strain (c_{6A}-OE). The construct pDKM-000 was used to create the strain c_{6A}-OE (section 3.2.2). Whole cells, chloroplasts, stroma, thylakoids and treated thylakoids (proteinase, proteinase + Triton) were obtained through subcellular fractionation and subjected to protein gel electrophoresis with subsequent immunoblotting. Four different compartment markers were utilised: RuBisCO (stroma), NDA2 (thylakoid membrane, stromal side), PSBO (thylakoid membrane, luminal side), and plastocyanin (thylakoid lumen). Two exposures of the anti-FLAG blot are shown, as well as the total protein visualisation as determined with the stain-free method (BioRad). 20 µg of protein (as determined with a Bradford assay) were loaded per fraction.

NDA2, localised in the thylakoid membrane facing the stromal side [38, 39], was detected with an NDA2 antibody in whole cells, chloroplasts and the thylakoid fraction but not in the stromal fraction, aligning with its known location. It was also absent from the treated thylakoid fractions, indicating digestion by proteinase with or without Triton.

The same pattern of distribution at just above 25 kDa was found for PSBO, a PSII subunit of the oxygen evolving enhancer associated with the thylakoid membrane on the luminal side [304]. However, the absence of PSBO in the proteinase treated thylakoid fraction (no Triton) suggested that luminal proteins were digested even without Triton, indicating potential damage to thylakoid membranes.

Lastly, plastocyanin was used as a soluble thylakoid lumen marker [330]. Bands at ~10 kDa corresponding with mature plastocyanin were found in whole cell, chloroplast, and stromal fractions, with a faint band in the untreated thylakoid fraction. The presence of plastocyanin in the stromal fraction suggested cross-contamination with soluble luminal proteins due to damaged thylakoids. Plastocyanin was undetectable in treated thylakoid fractions, further suggesting proteinase digestion of luminal proteins, consistent with damaged thylakoid membranes.

Using an anti-FLAG antibody, the presence of c_{6A}-FLAG in the isolated fractions was tested. Low exposure times during blot imaging revealed a c_{6A}-FLAG band around 15 kDa in whole cell, chloroplast, and stroma fractions but not in the thylakoid fractions. Longer exposure times showed an additional band at the expected size in the untreated thylakoid fraction and a very faint band in the proteinase-treated fraction but not in the proteinase+Triton fraction. Without taking into account the distribution pattern of the other proteins, from this subcellular fractionation analysis c_{6A} appeared to be localised mostly to the stroma and, in a much lower amount, to the lumen. The pattern observed for c_{6A}, however, was most similar to what was found for plastocyanin. Together with the indication of loss of membrane integrity, as observed in proteinase treated samples, this suggests that c_{6A} was more likely localised to the thylakoid lumen, the known localisation of plastocyanin.

Overall, two conclusions can be drawn from this experiment. First, the subcellular fractionation method employed here requires optimization to prevent thylakoid breakage and leakage of luminal proteins into the stroma fraction and to avoid proteinase treatments digesting luminal contents. Second, the distribution pattern of c_{6A}-FLAG looked most similar to that of plastocyanin distribution, suggesting that c_{6A} is actually located in the thylakoid lumen, despite a prominent band in the stromal fraction. More studies using complementary approaches to subcellular localisation are therefore needed to show this conclusively.

5.2.1.3 Immunofluorescence localisation studies of *C. reinhardtii* overexpressing c_{6A}-FLAG confirm a thylakoid luminal localisation of c_{6A}

A complementary method to subcellular fractionation for localisation studies, that also employs immunodetection, is immunofluorescence microscopy. Samples from cultures of the c_{6A}-FLAG overexpressing strain (c_{6A}-OE) and its background strain (c_{6A}-KO) grown under standard conditions were therefore probed with a FLAG-antibody, which was subsequently detected by a secondary antibody conjugated with the fluorescent dye AlexaFluor488. The fluorescence of AlexaFluor488, along with chlorophyll autofluorescence and a brightfield image, was recorded using a confocal microscope (two representative images are shown per strain in figure 5.7).

In the negative control (c_{6A}-KO), the brightfield images showed well-preserved cell structures, including flagella, pyrenoid, chloroplast, and cytoplasm, indicating that the fixation method was not overly harsh. Chlorophyll autofluorescence revealed the characteristic cup-shaped chloroplast structure and thylakoid membrane substructures, with a less fluorescent region corresponding to the pyrenoid (white arrows in c_{6A}-KO chlorophyll images in figure 5.7). The AlexaFluor488 signal in these cells was distinguishable from the background but did not show strong fluorescence. No specific staining of cell structures was found, as chloroplast, flagella and cytoplasm all exhibited fluorescence signal.

In the c_{6A}-FLAG overexpressing sample (c_{6A}-OE), brightfield images were similar to the background control, with intact cells displaying a distinguishable pyrenoid, chloroplast, cytoplasm, and flagella. The chlorophyll autofluorescence also mirrored the background control. However, the AlexaFluor488 fluorescence signal was more intense and more localised in the c_{6A}-OE strain than in c_{6A}-KO. The stain assumed the shape of the chloroplast and was not present in the cytoplasm or flagella, confirming chloroplast-specific localisation of c_{6A} [169]. Additionally, z-stack images were recorded, allowing deconvolution of the fluorescence signal and thereby increasing its resolution. This enabled the detection of a clear anti-FLAG signal from structures resembling pyrenoid-traversing thylakoids (red arrows in figure 5.7) [331], providing strong support for a thylakoid luminal localisation of c_{6A} in *C. reinhardtii*. Similar signals from pyrenoid-traversing thylakoids have been detected for other lumen localised proteins such as the PSII component PSBP3 [328], the PSII assembly factor HCF136, or plastocyanin [329]. While these signals were detected from Venus labelled proteins, Wang *et al.* (2023) were also able to show good agreement between localisation inferred from fluorescent protein and immunofluorescence studies [329].

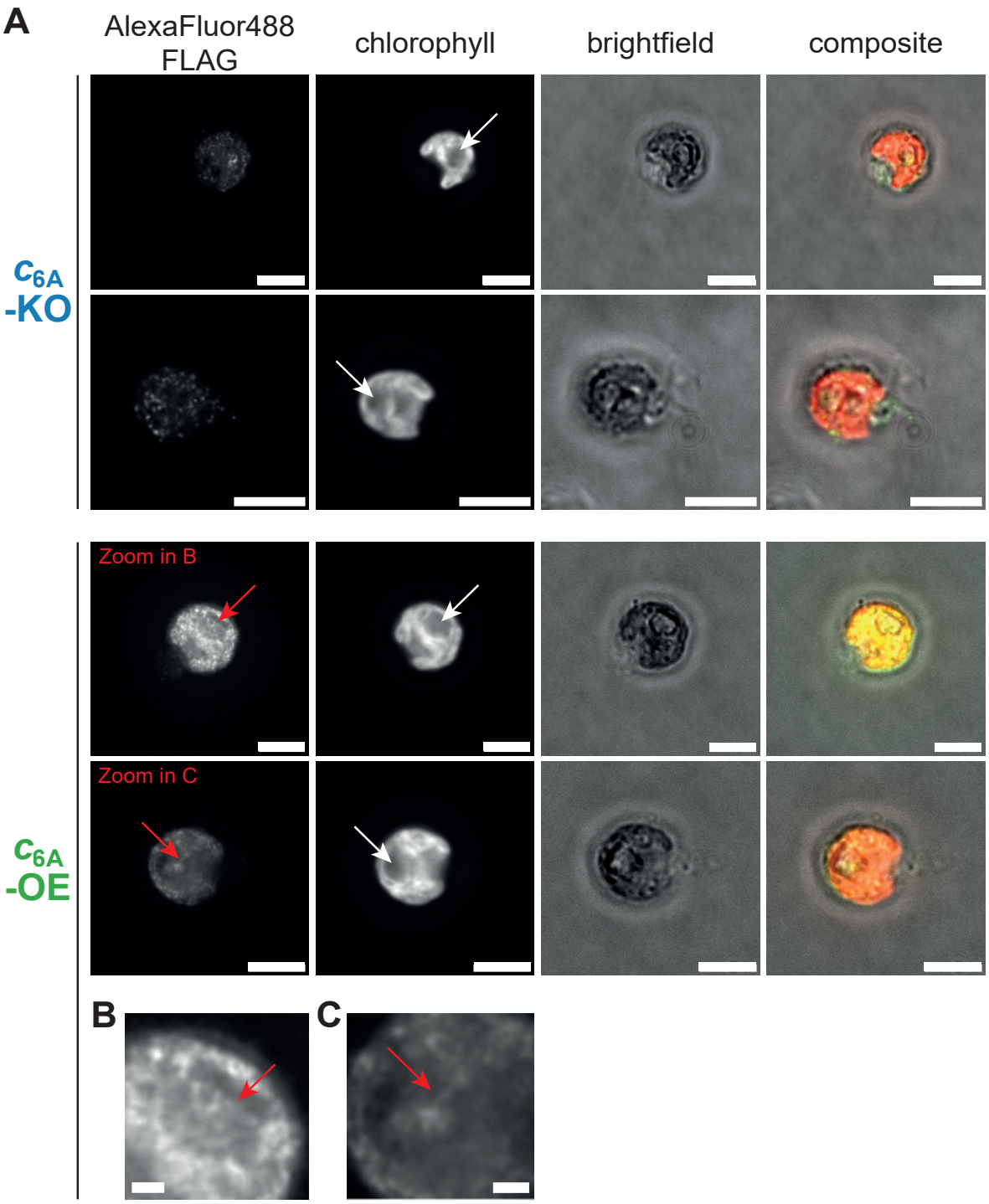


Figure 5.7: Immunofluorescence localisation of c_{6A}-FLAG using c_{6A}-OE and the untransformed background strain c_{6A}-KO. (**A**) Two representative cells are shown per strain. Samples were probed with an anti-FLAG antibody and a secondary anti-mouse antibody conjugated to AlexaFluor488 fluorescent dye. Using a 100x oil immersion lens, AlexaFluor488 (500 nm excitation, yellow emission filter, 500 ms exposure) and chlorophyll fluorescence (635 nm excitation, red filter, 500 ms exposure) were imaged in z-stacks and a brightfield image was recorded as well (scale bar = 5 µm). Images were subjected to fluorescence signal deconvolution to improve resolution and adjusted to the same brightness and contrast values. White arrows in the chlorophyll images indicate the location of the pyrenoid. In the composite, the AlexaFluor488 and chlorophyll fluorescence are shown in green and red, respectively. (**B** & **C**) Zoomed-in images of the AlexaFluor488 channel from c_{6A}-OE, where red arrows mark structures that resemble pyrenoid-traversing thylakoid membranes (scale bar = 1 µm).

Nevertheless, some limitations exist for the method employed here. First, c_{6A}-FLAG was expressed from a non-native promoter, because the native expression level of c_{6A} is very low [169, 172]. A highly increased amount of c_{6A} could potentially lead to mislocalisation. The detected c_{6A}-FLAG fluorescence was, however, not localised to multiple compartments, a regular symptom of mislocalisation, rendering it unlikely that c_{6A}-FLAG was mislocalised here. The use of indirect c_{6A} detection via the FLAG tag represents another limitation as unspecific fluorescence signal can lead to misinterpretation. To mitigate concerns about non-specific staining, the untransformed background strain c_{6A}-KO was used here to control for the background signal.

In summary, immunofluorescence microscopy showed a thylakoid luminal localisation for c_{6A} in *C. reinhardtii*. This further supports a role in photosynthesis as the thylakoid lumen is tightly linked to the function and regulation of the photosynthetic apparatus [125, 332].

5.2.2 Co-immunoprecipitation of putative interaction partners of c_{6A} in *C. reinhardtii* does not reveal any stable interactions

5.2.2.1 Co-IP of c_{6A} from *C. reinhardtii* cultures grown in continuous light

Having established the localisation of c_{6A} in *C. reinhardtii*, knowledge on interaction partners from the thylakoid lumen and membrane would provide further clues about c_{6A}'s function. Protein-protein interactions rely on proteins binding to each other, resulting in a great variety of methods for investigation of protein-protein interactions. Previously, Y2H assays were used to identify putative interaction partners of c_{6A}. However, Y2H is an *in vitro* method, in contrast to co-immunoprecipitation (co-IP). In the latter, putative interaction partners can be isolated under native physiological conditions *in vivo* [333]. In co-IP, the protein of interest is specifically isolated and all proteins that are bound to it can be regarded as putative interaction partners. Hence, a c_{6A}-FLAG overexpressing strain (pDKM-000) was subjected to co-IP analyses. The untransformed background strain (negative control) was used to control for unspecific binding excluding proteins as interaction candidates that also appear in the co-immunoprecipitate of the negative control. Cell lysates from exponential growth phase cultures grown under standard conditions were incubated with anti-FLAG antibody components covalently bound to agarose beads. After removal of lysate from the beads and multiple washes, proteins bound to the beads were eluted by incubation with denaturing sample buffer (figure 5.8A). Fractions were subsequently analysed by protein gel electrophoresis and immunoblotting (figure 5.8B).

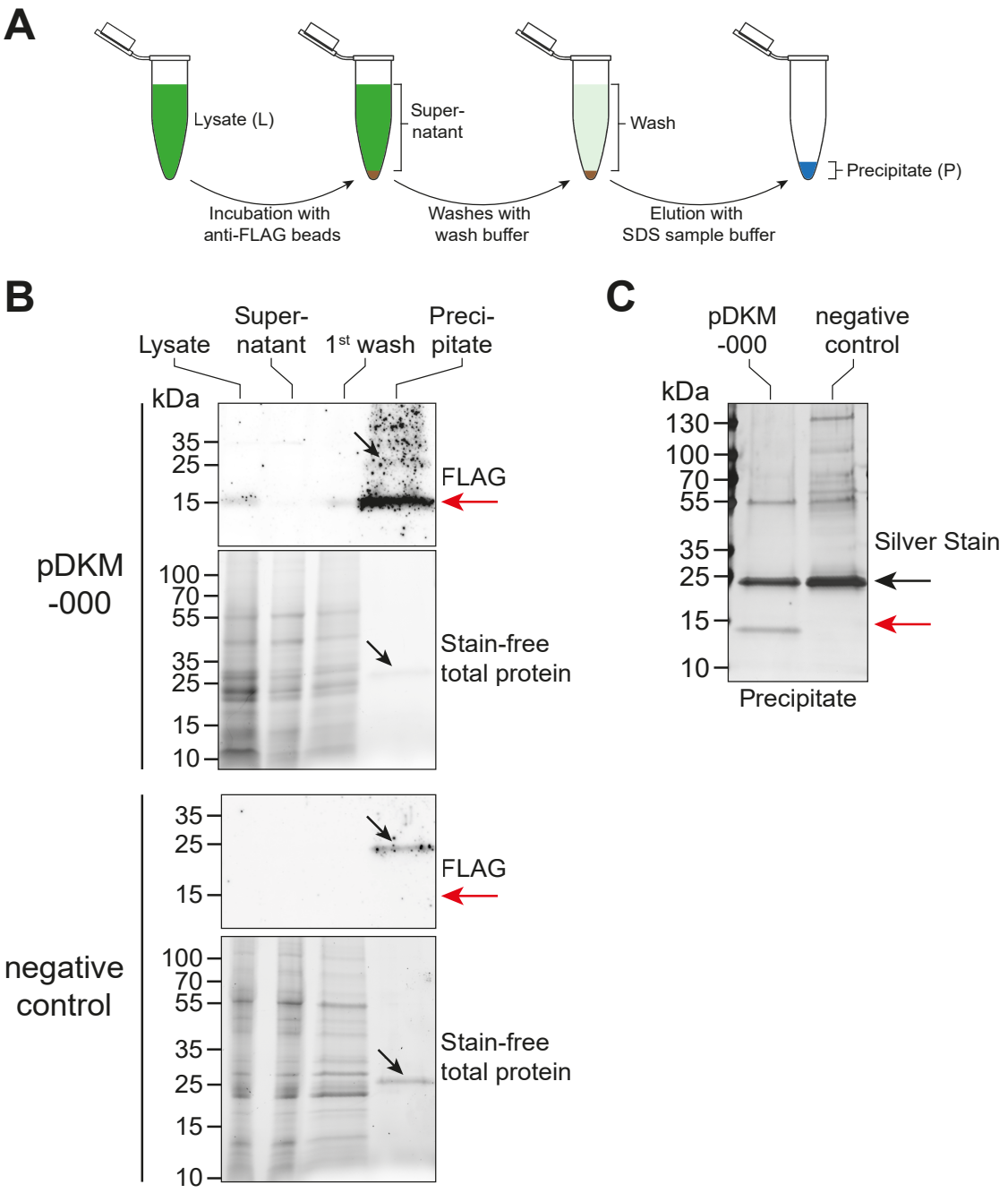


Figure 5.8: Co-immunoprecipitation of FLAG-tagged proteins from a c_{6A}-FLAG overexpression strain (pDKM-000) and an untransformed background strain (negative control) grown under standard conditions. (**A**) Co-IP relied on anti-FLAG antibody fragments that are covalently bound to agarose beads (brown), to pull down FLAG-tagged proteins from a cell lysate, yielding a precipitate (blue) after washes and elution. (**B**) Lysate, supernatant, 1st wash and precipitate of pDKM-000 and negative control were subjected to protein gel electrophoresis (stain-free total protein) and anti-FLAG immunoblotting. (**C**) An additional protein gel electrophoresis was carried out with the precipitates and the gel was stained for protein with a higher sensitivity silver stain. Red arrows mark the expected c_{6A}-FLAG size and black arrows point at a 25 kDa band discussed in the text.

In both strains, stain-free total protein visualisation showed similar patterns for lysate, supernatant and the first wash supernatant, indicating that most protein did not bind to the anti-FLAG coated beads. The precipitate of both strains also looked similar in the total protein stain with only one faint band visible at ~25 kDa (black arrows in figure 5.8B).
In contrast, immunodetection of FLAG showed significant differences between pDKM-000 and the negative control. In pDKM-000 (overexpressing c_{6A}-FLAG), bands at ~15 kDa were detected, in agreement with the expected size of mature c_{6A}-FLAG. A c_{6A}-FLAG band was found in lysate and first wash samples but not in the supernatant, indicating that the beads successfully precipitated c_{6A}-FLAG from the lysate. This was further supported by the intense band of c_{6A}-FLAG in the precipitate. Interestingly, further FLAG signal was detected in regions of 25 to 35 kDa.

A FLAG band at 25 kDa was also detected for the negative control sample, while no other bands were seen with that sample. The 25 kDa band corresponds to the band detected in the total protein stain in both samples and suggests that there was strong binding of unknown protein to the beads, as stringent washes were not enough to remove the protein. A blast search of the *C. reinhardtii* non-redundant protein database revealed no proteins in *C. reinhardtii* that contain the FLAG specific DYKDDDDK amino acid sequence. However, a few candidates with predicted molecular weights in the region of ~25 kDa were found with a motif similar to the FLAG motif that could have led to unspecific (i.e. not specific to c_{6A}-FLAG) pull-down of those proteins (table 5.1).

Table 5.1: Proteins from *C. reinhardtii* that could be unspecifically anti-FLAG immunoprecipitated from, their respective amino acid motif closest to the FLAG motif and predicted molecular weight (MW).

Identifier	Gene symbol	motif closest to DYKDDDDK	predicted MW (kDa)
Cre03.g201776	not assigned	DYEDDDDE	29.1
Cre03.g193300	*CPLD56*	DYADDDDE	30.8
Cre12.g545450	not assigned	DYKEDDYV	26.2
Cre03.g145607	*BET3*	PYKDDD*	21.2

As the total protein visualisation using the stain-free method did not reveal many bands, a higher sensitivity silver stain was employed to investigate the composition of the co-immunoprecipitate of pDKM-000 and the negative control (figure 5.8C) and identify any

putative interaction partners. The most prominent band in both samples was the previously described band at ~25 kDa. Another shared band was found at 55 kDa which could be RbcL, as RuBisCO is very abundant in *C. reinhardtii* [334]. The only band that was found in the c_{6A} overexpression sample and not in the control was the band associated with c_{6A}-FLAG (red arrow), indicating that no putative interaction partners could be isolated with co-IP with samples grown under continuous light.

5.2.2.2 Co-IP of c_{6A} from *C. reinhardtii* cultures grown in DISCO Light

A c_{6A}-dependent growth phenotype had been found under DISCO Light conditions, raising the possibility that under these conditions c_{6A} might engage in more interactions than under continuous light. Therefore, a FLAG-immunoprecipitation experiment was carried out comparing the c_{6A}-FLAG overexpressing strain c_{6A}-OE and its untransformed background strain c_{6A}-KO when grown in DISCO Light. Cultures were harvested at mid-exponential growth phase, where c_{6A}-OE exhibited 60% higher optical density of the culture than c_{6A}-KO, as expected from other growth experiments (section 3.2.3.2). Cell lysates (L) and precipitates (P) of c_{6A}-OE and c_{6A}-KO were compared with protein gel electrophoresis and immunoblotting (figure 5.9A).

Lysates of both strains showed similar patterns of protein in the total protein stain and no detectable bands in the precipitate fraction. An immunoblot probed with an anti-FLAG antibody revealed the expected c_{6A}-FLAG band at ~15 kDa in the lysate and - with a higher intensity - in the precipitate of c_{6A}-OE but not in c_{6A}-KO. There, a band at ~25 kDa was observed in the precipitate sample, which was also found in the c_{6A}-OE precipitate (black arrows in figure 5.9). Another band at around 35 kDa could be observed in the lysates of both strains. Overall, the samples appeared very similar to the ones from continuous light cultures.

For higher sensitivity of protein detection, a silver stain was employed to investigate the precipitates of c_{6A}-OE and c_{6A}-KO and identify putative interaction partners of c_{6A} under DISCO Light (figure 5.9B). Similar to the samples from continuous light, a band at ~25 kDa was the most prominent in both samples. The only band that was found in c_{6A}-OE but not in c_{6A}-KO was identified as the c_{6A}-FLAG itself from comparison with the immunoblot. Hence, no putative interaction partners were identified in samples grown under DISCO Light either.

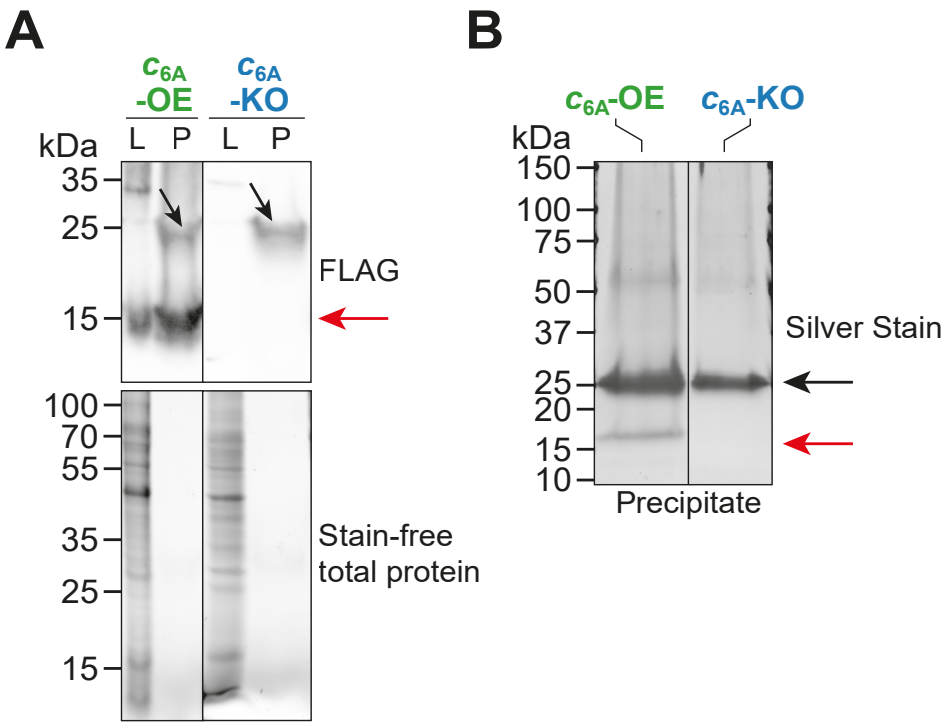


Figure 5.9: Co-immunoprecipitation of FLAG-tagged proteins from a c_{6A}-FLAG overexpression strain (c_{6A}-OE) and its untransformed background strain (c_{6A}-KO) grown photomixotrophically under DISCO Light conditions. (**A**) Lysates (L) and precipitates (P) were subjected to protein gel electrophoresis (stain-free total protein) and anti-FLAG immunoblotting. (**B**) An additional protein gel electrophoresis was carried out with the precipitates and gels were stained for protein with a higher sensitivity silver stain. Samples were run on the same gels and blots but not directly next to each other, as indicated by the black line in the middle of each gel or blot. Red arrows mark the expected c_{6A}-FLAG size and black arrows point at a 25 kDa band discussed in the text.

As co-IP can capture long-lasting interactions [335], it can be inferred that c_{6A} does not form stable complexes and is likely not associating with proteins for an extended period of time in continuous light and DISCO Light conditions. Interactions of c_{6A} are therefore likely of transient nature, in agreement with similar other small soluble electron carrier proteins, like cytochrome c_6, that also engage in transient interactions [336]. Addition of a crosslinking agent with subsequent co-IP might allow for identification of transient interaction partners of c_{6A} [333]. However, care needs to be taken when using cross-linking reagents to avoid recovering non-physiological interaction partners. Previously identified interaction partners of c_{6A} were found mainly using Y2H assays, which can also capture transient and weak interactions [337]. Hence, not finding interactions here is not in conflict with previous findings but indicates that the published identified candidates are interacting with c_{6A} more transiently than detectable with co-IP.

5.2.3 The effect of cytochrome c_{6A} on protein complexes of the thylakoid membrane in *C. reinhardtii*

5.2.3.1 Blue native PAGE analysis of thylakoids from c_{6A} mutants and WT

In *C. reinhardtii*, as in other photosynthetic organisms, the composition, distribution, and stoichiometry of thylakoid membrane complexes depends on environmental conditions. Studies of the thylakoid membrane protein composition of mutant strains have given insights into the functions of the affected proteins [318–326]. With the thylakoid luminal localisation confirmed, investigating the effect of c_{6A} on the complexes of the thylakoid membrane might help narrow down its functional involvement in photosynthesis. This was especially interesting in the light of the previously described c_{6A}-dependent difference in light harvesting balance between PSI and PSII (chapter 4). Thylakoids of WT, c_{6A}-KO and c_{6A}-OE were isolated from photomixotrophic cultures grown under continuous light, via passage through a syringe needle and a subsequent Percoll gradient. The protein composition of the thylakoid fraction was analysed employing blue native polyacrylamide gel electrophoresis (BN-PAGE) after membrane complex solubilisation with β-DM (figure 5.10).

Separation of native thylakoid membrane complexes resulted in a distinct pattern of eleven green and blue coloured bands, where blue bands contain protein and green appearance indicates the additional presence of chlorophyll. From comparison of the order of bands with published BN-PAGE analyses from *C. reinhardtii*, the bands found here could be assigned to photosystem complexes (supercomplexes, PSII-LHCII, PSI-LCHI, PSII dimer & PSII monomer), light-harvesting complexes (LHC trimers and monomers), and other non-chlorophyll containing complexes (ATP synthase, cytochrome b_6f & RuBisCO) [312, 318–324, 326]. While comparison with the literature is useful, some bands were not easily assignable, as the thylakoid isolation, solubilisation, and gel electrophoresis procedures are not standardised and experimental evidence for the assignment of bands is often lacking. For example, some authors found cytochrome b_6f or RuBisCO in their BN-PAGE while others did not. Despite this limitation, comparison of band presence and intensity between samples that were treated identically is still informative. Here, the presence of bands was the same in all strains, i.e. no band could be found in only one or two of the strains (figure 5.10A). A faint band for supercomplexes could be observed in most samples, indicating that the solubilisation with β-DM did not allow for stable supercomplexes to be isolated. PSII-LHCII and PSI-LCHI complexes appeared at similar intensities for all strains, rendering it unlikely that c_{6A} is involved in their assembly or turnover under standard conditions. The most noteworthy difference between the three strains was the intensity of an unassigned green band just below the PSI-LHCI band (III, red arrows in figure 5.10). Band III was found to be consistently more

prominent in c_{6A}-KO samples than in WT or c_{6A}-OE samples, indicating that this difference was due to c_{6A} absence. The band assigned to PSII dimers (band IV) also appeared slightly different between the strains, although not as consistently as band III. Band VII assigned to b_6f dimers and/or RuBisCO showed a slightly decreased intensity in c_{6A}-OE compared to c_{6A}-KO and WT. The remaining bands (assigned to ATP synthase, b_6f monomer, PSII monomers and LHCIIs) were not different between the strains.

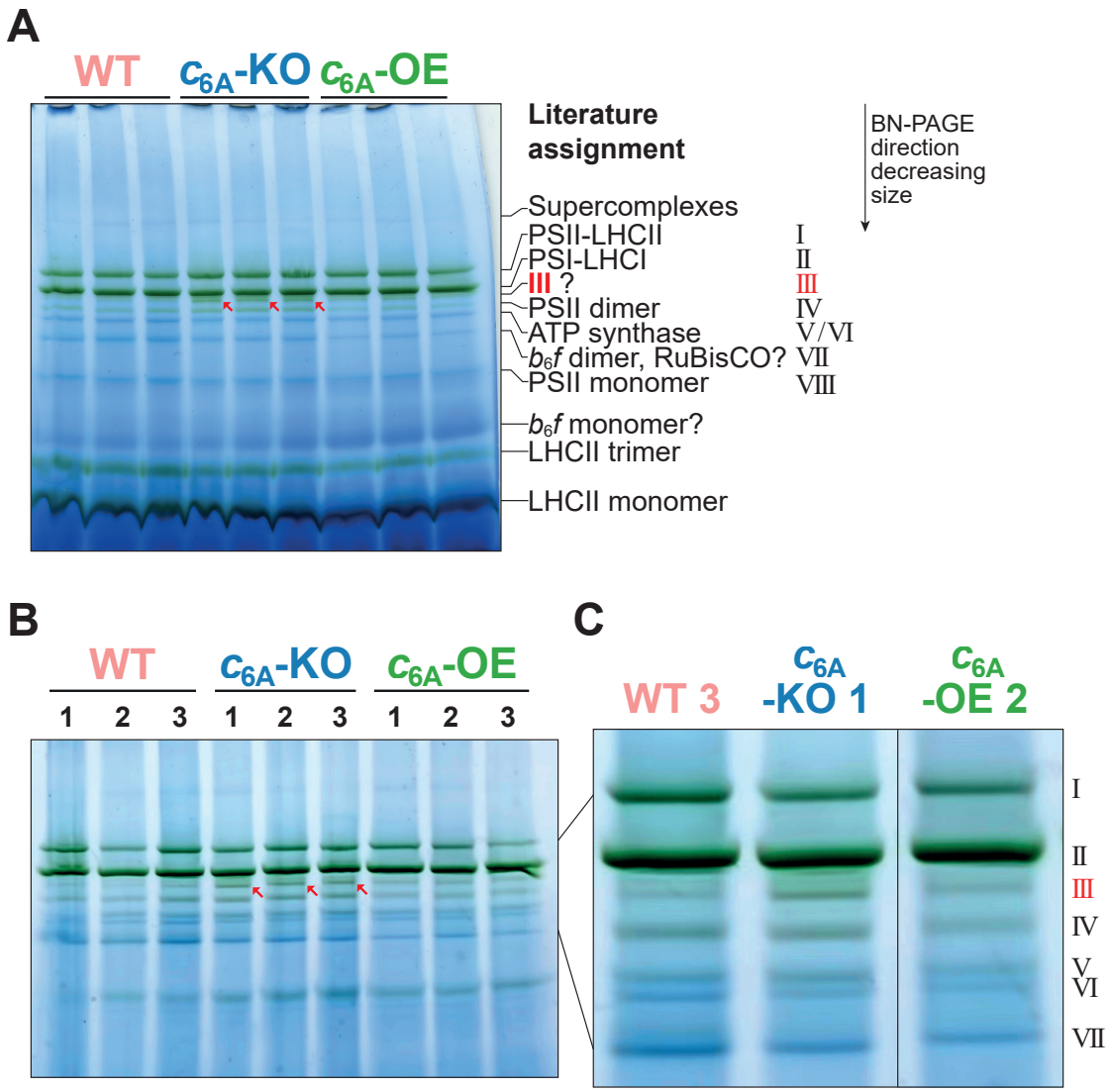


Figure 5.10: BN-PAGE analysis of c_{6A} mutant strains and WT thylakoid membrane complexes isolated from cultures grown in standard conditions. (**A**) Samples from three biological replicates (indicated by horizontal lines) per strain (0.53 µg/µL & 6 µg total chlorophyll) were solubilised in 1% β-DM and separated by electrophoresis. Thylakoid membrane complexes were assigned to bands according to the literature. (**B**) A second, longer run of the same samples was carried out to separate the marked band of interest (III, red arrows). An error led to decreased protein loading for sample WT 2. (**C**) For easier inspection, the area of interest with band III, from WT 3, c_{6A}-KO 1 and c_{6A}-OE 2 from (B) was enlarged.

To make sure that band III represents a separate complex from PSI-LHCI, the same samples were subjected to a prolonged run of BN-PAGE increasing the separation of complexes in the area of interest (figure 5.10B & C). A loading error leading to decreased protein amount in sample WT 2 did not prevent the conclusion that band III was indeed a separate complex. Band III was found in all strains but was significantly more prominent in c_{6A}-KO. The size and colour of the band led to the conclusion that band III contains a photosystem complex. Interestingly, the increased separation time also led to splitting of the band originally assigned to ATP synthase into bands V & VI.

Overall, the c_{6A}-dependent difference in intensity of band III indicates that c_{6A} influences the composition of photosystem complexes in the thylakoid membrane of *C. reinhardtii* even under conditions that did not cause a growth phenotype. However, to allow further conclusions about c_{6A}'s function regarding photosystem complexes, it was necessary to clarify the identity of band III.

5.2.3.2 2D-PAGE analysis of thylakoids from c_{6A}-KO

To investigate the identity of protein complexes separated with BN-PAGE, gel slices can be denatured and subjected to a second dimension SDS-PAGE. Protein subunits that are found in one complex will align in a vertical line underneath the band of the native complex. Components that can be found in multiple native complexes will align in a horizontal line on the SDS-PAGE according to their molecular weight. A BN-PAGE lane from c_{6A}-KO was subjected to a second dimension SDS-PAGE and the gel was silver stained to identify components of the complex in band III. Additionally, a simulation of mobility in the gel (R_f) of known thylakoid membrane complex components was carried out allowing comparison of patterns and thereby putative identification of complex components (figure 5.11).

Band I (literature assignment: PSII-LHCII) exhibited components in the size range of just under 15 kDa to over 25 kDa (yellow box) which could be LHC proteins (see R_f simulation). Further bands were found around 35 kDa (blue boxes) and represent shared components between bands I and II (literature assignment: PSI-LHCI). Band II additionally showed spots around 55 kDa, above 70 kDa, and below 15 kDa (red boxes) that were shared components with bands III and IV. Generally, bands III and IV seemed of the same composition, the size difference in the BN-PAGE could thus reflect multimers of the same complex. Band IV was assigned as PSII dimer from literature comparisons, suggesting that band III is also a PSII dimer but somewhat modified to be seen as separate band in the BN-PAGE. Interestingly, the components around 35 kDa seen in band I and II (blue boxes) could also be observed in bands V/VI and VIII, indicating that these bands contain complexes of the same proteins.

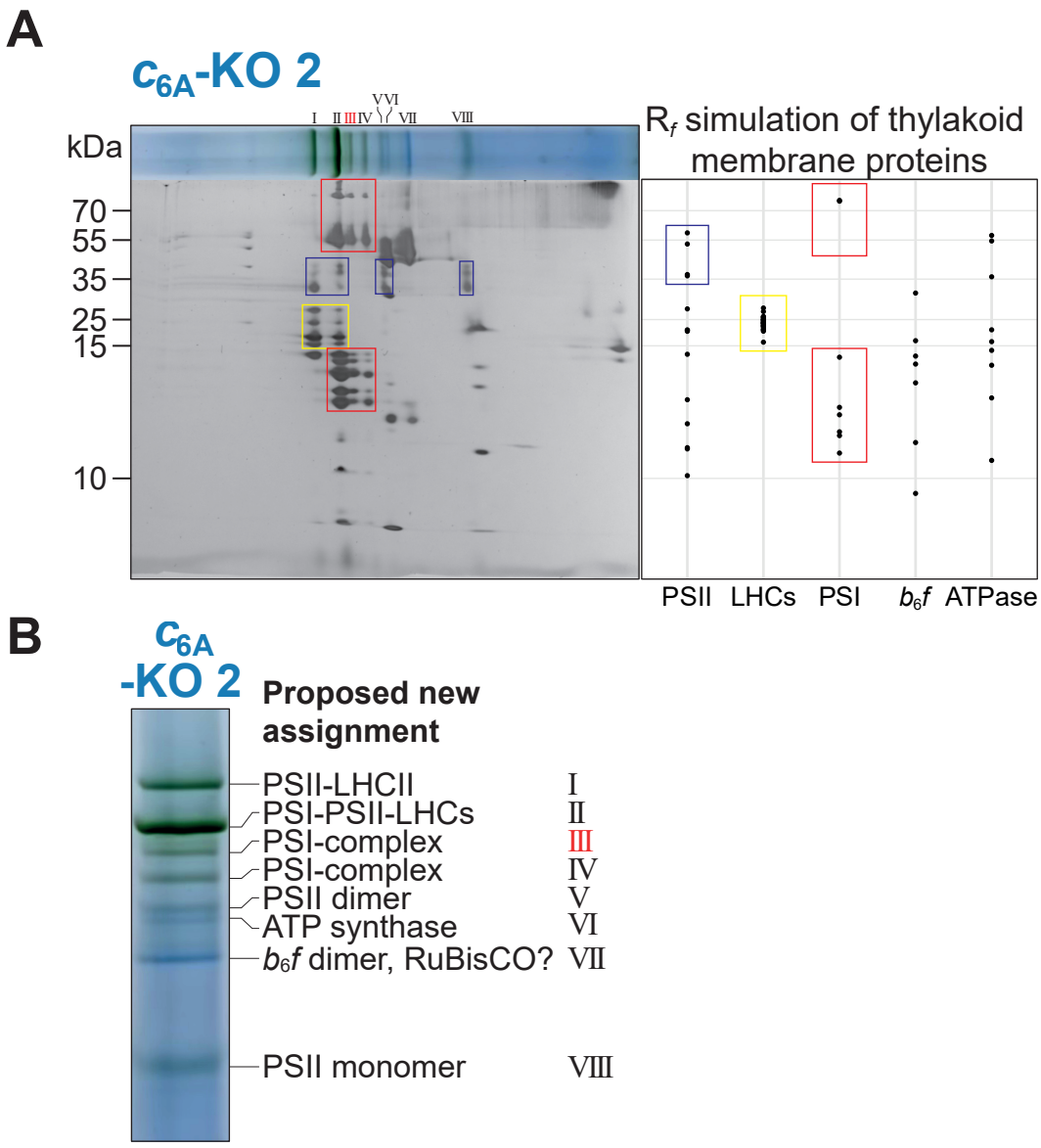


Figure 5.11: 2D-PAGE analysis of a BN-PAGE lane from c_{6A}-KO replicate 2 and the resulting proposed new assignment of bands. (**A**) Comparison of a two-dimensional BN-PAGE/SDS-PAGE analysis of c_{6A}-KO with calculated R_f values of known thylakoid membrane complex components. The R_f values of complex components were calculated using their known molecular weight and a linear regression of the distance of the protein standard in relation to the running front (r^2 = 0.98). More thylakoid membrane complexes exist than those shown here but here the focus was laid on complexes involved in photosynthesis and especially photosystems and antennae (LHCs), as the band of interest (III) was green. (**B**) The proposed new assignment of BN-PAGE bands on the basis of 2D-PAGE analysis and comparison with R_f values of known complex components.

For band IV, the absence of subunits found for bands I (PSII-LHCII) and VIII (PSII monomer) questions the literature assignment of PSII dimer. Band I and VIII share subunit spots around 35 kDa, making it more likely that bands III and IV actually do not contain PSII. Comparing the patterns of the BN-PAGE with the R_f simulation, the gap of spots from

bands III and IV between 15 and 55 kDa resembles the gap in PSI composition without bound LHC complexes. It is therefore proposed that bands III and IV compose PSI complexes without LHCI, while band I contains PSII-LHCII, band II a mixture of PSI-PSII-LHCs and bands V and VIII represent PSII complexes without LHCII (figure 5.11B). A LHC-less PSI complex as proposed for band III would be in agreement with earlier findings where in photomixotrophy PSI was found only without LHCI complexes [312]. However, complexome profiling of thylakoids from photomixotrophic cultures detected LHCI co-migrating with PSI core proteins [326]. There are some other difficulties with the interpretation of band and spot patterns presented above. For example, the presence of bands at 55 kDa and above 70 kDa for bands III and IV is not reflected in the R_f simulation, where only two spots (PsaA & PsaB) were expected above 70 kDa. However, previous mass spectrometric analyses have also found PsaA at two positions of different high molecular weight, too [312].

Despite the difficulties in correctly assigning the bands to photosynthetic complexes, the colour of band III indicates that it contains a photosynthetic complex while the size comparison of its components with known proteins suggests that band III lacks LHC proteins. Independent of which photosystem band III actually contains, this suggests that loss of c_{6A} leads to increased levels of a LHC-less photosynthetic complex. Unfortunately, due to the extended run time of the BN-PAGE to resolve band III, the LHC trimers were not resolved on the second dimension SDS-PAGE, so experimental confirmation of LHCs missing in band III is still needed. BN-PAGEs with different percentage gels might allow for comparison of LHC trimer and monomers while band III is still resolved.

5.2.3.3 Further 2D-PAGE analyses of thylakoids from c_{6A} mutant strains and WT and mass-spectrometric protein identification of selected spots

A second dimension SDS-PAGE was also carried out for WT, c_{6A}-OE and second c_{6A}-KO sample and the gels were silver stained in pairs to allow for comparison of abundances of components between WT and c_{6A}-KO or c_{6A}-OE and c_{6A}-KO. To aid the identification of band III and other bands further, selected spots were excised, and their peptide composition was analysed with LC-MS/MS (figure 5.12).

Comparing WT 3 and c_{6A}-KO 1 in figure 5.12A, a likely staining artifact led to decreased staining starting in the left top corner and going down across to band VII at the height of 15 kDa in both samples. Nevertheless, very similar patterns could be observed overall and no spots were unique to either strain. This indicates that c_{6A} is unlikely to be represented among the spots observed and that c_{6A} absence does not cause dramatically altered complex composition. Importantly, the abundance difference of band III also translated into increased

abundance of its components in c_{6A}-KO. A component of band VIII that was found at the same molecular weight but exhibited different mobility comparing c_{6A}-KO and WT in the first dimension is indicated by a yellow circle.

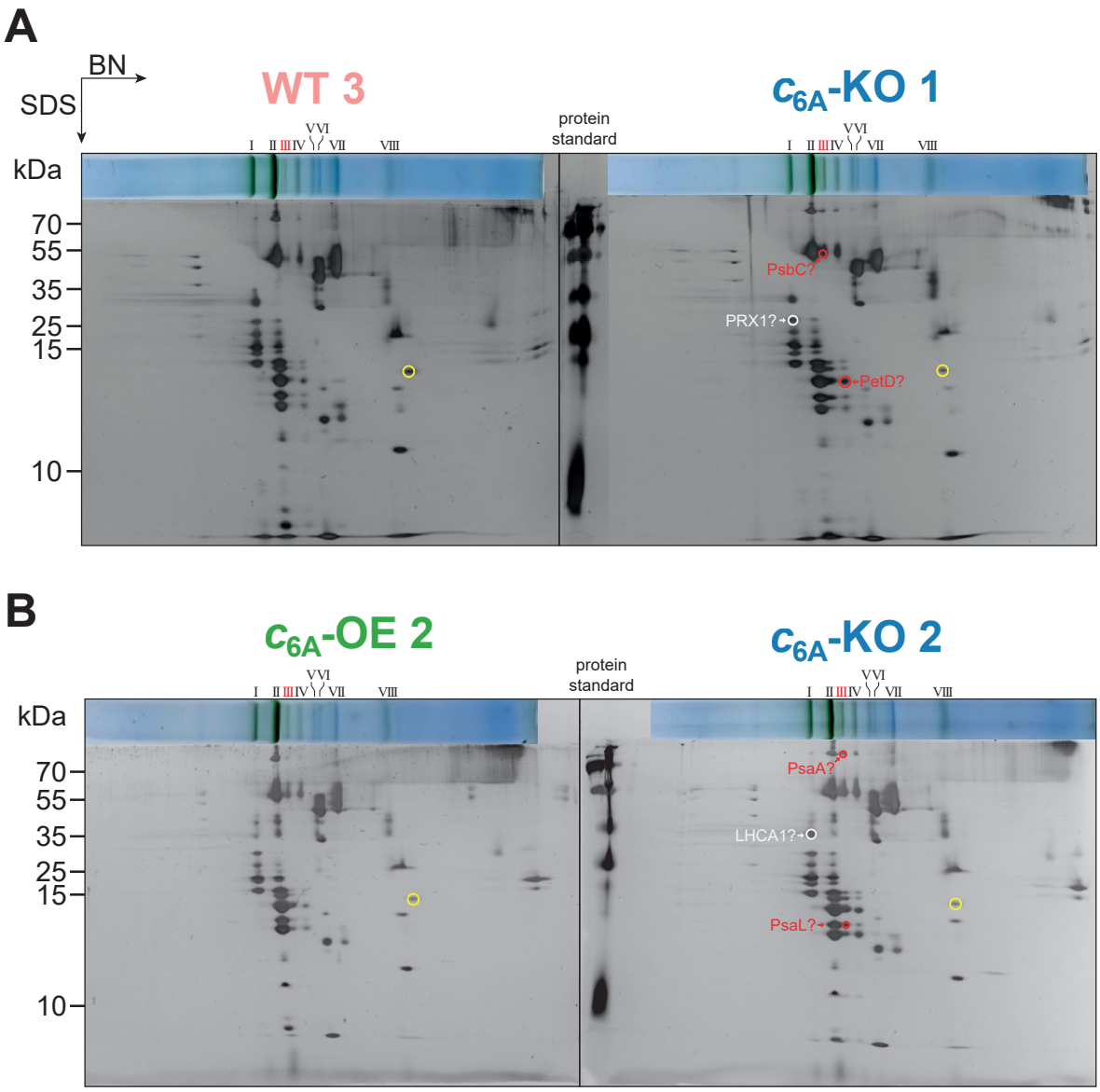


Figure 5.12: 2D-PAGE analyses of *C. reinhardtii* WT, c_{6A}-KO and c_{6A}-OE thylakoid membrane complexes isolated from cultures grown in standard conditions. (**A**) WT 3 and c_{6A}-KO 1 were run on separate gels but subjected to silver stain together. (**B**) The same procedure was repeated with c_{6A}-OE 2 and c_{6A}-KO 2. The horizontal BN-PAGE slices are the lanes from figure 5.10 and the 2D image of c_{6A}-KO 2 is the same as in figure 5.11. Bands from the BN-PAGE are indicated with roman numerals and the consistently different band III is marked red. Spots that were identified by LC-MS/MS are circled and labelled with their most likely identity. Spots labelled in red were found in band III, while spots labelled in white were not. Yellow circles mark spots that showed a c_{6A}-dependent mobility shift in the first dimension (BN-PAGE).

The comparison between c_{6A}-OE 2 and c_{6A}-KO 2 showed no staining artifacts and the region around 35 kDa displayed spots for bands I and II in both strains (figure 5.12B). Otherwise, a very similar pattern to WT vs c_{6A}-KO was found also in regard to the intensity of spots, with c_{6A}-OE resembling WT more than c_{6A}-KO. This was especially obvious for the prominence of band III associated spots. Similarly, the mobility in the first dimension of the yellow-circled band VIII component was found to be different between c_{6A}-OE and c_{6A}-KO, confirming this as a c_{6A}-dependent difference.

After the second dimension SDS-PAGE, selected spots were excised, and their protein composition was analysed with LC-MS/MS. Peptides found were searched against the *C. reinhardtii* proteome and the so-called CRAPome [338] to differentiate between contaminating and *C. reinhardtii* peptides. *C. reinhardtii* hits for the marked spots are shown in appendix tables C.1 to C.7. The most likely identity of each spot was assigned by filtering *C. reinhardtii* hits to fall in the range of the observed molecular weight ($\pm$10 kDa) and sorting by the total spectrum count of the detected protein fragments.

These analyses focussed mainly on proteins found in band III to test the hypothesis that band III is a PSI complex without LHCs. The highest molecular weight spot above 70 kDa was found to contain peptides that corresponded to PsaA, a subunit of PSI (figure 5.12 c_{6A}-KO 2). As this spot is found in band III, its likely identity supports the PSI assignment of band III. Fragments corresponding to other uncharacterised proteins (encoded by Cre06.g278255 and Cre06.g255100) were also detected at similarly high abundance as PsaA in this spot (appendix table C.1). However, the predicted molecular weights of these did not align as well as PsaA to the observed size of the spot.

A spot between 10 and 15 kDa was identified to contain mostly peptides of PsaL, another subunit from PSI, which would also be in agreement with the PSI assignment (figure 5.12 c_{6A}-KO 2). However, the observed size of the protein (~13 kDa) did not correspond well with the size of PsaL (20.3 kDa) and various ribosomal protein fragments were also detected (appendix table C.2).

Mass-spectrometric analysis of the spot around 55 kDa, which was thought to represent PSI subunits, was found to be made up of fragments corresponding to PsbC, the CP43 subunit of PSII (figure 5.12 c_{6A}-KO 1). However, the apparent size of the spot (~55 kDa) did not align well with the expected size of PsbC (43 kDa). The next most abundant protein by total peptide count was the fructose-1,6-bisphosphate aldolase FBA3 (appendix table C.3), which may be explained by its generally high abundance [339, 340]. If the 55 kDa spot were indeed composed of mostly PsbC, it would question the above hypothesis of band III being a PSI-related complex. Additionally, it would not align with the literature-based band

assignment, as the 55 kDa spot was found only in bands II, III and IV and not in bands originally assigned as PSII complexes.

Another spot that was found in band III was identified to contain fragments corresponding to PetD, a subunit of the cytochrome b_6f complex (figure 5.12 c_{6A}-KO 1). This would suggest that band III did not only contain a photosystem complex. However, with 6.25%, the sequence coverage of PetD from the detected fragments was low (appendix table C.4).

Two spots that were not found in band III but only in bands I and II contained fragments corresponding to LHCA1, a subunit of LHCI, and PRX1, a chloroplast localised thioredoxin-dependent peroxidase [341, 342], respectively (marked white in figure 5.12). It would be surprising if band I was indeed mostly LHCA1, as this band was originally assigned as PSII-LHCII complex according to the literature. As for other spots before, the observed size of the spot (~33 kDa) did not correspond well with the expected size of the protein (23 kDa for LHCA1). Identifying PRX1 was also unexpected, as it is unclear if this soluble protein is actually associated with photosystem complexes.

Analysis of the yellow-circled spot from WT 3 did not yield any candidates in the expected molecular weight region (appendix table C.7). However, mostly PSII-related peptides were found, indicating that the original assignment of band VIII as PSII monomer could be correct.

Overall, mass-spectrometric analyses did not yield conclusive evidence for the identification of band III. While the identification of protein fragments in some spots supported the hypothesis of band III containing a PSI complex, others did not. The sizes of many of the proteins assigned to the excised spots did not correspond well with the observed molecular weight of the spot, questioning the assignment. Furthermore, fragments from unexpected proteins were detected such as ribosomal proteins and PRX1, indicating possible contamination issues. Future studies could include the mass-spectrometric analysis of more spots, allowing to find a consensus between different spots of the same apparent molecular weight and thereby eliminating unexpected outliers.

5.3 Conclusion & Outlook

5.3.1 Summary of findings

The aim of this study was to test the proposed thylakoid luminal localisation of c_{6A} and subsequently characterise c_{6A}'s interactions and effect on thylakoid membrane complexes.

Overexpressing fluorescently tagged versions of c_{6A} did not lead to measurable fluorescence, which prevented any localisation studies with these strains (section 5.2.1.1) and prompted a move to two different immunodetection-based methods. First, subcellular fractionation with subsequent immunoblotting revealed that c_{6A}-FLAG was most similar in its distribution to plastocyanin, supporting a thylakoid luminal localisation (section 5.2.1.2). It should be noted that the strongest signal from both, c_{6A} and plastocyanin, was obtained from the stromal fraction. This indicated cross-contamination of stroma with soluble lumen proteins, although no contamination of thylakoid membranes with stromal proteins, including the highly-abundant RuBisCO, was seen. Nevertheless, the cross-contamination suggests caution is needed when interpreting these results. Finally, immunofluorescence microscopy of intact *C. reinhardtii* cells showed a thylakoid luminal localisation of c_{6A}-FLAG, as determined by co-localisation with chlorophyll fluorescence and signal from pyrenoid-traversing thylakoids (section 5.2.1.3). The thylakoid luminal localisation is in line with previous findings and further supports a role for c_{6A} in photosynthetic processes.

Co-IP of c_{6A}-FLAG delivered no interaction candidates under continuous light or DISCO Light, suggesting that c_{6A} does not form a stable complex with other proteins (section 5.2.2). This would be consistent with c_{6A} functioning through transient interactions.

The effect of c_{6A} on complexes of the thylakoid membrane was investigated with BN-PAGE of WT, c_{6A}-KO and c_{6A}-OE. Here, a chlorophyll-containing complex was found to be more abundant in absence of c_{6A}. Efforts to clarify the identity of this complex through 2D-PAGE and mass-spectrometric analyses of selected spots were inconclusive. However, comparison of 2D-PAGE with R_f values of known thylakoid membrane complex components resulted in the proposition that band III contained a LHC-less PSI complex. More LHC-less PSI in c_{6A}-KO could explain the observation of an altered light-harvesting balance towards PSII in the absence of c_{6A} (chapter 4) as without LHCs PSI would have a decreased relative fluorescence. More LHC-less PSI might also translate to less PSI-LHC complexes which were proposed to be found in band II. Band II did not exhibit an obvious decrease of intensity in c_{6A}-KO compared to WT/c_{6A}-OE, however this could be masked by the band's great overall intensity. If the light-harvesting balance phenotype were at least partly caused by the altered thylakoid membrane complex composition, BN-PAGE analyses of DISCO Light grown cultures should exhibit a stronger difference between c_{6A}-KO and WT/c_{6A}-OE similar to the increased difference observed in 77 K measurements (section 4.2.2.1).

5.3.2 Further work

To confirm the localisation of c_{6A} further, two approaches could be pursued. First, the expression of fluorescently tagged fusion proteins of c_{6A} should be optimised. This could entail screening other fluorescent tags or could be expanded to other tags that rely on extrinsically added fluorophores, like the HaloTag [343]. The latter could bring the advantage of a completely different protein fold compared to intrinsically fluorescent proteins that rely on a β-barrel secondary structure. Second, raising a specific c_{6A} antibody would allow confirmation of the results obtained with subcellular fractionation and immunofluorescence microscopy, without the need for a FLAG-tagged overexpression. However, the very low expression level of c_{6A} may present a challenge for this approach.

To identify putative transient interaction partners of c_{6A}, the co-IP procedure described above could be modified to include a crosslinking step. Crosslinking *in vivo* with formaldehyde or dithiobis(succinimidyl-propionate) (DSP) mostly relies on presence of lysine residues [333], five of which can be found in mature c_{6A} from *C. reinhardtii*, suggesting that either method should yield interaction candidates. However, it should be noted that careful titration of crosslinking reagents is essential in such studies. Alternatively, biotin-dependent proximity labelling has been established in *C. reinhardtii* in recent years and could provide valuable insights into the proxiome of c_{6A} [344, 345]. As this method relies on fusion proteins, their correct processing and localisation would need to be established prior to the labelling experiments.

While efforts were undertaken to identify the photosynthetic complex accumulating in absence of c_{6A}, further investigation would be beneficial to conclusively prove its identity. Using different gel densities should allow for separation of complexes without losing smaller components such as LHC monomers and thus would help assignment of complexes to bands. Furthermore, a more detailed analysis of complex components from 2D-PAGE using mass spectrometry and immunoblotting will ultimately reveal the composition of isolated thylakoid membrane complexes. Additionally, it would be interesting to investigate thylakoid membrane complexes from *C. reinhardtii* c_{6A} mutant strains when grown under DISCO Light. This could help to elucidate further why c_{6A} is important for growth of *C. reinhardtii* under these conditions. Finally, the comparison of protein levels of subunits from photosynthetic complexes and their associated transcript levels might reveal further insight into the composition of thylakoid membrane complexes under continuous light and DISCO Light (chapter 6).

6

Protein and transcript levels of cytochrome c_{6A} mutant strains in *C. reinhardtii*

6.1 Introduction

Given the effects of c_{6A} on the biophysical characteristics of components of the PETC, as well as on thylakoid membrane complex composition and growth, it was decided to study the abundance of a number of the relevant proteins. Furthermore, a transcriptomic analysis was conducted, as this might help to detect any broader effects of c_{6A} and DISCO Light in addition to those on photosynthesis directly.

6.1.1 Responses to stressful light in *C. reinhardtii*

Some light conditions, such as high light intensity, can lead to significant challenges for *C. reinhardtii*, primarily in the form of photooxidative stress. This type of stress occurs when light-excited states cannot be efficiently utilised for photochemical reactions within the PETC, resulting in the formation of ROS [346]. ROS, known for their damaging effects on nearby proteins and lipids, have been found to be generated at key sites within the photosynthetic apparatus, including PSII, the cytochrome b_6f complex, and PSI [60].

In response to short-term stress, *C. reinhardtii* employs various mechanisms to mitigate photooxidative damage. The electron transfer towards PSI can be slowed at the cytochrome b_6f complex via photosynthetic control to prevent excessive electron pressure on PSI [347]. Moreover, alternative electron pathways, such as the NADPH dehydrogenase activity of NDA2 or chlororespiration via PTOX2, can be modulated to prevent ROS generation [60]. NDA2 can reduce the PQ pool by oxidising NADPH, while PTOX2 can oxidise the PQ pool by reducing molecular oxygen. Lower NDA2 or higher PTOX2 activities or abundances

would lead to a more oxidised PQ pool relieving pressure from the PETC. Furthermore, flavodiiron proteins are associated with alleviating electron pressure on PSI and thereby preventing ROS generation [66]. Another strategy of ROS prevention involves adapting light-harvesting processes, notably through the action of LHCSR proteins. The rapidly reversible component of NPQ (qE) is particularly dependent on the LHC-like protein LHCSR3, which is upregulated under conditions that pose a risk of photooxidative stress, including exposure to light, especially high light [77], blue light [84], and UV-B light [348], low CO_2 [70, 349], low sulphur [350], low iron [351], and osmotic stress [352]. Additionally, a protective role has been suggested for LHCBM4/6/8 of LHCII [353]. Rather than preventing its generation, existing ROS can also be neutralised by scavenger proteins such as superoxide dismutase, ascorbate peroxidases, peroxiredoxins, and glutathione peroxidase [354]. Furthermore, lipid-soluble antioxidants such as tocopherols and carotenoids play a crucial role in detoxifying ROS and are also involved in preventing its production via quenching of excited chlorophylls [355].

Beyond these immediate responses, ROS also serve as signalling molecules that trigger longer-term stress adaptation mechanisms, including gene regulatory changes [57, 58, 356]. Another critical long-term response to environmental stress is autophagy, a process through which *C. reinhardtii* degrades intracellular material to maintain cellular homeostasis. Autophagy can be induced by various stress conditions, including nutrient limitations, heavy metal toxicity, salt stress, photooxidative stress, and exposure to high light [357, 358].

6.1.2 Effect of stress and other environmental conditions on transcript levels of cytochrome c_{6A}

Responses of *C. reinhardtii* to various stressful and other environmental conditions are an active area of research [13] and publicly available datasets often also include information on the expression of genes that were not the direct focus of those studies, for example c_{6A}. As a background to this chapter, a survey of studies was carried out and the resulting summary of differential expression of *CYC4* (encoding c_{6A}) under specific environmental conditions is shown in table 6.1.

A significant induction of c_{6A} expression was found when *C. reinhardtii* was exposed to high light (400 $\mu mol_{photons}\ m^{-2}\ s^{-1}$) for four hours [171]. This could indicate involvement of c_{6A} in the response to high light, even though this was a minor induction. Together with the low native expression levels of c_{6A} [169], which means that a small absolute change is proportionately large, it seemed that high light had a small effect on the actual number of c_{6A} transcripts.

Table 6.1: Summary of different conditions and their respective effect on transcript levels of *CYC4* in *C. reinhardtii*. "None" indicates no significant or trending on significant effect.

Condition	Effect on *CYC4* expression	Reference
High light (4 h 400 $\mu mol_{photons}$ m^{-2} s^{-1})	induction log_2FC = 0.69, p_{adj} = 1.14E-4	[171]
H_2O_2 treatment	repression log_2FC = -0.66, q-value = 0.017	[21]
H_2O_2 treatment	None	[18]
Sulphur deprivation	repression trend log_2FC = -0.51, q-value = 0.061	[21]
Diurnal cycle	None	[14, 15]
CO_2 (low and high)	None	[16]
Salt stress	None	[19]
Nitrogen deprivation	None	[21]
Iron deprivation	None	[21]
Copper deprivation	None	[21]

A trend of repression of c_{6A} expression was observed for sulphur deprivation and more significantly for H_2O_2 treatment. However, another study did not find c_{6A} downregulated by H_2O_2 treatment. It must be noted again that slight repression of the lowly expressed c_{6A} probably did not lead to noteworthy changes in absolute number of its transcripts. Interestingly, no differential expression of c_{6A} was reported in *C. reinhardtii* when exposed to diurnal cycles, different CO_2 conditions, salt stress, nitrogen, iron, or copper deprivation. The lack of effect of copper deprivation is especially interesting, as the c_{6A} homologue cytochrome c_6 shows a dramatic induction in the absence of copper (log_2FC = 15.5, q-value = 3.25E-5). This is expected as c_6 is a functional replacement for the copper protein plastocyanin and its expression is known to be regulated by copper responsive elements [359].

6.1.3 Aims

Although the literature did not indicate any conditions that drastically affected c_{6A} transcript levels, and which might therefore give an insight into its function, various previous experimental results, described in previous chapters, prompted further investigation of protein abundances. The apparently LHC-less PSI complex that was more abundant in c_{6A}-KO and the effect of c_{6A} absence on light-harvesting balance both raised the question whether absence of c_{6A} might alter the photosystem core protein levels. Furthermore, the increased NPQ levels in the absence of c_{6A} might be connected to changes in the abundance of LHCSR3. In addition, the altered redox kinetics of the *b* hemes seen in the absence of c_{6A} warranted protein level analysis of the abundance of the b_6f complex. Studying the abundances of proteins known to affect the PQ pool redox state, like NDA2 or PTOX2, might help to understand the more reduced PQ pool in c_{6A}-KO. Finally, examining the abundance of ATP synthase and RuBisCO might provide insights into the pmf and PSI acceptor side limitation measurements. Therefore, western blot analyses probing for all the above proteins were carried out from samples grown in continuous light and DISCO Light. To obtain a more comprehensive picture of the effect of c_{6A} on *C. reinhardtii* and the effects of DISCO Light, RNAseq was also carried out on the same cultures used for protein analysis.

6.2 Results & Discussion

To examine the effect of c_{6A} on protein and transcript levels in *C. reinhardtii* when grown under continuous light or DISCO Light, cultures were grown and protein and RNA samples were isolated as detailed in figure 6.1. The same cultures were used for RNA and protein sampling to allow better comparison between the levels detected. OD_{750nm} of cultures was measured during growth. All cultures were in exponential growth phase when sampled, to avoid differences due to growth phase, although this required sampling after different times for continuous light and DISCO Light. Protein samples of continuous light cultures were taken at late exponential growth phase (48 h) to match with the samples used for biophysical investigations. RNA samples were taken slightly earlier in mid-exponential phase (31 h), as proteins generally have a longer half-life than RNA, and to reduce the risk of effects on the transcriptome due to the onset of transition into stationary phase (rather than absence of c_{6A}). In DISCO Light, RNA samples were also taken in mid-exponential phase (54 h). Samples for proteins were taken at days 2 (48 h) and 4 (96 h) to match with the biophysical investigation of the light harvesting balance (section 4.2.2.1).

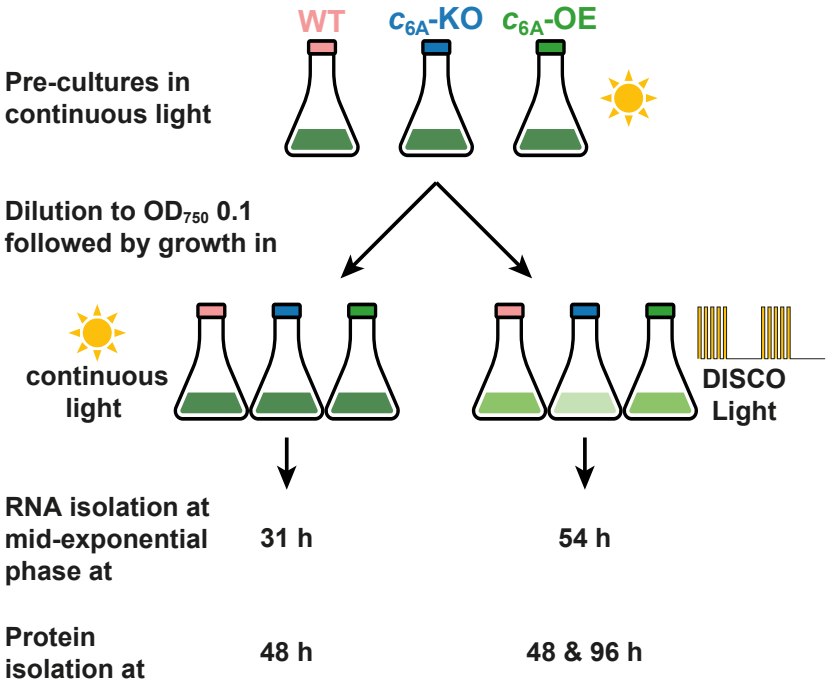


Figure 6.1: Experimental setup for the investigation of protein and transcript levels of c_{6A} mutant strains and WT grown in continuous light or DISCO Light. Three biological replicates per strain were pre-cultured in standard conditions, diluted with fresh photomixotrophic medium and exposed to standard continuous light (30 $\mu mol_{photons}\ m^{-2}\ s^{-1}$) or DISCO Light. RNA was harvested at mid-exponential growth phase for both conditions (continuous light: after 31 h; DISCO Light: after 54 h) and protein samples were taken at day 2 (continuous light & DISCO Light) and day 4 (DISCO Light only).

6.2.1 The effect of c_{6A} on the abundance of selected proteins associated with photosynthesis

6.2.1.1 Continuous light

To investigate if there were differences in protein abundances between WT and c_{6A} mutant strains under conditions that did not cause a growth phenotype, protein samples of all three strains grown photomixotrophically in continuous standard light were analysed. Protein samples (3 biological replicates per strain) were isolated in the late exponential growth phase after two days and their abundance was probed with specific antibodies on western blots. The studies were carried out with the same samples on multiple gels and membranes and some membranes were stripped of antibodies and re-exposed to a specific primary antibody that detected a protein of different size than the first primary antibody (figure 6.2, with membranes stained for total protein shown in appendix figure D.1).

Equal amounts of protein based on a Bradford assay were loaded, which was (along with

efficiency of transfer) confirmed by subsequent PonceauS staining (appendix figure D.1). The latter suggested a slightly lower amount of protein of c_{6A}-KO replicate 1 had been loaded on the membrane probed for PsbA, NDA2, and AtpB notwithstanding the Bradford assay.

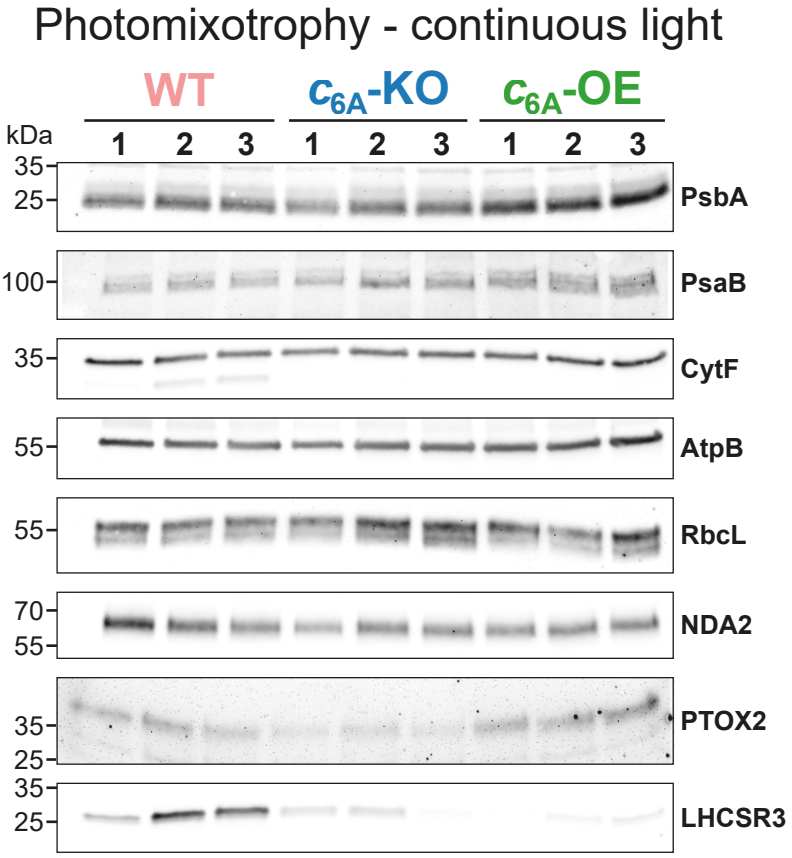


Figure 6.2: Immunoblot analyses of whole cell protein samples from c_{6A} mutant strains and WT probing for selected proteins associated with photosynthesis. Three biological replicates per strain (1-3) were grown photomixotrophically in continuous light and protein was isolated in the late exponential growth phase. Three individual SDS-PAGE gels and membranes were prepared from the same samples and some membranes were sliced in half to allow two separate protein detections per membrane. Antibodies were used to probe for eight different proteins (membrane 1: anti-PsbA & anti-NDA2, stripped and re-probed with anti-AtpB; membrane 2: anti-LHCSR3 & anti-RbcL, stripped and re-probed with anti-PsaB & anti-CytF; membrane 3: anti-PTOX2). Equal loading of total protein (except for c_{6A}-KO replicate 1) and successful transfer onto the membrane were confirmed with PonceauS total protein staining (appendix figure D.1). For reference, the protein ladder position for each membrane part is noted on the left.

PsbA, a core reaction centre protein of PSII, was detected at just above 25 kDa which was expected despite its molecular weight being ~38 kDa as the antibody manufacturer found that PsbA is apparent at 28-30 kDa (Agrisera, AS05084). Similar levels of PsbA were found between c_{6A}-KO and WT, however a slight increase in PsbA abundance was observed for c_{6A}-OE (figure 6.2). While decreased PSII subunit abundances are often observed under stress conditions like high light [323] and in assembly mutants [360], an increased amount

of PsbA is more unusual for a mutant strain. The c_{6A}-OE specific increase of PsbA protein suggests a slightly higher abundance of PSII in c_{6A}-OE, although no obvious difference could be found with BN-PAGE analyses (section 5.2.3). More PSII could indicate a lower level of photodamage when c_{6A} is overexpressed. Alternatively, increased c_{6A} levels could potentially cause altered PsbA turnover via interaction with proteases [361], influence its transcriptional regulation via interaction with proteins that bind *psbA* mRNA [362], ultimately leading to the increased abundance detected here.

PsaB, one of two core reaction centre proteins of PSI, showed slightly increased abundance in both c_{6A}-KO and c_{6A}-OE compared to WT. PsaB levels are especially interesting in the light of the c_{6A}-dependent difference detected in photosynthetic complexes, where a putatively LHC-less PSI complex was more abundant in c_{6A}-KO than in WT or c_{6A}-OE (section 5.2.3). More PSI core protein as seen here could help explain the increased abundance of this PSI complex in BN-PAGE studies of cultures from the same conditions. However, although c_{6A}-KO showed greater abundance of both PsaB and the complex than WT, the results were not consistent for c_{6A}-OE, where no increase of the PSI complex was found although PsaB levels were increased compared to WT. If the differences seen in the immunoblots are significant, this might suggest that c_{6A} plays a role in the assembly or stability of PSI-LHC complexes as well as affecting the abundance of PSI cores.

Cytochrome *f* (CytF) is a subunit of the cytochrome b_6f complex. Here, its protein levels appeared largely unaffected by c_{6A}, with only WT replicate 1 and c_{6A}-OE replicate 3 exhibiting slightly more intense bands than the rest. The two very faint bands below the 35 kDa band of CytF in WT samples were remaining signal from the LHCSR3 antibody (see below), as some blots were stripped of the bound antibodies and re-exposed to different antibodies. Given the similarity in CytF levels, cytochrome b_6f abundance seemed unaltered by c_{6A}, which indicates that the c_{6A}-dependent differences in *b* hemes redox kinetics (section 4.2.1.6) are unlikely to be caused by protein level differences but rather reflect differences in electron transfer activity of b_6f.

The abundance of AtpB, the beta-subunit of the chloroplastic ATP synthase, was similar across all samples with the exception of replicate 3 of c_{6A}-OE that appeared to have a slightly more intense band than the rest. The similarity between strains is consistent with the absence of any strain-dependent difference in proton conductivity as measured by ECS (sections 4.2.1.7 & 4.2.2.3) and supports the observation that ATP synthase activity is not affected by c_{6A}.

RbcL, the large subunit of RuBisCO, showed no consistent differences in abundance between the three strains, although some variation across replicates was observed. This is in line with the absence of a difference in acceptor side limitation of PSI (section 4.2.1.3).

Changed RuBisCO levels could lead to altered acceptor side limitation, as the CBB cycle is the major electron sink downstream of PSI.

NDA2 levels were similar between WT, c_{6A}-KO and c_{6A}-OE, with the exception of WT replicate 1 which showed a substantially more intense band (figure 6.2). It seems unlikely that NDA2 abundance could explain the c_{6A}-dependent difference of the PQ pool redox state, as c_{6A}-KO would have been expected to exhibit substantially more intense bands for NDA2 than WT and c_{6A}-OE.

PTOX2 levels were consistently lower in c_{6A}-KO samples than in WT and c_{6A}-OE, although a high background signal was observed. Lower abundance of PTOX2 in the absence of c_{6A} could help explain the c_{6A}-dependent difference of the PQ pool redox state, as decreased PTOX2 activity would lead to a more reduced PQ pool. An altered PTOX2 abundance could be caused by changes of transcript level, protein level or both. For *C. reinhardtii*, the PTOX2 transcript level was found to be upregulated by nitrogen deficiency [363] and in plants other environmental stresses like high light have been associated with increased PTOX protein levels [295, 364]. Less expression of PTOX2 was found in the knock-out mutant of the transcription factor PSR1 which regulates phosphate scavenging activities and is important for *C. reinhardtii* to manage excess light energy [365]. Consequently, if c_{6A} were a necessary signal for gene expression regulated by PSR1 (or some other transcription factor), c_{6A} absence would also lead to less PTOX2 transcription and thus decreased abundance as observed here. On the other hand, PTOX abundance in rice was found to be controlled not only at the transcript level but also through altered regulation of splicing, opening another possible route for involvement of c_{6A} [366]. In either case, it is likely that a downstream effector would be needed for c_{6A} to affect PTOX2 levels via a regulatory pathway, as c_{6A} is tentatively localised in the thylakoid lumen, PTOX2 is stromal localised, and the *PTOX2* gene is nuclear encoded. The difference in abundance of PTOX2 found here contrasts with the earlier studies on the influence of PTOX2 on the redox kinetics of *b* hemes or the oxygen gas exchange of the c_{6A} mutant strains. Those studies suggested involvement of PTOX2 in c_{6A}-dependent differences was unlikely (sections 4.2.1.6 & 4.2.1.8). However, as PTOX2 accounts for only a small percentage of PQ pool oxidation (~3% of the amount of linear electron flow [295]), it is possible that the effect of a lower PTOX2 abundance in c_{6A}-KO was not detectable with the methods used. To test if a decreased amount of PTOX2 is the cause of the more reduced PQ pool in c_{6A}-KO, OJIP measurements of WT and the c_{6A} mutant strains with added PTOX inhibitor n-propyl gallate could be employed.

Lastly, the protein abundance of LHCSR3, a stress related protein that is the major effector of the pH-dependent qE part of NPQ, was investigated. WT showed readily detectable bands albeit with some variation between replicates, while LHCSR3 abundance in c_{6A}-KO and

c_{6A}-OE was greatly reduced. A much lower abundance of LHCSR3 was also found for knock-out mutants of PGR5 and PGRL1 compared to their wild-type background when grown under continuous light [65]. Similar to c_{6A}, PGR5 and PGRL1 were found to be important for growth of *C. reinhardtii* under fluctuating light conditions. However, for PGR5 and PGRL1 knock-outs, the lower LHCSR3 abundance correlated with a decreased NPQ capacity. For c_{6A}, this was not the case as an increased NPQ capacity was found even though LHCSR3 levels were drastically reduced (sections 4.2.1.3 & 4.2.2.2). This suggests that the c_{6A}-dependent NPQ difference found does not rely on LHCSR3 activity but rather on the other NPQ components qT, qZ, and qI. If the NPQ difference seen is in fact independent of LHCSR3 activity (i.e. not pH dependent) addition of the ionophore nigericin during NPQ recordings should result in the same c_{6A}-dependent differences seen, compared to a disappearance of differences if LHCSR3 were involved [70].

Overall, the investigation of abundances of proteins associated with photosynthesis in continuous light uncovered subtle but notable differences between c_{6A}-KO and WT. The consistently lower abundance of PTOX2 and LHCSR3 in c_{6A}-KO was especially noteworthy. The c_{6A}-OE strain showed protein abundance similar to WT levels for PTOX2 but not for LHCSR3, indicating that a changed c_{6A} abundance can influence protein levels differently. The protein abundance differences found in continuous light might also affect how well WT and c_{6A} mutant strains cope with DISCO Light. The protein levels of cultures grown in DISCO Light were examined to provide further insight on this.

6.2.1.2 DISCO Light

In addition to protein levels in cultures grown in continuous light, protein levels of *C. reinhardtii* c_{6A} mutant strains and WT grown in DISCO Light were examined. Samples of three biological replicates per strain were taken at day 2 and day 4 of growth, where a clear c_{6A}-dependent difference in optical density of the cultures was visible (section 3.2.3.2). Immunoblots were carried out for the same proteins and following the same procedure as for continuous light (figures 6.3 & 6.4, with membranes stained for total protein shown in appendix figures D.2 & D.3).

6.2.1.2.1 DISCO Light Day 2

Focusing on investigation of protein abundances on day 2, equal protein loading between samples could be confirmed by PonceauS staining for all membranes (appendix figure D.2).

Similar to samples from continuous light, the PsbA levels from DISCO Light samples appeared to be slightly increased in c_{6A}-OE compared to WT (figure 6.3). Additionally, c_{6A}-KO also exhibited increased PsbA abundance compared to WT. For c_{6A}-KO increased PSII abundance could help explain the lowered PSI/PSII ratio observed in 77 K fluorescence measurements of cultures grown in DISCO Light (4.2.2.1). However, as c_{6A}-OE recovered the difference in 77 K fluorescence, it is unlikely that the c_{6A}-dependent difference in PSI/PSII ratio is solely due to altered PsbA levels and it could also depend on variations in LHC antennae binding to the photosystems.

PsaB levels were similar between the strains in both continuous light and DISCO Light with c_{6A}-KO and c_{6A}-OE exhibiting slightly increased band intensities compared to WT.

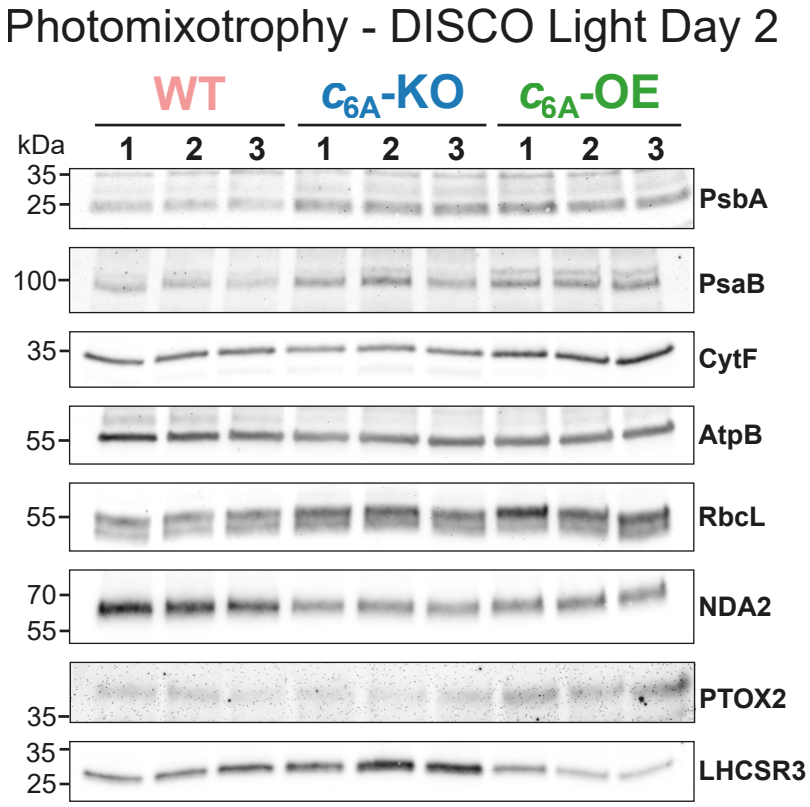


Figure 6.3: Immunoblot analyses of whole cell protein samples from c_{6A} mutant strains and WT probing for selected proteins associated with photosynthesis. Three biological replicates per strain (1-3) were grown photomixotrophically in DISCO Light and protein was isolated on day 2 of growth. Three individual SDS-PAGE gels and membranes were prepared from the same samples and some membranes were sliced in half to allow two separate protein detections per membrane. Antibodies were used to probe for eight different proteins (membrane 1: anti-PsbA & anti-NDA2, stripped and re-probed with anti-AtpB; membrane 2: anti-LHCSR3 & anti-RbcL, stripped and re-probed with anti-PsaB & anti-CytF; membrane 3: anti-PTOX2). Equal loading of total protein and successful transfer onto the membrane were confirmed with PonceauS total protein staining (appendix figure D.2). For reference, the protein ladder position for each membrane part is noted on the left.

The abundance of CytF seemed slightly affected by c_{6A} in DISCO Light grown cultures as c_{6A}-KO exhibited slightly less intense bands than WT and c_{6A}-OE, which was more obvious for c_{6A}-OE. Less CytF would likely indicate less cytochrome b_6f complex. It is possible that the more reduced *b* hemes in c_{6A}-KO may lead to increased ROS production at b_6f [367] which could damage the complex, decreasing its abundance.

AtpB abundance was not consistently different between the strains, although WT replicate 1 showed a slightly more intense band than the rest. As under continuous light, this is in line with the absence of an ATP synthase activity difference as determined by ECS measurements in DISCO Light (section 4.2.2.3).

In contrast to continuous light, DISCO Light samples exhibited a difference in abundance of RbcL, as c_{6A}-KO and c_{6A}-OE both showed slightly elevated band intensities from WT. RbcL abundance is regulated via various transcriptional and post-transcriptional mechanisms in response to environmental conditions [368]. It may be that high or low amounts of c_{6A} could influence this intricate regulatory system differently, leading to similar RbcL amounts in c_{6A}-KO and c_{6A}-OE that are changed from WT levels. An increased amount of RuBisCO, as suggested by higher RbcL levels in c_{6A}-KO could also lead to lower acceptor side limitation at PSI compared to WT. This was not the case for the first 40 min of DISCO Light exposure (section 4.2.2.4), although it is possible that after two days of growth in DISCO Light such an effect might emerge.

NDA2 abundance was consistently lower in c_{6A}-KO and c_{6A}-OE than in WT when grown in DISCO Light, contrasting the similar levels found in continuous light. NDA2 was found to be important in nitrogen deprivation and upregulated in sulphur deprived conditions [369, 370], connecting its activity to coping with stress conditions. A decreased abundance of NDA2 in c_{6A}-KO compared to WT might reflect a lack of adaptation to the stressful light condition of DISCO Light. However, c_{6A}-OE did not recover this protein's abundance to WT levels, preventing clear conclusions of c_{6A}'s effect on NDA2.

The c_{6A}-dependent difference in PTOX2 abundance found in continuous light, could also be observed in samples from DISCO Light. Here, c_{6A}-KO exhibited lower band intensities than WT and c_{6A}-OE, albeit a high background staining level. Interestingly, c_{6A}-OE showed even higher PTOX2 abundance than WT. Under stressful light conditions like DISCO Light, PTOX2 activity may be important to prevent over-reduction of the PQ pool by the short phases of high intensity light. A lower amount of PTOX2 in c_{6A}-KO in DISCO Light could therefore contribute to the observed growth penalty. In the light of the high background staining of PTOX2 western blots, optimisation of antibody exposure and estimation of transcript levels should be carried out.

LHCSR3 protein abundance was strikingly different in DISCO Light compared to continuous light. In DISCO Light, c_{6A}-KO exhibited the most intense bands compared to WT and c_{6A}-OE. Increased LHCSR3 abundance suggests higher stress levels in c_{6A}-KO compared to WT and c_{6A}-OE, in line with the observed growth phenotype and increased NPQ levels under DISCO Light (section 4.2.2.2). However, as mentioned before, it remains to be investigated if the observed NPQ differences are LHCSR3-dependent, or if they rely on other mechanisms of NPQ.

6.2.1.2.2 DISCO Light Day 4

For protein samples from DISCO Light grown cultures harvested at day 4, equal protein loading between samples could be confirmed by PonceauS staining for all membranes (appendix figure D.3).

For the two photosystem subunits PsbA and PsaB, similar patterns were obtained from day 4 samples as from day 2 samples (figure 6.4). Interestingly, two new bands above 15 kDa appeared when probing for PsbA. These bands were most prominent in c_{6A}-KO samples and are likely to correspond to C-terminal fragments of PsbA breakdown [112, 371]. These breakdown fragments appear when *C. reinhardtii* is photoinhibited [112]. The increased presence of breakdown product bands in c_{6A}-KO compared to WT and c_{6A}-OE suggests that c_{6A}-KO is more photoinhibited in DISCO Light, correlating with the observed growth phenotype. Interestingly, the degradation of PsbA is correlated with the dissociation of PSII subunits PSBO, PSBP, and PSBQ on the luminal side of PSII. This dissociation was found to possibly represent the rate-limiting step of PsbA degradation [113, 114]. For PSBO it has been shown that a disulphide in oxidised form is necessary for a stable protein [115]. Increased PsbA breakdown in the absence of c_{6A} might therefore also connect c_{6A} with thiol-based redox regulation.

CytF abundance was found to be not substantially affected by c_{6A}, as all samples exhibited similarly intense bands. Comparing this to the observation at day 2, where CytF levels were lower in c_{6A}-KO, may suggest an earlier onset of ROS damage in c_{6A}-KO, with all strains showing a similar level by day 4.

The c_{6A}-KO strain appeared to have slightly but consistently lower AtpB levels than WT and c_{6A}-OE on day 4 of DISCO Light growth. This may indicate that ATP synthesis is affected by absence of c_{6A} after 4 days of growth in DISCO Light. Similar to the increased PSII photoinhibition levels in c_{6A}-KO, an effect on ATP synthase could be a longer-term consequence of imbalances within the PETC and further supports the idea that c_{6A}-KO is more adversely affected in DISCO Light than WT and c_{6A}-OE.

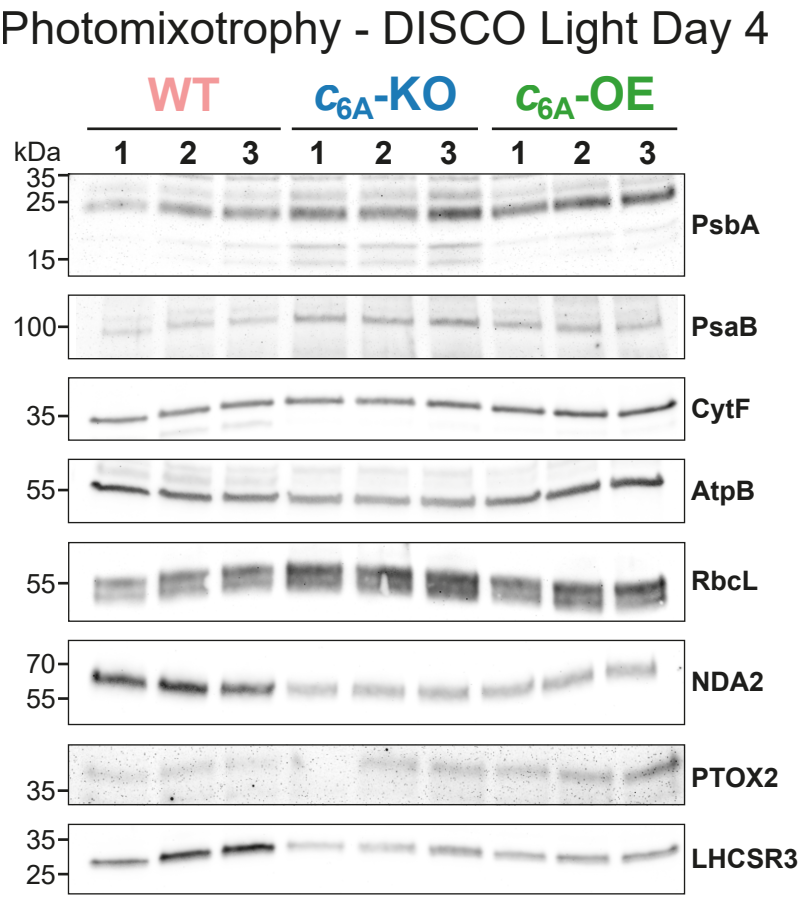


Figure 6.4: Immunoblot analyses of whole cell protein samples from c_{6A} mutant strains and WT probing for selected proteins associated with photosynthesis. Three biological replicates per strain (1-3) were grown photomixotrophically in DISCO Light and protein was isolated on day 4 of growth. Three individual SDS-PAGE gels and membranes were prepared from the same samples and some membranes were sliced in half to allow two separate protein detections per membrane. Antibodies were used to probe for eight different proteins (membrane 1: anti-PsbA & anti-NDA2, stripped and re-probed with anti-AtpB; membrane 2: anti-LHCSR3 & anti-RbcL, stripped and re-probed with anti-PsaB & anti-CytF; membrane 3: anti-PTOX2). Equal loading of total protein and successful transfer onto the membrane were confirmed with PonceauS total protein staining (appendix figure D.3). For reference, the protein ladder position for each membrane part is noted on the left.

The patterns of abundance for RbcL and NDA2 were similar between day 4 and day 2 samples with the c_{6A} mutant strains showing more intense and less intense bands than WT for RbcL and NDA2, respectively.

PTOX2 abundances were similar between c_{6A}-KO and WT at day 4 of DISCO Light, except for KO replicate 1 where an air bubble prevented successful protein transfer leading to a false negative detection (appendix figure D.3). The c_{6A}-OE strain showed marginally increased PTOX2 band intensity compared to c_{6A}-KO and WT. The similar levels between c_{6A}-KO and WT are in contrast to the c_{6A}-dependent difference observed before in continuous

light and DISCO Light day 2, indicating that over four days in DISCO Light, PTOX2 protein levels are unlikely to be solely affected by c_{6A} abundance.

Levels of LHCSR3 in DISCO Light day 4 samples resembled the abundance in samples from continuous light cultures more than the abundance pattern of DISCO Light day 2 samples. The c_{6A} mutant strains exhibited lower intensity bands than WT, although the difference between strains was not as pronounced as in samples from continuous light.

Overall, the investigation of abundances of proteins associated with photosynthesis in DISCO Light showed that c_{6A}-KO in particular is under considerable stress. This was evidenced by transient increases in LHCSR3 levels, the appearance of PSII breakdown products, and observed reductions in the abundance of cytochrome b_6f and ATP synthase compared to WT. While these findings provided valuable insights, it is important to note that western blotting is not a quantitative technique. To assess accurately how protein levels change within a single strain when comparing continuous light and DISCO Light conditions, additional immunoblot experiments would be necessary. Analyses comparing all three conditions for one strain on one membrane could offer additional insights into the differential regulation of photosynthetic protein abundance in response to DISCO Light and how c_{6A} affects such regulation. Moreover, examining these changes at the transcript level through RNAseq would provide further understanding of the underlying regulatory mechanisms (section 6.2.2).

6.2.1.3 Further Discussion

The investigation of protein levels led to the finding that, in some cases, c_{6A}-OE did not rescue the differences in protein abundance seen between c_{6A}-KO and WT back to WT level. These proteins included PsbA, PsaB, NDA2, RbcL, and LHCSR3 under either continuous or DISCO Light conditions.

The observation of protein levels of c_{6A}-OE that appeared uniquely altered compared to c_{6A}-KO and WT, or similar to the abundance in c_{6A}-KO, could be interpreted as an effect that is not dependent on c_{6A}. Instead, these differences may be symptomatic of other uncharacterised off-site variations between the strains. However, earlier whole genome sequencing (WGS) analysis concluded that the differences between WT and c_{6A}-KO (and by extension, c_{6A}-OE, which has a c_{6A}-KO background) are most significant at the c_{6A} gene, with no other regions showing such substantial differences (section 3.2.1).

Another plausible explanation is that *C. reinhardtii* may exhibit sensitivity to the precise amount of c_{6A} present. In this scenario, only the endogenous levels of c_{6A} in WT cells are

optimal for normal function, whereas both the absence (as in c_{6A}-KO) and overexpression (as in c_{6A}-OE, accepting the assumption that increased transcript levels translate to increased protein levels) of c_{6A} lead to the observed altered protein levels. This type of response, where low amounts of a stimulus lead to a different response than no stimulus or high amounts of it, is referred to as 'hormesis' [372]. While hormesis has traditionally been studied in the context of toxic compound exposure, similar complex dose-dependent responses can also occur in gene expression regulation, for example in so-called 'incoherent feed-forward loops' [373]. Especially when considering the identity of c_{6A} as a redox protein and the presence of its surface-exposed disulphide bridge, it is conceivable that c_{6A} could play a role in the intricate network of thiol-based redox signalling that influences protein activities and levels in the thylakoid [125]. Indeed, a hypothesis for c_{6A}'s function involving the oxidation of disulphide bridges of luminal proteins was proposed before [134] and could now be helpful for explaining the impact of c_{6A} on protein levels. For instance, in *A. thaliana*, disulphide bond formation, i.e. oxidation, is crucial for the stability of the PSBO protein, which would otherwise be degraded if left in its unfolded form, leading to reduced protein levels [115]. This suggests that c_{6A} could be involved in similar redox-dependent regulatory mechanisms that affect the stability and abundance of photosynthetic proteins in *C. reinhardtii*. Further investigation of c_{6A}'s potential involvement in redox signalling pathways should therefore be carried out.

In summary, protein level analyses suggested that c_{6A} could be involved in a complex (possibly thiol-based) regulatory system. Regulatory systems (including thiol-based redox regulation) can often also affect gene expression [374]. This, together with the need to understand how the transcriptome reacts to the loss of c_{6A} and DISCO Light, prompted a detailed analysis of the transcriptome of c_{6A} mutant strains in *C. reinhardtii*.

6.2.2 Transcriptomic analysis of *C. reinhardtii* c_{6A} mutant strains exposed to DISCO Light

Having investigated protein levels of c_{6A} mutant strains and WT of *C. reinhardtii*, transcriptomic analyses were carried out with RNAseq to further investigate a possible role of c_{6A} in regulation processes and to assess the impact of DISCO Light on the transcriptome. After extraction of RNA, its quality and suitability for RNAseq was determined. Subsequently, differential expression analysis was performed.

6.2.2.1 Quality assessments

RNA was extracted from the same cultures as used for the protein abundance studies during their respective mid-exponential growth phases (after 31 h in continuous light and after 54 h in DISCO Light, section 6.2.1). The quality of RNA samples was assessed by gel electrophoresis and Nanodrop measurements (appendix table E.1 and figure E.1) and found to be appropriate for analysis. Novogene, the company that carried out the sequencing, also confirmed the high quality of provided samples using the Agilent 5400 fragment analyzer (appendix table E.2). Following the sequencing of the samples, Novogene assessed the read quality by analysis of quality scores and determined low error rates with over 94% of all reads having less than 0.001% errors (Q30, appendix table E.3). The GC content of sequenced samples was found to be appropriate for *C. reinhardtii*, ranging between 59.30 and 62.79%, which is comparable to the GC content of the *C. reinhardtii* genome at 64% [11]. The obtained reads were then mapped to the latest *C. reinhardtii* genome assembly (CC-4532 v6.1, [11]) and reads for each gene were counted. Further quality measures of the alignment and assignment process indicated that the data were of high enough quality to proceed with further analysis (end of appendix E). The high read duplication rate for all samples signified that the sequencing depth was unnecessarily high but this did not pose a problem for further analysis.

As expected, read counts for *CYC4*, the gene coding for c_{6A}, were different between WT, c_{6A}-KO and c_{6A}-OE (figure 6.5). Under continuous light, no counts were found for c_{6A}-KO, again confirming the strain as a c_{6A} knock-out. The WT level of 246 counts on average was increased nearly 14-fold to 3405 on average in c_{6A}-OE, making c_{6A}-OE an overexpression (at least at transcript level) rather than a complementation strain. Similar counts of *CYC4* transcripts to those under continuous light for WT and c_{6A}-OE were found under DISCO Light conditions (200 and 3639 counts, respectively). Cytochrome c_{6A} is thus not differentially regulated in response to DISCO Light. While this may be unexpected in the light of the growth phenotype observed under DISCO Light, it aligns well with the overall very limited differential expression of c_{6A} under various conditions, as determined by database and literature searches (table 6.1). Surprisingly, two of three replicates of c_{6A}-KO had reads for *CYC4* in DISCO Light (9 and 77 read counts for replicates 2 and 3, respectively). Through examination of the read data at the *CYC4* locus for these replicates it could be confirmed that there were no reads in the knocked-out region, which includes the pivotal CxxCH heme binding motif. Expression of functional c_{6A} can therefore be excluded in these replicates of c_{6A}-KO.

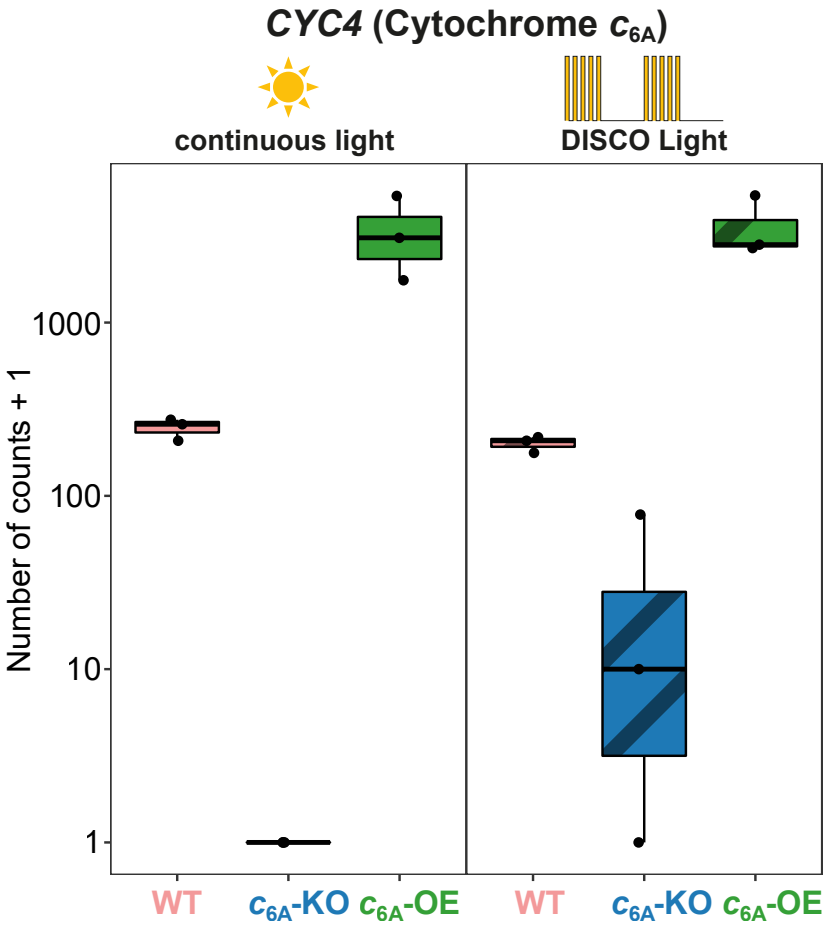


Figure 6.5: Counts of reads mapped to *CYC4* comparing WT and c_{6A} mutant strains when grown under continuous light or DISCO Light. Counts are presented on a logarithmic scale for which one read was manually added to samples that exhibited no reads (c_{6A}-KO).

A principal component analysis (PCA) of the count data of 18 individual samples was performed to estimate variance between strains and replicates (figure 6.6). Clustering of biological replicates was visible with c_{6A}-OE exhibiting the largest spread. Under continuous light conditions, c_{6A}-KO and WT clustered close to each other, indicating only little differential expression. The c_{6A}-OE strain was markedly different under continuous light from c_{6A}-KO and WT, although mostly in the dimension of principal component 2 (PC2) which accounted for only a small percentage of variability (16.73%). Principal component 1 (PC1) seemed to be substantially influenced by growth under DISCO Light, as all strains exhibited a shift towards positive values compared to continuous light. The distance in the PCA plot between c_{6A}-KO and WT was larger for the DISCO Light samples than for the continuous light samples, indicating more differential expression between strains under DISCO Light.

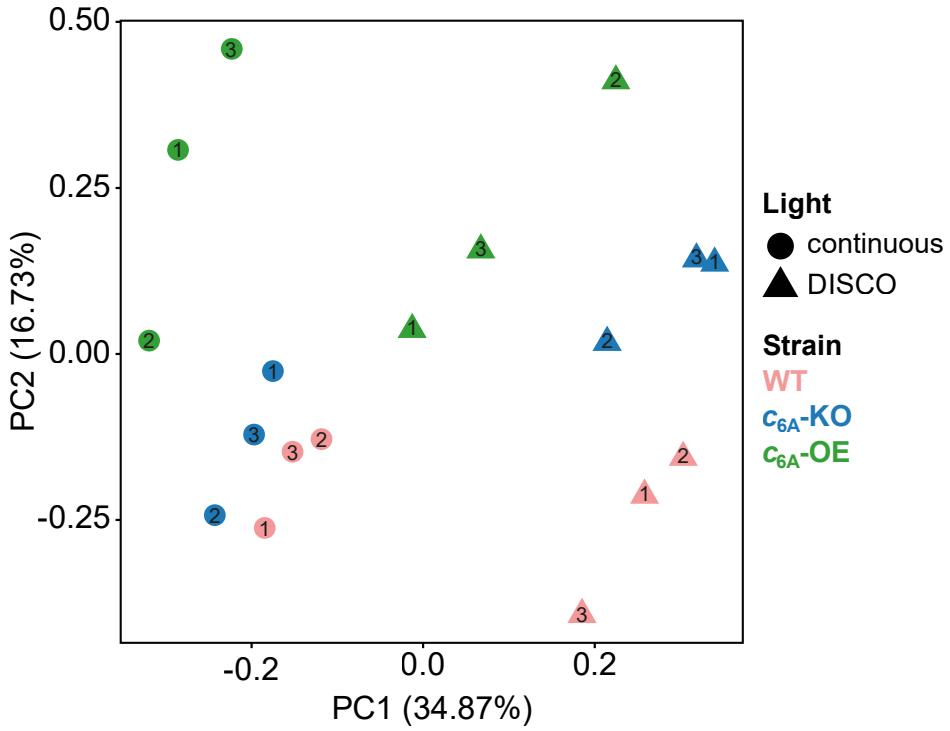


Figure 6.6: Principal Component Analysis (PCA) of the RNAseq count data. Samples are separated by strain and light condition used and the number in the symbol indicates the replicate.

Overall, the PCA uncovered that altered expression levels of c_{6A} seem to affect the transcriptome of *C. reinhardtii* differently as both c_{6A}-KO and c_{6A}-OE clustered distinctly from WT and from each other. Additionally, DISCO Light growth appeared to have caused a strong transcriptomic response, mostly independent of the strain. Differential expression analysis was carried out to explore these observations further.

6.2.2.2 Differential expression analysis of *C. reinhardtii* c_{6A} mutant strains grown in continuous light or DISCO Light

Analysis of differential expression was carried out with DESeq2 employing a model that included interaction terms describing the effect the strain had on the difference between continuous light and DISCO Light. This analysis provided twelve different comparisons (arrows + interaction terms in figure 6.7).

If not specified otherwise, the following results are all based on the differential expression analysis of 16828 expressed genes of *C. reinhardtii* with a total of at least 5 reads in at least 3 samples. "Differentially expressed genes" (DEGs) are specified as genes that showed an absolute $\log_2$ fold change ($\log_2$FC) larger than 1 and an adjusted p-value of less than 0.05. The overall number of DEGs for the different comparisons is shown in table 6.2.

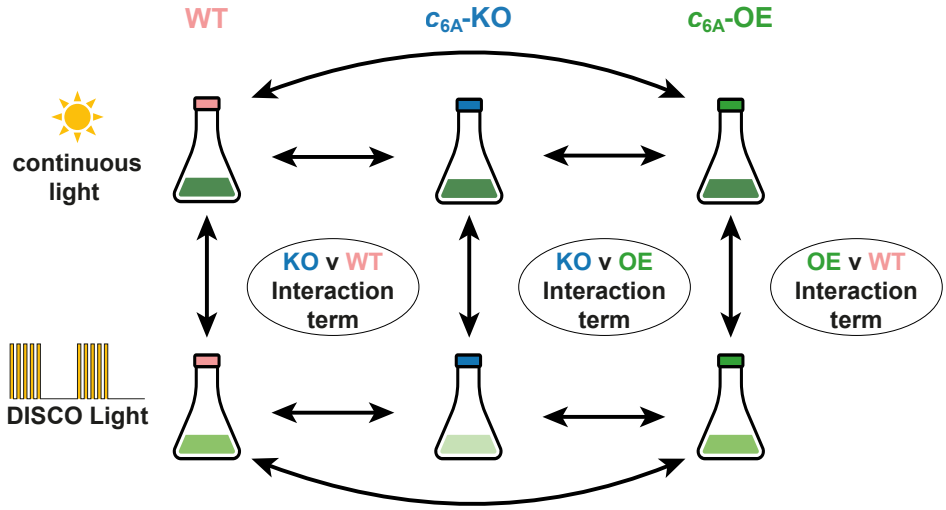


Figure 6.7: Comparisons of gene expression between strains and/or conditions as carried out with DESeq2.

Table 6.2: Number of DEGs ($|\log_2 FC| > 1$ & $p_{adjusted} < 0.05$) and the percentage out of all expressed genes (16828) per comparison.

Group	Comparison	#DEGs	% of all genes
Continuous light	KO vs WT continuous	225	1.3
	OE vs WT continuous	396	2.4
	KO vs OE continuous	368	2.2
DISCO light	KO vs WT DISCO	372	2.2
	OE vs WT DISCO	352	2.1
	KO vs OE DISCO	425	2.5
DISCO vs continuous	WT DISCO vs continuous	926	5.5
	KO DISCO vs continuous	1578	9.4
	OE DISCO vs continuous	753	4.5
Interaction DISCO vs continuous	KO vs WT	37	0.22
	OE vs WT	108	0.64
	KO vs OE	40	0.24

The numbers in table 6.2 confirmed two observations originating from the PCA. First, in continuous light c_{6A}-OE showed more DEGs compared to WT (2.4%) or c_{6A}-KO (2.2%) than c_{6A}-KO compared to WT (1.3%). Second, when comparing the group "DISCO vs continuous" (4.5-9.4% DEGs) with "DISCO Light" (2.1-2.5% DEGs) or "Continuous light" (1.3-2.4% DEGs) the effect of DISCO Light appeared larger than the effect of the genotype. Additionally, the low numbers of DEGs in the interaction terms (0.22-0.64% DEGs) suggested that c_{6A}'s effect on the transcriptomic reaction to DISCO Light is limited.

Five questions were formulated to investigate this RNAseq dataset further. First, how are transcript levels affected by the absence of c_{6A} in continuous light, i.e. conditions that did not cause a growth phenotype? Second, how are transcript levels affected by the absence of c_{6A} in DISCO Light? Third, how does the WT transcriptome change between continuous light and DISCO Light? Fourth, how does the transcriptomic response to DISCO light differ between c_{6A}-KO and WT? Last, what is the influence of c_{6A} on transcript levels of photosynthesis-related genes under continuous light or DISCO Light? While further questions could be formulated as well, these five appeared to be the most important and informative ones regarding the function of c_{6A}.

6.2.2.2.1 How are transcript levels affected by the absence of c_{6A} in continuous light?

225 genes were differentially expressed between c_{6A}-KO and WT in continuous light, representing 1.3% of all expressed genes. Of these DEGs, 132 (59%) had lower and 93 (41%) had higher expression levels in c_{6A}-KO than WT. The ten most significantly differentially expressed genes that were upregulated in c_{6A}-KO compared to WT, included two "Rhythm of Chloroplast" genes *ROC59* and *ROC15*, *HOPP1*, and seven other uncharacterised genes (table 6.3).

HOPP1 encodes a HORMA-domain containing protein. These proteins are crucial regulators of meiosis in a variety of species [375, 376]. An upregulation in the absence of c_{6A}, as observed here, might connect c_{6A} with the process of meiosis. However, HORMA-domain proteins and especially *HOPP1* have not been well studied in *C. reinhardtii*, preventing clear conclusions about c_{6A}'s involvement.

The "Rhythm of Chloroplast" genes were identified through mutant strains exhibiting an altered chloroplast circadian rhythm, as determined by expression of a bioluminescent reporter from the circadian regulated chloroplast *tufA* promoter [377]. ROC15, the transcript of which had higher expression levels in c_{6A}-KO than WT, was subsequently found to be a key transcription factor in the resetting of the circadian clock in *C. reinhardtii*. Its mRNA levels and protein amounts oscillate in a circadian manner and are regulated by light [378]. Together

with other ROC genes and proteins, ROC15 was proposed to form transcriptional feedback loops in the *C. reinhardtii* circadian clock. An elevated level of *ROC15* mRNA, as seen here for c_{6A}-KO, was also found for a mutant of CETL (Cre07.g357500, not annotated in the latest genome release), which has since been placed upstream of ROC15 in a circadian clock regulatory network [379]. Cytochrome c_{6A} could thus assume another position upstream of ROC15 similar to CETL, affecting the circadian rhythm. This could be tested by examining the light resetting ability and the light induced degradation of ROC15 in the c_{6A} mutant strains compared to WT. *ROC15* is a target of the transcription factor ROC75 that acts as a daytime repressor of the circadian clock in *C. reinhardtii* [380]. Interestingly, enrichment of putative ROC75 targets could be found in DEGs comparing c_{6A}-KO and WT in continuous light (7 found, expected: 0.94, 7.48-fold enrichment). This further supports a putative regulatory role for c_{6A} that is connected to the circadian clock in *C. reinhardtii*.

Table 6.3: Top 10 upregulated DEGs (by $p_{adjusted}$) when comparing c_{6A}-KO to WT in continuous light and the respective symbols, $\log_2$ fold changes, adjusted p-values, and descriptions.

Gene ID	Gene symbol	$\log_2$FC	$p_{adjusted}$	Description
Cre11.g478800		4.83	1.62E-77	
Cre10.g425050	*ROC59*	2.63	1.34E-41	Rhythm Of Chloroplast 59
Cre10.g452550	*HOPP1*	3.38	4.24E-26	Homologous-pairing protein 1
Cre15.g801749		3.23	5.16E-23	
Cre02.g141826		4.27	6.38E-20	
Cre09.g410450	*ROC15*	1.46	3.47E-19	Rhythm Of Chloroplast 15
Cre04.g217928		6.44	1.56E-18	
Cre12.g498850		1.00	1.43E-14	
Cre17.g716700		1.55	5.81E-14	
Cre16.g687400		1.57	7.11E-14	

The ten most significantly downregulated genes in c_{6A}-KO compared to WT included *PDC3*, *LHCBM8*, *FAD6*, *CPL20*, *PHT3A*, and five other undescribed genes (table 6.4).

The change in *PDC3* expression is intriguing, as this gene encodes the pyruvate decarboxylase PDC3 that is part of the ethanol fermentation pathway of *C. reinhardtii* under anaerobic conditions. This cytoplasmic protein catalyses the decarboxylation of pyruvate to acetaldehyde and CO_2 [381]. Its mRNA accumulation follows a circadian rhythm with a 24h period [382], further connecting c_{6A} with circadian regulation mechanisms. However, protein levels were not found to follow the same circadian pattern [381], making an additional posttranslational regulation process appear likely. Nevertheless, less *PDC3* mRNA as observed in the absence of c_{6A} might result in a lower capacity for fermentation. Under continuous light and aerobic conditions (as is the case for standard culturing conditions) this might be irrelevant, in line with the absence of a growth phenotype. However, in conditions that require more metabolic flexibility due to stress conditions, for example DISCO Light, lower fermentation capacity might prove detrimental for maintaining metabolic balance and could contribute to the observed c_{6A}-dependent growth phenotype.

The lower abundance of *LHCBM8* transcript in c_{6A}-KO compared to WT is noteworthy, as this gene encodes a subunit of the LHCII antenna. Altered LHCII antennae composition would be interesting in the light of the putative LHC-less PSI complex observed more prominently in c_{6A}-KO (section 5.2.3). As part of the trio LHCBM4/6/8 comprising very similar proteins, LHCBM8 mainly resides in a free LHCII pool within the thylakoid membrane that is not or only very poorly connected to PSII. LHCII that include LHCBM4/6/8 are therefore more likely to be involved in photoprotective mechanisms rather than being essential for light harvesting [353]. Interestingly, *LHCBM4* was also differentially expressed in c_{6A}-KO vs WT (log_2FC = -1.21, p_{adj} = 7.51E-14) while *LHCBM6* (log_2FC = -0.06, p_{adj} = 0.89) was unaffected. LHCBM4/6/8 have been suggested to be important for state 1 to 2 transitions and a reduction of LHCBM4/6/8 caused significant NPQ reduction and elevated ROS levels in *C. reinhardtii* [353]. While state transitions were not absent in c_{6A}-KO, the lowered *LHCBM8* expression is another reason for further investigation of state transition rates (section 4.2.1.2). Furthermore, lower LHCBM4/6/8 levels lead to decreased accumulation of LHCSR3, suggesting that LHCBM4/6/8 are important for stabilising LHCSR3 in the thylakoid membranes, although no stable complexes between LHCSR3 and LHCBMs were found [353]. Lower *LHCBM8* expression (as seen for c_{6A}-KO) could therefore help explain the decreased LHCSR3 protein levels observed in the absence of c_{6A} (section 6.2.1.1), while not accounting for the increased NPQ in c_{6A}-KO (section 4.2.1.3). Together with other *LHCBM*s, expression of *LHCBM8* was suggested to be under the control of the transcriptional repressor NAB1, which is known to affect *LHCBM6* expression when the linear photosynthetic electron flow is restricted by CO_2 limitation in photomixotrophy [353, 383]. However, the difference in

expression regulation found here between *LHCBM4/8* being downregulated and *LHCBM6* being unaffected suggests that there might be regulatory factors involved in addition to the joint regulation of *LHCBM4/6/8* via NAB1.

Table 6.4: Top 10 downregulated DEGs (by $p_{adjusted}$) when comparing c_{6A}-KO to WT in continuous light and the respective symbols, log_2 fold changes, adjusted p-values, and descriptions.

Gene ID	Gene symbol	log_2FC	$p_{adjusted}$	Description
Cre16.g686285		-4.74	5.13E-45	
Cre03.g165700	*PDC3*	-3.07	4.35E-30	Pyruvate decarboxylase
Cre06.g284250	*LHCBM8*	-2.04	4.29E-29	Light-harvesting Chlorophyll a/b binding protein of LHCII
Cre13.g590500	*FAD6*	-1.85	1.64E-25	Omega-6-fatty acid desaturase, chloroplast isoform
Cre15.g634650		-3.33	5.27E-25	
Cre16.g650400	*CPL20*	-2.05	3.34E-23	Hypothetical zinc-dependent DNA-binding protein
Cre15.g801845		-9.58	1.31E-19	
Cre03.g172300	*PHT3A*	-1.09	7.03E-18	Mitochondrial phosphate carrier protein
Cre07.g321750		-4.06	9.54E-17	
Cre12.g512300		-2.44	1.04E-15	

To examine if there are specific patterns of differential expression comparing c_{6A}-KO and WT, GO enrichment was employed. Gene ontology enrichment has the limitation that only 60.5% of the expressed genes in this dataset have at least one GO term annotation. Nevertheless, it can be useful to examine these annotations to obtain insights into already

described processes. Here, a significant enrichment was defined as having a false-discovery-rate adjusted p-value (FDR) of less than 0.05.

For the upregulated genes, 10 of 93 were associated with the GO term "signalling" (GO:0023052) representing a 3.4-fold enrichment. These genes included adenylate/guanylate cyclases and *PRR1*, a gene that encodes a pseudo-response regulator-like protein similar to the *A. thaliana* circadian clock protein TOC1. *PRR1* is also a putative target of the above-mentioned transcription factor ROC75 [380]. This finding further supports a possible involvement of c_{6A} in circadian clock regulation.

For the downregulated genes, a significant enrichment was found for the cellular component GO term "chloroplast thylakoid" (7 out of 132 genes, 9.45-fold enrichment, GO:0009534). Together with *LHCBM4/8* and *CYC4*, three more genes encoding thylakoid associated proteins were significantly downregulated: copper-regulated *CHL27A* which encodes a chlorophyll biosynthesis protein [384], *PRX6* encoding a thioredoxin dependent peroxiredoxin similar to PRXQ of *A. thaliana* [137, 385], *TRXF1* coding for a chloroplastic thioredoxin [386], and the chloroplastic gene *atpB* encoding the beta subunit of the chloroplastic ATP synthase. Lowered expression of peroxiredoxin and thioredoxin in the absence of c_{6A} implicates c_{6A} in thiol-based signalling mechanisms, as these proteins are part of the intricate thioredoxin mechanisms regulating various parts of photosynthesis [268]. This lends further support to the earlier suggestion of a possible involvement of c_{6A} in thiol-based regulation (section 6.2.1.3). Differentially expressed *atpB* was surprising, as no difference in protein levels of AtpB was found between c_{6A}-KO and WT (section 6.2.1.1). However, altered mRNA levels do not necessarily translate into changed protein levels, as post-transcriptional and -translational processes affect protein abundance. Additionally, as *atpB* is a chloroplast encoded gene and the RNAseq procedure enriched for poly-A tailed transcripts, caution has to be taken when interpreting this result.

To investigate the expression in c_{6A}-OE of genes that were DEGs when comparing c_{6A}-KO and WT in continuous light, a heatmap of all 225 DEGs was created containing all continuous light samples (figure 6.8).

Hierarchical clustering of the genes resulted in five distinct clusters, three of which exhibited downregulated genes comparing c_{6A}-KO with WT (cluster 1, 2 & 5), while the other two comprised upregulated genes in c_{6A}-KO versus WT (clusters 3 & 4). In cluster 5, four very lowly expressed genes could be found (read count mean over all samples: 7-13). For genes in clusters 2 and 3, c_{6A}-OE appeared to have similar expression as c_{6A}-KO. This phenomenon was also observed for abundances of some of the proteins investigated earlier (section 6.2.1) and could point to a complex dose-dependent regulation involving c_{6A}. Three

"Rhythm of Chloroplast" genes (*ROC15* and *ROC59* mentioned earlier and *ROC40*) also belong to these clusters. Notably, *ROC15* has already been identified as having a complex regulation [379], which may align with the proposed involvement of c_{6A}.

For genes in clusters 1 and 4, c_{6A}-OE showed reversal of the difference seen for c_{6A}-KO compared to WT. Expression of these 72 genes (58 in cluster 1, 14 in cluster 4) therefore appears more directly linked to presence or absence of c_{6A} than expression of genes in clusters 2 and 3. In clusters 1 and 4 many of the genes discussed above were found, including *CYC4*, *PDC3*, *LHCBM4*, *TRXF1* and *atpB*.

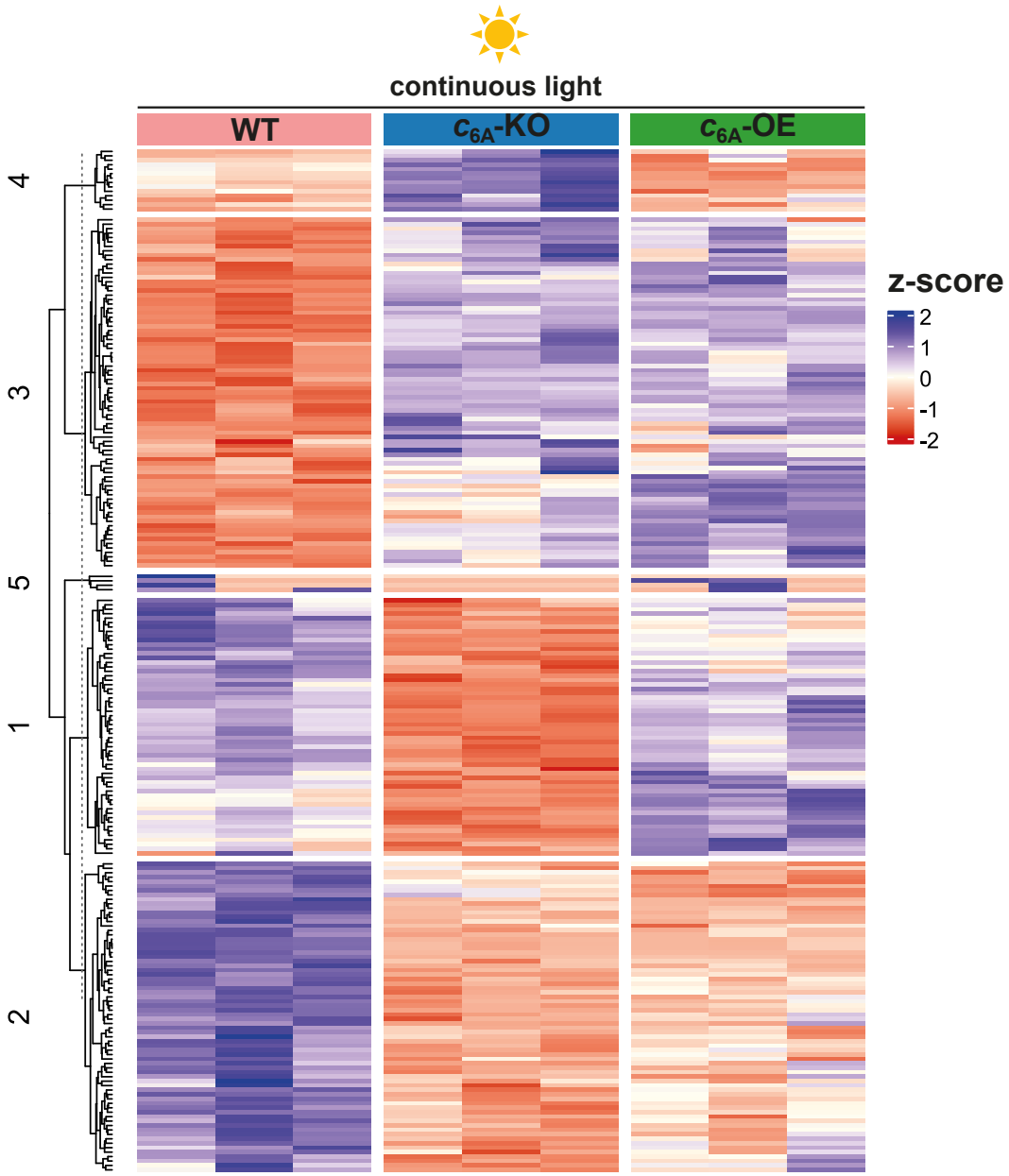


Figure 6.8: Heatmap of the 225 DEGs from the comparison c_{6A}-KO versus WT in continuous light. Each column represents one biological replicate and the read counts per gene (normalised to sample library size) were transformed into a z-score for visualisation. Hierarchical clustering led to the clusters indicated on the left.

Overall, the investigation of DEGs between c_{6A}-KO and WT in continuous light suggests that the absence of c_{6A} leads to significant transcriptomic changes, particularly affecting the circadian rhythm, genes regulated by it, and thylakoid proteins associated with stress responses like *LHCBM4/8* and redoxins. A possible role for c_{6A} in regulatory processes via its disulphide bridge was further supported, as some genes involved in thioredoxin signalling were downregulated in the absence of c_{6A}. The absence of a growth phenotype under continuous light suggests that these differentially expressed genes are likely to have only a small effect on the overall fitness of *C. reinhardtii*. However, a small effect under continuous light could potentially translate into a large change when *C. reinhardtii* is grown in the stressful DISCO Light. Therefore, differential expression between c_{6A}-KO and WT was investigated under DISCO Light conditions as well.

6.2.2.2.2 How are transcript levels affected by the absence of c_{6A} in DISCO Light?

372 genes were differentially expressed between c_{6A}-KO and WT in DISCO Light, representing 2.2% of all expressed genes. Of these DEGs, 276 (74%) had lower and 96 (26%) had higher expression levels in c_{6A}-KO than WT. When comparing the DEGs found for c_{6A}-KO vs WT in continuous light, with the ones found for the same comparison under DISCO Light, it became clear that the differences in DISCO Light were greater and included many genes that were differentially expressed in continuous light as well. The shared DEGs included for example *HOPP1*, *PDC3*, and *ROC40*. Some DEGs were found to be unique to continuous light (figure 6.9). Importantly, of the genes that were DEGs uniquely in continuous light, many showed significant expression changes in the same direction in DISCO Light as under continuous light albeit not reaching the $\log_2$FC threshold. These genes included *ROC59*, *ROC15*, *LHCBM4*, *LHCBM8* and *PRX6*, discussed above.

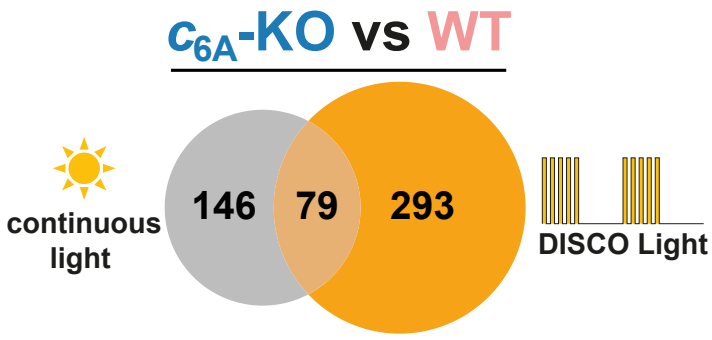


Figure 6.9: Venn diagram of DEGs from c_{6A}-KO versus WT in continuous light or DISCO Light.

The ten most significantly upregulated genes in c_{6A}-KO compared to WT in DISCO Light, included *HCP2*, *HOPP1*, *MOCOCP1*, *DIV39*, and six other undescribed genes (table 6.5).

Table 6.5: Top 10 upregulated DEGs (by $p_{adjusted}$) when comparing c_{6A}-KO to WT in DISCO light and the respective symbols, $\log_2$ fold changes, adjusted p-values, and descriptions. Gene symbols marked with an asterisk are from the earlier v5.6 genome assembly and do not have a gene symbol in v6.1.

Gene ID	Gene symbol	$\log_2$FC	$p_{adjusted}$	Description
Cre11.g478800		3.82	5.21E-49	
Cre09.g393543	*HCP2*	2.46	6.89E-36	Hybrid-cluster protein
Cre10.g452550	*HOPP1*	3.31	2.21E-24	Homologous-pairing protein 1
Cre09.g390050	*MOCOCP1*	2.42	1.19E-22	Molybdenum cofactor carrier protein
Cre09.g395100	*MKP3**	1.79	8.49E-22	Dual-specificity protein phosphatase
Cre15.g801749		2.63	1.59E-16	
Cre10.g462050	*PTK20**	3.04	1.59E-16	Protein tyrosine kinase
Cre09.g407110		2.42	2.61E-15	
Cre06.g250500		2.78	3.59E-15	
Cre09.g396661	*DIV39*	1.98	5.06E-14	

HCP2 encodes a hybrid cluster protein. As such, HCP2 contains an iron-sulphur-oxygen cluster and has been proposed to be a redox-active nitrate-dependent S-nitrosylase potentially involved in signalling processes in *C. reinhardtii* [387]. Upregulation of *HCP2* in the absence of c_{6A} could thus further support a possible role in signalling processes for c_{6A}. *MOCOCP1*, encoding the molybdenum cofactor carrier protein, is somewhat connected to HCP2 via nitrogen metabolism where molybdenum cofactors are essential for nitrogen assimilation [388]. The phosphatase encoded by *MKP3* dephosphorylates and inactivates mitogen activated protein (MAP) kinases and has been implicated in ciliogenesis [389]. The association with MAP kinases that are signal transducers for the regulation of stress responses as well as cell development and proliferation in eukaryotes [390], further supports an involvement of c_{6A} in signalling processes. Similarly to *MKP3*, the gene product of *PTK20* could be involved in signalling processes, as it is predicted to function as a tyrosine kinase which was determined

from a multi-level hidden Markov model library for kinase classification [391]. With *DIV39* a cell cycle regulator [392] has also been found to be more highly expressed in the absence of c_{6A}, further supporting a possible effect of c_{6A} abundance on signalling processes.

Table 6.6: Top 10 downregulated DEGs (by $p_{adjusted}$) when comparing c_{6A}-KO to WT in DISCO light and the respective symbols, log_2 fold changes, adjusted p-values, and descriptions.

Gene ID	Gene symbol	log_2FC	$p_{adjusted}$	Description
Cre17.g722650		-1.68	2.17E-21	
Cre09.g397850		-2.90	2.77E-15	
Cre03.g166050	*SBD1*	-1.35	4.13E-15	Selenium binding protein
Cre06.g800714		-2.93	8.73E-15	
Cre02.g077750	*FAP211*	-1.78	9.99E-15	Flagellar Associated Protein 211
Cre01.g045200		-2.28	1.13E-14	
Cre03.g165700	*PDC3*	-2.10	1.46E-14	Pyruvate decarboxylase
Cre16.g686285		-2.56	1.63E-14	
Cre03.g144364		-1.33	5.57E-14	
Cre15.g801845		-7.90	1.21E-13	

The ten most significantly downregulated genes in c_{6A}-KO compared to WT in DISCO Light, included *SBD1*, *FAP211*, *PDC3*, and seven other undescribed genes. Of these only *SBD1* exhibited a downregulation in c_{6A}-KO under DISCO Light but not in continuous light. This selenium binding protein was recently found to be a stress response regulator in *C. reinhardtii* important for the response to oxidative stress conditions [393]. A lower abundance of its mRNA in the absence of c_{6A} in DISCO Light could therefore indicate that under those conditions, c_{6A}-KO cannot react appropriately to oxidative stress. As DISCO Light is likely to cause photooxidative stress for *C. reinhardtii*, a missing response to it could contribute to the observed c_{6A}-dependent growth phenotype.

Other notable downregulated genes that were not differentially expressed in continuous light included *ROC75*, *LHCBM9* and *PRX2* (table 6.7). The gene product of *ROC75* was introduced above as a transcriptional regulator of other circadian clock associated *ROC* genes. Its lower mRNA abundance in c_{6A}-KO than WT in DISCO Light was detected because WT levels increased between continuous light and DISCO Light while levels in c_{6A}-KO decreased slightly. This could indicate, as proposed before, that in the absence of c_{6A}, circadian clock regulation is affected via *ROC* genes and that this regulation becomes more important in the stressful DISCO Light conditions. *LHCBM9* encodes another LHCII subunit from the same LHCII subunit group as the above-mentioned *LHCBM4/6/8* [394]. A downregulation of LHCBMs in absence of c_{6A} could also contribute to the observed growth phenotype in stressful light conditions, as these proteins are more likely involved in photoprotective mechanisms rather than being essential for light harvesting [353]. *PRX2* encodes another peroxiredoxin belonging to the same family as the already introduced PRX6 and further supports a possible involvement of c_{6A} in thioredoxin-based signalling.

Table 6.7: Other notable downregulated genes between c_{6A}-KO to WT in DISCO light that were not differentially expressed in the same comparison under continuous light, the respective symbols, $\log_2$ fold changes, adjusted p-values, and descriptions.

Gene ID	Gene symbol	$\log_2$FC	$p_{adjusted}$	Description
Cre02.g083750	*ROC75*	-2.13	8.38E-05	Rhythm Of Chloroplast 75
Cre06.g284200	*LHCBM9*	-1.79	2.06E-04	Light-harvesting Chlorophyll a/b binding protein of LHCII
Cre02.g114600	*PRX2*	-1.04	1.41E-04	2-cys Peroxiredoxin

GO enrichment analysis of the upregulated genes did not yield any significant enrichments. However, for downregulated genes GO enrichment analysis resulted in a significant enrichment of the term "response to oxidative stress" (GO: 0006797, 7 of 276 downregulated genes, 6.73-fold enrichment). These genes encoded for two heat shock proteins (HSP22E & F) and various proteins involved in the response to ROS, for example the above-mentioned PRX2, ascorbate peroxidase-like protein APX4 and superoxide dismutase MID3. A smaller response to oxidative stress may contribute to the observed growth penalty for c_{6A}-KO under DISCO Light.

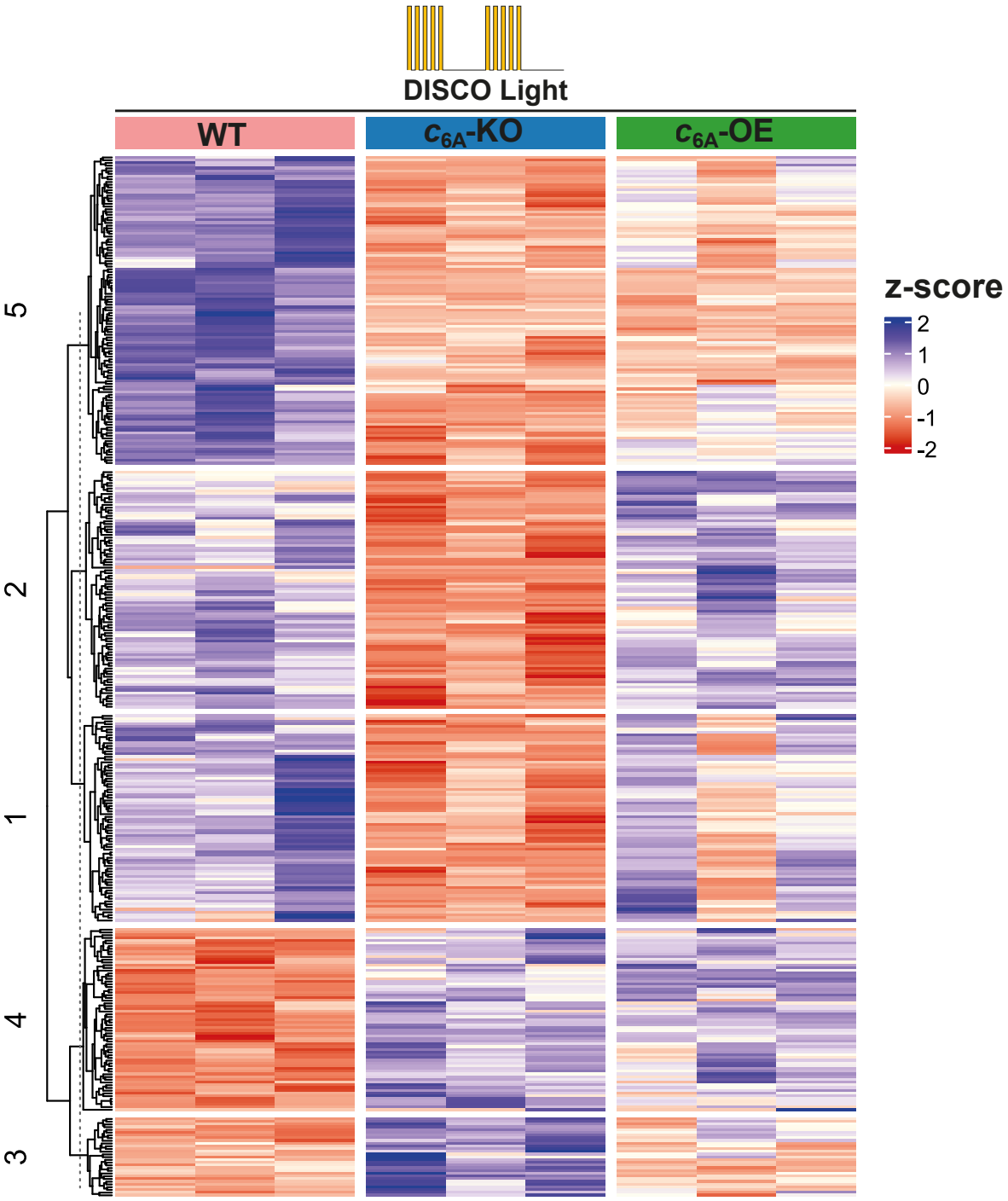


Figure 6.10: Heatmap of the 372 DEGs from the comparison c_{6A}-KO versus WT in DISCO light. Each column represents one biological replicate and the read counts per gene (normalised to sample library size) were transformed into a z-score for visualisation. Hierarchical clustering led to the clusters indicated on the left.

A heatmap with all 372 DEGs comparing c_{6A}-KO and WT in DISCO Light was created to assess the expression of these genes in c_{6A}-OE (figure 6.10). Similar to continuous light samples, some DEGs were recovered to WT expression levels in c_{6A}-OE (clusters 1 (not consistently for c_{6A}-OE replicate 2), 2 and 3) while others had expression more similar to

c_{6A}-KO (clusters 4 and 5). Cluster 2 included the genes *PDC3* and *ROC75*, signifying a more direct connection with c_{6A} abundance. *SBD1*, *MOMOCP1*, and *HCP2* were found in clusters 5, 4, and 4, respectively which could be explained by more complex regulation mechanisms as discussed above (section 6.2.1.3).

Taken together, differential expression analysis of c_{6A}-KO and WT in DISCO Light conditions supported and expanded on c_{6A}-dependent differences observed under continuous light, such as c_{6A}'s effect on LHCBMs and thioredoxin-related proteins or genes involved in circadian rhythm. Furthermore, the downregulation of oxidative stress response genes compared to WT indicated a possible explanation for the observed growth phenotype under DISCO Light.

6.2.2.2.3 How does the WT transcriptome change between continuous light and DISCO Light?

From the PCA plot (figure 6.6), it could be inferred that DISCO Light growth has a substantial influence on the transcriptome of *C. reinhardtii*. Differential expression analysis comparing WT in DISCO Light versus continuous light was therefore carried out to characterise this influence.
In WT, 926 genes were found to be significantly differentially expressed in DISCO Light compared to continuous light, 722 (78%) thereof were upregulated and 204 (22%) downregulated. To analyse this great number of genes, GO enrichment analysis was performed and the resulting top 15 significantly enriched terms were clustered by semantic similarity (figure 6.11).

For the 722 upregulated genes, three GO term clusters were found with the themes of "catabolism", "autophagy", and "proteolysis regulation". Especially, “amino acid catabolism” was found to be enriched. This process has been shown to be upregulated when *C. reinhardtii* cells are photosynthesis impaired and rely more on their ability to survive heterotrophically [395, 396]. Proteins can then be broken down and amino acids are oxidised providing tricarboxylic acid (TCA) cycle substrates for energy generation. The upregulation of amino acid catabolism in DISCO Light therefore suggests that in DISCO Light photosynthetic energy production is impaired. This is consistent with the absence of photoautotrophic growth in DISCO Light (section 3.2.3.2). As DISCO Light leads to the induction of genes involved in autophagy, it can be inferred that DISCO Light causes substantial stress in *C. reinhardtii*. This is consistent with the slower growth even of WT under DISCO Light compared to continuous light conditions. The genes encoding light harvesting stress related proteins LHCSR1&3 were specifically examined for differential expression given their involvement in photo-oxidative stress responses. The three related genes *LHCSR1*, *LHCSR3A* & *LHCSR3B* were found within

the 722 upregulated DEGs. The over 15-fold upregulation in DISCO Light compared to continuous light of each of the genes further supported that DISCO Light causes photo-oxidative stress.

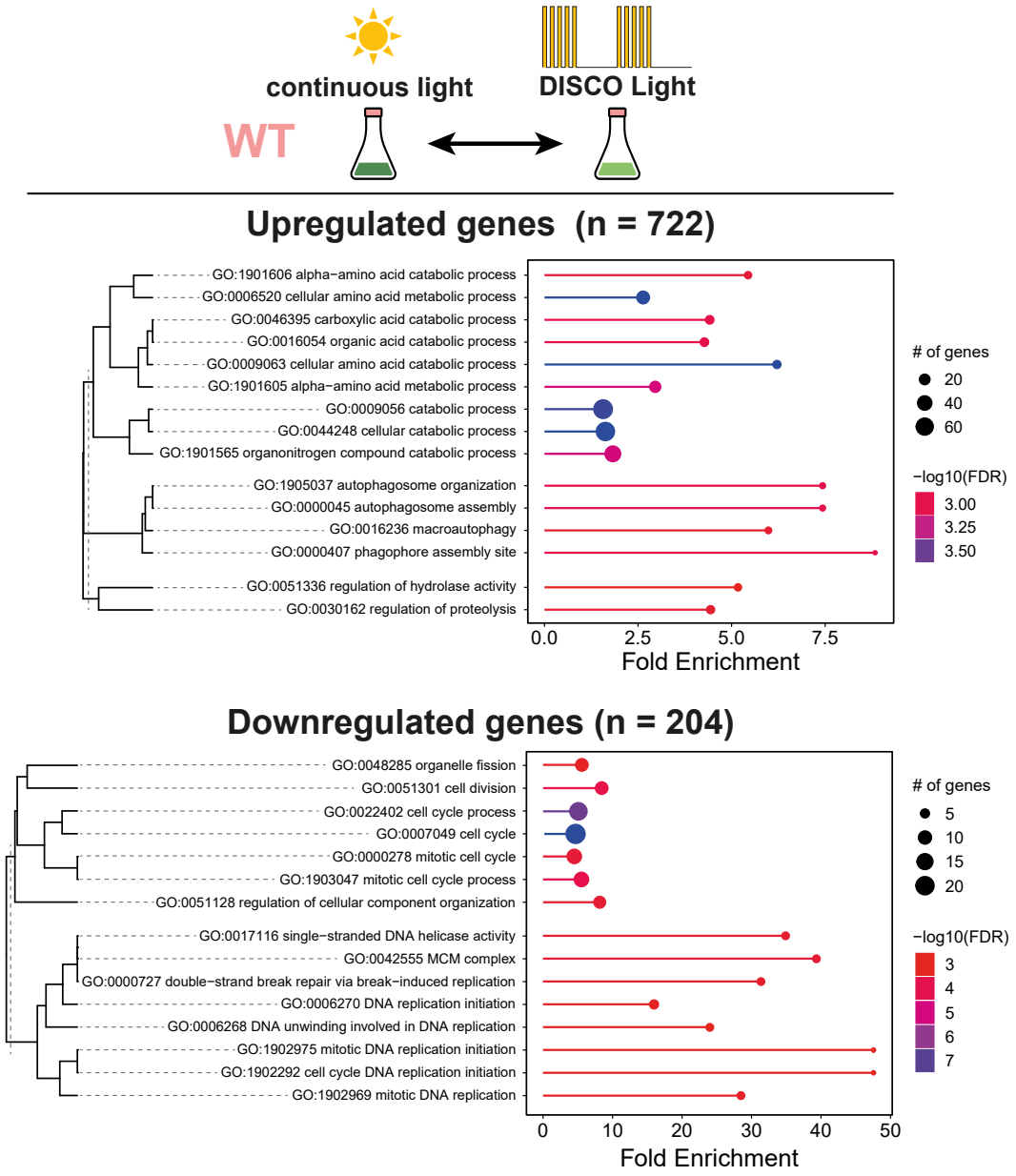


Figure 6.11: GO enrichment analysis for DEGs from WT comparing DISCO Light versus continuous light. Top 15 most significantly enriched GO terms were clustered by their semantic similarity and include GO terms from the categories "biological process", "molecular function", and "cellular component".

For the 204 downregulated genes, two GO term clusters could be found that were related to each other and aggregated under the themes "cell cycle" and "DNA replication". Expression of cell cycle genes is tightly linked to the circadian rhythm of *C. reinhardtii* and shows natural fluctuations with downregulation of cell cycle genes in darkness [15]. This phenomenon

would be observable in transcriptomic analyses with synchronised cultures where cells are in the same stage of the cell cycle. The cultures used here were not synchronised as they were grown under continuous light or DISCO Light without a diurnal cycle, likely resulting in cells distributed across all stages of the cell cycle [397]. A difference in cell cycle stage as origin of the downregulated cell cycle genes in DISCO Light therefore seems unlikely. Downregulation of cell cycle genes has also been found for *C. reinhardtii* under stress conditions, such as nitrogen deprivation [398]. While nitrogen deprivation is very unlikely to be present here, DISCO Light causes substantial stress for *C. reinhardtii* and thus presents another condition where cell cycle gene expression is downregulated. This may be related to the slowed growth in DISCO Light compared to continuous light, indicating that cell division also occurs more slowly.

Taken together, differential expression analysis of DISCO Light versus continuous light in WT supported the finding that *C. reinhardtii* is severely stressed when grown in DISCO Light. This was reflected in upregulation of stress response mechanisms like amino acid catabolism and autophagy as well as in downregulation of cell cycle genes.

6.2.2.2.4 How does the transcriptomic response to DISCO light differ between c_{6A}-KO and WT?

Comparing the number of DEGs from "WT DISCO vs continuous" and "KO DISCO vs continuous" (table 6.2), it appeared that c_{6A}-KO had a different reaction to DISCO Light than WT. However, this could not be confirmed from GO enrichment analyses, which resulted in very similar significantly enriched terms for both up- and downregulated genes (figure 6.12).

While autophagy-associated terms were not included in the top 15 most significantly enriched GO terms for c_{6A}-KO, associated genes still showed significant changes while some did not pass the $\log_2$FC threshold. The overall very similar reaction to DISCO Light between c_{6A}-KO and WT is consistent with observations from the PCA plot, where the influence of DISCO Light appeared much larger than that of the c_{6A}-genotype. Indeed, when examining 931 unique DEGs from "KO DISCO vs continuous" (i.e. DEGs that were not found in "WT DISCO vs continuous") with heatmaps, it became clear that most of the unique genes still showed altered expression in WT similar to c_{6A}-KO in response to DISCO Light (figure 6.13). However, in WT these genes did not pass the $\log_2$FC threshold leading to a much greater number of DEGs in "KO DISCO vs continuous" than in "WT DISCO vs continuous", especially for downregulated genes.

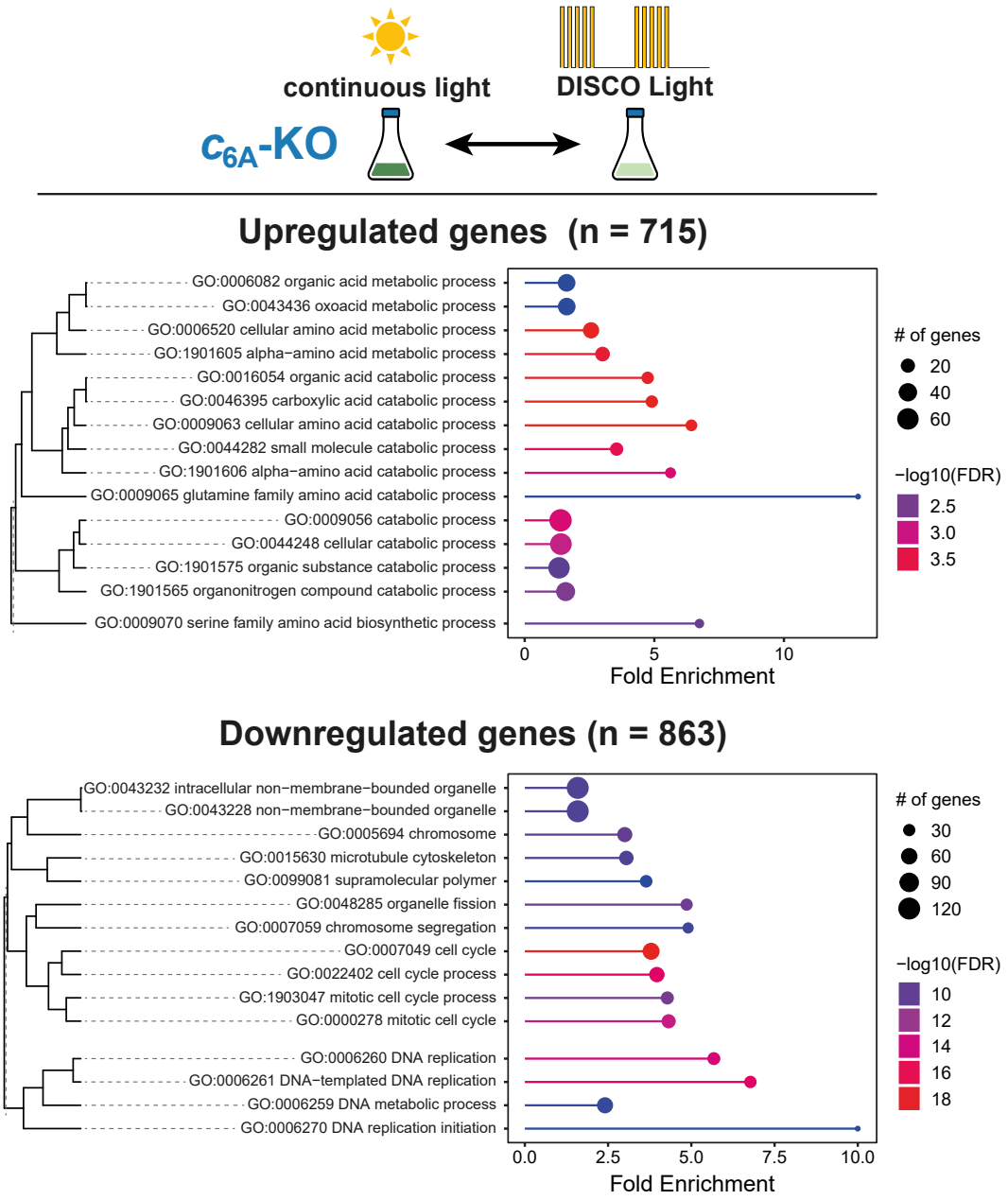


Figure 6.12: GO enrichment analysis for DEGs from c_{6A}-KO comparing DISCO Light versus continuous light. Top 15 most significantly enriched GO terms were clustered by their semantic similarity and include GO terms from the categories "biological process", "molecular function", and "cellular component".

It could be concluded that c_{6A}-KO's response to DISCO Light was slightly larger in magnitude but not completely altered. This is also in agreement with the low number of genes that were DEGs in the interaction term comparing c_{6A}-KO's and WT's difference between DISCO Light and continuous light (37 DEGs in total). Nevertheless, these 37 genes included relevant genes that were already discussed, including *LHCBM8*, *ROC59* and *HCP2*. For these genes an altered difference between DISCO Light and continuous light in the absence of c_{6A} could be found, further supporting a possible role for c_{6A} in their transcriptional regulation.

As c_{6A} was found in the thylakoid lumen, a signal for transcriptional regulation of these nuclear genes from c_{6A} would have to be forwarded via other retrograde effectors.

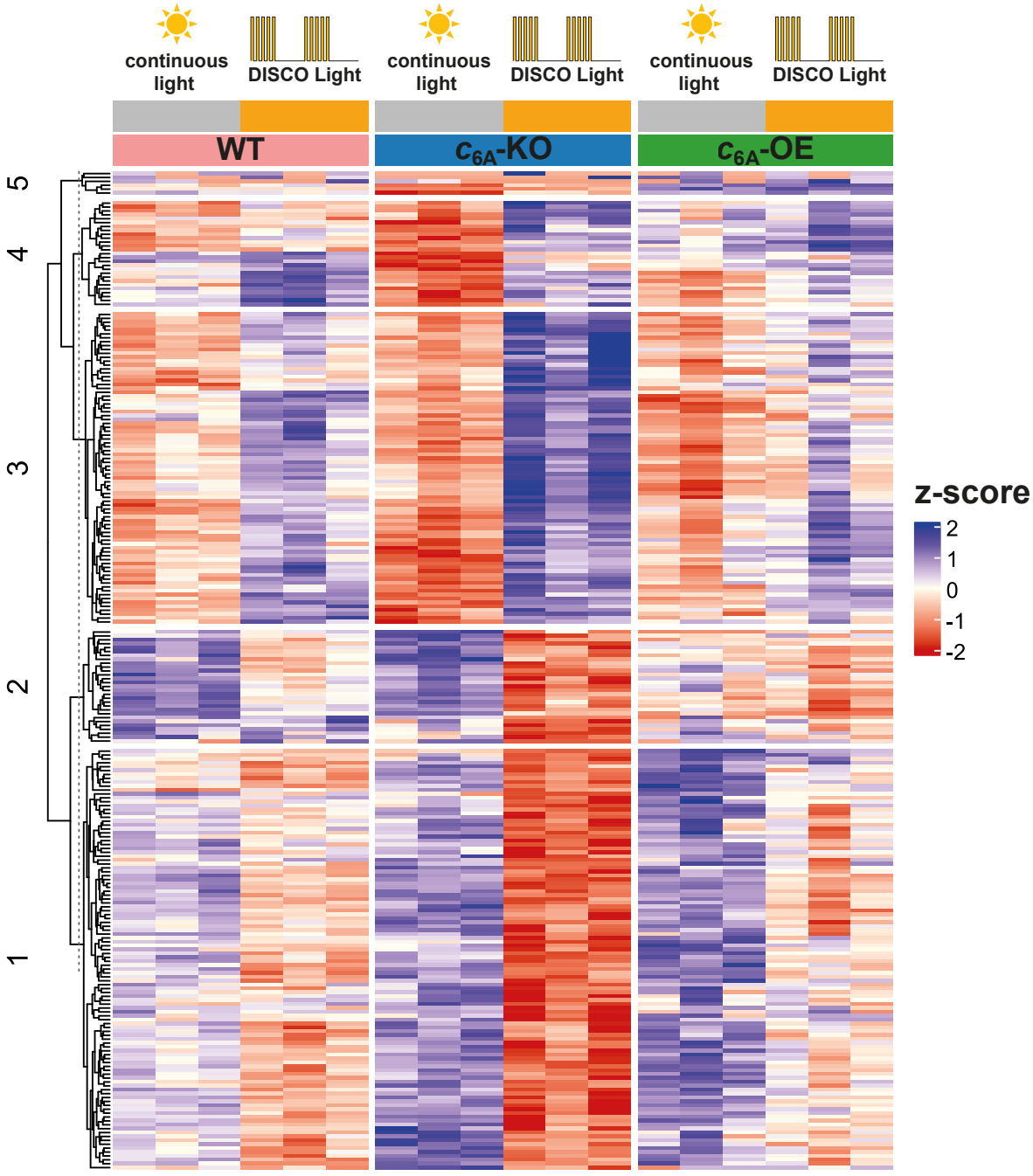


Figure 6.13: Heatmap of the top 250 most significant DEGs that were unique to "c_{6A}-KO DISCO vs continuous light" and not DEGs in WT or c_{6A}-OE. Each column represents one biological replicate and the read counts per gene (normalised to sample library size) were transformed into a z-score for visualisation. Hierarchical clustering led to the clusters indicated on the left.

6.2.2.2.5 What is the influence of c_{6A} on transcript levels of photosynthesis-related genes under continuous light or DISCO Light?

Some of the *LHCBM* genes encoding light harvesting proteins were found to be DEGs comparing c_{6A}-KO with WT, both in continuous light and DISCO Light. Given the other photosynthesis-related phenotypes examined with biophysical methods (chapter 4), this prompted a more general investigation of c_{6A}'s effect on the expression of genes associated with photosynthesis. A heatmap of read counts for all samples, normalised to the size of each sample library, was prepared comprising photosynthesis genes with a focus on the main complexes of the PETC: PSII + associated antennae, cytochrome b_6f, PSI + associated antennae, and ATP synthase (figure 6.14). It should be noted that many genes depicted here are located in the chloroplast genome of *C. reinhardtii*. As the RNAseq procedure enriched for poly-A tailed transcripts to increase the fraction of mRNA versus ribosomal RNA, the abundance of chloroplast transcripts, which lack poly-A tails, was also decreased. The obtained read counts do not reflect the total abundance in the cell, however, this under-representation would not be expected to be influenced by the conditions or genotype. Nevertheless, any findings regarding chloroplast encoded genes should be confirmed again on the same RNA samples using quantitative PCR.

Overall, 81 photosynthesis genes were investigated. Many of them were highly expressed including plastocyanin (*PCY1*), the seventh most highly expressed gene detected across all samples. Only nine of these 81 genes were DEGs comparing c_{6A}-KO and WT in either continuous light or DISCO Light. Hence, the impact of c_{6A} on expression of photosynthesis genes seemed limited. In continuous light, only the above-mentioned genes *LHCBM4*, *LHCBM8* and *atpB* (section 6.2.2.2.1) were expressed at significantly lower levels in c_{6A}-KO than in WT (blue asterisks in continuous light in figure 6.14). In DISCO Light, six DEGs were found when comparing c_{6A}-KO and WT (blue asterisks in DISCO Light in figure 6.14), one of which was *LHCBM9* (section 6.2.2.2.2). Additionally, lower expression levels of genes encoding PSII core subunit PsbB, b_6f subunits PetD and PetG, as well as ATP synthase subunits AtpF and AtpH were detected. This difference could be a consequence of DISCO Light exposure causing more stress in c_{6A}-KO than in WT, preventing the accumulation of WT levels of some chloroplastic mRNAs.

Regarding the altered light-harvesting balance in favour of PSII in the absence of c_{6A} (section 4.2.1.1), the lack of increased PSII or LHCII transcripts, or decreased PSI or LHCI transcripts in c_{6A}-KO compared to WT, suggests that the light harvesting phenotype is likely to be due to altered antennae binding rather than changed complex abundances.

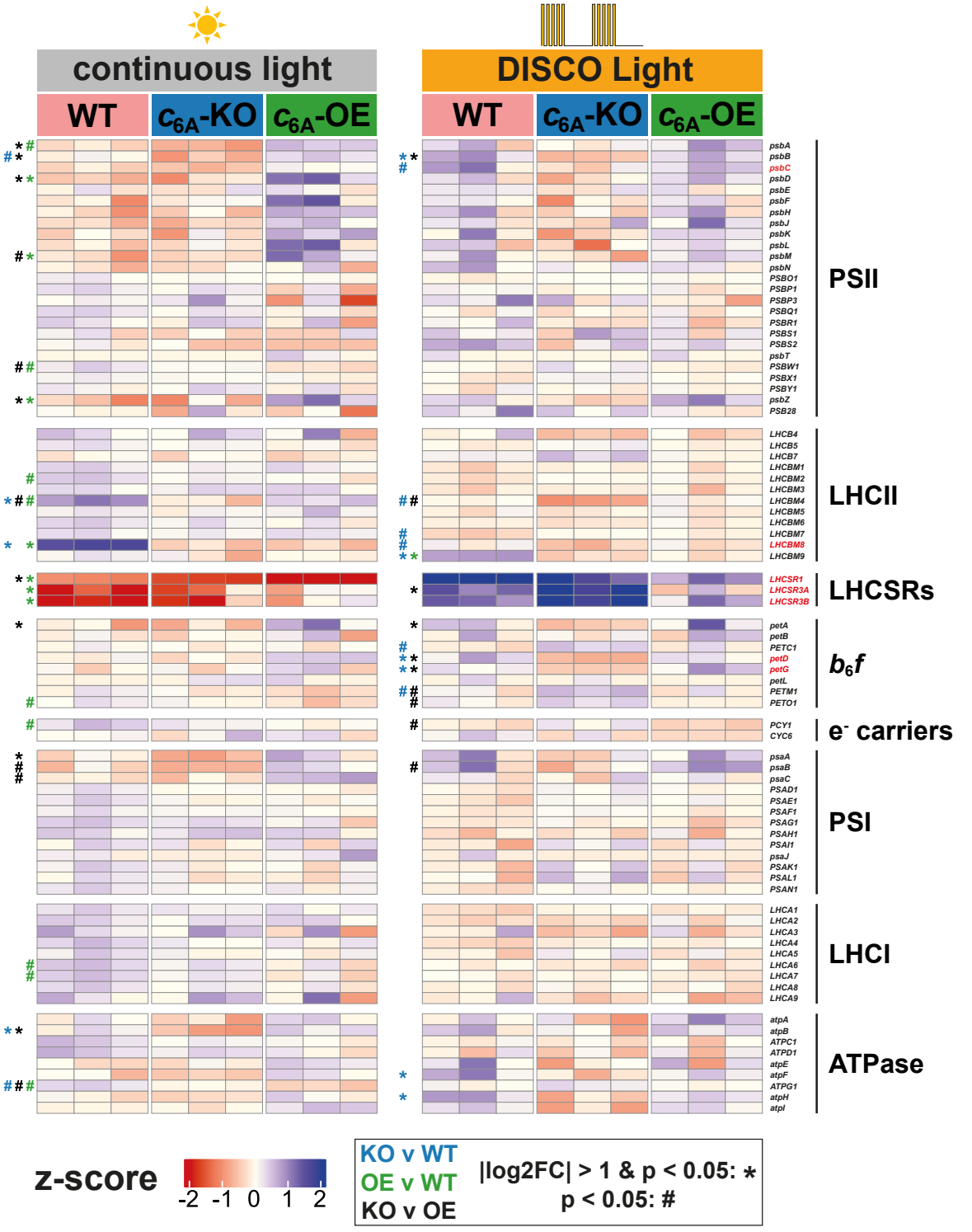


Figure 6.14: Heatmap of genes encoding proteins associated with photosynthesis in *C. reinhardtii* comparing c_{6A} mutant strains and WT in continuous light and DISCO Light. Three biological replicates per strain are shown for which individual read counts per gene (normalised to sample library size) were transformed into a z-score for visualisation. Significance of differential expression analysis between strains in each light condition is marked on the left of each light condition with asterisks indicating a DEG and hash signs representing significant differential expression ($p_{adj} < 0.05$) without meeting the $\log_2$FC threshold. Genes that were DEGs comparing DISCO Light versus continuous light in any of the strains are marked in red (see text for details).

Interestingly, comparing DISCO Light versus continuous light also led to only a small number of DEGs. Seven genes were DEGs in either of the three strains: *LHCSR1* in all three strains, *LHCSR3A & B* in c_{6A}-KO and WT, *LHCBM8* and *psbC* in WT only; and *petD & G* in c_{6A}-KO only (gene symbol marked in red in figure 6.14). From those genes, the *LHCSR* genes exhibited the most prominent difference with more than 15-fold upregulation in DISCO Light compared to continuous light, translating into the largest colour difference between light conditions of all genes on the heatmap. Notably, this drastic upregulation was not the case for *LHCSR3* genes in c_{6A}-OE which did not show significant alterations of transcript abundance comparing DISCO Light and continuous light. This can be explained at least partly by an elevated LHCSR3 transcript abundance in c_{6A}-OE compared to WT already under continuous light (green asterisks in figure 6.14). Regarding *LHCSR3* transcription, c_{6A}-OE thus appeared pre-adapted to DISCO Light conditions in contrast to c_{6A}-KO and WT. The expression levels of the *LHCSR* were not significantly different between c_{6A}-KO and WT in either continuous light or DISCO Light, although one c_{6A}-KO replicate showed higher transcript levels than WT for *LHCSR3A & B* in continuous light (fainter red boxes for *LHCSR3A & B* in c_{6A}-KO continuous light in figure 6.14).

Taken together, these data show that absence of c_{6A} only affected expression of specific photosynthesis genes like *LHCBMs* but did not lead to major alterations of photosynthesis gene expression.

6.2.3 Comparison of protein and transcript levels of *C. reinhardtii* c_{6A} mutant strains

For the investigation of protein and transcript levels, samples from the same cultures were isolated (figure 6.1). While the isolation time points were not exactly the same, the growth phases of each culture were similar between RNA and protein isolation. This enabled the comparison of transcript and protein levels side-by-side to investigate if differences between strains on protein level (section 6.2.1) are reflected on transcript level. A heatmap of transcript levels of genes encoding the proteins investigated earlier was aligned with the western blot results of continuous light and DISCO Light day 2 cultures from section 6.2.1. Protein band intensities were compared with transcript abundances for any one strain in relation to the others (figure 6.15).

When comparing protein and transcript differences within one light condition, some genes and their products showed consistent patterns. In continuous light, c_{6A}-OE had a higher abundance of PsbA and its transcript compared to c_{6A}-KO and WT, expression of RbcL was unaffected by c_{6A}, and PTOX2 protein and transcript was less abundant in c_{6A}-KO than in c_{6A}-

OE. For *PTOX2* however, the difference in transcript abundance was small comparing c_{6A}-KO and c_{6A}-OE and not statistically significant when comparing c_{6A}-KO and WT (black hash at *PTOX2* in continuous light in figure 6.15). Further validation of *PTOX2* gene expression through qPCR could help clarify if the difference in protein levels actually originates from altered transcript abundance or is connected to post-transcriptional regulation.

In DISCO Light, differential protein abundance of CytF (encoded by *petA*), AtpB, NDA2, and LHCSR3 between strains were consistent with their respective differential transcript expression. For example, *petA* had significantly lower expression in c_{6A}-KO than in c_{6A}-OE (black asterisks at *petA* in DISCO Light in figure 6.15), in agreement with the altered protein abundance. AtpB abundance was not changed between the strains on either protein or transcript level, while NDA2 was clearly more abundant in WT than the c_{6A} mutant strains, which is reflected in higher *NDA2* transcript levels (green and blue symbols at *NDA2* in DISCO Light in figure 6.15). Finally, LHCSR3 protein abundance, which was investigated with an antibody that detects both gene products of *LHCSR3A* and *LHCSR3B*, was more prominent in c_{6A}-KO especially compared to c_{6A}-OE. This was consistent with a significantly higher transcript level of *LHCSR3A* in c_{6A}-KO compared to c_{6A}-OE (black asterisks at *LHCSR3A* in DISCO Light in figure 6.15).

Many differences in protein level between the strains were not consistent with differences in transcript abundance. Most prominently that was the case for LHCSR3 in continuous light. Here, LHCSR3 protein was most prominent in WT, while transcript levels of *LHCSR3* indicated the opposite with WT having the lowest transcript levels on average, with the difference being significant comparing c_{6A}-OE and WT (green asterisks at *LHCSR3A*/*B* in continuous light in figure 6.15). This might indicate that the LHCSR3 protein is more stable in WT than in the c_{6A} mutant strains, resulting in increased protein levels despite lower transcript accumulation. An inconsistent pattern between protein and transcript abundance was also found for PsaB, PetA, AtpB, and NDA2 in continuous light, and PsbA, RbcL, PsaB, and PTOX2 in DISCO Light. This suggests that these proteins undergo post-transcriptional regulation of abundance that may be influenced by c_{6A}. If c_{6A} strictly had an influence on the transcriptome only, the same patterns between transcripts and protein levels would have been expected. Similarly, if c_{6A} only affected post-transcriptional processes such as translation or protein stability, similar patterns between transcript and protein levels would have been unlikely. As both similar and different patterns can be observed here, c_{6A} appears to influence both gene expression and post-transcriptional control of protein abundance. This effect might originate in c_{6A} directly as source of a signal (as discussed with thiol-based regulation) or be a reaction of the cell to different abundances of c_{6A}.

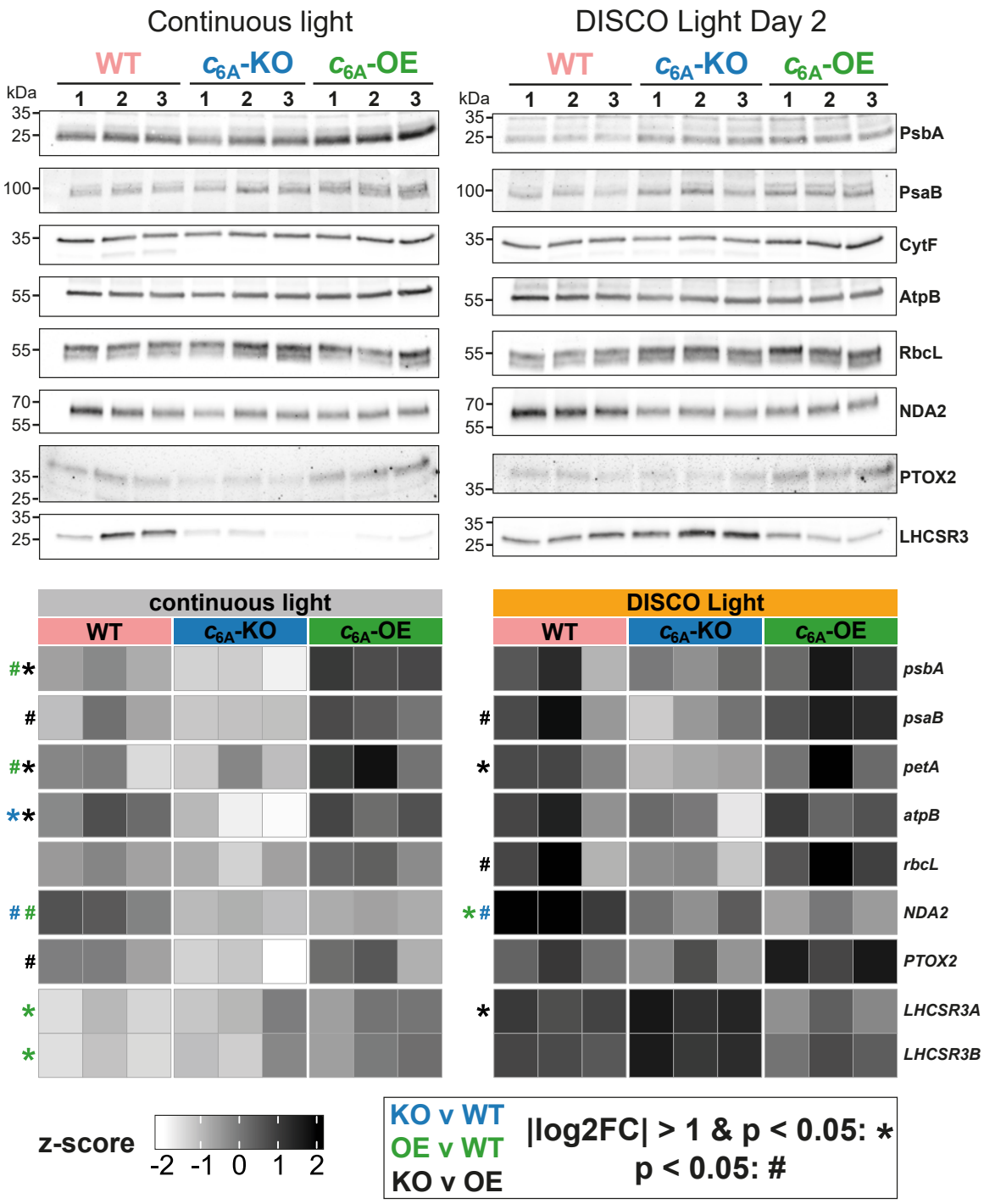


Figure 6.15: Comparison of protein and transcript levels of selected genes and their products associated with photosynthesis. WT and c_{6A} mutant strains were compared between continuous light and DISCO Light growth. The western blot images are the same as in section 6.2.1. The heatmap of transcript levels includes the same three biological replicates per strain as the protein level data. Individual read counts were transformed into a z-score and plotted along a white-to-black gradient for easier comparison with western blot band intensity. Significance of differential expression analyses is indicated on the left of each light condition with asterisks indicating a DEG and hash signs representing significant differential expression ($p_{adj} < 0.05$) without meeting the $\log_2$FC threshold. CytF is encoded by *petA*.

DISCO Light and continuous light samples were not compared for protein levels, as the samples from different light conditions were analysed on different membranes. However, transcript levels could be compared between DISCO Light and continuous light for all three strains where, of the selected genes, only *LHCSR3A/B* were found to be DEGs (table 6.8). However, while not exhibiting an absolute $\log_2$FC above 1, *NDA2* also exhibited significant upregulation in response to DISCO Light in both c_{6A}-KO and WT. As NDA2 is involved in alternative electron pathways, an upregulation in DISCO Light could help alleviate pressure on the PETC. Interestingly, c_{6A}-OE did not exhibit any DISCO Light induced *NDA2* upregulation, which could be explained by less need for stress responses as c_{6A}-OE already appeared pre-adapted to more stressful conditions as evidenced by elevated transcript levels of *LHCSR3A/B*.

Table 6.8: Differential expression values ($\log_2$FC & $p_{adjusted}$) for selected genes associated with photosynthesis when comparing DISCO Light versus continuous light (cont) in WT, c_{6A}-KO, or c_{6A}-OE. Values that reached the threshold of $|\log_2 FC| > 1$ or $p_{adjusted} < 0.05$ are printed bold.

	WT DISCO vs cont		**KO DISCO vs cont**		**OE DISCO vs cont**	
Gene symbol	$\log_2$FC	$p_{adjusted}$	$\log_2$FC	$p_{adjusted}$	$\log_2$FC	$p_{adjusted}$
psbA	0.41	0.10	0.73	**6.43E-03**	0.06	0.89
psaB	0.75	**0.03**	0.44	0.26	0.28	0.42
petA	0.44	0.21	0.00	0.99	-0.01	0.99
atpB	0.15	0.70	0.86	**0.04**	0.02	0.96
rbcL	0.57	0.09	0.20	0.65	0.38	0.27
NDA2	0.66	**2.88E-4**	0.51	**0.01**	0.15	0.55
PTOX2	0.20	0.36	0.45	0.02	0.36	0.05
LHCSR3A	**3.95**	**1.35E-09**	**3.01**	**1.09E-06**	0.05	0.91
LHCSR3B	**4.06**	**3.72E-11**	**3.47**	**4.81E-09**	0.40	0.27

In summary, the comparison of protein and transcript levels across different light conditions revealed both consistent and inconsistent patterns between strains. While some proteins, such as PsbA, CytF, and NDA2, exhibited changes in abundance that aligned with their respective transcript levels, others, including LHCSR3 and PTOX2, showed discrepancies

suggesting post-transcriptional regulation. While these differences may be related to the different sampling time points for RNA and protein, these results also highlight the potential role of c_{6A} in influencing protein abundance beyond transcriptional control. Further validation is needed to clarify any putative regulatory mechanisms.

6.3 Conclusion & Outlook

6.3.1 Summary of findings

The aim of this study was to characterise the effects of c_{6A} on the abundance of specific photosynthesis-associated proteins and on the overall transcriptome of *C. reinhardtii*, both under continuous light and DISCO Light conditions. This investigation was prompted by previous findings that suggested c_{6A} influences photosynthesis and the goal was also to search for further explanations for the growth phenotype observed under DISCO Light.

In continuous light, the analysis revealed several important findings (section 6.2.1.1): the PSI core abundance changed only when c_{6A} was overexpressed, suggesting that the likely LHC-less PSI complex observed in c_{6A}-KO was not due to changes in PSI core protein abundance. Additionally, differences in the PQ pool redox state were probably unrelated to NDA2 levels but possibly linked to a consistent decrease in PTOX2 levels in c_{6A}-KO. LHCSR3 showed altered levels from WT in both c_{6A}-KO and c_{6A}-OE, highlighting the need for further investigation into whether the c_{6A}-dependent difference in NPQ relies on qE or another mechanism. The RNAseq data added complexity by showing that the transcript levels of LHCSR3 and PTOX2 did not align with their protein levels, indicating a potential post-transcriptional effect of c_{6A} beyond its impact on transcript levels (section 6.2.3). More broadly, RNAseq of continuous light samples revealed c_{6A}-dependent changes in the transcript levels of genes associated with circadian rhythm, chloroplast thylakoid components including light-harvesting complex subunits, and thiol-based redox regulation (section 6.2.2.2.1).

Under DISCO Light, these trends persisted, alongside a decreased expression of oxidative stress response genes in c_{6A}-KO compared to WT, which could help explain the observed growth phenotype (section 6.2.2.2.2). Correspondingly, the transient increase in LHCSR3 protein abundance, lowered CytF abundance and the prominent emergence of PsbA breakdown products in c_{6A}-KO by day 4 in DISCO Light also indicated increased oxidative stress (section 6.2.1.2).

Overall, DISCO Light significantly affected the *C. reinhardtii* transcriptome, with similar patterns observed in both c_{6A}-KO and WT. Stress-related mechanisms such as amino acid catabolism and autophagy were upregulated, while cell cycle gene expression was downregulated compared to continuous light samples (section 6.2.2.2.3). Finally, taking c_{6A}-OE into account suggested that c_{6A} is part of complex regulatory networks, as its overexpression did not merely restore transcript or protein abundances to WT levels but also displayed unique characteristics.

6.3.2 Further work

Future work can be divided into two main areas: further analysis of existing samples and investigations into new hypotheses generated from the current findings.

For the existing samples, several experiments should be undertaken. First, optimising the PTOX2 western blot to lower the background signal is essential to confirm the c_{6A}-dependent differences observed. Additionally, it would be beneficial to examine the protein levels of chloroplast rhythm proteins, those involved in thiol-based regulation, and LHCBMs, along with other antenna proteins like LHCA. Even though there was no observed change at the transcript level for LHCAs, investigating these proteins is especially interesting in the light of the likely LHC-less PSI complex being more prominent in c_{6A}-KO. Moreover, conducting western blots on samples comparing the strains' differences between continuous light and DISCO Light on days 2 and 4, will aid in characterising c_{6A}'s effect more thoroughly. Performing qPCR on chloroplast genes such as atpB and petA (which codes for CytF) would be necessary to confirm their differential expression.

The second area of future work involves exploring hypotheses that arose from the analyses but are not directly related to the samples used in this study. One such hypothesis is that PTOX2 may be responsible for the more reduced PQ pool in c_{6A}-KO, which could be tested through PQ pool measurements with or without its inhibitor n-PG. Another avenue is to investigate the hypothesis that c_{6A} is involved in thiol-based regulation by complementing c_{6A}-KO with a *CYC4* gene carrying mutated residues making a disulphide bridge impossible. With a strain like this, protein level and biophysical characteristics could be analysed and the importance of c_{6A}'s disulphide bridge clarified.

The suggested role of the gene products of *LHCBM4*/*8*, which were DEGs in c_{6A}-KO compared to WT, in state transitions warrants further investigation. These investigations should focus on the rate of state transitions and phosphorylation states as it was shown earlier that absence of c_{6A} does not stop state transitions (section 4.2.1.2).

The proposed difference in LHCSR3 stability between WT and c_{6A} mutant strains could also be further examined. Sampling cultures at more time points might give a first indication if the observed difference is part of a consistent trend. Furthermore, pulse-chase experiments with radioactively labelled amino acids like [^{35}S]-methionine or [^{35}S]-cysteine [399] could be employed to assess the half-life of LHCRS3 in the different strains, similar to the work by Cecchin *et al.* (2021) on the turnover rate of PSII subunits in *C. reinhardtii* [360].

Finally, the oxidative stress observed under DISCO Light could be assessed by comparing ROS levels of c_{6A} mutant strains and WT using ROS probes like dichlorofluorescein diacetate (DCFH-DA), as carried out by Devadesu *et al.* (2021) [320].

7

General Conclusions & Outlook

7.1 Summary of findings

The electron transfer protein cytochrome c_6 was believed to have been lost in plants until a ubiquitous and highly conserved homologue, named cytochrome c_{6A}, was identified throughout the plant and green algal lineages. Despite its homology to c_6, c_{6A} cannot replace c_6 (or plastocyanin) functionally in the PETC. The function of c_{6A} in green photosynthetic eukaryotes therefore remained unclear, motivating this study. A short summary of the results obtained in the study is given below and in table 7.1 in preparation for discussing their functional implications.

Comparing a knock-out and an overexpression strain of c_{6A} in *C. reinhardtii* to the wild type background, a growth penalty was observed in the absence of c_{6A} only under a harsh fluctuating light regime, named DISCO Light, and in photomixotrophic conditions. No growth phenotype was seen in continuous light, continuous darkness, or other fluctuating light regimes in photoautotrophic or photomixotrophic conditions (chapter 3).

The light dependency of the growth phenotype prompted in depth analyses of the PETC with a wide range of absorbance and fluorescence spectrometry methods (chapter 4). Cytochrome c_{6A} was found to be important for a normal light harvesting balance between PSI and PSII and maintaining a normal PQ pool redox state when cells were grown photomixotrophically, even in light conditions that did not cause a growth phenotype. In the absence of c_{6A} light harvesting was shifted in favour of PSII while state transitions were at least in principle functional. However, the shift in light harvesting towards PSII in the absence of c_{6A} was still present in conditions that normally lead to state 1 or state 2. While PSI was largely unaffected by the absence of c_{6A}, PSII fluorescence measurements revealed elevated NPQ and a more reduced PQ pool in the absence of c_{6A}. The more reduced PQ pool was found to affect most prominently the redox kinetics of *b* hemes in the cytochrome b_6f complex in response to light, while the Q cycle appeared functional. When exposed to DISCO Light, the c_{6A}-dependent light harvesting balance phenotype was amplified and PSII showed lower photochemical

activity in the absence of c_{6A}. Together with elevated NPQ levels this suggested increased stress levels in the c_{6A}-KO. These insights explain the observed growth penalty which could be caused by the altered light harvesting balance, leading to a more reduced PQ pool, and ultimately increased damage through photooxidative stress in the absence of c_{6A}.

Localisation of c_{6A} in the thylakoid lumen was confirmed by subcellular fractionation and immunofluorescence microscopy, further supporting the association of c_{6A} with photosynthesis (chapter 5). Co-immunoprecipitation studies did not reveal any stable complexes, consistent with a function for c_{6A} through transient interactions. Examination of the effect of the absence of c_{6A} on complexes of the thylakoid membrane indicated an increased prominence of a PSI complex apparently lacking LHC. This could help explain the effect of c_{6A} on the light harvesting balance and thus the PQ pool redox state.

Protein and transcript abundance analyses were carried out with western blots and RNAseq, respectively (chapter 6). In continuous light, the abundances of PSI and PSII core proteins were unlikely to account for the increased presence of the proposed LHC-less PSI complex in the absence of c_{6A}. Notably, the abundance of PTOX2 was reduced in the absence of c_{6A}, potentially contributing to the observed difference in PQ pool redox state. RNAseq revealed c_{6A}-dependent changes in continuous light in the transcript levels of genes associated with circadian rhythm, chloroplast thylakoid components including light-harvesting complex subunits, and thiol-based redox regulation. In DISCO Light, these trends persisted, alongside a decreased expression of oxidative stress response genes in c_{6A}-KO compared to WT, which could further contribute to the observed growth phenotype. Correspondingly, a transient increase in LHCSR3 protein abundance, lowered CytF abundance and the prominent emergence of PsbA breakdown products in c_{6A}-KO in DISCO Light also indicated increased oxidative stress.

Table 7.1: Summary of findings of this study, listed together with the section they were discussed in and the experimental method used. The section numbers link to the corresponding page in the document.

Section	Method	Finding
3.2.1	PCR, WGS	A CRISPR edited strain confirmed as c_{6A}-KO
3.2.2	PCR, western blot	A c_{6A}-overexpression strain created and confirmed (supported by RNAseq)
3.2.3.1	Growth curves	No c_{6A}-dependent growth phenotype under continuous light
3.2.3.2	Growth curves	c_{6A}-dependent growth phenotype under DISCO Light (absence $\rightarrow$ less growth)
3.2.3.3	Growth curves	No c_{6A}-dependent growth phenotype under darkness or other fluctuating light
3.2.3.4	Acetate and chlorophyll measurements	Acetate and chlorophyll contents reflect DISCO Light phenotype
4.2.1.1	77 K fluorescence	No c_{6A}-dependent effect on PSI/PSII ratio under standard conditions in autotrophy
4.2.1.1	77 K fluorescence	c_{6A}-dependent light harvesting balance phenotype under normal conditions in photomixotrophy (absence $\rightarrow$ lower PSI/PSII ratio)
4.2.1.2	77 K fluorescence	Ability for state transitions is still present but c_{6A}-KO always had lower PSI/PSII ratio in either state in photomixotrophy
4.2.1.3	DUAL-PAM light curves	c_{6A}-dependent difference in NPQ in continuous light (absence $\rightarrow$ slightly elevated NPQ)
4.2.1.3	DUAL-PAM light curves	c_{6A}-dependent difference in PQ pool redox state in continuous light (absence $\rightarrow$ more reduced PQ pool)
4.2.1.3	DUAL-PAM light curves	Slightly increased Y(II) in c_{6A}-OE

Section	Method	Finding
4.2.1.3 & 4.2.1.4	as 4.2.1.3 & DUAL-KLAS-NIR	No major impact of c_{6A} on PSI
4.2.1.5	OJIP curves	More reduced PQ pool in the absence of c_{6A}
4.2.1.6	JTS	Light-induced oxidation of *b* hemes (esp. in photomixotrophy) in the absence of c_{6A}, no major influence on cytochrome *f*, Pc signal drifted
4.2.1.6	JTS	DCMU addition: some decrease in c_{6A}-dependent difference in *b* hemes but still least reduction in the absence of c_{6A}
4.2.1.6	JTS	MV addition: some decrease in of c_{6A}-dependent differences in *b* hemes but still least reduction in the absence of c_{6A}
4.2.1.6	JTS	n-PG addition: c_{6A}-dependent *b* hemes differences are similar to without n-PG addition
4.2.1.6	JTS	DBMIB addition: absence of c_{6A}-dependent differences and oxidation of *b* hemes in all strains
4.2.1.7	ECS	No c_{6A}-dependent difference in pmf, gH^+, vH^+ in continuous light and photomixotrophy
4.2.1.8	MIMS	No c_{6A}-dependent difference in oxygen flows under continuous light in photomixotrophy
4.2.2.1	77 K fluorescence	c_{6A}-dependent light harvesting phenotype amplified by DISCO Light and shifted further towards PSII (absence $\rightarrow$ lower PSI/PSII ratio)
4.2.2.2	DUAL-PAM fluorescence	Lower Y(II) in light phases of DISCO Light in the absence of c_{6A}
4.2.2.2	DUAL-PAM fluorescence	Higher Y(NPQ) in DISCO Light in the absence of c_{6A} over 40 min
4.2.2.2	DUAL-PAM fluorescence	More reduced PQ pool in DISCO Light in the absence of c_{6A}

Section	Method	Finding
4.2.2.3	ECS measurements	No c_{6A}-dependent difference in pmf, gH^+, vH^+ in DISCO Light
4.2.2.4	DUAL-PAM P700	Increasing Y(NA) over the course of 40 min DISCO Light independent of c_{6A}
4.2.2.4	DUAL-PAM P700	Lower Y(ND) in the absence of c_{6A} in DISCO Light
5.2.1.1	Microscopy	No fluorescence from c_{6A}-mVenus transformants
5.2.1.2	Subcellular fractionation	c_{6A} probably thylakoid luminal localised
5.2.1.3	Immuno-fluorescence	c_{6A} likely thylakoid luminal localised
5.2.2	Co-IP	No stable complexes of c_{6A} with other proteins
5.2.3	BN-PAGE and 2D-PAGE	c_{6A}-dependent difference in accumulation of a proposed LHC-less PSI complex (absence $\rightarrow$ more prominent complex)
6.2.1.1	Western blot	PTOX2: less in KO than WT/OE
6.2.1.1	continuous light samples	LHCSR3: much more in WT than KO/OE
6.2.1.2	Western blot	PsbA degradation products only day 4: much more in KO than WT/OE
6.2.1.2	DISCO	CytF only day 2: less in KO than WT/OE
6.2.1.2	Light	NDA2: more in WT than KO/OE
6.2.1.2	samples	PTOX2: less in KO than WT/OE
6.2.1.2	from day 2	LHCSR3 day 2: most in KO, then WT, then OE
6.2.1.2	and day 4	LHCSR3 day 4: more in WT than KO/OE

Section	Method	Finding
6.2.2.1	RNAseq	No induction of c_{6A} transcript levels in DISCO light
6.2.2.2	RNAseq	Limited effect of c_{6A} on the transcriptomic reaction to DISCO Light
6.2.2.2.1	RNAseq	c_{6A}-dependent transcriptome differences in continuous light: genes associated with circadian clock, stress related LHCII antennae, peroxi-& thioredoxin
6.2.2.2.2	RNAseq	c_{6A}-dependent transcriptome differences in DISCO Light: as in 6.2.2.2.1 + response to oxidative stress
6.2.2.2.3	RNAseq	Large transcriptomic reaction to DISCO Light independent of c_{6A}
6.2.2.2.5	RNAseq	No major c_{6A}-dependent effect on expression of photosynthesis genes except for previously mentioned
6.2.3	RNAseq & western blot	Some incongruence in c_{6A}-dependent differences in protein and transcript levels

7.2 Findings in the light of proposed functions

Overall, absence of c_{6A} did not cause drastic phenotypes. Even under stressful conditions such as DISCO Light, the observed c_{6A}-dependent differences were rather subtle. This aligns with the long-standing difficulty in pinpointing the function of this protein and suggests that its role may be more associated with photosynthesis rather than directly involved in electron transfer mechanisms. Nevertheless, the results obtained showed multiple c_{6A}-dependent differences which offer a valuable foundation for functional hypotheses of c_{6A}. As some functions have been proposed in the past, the results obtained here are discussed in the light of these hypotheses before an updated working hypothesis is presented.

7.2.1 Cytochrome c_{6A} as a replacement for plastocyanin?

The hypothesis that c_{6A} might function as a replacement for plastocyanin was initially suggested by Gupta *et al.* (2002) [146] but had been questioned early on by Wastl *et al.* (2002) in their independent report on the existence of c_{6A} [144]. Since then, the hypothesis has been largely found unlikely by several pieces of evidence (section 1.4.5) [172]. Despite the unlikeliness of this hypothesis representing the actual function of c_{6A}, it remains valuable to compare it to the findings of this study.

Several observations could support the idea of c_{6A} having a functional role similar to plastocyanin. First, the luminal localisation of c_{6A} and the likely transient nature of its interactions would support this possibility. The absence of a growth phenotype under standard conditions could also be expected, as in c_{6A}-KO plastocyanin is still present in large quantities, at least by transcript level. Additionally, the more reduced PQ pool in the absence of c_{6A} would align with a role of c_{6A} similar to plastocyanin. The effect of overexpressing c_{6A} supports this further, as a less reduced PQ pool and a slightly increased PSII quantum yield was found as a result.

However, several lines of evidence contradict the hypothesis. Importantly, in WT the transcript level of c_{6A} was three orders of magnitude lower than that of plastocyanin, making replacement unlikely, at least under the growth conditions used here. Additionally, if the presence of plastocyanin prevented emergence of a phenotype under continuous light, a phenotype would also not be expected under any other conditions with normal or elevated plastocyanin expression. Under DISCO Light plastocyanin exhibited the seventh highest level of all transcripts found and would thus make the emergence of the c_{6A}-dependent growth phenotype under DISCO Light unlikely. Furthermore, a more reduced PQ pool caused by the absence of c_{6A} under this model should theoretically lead to greater PSI fluorescence relative to PSII fluorescence at 77 K in the absence of c_{6A} but this was not observed. Additionally, the lack of any change in the redox kinetics of cytochrome *f*, which would be expected if c_{6A} were replacing plastocyanin under the conditions used here, further undermines this hypothesis. Finally, the donor-side limitation in PSI was lower in c_{6A}-KO under DISCO Light, whereas increased limitation would be anticipated if a replacement of plastocyanin were absent.

Taken together, more evidence was found that contradicts the hypothesis of functional replacement for plastocyanin than supports it. Additionally, the observations in agreement with the hypothesis do not support this hypothesis alone but are also consistent with other hypotheses, as discussed below.

7.2.2 Cytochrome c_{6A} as part of a high light signalling response?

The hypothesis that c_{6A} plays a role in high light signalling was proposed based on RNAseq analysis, which compared the response of *C. reinhardtii* lacking c_{6A} to that of WT under high light conditions [171]. While this hypothesis was not explicitly tested here, it gains relevance from the fact that the DISCO Light used in this study included phases of high light exposure, potentially inducing a similar stress response.

In support of this hypothesis, some genes involved in the oxidative stress response, which is closely tied to the high light stress response, were found to be differentially expressed in a c_{6A}-dependent manner. However, there are other factors that challenge the idea of c_{6A} being a key player in high light signalling. One piece of evidence against this hypothesis is the lack of major effects of c_{6A} deficiency on the expression of *LHCSR3*, which encodes a well-known photoprotective protein playing a critical role in high light acclimation. Even under DISCO Light, where *LHCSR3* expression is dramatically increased, the absence of c_{6A} did not influence its expression levels significantly. Furthermore, the overall transcriptomic response to DISCO Light showed relatively minor changes in the absence of c_{6A}, suggesting that while c_{6A} might have some role in stress responses, its impact on high light signalling specifically appears to be limited. The absence of a growth phenotype under high light in both photoautotrophy and photomixotrophy also contrasts this hypothesis.

In conclusion, while there is evidence suggesting that c_{6A} may be involved in stress responses that overlap with high light signalling, its role in mediating signals remains uncertain and would require more targeted experiments to clarify.

7.2.3 Cytochrome c_{6A} as safety valve for excess electrons?

Another hypothesis proposed that c_{6A} might function as a 'safety valve' in the PETC, taking on excess electrons under difficult light conditions [172]. This would be similar to the likely role of PTOX2, which has been shown to mitigate the effects of excess light energy by redirecting electrons from the PETC in stressful conditions [51, 53].

Several observations support this hypothesis. First, *C. reinhardtii* lacking c_{6A} exhibited worse growth under stressful DISCO Light, suggesting that c_{6A} might play a protective role. In line with this, the absence of c_{6A} also led to a more reduced PQ pool, which would be expected from the absence of a 'safety valve'. Additionally, c_{6A} is localised to the thylakoid lumen and likely interacts with other proteins transiently, which would be appropriate for a protein involved in dissipating excess electrons.

However, there are several counterarguments to this hypothesis. One major issue is the generally low expression level of c_{6A}, which was confirmed again on transcript level in this study. If c_{6A} were acting as a crucial safety valve, it would be expected to show higher expression under stressful light conditions such as DISCO Light but no such increase was observed. Similar to the arguments against c_{6A} functioning as a plastocyanin replacement, a more reduced PQ pool would typically lead to increased relative PSI fluorescence at 77 K in the absence of c_{6A} assuming state transitions are unaffected. However, this fluorescence increase was not observed. Additionally, PTOX2, which is involved in a similar electron dissipation process, was less abundant in the absence of c_{6A}. If c_{6A} were acting as an alternative safety valve, increased PTOX2 levels would be expected rather than a decrease, to compensate for the loss of c_{6A}.

In summary, the 'safety valve' hypothesis did not receive much support from this study with evidence in agreement also being relevant for other functional hypotheses. While a 'safety valve' function cannot be excluded for conditions where c_{6A} expression may be higher, these conditions have not yet been identified (table 6.1).

7.2.4 Cytochrome c_{6A} as part of thiol-based redox regulation?

The hypothesis that c_{6A} is involved in thiol-based redox regulation was brought forward as c_{6A} possesses two evolutionarily conserved cysteine residues that can form a disulphide bridge on the surface exposed LIP (section 1.4.2). It was suggested that c_{6A} would interact with other luminal proteins with a disulphide bridge and maintain them in their oxidised and therefore active state [145]. FKBP13 was identified as a possible target when c_{6A} was discovered, as a Y2H screen using FKBP13 showed interaction with c_{6A} [146]. The electrons obtained from such interactions were then proposed to be funnelled back into the PETC via plastocyanin [134].

There are several arguments supporting this hypothesis. First, c_{6A} is localised to the thylakoid lumen, where thiol-based redox regulation is known to occur and control activity of various proteins (section 1.2.5). Additionally, the likely transient nature of c_{6A}'s interactions also aligns with a regulatory role. If c_{6A} were to help maintain target proteins in an oxidised state, that would make its function more important under highly reducing conditions, such as photomixotrophy and DISCO Light that leads to PSI acceptor side limitation. This would be in line with the absence of a growth phenotype under standard and photoautotrophic conditions and the emergence of a difference in DISCO Light. Additionally, RuBP regeneration was identified as a potential problem for c_{6A}-KO cells in DISCO Light and this regeneration process involves several thioredoxin-regulated components. However, it is important to note

that c_{6A} is located in the lumen, while the ferredoxin/thioredoxin system regulating the activity of various CBB cycle enzymes operates in the stroma [123]. The evidence of increased stress in the absence of c_{6A} under DISCO Light would be in agreement with a regulatory role for c_{6A} suggesting a lack of stress response in c_{6A}-KO. The existing connection between thiol-based regulation and state transitions via the conserved cysteine residues of the state transition kinase STT7 [102] could help explain why in the absence of c_{6A} the light-harvesting balance is skewed in favour of PSII compared to WT despite a more reduced PQ pool. Furthermore, a putative connection of c_{6A} with thiol-based regulation of the PSII subunit PSBO was proposed [134]. This connection could help explain the observed differences in NPQ and appearance of PsbA breakdown products. PSBO is more stable when its luminal disulphide bridge is oxidised [115], while its detachment from PSII due to instability is associated with the PSII repair cycle and thus qI quenching and PsbA degradation [113, 114]. Lastly, the complex responses observed at both the protein and transcript level when c_{6A} is absent or overexpressed could also be linked to thiol-based regulation, which is a complex regulatory network of activating and inhibiting effectors. Such regulation could affect not only protein stability but also gene expression, for example as observed for the c_{6A}-dependent differences in transcript levels of thioredoxins and peroxiredoxins.

One example where c_{6A} was found to be unlikely to participate in luminal thiol-based redox regulation is the case of PSAF. PSAF has been suggested as a key target in PSI for the redox regulation of ROS formation [138]. In the authors' model, PSAF with an oxidised disulphide bond results in less superoxide formation in PSI. A c_{6A}-KO in *A. thaliana* did not support any involvement of c_{6A} in this regulation, as determined by electron paramagnetic resonance (EPR) spectroscopy of ROS abundance. Despite this, other luminal proteins could still be targets of c_{6A}-mediated redox regulation.

Open questions and challenges remain to explain fully a role of c_{6A} in the context of thiol-based redox regulation. These include how c_{6A} can reduce plastocyanin *in vitro* at a rate that could be physiologically relevant [152], although interaction of c_{6A} and plastocyanin could not be found in a Y2H assay [148]. The question remains if there are any other routes for the electrons obtained by c_{6A} to be transferred to oxidising mediators. Additionally, the observed lower abundance of PTOX2 in the absence of c_{6A} remains to be explained in the context of this hypothesis.

Despite these uncertainties, the thiol-based redox regulation hypothesis remains a most interesting and plausible proposed function for c_{6A}. Further discussion of its implications is presented below, together with an updated working hypothesis of the function of c_{6A} in the context of thiol-based redox regulation in the thylakoid lumen.

7.3 Working hypothesis for the function of cytochrome c_{6A}

Figure 7.1 shows a selection of known connections between proteins involved in the luminal network of thiol-based redox regulation. At first, c_{6A} is omitted for clarity and is introduced later with the discussion of the role proposed here. The figures of this section represent a hypothetical model for the function of c_{6A} but do not aim to include all luminal proteins that may be involved in, or affected by, thiol-based redox regulation. Rather, they focus on the putative target proteins of c_{6A} specifically. There might be more target proteins of c_{6A} than shown, but most of the findings from this study can be explained with the selection in figure 7.1. Interactions that have been suggested by other researchers or the author are represented as broken lines, while connections determined experimentally *in vivo* or *in vitro* in *C. reinhardtii* or *A. thaliana* are shown as solid lines.

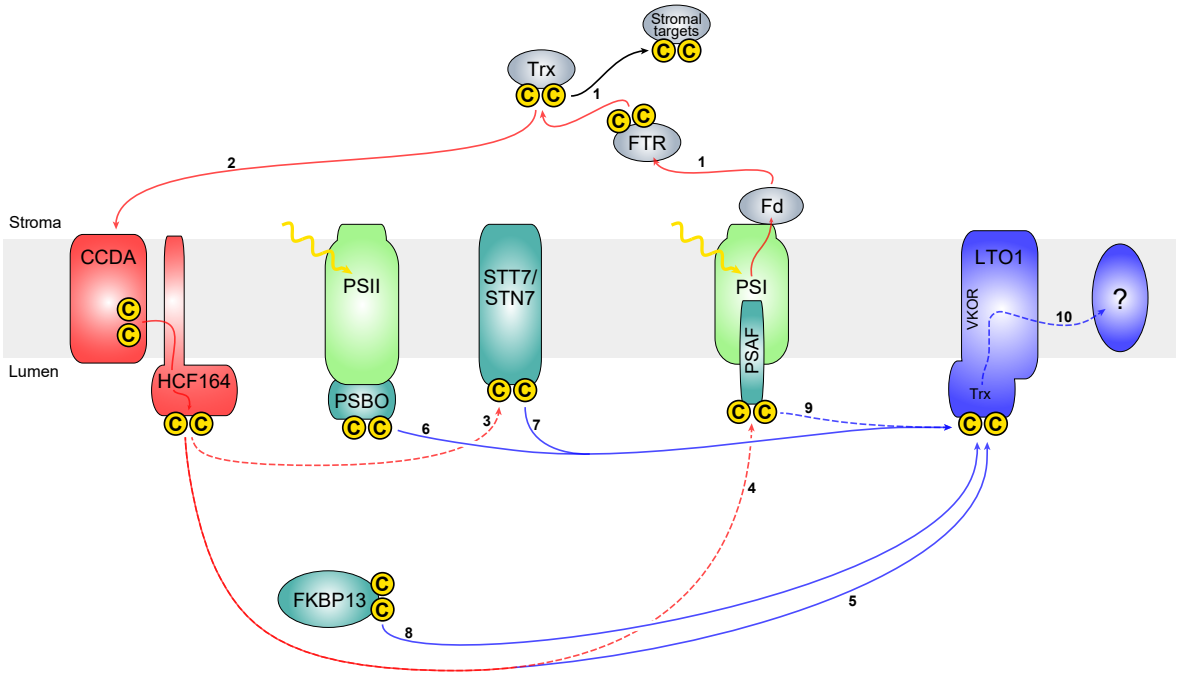


Figure 7.1: Selected known components of thiol-based redox regulation in the thylakoid lumen of plants and algae. Luminal target proteins of thiol-based regulation are shown in turquoise (PSBO, STT7/STN7, FKBP13, PSAF), the reductive pathway via CCDA and HCF164 influencing the redox state of the thiol(s)/disulphide(s) (yellow C for cysteine) is marked red and the oxidative pathway via LTO1 is shown in blue. The numbers on the arrows are referred to in the text and connections suggested by other researchers or the author with limited experimental evidence are represented as broken lines.

The stromal ferredoxin (Fd)/thioredoxin (Trx) system is well-known for regulating various stromal targets, such as CBB cycle enzymes and electron transfer from ferredoxin to thioredoxin is mediated by the ferredoxin-thioredoxin reductase (FTR) (figure 7.1 **1**) [123]. For luminal target proteins, the reductive system (red) relies on the introduction of reduction

equivalents from thioredoxin into the lumen via CCDA and HCF164 (figure 7.1 **2**) [124]. HCF164 has been suggested to be the reductive effector for various target proteins. The observation that overexpression of thioredoxin results in a more reduced state for STN7 [131] led to the suggestion that HCF164 can reduce STN7/STT7 (figure 7.1 **3**). Furthermore, HCF164 was also proposed to be the reducing mediator of PSAF in the regulation of ROS generation at PSI (figure 7.1 **4**) [138].

The oxidative system for luminal target protein (blue) is primarily driven by the membrane protein LTO1, which has a luminal thioredoxin (Trx) domain and a membrane-embedded VKOR (vitamin K epoxide reductase) domain. Interestingly, the reductive and oxidative systems appear to be directly connected, as interaction between HCF164 and LTO1 has been found in a Y2H assay and oxidation of HCF164 by LTO1 could be observed *in vitro* (figure 7.1 **5**) [133]. This interaction could represent a short-circuit in the redox regulation system within the lumen or function as a balancing switch between the reductive and oxidative pathways. LTO1 has been shown to oxidise PSBO *in vitro* (figure 7.1 **6**) [132]. Additionally, STN7 was found to be oxidised by LTO1 *in vitro* and diminished state transitions were observed *in vivo* in *A. thaliana* lacking LTO1 (figure 7.1 **7**) [105]. The luminal immunophilin FKBP13 exhibited interaction with LTO1 in a Y2H and thus represents another putative target of LTO1 (figure 7.1 **8**) [133]. Finally, PSAF has been suggested to be oxidised by LTO1 as ROS generation at PSI was affected in an *A. thaliana* LTO1 knock-out (figure 7.1 **9**) [138]. The fate of electrons obtained by LTO1 from oxidising target proteins remains to be determined. However, it was speculated that they are transferred to a different unknown oxidising mediator that could potentially lead to reduction of hydrogen peroxide to water (figure 7.1 **10**) [124].

7.3.1 Putative regulation targets of c_{6A}

7.3.1.1 STT7/STN7

The state transition kinase STT7/STN7 is regulated by conserved cysteine residues that need to be in an oxidised state for kinase activity [93, 102]. While LTO1 was found to be closely associated with the thiol-based regulation of STN7, state transitions were not completely abolished in LTO1 knock-out mutants, suggesting that additional factors may contribute to maintaining the oxidised state of STN7 [105].

Cytochrome c_{6A} could potentially take on this role and help maintain STT7/STN7 in its oxidised, active state (figure 7.2 **11**). In the absence of c_{6A}, this would result in a less active STT7 kinase on average. If the oxidising effect of c_{6A} on STT7/STN7 were small, state transitions could still occur, as seen in 77 K fluorescence measurements of c_{6A}-KO

mutants, although their rate might be slower, or the overall phosphorylation of LHCII could be reduced. This would lead to less LHCII attachment to PSI, resulting in the observed lower relative PSI fluorescence at 77 K. Additionally, this reduction in LHCII phosphorylation could result in increased abundance of PSI complexes lacking LHCII, which could be related to the proposed LHC-less PSI complex observed in 2D-PAGE. Consequently, the altered light-harvesting balance, favouring PSII over PSI, would contribute to a more reduced PQ pool in the absence of c_{6A}, aligning with the observed differences in PQ pool redox states and the altered redox kinetics of *b* hemes in the absence of c_{6A}. A more reduced PQ pool might not be detrimental under standard conditions where relatively low light intensity is unlikely to cause damage. However, in DISCO Light with its high light phases, it might lead to increased damage exacerbated by downstream electron sinks not being available. This damage could be one of the reasons for the observed growth phenotype under DISCO Light in absence of c_{6A}. Longer term, the combination of imbalances in light harvesting and PQ pool with DISCO Light could also lead to an imbalance of ATP/NADPH ratio and thus further cause a growth deficit in the absence of c_{6A}.

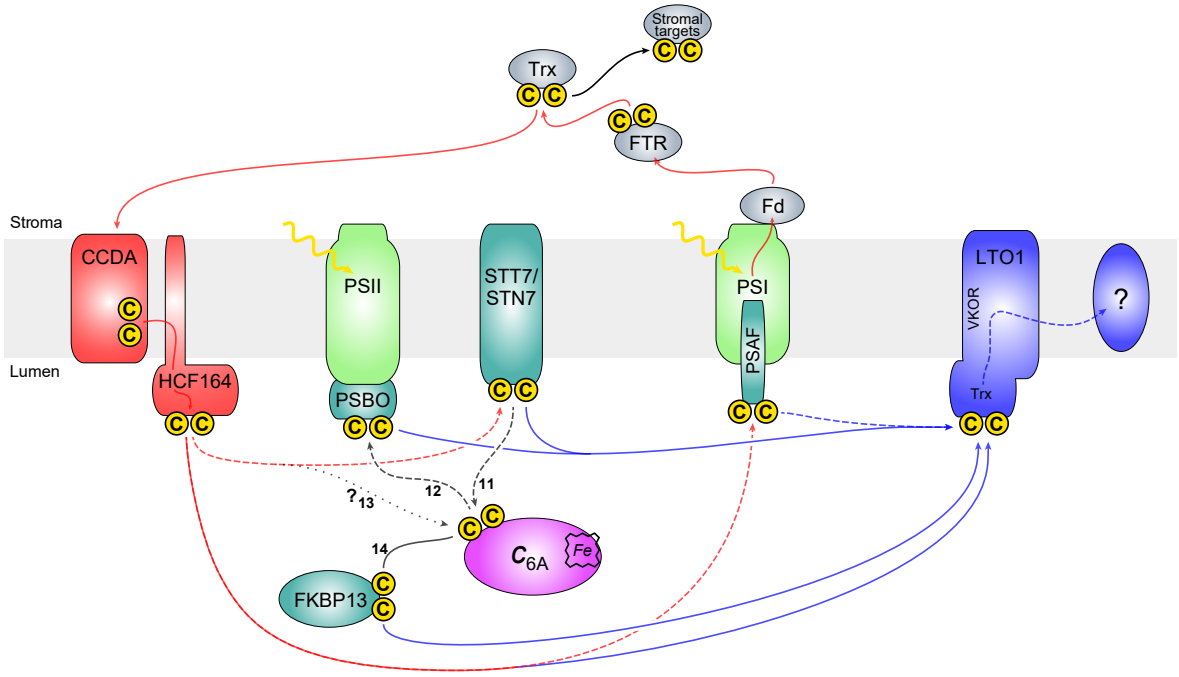


Figure 7.2: Putative targets of c_{6A} in thiol-based redox regulation in the thylakoid lumen. Luminal target proteins of thiol-based regulation are shown in turquoise (PSBO, STT7/STN7, FKBP13, PSAF), the reductive pathway via CCDA and HCF164 influencing the redox state of the thiol(s)/disulphide(s) (yellow C for cysteine) is marked red and the oxidative pathway via LTO1 is shown in blue. The heme of c_{6A} is indicated by a framed "Fe" and interactions with c_{6A} are marked with grey arrows. The numbers on the arrows are referred to in the text and connections suggested by other researchers or the author with limited experimental evidence are represented as broken lines. The dotted line with a question mark indicates a speculation.

7.3.1.2 PSBO

Another potential target of c_{6A} is PSBO, which requires two conserved cysteines to be oxidised in order to maintain its stability [115]. If these cysteines are reduced, the PSII reaction centre becomes more accessible to degradation by the FTSH protease, leading to an increase in PSII breakdown products [114]. PSBO has been shown to be oxidised by LTO1 [132] but the reductive pathway for PSBO is yet to be uncovered [124].

According to the previous thiol-based regulation hypothesis (section 7.2.4), c_{6A} would be involved in maintaining PSBO in its oxidised state. Consequently, more PSII degradation in the absence of c_{6A} would be expected, which correlates with the increased PsbA degradation observed after four days under DISCO Light in c_{6A}-KO. However, a reduction of the photoinhibition qI element of NPQ would also be anticipated for c_{6A}-KO, as PSBO would probably be less stable and thus make PSII repair easier, allowing the faster exchange of PsbA subunits and thus lowering the contribution of qI quenching. Rather than a decrease in NPQ in the absence of c_{6A}, an increase in NPQ was observed (sections 4.2.1.3 & 4.2.2.2). This increase was found not to depend on a difference in pmf (as determined by ECS measurements) and was not in agreement with altered LHCSR3 protein levels. Hence, it was unlikely to be related to the energy-dependent quenching qE. The likely exclusion of qE raised the question if c_{6A} could influence other quenching mechanisms, such as qZ, qT or qI. Zeaxanthin-dependent quenching qZ in *C. reinhardtii* is dependent on the activity of CVDE, which is a stromal protein [88], unlikely to be thiol-regulated [89] and thus less likely to be a direct target of c_{6A} regulation. State transition quenching qT could be involved as well and c_{6A}'s putative effect on the main state transition effector STT7 was discussed above. This leaves qI as another possible target of c_{6A} regulation.

If, rather than oxidising PSBO, c_{6A} were to play a role in reducing PSBO (figure 7.2 **12**), its absence would lead to a higher proportion of oxidised PSBO, which could slow the repair process of PSII. A slower PsbA turnover would result in increased qI NPQ, observable over minutes to hours. This would align with the higher NPQ levels seen in c_{6A}-KO under DISCO Light conditions where NPQ levels rise above WT levels over the course of 40 min. In the case of c_{6A} reducing PSBO, the increased PsbA breakdown after four days under DISCO Light would not be directly related to the redox state of PSBO but rather a consequence of the overall stress experienced by the cells. This would be in agreement with the finding that PsbA repair is also influenced by other factors, such as phosphorylation state of core proteins [96] or protease activity [113] that may be affected under stress conditions. As the redox midpoint potentials of the thiols/disulphides on c_{6A} and PSBO are unknown, the likely direction of reduction remains to be determined.

If c_{6A} were indeed helping to oxidise STT7/STN7 and reduce PSBO, this might suggest a regulatory link between the qI and qT mechanisms of NPQ. In fact, in *C. reinhardtii* a knock-out of STT7 accumulated more PsbA under high light conditions compared to wild-type [96]. This would be expected if a c_{6A}-dependent reduction of PSBO and thus ultimately PsbA degradation, required electrons from the STT7/STN7 thiols. However, in an *A. thaliana* STN7 knock-out, no significant difference in the PsbA repair cycle compared to wild type was observed [400], suggesting that STN7/STT7 might not be the only electron donor to c_{6A} in this model. It is conceivable that HCF164 could act as the electron donor to c_{6A} allowing the reduction of PSBO in the absence of STT7/STN7 (figure 7.2 **13**).

7.3.1.3 FKBP13

FKBP13 is a soluble thylakoid luminal protein [135] that has been identified as a putative interaction partner of c_{6A} in a Y2H assay (figure 7.2 **14**) [146]. The redox midpoint potential of the FKBP13 thiol/disulphide has not been determined yet, preventing a clear conclusion on c_{6A}'s theoretical ability to reduce or oxidise FKBP13. In any case, a thiol/disulphide exchange between c_{6A} and FKBP13 would indicate that FKBP13 may, at least somewhat, replace the function of c_{6A} as a soluble thiol-based redox mediator. If FKBP13 were to accept electrons from targets like STT7/STN7 as well, this would further explain the absence of a clear phenotype of c_{6A}-KO under standard conditions.

7.3.1.4 PSAF

PSAF has been suggested to play a role in the redox regulation of ROS formation at PSI, potentially through its interaction with LTO1 [138]. In studies relying on *A. thaliana*, c_{6A} was found not to be involved [138], making PSAF an unlikely target protein in the model presented here. If c_{6A} were involved in PSAF regulation, a change in Y(I) and Y(NA) would be expected in the absence of c_{6A}, as ferredoxin reduction becomes less or more efficient when the PSAF subunit has a reduced or oxidised disulphide bond, respectively [138]. This was not observed in P700 measurements. The lack of significant c_{6A}-dependent differences in PSI parameters thus aligns with the conclusion that c_{6A} does not participate in PSAF regulation.

7.3.2 Putative downstream electron acceptors from c_{6A}

Apart from reducing PSBO, the electrons c_{6A} obtains in this model from oxidising target proteins such as STT7/STN7, could be transferred to multiple other proteins. These transfers are either reliant on the heme in addition to the cysteine residues, or solely on the cysteine residues in the LIP of c_{6A}.

7.3.2.1 Electron transfers dependent on the heme group

For the routes involving the heme group, electron transfer from the thiols in the LIP to the heme is required. Structural investigation of c_{6A} confirmed that this is, in principle, possible as the two are close enough for electron transfer to occur (figure 7.3 **15**) [152]. Subsequently, as proposed in the previous thiol-based regulation hypothesis, electrons from c_{6A} could be funnelled back into the PETC via plastocyanin [134]. Plastocyanin reduction by c_{6A} was shown *in vitro* and found to be physiologically relevant by examining the rate constant k_2, which includes binding, electron transfer and dissociation. The k_2 rate for this reaction amounted to more than 13% of the same rate constant for the essential reaction between plastocyanin and PSI (figure 7.3 **16**) [152]. Such an interaction between c_{6A} and plastocyanin may also provide an explanation for the observation that in *A. thaliana* a plastocyanin knock-down that is additionally deficient in c_{6A} is lethal, while it is only drastically growth impaired when c_{6A} is expressed [146]. Low levels of plastocyanin would be likely to result in a highly reduced PQ pool because of the impaired electron transfer to PSI. A highly reduced PQ pool would induce state transitions towards state 2. If c_{6A} were important for oxidising STT7, as suggested above, state transitions might be impaired under these conditions. This could further exacerbate the reduction of the PQ pool and lead to severe photooxidative stress at PSII, ultimately causing lethality.

Another route of electron transfer, bypassing plastocyanin, sees c_{6A} directly transferring electrons to PSI (figure 7.3 **17**). This electron transfer was found to be orders of magnitude slower than the rate of PSI reduction by plastocyanin or c_6 and serves as an argument against the functional hypothesis of replacing plastocyanin [147, 156]. However, it can be assumed that the electron flow through the PETC is much larger than the one originating from oxidising thiols in the lumen, so the slow reduction rate of PSI by c_{6A} could be sufficient for c_{6A} to perform its proposed function in thiol-based redox regulation. With the relatively minor contribution to PSI reduction compared to the reduction by plastocyanin, no major differences between c_{6A} mutant strains and WT would be expected when examining biophysical PSI parameters, in line with the findings of this study.

7.3.2.2 Electron transfer via thiol/disulphide exchange

Another potential electron acceptor for c_{6A}, without involving the heme, is LTO1. In this case, c_{6A} would transfer electrons via a thiol/disulphide exchange. Whether c_{6A} could donate electrons to LTO1 depends on the redox midpoint potentials of the disulphide bonds in both proteins. For the soluble thioredoxin domain of LTO1 a redox midpoint potential of -180 mV (pH 7) was determined [401], while no potential has been recorded for c_{6A}'s thiol/disulphide yet. If the c_{6A} thiol/disulphide potential were more negative than this, it would be conceivable that c_{6A} functions within the oxidative pathway by transferring electrons to LTO1. Experimental evidence provides some support for this interaction, as a Y2H assay recovered interaction between LTO1 and c_{6A} (figure 7.3 **18**). A surface plasmon resonance experiment performed subsequently did not detect a direct interaction, although the authors noted that this is likely to have been impacted by the formation of inclusion bodies during heterologous expression of c_{6A} [133].

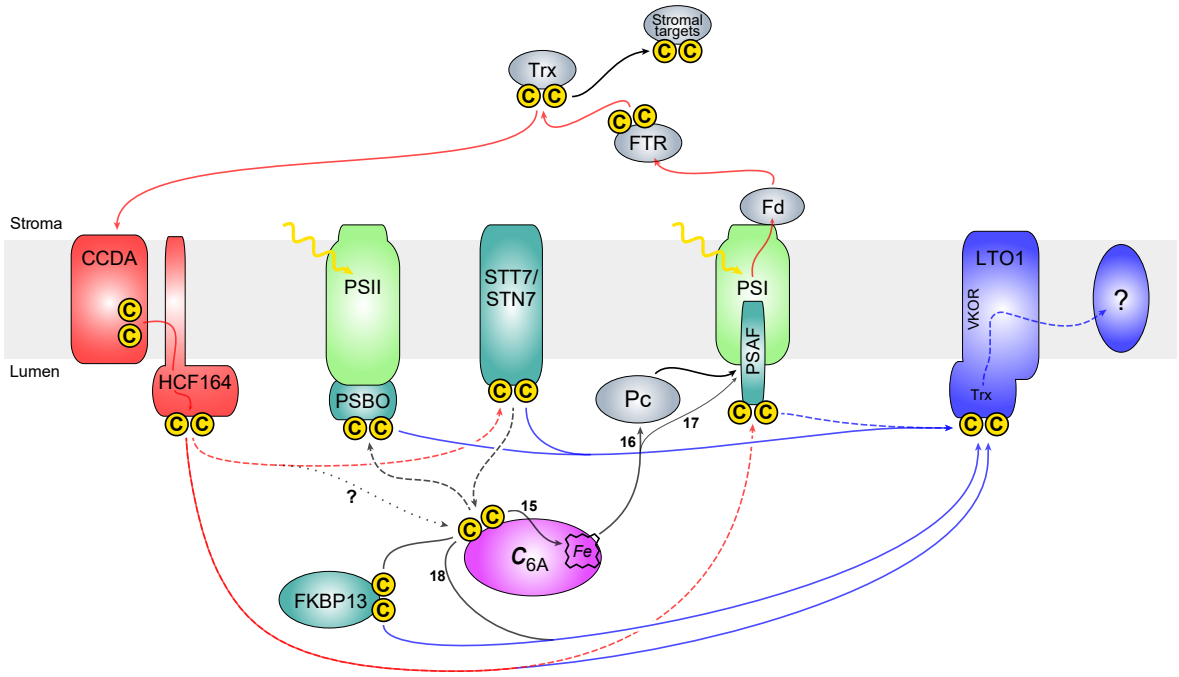


Figure 7.3: Putative downstream electron acceptors of c_{6A} in the model of c_{6A} being involved in thiol-based redox regulation in the thylakoid lumen. Luminal target proteins of thiol-based regulation are shown in turquoise (PSBO, STT7/STN7, FKBP13, PSAF), the reductive pathway via CCDA and HCF164 influencing the redox state of the thiol(s)/disulphide(s) (yellow C for cysteine) is marked red and the oxidative pathway via LTO1 is shown in blue. The heme of c_{6A} is indicated by a framed "Fe" and interactions with c_{6A} are marked with grey arrows. The numbers on the arrows are referred to in the text and connections suggested by other researchers or the author with limited experimental evidence are represented as broken lines. The dotted line with a question mark indicates a speculation.

Experiments investigating if LTO1 can be reduced by c_{6A} *in vitro* are yet to be carried out. Interestingly, in *A. thaliana*, LTO1 was found to be specific to sensory plastids, which is also the case for c_{6A} [165]. This shared localisation further supports the possibility of an interaction between the two proteins, as both may participate in redox regulation within these specialised plastids.

It remains an open question whether c_{6A} has a single primary electron acceptor or could transfer electrons to multiple targets, such as LTO1, plastocyanin, and PSI, depending on the specific physiological context. It is worth noting that state transitions are not entirely abolished in LTO1 knock-out mutants [105], indicating that if c_{6A} were involved in keeping STT7/STN7 oxidised and transferring those electrons to LTO1, alternative pathways oxidising c_{6A} must exist. This redundancy could provide flexibility to the system, ensuring that thiol-based redox regulation and state transitions can continue somewhat even under stressful environmental conditions such as DISCO Light or if LTO1 or c_{6A} were absent. Especially regarding the light-dependent generation of a proton gradient, multiple routes of electron transfer may be important, because the redox midpoint potentials of proteins are affected by the surrounding pH [124].

7.3.2.3 Putative electron acceptors from LTO1 and downstream effects

The fate of electrons transferred to LTO1 remains a key part of understanding thiol-based redox regulation in the thylakoid lumen. One possible route is through an unknown mediator that was recently proposed to reduce hydrogen peroxide to water [124] (figure 7.4 **10**). Another possible route is through the VKOR domain of LTO1. Structural studies of a cyanobacterial homologue of LTO1 have clarified the mechanism of electron transfer from the Trx domain to the VKOR (vitamin K epoxide reductase) domain via intramolecular thiol/disulphide exchanges towards the active site of the VKOR domain [402, 403]. This makes the quinone substrate of the VKOR domain another likely electron acceptor. There are various possible identities for this quinone substrate, and a number of quinones, such as phylloquinone (also known as vitamin K_1) have been detected in addition to plastoquinone in plant tissues [404]. Studies using yeast microsomal preparations have shown that the VKOR domain from *A. thaliana* LTO1 can reduce phylloquinone (PhyQ, figure 7.4 **19**) but not plastoquinone [401].

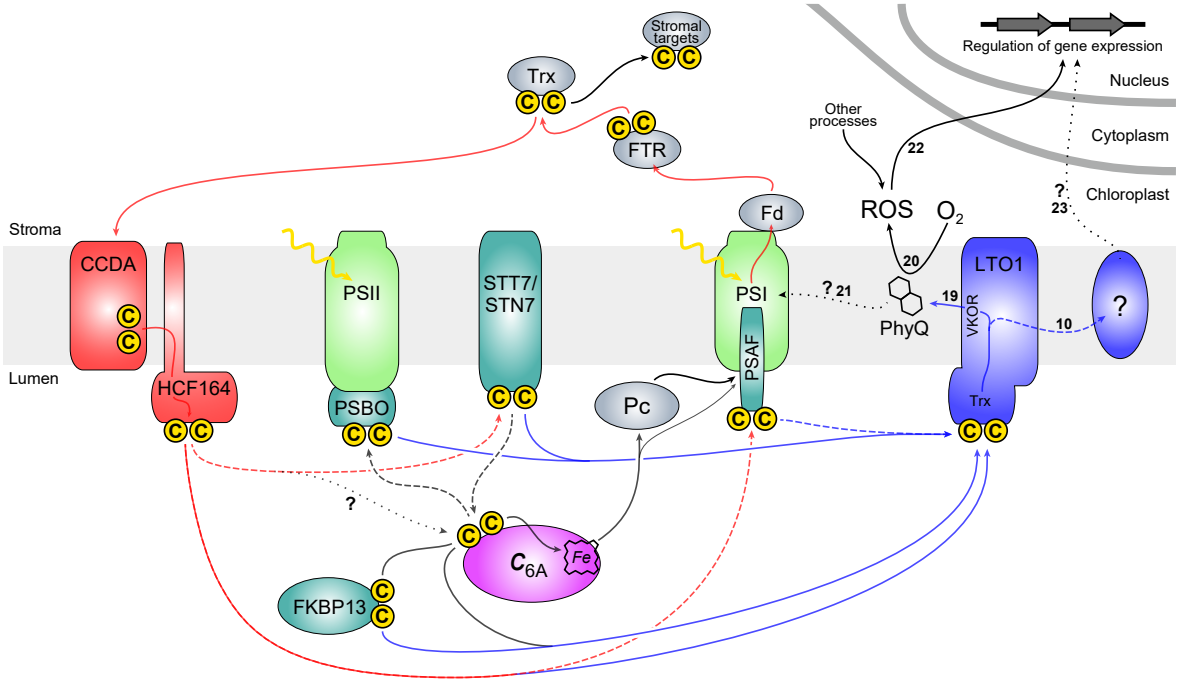


Figure 7.4: Putative electron acceptors of LTO1 in the model of c_{6A} being involved in thiol-based redox regulation in the thylakoid lumen. Luminal target proteins of thiol-based regulation are shown in turquoise (PSBO, STT7/STN7, FKBP13, PSAF), the reductive pathway via CCDA and HCF164 influencing the redox state of the thiol(s)/disulphide(s) (yellow C for cysteine) is marked red and the oxidative pathway via LTO1 is shown in blue. The heme of c_{6A} is indicated by a framed "Fe" and interactions with c_{6A} are marked with grey arrows. The numbers on the arrows are referred to in the text and connections suggested by other researchers or the author with limited experimental evidence are represented as broken lines. The dotted lines with a question mark indicate speculations.

Once reduced, phylloquinone can transfer its electrons to oxygen, leading to the production of ROS (figure 7.4 **20**) [405]. The A_{1A} phylloquinone of PSI was also found to be a major site of ROS generation as part of the Mehler reaction [406], although an interaction with LTO1 seems unlikely given the position of A_{1A} within the PSI core (figure 7.4 **21**). Any ROS generated from the reduction of oxygen by phylloquinone could subsequently be detoxified by superoxide dismutase or other ROS-scavenging enzymes. However, these ROS might also play a signalling role, influencing chloroplast-to-nucleus communication (figure 7.4 **22**) [57, 58]. Such a model would be consistent with the observation of changes in gene expression in the absence of c_{6A}. If LTO1 is involved in transmitting signals from the thylakoid lumen to the nucleus through ROS production, the absence of c_{6A} could limit the effect of this signalling pathway, resulting in the observed lower expression of ROS response genes under DISCO Light conditions. This hypothesis thus links the redox status of the lumen as perceived by thiol-containing proteins to gene expression in the nucleus. This linkage could also be connected to the observed altered regulation of the expression of circadian rhythm genes, some of which were shown to be regulated by light [378]. It should be noted, however, that many

other processes in the chloroplast influence the level of ROS accumulation [58]. Additionally, phylloquinone is not necessarily oxidised only by molecular oxygen. In studies investigating the chloroplastic phylloquinone pool, authors speculated that there likely are enzymes re-oxidising reduced phylloquinone and that these enzymes could potentially relay the redox state of the phylloquinone pool as a signal to downstream effectors (figure 7.4 **23**) [401, 404].

7.3.3 Cytochrome c_{6A} is a soluble mediator in the complex thiol-based redox regulation network in the thylakoid lumen and fine-tunes STT7 activity and PSBO stability

Considering the wider model, *in vivo* interactions between many of the proteins involved in the proposed redox regulation network are unclear. Given that many of the proteins involved are membrane-embedded or membrane-bound, it remains to be investigated whether these proteins are even in close enough proximity to facilitate electron transfer. The presence of a soluble redox mediator like c_{6A} could be a valuable addition, making co-localisation of membrane proteins less important.

Summarising the sections above, it is proposed that c_{6A} functions as a soluble mediator for thiol-based redox regulation in the thylakoid lumen (figure 7.4). As such, it would provide a diffusible component linking known membrane-embedded and membrane-bound effector and target proteins. The hypothesis suggests that c_{6A} fine-tunes STT7/STN7 activity and PSBO stability. Additionally, c_{6A} may interact with FKBP13. Electrons obtained by c_{6A} from interaction with target proteins may be transferred to plastocyanin, PSI, and LTO1, providing important regulatory flexibility. Finally, via LTO1 and downstream signalling effectors such as ROS, c_{6A} may in addition influence gene expression in the nucleus.

7.3.4 Challenges to the hypothesis and open questions

One of the key challenges is found in a previous structural analysis by Worrall *et al.* (2008) that predicted the disulphide bridge of the LIP in c_{6A} to be rather of structural importance than being catalytic [153]. This prediction solely relies on the comparison of the angles of the disulphide-bond with disulphide bonds of known catalytic enzymes [407]. Especially for proteins of the thylakoid lumen that are exposed to a wide range of pH, it may be important to take into account the influence of such environmental changes on the characteristics of a chemical bond such as disulphide bridges. Similar to the conclusion of Worrall *et al.* (2008), it remains to be experimentally tested if the disulphide bond of c_{6A} is catalytically active or

not. With the interaction partners proposed here, experiments to investigate this could be carried out *in vitro*, as described in the future work section (section 7.4.1).

Another challenge to the hypothesis is the proposed connection of c_{6A} with the regulation of gene expression via LTO1 and ROS generation from phylloquinones. In this model, the absence of c_{6A} would reduce the transcriptomic response to ROS, as observed in the RNAseq data from DISCO Light conditions. However, this would be inconsistent with the putative increase in ROS generation that could be caused by the imbalances in light harvesting and PQ pool redox state. This was suggested to contribute to the emergence of the growth phenotype in DISCO Light. The hypothesis of an alternative, unknown oxidising mediator downstream of LTO1 [124], possibly involving the oxidation of reduced phylloquinone [401, 404], could help resolve this inconsistency if such a mediator were involved in signalling processes that led to changes in gene expression.

Several open questions remain regarding the hypothesised model. For example, some known targets of thiol-based redox regulation in the lumen have been left out of the model. Cytochrome b_6f components, such as the Rieske protein and cytochrome *f* are known targets of HCF164 [130] and FKBP13 [135, 408]. These interactions are important for the biogenesis of the b_6f complex and could potentially be linked to c_{6A}'s proposed function. Perhaps consistent with this, a small c_{6A}-dependent difference in cytochrome *f* abundance was detected on day 2 of DISCO Light exposure. However, no other significant c_{6A}-dependent phenotypes related to these proteins, such as altered redox kinetics of cytochrome *f*, were observed. This may warrant for the exclusion of these proteins from the model.

The violaxanthin de-epoxidase CVDE has also been excluded from this model because in *C. reinhardtii* it is located in the stroma [88] and is unlikely to be thiol-regulated [89]. However, in plants, VDE is luminal, known to be thiol-regulated and most stable when its cysteine residues form six disulphide bridges [86, 87]. Additional to the pmf, LTO1 has been suggested as a regulator of VDE activity [409]. CCDA and HCF164 were also found to be involved in regulation of VDE activity [128, 130]. In this context, c_{6A} could either help keep VDE oxidised or participate in its reduction. The absence of c_{6A} in plants could then affect the qZ quenching mechanism by altering VDE activity, a regulatory pathway that this model does not include.

The protein abundance of PTOX2 comparing WT and c_{6A} mutant strains are challenging to place within the proposed model. In the absence of c_{6A} lower PTOX2 protein levels were found in continuous light and DISCO Light. While the absence of PTOX2 would be likely to lead to a more reduced PQ pool, as observed for c_{6A}-KO, this should result also in increased relative PSI fluorescence if state transitions are unaffected. As a relative decrease of PSI

fluorescence was observed, it can be concluded that the difference in PTOX2 abundance does not account for all observed effects of the absence of c_{6A}. How the stromal localised PTOX2 might be affected by absence of the luminal c_{6A} is not immediately clear. However, the ROS-dependent gene regulation included in the model might help to explain the PTOX2 protein levels. If a signal from LTO1 or phylloquinone (as discussed above) affected the activity of the transcriptional regulator PSR1 that influences PTOX2 expression [365], it would be conceivable that PTOX2 abundance is downregulated at the transcriptional level in the absence of c_{6A}. This was indeed observed as a significantly lower PTOX2 transcript abundance in c_{6A}-KO than in c_{6A}-OE under continuous light, although the difference did not meet the $\log_2$FC threshold.

The altered protein abundance of LHCSR3, a key photoprotective protein, is also not explained by this model. However, it is possible that LHCSR3 expression is peripheral to the function of c_{6A}, merely reflecting the stress conditions in the absence of c_{6A}, in line with LHCSR3 expression being induced by a multitude of stresses (section 6.1.1).

7.4 Further work

Several experiments have been proposed throughout this study, each aimed at further investigating the function of c_{6A} within the specific contexts discussed in individual chapters. In this section, additional avenues for future research are outlined, with a particular focus on testing the hypothesis of c_{6A}'s involvement in thiol-based redox regulation in the thylakoid lumen. Additionally, experiments to explore the role of c_{6A} in other green eukaryotes are suggested and potential research directions for other cytochrome c_6-like proteins are presented.

7.4.1 Testing the thiol-based redox regulation hypothesis

A straightforward method to test the involvement of c_{6A} in thiol-based redox regulation in the thylakoid lumen would be to transform the *C. reinhardtii* c_{6A}-KO strain with a construct of c_{6A} with the relevant cysteine residues mutated to alanine residues. Those mutation studies are a well-known tool for the investigation of the importance of cysteine residues in redox activity and structure of proteins [105, 136, 402]. A transformant expressing mature c_{6A} but with alanine instead of cysteine residues could be tested for the observed c_{6A}-dependent phenotypes, for example by employing growth curves in DISCO Light, 77 K fluorescence spectrometry to examine the light harvesting balance, and PQ pool measurements by OJIP or more indirectly via measurements of the redox kinetics of *b* hemes. If an alanine mutant strain

expressed a structurally unaffected c_{6A} and behaved in the same way as c_{6A}-KO, it would provide strong evidence for the involvement of the cysteine residues in c_{6A}'s function. If c_{6A}-dependent phenotypes were complemented to WT characteristics, the proposed hypothesis would appear unlikely.

Further experiments could investigate whether c_{6A} oxidises STT7 *in vitro*, similar to the work by Wu *et al.* (2021) [105]. There, *in vitro* oxidation of STN7 by LTO1 could be shown by incubating reduced STN7 with oxidised LTO1 and trapping the oxidation state of the cysteine residues with ice-cold trichloroacetic acid. Free thiols were then modified with the alkylation agent acetamido-maleimidylstilbene-disulphonic acid (AMS) which led to an increase in molecular mass of the affected protein, making oxidised and reduced forms distinguishable by gel electrophoresis [105]. This method should also be applied to test if c_{6A} can reduce PSBO and LTO1. If c_{6A} led to more reduction of PSBO, absence of c_{6A} should lead to an increased protein abundance of PSBO, as it is more stable when its cysteine residues are oxidised. This could be tested with immunoblots utilising the samples obtained for the transcript and protein level study presented in chapter 6.

To test if c_{6A} allows the residual state transition activity observed in a LTO1 knock-out [105], a double mutant lacking both c_{6A} and LTO1 could be examined for its state transition ability utilising 77 K fluorescence spectrometry. This could clarify the extent of their interactions, as the complete absence of state transitions would be expected in this double mutant if both proteins were involved in STT7 activation. Additionally, the phosphorylation of LHCII proteins should be analysed with immunoblots. The single mutants as well as the established *stt7* mutant strain, deficient in state transitions, could serve as controls. It would also be particularly interesting to examine the growth of this *stt7* mutant under DISCO Light conditions. Similar to c_{6A}-KO, no phenotype has been observed for *stt7* under more consistent fluctuating light than DISCO Light (cycles of 1, 10 or 30 min 620 $\mu mol_{photons}\ m^{-2}\ s^{-1}$light/dark) [235]. If a growth penalty similar to c_{6A}-KO compared to the background strain were to become apparent in DISCO Light, this would support the hypothesis that effects on state transitions contribute to the c_{6A}-dependent phenotype.

The hypothesis also predicts that in the absence of c_{6A}, there would be less qT (due to STT7 being more reduced) and more qI (due to PSBO being more oxidised), indications for which were observed in this study. Time-resolved measurements of qT and qI could be employed to test this prediction in more detail. Various chlorophyll fluorescence-based methods are available to examine the levels of qI [113] and qT [98] in *C. reinhardtii*.

Another unknown in the proposed hypothesis are the redox midpoint potentials of the cysteine residues in c_{6A}, FKBP13, STT7/STN7, and PSBO. Determining these would clarify

whether c_{6A} is theoretically able to oxidise or reduce its putative target proteins. It is important to note that the redox-active heme group of c_{6A} may interfere with redox midpoint potential measurements aimed at the thiol/disulphide, especially if electron transfer from the LIP thiols to the heme occurs. The redox midpoint potential of the heme in c_{6A} has been measured with redox titrations of the protein [156] or protein film cyclic voltammetry [155], both of which could only be employed to determine the potential of the cysteine residues if utilising a heme-less c_{6A}. As maturation of *c*-type cytochromes in *Escherichia coli* (*E. coli*) requires the ccm operon machinery [410] which is usually provided by co-transformation of a plasmid encoding it [152], expression of heterologous c_{6A} in an *E. coli* strain without a co-transformed ccm operon should result in a heme-less c_{6A}. Under the assumption that the folding of c_{6A} is unaffected without the heme, protein film voltammetry could then be carried out to determine the redox midpoint potential of the cysteine residues. This method has also been used to determine potentials of thioredoxins [411], and could thus be readily applied to the proposed interaction partners FKBP13, STT7/STN7, and PSBO. Additionally, studies could test if c_{6A} can be reduced *in vitro*, e.g. by dithiothreitol (DTT) employing a similar assay as described above involving the modification of cysteine residues with AMS. If reduction were observed, the concentrations needed to reduce a heme-containing or a heme-less c_{6A} could indicate if electron transfer from the thiol/disulphide to the heme occurs. If similar concentrations were needed, that would indicate that electron transfer to the heme is unlikely, while increased concentrations for the heme-containing protein would correlate with an increased oxidation capacity rendering transfer from the thiol/disulphide to the heme more likely.

Moreover, the kinetics of electron transfer, along with distribution of thylakoid membrane proteins, interaction strength, and diffusion rates of soluble proteins, are all factors that could influence the overall redox homeostasis in the thylakoid lumen but are yet to be comprehensively characterised. Once more data are available on these, a comprehensive model of thiol-based electron transfer in the thylakoid lumen could help uncover the role of c_{6A} in the homeostasis of thiol-based redox regulation.

7.4.2 The function of c_{6A} beyond *C. reinhardtii*

The sequence of c_{6A} is highly conserved across the green lineage (section 1.4.3) which indicates that its function may be also highly conserved. To assess this, the function of c_{6A} in other green eukaryotes such as plants could be investigated using the findings of this study as a guideline. A logical starting point would be *A. thaliana*, as mutant lines of c_{6A} exist as SALK T-DNA insertion mutants [412]. These mutants have been used before in other studies [148, 170, 174] and provide a valuable resource for testing the impact

of c_{6A} absence in land plants especially under conditions of light stress, such as DISCO Light. Testing for phenotypes under these conditions, particularly regarding growth and photosynthetic parameters, could reveal whether c_{6A} plays a similar role in plants to that in *C. reinhardtii*. The biophysical measurements that have been used here for *C. reinhardtii* can also be readily applied to plant samples. In fact, certain measurements, such as state transitions via chlorophyll fluorescence [268], may be easier in plants because light conditions tend to have a greater influence on state transitions in plants than in *C. reinhardtii* [108]. Another valuable experiment to test functional conservation would be to express the *A. thaliana* c_{6A} gene in the *C. reinhardtii* c_{6A}-KO. If the *A. thaliana* gene rescued the c_{6A}-KO phenotype in *C. reinhardtii*, this would suggest a conserved function between algae and plants. Alternatively, if the rescue were incomplete or absent, this might indicate evolutionary divergence in the function or interactions of c_{6A} between different photosynthetic organisms.

An intriguing area for investigation in *A. thaliana* is the potential connection between c_{6A} and LTO1 and their shared unique localisation in sensory plastids [165]. Further characterisation of signalling pathways from sensory plastids towards the nucleus and other cells might reveal the identity of suggested components such as the unknown oxidising mediator accepting electrons from LTO1 (figure 7.4).

Furthermore, the observed impact of c_{6A} on the abundance of PTOX2 warrants additional investigation. In *A. thaliana*, there is evidence suggesting that PTOX activity is regulated in a light-dependent manner via cysteine residues at its C-terminus [54]. This thiol regulation is absent in *C. reinhardtii* PTOX2 due to the lack of the C-terminal domain, making *A. thaliana* a more appropriate model organism for exploring a connection between c_{6A} and PTOX. To investigate this possible connection, PTOX activity in *A. thaliana* could be compared between plants with or without functional c_{6A}, e.g. by measuring oxygen flux.

Beyond *A. thaliana*, other genetically tractable plant species could also be considered for these studies. For example, the well-characterised liverwort *Marchantia polymorpha* is phylogenetically positioned between *A. thaliana* and *C. reinhardtii*, making it an excellent candidate for comparative studies [413]. Collecting data on c_{6A}'s function across a range of organisms will help assess the degree of functional conservation of this protein. It may also reveal interesting differences in how c_{6A} operates in various photosynthetic systems, potentially uncovering novel aspects of its proposed role in thiol-based redox regulation.

7.4.3 The function of other c_6-like cytochromes

In addition to c_{6A} in Viridiplantae, another homologue of c_6, referred to as c_{6B}, has been identified in cyanobacteria [159]. Cytochrome c_{6B} shares a similarly low redox midpoint potential with c_{6A} and phylogenetic analyses have shown that c_{6A} forms a monophyletic group within the broader c_{6B} clade [162]. This could indicate that c_{6A} and c_{6B} are functionally conserved between cyanobacteria and Viridiplantae. However, an important difference between the two proteins is that c_{6B} lacks the LIP with the conserved cysteine residues found in c_{6A}. The model proposed here for c_{6A}'s function in thiol-based redox regulation relies heavily on these cysteines. Following the model, c_{6A} and c_{6B} would likely have distinct functions or at least differ in their mechanisms of influencing similar targets. An argument for functional divergence is c_{6A}'s proposed role in state transitions. Cyanobacteria do not seem to rely on kinase-driven state transitions as plants and green algae do [414]. Instead of LHC proteins, they use phycobilisomes as their primary light-harvesting complexes and the mechanism of state transitions in cyanobacteria remains a topic of debate [415].

To explore this potential functional divergence, c_{6B} mutant strains in cyanobacteria could be tested for the phenotypes observed in plants and algae mutant in c_{6A}. For example, *Synechococcus elongatus* PCC 7942, which contains a c_{6B} sequence, could be used to generate c_{6B} knockdown mutants employing CRISPR interference (CRISPRi)-mediated genome modification [416, 417]. Testing these mutants under DISCO Light conditions would be straightforward and could help assess whether c_{6B} plays a role similar to c_{6A} in supporting survival under such stressful light conditions. However, investigating the light-harvesting balance between photosystems, where a c_{6A}-dependent phenotype was observed in *C. reinhardtii*, might be more challenging in cyanobacteria due to the differences in their photosynthetic machinery and state transition mechanisms compared to plants and algae. Another informative approach would be a rescue experiment in which a c_{6A}-KO mutant of *C. reinhardtii* is transformed with an overexpression construct of cyanobacterial c_{6B}. If c_{6B} could rescue the c_{6A}-KO phenotype, this would suggest some degree of functional overlap between the two proteins and provide evidence contrasting the presented working hypothesis. However, if c_{6B} were unable to compensate for the loss of c_{6A}, it would imply that c_{6A} has evolved distinct functions (or has different residues involved in interactions) in the green lineage, possibly in relation to the proposed thiol-based redox regulation and state transitions.

Interestingly, c_{6B} has also been retained in red algae [162], which, like cyanobacteria, rely on phycobilisomes for light harvesting and do not exhibit phosphorylation of their light-harvesting complexes [418]. This raises an interesting hypothesis: as the green lineage evolved and the phycobilisome was lost, the need for a different mode of regulation of state

transitions may have driven the development of a specialised cytochrome like c_{6A} alongside the emergence of LHC proteins and STT7/STN7. Such a c_{6A} protein, with the low redox midpoint potential it inherited from c_{6B} could avoid accepting electrons from cytochrome *f*, allowing it to remain oxidised rather than being constitutively reduced in the light. This would help maintain oxidised disulphides in the thylakoid lumen, important for the redox regulation of state transitions.

Additionally, a comprehensive search for c_{6A} homologues across photosynthetic organisms has uncovered c_{6A}- and c_{6B}-like sequences in various dinoflagellate species [162]. These included putative c_{6A} sequences in *Symbiodinium microadriaticum*, a peridinin dinoflagellate of particular research interest due to its symbiotic association with coral. A c_{6A}-like sequence in a peridinin dinoflagellate is intriguing, as they are thought to have acquired their plastids from the red algal lineage [419] and thus would be expected to possess c_{6B} rather than c_{6A}. As these sequences contain insertions similar to the LIP with conserved cysteines but slightly different in length, a second independent origin of a LIP insertion was proposed [162]. Little is known about state transitions in dinoflagellates [420]. However, given the presence of a c_{6A}-like sequence with a LIP-like insertion containing two cysteine residues, exploring a putative ability for state transitions in *Symbiodinium microadriaticum* could provide an interesting perspective on the function of c_{6A} and its conserved disulphide bridge.

Understanding how the members of this enigmatic protein family operate in different organisms will provide valuable insights into their role in photosynthesis across a wide range of ecosystems.

References

[1] A. Dodel-Port and C. Dodel-Port, *Erläuternder Text zum Anatomisch-physiologischen Atlas der Botanik für Hoch- und Mittelschulen* (J. F. Schreiber, Esslingen a. N., 1883).

[2] One Thousand Plant Transcriptomes Initiative, "One thousand plant transcriptomes and the phylogenomics of green plants", Nature **574**, 679–685 (2019).

[3] P. J. Keeling, "The endosymbiotic origin, diversification and fate of plastids", Philosophical Transactions of the Royal Society B: Biological Sciences **365**, 729–748 (2010).

[4] Z. Yang, X. Ma, Q. Wang, X. Tian, J. Sun, Z. Zhang, S. Xiao, O. De Clerck, F. Leliaert, and B. Zhong, "Phylotranscriptomics unveil a Paleoproterozoic-Mesoproterozoic origin and deep relationships of the Viridiplantae", Nature Communications **14**, 5542 (2023).

[5] F. Leliaert, D. R. Smith, H. Moreau, M. D. Herron, H. Verbruggen, C. F. Delwiche, and O. De Clerck, "Phylogeny and Molecular Evolution of the Green Algae", Critical Reviews in Plant Sciences **31**, 1–46 (2012).

[6] F. Leliaert, H. Verbruggen, and F. W. Zechman, "Into the deep: New discoveries at the base of the green plant phylogeny", BioEssays **33**, 683–692 (2011).

[7] C. G. Ehrenberg, *Die Infusionsthierchen als vollkommene Organismen: Ein Blick in das tiefere organische Leben der Natur* (L. Voss, Leipzig, 1838).

[8] T. Pröschold and T. Darienko, "The genus *Chlamydomonas*", in *The Chlamydomonas Sourcebook: Volume 1: Introduction to Chlamydomonas and Its Laboratory Use*, 3rd edition (Academic Press, 2023), pp. 1–15.

[9] P. A. Salomé and S. S. Merchant, "A Series of Fortunate Events: Introducing *Chlamydomonas* as a Reference Organism", The Plant Cell **31**, 1682–1707 (2019).

[10] E. H. Harris, "*Chlamydomonas* as a model organism", Annual Review of Plant Physiology and Plant Molecular Biology **52**, 363–406 (2001).

[11] R. J. Craig et al., "The *Chlamydomonas* Genome Project, version 6: Reference assemblies for mating-type plus and minus strains reveal extensive structural mutation in the laboratory", Plant Cell **35**, 644–672 (2023).

[12] S. S. Merchant et al., "The *Chlamydomonas* Genome Reveals the Evolution of Key Animal and Plant Functions", Science **318**, 245–250 (2007).

[13] I. K. Blaby, M. J. Soto, and C. E. Blaby-Haas, "Functional genomics of *Chlamydomonas reinhardtii*", in *The Chlamydomonas Sourcebook: Volume 1: Introduction to Chlamydomonas and Its Laboratory Use*, 3rd edition (Academic Press, 2023), pp. 65–84.

[14] D. Strenkert, S. Schmollinger, S. D. Gallaher, P. A. Salomé, S. O. Purvine, C. D. Nicora, T. Mettler-Altmann, E. Soubeyrand, A. P. M. Weber, M. S. Lipton, G. J. Basset, and S. S. Merchant, "Multiomics resolution of molecular events during a day in the life of *Chlamydomonas*", Proceedings of the National Academy of Sciences **116**, 2374–2383 (2019).

[15] J. M. Zones, I. K. Blaby, S. S. Merchant, and J. G. Umen, "High-resolution profiling of a synchronized diurnal transcriptome from *Chlamydomonas reinhardtii* reveals continuous cell and metabolic differentiation", Plant Cell **27**, 2743–2769 (2015).

[16] W. Fang, Y. Si, S. Douglass, D. Casero, S. S. Merchant, M. Pellegrini, I. Ladunga, P. Liu, and M. H. Spalding, "Transcriptome-Wide Changes in *Chlamydomonas reinhardtii* Gene Expression Regulated by Carbon Dioxide and the CO_2-Concentrating Mechanism Regulator CIA5 / CCM1", The Plant Cell **24**, 1876–1893 (2012).

[17] S. Schmollinger et al., "Nitrogen-Sparing Mechanisms in *Chlamydomonas* Affect the Transcriptome, the Proteome, and Photosynthetic Metabolism", The Plant Cell **26**, 1410–1435 (2014).

[18] I. K. Blaby, C. E. Blaby-Haas, M. E. Pérez-Pérez, S. Schmollinger, S. Fitz-Gibbon, S. D. Lemaire, and S. S. Merchant, "Genome-wide analysis on *Chlamydomonas reinhardtii* reveals the impact of hydrogen peroxide on protein stress responses and overlap with other stress transcriptomes", The Plant Journal **84**, 974–988 (2015).

[19] N. Wang, Z. Qian, M. Luo, S. Fan, X. Zhang, and L. Zhang, "Identification of Salt Stress Responding Genes Using Transcriptome Analysis in Green Alga *Chlamydomonas reinhardtii*", International Journal of Molecular Sciences **19**, 3359 (2018).

[20] U. Goodenough, I. Blaby, D. Casero, S. D. Gallaher, C. Goodson, S. Johnson, J.-H. Lee, S. S. Merchant, M. Pellegrini, R. Roth, J. Rusch, M. Singh, J. G. Umen, T. L. Weiss, and T. Wulan, "The Path to Triacylglyceride Obesity in the *sta6* Strain of *Chlamydomonas reinhardtii*", Eukaryotic Cell **13**, 591–613 (2014).

[21] F. J. Romero-Campero, I. Perez-Hurtado, E. Lucas-Reina, J. M. Romero, and F. Valverde, "ChlamyNET: a *Chlamydomonas* gene co-expression network reveals global properties of the transcriptome and the early setup of key co-expression patterns in the green lineage", BMC Genomics **17**, 227 (2016).

[22] D. P. Weeks, "Genetic transformation of *Chlamydomonas* nuclear, chloroplast, and mitochondrial genomes", in *The Chlamydomonas Sourcebook: Volume 1: Introduction to Chlamydomonas and Its Laboratory Use*, 3rd edition (Academic Press, 2023), pp. 325–343.

[23] O. Baidukova, S. Kelterborn, I. Sizova, and P. Hegemann, "Reverse genetics", in *The Chlamydomonas Sourcebook: Volume 1: Introduction to Chlamydomonas and Its Laboratory Use*, 3rd edition (Academic Press, 2023), pp. 421–430.

[24] M.-P. Zhang, M. Wang, and C. Wang, "Nuclear transformation of *Chlamydomonas reinhardtii*: A review", Biochimie **181**, 1–11 (2021).

[25] A. Ferenczi, D. E. Pyott, A. Xipnitou, and A. Molnar, "Efficient targeted DNA editing and replacement in *Chlamydomonas reinhardtii* using Cpf1 ribonucleoproteins and single-stranded DNA", Proceedings of the National Academy of Sciences **114**, 13567–13572 (2017).

[26] P. Crozet et al., "Birth of a Photosynthetic Chassis: A MoClo Toolkit Enabling Synthetic Biology in the Microalga *Chlamydomonas reinhardtii*", ACS Synthetic Biology **7**, 2074–2086 (2018).

[27] R. E. Blankenship, *Molecular Mechanisms of Photosynthesis*, 2nd (Wiley, 2014).

[28] K. E. Redding and S. Santabarbara, "Photosystems I and II", in *The Chlamydomonas Sourcebook: Volume 2: Organellar and Metabolic Processes*, 3rd edition (Academic Press, 2023), pp. 525–560.

[29] L. A. Malone, M. S. Proctor, A. Hitchcock, C. N. Hunter, and M. P. Johnson, "Cytochrome b_6f – Orchestrator of photosynthetic electron transfer", Biochimica et Biophysica Acta (BBA) - Bioenergetics **1862**, 148380 (2021).

[30] M. Sarewicz, S. Pintscher, R. Pietras, A. Borek, Ł. Bujnowicz, G. Hanke, W. A. Cramer, G. Finazzi, and A. Osyczka, "Catalytic Reactions and Energy Conservation in the Cytochrome bc_1 and b_6f Complexes of Energy-Transducing Membranes", Chemical Reviews **121**, 2020–2108 (2021).

[31] A. N. Tikhonov, "The cytochrome b_6f complex at the crossroad of photosynthetic electron transport pathways", Plant Physiology and Biochemistry **81**, 163–183 (2014).

[32] M. Szwalec, Ł. Bujnowicz, M. Sarewicz, and A. Osyczka, "Unexpected Heme Redox Potential Values Implicate an Uphill Step in Cytochrome b_6f", The Journal of Physical Chemistry B **126**, 9771–9780 (2022).

[33] T. Le Moigne, N. D. Boisset, F. de Carpentier, P. Crozet, A. Danon, J. Henri, C. H. Marchand, S. D. Lemaire, and X. Johnson, "Photoproduction of reducing power and the Calvin-Benson cycle", in *The Chlamydomonas Sourcebook: Volume 2: Organellar and Metabolic Processes*, 3rd edition (Academic Press, 2023), pp. 273–315.

[34] F. Buchert and F. Zito, "Chloroplast ATP synthase and the cytochrome b_6f complex", in *The Chlamydomonas Sourcebook: Volume 2: Organellar and Metabolic Processes*, 3rd edition (Academic Press, 2023), pp. 561–589.

[35] P. Turina, J. Petersen, and P. Gräber, "Thermodynamics of proton transport coupled ATP synthesis", Biochimica et Biophysica Acta (BBA) - Bioenergetics **1857**, 653–664 (2016).

[36] C. A. Raines, "Improving plant productivity by re-tuning the regeneration of RuBP in the Calvin–Benson–Bassham cycle", New Phytologist **236**, 350–356 (2022).

[37] P. C. Maxwell and J. Biggins, "Role of Cyclic Electron Transport in Photosynthesis as Measured by the Photoinduced Turnover of P700 *in Vivo*", Biochemistry **15**, 3975–3981 (1976).

[38] C. Desplats, F. Mus, S. Cuiné, E. Billon, L. Cournac, and G. Peltier, "Characterization of Nda2, a plastoquinone-reducing type II NAD(P)H dehydrogenase in *Chlamydomonas* chloroplasts", Journal of Biological Chemistry **284**, 4148–4157 (2009).

[39] F. Jans, E. Mignolet, P.-A. Houyoux, P. Cardol, B. Ghysels, S. Cuiné, L. Cournac, G. Peltier, C. Remacle, and F. Franck, "A type II NAD(P)H dehydrogenase mediates light-independent plastoquinone reduction in the chloroplast of *Chlamydomonas*", Proceedings of the National Academy of Sciences **105**, 20546–20551 (2008).

[40] G. DalCorso, P. Pesaresi, S. Masiero, E. Aseeva, D. Schünemann, G. Finazzi, P. Joliot, R. Barbato, and D. Leister, "A Complex Containing PGRL1 and PGR5 Is Involved in the Switch between Linear and Cyclic Electron Flow in *Arabidopsis*", Cell **132**, 273–285 (2008).

[41] A. P. Hertle, T. Blunder, T. Wunder, P. Pesaresi, M. Pribil, U. Armbruster, and D. Leister, "PGRL1 Is the Elusive Ferredoxin-Plastoquinone Reductase in Photosynthetic Cyclic Electron Flow", Molecular Cell **49**, 511–523 (2013).

[42] Y. Munekage, M. Hojo, J. Meurer, T. Endo, M. Tasaka, and T. Shikanai, "PGR5 is involved in cyclic electron flow around photosystem I and is essential for photoprotection in *Arabidopsis*", Cell **110**, 361–371 (2002).

[43] W. J. Nawrocki, B. Bailleul, D. Picot, P. Cardol, F. Rappaport, F. A. Wollman, and P. Joliot, "The mechanism of cyclic electron flow", Biochimica et Biophysica Acta - Bioenergetics **1860**, 433–438 (2019).

[44] T. Shikanai, "Molecular Genetic Dissection of the Regulatory Network of Proton Motive Force in Chloroplasts", Plant And Cell Physiology **65**, 537–550 (2024).

[45] M. Iwai, K. Takizawa, R. Tokutsu, A. Okamuro, Y. Takahashi, and J. Minagawa, "Isolation of the elusive supercomplex that drives cyclic electron flow in photosynthesis", Nature **464**, 1210–1213 (2010).

[46] J. Steinbeck, I. L. Ross, R. Rothnagel, P. Gäbelein, S. Schulze, N. Giles, R. Ali, R. Drysdale, E. Sierecki, Y. Gambin, H. Stahlberg, Y. Takahashi, M. Hippler, and B. Hankamer, "Structure of a PSI–LHCI–cyt b_6f supercomplex in *Chlamydomonas reinhardtii* promoting cyclic electron flow under anaerobic conditions", Proceedings of the National Academy of Sciences **115**, 10517–10522 (2018).

[47] L. A. Malone, P. Qian, G. E. Mayneord, A. Hitchcock, D. A. Farmer, R. F. Thompson, D. J. K. Swainsbury, N. A. Ranson, C. N. Hunter, and M. P. Johnson, "Cryo-EM structure of the spinach cytochrome b_6f complex at 3.6 Å resolution", Nature **575**, 535–539 (2019).

[48] D. Stroebel, Y. Choquet, J.-L. Popot, and D. Picot, "An atypical haem in the cytochrome b_6f complex", Nature **426**, 413–418 (2003).

[49] P. Mitchell, "The protonmotive Q cycle: A general formulation", FEBS Letters **59**, 137–139 (1975).

[50] F. Buchert, L. Mosebach, P. Gäbelein, and M. Hippler, "PGR5 is required for efficient Q cycle in the cytochrome b_6f complex during cyclic electron flow", Biochemical Journal **477**, 1631–1650 (2020).

[51] L. Houille-Vernes, F. Rappaport, F. A. Wollman, J. Alric, and X. Johnson, "Plastid terminal oxidase 2 (PTOX2) is the major oxidase involved in chlororespiration in *Chlamydomonas*", Proceedings of the National Academy of Sciences **108**, 20820–20825 (2011).

[52] A. M. Lennon, P. Prommeenate, and P. J. Nixon, "Location, expression and orientation of the putative chlororespiratory enzymes, Ndh and IMMUTANS, in higher-plant plastids", Planta **218**, 254–260 (2003).

[53] W. J. Nawrocki, F. Buchert, P. Joliot, F. Rappaport, B. Bailleul, and F.-A. Wollman, "Chlororespiration Controls Growth Under Intermittent Light", Plant Physiology **179**, 630–639 (2019).

[54] I. Rog, A. K. Chaturvedi, V. Tiwari, and A. Danon, "Low light-regulated intramolecular disulfide fine-tunes the role of PTOX in *Arabidopsis*", The Plant Journal **109**, 585–597 (2022).

[55] A. H. Mehler, "Studies on reactions of illuminated chloroplasts. II. Stimulation and inhibition of the reaction with molecular oxygen", Archives of Biochemistry and Biophysics **34**, 339–351 (1951).

[56] K. Ogawa, S. Kanematsu, K. Takabe, and K. Asada, "Attachment of CuZn-Superoxide Dismutase to Thylakoid Membranes at the Site of Superoxide Generation (PSI) in Spinach Chloroplasts: Detection by Immuno-Gold Labeling After Rapid Freezing and Substitution Method", Plant and Cell Physiology **36**, 565–573 (1995).

[57] K. X. Chan, S. Y. Phua, P. Crisp, R. McQuinn, and B. J. Pogson, "Learning the Languages of the Chloroplast: Retrograde Signaling and Beyond", Annual Review of Plant Biology **67**, 25–53 (2016).

[58] C. H. Foyer and G. Hanke, "ROS production and signalling in chloroplasts: cornerstones and evolving concepts", The Plant Journal **111**, 642–661 (2022).

[59] K. Asada, "The water-water cycle in chloroplasts: Scavenging of active oxygens and dissipation of excess photons", Annual Review of Plant Biology **50**, 601–639 (1999).

[60] A. Krieger-Liszkay and G. Shimakawa, "Regulation of the generation of reactive oxygen species during photosynthetic electron transport", Biochemical Society Transactions **50**, 1025–1034 (2022).

[61] Y. Helman, D. Tchernov, L. Reinhold, M. Shibata, T. Ogawa, R. Schwarz, I. Ohad, and A. Kaplan, "Genes Encoding A-Type Flavoproteins Are Essential for Photoreduction of O_2 in Cyanobacteria", Current Biology **13**, 230–235 (2003).

[62] A. Santana-Sanchez, D. Solymosi, H. Mustila, L. Bersanini, E. M. Aro, and Y. Allahverdiyeva, "Flavodiiron proteins 1–to-4 function in versatile combinations in O_2 photoreduction in cyanobacteria", eLife **8**, 1–22 (2019).

[63] Y. Allahverdiyeva, H. Mustila, M. Ermakova, L. Bersanini, P. Richaud, G. Ajlani, N. Battchikova, L. Cournac, and E.-M. Aro, "Flavodiiron proteins Flv1 and Flv3 enable cyanobacterial growth and photosynthesis under fluctuating light", Proceedings of the National Academy of Sciences **110**, 4111–4116 (2013).

[64] G. Peltier, D. Tolleter, E. Billon, and L. Cournac, "Auxiliary electron transport pathways in chloroplasts of microalgae", Photosynthesis Research **106**, 19–31 (2010).

[65] M. Jokel, X. Johnson, G. Peltier, E. M. Aro, and Y. Allahverdiyeva, "Hunting the main player enabling *Chlamydomonas reinhardtii* growth under fluctuating light", Plant Journal **94**, 822–835 (2018).

[66] F. Chaux, A. Burlacot, M. Mekhalfi, P. Auroy, S. Blangy, P. Richaud, and G. Peltier, "Flavodiiron Proteins Promote Fast and Transient O_2 Photoreduction in *Chlamydomonas*", Plant Physiology **174**, 1825–1836 (2017).

[67] P. Sétif, G. Shimakawa, A. Krieger-Liszkay, and C. Miyake, "Identification of the electron donor to flavodiiron proteins in *Synechocystis* sp. PCC 6803 by *in vivo* spectroscopy", Biochimica et Biophysica Acta - Bioenergetics **1861**, 148256 (2020).

[68] L. Nikkanen, S. Vakal, A. Santana-Sánchez, M. Hubacek, Y. Wang, M. Böhm, K. Gutekunst, T. A. Salminen, and Y. Allahverdiyeva, "Proton motive force dissipation drives flavodiiron proteins to the thylakoid membrane for ferredoxin-powered O_2 photoreduction", bioRxiv, https://doi.org/10.1101/2023.05.19.541409 (2023).

[69] J. Selinski and R. Scheibe, "Malate valves: old shuttles with new perspectives", Plant Biology **21**, 21–30 (2019).

[70] A. Burlacot, O. Dao, P. Auroy, S. Cuiné, Y. Li-Beisson, and G. Peltier, "Alternative photosynthesis pathways drive the algal CO_2-concentrating mechanism", Nature **605**, 366–371 (2022).

[71] E. Erickson, S. Wakao, and K. K. Niyogi, "Light stress and photoprotection in *Chlamydomonas reinhardtii*", The Plant Journal **82**, 449–465 (2015).

[72] M. Iwai, S. Wakao, and K. K. Niyogi, "Photoprotection", in *The Chlamydomonas Sourcebook: Volume 2 : Organellar and Metabolic Processes*, 3rd edition (Academic Press, 2023), pp. 807–828.

[73] A. Malnoë, "Photoinhibition or photoprotection of photosynthesis? Update on the (newly termed) sustained quenching component qH", Environmental and Experimental Botany **154**, 123–133 (2018).

[74] A. Malnoë, A. Schultink, S. Shahrasbi, D. Rumeau, M. Havaux, and K. K. Niyogi, "The Plastid Lipocalin LCNP Is Required for Sustained Photoprotective Energy Dissipation in *Arabidopsis*", The Plant Cell **30**, 196–208 (2018).

[75] P. Redekop, N. Rothhausen, N. Rothhausen, M. Melzer, L. Mosebach, E. Dülger, A. Bovdilova, S. Caffarri, M. Hippler, and P. Jahns, "PsbS contributes to photoprotection in *Chlamydomonas reinhardtii* independently of energy dissipation", Biochimica et Biophysica Acta (BBA) - Bioenergetics **1861** (2020).

[76] G. Bonente, M. Ballottari, T. B. Truong, T. Morosinotto, T. K. Ahn, G. R. Fleming, K. K. Niyogi, and R. Bassi, "Analysis of LhcSR3, a Protein Essential for Feedback De-Excitation in the Green Alga *Chlamydomonas reinhardtii*", PLoS Biology **9** (2011).

[77] G. Peers, T. B. Truong, E. Ostendorf, A. Busch, D. Elrad, A. R. Grossman, M. Hippler, and K. K. Niyogi, "An ancient light-harvesting protein is critical for the regulation of algal photosynthesis", Nature **462**, 518–521 (2009).

[78] T. B. Truong, "Investigating the Role(s) of LHCSRs in *Chlamydomonas reinhardtii*", PhD thesis, University of California, Berkeley (2011).

[79] M. Ballottari, T. B. Truong, E. De Re, E. Erickson, G. R. Stella, G. R. Fleming, R. Bassi, and K. K. Niyogi, "Identification of pH-sensing Sites in the Light Harvesting Complex Stress-related 3 Protein Essential for Triggering Non-photochemical Quenching in *Chlamydomonas reinhardtii*", Journal of Biological Chemistry **291**, 7334–7346 (2016).

[80] R. Tokutsu and J. Minagawa, "Energy-dissipative supercomplex of photosystem II associated with LHCSR3 in *Chlamydomonas reinhardtii*", Proceedings of the National Academy of Sciences **110**, 10016–10021 (2013).

[81] L. Girolomoni, S. Cazzaniga, A. Pinnola, F. Perozeni, M. Ballottari, and R. Bassi, "LHCSR3 is a nonphotochemical quencher of both photosystems in *Chlamydomonas reinhardtii*", Proceedings of the National Academy of Sciences **116**, 4212–4217 (2019).

[82] J. M. Troiano, F. Perozeni, R. Moya, L. Zuliani, K. Baek, E. Jin, S. Cazzaniga, M. Ballottari, and G. S. Schlau-Cohen, "Identification of distinct pH- and zeaxanthin-dependent quenching in LHCSR3 from *Chlamydomonas reinhardtii*", eLife **10**, 1–59 (2021).

[83] G. Gagné and M. Guertin, "The early genetic response to light in the green unicellular alga *Chlamydomonas eugametos* grown under light/dark cycles involves genes that represent direct responses to light and photosynthesis", Plant Molecular Biology **18**, 429–445 (1992).

[84] D. Petroutsos, R. Tokutsu, S. Maruyama, S. Flori, A. Greiner, L. Magneschi, L. Cusant, T. Kottke, M. Mittag, P. Hegemann, G. Finazzi, and J. Minagawa, "A blue-light photoreceptor mediates the feedback regulation of photosynthesis", Nature **537**, 563–566 (2016).

[85] D. Petroutsos, A. Busch, I. Janßen, K. Trompelt, S. V. Bergner, S. Weinl, M. Holtkamp, U. Karst, J. Kudla, and M. Hippler, "The Chloroplast Calcium Sensor CAS Is Required for Photoacclimation in *Chlamydomonas reinhardtii*", The Plant Cell **23**, 2950–2963 (2011).

[86] E. I. Hallin, K. Guo, and H.-E. Åkerlund, "Violaxanthin de-epoxidase disulphides and their role in activity and thermal stability", Photosynthesis Research **124**, 191–198 (2015).

[87] D. Simionato, S. Basso, M. Zaffagnini, T. Lana, F. Marzotto, P. Trost, and T. Morosinotto, "Protein redox regulation in the thylakoid lumen: The importance of disulfide bonds for violaxanthin de-epoxidase", FEBS Letters **589**, 919–923 (2015).

[88] Z. Li, G. Peers, R. M. Dent, Y. Bai, S. Y. Yang, W. Apel, L. Leonelli, and K. K. Niyogi, "Evolution of an atypical de-epoxidase for photoprotection in the green lineage", Nature Plants **2**, 16140 (2016).

[89] T. Quaas, S. Berteotti, M. Ballottari, K. Flieger, R. Bassi, C. Wilhelm, and R. Goss, "Non-photochemical quenching and xanthophyll cycle activities in six green algal species suggest mechanistic differences in the process of excess energy dissipation", Journal of Plant Physiology **172**, 92–103 (2015).

[90] M. Goldschmidt-Clermont, "State transitions", in *The Chlamydomonas Sourcebook: Volume 2: Organellar and Metabolic Processes*, 3rd edition (Academic Press, 2023), pp. 787–805.

[91] E. Wientjes, H. van Amerongen, and R. Croce, "LHCII is an antenna of both photosystems after long-term acclimation", Biochimica et Biophysica Acta (BBA) - Bioenergetics **1827**, 420–426 (2013).

[92] N. Depège, S. Bellafiore, and J.-D. Rochaix, "Role of Chloroplast Protein Kinase Stt7 in LHCII Phosphorylation and State Transition in *Chlamydomonas*", Science **299**, 1572–1575 (2003).

[93] S. Lemeille, A. Willig, N. Depège-Fargeix, C. Delessert, R. Bassi, and J. D. Rochaix, "Analysis of the Chloroplast Protein Kinase Stt7 during State Transitions", PLoS Biology **7** (2009).

[94] R. Delosme, J. Olive, and F.-A. Wollman, "Changes in light energy distribution upon state transitions: an *in vivo* photoacoustic study of the wild type and photosynthesis mutants from *Chlamydomonas reinhardtii*", Biochimica et Biophysica Acta (BBA) - Bioenergetics **1273**, 150–158 (1996).

[95] C. Ünlü, B. Drop, R. Croce, and H. van Amerongen, "State transitions in *Chlamydomonas reinhardtii* strongly modulate the functional size of photosystem II but not of photosystem I", Proceedings of the National Academy of Sciences **111**, 3460–3465 (2014).

[96] S. V. Bergner, M. Scholz, K. Trompelt, J. Barth, P. Gäbelein, J. Steinbeck, H. Xue, S. Clowez, G. Fucile, M. Goldschmidt-Clermont, C. Fufezan, and M. Hippler, "STATE TRANSITION7-Dependent Phosphorylation Is Modulated by Changing Environmental Conditions, and Its Absence Triggers Remodeling of Photosynthetic Protein Complexes", Plant Physiology **168**, 615–634 (2015).

[97] L. Dumas, F. Zito, S. Blangy, P. Auroy, X. Johnson, G. Peltier, and J. Alric, "A stromal region of cytochrome b_6f subunit IV is involved in the activation of the Stt7 kinase in *Chlamydomonas*", Proceedings of the National Academy of Sciences **114**, 12063–12068 (2017).

[98] S. Lemeille, M. V. Turkina, A. V. Vener, and J. D. Rochaix, "Stt7-dependent phosphorylation during state transitions in the green alga *Chlamydomonas reinhardtii*", Molecular and Cellular Proteomics **9**, 1281–1295 (2010).

[99] P. Hamel, J. Olive, Y. Pierre, F.-A. Wollman, and C. de Vitry, "A New Subunit of Cytochrome b_6f Complex Undergoes Reversible Phosphorylation upon State Transition", Journal of Biological Chemistry **275**, 17072–17079 (2000).

[100] F. Cariti, M. Chazaux, L. Lefebvre-Legendre, P. Longoni, B. Ghysels, X. Johnson, and M. Goldschmidt-Clermont, "Regulation of Light Harvesting in *Chlamydomonas reinhardtii* Two Protein Phosphatases Are Involved in State Transitions", Plant Physiology **183**, 1749–1764 (2020).

[101] A. de Lacroix de Lavalette, G. Finazzi, and F. Zito, "b_6f-associated chlorophyll: structural and dynamic contribution to the different cytochrome functions", Biochemistry **47**, 5259–5265 (2008).

[102] A. Shapiguzov, X. Chai, G. Fucile, P. Longoni, L. Zhang, and J.-D. Rochaix, "Activation of the Stt7/STN7 Kinase through Dynamic Interactions with the Cytochrome b_6f Complex", Plant Physiology **171**, 82–92 (2016).

[103] G. Schuster, M. Dewit, L. A. Staehelin, and I. Ohad, "Transient inactivation of the thylakoid photosystem II light-harvesting protein kinase system and concomitant changes in intramembrane particle size during photoinhibition of *Chlamydomonas reinhardtii*.", The Journal of Cell Biology **103**, 71–80 (1986).

[104] S. Lemeille and J.-D. Rochaix, "State transitions at the crossroad of thylakoid signalling pathways", Photosynthesis Research **106**, 33–46 (2010).

[105] J. Wu, L. Rong, W. Lin, L. Kong, D. Wei, L. Zhang, J.-D. Rochaix, and X. Xu, "Functional redox links between lumen thiol oxidoreductase1 and serine/threonine-protein kinase STN7", Plant Physiology **186**, 964–976 (2021).

[106] W. J. Nawrocki, S. Santabarbara, L. Mosebach, F.-A. Wollman, and F. Rappaport, "State transitions redistribute rather than dissipate energy between the two photosystems in *Chlamydomonas*", Nature Plants **2**, 16031 (2016).

[107] L. Bulté, P. Gans, F. Rebéillé, and F.-A. Wollman, "ATP control on state transitions *in vivo* in *Chlamydomonas reinhardtii*", Biochimica et Biophysica Acta (BBA) - Bioenergetics **1020**, 72–80 (1990).

[108] F. A. Wollman and P. Delepelaire, "Correlation between changes in light energy distribution and changes in thylakoid membrane polypeptide phosphorylation in *Chlamydomonas reinhardtii*.", The Journal of cell biology **98**, 1–7 (1984).

[109] B. Kok, "On the inhibition of photosynthesis by intense light", Biochimica et Biophysica Acta **21**, 234–244 (1956).

[110] J. Nickelsen and B. Rengstl, "Photosystem II Assembly: From Cyanobacteria to Plants", Annual Review of Plant Biology **64**, 609–635 (2013).

[111] N. Murata, S. I. Allakhverdiev, and Y. Nishiyama, "The mechanism of photoinhibition in vivo: Re-evaluation of the roles of catalase, α-tocopherol, non-photochemical quenching, and electron transport", Biochimica et Biophysica Acta (BBA) - Bioenergetics **1817**, 1127–1133 (2012).

[112] A. Malnoë, F. Wang, J. Girard-Bascou, F.-A. Wollman, and C. de Vitry, "Thylakoid FtsH Protease Contributes to Photosystem II and Cytochrome b_6f Remodeling in *Chlamydomonas reinhardtii* under Stress Conditions", The Plant Cell **26**, 373–390 (2014).

[113] W. J. Nawrocki, X. Liu, B. Raber, C. Hu, C. de Vitry, D. I. G. Bennett, and R. Croce, "Molecular origins of induction and loss of photoinhibition-related energy dissipation q_I", Science Advances **7**, 1–13 (2021).

[114] Y. Eisenberg-Domovich, R. Oelmüller, R. G. Herrmann, and I. Ohad, "Role of the RCII-D1 Protein in the Reversible Association of the Oxygen-evolving Complex Proteins with the Lumenal Side of Photosystem II", Journal of Biological Chemistry **270**, 30181–30186 (1995).

[115] M. Hall, A. Mata-Cabana, H.-E. Åkerlund, F. J. Florencio, W. P. Schröder, M. Lindahl, and T. Kieselbach, "Thioredoxin targets of the plant chloroplast lumen and their implications for plastid function", Proteomics **10**, 987–1001 (2010).

[116] J. P. Fett and J. R. Coleman, "Regulation of Periplasmic Carbonic Anhydrase Expression in *Chlamydomonas reinhardtii* by Acetate and pH", Plant Physiology **106**, 103–108 (1994).

[117] P. B. Heifetz, B. Förster, C. B. Osmond, L. J. Giles, and J. E. Boynton, "Effects of acetate on facultative autotrophy in *Chlamydomonas reinhardtii* assessed by photosynthetic measurements and stable isotope analyses", Plant Physiology **122**, 1439–1445 (2000).

[118] T. Endo and K. Asada, "Dark Induction of the Non-Photochemical Quenching of Chlorophyll Fluorescence by Acetate in *Chlamydomonas reinhardtii*", Plant and Cell Physiology **37**, 551–555 (1996).

[119] L. Kovács, W. Wiessner, M. Kis, F. Nagy, D. Mende, and S. Demeter, "Short- and long-term redox regulation of photosynthetic light energy distribution and photosystem stoichiometry by acetate metabolism in the green alga, *Chlamydobotrys stellata*", Photosynthesis Research **65**, 231–247 (2000).

[120] T. Roach, A. Sedoud, and A. Krieger-Liszkay, "Acetate in mixotrophic growth medium affects photosystem II in *Chlamydomonas reinhardtii* and protects against photoinhibition", Biochimica et Biophysica Acta (BBA) - Bioenergetics **1827**, 1183–1190 (2013).

[121] S. P. Chapman, C. M. Paget, G. N. Johnson, and J. M. Schwartz, "Flux balance analysis reveals acetate metabolism modulates cyclic electron flow and alternative glycolytic pathways in *Chlamydomonas reinhardtii*", Frontiers in Plant Science **6** (2015).

[122] H. Kühne, V. A. Szalai, and G. W. Brudvig, "Competitive Binding of Acetate and Chloride in Photosystem II", Biochemistry **38**, 6604–6613 (1999).

[123] M. Zaffagnini, S. Fermani, C. H. Marchand, A. Costa, F. Sparla, N. Rouhier, P. Geigenberger, S. D. Lemaire, and P. Trost, "Redox Homeostasis in Photosynthetic Organisms: Novel and Established Thiol-Based Molecular Mechanisms", Antioxidants & Redox Signaling **31**, 155–210 (2019).

[124] D. Hoh, J. E. Froehlich, and D. M. Kramer, "Redox regulation in chloroplast thylakoid lumen: The pmf changes everything, again", Plant, Cell & Environment **47**, 2749–2765 (2024).

[125] S. Järvi, P. J. Gollan, and E.-M. Aro, "Understanding the roles of the thylakoid lumen in photosynthesis regulation", Frontiers in Plant Science **4** (2013).

[126] B. B. Buchanan and S. Luan, "Redox regulation in the chloroplast thylakoid lumen: A new frontier in photosynthesis research", Journal of Experimental Botany **56**, 1439–1447 (2005).

[127] K. Lennartz, H. Plücken, A. Seidler, P. Westhoff, N. Bechtold, and K. Meierhoff, "HCF164 Encodes a Thioredoxin-Like Protein Involved in the Biogenesis of the Cytochrome b_6f Complex in *Arabidopsis*", The Plant Cell **13**, 2539–2551 (2001).

[128] K. Motohashi and T. Hisabori, "HCF164 Receives Reducing Equivalents from Stromal Thioredoxin across the Thylakoid Membrane and Mediates Reduction of Target Proteins in the Thylakoid Lumen", Journal of Biological Chemistry **281**, 35039–35047 (2006).

[129] A. Das, N. Subrahmanian, S. T. Gabilly, E. P. Andrianova, I. B. Zhulin, K. Motohashi, and P. P. Hamel, "Two disulfide-reducing pathways are required for the maturation of plastid c -type cytochromes in *Chlamydomonas reinhardtii*", Genetics **225**, 1–13 (2023).

[130] K. Motohashi and T. Hisabori, "CcdA Is a Thylakoid Membrane Protein Required for the Transfer of Reducing Equivalents from Stroma to Thylakoid Lumen in the Higher Plant Chloroplast", Antioxidants & Redox Signaling **13**, 1169–1176 (2010).

[131] M. Ancín, A. Fernández-San Millán, L. Larraya, F. Morales, J. Veramendi, I. Aranjuelo, and I. Farran, "Overexpression of thioredoxin m in tobacco chloroplasts inhibits the protein kinase STN7 and alters photosynthetic performance", Journal of Experimental Botany **70**, 1005–1016 (2019).

[132] M. Karamoko, S. Cline, K. Redding, N. Ruiz, and P. P. Hamel, "Lumen Thiol Oxidoreductase1, a Disulfide Bond-Forming Catalyst, Is Required for the Assembly of Photosystem II in *Arabidopsis*", The Plant Cell **23**, 4462–4475 (2011).

[133] Y. Lu, J.-J. Du, Z.-B. Yu, J.-J. Peng, J.-N. Xu, and X.-Y. Wang, "Identification of Potential Targets for Thylakoid Oxidoreductase AtVKOR/LTO1 in Chloroplasts", Protein & Peptide Letters **22**, 219–225 (2015).

[134] B. G. Schlarb-Ridley, R. H. Nimmo, S. Purton, C. J. Howe, and D. S. Bendall, "Cytochrome c_{6A} is a funnel for thiol oxidation in the thylakoid lumen", FEBS Letters **580**, 2166–2169 (2006).

[135] R. Gupta, R. M. Mould, Z. He, and S. Luan, "A chloroplast FKBP interacts with and affects the accumulation of Rieske subunit of cytochrome *bf* complex", Proceedings of the National Academy of Sciences **99**, 15806–15811 (2002).

[136] G. Gopalan, Z. He, K. P. Battaile, S. Luan, and K. Swaminathan, "Structural comparison of oxidized and reduced FKBP13 from *Arabidopsis thaliana*", Proteins: Structure, Function, and Bioinformatics **65**, 789–795 (2006).

[137] U. A. Petersson, T. Kieselbach, J. G. García-Cerdán, and W. P. Schröder, "The Prx Q protein of *Arabidopsis thaliana* is a member of the luminal chloroplast proteome", FEBS Letters **580**, 6055–6061 (2006).

[138] U. Hani, B. Naranjo, G. Shimakawa, C. Espinasse, H. Vanacker, P. Sétif, E. Rintamäki, E. Issakidis-Bourguet, and A. Krieger-Liszkay, "A complex and dynamic redox network regulating oxygen reduction at photosystem I", bioRxiv, https://doi.org/10.1101/2023.09.28.559979 (2023).

[139] W. Bialek, A. Szczepaniak, P. Kolesinski, and T. Kallas, "Cryptic c_6-Like and c_M Cytochromes of Cyanobacteria", in *Cytochrome complexes: evolution, structures, energy transduction, and signaling*, edited by W. A. Cramer and T. Kallas (Springer Netherlands, Dordrecht, 2016), pp. 713–734.

[140] J. A. Navarro, M. Hervás, and M. A. De la Rosa, "Co-evolution of cytochrome c_6 and plastocyanin, mobile proteins transferring electrons from cytochrome b_6f to photosystem I", JBIC Journal of Biological Inorganic Chemistry **2**, 11–22 (1997).

[141] P. M. Wood, "Interchangeable Copper and Iron Proteins in Algal Photosynthesis. Studies on Plastocyanin and Cytochrome *c*-552 in *Chlamydomonas*", European Journal of Biochemistry **87**, 9–19 (1978).

[142] M. Reith and J. Munholland, "Complete nucleotide sequence of the *Porphyra purpurea* chloroplast genome", Plant Molecular Biology Reporter **13**, 333–335 (1995).

[143] C. Frazão, C. Soares, M. Carrondo, E. Pohl, Z. Dauter, K. Wilson, M. Hervés, J. Navarro, M. De la Rosa, and G. Sheldrick, "Ab initio determination of the crystal structure of cytochrome c_6 and comparison with plastocyanin", Structure **3**, 1159–1169 (1995).

[144] J. Wastl, D. S. Bendall, and C. J. Howe, "Higher plants contain a modified cytochrome c_6", Trends in Plant Science **7**, 244–245 (2002).

[145] C. J. Howe, B. G. Schlarb-Ridley, J. Wastl, S. Purton, and D. S. Bendall, "The novel cytochrome c_6 of chloroplasts: a case of evolutionary bricolage?", Journal of Experimental Botany **57**, 13–22 (2006).

[146] R. Gupta, Z. He, and S. Luan, "Functional relationship of cytochrome c_6 and plastocyanin in *Arabidopsis*", Nature **417**, 567–571 (2002).

[147] F. P. Molina-Heredia, J. Wastl, J. A. Navarro, D. S. Bendall, M. Hervás, C. J. Howe, and M. A. De la Rosa, "A new function for an old cytochrome?", Nature **424**, 33–34 (2003).

[148] P. Pesaresi, M. Scharfenberg, M. Weigel, I. Granlund, W. P. Schröder, G. Finazzi, F. Rappaport, S. Masiero, A. Furini, P. Jahns, and D. Leister, "Mutants, overexpressors, and interactors of *Arabidopsis* plastocyanin isoforms: Revised roles of plastocyanin in photosynthetic electron flow and thylakoid redox state", Molecular Plant **2**, 236–248 (2009).

[149] M. Weigel, C. Varotto, P. Pesaresi, G. Finazzi, F. Rappaport, F. Salamini, and D. Leister, "Plastocyanin Is Indispensable for Photosynthetic Electron Flow in *Arabidopsis thaliana*", Journal of Biological Chemistry **278**, 31286–31289 (2003).

[150] J. Wastl, S. Purton, D. S. Bendall, and C. J. Howe, "Two forms of cytochrome c_6 in a single eukaryote", Trends in Plant Science **9**, 474–476 (2004).

[151] H. Chida, T. Yokoyama, F. Kawai, A. Nakazawa, H. Akazaki, Y. Takayama, T. Hirano, K. Suruga, T. Satoh, S. Yamada, R. Kawachi, S. Unzai, T. Nishio, S.-Y. Park, and T. Oku, "Crystal structure of oxidized cytochrome c_{6A} from *Arabidopsis thaliana*", FEBS Letters **580**, 3763–3768 (2006).

[152] M. J. Marcaida, B. G. Schlarb-Ridley, J. A. Worrall, J. Wastl, T. J. Evans, D. S. Bendall, B. F. Luisi, and C. J. Howe, "Structure of Cytochrome c_{6A}, a Novel Dithiocytochrome of *Arabidopsis thaliana*, and its Reactivity with Plastocyanin: Implications for Function", Journal of Molecular Biology **360**, 968–977 (2006).

[153] J. A. Worrall, B. F. Luisi, B. G. Schlarb-Ridley, D. S. Bendall, and C. J. Howe, "Cytochrome c_{6A}: discovery, structure and properties responsible for its low haem redox potential", Biochemical Society Transactions **36**, 1175–1179 (2008).

[154] J. M. Mason, D. S. Bendall, C. J. Howe, and J. A. Worrall, "The role of a disulfide bridge in the stability and folding kinetics of *Arabidopsis thaliana* cytochrome c_{6A}", Biochimica et Biophysica Acta (BBA) - Proteins and Proteomics **1824**, 311–318 (2012).

[155] J. A. R. Worrall, B. G. Schlarb-Ridley, T. Reda, M. J. Marcaida, R. J. Moorlen, J. Wastl, J. Hirst, D. S. Bendall, B. F. Luisi, and C. J. Howe, "Modulation of Heme Redox Potential in the Cytochrome c_6 Family", Journal of the American Chemical Society **129**, 9468–9475 (2007).

[156] J. Wastl, F. P. Molina-Heredia, M. Hervás, J. A. Navarro, M. A. De la Rosa, D. S. Bendall, and C. J. Howe, "Redox properties of *Arabidopsis* cytochrome c_6 are independent of the loop extension specific to higher plants", Biochimica et Biophysica Acta (BBA) - Bioenergetics **1657**, 115–120 (2004).

[157] C. A. Kerfeld, H. P. Anwar, R. Interrante, S. Merchant, and T. O. Yeates, "The Structure of Chloroplast Cytochrome c_6 at 1.9 Å Resolution: Evidence for Functional Oligomerization", Journal of Molecular Biology **250**, 627–647 (1995).

[158] W. Bialek, M. Nelson, K. Tamiola, T. Kallas, and A. Szczepaniak, "Deeply Branching c_6-like Cytochromes of Cyanobacteria", Biochemistry **47**, 5515–5522 (2008).

[159] W. Bialek, S. Krzywda, P. Zatwarnicki, M. Jaskolski, P. Kolesinski, and A. Szczepaniak, "Insights into the relationship between the haem-binding pocket and the redox potential of c_6 cytochromes: four atomic resolution structures of c_6 and c_6-like proteins from Synechococcus sp. PCC 7002", Acta Crystallographica Section D Biological Crystallography **70**, 2823–2832 (2014).

[160] F. M. Reyes-Sosa, J. Gil-Martínez, and F. P. Molina-Heredia, "Cytochrome c_6-like protein as a putative donor of electrons to photosystem I in the cyanobacterium *Nostoc* sp. PCC 7119", Photosynthesis Research **110**, 61–72 (2011).

[161] P. Zatwarnicki, J. Barciszewski, S. Krzywda, M. Jaskolski, P. Kolesinski, and A. Szczepaniak, "Cytochrome c_{6B} of *Synechococcus* sp. WH 8102 – Crystal structure and basic properties of novel c_6-like family representative", Biochemical and Biophysical Research Communications **443**, 1131–1135 (2014).

[162] B. Slater, D. Kosmützky, R. E. R. Nisbet, and C. J. Howe, "The Evolution of the Cytochrome c_6 Family of Photosynthetic Electron Transfer Proteins", Genome Biology and Evolution **13**, 1–12 (2021).

[163] A. Torrado, M. Iniesta-Pallarés, A. Velázquez-Campoy, C. Álvarez, V. Mariscal, and F. P. Molina-Heredia, "Phylogenetic and functional analysis of cyanobacterial Cytochrome c_6-like proteins", Frontiers in Plant Science **14** (2023).

[164] A. Torrado, A. Valladares, L. Puerto-Galán, M. Hervás, J. A. Navarro, and F. P. Molina-Heredia, "Cyt $c_{6\text{-}3}$: A New Isoform of Photosynthetic Cyt c_6 Exclusive to Heterocyst-Forming Cyanobacteria", Plant and Cell Physiology **58**, pcw184 (2016).

[165] J. Beltrán, Y. Wamboldt, R. Sanchez, E. W. LaBrant, H. Kundariya, K. S. Virdi, C. Elowsky, and S. A. Mackenzie, "Specialized Plastids Trigger Tissue-Specific Signaling for Systemic Stress Response in Plants", Plant Physiology **178**, 672–683 (2018).

[166] S. A. Mackenzie and P. M. Mullineaux, "Plant environmental sensing relies on specialized plastids", Journal of Experimental Botany **73**, 7155–7164 (2022).

[167] I. J. Dopp, X. Yang, and S. A. Mackenzie, "A new take on organelle-mediated stress sensing in plants", New Phytologist **230**, 2148–2153 (2021).

[168] P. J. Gollan, A. Trotta, A. A. Bajwa, I. Mancini, and E.-M. Aro, "Characterization of the Free and Membrane-Associated Fractions of the Thylakoid Lumen Proteome in *Arabidopsis thaliana*", International Journal of Molecular Sciences **22**, 8126 (2021).

[169] I. Nimmo, "Location and function of cytochrome c_{6A}", PhD thesis, University of Cambridge (2011).

[170] M. Scharfenberg, "Cytochrome c_{6A} – Functional Evolution of a Plastidial Protein", PhD thesis, Ludwig-Maximilians-Universität München (2011).

[171] B. A. Slater, "The ancestry and function of cytochrome c_{6A}", PhD thesis, University of Cambridge (2020).

[172] C. J. Howe, R. H. Nimmo, A. C. Barbrook, and D. S. Bendall, "Cytochrome c_{6A} of Chloroplasts", in *Cytochrome complexes: evolution structures, energy transduction and signaling*, Vol. 41, edited by W. A. Cramer and T. Kallas, Advances in Photosynthesis and Respiration (Springer Science+Business Media, Dordrecht, 2016).

[173] I. M. Ibrahim, H. Wu, R. Ezhov, G. E. Kayanja, S. D. Zakharov, Y. Du, W. A. Tao, Y. Pushkar, W. A. Cramer, and S. Puthiyaveetil, "An evolutionarily conserved iron-sulfur cluster underlies redox sensory function of the Chloroplast Sensor Kinase", Communications Biology **3**, 13 (2020).

[174] R. Vasudevan, "Characterization of low molecular weight *c*-type cytochromes in cyanobacteria and plants", PhD thesis, University of Cambridge (2019).

[175] S. H. Hutner, L. Provasoli, A. Schnatz, and C. Haskins, "Some Approaches to the Study of the Role of Metals in the Metabolism of Microorganisms", Proceedings of the American Philosophical Society **94**, 152–170 (1950).

[176] E. Weber, C. Engler, R. Gruetzner, S. Werner, and S. Marillonnet, "A modular cloning system for standardized assembly of multigene constructs", PLoS ONE **6**, 1–11 (2011).

[177] D. I. Arnon, "Copper Enzymes in Isolated Chloroplasts. Polyphenoloxidase in *Beta Vulgaris*", Plant Physiology **24**, 1–15 (1949).

[178] C. B. Mason, T. M. Bricker, and J. V. Moroney, "A rapid method for chloroplast isolation from the green alga *Chlamydomonas reinhardtii*", Nature Protocols **1**, 2227–2230 (2006).

[179] W. Zerges and J. D. Rochaix, "Low density membranes are associated with RNA-binding proteins and thylakoids in the chloroplast of *Chlamydomonas reinhardtii*", Journal of Cell Biology **140**, 101–110 (1998).

[180] Cold Spring Harbor Laboratory, "RIPA Lysis Buffer", Cold Spring Harbor Protocols **2017**, pdb.rec101428 (2017).

[181] M. M. Bradford, "A rapid and sensitive method for the quantitation of microgram quantities of protein utilizing the principle of protein-dye binding", Analytical Biochemistry **72**, 248–254 (1976).

[182] U. K. Laemmli, "Cleavage of Structural Proteins during the Assembly of the Head of Bacteriophage T4", Nature **227**, 680–685 (1970).

[183] S. Järvi, M. Suorsa, V. Paakkarinen, and E. M. Aro, "Optimized native gel systems for separation of thylakoid protein complexes: Novel super- and mega-complexes", Biochemical Journal **439**, 207–214 (2011).

[184] M. Rantala, V. Paakkarinen, and E. M. Aro, "Analysis of thylakoid membrane protein complexes by blue native gel electrophoresis", Journal of Visualized Experiments **2018**, 1–6 (2018).

[185] T. Yamano and H. Fukuzawa, "Indirect Immunofluorescence Assay in *Chlamydomonas reinhardtii*", Bio-protocol **6**, e1864 (2016).

[186] C. Klughammer and U. Schreiber, "Complementary PS II quantum yields calculated from simple fluorescence parameters measured by PAM fluorometry and the Saturation Pulse method", PAM Application Notes **1**, 27–35 (2008).

[187] H. M. Kalaji et al., "Frequently asked questions about chlorophyll fluorescence, the sequel", Photosynthesis Research **132**, 13–66 (2017).

[188] C. Klughammer and U. Schreiber, "Saturation Pulse method for assessment of energy conversion in PS I", PAM Application Notes **1**, 11–14 (2008).

[189] C. Klughammer and U. Schreiber, "Deconvolution of ferredoxin, plastocyanin, and P700 transmittance changes in intact leaves with a new type of kinetic LED array spectrophotometer", Photosynthesis Research **128**, 195–214 (2016).

[190] U. Schreiber, "Redox changes of ferredoxin, P700, and plastocyanin measured simultaneously in intact leaves", Photosynthesis Research **134**, 343–360 (2017).

[191] P. Sétif, A. Boussac, and A. Krieger-Liszkay, "Near-infrared *in vitro* measurements of photosystem I cofactors and electron-transfer partners with a recently developed spectrophotometer", Photosynthesis Research **142**, 307–319 (2019).

[192] A. Savitzky and M. J. E. Golay, "Smoothing and Differentiation of Data", Anal. Chem **36**, 1627–1639 (1964).

[193] J. Alric, J. Lavergne, and F. Rappaport, "Redox and ATP control of photosynthetic cyclic electron flow in *Chlamydomonas reinhardtii* (I) aerobic conditions", Biochimica et Biophysica Acta - Bioenergetics **1797**, 44–51 (2010).

[194] P. Bennoun, "Chlororespiration and the process of carotenoid biosynthesis", Biochimica et Biophysica Acta - Bioenergetics **1506**, 133–142 (2001).

[195] A. Kanazawa and D. M. Kramer, "*In vivo* modulation of nonphotochemical exciton quenching (npq) by regulation of the chloroplast atp synthase", Proceedings of the National Academy of Sciences **99**, 12789–12794 (2002).

[196] K. Kohzuma, C. Dal Bosco, J. Meurer, and D. M. Kramer, "Light- and metabolism-related regulation of the chloroplast ATP synthase has distinct mechanisms and functions", Journal of Biological Chemistry **288**, 13156–13163 (2013).

[197] D. M. Kramer and A. R. Crofts, "Activation of the chloroplast ATPase measured by the electrochromic change in leaves of intact plants", BBA - Bioenergetics **976**, 28–41 (1989).

[198] B. Bailleul, P. Cardol, C. Breyton, and G. Finazzi, "Electrochromism: A useful probe to study algal photosynthesis", Photosynthesis Research **106**, 179–189 (2010).

[199] J. A. Cruz, C. A. Sacksteder, A. Kanazawa, and D. M. Kramer, "Contribution of electric field ($\Delta\psi$) to steady-state transthylakoid proton motive force (pmf) *in vitro* and *in vivo*. Control of pmf parsing into $\Delta\psi$ and ΔpH by ionic strength", Biochemistry **40**, 1226–1237 (2001).

[200] P. Joliot and A. Joliot, "Cyclic electron transfer in plant leaf", Proceedings of the National Academy of Sciences **99**, 10209–10214 (2002).

[201] L. Nikkanen, A. Santana Sánchez, M. Ermakova, M. Rögner, L. Cournac, and Y. Allahverdiyeva, "Functional redundancy between flavodiiron proteins and NDH-1 in *Synechocystis* sp. PCC 6803", Plant Journal **103**, 1460–1476 (2020).

[202] D. Solymosi, L. Nikkanen, D. Muth-Pawlak, D. Fitzpatrick, R. Vasudevan, C. J. Howe, D. J. Lea-Smith, and Y. Allahverdiyeva, "Cytochrome c_M decreases photosynthesis under photomixotrophy in *Synechocystis* sp. PCC 6803", Plant Physiology **183**, 700–716 (2020).

[203] K. Beckmann, J. Messinger, M. R. Badger, T. Wydrzynski, and W. Hillier, "On-line mass spectrometry: Membrane inlet sampling", Photosynthesis Research **102**, 511–522 (2009).

[204] G. Hoch and B. Kok, "A mass spectrometer inlet system for sampling gases dissolved in liquid phases", Archives of Biochemistry and Biophysics **101**, 160–170 (1963).

[205] R Core Team, *R: A Language and Environment for Statistical Computing*, Vienna, Austria, 2024.

[206] Posit team, *RStudio: Integrated Development Environment for R*, Boston, MA, 2024.

[207] H. Wickham et al., "Welcome to the tidyverse", Journal of Open Source Software **4**, 1686 (2019).

[208] H. Wickham, *ggplot2: Elegant Graphics for Data Analysis* (Springer-Verlag New York, 2016).

[209] A. Kassambara, *ggpubr: 'ggplot2' Based Publication Ready Plots*, 2023.

[210] A. Kassambara, *rstatix: Pipe-Friendly Framework for Basic Statistical Tests*, 2023.

[211] S. Andrews, *FastQC: A Quality Control Tool for High Throughput Sequence Data*, 2010.

[212] S. Andrews and L. Biggins, *SeqMonk: A tool to visualise and analyse high throughput mapped sequence data*, Cambridge, 2021.

[213] J. T. Robinson, H. Thorvaldsdóttir, W. Winckler, M. Guttman, E. S. Lander, G. Getz, and J. P. Mesirov, "Integrative genomics viewer", Nature Biotechnology **29**, 24–26 (2011).

[214] D. Kim, J. M. Paggi, C. Park, C. Bennett, and S. L. Salzberg, *Graph-based genome alignment and genotyping with HISAT2 and HISAT-genotype*, 2019.

[215] Broad Institute, *Picard Tools*, 2024.

[216] P. Ewels, M. Magnusson, S. Lundin, and M. Käller, "MultiQC: Summarize analysis results for multiple tools and samples in a single report", Bioinformatics **32**, 3047–3048 (2016).

[217] Y. Liao, G. K. Smyth, and W. Shi, "FeatureCounts: An efficient general purpose program for assigning sequence reads to genomic features", Bioinformatics **30**, 923–930 (2014).

[218] M. I. Love, W. Huber, and S. Anders, "Moderated estimation of fold change and dispersion for RNA-seq data with DESeq2", Genome Biology **15**, 1–21 (2014).

[219] Z. Gu, "Complex heatmap visualization", iMeta **1**, 1–15 (2022).

[220] S. X. Ge, D. Jung, and R. Yao, "ShinyGO: a graphical gene-set enrichment tool for animals and plants", Bioinformatics **36**, 2628–2629 (2020).

[221] A. Alexa and J. Rahnenfuhrer, *topGO: Enrichment Analysis for Gene Ontology*, R package version 2.56.0, 2024.

[222] Chlamydomonas Resource Center, *CC-1883 cw15 NIT+ mt-*, 2024.

[223] E. H. Harris, "The Genus *Chlamydomonas*", in *The Chlamydomonas Sourcebook*, edited by E. H. Harris, D. B. Stern, and G. B. Witman, 2nd edition (Academic Press, 2009), pp. 1–24.

[224] Chlamydomonas Resource Center, *CC-4532 Mets strain 2137 mt-*, 2024.

[225] E. H. Harris, "The Life of an Acetate Flagellate", in *The Chlamydomonas Sourcebook*, edited by E. H. Harris, D. B. Stern, and G. B. Witman, 2nd edition (Academic Press, 2009), pp. 159–210.

[226] X. Johnson and J. Alric, "Central Carbon Metabolism and Electron Transport in *Chlamydomonas reinhardtii*: Metabolic Constraints for Carbon Partitioning between Oil and Starch", Eukaryotic Cell **12**, 776–793 (2013).

[227] X. Johnson and J. Alric, "Interaction between Starch Breakdown, Acetate Assimilation, and Photosynthetic Cyclic Electron Flow in *Chlamydomonas reinhardtii*", Journal of Biological Chemistry **287**, 26445–26452 (2012).

[228] K. A. Bogaert, E. Perez, J. Rumin, A. Giltay, M. Carone, N. Coosemans, M. Radoux, G. Eppe, R. D. Levine, F. Remacle, and C. Remacle, "Metabolic, physiological, and transcriptomics analysis of batch cultures of the green microalga *Chlamydomonas* grown on different acetate concentrations", Cells **8**, 1–21 (2019).

[229] F. Mus, L. Cournac, V. Cardettini, A. Caruana, and G. Peltier, "Inhibitor studies on non-photochemical plastoquinone reduction and H_2 photoproduction in *Chlamydomonas reinhardtii*", Biochimica et Biophysica Acta - Bioenergetics **1708**, 322–332 (2005).

[230] S. Sasso, H. Stibor, M. Mittag, and A. R. Grossman, "From molecular manipulation of domesticated *Chlamydomonas reinhardtii* to survival in nature", eLife **7**, 363–406 (2018).

[231] S. Abu-Ghosh, D. Fixler, Z. Dubinsky, and D. Iluz, "Flashing light in microalgae biotechnology", Bioresource Technology **203**, 357–363 (2016).

[232] M. Janssen, M. Janssen, M. De Winter, J. Tramper, L. R. Mur, J. Snel, and R. H. Wijffels, "Efficiency of light utilization of *Chlamydomonas reinhardtii* under medium-duration light/dark cycles", Journal of Biotechnology **78**, 123–137 (2000).

[233] P. J. Graham, B. Nguyen, T. Burdyny, and D. Sinton, "A penalty on photosynthetic growth in fluctuating light", Scientific Reports **7**, 1–11 (2017).

[234] A. Caccamo, "The role of ascorbate peroxidase 2 and protein cysteine modifications in the green alga *Chlamydomonas reinhardtii*", PhD thesis, Vrije Universiteit Brussel & University of Liege (2024).

[235] C. J. Steen, A. Burlacot, A. H. Short, K. K. Niyogi, and G. R. Fleming, "Interplay between LHCSR proteins and state transitions governs the NPQ response in *Chlamydomonas* during light fluctuations", Plant Cell and Environment **45**, 2428–2445 (2022).

[236] M. Grieco, M. Tikkanen, V. Paakkarinen, S. Kangasjärvi, and E.-M. Aro, "Steady-State Phosphorylation of Light-Harvesting Complex II Proteins Preserves Photosystem I under Fluctuating White Light", Plant Physiology **160**, 1896–1910 (2012).

[237] S. Bellafiore, F. Barneche, G. Peltier, and J.-D. Rochaix, "State transitions and light adaptation require chloroplast thylakoid protein kinase STN7", Nature **433**, 892–895 (2005).

[238] T. Roach, "LHCSR3-Type NPQ Prevents Photoinhibition and Slowed Growth under Fluctuating Light in *Chlamydomonas reinhardtii*", Plants **9**, 1604 (2020).

[239] S. Saroussi, D. A. J. Karns, D. C. Thomas, C. Bloszies, O. Fiehn, M. C. Posewitz, and A. R. Grossman, "Alternative outlets for sustaining photosynthetic electron transport during dark-to-light transitions", Proceedings of the National Academy of Sciences **116**, 11518–11527 (2019).

[240] A. Caccamo, F. Vega de Luna, A. E. Misztak, S. Pyr dit Ruys, D. Vertommen, P. Cardol, J. Messens, and C. Remacle, "APX2 Is an Ascorbate Peroxidase–Related Protein that Regulates the Levels of Plastocyanin in *Chlamydomonas*", Plant And Cell Physiology **65**, 644–656 (2024).

[241] E. Wientjes, B. Drop, R. Kouřil, E. J. Boekema, and R. Croce, "During State 1 to State 2 Transition in *Arabidopsis thaliana*, the Photosystem II Supercomplex Gets Phosphorylated but Does Not Disassemble", Journal of Biological Chemistry **288**, 32821–32826 (2013).

[242] S. D. Gallaher, S. T. Fitz-Gibbon, A. G. Glaesener, M. Pellegrini, and S. S. Merchant, "*Chlamydomonas* genome resource for laboratory strains reveals a mosaic of sequence variation, identifies true strain histories, and enables strain-specific studies", Plant Cell **27**, 2335–2352 (2015).

[243] D. Karcher, D. Köster, A. Schadach, A. Klevesath, and R. Bock, "The *Chlamydomonas* chloroplast HLP protein is required for nucleoid organization and genome maintenance", Molecular Plant **2**, 1223–1232 (2009).

[244] E. Kaiser, A. Morales, J. Harbinson, J. Kromdijk, E. Heuvelink, and L. F. Marcelis, "Dynamic photosynthesis in different environmental conditions", Journal of Experimental Botany **66**, 2415–2426 (2015).

[245] C. Schiphorst, C. Koeman, L. Caracciolo, K. Staring, T. P. Theeuwen, S. M. Driever, J. Harbinson, and E. Wientjes, "The effects of different daily irradiance profiles on *Arabidopsis* growth, with special attention to the role of PsbS", Frontiers in Plant Science **14** (2023).

[246] T. von Bismarck, K. Korkmaz, J. Ruß, K. Skurk, E. Kaiser, V. Correa Galvis, J. A. Cruz, D. D. Strand, K. Köhl, J. Eirich, I. Finkemeier, P. Jahns, D. M. Kramer, and U. Armbruster, "Light acclimation interacts with thylakoid ion transport to govern the dynamics of photosynthesis in *Arabidopsis*", New Phytologist **237**, 160–176 (2023).

[247] H. M. Kalaji et al., "Frequently asked questions about *in vivo* chlorophyll fluorescence: practical issues", Photosynthesis Research **122**, 121–158 (2014).

[248] E. G. Andrizhiyevskaya, A. Chojnicka, J. A. Bautista, B. A. Diner, R. van Grondelle, and J. P. Dekker, "Origin of the F685 and F695 fluorescence in Photosystem II", Photosynthesis Research **84**, 173–180 (2005).

[249] M. L. Groot, R. N. Frese, F. L. De Weerd, K. Bromek, Å. Pettersson, E. J. Peterman, I. H. Van Stokkum, R. Van Grondelle, and J. P. Dekker, "Spectroscopic properties of the CP43 core antenna protein of photosystem II", Biophysical Journal **77**, 3328–3340 (1999).

[250] L. Ferroni, C. Baldisserotto, M. Giovanardi, L. Pantaleoni, T. Morosinotto, and S. Pancaldi, "Revised assignment of room-temperature chlorophyll fluorescence emission bands in single living cells of *Chlamydomonas reinhardtii*", Journal of Bioenergetics and Biomembranes **43**, 163–173 (2011).

[251] J. Garnier, J. Maroc, and D. Guyon, "Low-temperature fluorescence emission spectra and chlorophyll-protein complexes in mutants of *Chlamydomonas reinhardtii*: Evidence for a new chlorophyll-a-protein complex related to Photosystem I", BBA - Bioenergetics **851**, 395–406 (1986).

[252] P. W. Hemelrijk, S. L. Kwa, R. van Grondelle, and J. P. Dekker, "Spectroscopic properties of LHC-II, the main light-harvesting chlorophyll a/b protein complex from chloroplast membranes", Biochimica et Biophysica Acta (BBA) - Bioenergetics **1098**, 159–166 (1992).

[253] J. Kargul, J. Nield, and J. Barber, "Three-dimensional reconstruction of a light-harvesting complex I-photosystem I (LHCI-PSI) supercomplex from the green alga *Chlamydomonas reinhardtii*: Insights into light harvesting for PSI", Journal of Biological Chemistry **278**, 16135–16141 (2003).

[254] B. Drop, S. Yadav K.N., E. J. Boekema, and R. Croce, "Consequences of state transitions on the structural and functional organization of Photosystem I in the green alga *Chlamydomonas reinhardtii*", The Plant Journal **78**, 181–191 (2014).

[255] G. C. Papageorgiou and Govindjee, "Photosystem II fluorescence: Slow changes – Scaling from the past", Journal of Photochemistry and Photobiology B: Biology **104**, 258–270 (2011).

[256] N. R. Baker, "Chlorophyll Fluorescence: A Probe of Photosynthesis In Vivo", Annual Review of Plant Biology **59**, 89–113 (2008).

[257] K. Maxwell and G. N. Johnson, "Chlorophyll fluorescence - A practical guide", Journal of Experimental Botany **51**, 659–668 (2000).

[258] U. Schreiber, "Pulse-Amplitude-Modulation (PAM) Fluorometry and Saturation Pulse Method: An Overview", in *Chlorophyll a fluorescence: a signature of photosynthesis*, edited by G. C. Papageorgiou and Govindjee (Springer Netherlands, 2004), pp. 279–319.

[259] K. Oxborough and N. R. Baker, "Resolving chlorophyll *a* fluorescence images of photosynthetic efficiency into photochemical and non-photochemical components - Calculation of *qP* and *Fv'/Fm'* without measuring *Fo'*", Photosynthesis Research **54**, 135–142 (1997).

[260] M. Tikkanen, S. Rantala, M. Grieco, and E. M. Aro, "Comparative analysis of mutant plants impaired in the main regulatory mechanisms of photosynthetic light reactions - From biophysical measurements to molecular mechanisms", Plant Physiology and Biochemistry **112**, 290–301 (2017).

[261] D. M. Kramer, G. Johnson, O. Kiirats, and G. E. Edwards, "New Fluorescence Parameters for the Determination of Q_A Redox State and Excitation Energy Fluxes", Photosynthesis Research **79**, 209–218 (2004).

[262] P. J. Ralph and R. Gademann, "Rapid light curves: A powerful tool to assess photosynthetic activity", Aquatic Botany **82**, 222–237 (2005).

[263] B. A. Diner, "Dependence of the deactivation reactions of Photosystem II on the redox state of plastoquinone pool a varied under anaerobic conditions. Equilibria on the acceptor side of Photosystem II", Biochimica et Biophysica Acta (BBA) - Bioenergetics **460**, 247–258 (1977).

[264] S. Z. Tóth, G. Schansker, and R. J. Strasser, "A non-invasive assay of the plastoquinone pool redox state based on the OJIP-transient", Photosynthesis Research **93**, 193 (2007).

[265] M. G. Ceppi, A. Oukarroum, N. Çiçek, R. J. Strasser, and G. Schansker, "The IP amplitude of the fluorescence rise OJIP is sensitive to changes in the photosystem I content of leaves: a study on plants exposed to magnesium and sulfate deficiencies, drought stress and salt stress", Physiologia Plantarum **144**, 277–288 (2012).

[266] C. Klughammer and U. Schreiber, "Analysis of Light-Induced Absorbance Changes in the Near-Infrared Spectral Region I. Characterization of Various Components in Isolated Chloroplasts", Zeitschrift fur Naturforschung - Section C Journal of Biosciences **46**, 233–244 (1991).

[267] C. Klughammer and U. Schreiber, "An improved method, using saturating light pulses, for the determination of photosystem I quantum yield via $P700^+$-absorbance changes at 830 nm", Planta **192**, 261–268 (1994).

[268] L. Nikkanen, M. Guinea Diaz, J. Toivola, A. Tiwari, and E. Rintamäki, "Multilevel regulation of non-photochemical quenching and state transitions by chloroplast NADPH-dependent thioredoxin reductase", Physiologia Plantarum **166**, 211–225 (2019).

[269] L. Nikkanen, J. Toivola, A. Trotta, M. G. Diaz, M. Tikkanen, E. M. Aro, and E. Rintamäki, "Regulation of cyclic electron flow by chloroplast NADPH-dependent thioredoxin system", Plant Direct **2** (2018).

[270] G. Shimakawa, P. Sétif, and A. Krieger-Liszkay, "Near-infrared *in vivo* measurements of photosystem I and its lumenal electron donors with a recently developed spectrophotometer", Photosynthesis Research **144**, 63–72 (2020).

[271] P. Ortega-Martínez, L. Nikkanen, L. T. Wey, F. J. Florencio, Y. Allahverdiyeva, and S. Díaz-Troya, "Glycogen synthesis prevents metabolic imbalance and disruption of photosynthetic electron transport from photosystem II during transition to photomixotrophy in *Synechocystis* sp. PCC 6803", New Phytologist **243**, 162–179 (2024).

[272] M. L. Theune, S. Hildebrandt, A. Steffen-Heins, W. Bilger, K. Gutekunst, and J. Appel, "In-vivo quantification of electron flow through photosystem I – Cyclic electron transport makes up about 35% in a cyanobacterium", Biochimica et Biophysica Acta - Bioenergetics **1862**, 148353 (2021).

[273] BioLogics, "JTS-150 user manual", (2021).

[274] F. Buchert, M. Scholz, and M. Hippler, "Electron transfer via cytochrome b_6f complex displays sensitivity to antimycin A upon STT7 kinase activation", Biochemical Journal **479**, 111–127 (2022).

[275] A. Malnoë, F.-A. Wollman, C. de Vitry, and F. Rappaport, "Photosynthetic growth despite a broken Q-cycle", Nature Communications **2**, 301 (2011).

[276] S. Saroussi, P. Redekop, D. A. J. Karns, D. C. Thomas, T. M. Wittkopp, M. C. Posewitz, and A. R. Grossman, "Restricting electron flow at cytochrome b_6f when downstream electron acceptors are severely limited", Plant Physiology, 1–16 (2023).

[277] D. M. Kramer, J. A. Cruz, and A. Kanazawa, "Balancing the central roles of the thylakoid proton gradient", Trends in Plant Science **8**, 27–32 (2003).

[278] L. N. M. Duysens, "Reversible Changes in the Absorption Spectrum of *Chlorella* upon Irradiation", Science **120**, 353–354 (1954).

[279] C. A. Sacksteder and D. M. Kramer, "Dark-interval relaxation kinetics (DIRK) of absorbance changes as a quantitative probe of steady-state electron transfer", Photosynthesis Research **66**, 145–158 (2000).

[280] T. J. Avenson, A. Kanazawa, J. A. Cruz, K. Takizawa, W. E. Ettinger, and D. M. Kramer, "Integrating the proton circuit into photosynthesis: progress and challenges", Plant, Cell & Environment **28**, 97–109 (2005).

[281] P. Joliot and A. Joliot, "Quantification of the electrochemical proton gradient and activation of ATP synthase in leaves", Biochimica et Biophysica Acta - Bioenergetics **1777**, 676–683 (2008).

[282] C. Wang, H. Yamamoto, and T. Shikanai, "Role of cyclic electron transport around photosystem I in regulating proton motive force", Biochimica et Biophysica Acta - Bioenergetics **1847**, 931–938 (2015).

[283] A. Santana-Sánchez, L. Nikkanen, E. Werner, G. Tóth, M. Ermakova, S. Kosourov, J. Walter, M. He, E.-M. Aro, and Y. Allahverdiyeva, "Flv3A facilitates O_2 photoreduction and affects H_2 photoproduction independently of Flv1A in diazotrophic *Anabaena* filaments", New Phytologist **237**, 126–139 (2023).

[284] C. Mathiot and J. Alric, "Standard units for ElectroChromic Shift measurements in plant biology", Journal of Experimental Botany **72**, 6467–6473 (2021).

[285] P. Joliot and R. Delosme, "Flash-induced 519 nm absorption change in green algae", Biochimica et Biophysica Acta (BBA) - Bioenergetics **357**, 267–284 (1974).

[286] U. Armbruster, L. R. Carrillo, K. Venema, L. Pavlovic, E. Schmidtmann, A. Kornfeld, P. Jahns, J. A. Berry, D. M. Kramer, and M. C. Jonikas, "Ion antiport accelerates photosynthetic acclimation in fluctuating light environments", Nature Communications **5**, 5439 (2014).

[287] A. Burlacot, F. Burlacot, Y. Li-Beisson, and G. Peltier, "Membrane Inlet Mass Spectrometry: A Powerful Tool for Algal Research", Frontiers in Plant Science **11** (2020).

[288] A. V. Ruban and M. P. Johnson, "Dynamics of higher plant photosystem cross-section associated with state transitions", Photosynthesis Research **99**, 173–183 (2009).

[289] P. Joliot and A. Joliot, "Proton pumping and electron transfer in the cytochrome *b/f* complex of algae", Biochimica et Biophysica Acta (BBA) - Bioenergetics **849**, 211–222 (1986).

[290] P. Bennoun, "Réoxydation du quencher de fluorescence "Q" en présence de 3-(3,4-dichlorophényl)-1,1-diméthylurée", Biochimica et Biophysica Acta (BBA) - Bioenergetics **216**, 357–363 (1970).

[291] T. Fujii, E.-i. Yokoyama, K. Inoue, and H. Sakurai, "The sites of electron donation of Photosystem I to methyl viologen", Biochimica et Biophysica Acta (BBA) - Bioenergetics **1015**, 41–48 (1990).

[292] A. G. Roberts and D. M. Kramer, "Inhibitor "Double Occupancy" in the Q_O Pocket of the Chloroplast Cytochrome b_6f Complex", Biochemistry **40**, 13407–13412 (2001).

[293] A. Belatik, D. Joly, S. Hotchandani, and R. Carpentier, "Re-evaluation of the side effects of cytochrome b_6f inhibitor dibromothymoquinone on photosystem II excitation and electron transfer", Photosynthesis Research **117**, 489–496 (2013).

[294] G. Peltier, C. Stoffel, J. Findinier, S. K. Madireddi, O. Dao, V. Epting, A. Morin, A. Grossman, Y. Li-Beisson, and A. Burlacot, "Alternative electron pathways of photosynthesis power green algal CO_2 capture", The Plant Cell **00**, 1–11 (2024).

[295] W. J. Nawrocki, N. J. Tourasse, A. Taly, F. Rappaport, and F.-A. Wollman, "The Plastid Terminal Oxidase: Its Elusive Function Points to Multiple Contributions to Plastid Physiology", Annual Review of Plant Biology **66**, 49–74 (2015).

[296] W. Huang, A. Krishnan, A. Plett, M. Meagher, N. Linka, Y. Wang, B. Ren, J. Findinier, P. Redekop, N. Fakhimi, R. G. Kim, D. A. Karns, N. Boyle, M. C. Posewitz, and A. R. Grossman, "*Chlamydomonas* mutants lacking chloroplast triose phosphate transporter3 are metabolically compromised and light sensitive", The Plant Cell **35**, 2592–2614 (2023).

[297] I. Vass, S. Styring, T. Hundal, A. Koivuniemi, E. Aro, and B. Andersson, "Reversible and irreversible intermediates during photoinhibition of photosystem II: stable reduced Q_A species promote chlorophyll triplet formation.", Proceedings of the National Academy of Sciences **89**, 1408–1412 (1992).

[298] O. Virtanen and E. Tyystjärvi, "Plastoquinone pool redox state and control of state transitions in *Chlamydomonas reinhardtii* in darkness and under illumination", Photosynthesis Research **155**, 59–76 (2023).

[299] U. Goodenough and B. D. Engel, "Cell ultrastructure", in *The Chlamydomonas Sourcebook: Volume 1: Introduction to Chlamydomonas and Its Laboratory Use*, 3rd edition (Academic Press, 2023), pp. 17–40.

[300] W. Wietrzynski and B. D. Engel, "Supramolecular organization of chloroplast membranes", in *The Chlamydomonas Sourcebook: Volume 2: Organellar and Metabolic Processes*, 3rd edition (Academic Press, 2023), pp. 763–785.

[301] W. Wietrzynski, M. Schaffer, D. Tegunov, S. Albert, A. Kanazawa, J. M. Plitzko, W. Baumeister, and B. D. Engel, "Charting the native architecture of *Chlamydomonas* thylakoid membranes with single-molecule precision", eLife **9**, 1–18 (2020).

[302] E. Morita, H. Kuroiwa, T. Kuroiwa, and H. Nozaki, "High Localization of Ribulose-1,5-bisphosphate Carboxylase/oxygenase in the Pyrenoids of *Chlamydomonas reinhardtii* (Chlorophyta), as Revealed by Cryofixation and Immunogold Electron Microscopy", Journal of Phycology **33**, 68–72 (1997).

[303] H. Kirchhoff, U. Mukherjee, and H.-J. Galla, "Molecular Architecture of the Thylakoid Membrane: Lipid Diffusion Space for Plastoquinone", Biochemistry **41**, 4872–4882 (2002).

[304] J. L. Roose, L. K. Frankel, M. P. Mummadisetti, and T. M. Bricker, "The extrinsic proteins of photosystem II: update", Planta **243**, 889–908 (2016).

[305] L. Shen, Z. Huang, S. Chang, W. Wang, J. Wang, T. Kuang, G. Han, J.-R. Shen, and X. Zhang, "Structure of a $C_2S_2M_2N_2$-type PSII–LHCII supercomplex from the green alga *Chlamydomonas reinhardtii*", Proceedings of the National Academy of Sciences **116**, 21246–21255 (2019).

[306] R. N. Burton-Smith, A. Watanabe, R. Tokutsu, C. Song, K. Murata, and J. Minagawa, "Structural determination of the large photosystem II–light-harvesting complex II supercomplex of *Chlamydomonas reinhardtii* using nonionic amphipol", Journal of Biological Chemistry **294**, 15003–15013 (2019).

[307] C. Le Quiniou, L. Tian, B. Drop, E. Wientjes, I. H. van Stokkum, B. van Oort, and R. Croce, "PSI–LHCI of *Chlamydomonas reinhardtii*: Increasing the absorption cross section without losing efficiency", Biochimica et Biophysica Acta (BBA) - Bioenergetics **1847**, 458–467 (2015).

[308] X. Su, J. Ma, X. Pan, X. Zhao, W. Chang, Z. Liu, X. Zhang, and M. Li, "Antenna arrangement and energy transfer pathways of a green algal photosystem-I–LHCI supercomplex", Nature Plants **5**, 273–281 (2019).

[309] M. Suga, S.-I. Ozawa, K. Yoshida-Motomura, F. Akita, N. Miyazaki, and Y. Takahashi, "Structure of the green algal photosystem I supercomplex with a decameric light-harvesting complex I", Nature Plants **5**, 626–636 (2019).

[310] Z. Huang, L. Shen, W. Wang, Z. Mao, X. Yi, T. Kuang, J. R. Shen, X. Zhang, and G. Han, "Structure of photosystem I-LHCI-LHCII from the green alga *Chlamydomonas reinhardtii* in State 2", Nature Communications **12**, 1–14 (2021).

[311] A. Naschberger, L. Mosebach, V. Tobiasson, S. Kuhlgert, M. Scholz, A. Perez-Boerema, T. T. H. Ho, A. Vidal-Meireles, Y. Takahashi, M. Hippler, and A. Amunts, "Algal photosystem I dimer and high-resolution model of PSI-plastocyanin complex", Nature Plants **8**, 1191–1201 (2022).

[312] S. Rexroth, J. M. Meyer zu Tittingdorf, F. Krause, N. A. Dencher, and H. Seelert, "Thylakoid membrane at altered metabolic state: Challenging the forgotten realms of the proteome", Electrophoresis **24**, 2814–2823 (2003).

[313] Y. Choquet and F. A. Wollman, "The assembly of photosynthetic proteins", in *The Chlamydomonas Sourcebook: Volume 2: Organellar and Metabolic Processes*, 3rd edition (Academic Press, 2023), pp. 615–646.

[314] H. Heide, L. Bleier, M. Steger, J. Ackermann, S. Dröse, B. Schwamb, M. Zörnig, A. S. Reichert, I. Koch, I. Wittig, and U. Brandt, "Complexome Profiling Identifies TMEM126B as a Component of the Mitochondrial Complex I Assembly Complex", Cell Metabolism **16**, 538–549 (2012).

[315] H. Heide and I. Wittig, "Methods to analyse composition and dynamics of macromolecular complexes", Biochemical Society Transactions **41**, 1235–1241 (2013).

[316] E. M. Aro, M. Suorsa, A. Rokka, Y. Allahverdiyeva, V. Paakkarinen, A. Saleem, N. Battchikova, and E. Rintamäki, "Dynamics of photosystem II: A proteomic approach to thylakoid protein complexes", Journal of Experimental Botany **56**, 347–356 (2005).

[317] M. Herranen, N. Battchikova, P. Zhang, A. Graf, S. Sirpiö, V. Paakkarinen, and E. M. Aro, "Towards Functional Proteomics of Membrane Protein Complexes in *Synechocystis* sp. PCC 6803", Plant Physiology **134**, 470–481 (2004).

[318] F. Ossenbühl, V. Göhre, J. Meurer, A. Krieger-Liszkay, J. D. Rochaix, and L. A. Eichacker, "Efficient assembly of photosystem II in *Chlamydomonas reinhardtii* requires Alb3.1p, a homolog of *Arabidopsis* ALBINO3", Plant Cell **16**, 1790–1800 (2004).

[319] E. Devadasu, S. D. Kanna, S. Neelam, R. M. Yadav, S. Nama, P. Akhtar, T. F. Polgár, B. Ughy, G. Garab, P. H. Lambrev, and R. Subramanyam, "Long- and short-term acclimation of the photosynthetic apparatus to salinity in *Chlamydomonas reinhardtii*. The role of Stt7 protein kinase", Frontiers in Plant Science **14** (2023).

[320] E. Devadasu, J. Pandey, K. Dhokne, and R. Subramanyam, "Restoration of photosynthetic activity and supercomplexes from severe iron starvation in *Chlamydomonas reinhardtii*", Biochimica et Biophysica Acta - Bioenergetics **1862**, 148331 (2021).

[321] J. G. García-Cerdán, A. L. Furst, K. L. McDonald, D. Schünemann, M. B. Francis, and K. K. Niyogi, "A thylakoid membrane-bound and redox-active rubredoxin (RBD1) functions in de novo assembly and repair of photosystem II", Proceedings of the National Academy of Sciences **116**, 16631–16640 (2019).

[322] S. K. Madireddi, S. Nama, E. R. Devadasu, and R. Subramanyam, "Photosynthetic membrane organization and role of state transition in *cyt*, *cpII*, *stt7* and *npq* mutants of *Chlamydomonas reinhardtii*", Journal of Photochemistry and Photobiology B: Biology **137**, 77–83 (2014).

[323] S. Nama, S. K. Madireddi, E. R. Devadasu, and R. Subramanyam, "High light induced changes in organization, protein profile and function of photosynthetic machinery in *Chlamydomonas reinhardtii*", Journal of Photochemistry and Photobiology B: Biology **152**, 367–376 (2015).

[324] R. M. Yadav, S. Marriboina, M. Y. Zamal, J. Pandey, and R. Subramanyam, "High light-induced changes in whole-cell proteomic profile and its correlation with the organization of thylakoid super-complex in cyclic electron transport mutants of *Chlamydomonas reinhardtii*", Frontiers in Plant Science **14** (2023).

[325] J. Lang et al., "Complexome profiling of the *Chlamydomonas psb28* mutant reveals THYLAKOID ENRICHED FRACTION 5 as an early photosystem II assembly factor", bioRxiv, https://doi.org/10.1101/2024.06.24.600430 (2024).

[326] B. Spaniol, J. Lang, B. Venn, L. Schake, F. Sommer, M. Mustas, S. Geimer, F. A. Wollman, Y. Choquet, T. Mühlhaus, and M. Schroda, "Complexome profiling on the *Chlamydomonas lpa2* mutant reveals insights into PSII biogenesis and new PSII associated proteins", Journal of Experimental Botany **73**, 245–262 (2022).

[327] K. J. Lauersen, O. Kruse, and J. H. Mussgnug, "Targeted expression of nuclear transgenes in *Chlamydomonas reinhardtii* with a versatile, modular vector toolkit", Applied Microbiology and Biotechnology **99**, 3491–3503 (2015).

[328] L. C. Mackinder, C. Chen, R. D. Leib, W. Patena, S. R. Blum, M. Rodman, S. Ramundo, C. M. Adams, and M. C. Jonikas, "A Spatial Interactome Reveals the Protein Organization of the Algal CO_2-Concentrating Mechanism", Cell **171**, 133–147 (2017).

[329] L. Wang et al., "A chloroplast protein atlas reveals punctate structures and spatial organization of biosynthetic pathways", Cell **186**, 3499–3518.e14 (2023).

[330] M. R. Redinbo, D. Cascio, M. K. Choukair, D. Rice, S. Merchant, and T. O. Yeates, "The 1.5-Å Crystal Structure of Plastocyanin from the Green Alga *Chlamydomonas reinhardtii*", Biochemistry **32**, 10560–10567 (1993).

[331] B. D. Engel, M. Schaffer, L. Kuhn Cuellar, E. Villa, J. M. Plitzko, and W. Baumeister, "Native architecture of the *Chlamydomonas* chloroplast revealed by in situ cryo-electron tomography", eLife **4**, 1–29 (2015).

[332] D. Farci and W. P. Schröder, "Thylakoid Lumen; from "proton bag" to photosynthetic functionally important compartment", Frontiers in Plant Physiology **1** (2023).

[333] A. G. Ngounou Wetie, I. Sokolowska, A. G. Woods, U. Roy, J. A. Loo, and C. C. Darie, "Investigation of stable and transient protein–protein interactions: Past, present, and future", Proteomics **13**, 538–557 (2013).

[334] A. Hammel, D. Zimmer, F. Sommer, T. Mühlhaus, and M. Schroda, "Absolute Quantification of Major Photosynthetic Protein Complexes in *Chlamydomonas reinhardtii* Using Quantification Concatamers (QconCATs)", Frontiers in Plant Science **9** (2018).

[335] C. L. de Hoog and M. Mann, "Proteomics", Annual Review of Genomics and Human Genetics **5**, 267–293 (2004).

[336] A. Kölsch, C. Radon, M. Golub, A. Baumert, J. Bürger, T. Mielke, F. Lisdat, A. Feoktystov, J. Pieper, A. Zouni, and P. Wendler, "Current limits of structural biology: The transient interaction between cytochrome c_6 and photosystem I", Current Research in Structural Biology **2**, 171–179 (2020).

[337] J. Mehla, J. Caufield, N. Sakhawalkar, and P. Uetz, "A Comparison of Two-Hybrid Approaches for Detecting Protein–Protein Interactions", in *Methods in enzymology*, Vol. 586, 1st ed. (Elsevier, 2017), pp. 333–358.

[338] D. Mellacheruvu et al., "The CRAPome: a contaminant repository for affinity purification–mass spectrometry data", Nature Methods **10**, 730–736 (2013).

[339] T. Le Moigne, E. Sarti, A. Nourisson, M. Zaffagnini, A. Carbone, S. D. Lemaire, and J. Henri, "Crystal structure of chloroplast fructose-1,6-bisphosphate aldolase from the green alga *Chlamydomonas reinhardtii*", Journal of Structural Biology **214**, 107873 (2022).

[340] M. Schroda, D. Hemme, and T. Mühlhaus, "The *Chlamydomonas* heat stress response", Plant Journal **82**, 466–480 (2015).

[341] R. Dayer, B. B. Fischer, R. I. L. Eggen, and S. D. Lemaire, "The Peroxiredoxin and Glutathione Peroxidase Families in *Chlamydomonas reinhardtii*", Genetics **179**, 41–57 (2008).

[342] A. Goyer, C. Haslekås, M. Miginiac-Maslow, U. Klein, P. Le Marechal, J.-P. Jacquot, and P. Decottignies, "Isolation and characterization of a thioredoxin-dependent peroxidase from *Chlamydomonas reinhardtii*", European Journal of Biochemistry **269**, 272–282 (2002).

[343] G. V. Los et al., "HaloTag: A Novel Protein Labeling Technology for Cell Imaging and Protein Analysis", ACS Chemical Biology **3**, 373–382 (2008).

[344] E. Kreis, K. König, M. Misir, J. Niemeyer, F. Sommer, and M. Schroda, "TurboID reveals the proxiomes of *Chlamydomonas* proteins involved in thylakoid biogenesis and stress response", Plant Physiology **193**, 1772–1796 (2023).

[345] C. S. Lau, A. Dowle, G. H. Thomas, P. Girr, and L. C. M. Mackinder, "A phase-separated CO_2-fixing pyrenoid proteome determined by TurboID in *Chlamydomonas reinhardtii*", The Plant Cell **35**, 3260–3279 (2023).

[346] S. Wakao and K. K. Niyogi, "*Chlamydomonas* as a model for reactive oxygen species signaling and thiol redox regulation in the green lineage", Plant Physiology **187**, 687–698 (2021).

[347] C. H. Foyer, J. Neukermans, G. Queval, G. Noctor, and J. Harbinson, "Photosynthetic control of electron transport and the regulation of gene expression", Journal of Experimental Botany **63**, 1637–1661 (2012).

[348] G. Allorent, L. Lefebvre-Legendre, R. Chappuis, M. Kuntz, T. B. Truong, K. K. Niyogi, R. Ulm, and M. Goldschmidt-Clermont, "UV-B photoreceptor-mediated protection of the photosynthetic machinery in *Chlamydomonas reinhardtii*", Proceedings of the National Academy of Sciences **113**, 14864–14869 (2016).

[349] S. Maruyama, R. Tokutsu, and J. Minagawa, "Transcriptional regulation of the stress-responsive light harvesting complex genes in *Chlamydomonas reinhardtii*", Plant and Cell Physiology **55**, 1304–1310 (2014).

[350] Z. Zhang, J. Shrager, M. Jain, C.-W. Chang, O. Vallon, and A. R. Grossman, "Insights into the Survival of *Chlamydomonas reinhardtii* during Sulfur Starvation Based on Microarray Analysis of Gene Expression", Eukaryotic Cell **3**, 1331–1348 (2004).

[351] B. Naumann, A. Busch, J. Allmer, E. Ostendorf, M. Zeller, H. Kirchhoff, and M. Hippler, "Comparative quantitative proteomics to investigate the remodeling of bioenergetic pathways under iron deficiency in *Chlamydomonas reinhardtii*", Proteomics **7**, 3964–3979 (2007).

[352] S. K. Madireddi, R. M. Yadav, M. Y. Zamal, P. Bag, J. X. Gunasekaran, and R. Subramanyam, "Exploring LHCSR3 expression and its role in *Chlamydomonas reinhardtii* under osmotic stress: Implications for non-photochemical quenching mechanism", Journal of Photochemistry and Photobiology B: Biology **256**, 112941 (2024).

[353] L. Girolomoni, P. Ferrante, S. Berteotti, G. Giuliano, R. Bassi, and M. Ballottari, "The function of LHCBM4/6/8 antenna proteins in *Chlamydomonas reinhardtii*", Journal of Experimental Botany **68**, erw462 (2016).

[354] N. Smirnoff and D. Arnaud, "Hydrogen peroxide metabolism and functions in plants", New Phytologist **221**, 1197–1214 (2019).

[355] B. Nowicka, A. Trela-Makowej, D. Latowski, K. Strzalka, and R. Szymańska, "Antioxidant and signaling role of plastid-derived isoprenoid quinones and chromanols", International Journal of Molecular Sciences **22**, 1–25 (2021).

[356] B. B. Fischer, A. Krieger-Liszkay, É. Hideg, I. Šnyrychová, M. Wiesendanger, and R. I. Eggen, "Role of singlet oxygen in chloroplast to nucleus retrograde signaling in *Chlamydomonas reinhardtii*", FEBS Letters **581**, 5555–5560 (2007).

[357] N. Chouhan, E. Devadasu, R. M. Yadav, and R. Subramanyam, "Autophagy Induced Accumulation of Lipids in pgrl1 and pgr5 of *Chlamydomonas reinhardtii* Under High Light", Frontiers in Plant Science **12** (2022).

[358] M. Pérez-Pérez, I. Couso, L. Heredia-Martínez, and J. Crespo, "Monitoring Autophagy in the Model Green Microalga *Chlamydomonas reinhardtii*", Cells **6**, 36 (2017).

[359] J. M. Quinn and S. Merchant, "Two copper-responsive elements associated with the *Chlamydomonas CYC6* gene function as targets for transcriptional activators.", The Plant Cell **7**, 623–628 (1995).

[360] M. Cecchin, J. Jeong, W. Son, M. Kim, S. Park, L. Zuliani, S. Cazzaniga, A. Pompa, C. Young Kang, S. Bae, M. Ballottari, and E. Jin, "LPA2 protein is involved in photosystem II assembly in *Chlamydomonas reinhardtii*", The Plant Journal **107**, 1648–1662 (2021).

[361] L. Li, E. M. Aro, and A. H. Millar, "Mechanisms of Photodamage and Protein Turnover in Photoinhibition", Trends in Plant Science **23**, 667–676 (2018).

[362] P. Mulo, I. Sakurai, and E. M. Aro, "Strategies for *psbA* gene expression in cyanobacteria, green algae and higher plants: From transcription to PSII repair", Biochimica et Biophysica Acta - Bioenergetics **1817**, 247–257 (2012).

[363] L. Wei, B. Derrien, A. Gautier, L. Houille-Vernes, A. Boulouis, D. Saint-Marcoux, A. Malnoë, F. Rappaport, C. de Vitry, O. Vallon, Y. Choquet, and F.-A. Wollman, "Nitric Oxide–Triggered Remodeling of Chloroplast Bioenergetics and Thylakoid Proteins upon Nitrogen Starvation in *Chlamydomonas reinhardtii*", The Plant Cell **26**, 353–372 (2014).

[364] M. Díaz, V. de Haro, R. Muñoz, and M. J. Quiles, "Chlororespiration is involved in the adaptation of *Brassica* plants to heat and high light intensity", Plant, Cell and Environment **30**, 1578–85 (2007).

[365] J. L. Moseley, C.-W. Chang, and A. R. Grossman, "Genome-Based Approaches to Understanding Phosphorus Deprivation Responses and PSR1 Control in *Chlamydomonas reinhardtii*", Eukaryotic Cell **5**, 26–44 (2006).

[366] X. Sun and T. Wen, "Physiological roles of plastid terminal oxidase in plant stress responses", Journal of Biosciences **36**, 951–956 (2011).

[367] D. Baniulis, S. S. Hasan, J. T. Stofleth, and W. A. Cramer, "Mechanism of Enhanced Superoxide Production in the Cytochrome 6f Complex of Oxygenic Photosynthesis", Biochemistry **52**, 8975–8983 (2013).

[368] K. Wostrikoff and L. C. Mackinder, "Rubisco and inorganic carbon assimilation", in *The Chlamydomonas Sourcebook: Volume 2: Organellar and Metabolic Processes*, 3rd edition (Academic Press, 2023), pp. 223–271.

[369] S. I. Saroussi, T. M. Wittkopp, and A. R. Grossman, "The Type II NADPH Dehydrogenase Facilitates Cyclic Electron Flow, Energy-Dependent Quenching, and Chlororespiratory Metabolism during Acclimation of *Chlamydomonas reinhardtii* to Nitrogen Deprivation", Plant Physiology **170**, 1975–1988 (2016).

[370] E. Mignolet, R. Lecler, B. Ghysels, C. Remacle, and F. Franck, "Function of the chloroplastic NAD(P)H dehydrogenase Nda2 for H_2 photoproduction in sulphur-deprived *Chlamydomonas reinhardtii*", Journal of Biotechnology **162**, 81–88 (2012).

[371] J. De Las Rivas, B. Andersson, and J. Barber, "Two sites of primary degradation of the D1-protein induced by acceptor or donor side photo-inhibition in photosystem II core complexes", FEBS Letters **301**, 246–252 (1992).

[372] E. J. Calabrese and M. P. Mattson, "How does hormesis impact biology, toxicology, and medicine?", npj Aging and Mechanisms of Disease **3**, 13 (2017).

[373] Y. Schaerli, A. Munteanu, M. Gili, J. Cotterell, J. Sharpe, and M. Isalan, "A unified design space of synthetic stripe-forming networks", Nature Communications **5**, 4905 (2014).

[374] L. Martins, J. A. Trujillo-Hernandez, and J.-P. Reichheld, "Thiol Based Redox Signaling in Plant Nucleus", Frontiers in Plant Science **9**, 1–9 (2018).

[375] C. R. Milano, S. N. Ur, Y. Gu, J. Zhang, R. Allison, G. Brown, M. J. Neale, E. C. Tromer, K. D. Corbett, and A. Hochwagen, "Chromatin binding by HORMAD proteins regulates meiotic recombination initiation", The EMBO Journal **43**, 836–867 (2024).

[376] J. P. Prince and E. Martinez-Perez, "Functions and Regulation of Meiotic HORMA-Domain Proteins", Genes **13**, 777 (2022).

[377] T. Matsuo, K. Okamoto, K. Onai, Y. Niwa, K. Shimogawara, and M. Ishiura, "A systematic forward genetic analysis identified components of the *Chlamydomonas* circadian system", Genes & Development **22**, 918–930 (2008).

[378] Y. Niwa, T. Matsuo, K. Onai, D. Kato, M. Tachikawa, and M. Ishiura, "Phase-resetting mechanism of the circadian clock in *Chlamydomonas reinhardtii*", Proceedings of the National Academy of Sciences **110**, 13666–13671 (2013).

[379] M. Gururaj, A. Ohmura, M. Ozawa, T. Yamano, H. Fukuzawa, and T. Matsuo, "A potential EARLY FLOWERING 3 homolog in *Chlamydomonas* is involved in the red/violet and blue light signaling pathways for the degradation of RHYTHM OF CHLOROPLAST 15", PLOS Genetics **18** (2022).

[380] T. Matsuo, T. Iida, A. Ohmura, M. Gururaj, D. Kato, R. Mutoh, K. Ihara, and M. Ishiura, "The role of ROC75 as a daytime component of the circadian oscillator in *Chlamydomonas reinhardtii*", PLOS Genetics **16** (2020).

[381] S. J. Burgess, H. Taha, J. A. Yeoman, O. Iamshanova, K. X. Chan, M. Boehm, V. Behrends, J. G. Bundy, W. Bialek, J. W. Murray, and P. J. Nixon, "Identification of the elusive pyruvate reductase of *Chlamydomonas reinhardtii* chloroplasts", Plant and Cell Physiology **57**, 82–94 (2016).

[382] L. A. Swirsky Whitney, G. Novi, P. Perata, and E. Loreti, "Distinct Mechanisms Regulating Gene Expression Coexist within the Fermentative Pathways in *Chlamydomonas reinhardtii*", The Scientific World Journal **2012**, 1–9 (2012).

[383] H. Berger, O. Blifernez-Klassen, M. Ballottari, R. Bassi, L. Wobbe, and O. Kruse, "Integration of Carbon Assimilation Modes with Photosynthetic Light Capture in the Green Alga *Chlamydomonas reinhardtii*", Molecular Plant **7**, 1545–1559 (2014).

[384] S. S. Merchant, S. Schmollinger, D. Strenkert, J. L. Moseley, and C. E. Blaby-Haas, "From economy to luxury: Copper homeostasis in *Chlamydomonas* and other algae", Biochimica et Biophysica Acta (BBA) - Molecular Cell Research **1867**, 118822 (2020).

[385] P. Lamkemeyer, M. Laxa, V. Collin, W. Li, I. Finkemeier, M. A. Schöttler, V. Holtkamp, V. B. Tognetti, E. Issakidis-Bourguet, A. Kandlbinder, E. Weis, M. Miginiac-Maslow, and K.-J. Dietz, "Peroxiredoxin Q of *Arabidopsis thaliana* is attached to the thylakoids and functions in context of photosynthesis", The Plant Journal **45**, 968–981 (2006).

[386] K. Chibani, G. Wingsle, J.-P. Jacquot, E. Gelhaye, and N. Rouhier, "Comparative Genomic Study of the Thioredoxin Family in Photosynthetic Organisms with Emphasis on *Populus trichocarpa*", Molecular Plant **2**, 308–322 (2009).

[387] R. van Lis, S. Brugière, C. Baffert, Y. Couté, W. Nitschke, and A. Atteia, "Hybrid cluster proteins in a photosynthetic microalga", The FEBS Journal **287**, 721–735 (2020).

[388] V. Calatrava, M. Tejada-Jimenez, E. Sanz-Luque, E. Fernandez, and A. Galvan, "Nitrogen metabolism in *Chlamydomonas*", in *The Chlamydomonas Sourcebook: Volume 2: Organellar and Metabolic Processes*, 3rd edition (Academic Press, 2023), pp. 99–128.

[389] L. L. Dougherty, S. Dutta, and P. Avasthi, "The ERK activator, BCI, inhibits ciliogenesis and causes defects in motor behavior, ciliary gating, and cytoskeletal rearrangement", Life Science Alliance **6** (2023).

[390] G. T. Huang, S. L. Ma, L. P. Bai, L. Zhang, H. Ma, P. Jia, J. Liu, M. Zhong, and Z. F. Guo, "Signal transduction during cold, salt, and drought stresses in plants", Molecular Biology Reports **39**, 969–987 (2012).

[391] D. Miranda-Saavedra and G. J. Barton, "Classification and functional annotation of eukaryotic protein kinases", Proteins: Structure, Function, and Bioinformatics **68**, 893–914 (2007).

[392] F. Tulin and F. R. Cross, "A Microbial Avenue to Cell Cycle Control in the Plant Superkingdom", The Plant Cell **26**, 4019–4038 (2014).

[393] A. Koletti, I. Dervisi, C. Kalloniati, M. E. Zografaki, H. Rennenberg, A. Roussis, and E. Flemetakis, "Selenium-binding Protein 1 (SBD1): A stress response regulator in *Chlamydomonas reinhardtii*", Plant Physiology **189**, 2368–2381 (2022).

[394] J. Minagawa and Y. Takahashi, "Structure, function and assembly of Photosystem II and its light-harvesting proteins", Photosynthesis Research **82**, 241–263 (2004).

[395] M. Esperanza, M. Seoane, C. Rioboo, C. Herrero, and Á. Cid, "*Chlamydomonas reinhardtii* cells adjust the metabolism to maintain viability in response to atrazine stress", Aquatic Toxicology **165**, 64–72 (2015).

[396] M. Esperanza, M. Blanes-Rodríguez, Á. Cid, and M. Seoane, "Analysis of the effects of BP-3 and BP-4 on the transcriptome of *Chlamydomonas reinhardtii*: An RNA-Seq approach", Journal of Applied Phycology **35**, 1251–1262 (2023).

[397] F. R. Cross and J. G. Umen, "The *Chlamydomonas* cell cycle", The Plant Journal **82**, 370–392 (2015).

[398] Y.-T. Lin, T. Takeuchi, B. Youk, J. Umen, B. B. Sears, and C. Benning, "*Chlamydomonas* cht7 is involved in repressing dna replication and mitotic genes during synchronous growth", G3 Genes|Genomes|Genetics **12** (2022).

[399] E. Simon and D. Kornitzer, "Pulse-Chase Analysis to Measure Protein Degradation", in *Methods in enzymology*, Vol. 536, 1st ed. (Elsevier Inc., 2014), pp. 65–75.

[400] V. Bonardi, P. Pesaresi, T. Becker, E. Schleiff, R. Wagner, T. Pfannschmidt, P. Jahns, and D. Leister, "Photosystem II core phosphorylation and photosynthetic acclimation require two different protein kinases", Nature **437**, 1179–1182 (2005).

[401] F. Furt, C. V. Oostende, J. R. Widhalm, M. A. Dale, J. Wertz, and G. J. C. Basset, "A bimodular oxidoreductase mediates the specific reduction of phylloquinone (vitamin K1) in chloroplasts", The Plant Journal **64**, no–no (2010).

[402] W. Li, S. Schulman, R. J. Dutton, D. Boyd, J. Beckwith, and T. A. Rapoport, "Structure of a bacterial homologue of vitamin K epoxide reductase", Nature **463**, 507–512 (2010).

[403] S. Liu, W. Cheng, R. Fowle Grider, G. Shen, and W. Li, "Structures of an intramembrane vitamin K epoxide reductase homolog reveal control mechanisms for electron transfer", Nature Communications **5**, 3110 (2014).

[404] C. van Oostende, J. R. Widhalm, and G. J. Basset, "Detection and quantification of vitamin K1 quinol in leaf tissues", Phytochemistry **69**, 2457–2462 (2008).

[405] G. Silveira-Dorta, D. M. Monzón, F. P. Crisóstomo, T. Martín, V. S. Martín, and R. Carrillo, "Oxidation with air by ascorbate-driven quinone redox cycling", Chemical Communications **51**, 7027–7030 (2015).

[406] M. Kozuleva, A. Petrova, Y. Milrad, A. Semenov, B. Ivanov, K. E. Redding, and I. Yacoby, "Phylloquinone is the principal Mehler reaction site within photosystem I in high light", Plant Physiology **186**, 1848–1858 (2021).

[407] B. Schmidt, L. Ho, and P. J. Hogg, "Allosteric Disulfide Bonds", Biochemistry **45**, 7429–7433 (2006).

[408] G. Gopalan, Z. He, Y. Balmer, P. Romano, R. Gupta, A. Héroux, B. B. Buchanan, K. Swaminathan, and S. Luan, "Structural analysis uncovers a role for redox in regulating FKBP13, an immunophilin of the chloroplast thylakoid lumen", Proceedings of the National Academy of Sciences **101**, 13945–13950 (2004).

[409] Z.-B. Yu, Y. Lu, J.-J. Du, J.-J. Peng, and X.-Y. Wang, "The chloroplast protein LTO1/AtVKOR is involved in the xanthophyll cycle and the acceleration of D1 protein degradation", Journal of Photochemistry and Photobiology B: Biology **130**, 68–75 (2014).

[410] H. Schulz, R. A. Fabianek, E. C. Pellicioli, H. Hennecke, and L. Thöny-Meyer, "Heme transfer to the heme chaperone CcmE during cytochrome *c* maturation requires the CcmC protein, which may function independently of the ABC-transporter CcmAB", Proceedings of the National Academy of Sciences **96**, 6462–6467 (1999).

[411] S. E. Chobot, H. H. Hernandez, C. L. Drennan, and S. J. Elliott, "Direct Electrochemical Characterization of Archaeal Thioredoxins", Angewandte Chemie International Edition **46**, 4145–4147 (2007).

[412] J. M. Alonso et al., "Genome-Wide Insertional Mutagenesis of *Arabidopsis thaliana*", Science **301**, 653–657 (2003).

[413] J. L. Bowman et al., "The renaissance and enlightenment of *Marchantia* as a model system", The Plant Cell **34**, 3512–3542 (2022).

[414] P. I. Calzadilla, J. Zhan, P. Sétif, C. Lemaire, D. Solymosi, N. Battchikova, Q. Wang, and D. Kirilovsky, "The Cytochrome b_6f Complex Is Not Involved in Cyanobacterial State Transitions", The Plant Cell **31**, 911–931 (2019).

[415] P. I. Calzadilla and D. Kirilovsky, "Revisiting cyanobacterial state transitions", Photochemical & Photobiological Sciences **19**, 585–603 (2020).

[416] C.-H. Huang, C. R. Shen, H. Li, L.-Y. Sung, M.-Y. Wu, and Y.-C. Hu, "CRISPR interference (CRISPRi) for gene regulation and succinate production in cyanobacterium *S. elongatus* PCC 7942", Microbial Cell Factories **15**, 196 (2016).

[417] J. M. Lawrence, "Tools for analysing and engineering bioenergetic processes in cyanobacteria", PhD thesis, University of Cambridge (2023).

[418] B. R. Green, "What Happened to the Phycobilisome?", Biomolecules **9**, 748 (2019).

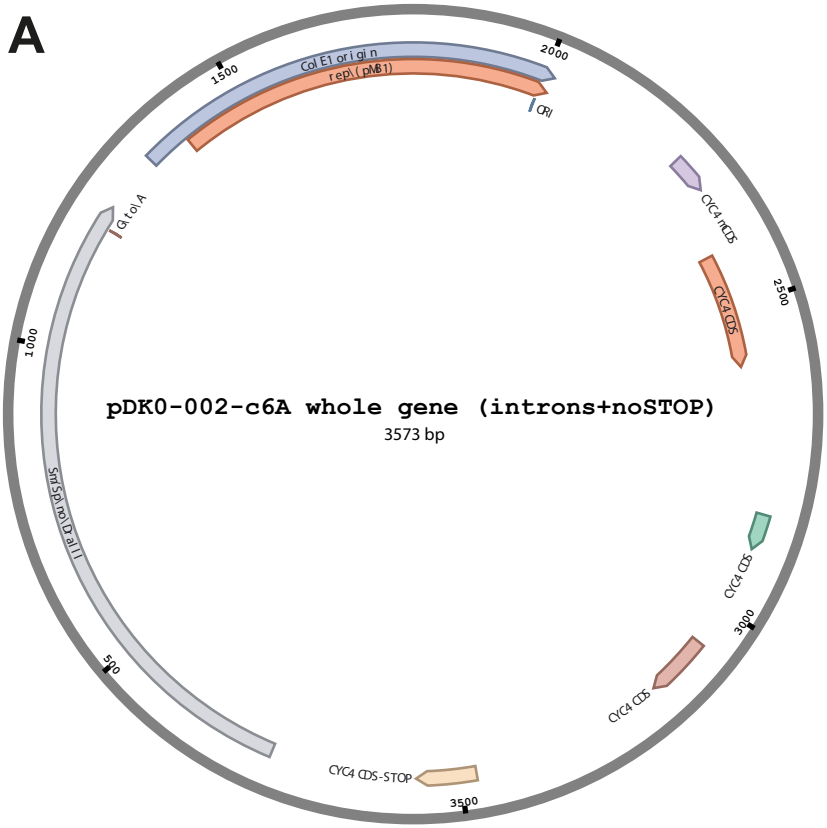
[419] R. G. Dorrell and C. J. Howe, "Integration of plastids with their hosts: Lessons learned from dinoflagellates", Proceedings of the National Academy of Sciences **112**, 10247–10254 (2015).

[420] A. Kanazawa, G. J. Blanchard, M. Szabó, P. J. Ralph, and D. M. Kramer, "The site of regulation of light capture in *Symbiodinium*: Does the peridinin–chlorophyll *a*–protein detach to regulate light capture?", Biochimica et Biophysica Acta (BBA) - Bioenergetics **1837**, 1227–1234 (2014).

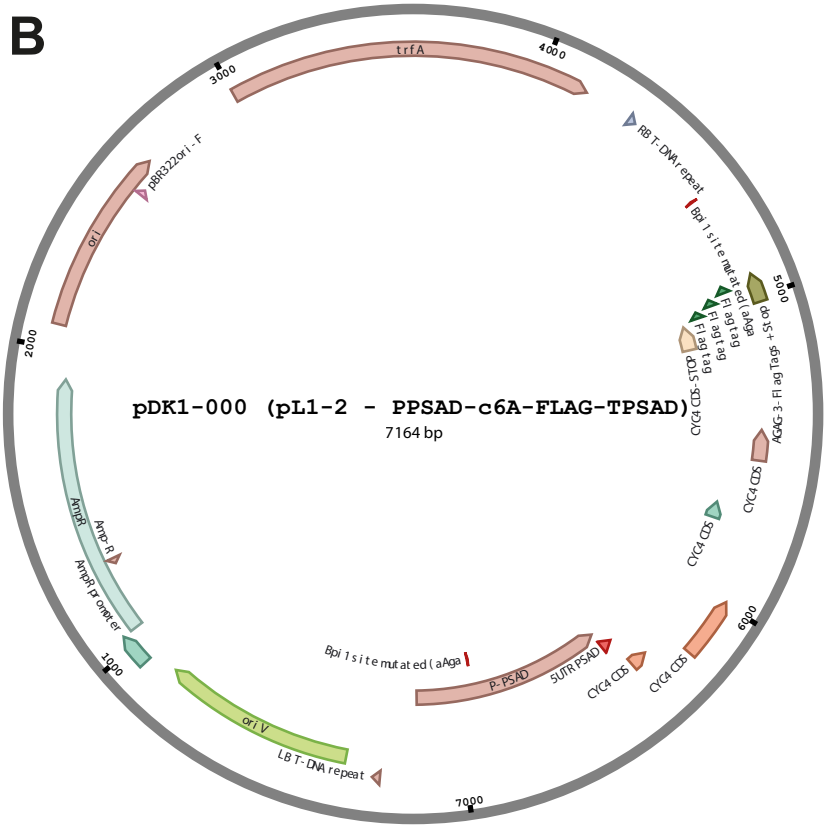
A

Plasmid maps

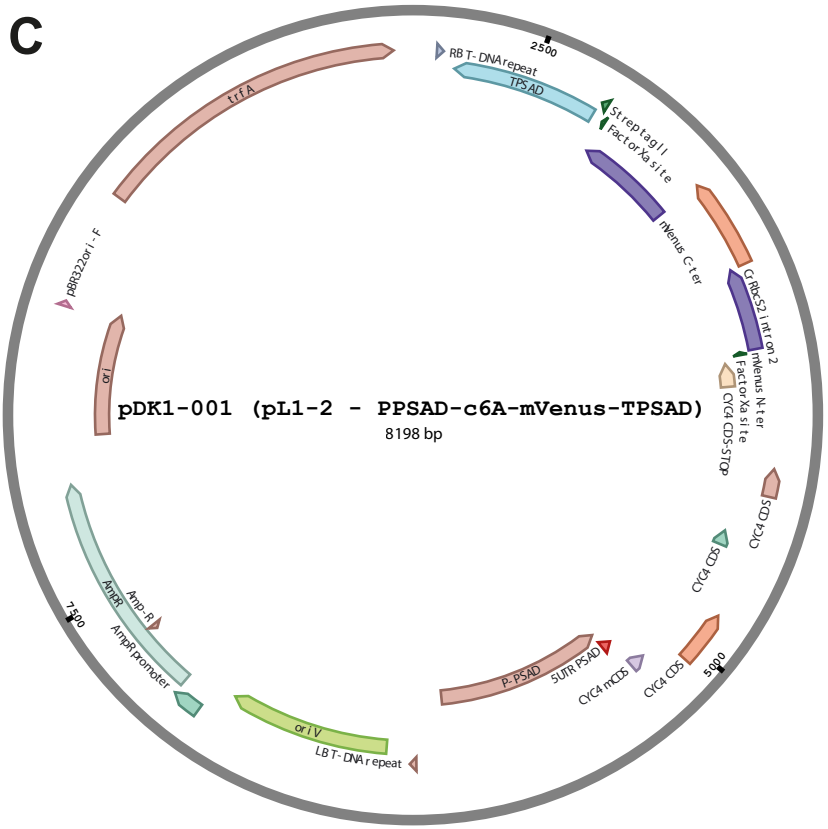
A


pDK0-002-c6A whole gene (introns+noSTOP)
3573 bp
Col E1 origin
repA (pMB1)
ORI
CYC4 nCDS
CYC4 CDS
CYC4 CDS
CYC4 CDS
CYC4 CDS-STOP
Sma I Sph I Not I Dra III I
G to A
500
1000
1500
2000
2500
3000
3500

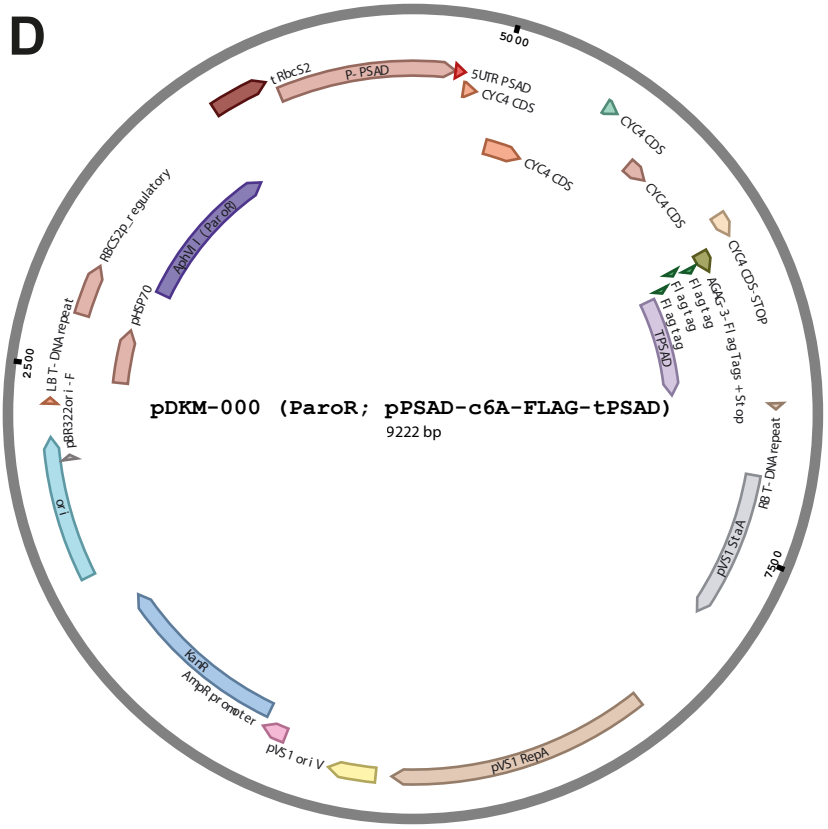
B


pDK1-000 (pL1-2 - PPSAD-c6A-FLAG-TPSAD)
7164 bp
trfA
RB T-DNA repeat
Bpi I site mutated (aAga
Flag tag
Flag tag
Flag tag
dCYC4 CDS-STOP
AGAG-3-Flag Tags+St dp
CYC4 CDS
CYC4 CDS
CYC4 CDS
CYC4 CDS
P-PSAD
SUTR PSAD
Bpi I site mutated (aAga
LB T-DNA repeat
orf V
AmpR promoter
AmpR
Amp R f1
ori
pBR322 ori - F
1000
2000
3000
4000
5000
6000
7000

C


pDK1-001 (pL1-2 - PPSAD-c6A-mVenus-TPSAD)
8198 bp
2500
5000
7500
RB T- DNA repeat
TPSAD
Strep tag II
Factor Xa site
mVenus C-ter
Cr.RbcS2 intron 2
mVenus N-ter
Factor Xa site
CYC4 CDS-STOP
SCD CYC6
CYC4 CDS
CYC4 mCDS
5UTR PSAD
P- PSAD
CYC4 CDS
ori V
LB T- DNA repeat
AmpR promoter
AmpR
Amp-R
ori
pBR322ori - F
trfA

D


pDKM-000 (ParoR; pPSAD-c6A-FLAG-tPSAD)
9222 bp
2500
5000
7500
LB T- DNA repeat
pBR322ori - F
ori
KanR
AmpR promoter
pVS1 ori V
pVS1 RepA
pVS1 StaA
RB T- DNA repeat
AGAG-3-Flag Tags + Stop
Flag tag
Flag tag
Flag tag
TPSAD
CYC4 CDS-STOP
CYC4 CDS
CYC4 CDS
CYC4 CDS
5UTR PSAD
CYC4 CDS
P- PSAD
tRbcS2
RBCS2p_regulatory
pPSP70
AqNVL (ParoR)

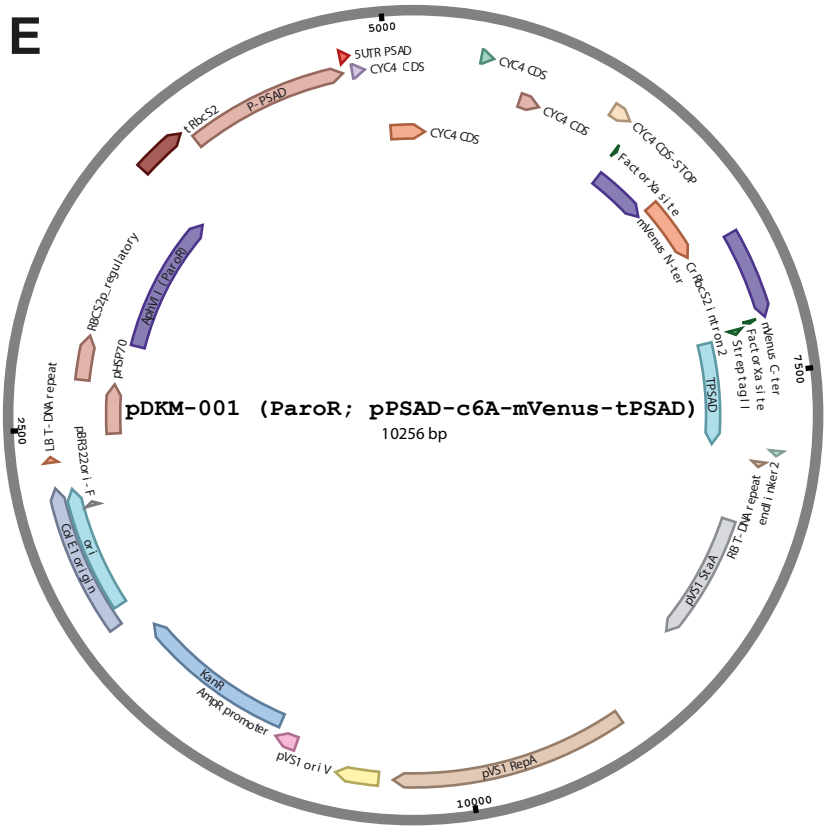


Figure A.1: Plasmid maps of pDK plasmids. (**A**) Level 0 plasmids pDK0-002 containing the *CYC4* gene with introns, two intronic *Bsa*I restriction sites altered (GAGACC $\rightarrow$ GAAACC) and the Stop codon removed. The plasmid confers a spectinomycin resistance (Sm/Sp). (**B**) Level 1 plasmid pDK1-000 containing a C-terminally FLAG-tagged *CYC4* gene (pDK0-002) under the control of the *PSAD* promoter and terminator. The plasmid also confers a resistance to Ampicillin (AmpR). (**C**) Level 1 plasmid pDK1-001 containing a C-terminally mVenus-tagged (with a *RBCS2* intron 2 artificially inserted) *CYC4* gene (pDK0-002) under the control of the *PSAD* promoter and terminator. The plasmid also confers a resistance to Ampicillin (AmpR). (**D**) Level M plasmid pDKM-000 combining pDK1-000 with a paromomycin resistance cassette (pHSP70, RBCS2p_regulatory, AphVII (ParoR), and tRbcS2). The plasmid also confers a resistance to kanamycin (KanR). (**E**) Level M plasmid pDKM-001 combining pDK1-001 with the same paromomycin resistance cassette as in (D). The plasmid also confers a resistance to kanamycin (KanR).

B

Additional WGS data

Table B.1: Results of fastQC quality assessment of the whole genome sequencing data presented in chapter 3.

Sample Name	Duplicates (%)	GC content (%)	# of sequences (million)
Edincw15_-EKDN230023760-1A_-HFLT3DSX7_L3_1	34.6	62	50.5
Edincw15_-EKDN230023760-1A_-HFLT3DSX7_L3_2	33.3	62	50.5
Uex55_-EKDN230022229-1A_-HF557DSX7_L1_1	31.2	61	44.1
Uex55_-EKDN230022229-1A_-HF557DSX7_L1_2	29.6	62	44.1

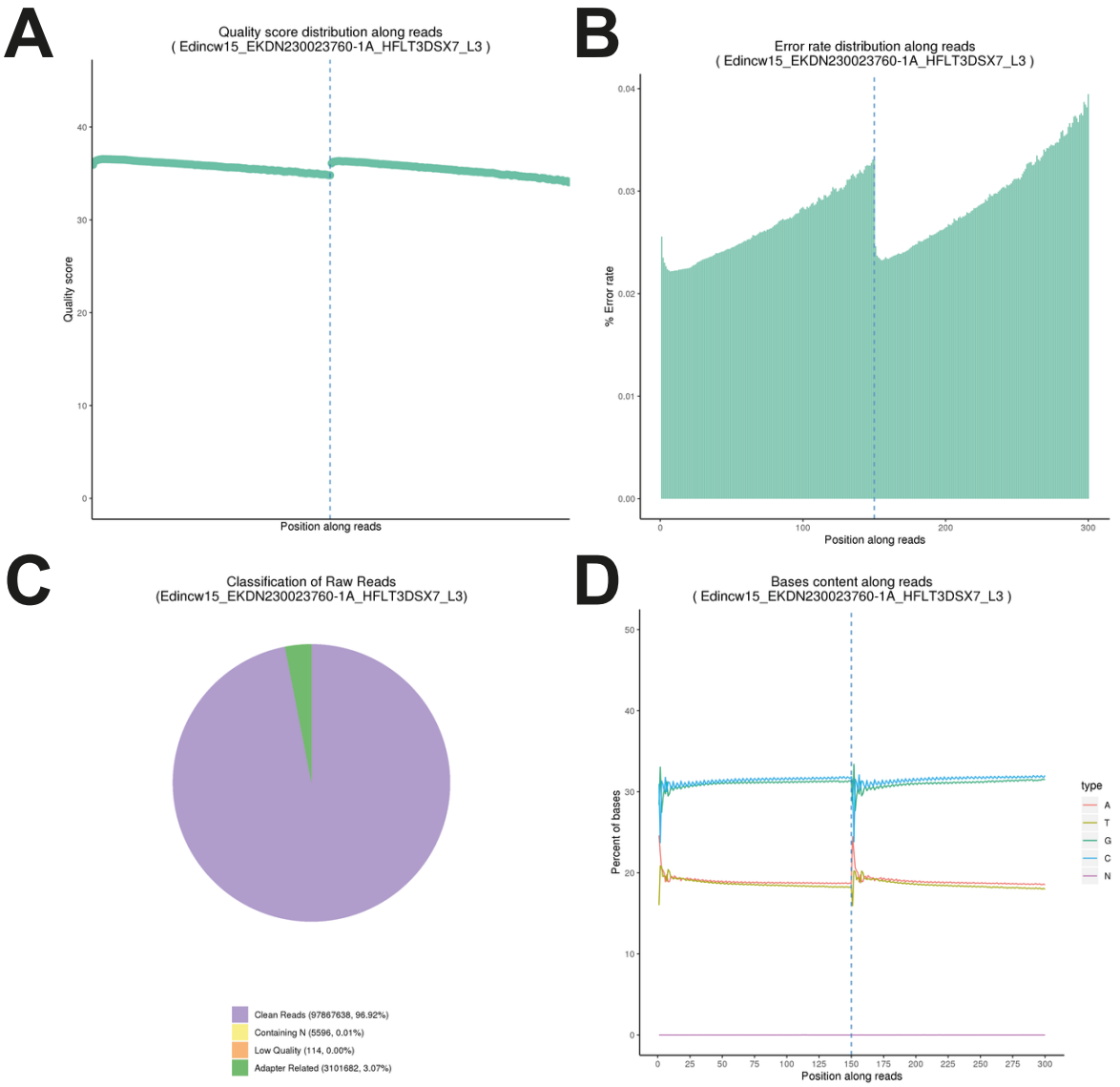


Figure B.1: Quality assessment graphs of whole genome sequencing data on WT ("Edincw15") as obtained from Novogene. Quality score distribution along reads (**A**), error rate distribution along reads (**B**), classification of reads (**C**), and bases content along reads (**D**) all confirmed high data quality.

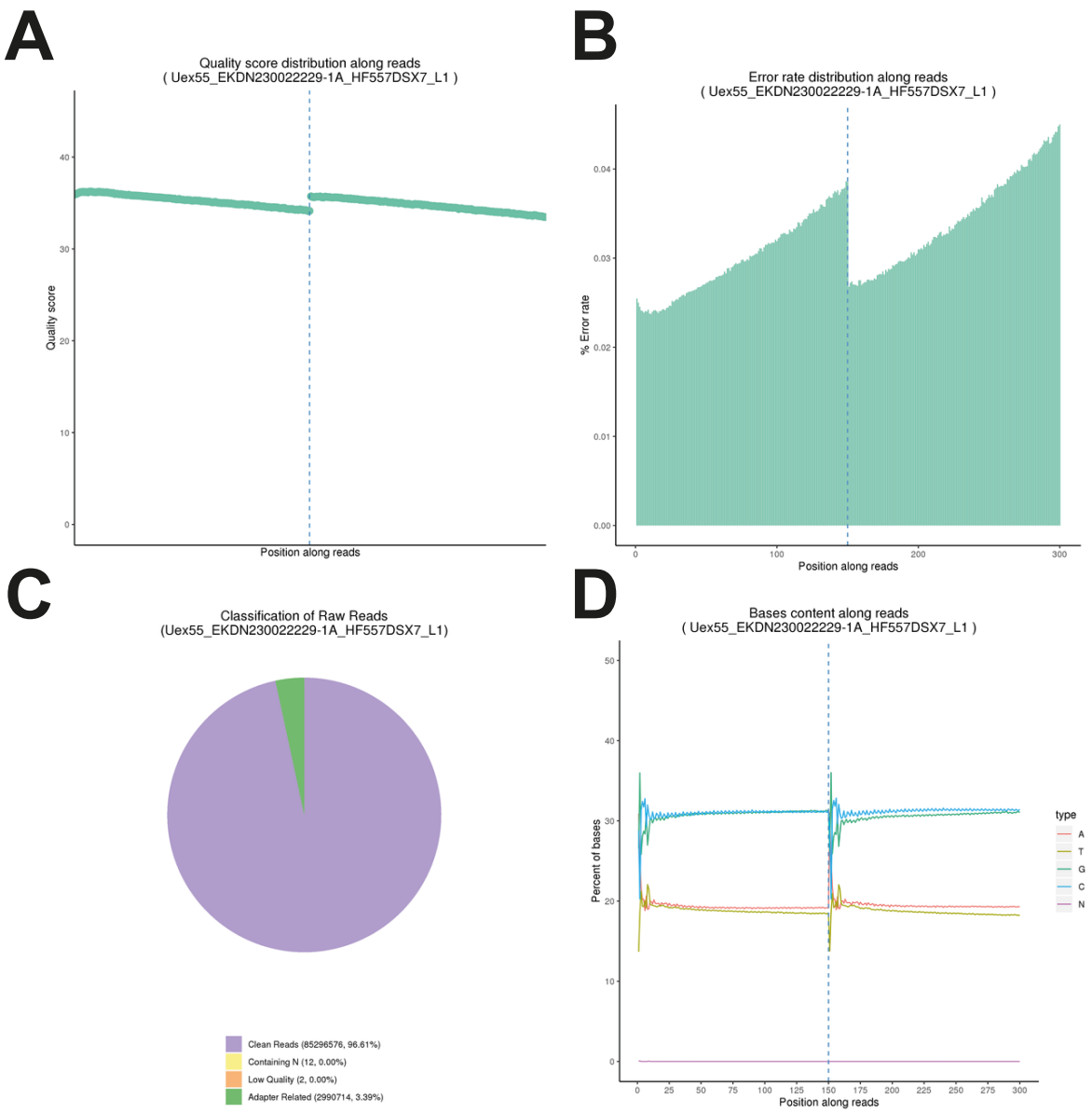


Figure B.2: Quality assessment graphs of whole genome sequencing data on c_{6A}-KO ("Uex55") as obtained from Novogene. Quality score distribution along reads (**A**), error rate distribution along reads (**B**), classification of reads (**C**), and bases content along reads (**D**) all confirmed high data quality.

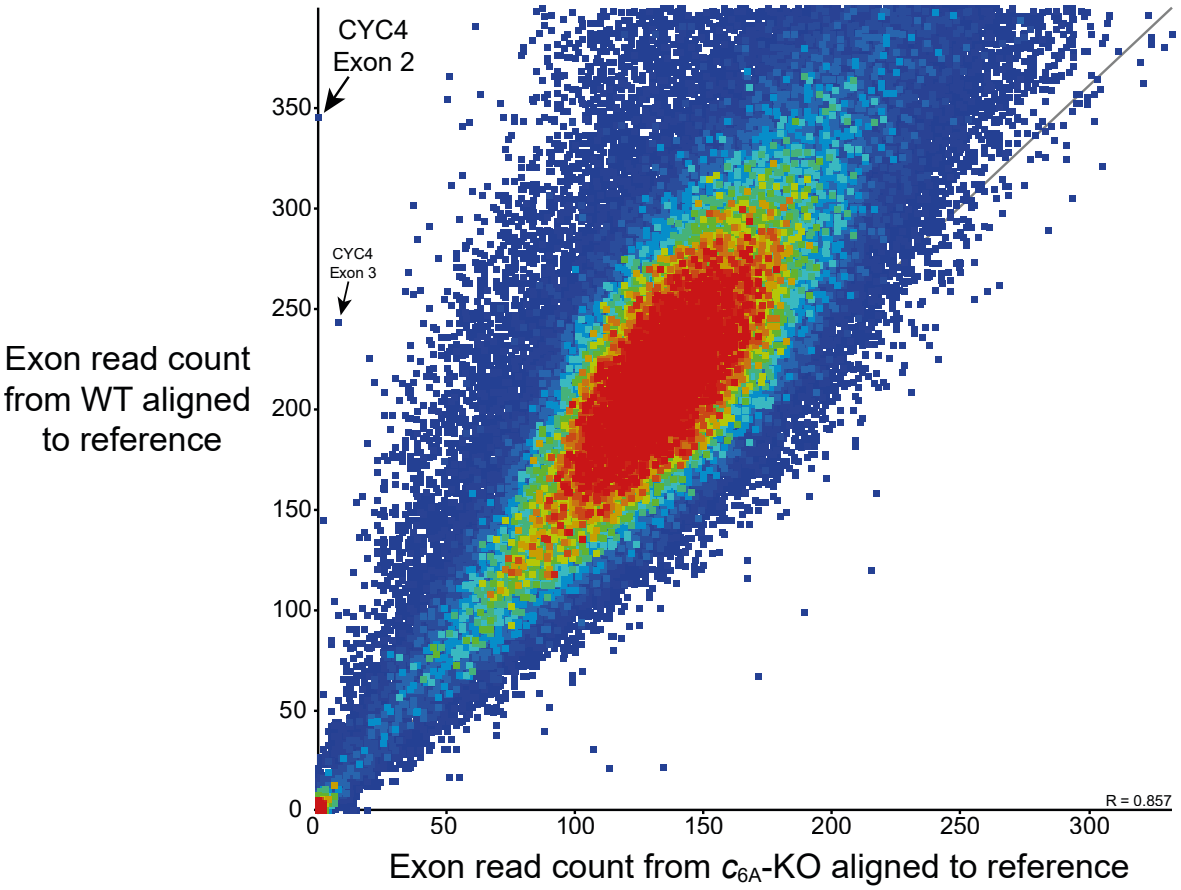


Figure B.3: Exon read count comparison between WT and c_{6A}-KO. *CYC4* exon 2 (marked with an arrow) shows no reads in c_{6A}-KO but around 350 reads in WT. No other exon was found to show a similar imbalance as found for *CYC4*. Each data point represents one exon and colours are indicating where data points are overlaying.

C

Additional mass-spectrometric data of 2D-PAGE spots

Table C.1: Identified proteins from peptides found in the spot assigned to PsaA in figure 5.12 (apparent MW in gel:~85 kDa), their molecular weight (MW), the number of exclusive unique peptides found for this protein, the number of total peptides found for this protein, the fraction of the total peptides of this protein compared to all peptides found, and the percentage of the protein amino acid sequence covered by the detected peptides. These top 10 results are ordered from highest to lowest total peptide count. The protein assigned to the spot as its most likely identity is marked in bold.

Identifier	MW (kDa)	Exclusive unique peptide count	Total peptide count	% of all peptides	Sequence coverage (%)
Cre06.g278255	107.0	21	21	0.39	21.50
PsaA	84.2	10	18	0.34	12.60
Cre06.g255100	94.1	10	10	0.19	11.70
EIF3C	99.6	8	8	0.15	6.59
MPPA2	49.6	6	6	0.11	10.70
PsaB	82.1	4	6	0.11	6.12
Cre01.g054500	112.3	5	5	0.09	4.57
ADH1	102.2	4	4	0.07	4.40
Cre17.g720450	107.1	4	4	0.07	3.71
RPL4	44.9	3	3	0.06	8.05

Table C.2: Identified proteins from peptides found in the spot assigned to PSAL in figure 5.12 (apparent MW in gel:~13 kDa), their molecular weight (MW), the number of exclusive unique peptides found for this protein, the number of total peptides found for this protein, the fraction of the total peptides of this protein compared to all peptides found, and the percentage of the protein amino acid sequence covered by the detected peptides. These top 10 results are ordered from highest to lowest total peptide count. The protein assigned to the spot as its most likely identity is marked in bold.

Identifier	MW (kDa)	Exclusive unique peptide count	Total peptide count	% of all peptides	Sequence coverage (%)
PSAL	20.3	2	12	0.18	13.30
RPL14	15.3	6	7	0.11	38.70
PRPL7	13.8	4	4	0.06	21.60
RPS16	16.0	3	3	0.05	16.90
PSAH	14.2	3	3	0.05	22.30
PSAE	10.8	1	3	0.05	23.70
PsbA	39.2	2	2	0.03	5.40
COX2B	16.8	2	2	0.03	22.90
PsaC	8.9	2	2	0.03	27.20
LHCB4	29.9	2	2	0.03	7.50

Table C.3: Identified proteins from peptides found in the spot assigned to PsbC in figure 5.12 (apparent MW in gel:~55 kDa), their molecular weight (MW), the number of exclusive unique peptides found for this protein, the number of total peptides found for this protein, the fraction of the total peptides of this protein compared to all peptides found, and the percentage of the protein amino acid sequence covered by the detected peptides. These top 10 results are ordered from highest to lowest total peptide count. The protein assigned to the spot as its most likely identity is marked in bold.

Identifier	MW (kDa)	Exclusive unique peptide count	Total peptide count	% of all peptides	Sequence coverage (%)
PsbC	50.6	14	98	1.45	32.10
FBA3	41.0	16	29	0.43	36.60
NUOA9	43.7	10	10	0.15	25.20
PsbD	39.4	6	9	0.13	18.20
GAP3	40.3	8	8	0.12	25.40
PST1	44.1	5	7	0.10	18.80
PsbB	56.0	5	5	0.07	9.84
CSP41A	48.0	5	5	0.07	12.30
NUO7	52.6	5	5	0.07	13.10
PGL1	38.9	4	4	0.06	8.65

Table C.4: Identified proteins from peptides found in the spot assigned to PetD in figure 5.12 (apparent MW in gel:~13.5 kDa), their molecular weight (MW), the number of exclusive unique peptides found for this protein, the number of total peptides found for this protein, the fraction of the total peptides of this protein compared to all peptides found, and the percentage of the protein amino acid sequence covered by the detected peptides. These top 10 results are ordered from highest to lowest total peptide count. The protein assigned to the spot as its most likely identity is marked in bold.

Identifier	MW (kDa)	Exclusive unique peptide count	Total peptide count	% of all peptides	Sequence coverage (%)
PetD	11.5	1	14	0.20	6.25
LHCA8	25.9	7	9	0.13	42.00
LHCA2	26.9	3	7	0.10	16.30
PRPL7	13.8	4	4	0.06	21.60
LHCB5	30.7	2	2	0.03	11.80
PSAH	14.2	2	2	0.03	16.20
PSBQ	21.8	2	2	0.03	9.55
ATPD	24.0	2	2	0.03	9.13
PRPL11	18.5	2	2	0.03	9.66
CPLD45	19.1	1	1	0.01	6.18

Table C.5: Identified proteins from peptides found in the spot assigned to LHCA1 in figure 5.12 (apparent MW in gel:~33 kDa), their molecular weight (MW), the number of exclusive unique peptides found for this protein, the number of total peptides found for this protein, the fraction of the total peptides of this protein compared to all peptides found, and the percentage of the protein amino acid sequence covered by the detected peptides. These top 10 results are ordered from highest to lowest total peptide count. The protein assigned to the spot as its most likely identity is marked in bold.

Identifier	MW (kDa)	Exclusive unique peptide count	Total peptide count	% of all peptides	Sequence coverage (%)
LHCA1	23.5	5	47	0.56	36.80
PsaD	21.3	8	31	0.37	30.60
PSAF	24.1	6	13	0.16	30.40
RPL13A	20.7	7	11	0.13	35.70
PsaC	8.9	5	6	0.07	64.20
PBA1	22.6	4	5	0.06	21.30
COX12	17.3	3	4	0.05	23.60
RPL18A	21.4	4	4	0.05	24.20
LHCA9	23.9	2	4	0.05	21.60
PSAE	10.8	2	4	0.05	34.00

Table C.6: Identified proteins from peptides found in the spot assigned to PRX1 in figure 5.12 (apparent MW in gel:~25 kDa), their molecular weight (MW), the number of exclusive unique peptides found for this protein, the number of total peptides found for this protein, the fraction of the total peptides of this protein compared to all peptides found, and the percentage of the protein amino acid sequence covered by the detected peptides. These top 10 results are ordered from highest to lowest total peptide count. The protein assigned to the spot as its most likely identity is marked in bold.

Identifier	MW (kDa)	Exclusive unique peptide count	Total peptide count	% of all peptides	Sequence coverage (%)
PRX1	22.3	3	100	1.01	60.90
PRPL10	25.9	12	16	0.16	46.80
PSRP-1	31.8	6	9	0.09	24.60
TOM20	21.7	5	7	0.07	24.90
TEF2	38.9	5	7	0.07	19.00
Cre01.g007600	28.1	6	6	0.06	31.20
Rpl5	20.2	5	6	0.06	27.90
ATPD	24.0	4	6	0.06	22.80
Rps9	21.0	5	5	0.05	26.20
CGL93	29.2	4	5	0.05	20.50

Table C.7: Identified proteins from peptides found in the yellow circled spot in figure 5.12 WT3 (apparent MW in gel:~14 kDa), their molecular weight (MW), the number of exclusive unique peptides found for this protein, the number of total peptides found for this protein, the fraction of the total peptides of this protein compared to all peptides found, and the percentage of the protein amino acid sequence covered by the detected peptides. These top 10 results are ordered from highest to lowest total peptide count. None of the proteins detected were in range of $\pm$ 10 kDa of the apparent molecular weight of the spot.

Identifier	MW (kDa)	Exclusive unique peptide count	Total peptide count	% of all peptides	Sequence coverage (%)
LHCB5	30.7	12	72	0.83	45.70
PsbD	39.4	7	35	0.40	23.60
LHCB4	29.9	12	21	0.24	51.80
PSRP3	33.4	8	8	0.09	30.50
PsbA	39.2	4	6	0.07	11.90
Cre11.g469150	29.9	4	6	0.07	20.40
PGM12	38.9	5	6	0.07	17.40
PSBO	30.5	5	5	0.06	22.30
ATPVE1	26.2	5	5	0.06	22.40
MDH4	38.5	4	4	0.05	11.10

D

PonceauS stains of membranes used for western blots

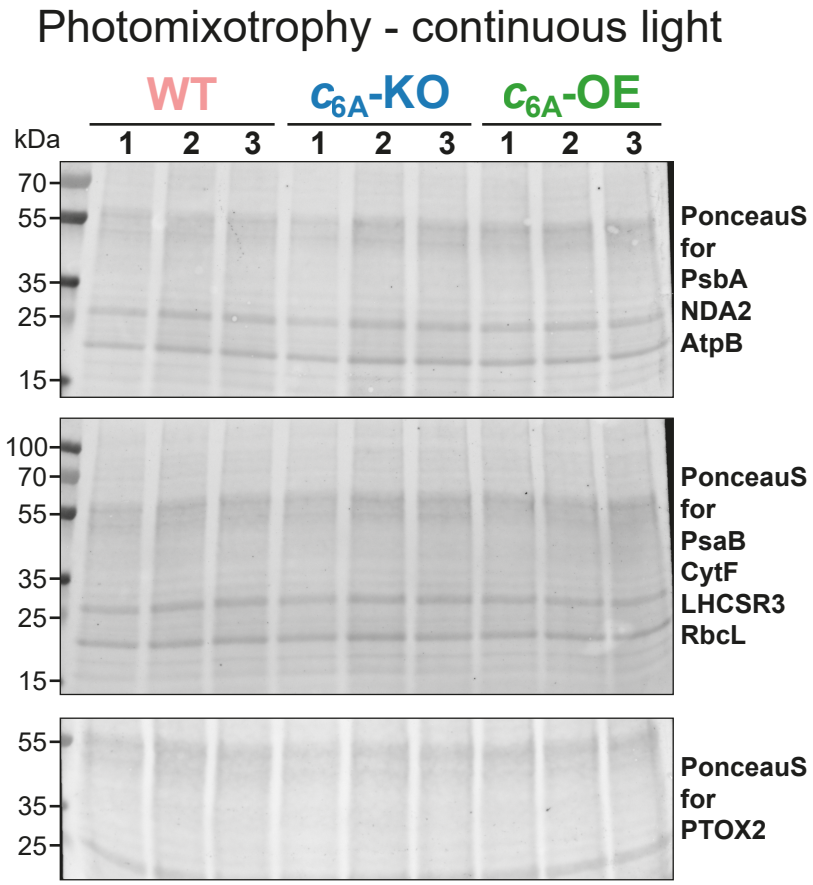


Figure D.1: PonceauS total protein stain of whole cell protein samples from WT and c_{6A} mutant strains. Three biological replicates per strain (1-3) were grown photomixotrophically in continuous light and protein was isolated in late exponential growth phase. Three individual SDS-PAGE gels and membranes were prepared from the same samples and the proteins probed for using the membrane are noted on the right. The relevant molecular weight areas where the antibodies detected proteins are shown and the protein ladder position for each membrane is noted on the left.

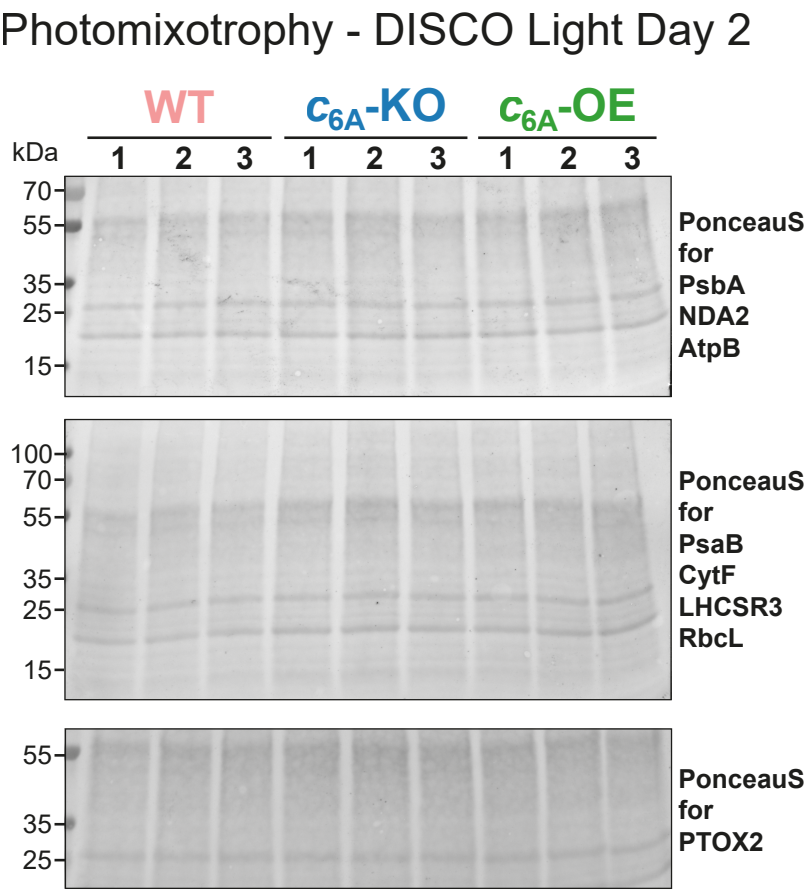


Figure D.2: PonceauS total protein stain of whole cell protein samples from WT and c_{6A} mutant strains. Three biological replicates per strain (1-3) were grown photomixotrophically in DISCO Light and protein was isolated on Day 2. Three individual SDS-PAGE gels and membranes were prepared from the same samples and the proteins probed for using the membrane are noted on the right. The relevant molecular weight areas where the antibodies detected proteins are shown and the protein ladder position for each membrane is noted on the left.

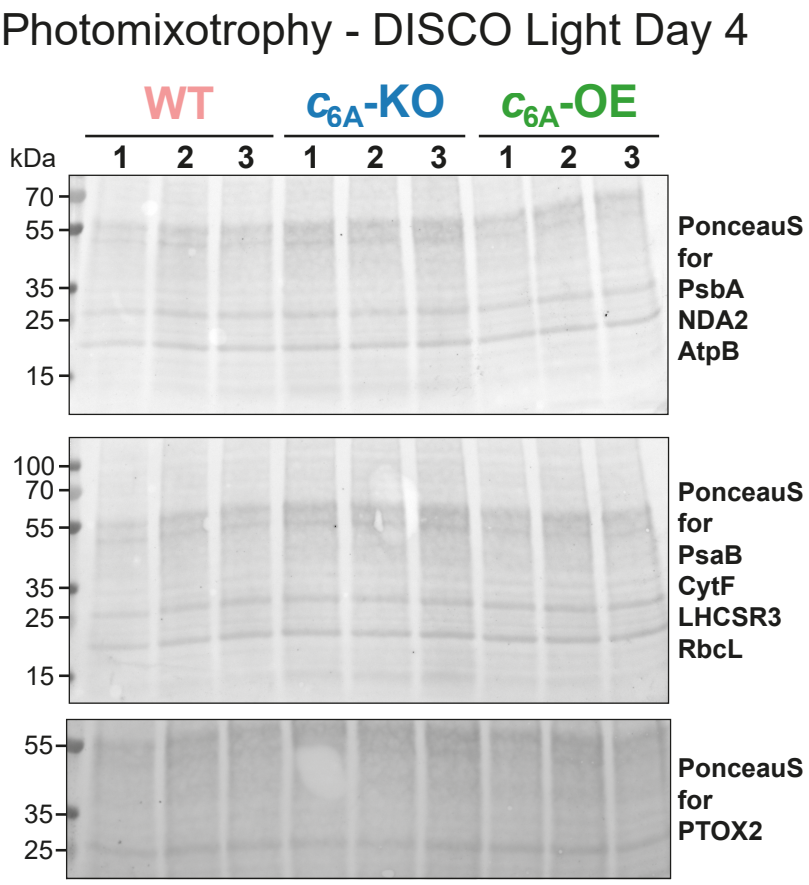


Figure D.3: PonceauS total protein stain of whole cell protein samples from WT and c_{6A} mutant strains. Three biological replicates per strain (1-3) were grown photomixotrophically in DISCO Light and protein was isolated on day 4. Three individual SDS-PAGE gels and membranes were prepared from the same samples and the proteins probed for using the membrane are noted on the right. The relevant molecular weight areas where the antibodies detected proteins are shown and the protein ladder position for each membrane is noted on the left.

E

RNAseq quality control details

Table E.1: Nanodrop measurements (concentration, 260/280 & 260/230 ratios) of RNA samples used for RNAseq (section 6.2.2).

strain	replicate	light condition	concentration (ng/µL)	260/280 ratio	260/230 ratio
c_{6A}-KO	I	continuous	790.6	2.11	1.53
c_{6A}-KO	II	continuous	920.6	2.13	2.28
c_{6A}-KO	III	continuous	897.6	2.14	2.35
c_{6A}-OE	I	continuous	850.1	2.13	2.34
c_{6A}-OE	II	continuous	1009	2.13	2.34
c_{6A}-OE	III	continuous	938.8	2.14	2.29
WT	I	continuous	1877	2.12	2.34
WT	II	continuous	1525.9	2.12	2.35
WT	III	continuous	1664.8	2.13	2.35
c_{6A}-KO	I	DISCO	1254.9	2.1	2.33
c_{6A}-KO	II	DISCO	1508.2	2.12	2.34
c_{6A}-KO	III	DISCO	1528.2	2.1	2.31
c_{6A}-OE	I	DISCO	1179.6	2.13	2.12
c_{6A}-OE	II	DISCO	1119.8	2.12	2.35
c_{6A}-OE	III	DISCO	1443.6	2.11	2.33
WT	I	DISCO	2344.2	2.13	2.29
WT	II	DISCO	2204.4	2.12	2.34
WT	III	DISCO	1625.2	2.11	2.36

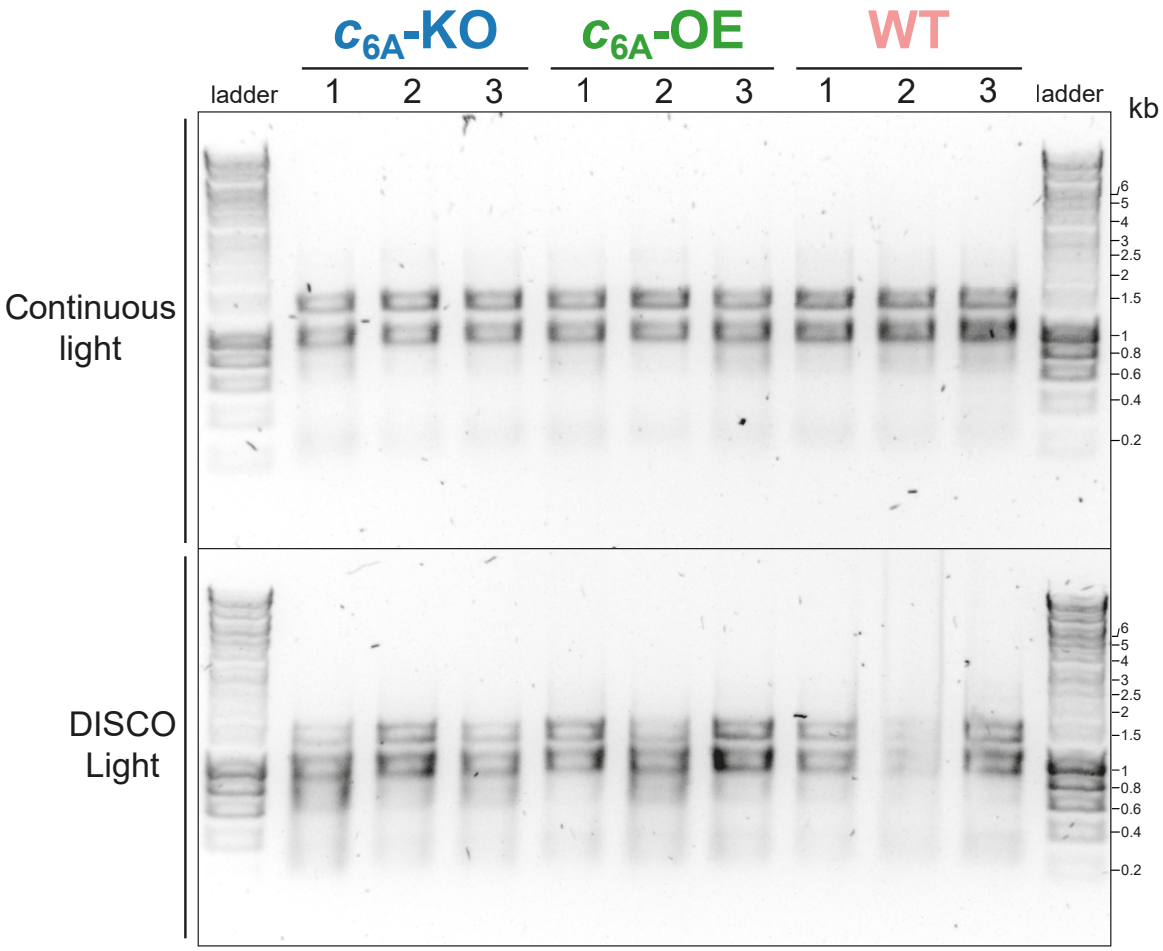


Figure E.1: Gel electrophoresis of RNA samples. RNA from three biological replicates per strain (1-3) was isolated from cultures grown photomixotrophically in continuous light or DISCO Light. Integrity of isolated RNA was confirmed visually by the presence of distinct bands corresponding to ribosomal RNA. 400 ng of RNA (as determined by Nanodrop) were loaded, except for sample WT 2 DISCO, where a loading error occurred. Sufficient quality for RNAseq of this sample was later confirmed by Novogene (table E.2.

Table E.2: RNA sample quality as determined by Novogene using an Agilent 5400 fragment analyzer. RIN: RNA integrity number.

Sample Name	Concentration (ng/µL)	Volume (µL)	Total amount (µg)	RIN	Sample QC Result
KO_I_cont	1210.05	23	27.83106	8.1	Pass
KO_II_cont	1180.38	12	14.16453	8.9	Pass
KO_III_cont	1231.99	12	14.78385	8.6	Pass
OE_I_cont	1297.02	12	15.56423	8.4	Pass
OE_II_cont	1510.61	9	13.59545	8.7	Pass
OE_III_cont	2206.53	12	26.47837	7.8	Pass
WT_I_cont	3115.2	12	37.38242	8.6	Pass
WT_II_cont	2178.41	12	26.14096	8.1	Pass
WT_III_cont	1973.55	12	23.68263	8.4	Pass
KO_I_Disco	2159.08	12	25.90896	5.7	Pass
KO_II_Disco	5637.5	12	67.64997	6.4	Pass
KO_III_Disco	2558.37	8	20.46697	5.7	Pass
OE_I_Disco	1527.37	12	18.32841	8.5	Pass
OE_II_Disco	1590.7	12	19.08842	5.9	Pass
OE_III_Disco	1879.95	12	22.55936	8.2	Pass
WT_I_Disco	2875.48	12	34.50571	7.4	Pass
WT_II_Disco	3250.49	12	39.00587	6.8	Pass
WT_III_Disco	2538.57	11	27.92426	8.2	Pass

Table E.3: Read quality measures of RNAseq samples as determined by Novogene (section 6.2.2). Raw reads: total amount of reads of raw data. Raw data: (Raw reads) * (sequence length), calculating in gigabyte (GB). Effective: (Clean reads/Raw reads)*100%. Error: base error rate. Q20, Q30: (Base count of Phred value > 20 or 30) / (Total base count). GC: (G & C base count) / (Total base count).

Sample	Raw reads	Raw data (GB)	Effective (%)	Error (%)	Q20 (%)	Q30 (%)	GC (%)
KO_I_cont	106266078	15.9	97.89	0.01	98.24	95.38	60.99
KO_II_cont	102014098	15.3	98.03	0.01	98.23	95.35	62.60
KO_III_cont	99375720	14.9	98.27	0.01	98.22	95.34	62.01
OE_I_cont	107668590	16.2	97.84	0.01	98.21	95.31	60.86
OE_II_cont	66177086	9.9	98.21	0.01	98.01	94.81	62.51
OE_III_cont	87108702	13.1	97.56	0.01	98.21	95.36	59.77
WT_I_cont	85885408	12.9	97.99	0.01	98.25	95.40	62.28
WT_II_cont	95404034	14.3	98.05	0.01	98.23	95.36	61.42
WT_III_cont	81507388	12.2	98.11	0.01	98.25	95.41	61.22
KO_I_Disco	68462624	10.3	96.71	0.01	98.23	95.35	59.64
KO_II_Disco	85548950	12.8	97.83	0.01	98.20	95.29	61.70
KO_III_Disco	90695814	13.6	97.44	0.01	98.20	95.32	59.54
OE_I_Disco	90026202	13.5	98.05	0.01	98.17	95.22	62.15
OE_II_Disco	87012834	13.1	96.81	0.01	98.14	95.23	59.30
OE_III_Disco	78482734	11.8	97.95	0.01	98.17	95.25	61.45
WT_I_Disco	90018034	13.5	98.09	0.01	98.20	95.29	61.51
WT_II_Disco	72826354	10.9	98.05	0.01	97.93	94.56	60.54
WT_III_Disco	86252036	12.9	98.03	0.01	98.21	95.31	62.79

MultiQC

A modular tool to aggregate results from bioinformatics analyses across many samples into a single report.

Report generated on 2024-05-05, 19:02 BST based on data in: `/mnt/d/Darius/X204SC24013263-Z01-F001/X204SC24013263-Z01-F001/analysis`

General Statistics

Copy table | Configure Columns | Plot | Showing 54/72 rows and 8/12 columns.

Sample Name	M Assigned	% rRNA	% mRNA	% Aligned	% Dups	% Dups	% GC	M Seqs
KO_III_Disco_EKRN240002943-1A_222T7HLT4_L2			86.7%	85%	97.6%			
KO_III_Disco_EKRN240002943-1A_222T7HLT4_L2_1						95.3%	59%	45.3
KO_III_Disco_EKRN240002943-1A_222T7HLT4_L2_2						94.6%	59%	45.3
KO_III_cont_EKRN240002934-1A_222T7HLT4_L2			87.7%	94%	90.9%			
KO_III_cont_EKRN240002934-1A_222T7HLT4_L2_1						91.7%	61%	49.7
KO_III_cont_EKRN240002934-1A_222T7HLT4_L2_2						90.9%	62%	49.7
KO_II_Disco_EKRN240002942-1A_222T7HLT4_L2			87.7%	94%	90.8%			
KO_II_Disco_EKRN240002942-1A_222T7HLT4_L2_1						91.8%	61%	42.8
KO_II_Disco_EKRN240002942-1A_222T7HLT4_L2_2						91.0%	62%	42.8
KO_II_cont_EKRN240002933-1A_222T7HLT4_L2			88.2%	94%	89.4%			
KO_II_cont_EKRN240002933-1A_222T7HLT4_L2_1						90.9%	62%	51.0
KO_II_cont_EKRN240002933-1A_222T7HLT4_L2_2						90.4%	62%	51.0
KO_I_Disco_EKRN240002941-1A_222T7HLT4_L2			87.0%	84%	97.0%			
KO_I_Disco_EKRN240002941-1A_222T7HLT4_L2_1						94.8%	59%	34.2
KO_I_Disco_EKRN240002941-1A_222T7HLT4_L2_2						94.1%	60%	34.2
KO_I_cont_EKRN240002932-1A_222T7HLT4_L2			86.3%	92%	95.7%			
KO_I_cont_EKRN240002932-1A_222T7HLT4_L2_1						94.3%	60%	53.1
KO_I_cont_EKRN240002932-1A_222T7HLT4_L2_2						93.5%	61%	53.1
OE_III_Disco_EKRN240002946-1A_222T7HLT4_L2			86.4%	93%	91.6%			
OE_III_Disco_EKRN240002946-1A_222T7HLT4_L2_1						91.8%	61%	39.2
OE_III_Disco_EKRN240002946-1A_222T7HLT4_L2_2						91.2%	61%	39.2
OE_III_cont_EKRN240002937-1A_222T7HLT4_L2			85.2%	88%	96.6%			
OE_III_cont_EKRN240002937-1A_222T7HLT4_L2_1						94.7%	59%	43.6
OE_III_cont_EKRN240002937-1A_222T7HLT4_L2_2						93.8%	60%	43.6
OE_II_Disco_EKRN240002945-1A_222T7HLT4_L2			85.3%	82%	97.9%			
OE_II_Disco_EKRN240002945-1A_222T7HLT4_L2_1						95.5%	59%	43.5
OE_II_Disco_EKRN240002945-1A_222T7HLT4_L2_2						94.6%	59%	43.5
OE_II_cont_EKRN240002936-1A_222T7HLT4_L2			88.8%	93%	84.5%			
OE_II_cont_EKRN240002936-1A_222T7HLT4_L2_1						87.4%	62%	33.1
OE_II_cont_EKRN240002936-1A_222T7HLT4_L2_2						86.1%	62%	33.1
OE_I_Disco_EKRN240002944-1A_222T7HLT4_L2			87.3%	94%	89.5%			
OE_I_Disco_EKRN240002944-1A_222T7HLT4_L2_1						90.7%	62%	45.0
OE_I_Disco_EKRN240002944-1A_222T7HLT4_L2_2						89.8%	62%	45.0
OE_I_cont_EKRN240002935-1A_222T7HLT4_L2			86.4%	91%	95.0%			
OE_I_cont_EKRN240002935-1A_222T7HLT4_L2_1						93.8%	60%	53.8
OE_I_cont_EKRN240002935-1A_222T7HLT4_L2_2						93.0%	61%	53.8
WT_III_Disco_EKRN240002949-1A_222T7HLT4_L2			87.9%	95%	81.9%			
WT_III_Disco_EKRN240002949-1A_222T7HLT4_L2_1						87.2%	62%	43.1
WT_III_Disco_EKRN240002949-1A_222T7HLT4_L2_2						86.6%	62%	43.1
WT_III_cont_EKRN240002940-1A_222T7HLT4_L2			86.4%	94%	90.1%			
WT_III_cont_EKRN240002940-1A_222T7HLT4_L2_1						91.7%	61%	40.8
WT_III_cont_EKRN240002940-1A_222T7HLT4_L2_2						90.6%	61%	40.8
WT_II_Disco_EKRN240002948-1A_222T7HLT4_L2			86.2%	89%	93.6%			
WT_II_Disco_EKRN240002948-1A_222T7HLT4_L2_1						92.8%	60%	36.4
WT_II_Disco_EKRN240002948-1A_222T7HLT4_L2_2						90.7%	61%	36.4
WT_II_cont_EKRN240002939-1A_222T7HLT4_L2			87.0%	94%	91.4%			
WT_II_cont_EKRN240002939-1A_222T7HLT4_L2_1						92.3%	61%	47.7
WT_II_cont_EKRN240002939-1A_222T7HLT4_L2_2						91.5%	61%	47.7
WT_I_Disco_EKRN240002947-1A_222T7HLT4_L2			87.0%	93%	91.0%			
WT_I_Disco_EKRN240002947-1A_222T7HLT4_L2_1						91.7%	61%	45.0
WT_I_Disco_EKRN240002947-1A_222T7HLT4_L2_2						90.8%	61%	45.0
WT_I_cont_EKRN240002938-1A_222T7HLT4_L2			87.8%	95%	82.7%			
WT_I_cont_EKRN240002938-1A_222T7HLT4_L2_1						88.2%	62%	42.9
WT_I_cont_EKRN240002938-1A_222T7HLT4_L2_2						87.5%	62%	42.9

featureCounts

Subread featureCounts is a highly efficient general-purpose read summarization program that counts mapped reads for genomic features such as genes, exons, promoter, gene bodies, genomic bins and chromosomal locations. *DOI: 10.1093/bioinformatics/btt656.*

Warning: 18 samples hidden. **See toolbox.**

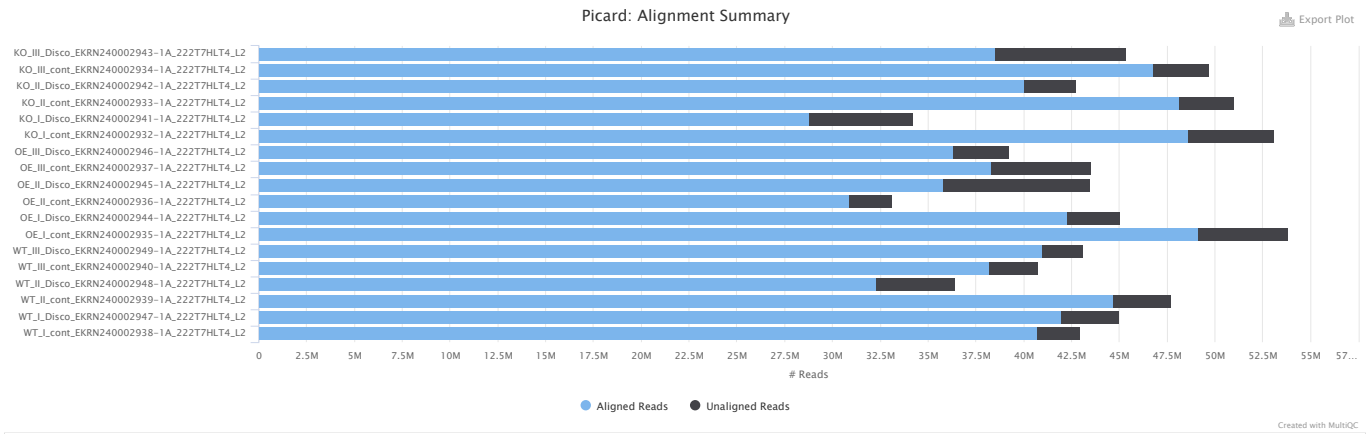
Picard

Picard is a set of Java command line tools for manipulating high-throughput sequencing data.

Alignment Summary

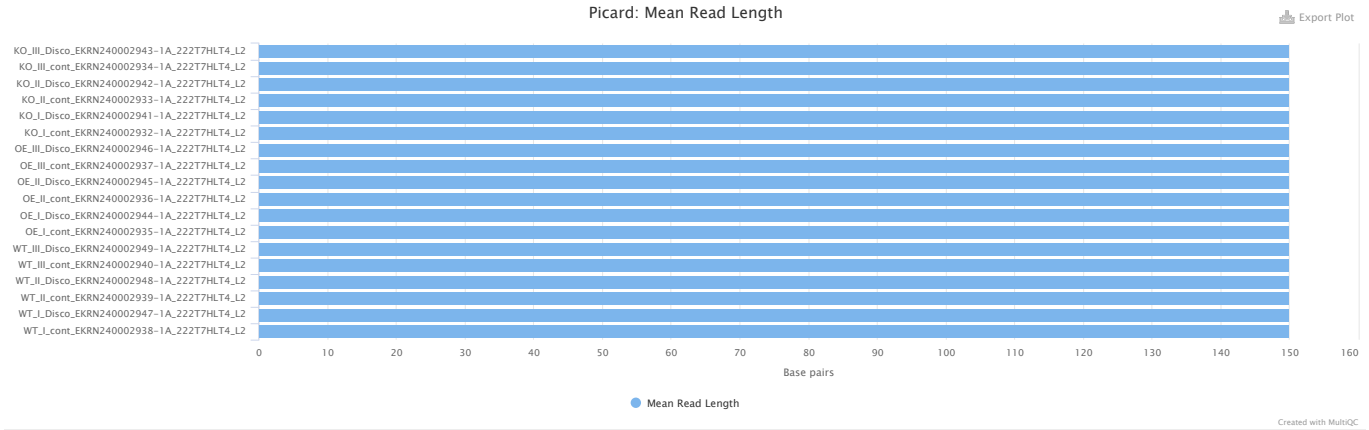
Please note that Picard's read counts are divided by two for paired-end data. Total bases (including unaligned) is not provided.

Counts | Percentages | Aligned Reads | Aligned Bases



Mean read length

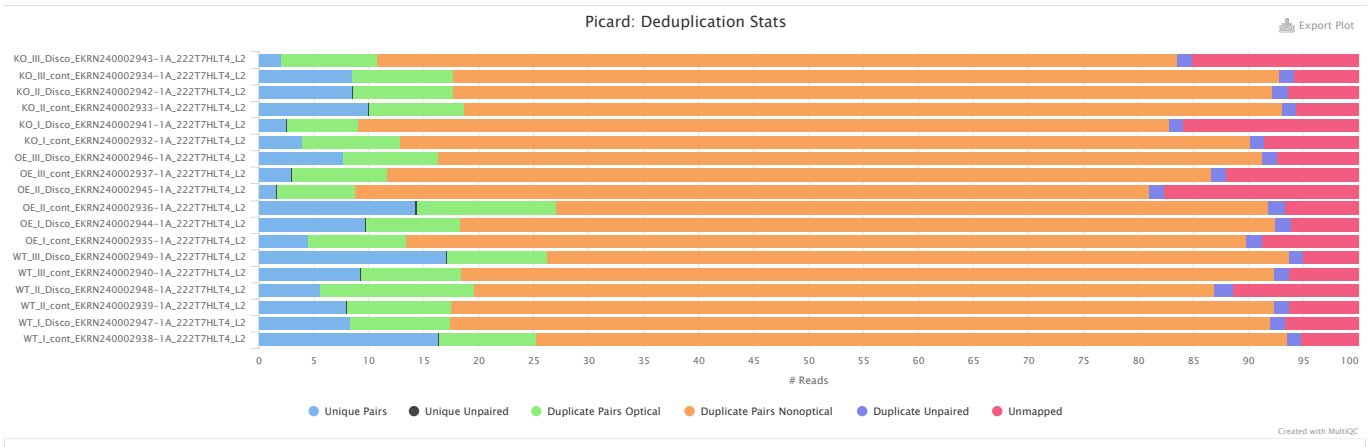
The mean read length of the set of reads examined.



Mark Duplicates

Number of reads, categorised by duplication state. **Pair counts are doubled** - see help text for details.

Number of Reads | Percentages

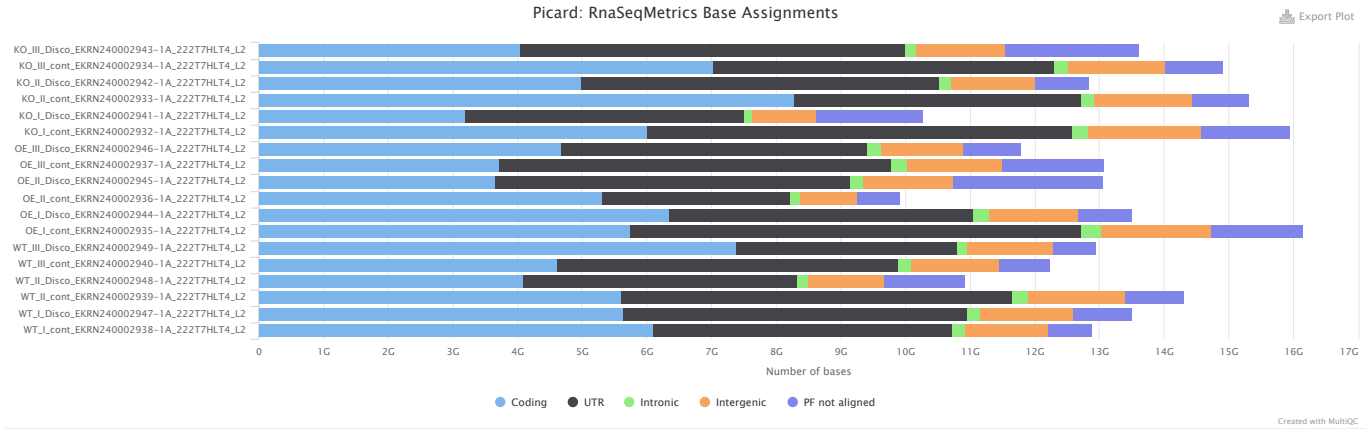


RnaSeqMetrics Assignment

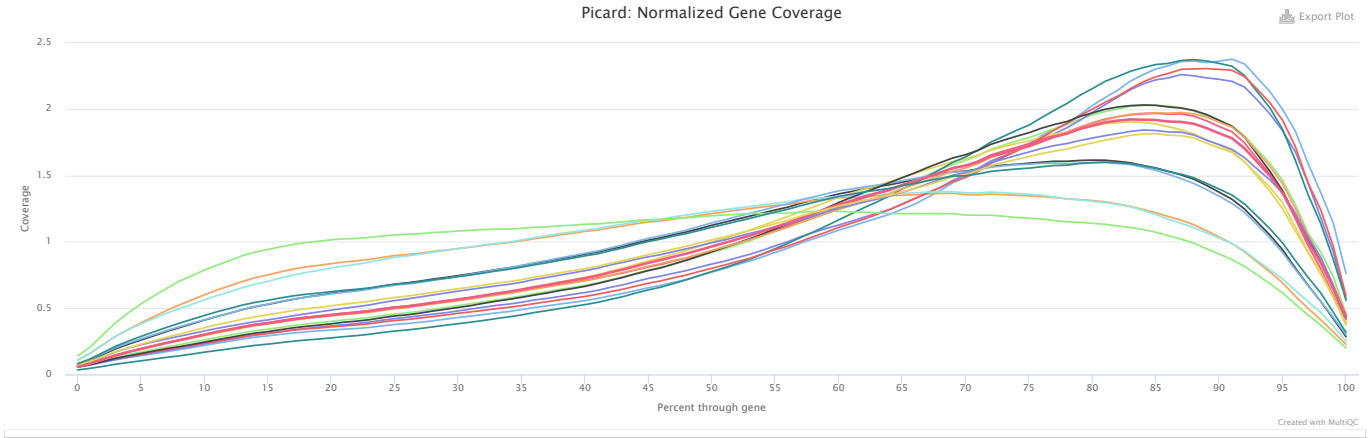
Number of bases in primary alignments that align to regions in the reference genome.

⚠ Picard was run without an rRNA annotation file **18 samples**, therefore the ribosomal assignment is not available. To correct, rerun with the `RIBOSOMAL_INTERVALS` parameter, as documented here.

Counts | Percentages



Gene Coverage



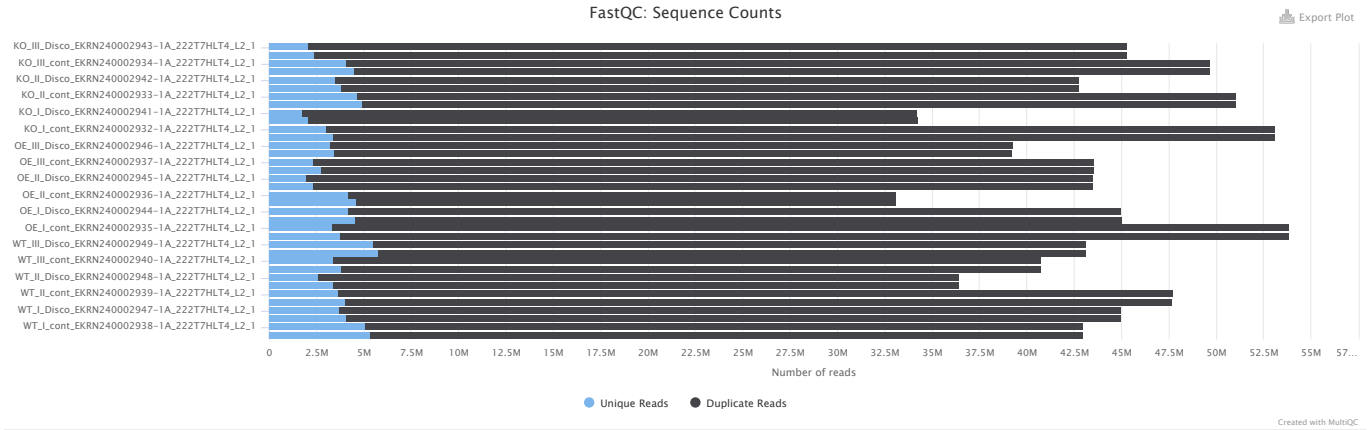
FastQC

FastQC is a quality control tool for high throughput sequence data, written by Simon Andrews at the Babraham Institute in Cambridge.

Sequence Counts

Sequence counts for each sample. Duplicate read counts are an estimate only.

Number of reads | Percentages



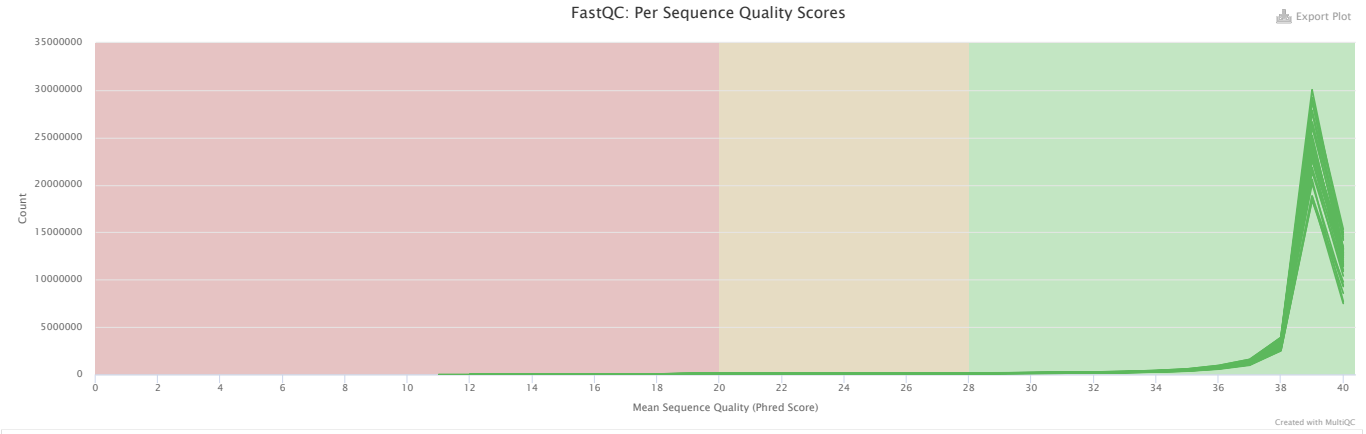
Sequence Quality Histograms 36

The mean quality value across each base position in the read.



Per Sequence Quality Scores 36

The number of reads with average quality scores. Shows if a subset of reads has poor quality.



Per Base Sequence Content 19

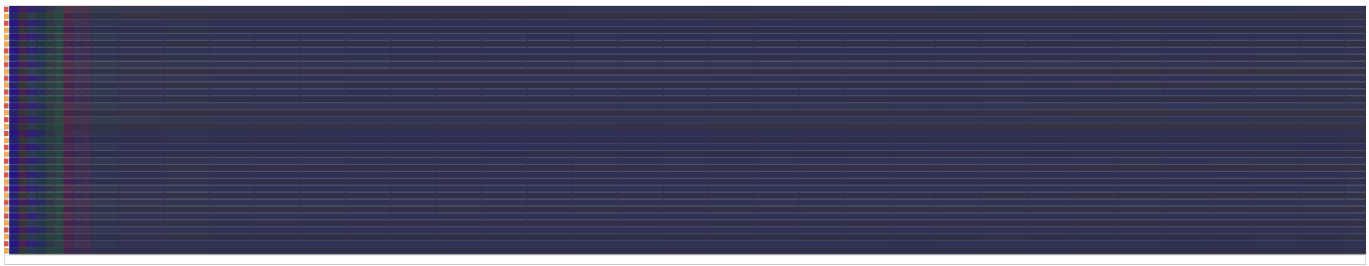
The proportion of each base position for which each of the four normal DNA bases has been called.

Click a sample row to see a line plot for that dataset.

Rollover for sample name

Position: - %T: - %C: - %A: - %G: -

Export Plot

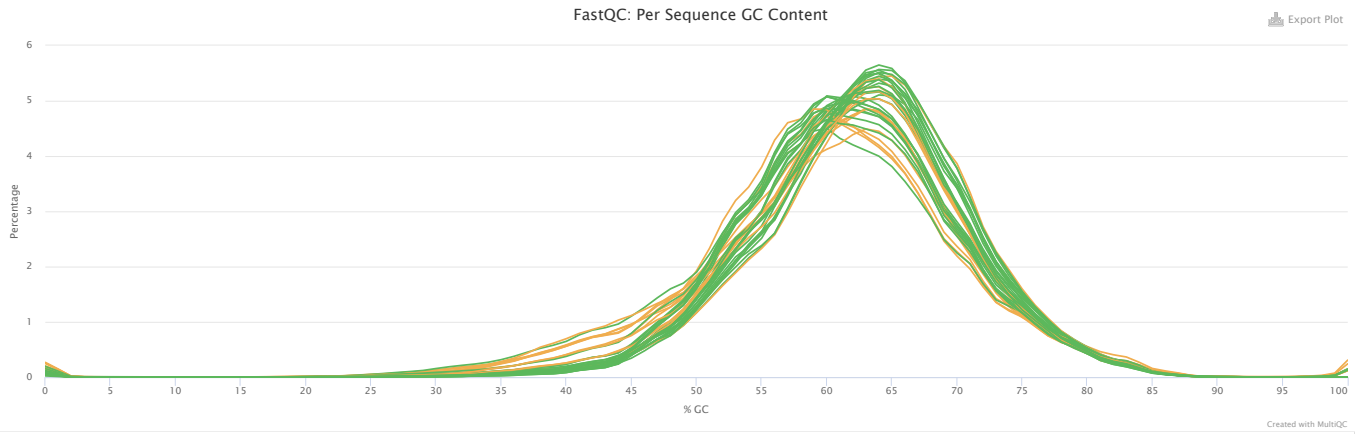


Per Sequence GC Content

24 12

The average GC content of reads. Normal random library typically have a roughly normal distribution of GC content.

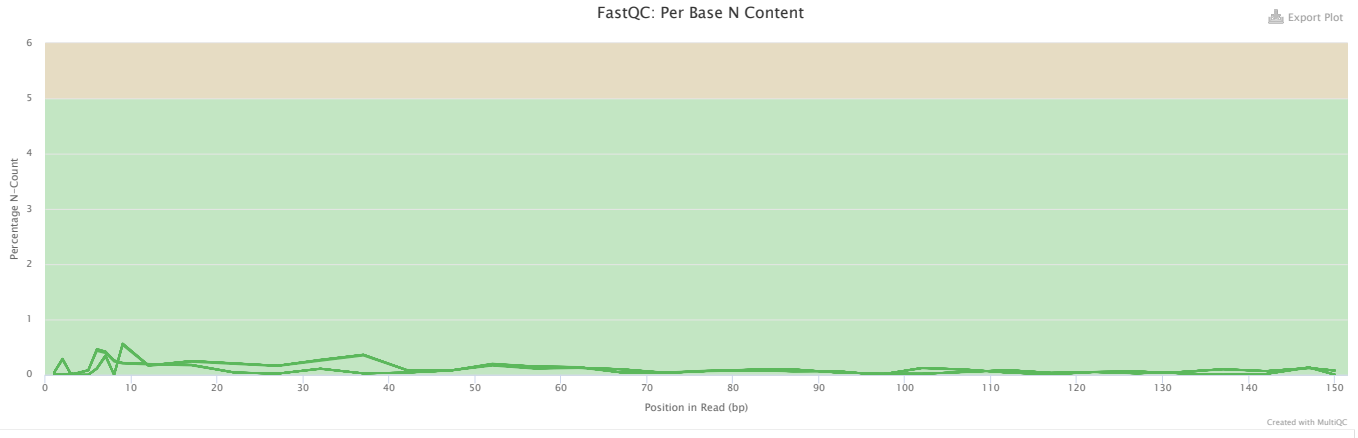
Percentages | Counts



Per Base N Content

36

The percentage of base calls at each position for which an N was called.



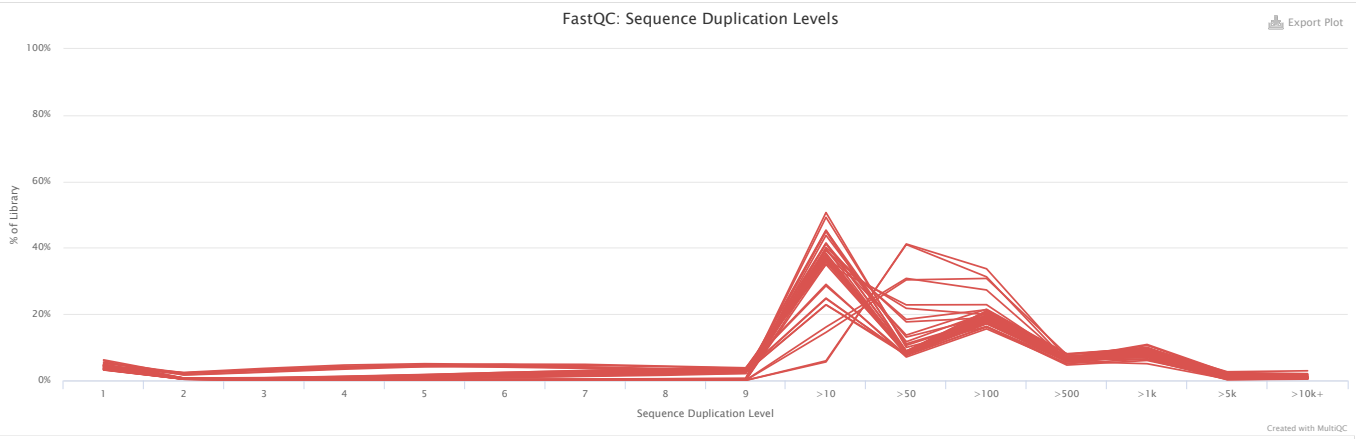
Sequence Length Distribution

36

All samples have sequences of a single length (150bp).

Sequence Duplication Levels

The relative level of duplication found for every sequence.



Overrepresented sequences

7 29

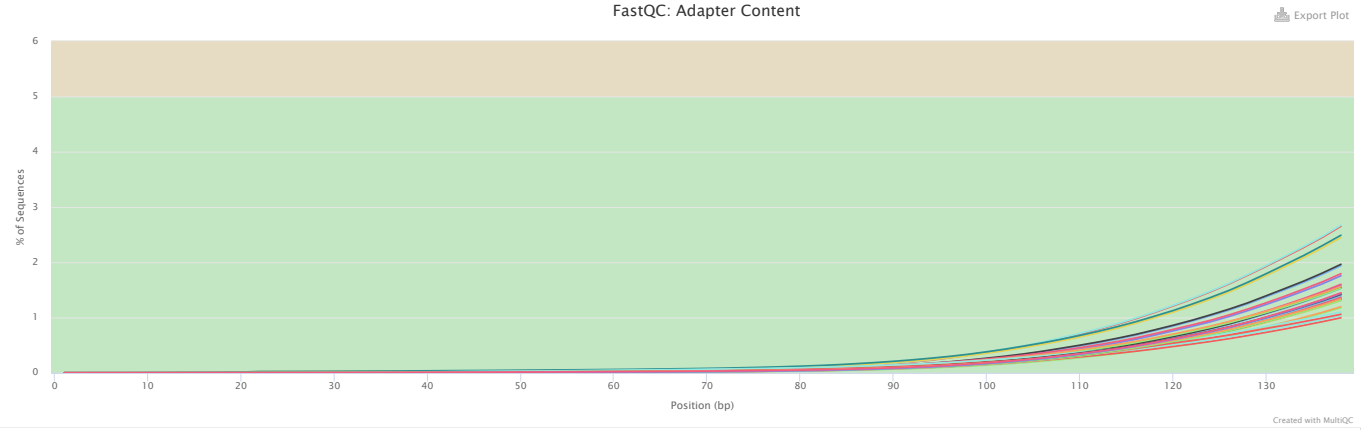
The total amount of overrepresented sequences found in each library.

36 samples had less than 1% of reads made up of overrepresented sequences

Adapter Content

36

The cumulative percentage count of the proportion of your library which has seen each of the adapter sequences at each position.



Status Checks

Status for each FastQC section showing whether results seem entirely normal (green), slightly abnormal (orange) or very unusual (red).

Sort by highlight Min: 0 Max: 1

